

Final Report

**METEOROLOGICAL MODELING FOR
THE SOUTHERN APPALACHIAN MOUNTAINS INITIATIVE (SAMI)**

Prepared by:

Kevin Doty
University of Alabama in Huntsville
320 Sparkman Drive
Huntsville, AL 35805

Thomas W. Tesche and Dennis E. McNally
Alpine Geophysics, LLC
3479 Reeves Dr.
Ft. Wright, KY 41017

Brian Timin
U.S. Environmental Protection Agency
Office of Air Quality Planning and Standards
Air Quality Modeling Group, MD 14
Research Triangle Park, NC 27711

Stephen F. Mueller
Tennessee Valley Authority
Energy Research & Technology Applications
P.O. Box 1010
Muscle Shoals, AL 35662-1010

July 2002

EXECUTIVE SUMMARY

1	INTRODUCTION	10
1.1	OVERVIEW	10
1.2	EPISODE SELECTION CRITERIA	10
1.3	METEOROLOGICAL MODEL EVALUATION	11
1.3.1	<i>The Importance of Meteorological Model Performance Evaluation</i>	11
1.3.2	<i>Evaluation Objectives</i>	12
1.3.3	<i>The Evaluation Process</i>	13
1.3.4	<i>Complementary Perspectives Brought to this Evaluation</i>	14
1.3.5	<i>Structure of Report</i>	15
2.0	THE METEOROLOGICAL MODEL	15
2.1	OVERVIEW OF RAMS	15
2.2	RAMS HORIZONTAL GRID STRUCTURE	15
2.3	RAMS VERTICAL GRID STRUCTURE	17
2.4	RAMS MODEL MODIFICATIONS	19
2.4.1	<i>Surface Grid Files</i>	19
2.4.2	<i>Model Physics Changes</i>	20
2.5	OTHER DIFFERENCES WITH RESPECT TO METEOROLOGICAL MODELING PROTOCOL	30
2.6	RAMSIN SELECTIONS	30
3.0	OVERVIEW OF RAMS SIMULATION PROCESS	33
3.1	NCEP/NCAR REANALYSIS DATA	33
3.2	PREPARATION OF RAMS INPUT AND NUDGING FILES	33
4.0	THE SAMI MODELING EPISODES	35
4.1	SAMI EPISODE SELECTION	35
4.1.2	<i>Important Meteorological and Air Quality Variables</i>	39
4.1.3	<i>CART Performance</i>	40
4.1.4	<i>Episode Selection Software</i>	40
4.1.5	<i>Episode Software “Theory”</i>	41
4.1.6	<i>Episode Software Rules</i>	42
4.1.7	<i>Episode Selection Error Terms</i>	42
4.1.8	<i>Biased (Unscaled) Error</i>	43
4.1.9	<i>Distance (Scaled) Error</i>	43
4.1.10	<i>Reproducing the Annual and Seasonal Metrics</i>	45
4.2	THE 11-19 JULY 1995 EPISODE	50
4.3	THE 9-18 MAY 1993 EPISODE	56
4.4	THE 21 MARCH - 1 APRIL 1993 EPISODE	62
4.5	THE 6-14 FEBRUARY 1994 EPISODE	68
4.6	THE 21 JULY - 1 AUGUST 1991 EPISODE	74
4.7	THE 3-12 AUGUST 1993 EPISODE	80
4.8	THE 22-29 JUNE 1992 EPISODE	81
4.9	THE 24 APRIL – 3 MAY 1995 EPISODE	82
4.10	THE 22-30 MAY 1995 EPISODE	97
4.10	THE 22-30 MAY 1995 EPISODE	98
5.0	TECHNICAL APPROACH TO THE MODEL PERFORMANCE EVALUATION	104
5.0	TECHNICAL APPROACH TO THE MODEL PERFORMANCE EVALUATION	104
5.1	COMPONENTS OF THE RAMS EVALUATION	104
5.2	DATA SUPPORTING MODEL EVALUATION	104
5.3	STATISTICAL AND GRAPHICAL EVALUATION TOOLS	105
5.3.1	<i>Mean and Global Statistics</i>	105
5.3.2	<i>Difference Statistics</i>	106
5.3.3	<i>Skill Measures</i>	109

5.3.4	<i>Graphical Tools</i>	110
6.0	EVALUATION OF SURFACE METEOROLOGICAL FIELDS	113
6.1	11-19 JULY 1995 EPISODE RESULTS	114
6.1.1	<i>48-km Results</i>	116
6.1.2	<i>12-km Results</i>	122
6.2	22-30 MAY 1995 EPISODE RESULTS.....	126
6.2.1	<i>96-km Results</i>	126
6.2.2	<i>12-km Results</i>	132
6.3	9-18 MAY 1993 EPISODE RESULTS.....	136
6.3.1	<i>96-km Results</i>	136
6.3.2	<i>12-km Results</i>	142
6.4	21 MARCH TO 1 APRIL 1993 EPISODE RESULTS	145
6.4.1	<i>96-km Results</i>	145
6.4.2	<i>12-km Results</i>	152
6.5	6-14 FEBRUARY 1994 EPISODE RESULTS	155
6.5.1	<i>96-km Results</i>	155
1.1.1	<i>6.5.2 12-km Results</i>	162
1.1.1	<i>6.5.2 12-km Results</i>	162
6.6	21 JULY - 1 AUGUST 1991 EPISODE RESULTS	166
6.6.1	<i>96-km Results</i>	166
6.6.2	<i>12-km Results</i>	172
6.7	3-12 AUGUST 1993 EPISODE RESULTS.....	177
6.7.1	<i>Surface Temperatures</i>	177
6.7.2	<i>Surface Wind Speed and Direction</i>	178
6.7.3	<i>Mixing Ratios</i>	180
6.7.4	<i>Precipitation</i>	180
6.8	22-29 JUNE 1992 EPISODE RESULTS	204
6.8.1	<i>Surface Temperatures</i>	204
6.8.2	<i>Surface Wind Speed and Direction</i>	205
6.8.3	<i>Mixing Ratios</i>	207
6.8.4	<i>Precipitation</i>	208
6.9	24 APRIL – 3 MAY 1995 EPISODE RESULTS.....	232
6.9.1	<i>Surface Temperatures</i>	232
6.9.2	<i>Surface Wind Speed and Direction</i>	233
6.9.3	<i>Mixing Ratios</i>	234
6.9.4	<i>Precipitation</i>	236
7.0	EVALUATION OF ALOFT METEOROLOGICAL FIELDS	259
7.1	11-19 JULY 1995 EPISODE	260
7.2	22-30 MAY 1995 EPISODE.....	264
7.3	9-18 MAY 1993 EPISODE.....	268
7.4	21 MARCH TO 1 APRIL 1993 EPISODE RESULTS	272
7.5	6-14 FEBRUARY 1994 EPISODE RESULTS	276
7.6	21 JULY - 1 AUGUST 1991 EPISODE RESULTS	280
7.7	3-12 AUGUST 1993 EPISODE RESULTS.....	284
7.7.1	<i>Statistics of Aloft Predictions of Temperatures and Winds</i>	284
7.7.2	<i>Vertical Profiles of Mixing Ratios, Temperatures and Winds</i>	285
7.8	23-29 JUNE 1992 EPISODE RESULTS	285
7.8.1	<i>Statistics of Aloft Predictions of Temperatures and Winds</i>	285
7.8.2	<i>Vertical Profiles of Mixing Ratios, Temperatures and Winds</i>	285
7.9	24 APRIL – 3 MAY 1995 EPISODE RESULTS.....	286
7.9.1	<i>Statistics of Aloft Predictions of Temperatures and Winds</i>	286
7.9.2	<i>Vertical Profiles of Mixing Ratios, Temperatures and Winds</i>	286

8.0	RAMS PERFORMANCE ACROSS SAMI EPISODES	291
8.1	EPISODE COMPOSITE NEAR-GROUND LEVEL PERFORMANCE MEASURES	291
8.1.1	<i>Bias and Error in Mean 2 m Temperatures</i>	291
8.1.2	<i>Bias and Error in Mean 10 m Wind Speeds</i>	291
8.1.3	<i>Bias and Error in Mean 10 m Wind Directions</i>	292
8.1.4	<i>Bias and Error in 2 m Mixing Ratios</i>	292
8.2	TIME SERIES OF SPATIAL MEAN SURFACE WINDS, TEMPERATURE AND MIXING RATIOS	292
8.2.1	<i>Spatial Mean Temperatures</i>	293
8.2.2	<i>Vector Mean Wind Speeds</i>	293
8.2.3	<i>Mean Wind Direction Differences</i>	293
8.2.4	<i>Index of Agreement</i>	293
8.2.5	<i>RMSE Errors</i>	294
8.2.6	<i>Spatial Mean Mixing Ratios</i>	294
8.3	COMPARISON WITH OTHER PROGNOSTIC MODEL EVALUATION STUDIES	294
8.3.1	<i>Bias and Error in Mean Temperatures</i>	294
8.3.2	<i>Bias and Error in Mean Mixing Ratios</i>	295
8.3.3	<i>Average Discrepancy in Mean Wind Speed</i>	295
8.3.4	<i>RMSE Errors</i>	295
8.3.5	<i>Index of Agreement</i>	296
8.3.6	<i>Average Discrepancy in Mean Wind Direction</i>	296
9.0	SUMMARY AND CONCLUSIONS	333
9.1	OPERATIONAL EVALUATION SUMMARY	333
9.1.1	<i>9-20 July 1995</i>	333
9.1.2	<i>22-30 May 1995</i>	333
9.1.3	<i>9-18 May 1993</i>	334
9.1.4	<i>21 March - 1 April 1993</i>	334
9.1.5	<i>6-14 February 1994</i>	334
9.1.6	<i>21 July - 1 August 1991</i>	335
9.1.7	<i>22-29 June 1992</i>	337
9.1.8	<i>24 April - 3 May 1995</i>	338
9.2	SCIENTIFIC EVALUATION SUMMARY	339
9.2.1	<i>3-12 August 1993</i>	340
9.2.2	<i>22-29 June 1992</i>	341
9.2.3	<i>24 April - 3 May 1995</i>	341
9.3	CONCLUSIONS	341
9.3.1	<i>Aloft Winds and Temperatures</i>	346
9.4	ADEQUACY OF THE SAMI METEOROLOGICAL MODELING FOR AIR QUALITY MODELING	347
9.4.1	<i>Framing the Questions to Be Addressed</i>	347
9.4.2	<i>Comparison of SAMI RAMS Performance Against Newly Proposed Meteorological Model Performance Benchmarks</i>	353
9.4.3	<i>Concluding Assessment of the SAMI RAMS Application</i>	354
9.5	IN SUMMARY	361
9	REFERENCES	364
10.	APPENDIX 1:.....	391
11.	APPENDIX 2:.....	406
12.	APPENDIX 3:.....	418
13.	APPENDIX 4:.....	414
1.	Introduction	415
2.	Meteorological Model Domain and Grid Configuration.....	416
2.1	METEOROLOGICAL MODEL DOMAIN.....	416
2.1.1	<i>Horizontal Extent of Meteorological Domain</i>	416
2.1.2	<i>Vertical Extent of Domain</i>	417

2.2	GRID CONFIGURATION	417
2.2.1	<i>Horizontal Grid Configuration</i>	417
2.2.3	<i>Vertical Grid Configuration</i>	418
3.	Model Inputs	418
3.1	ATMOSPHERIC DATA	418
3.2	SURFACE CHARACTERISTICS.....	419
4.	Model Configuration.....	419
4.1	NESTING VS. STAND-ALONE DOMAINS.....	419
4.2	MOIST PROCESSES	420
4.2.1	<i>Cumulus Parameterization</i>	420
4.2.2	<i>Grid-scale Moist Processes</i>	420
4.3	FOUR-DIMENSIONAL DATA ASSIMILATION (FDDA).....	420
4.4	OTHER CONFIGURATION CONSIDERATIONS	421
4.4.1	<i>Model Physics</i>	421
4.4.2	<i>Finite-Difference Formulation</i>	421
4.4.3	<i>Diffusion</i>	421
4.4.4	<i>Radiation</i>	421
4.4.5	<i>Soil Model</i>	422
4.4.6	<i>Model Physics Changes</i>	422
5.	Model Output.....	422
6.	Evaluation of Meteorological Fields	422
6.1	ROUTINE OBSERVATIONS	423
6.2	COMPARISON WITH WIND/TEMPERATURE PROFILER MEASUREMENTS	423
6.3	COMPARISON OF CLOUD FIELDS WITH SATELLITE IMAGES	423
6.4	COMPARISON WITH MM5 OUTPUT	424
6.5	LAGRANGIAN PARTICLE MODEL TRAJECTORY VISUALIZATIONS	424
7.	Post-Processing of Meteorological Fields	424
7.1	MAP PROJECTIONS	424
7.2	INTERPOLATION OF RAMS FIELDS TO THE URM-1ATM GRID.....	425
7.3	CONSERVATION OF MASS	425
8.	Computational Considerations.....	425
9.	Quality Assurance	425
9.1	APPROPRIATENESS OF INPUT DATA SETS	425
9.2	FILE DOCUMENTATION.....	427

EXECUTIVE SUMMARY

Environmental assessments made by the Southern Appalachian Mountains Initiative (SAMI) are based on chemical transport modeling conducted by the Georgia Institute of Technology (GIT) and the Tennessee Valley Authority (TVA). For this work GIT and TVA used the GIT Urban-Regional Multiscale URM-1ATM model. Both GIT and TVA used subcontractors—University of Alabama in Huntsville (UAH) and Alpine Geophysics, LLC (AG), respectively—to do the meteorological modeling. This was done using a version of the RAMS meteorological model that was modified and tested by Dr. Kevin Doty at UAH.

Simulated meteorological fields were produced to drive the transport, diffusion and chemical reactions in the URM-1ATM model. SAMI recognized early that, in an effort to address multiple air quality-related impacts from ozone, fine aerosols (visibility) and acid deposition, it had to examine multiple pollutants over relatively long time periods. This required a methodology for estimating seasonal (for ozone) to annual (for visibility and deposition) pollutant levels. Simulations of 7-12 months in length were impractical for studying multiple emission scenarios given the schedule and budget for the SAMI assessment. Therefore, SAMI chose to build its assessment using episodic modeling.

A contractor to SAMI classified as many days as possible during the 1991-1995 period according to meteorology and levels of ozone, aerosols and wet deposition observed at two target sites: Great Smoky Mountains National Park and Shenandoah National Park. Key time periods, or episodes, were identified from these classifications as being representative of similar conditions over the entire 5-year period. Weights were assigned to the episodes (either by day or week, depending on pollutant), enabling SAMI to scale up episodic model results to seasonal and annual average conditions at the target sites. Consequently, 69 days in nine individual episodes were selected to represent seasonal or annual pollutant conditions with a minimum of bias. Two episodes occurred in winter (outside the ozone season), two were in spring and four were in summer. Episodes were 6 to 9 days long.

Individual days were classified, when data were available, as falling into one of four ozone classes ranging from low to very high ozone levels. Similarly, days were classified as falling into one of five visibility classes based on fine aerosol mass. Weeks were classified as falling into one of four wet deposition categories based on the sum of major cation and anion wet deposition species. Each target site had its own separate set of classified days and weeks. Each modeling episode experienced precipitation, but some weeks had only light amounts and others experienced moderate or heavy amounts. Ozone season episodes experienced a wide range of daily ozone levels. However, visibility conditions (total aerosol mass) exhibited less variation within each episode.

UAH experimented with different model options and input data before selecting a common set to be applied across all episodes. A modeling domain was designed that, except for one episode, covered all the continental United States. The lone exception was the first episode modeled: a summer period that, because of light winds, was adequately simulated using a somewhat smaller grid. Initial and boundary nudging fields were derived using the NCEP Reanalysis data set. Nested model grids of different spatial resolution were used. In all cases the finest had a grid cell spacing of 12 km.

Several problems were experienced early in the modeling. One critical problem was achieving surface temperature and water vapor mixing ratio values that were unbiased, on average, across the modeling domain. Selective, non-uniform surface nudging was implemented in the model. Note that no direct nudging of meteorological variables was done in the lower portion of the finest (12-km) grid. However, a unique form of surface heat and moisture flux nudging on the finest grid was applied to improve model performance. Another critical problem was initiating convective precipitation in regions where the predominant forcing mechanism was active at sub-grid scales. In general, convective precipitation was difficult to reproduce. Problems with precipitation modeling caused significant delays in selecting the final version of the model. Some changes were made to the standard RAMS convective parameterization scheme, and for one episode an entirely different scheme was substituted. Other adjustments were made to standard RAMS microphysics, radiation schemes, the water vapor diffusion scheme, the soil moisture initialization process and a few other physical parameterizations. All changes were made after efforts to model an episode indicated biases in various output variables.

Each meteorological simulation was evaluated against observations. Standard National Weather Service (NWS) surface observations were used to compute a suite of statistical metrics of surface model performance for temperature, mixing ratio, and wind speed and direction. NWS and TVA precipitation measurements were used to compute errors in model precipitation amount. NWS upper air data were used to evaluate model performance. These latter data heavily influenced the nudging fields. Thus, upper level comparisons with model results only indicated how well the model nudging was able to maintain consistency with the nudging fields.

Grid-averaged model bias, gross error, and other metrics were analyzed for the 12-km grid. Two different techniques were used to estimate grid-wide metrics. One method first produced a gridded field of observations by interpolating from the surface observations and then comparing vertically interpolated (to correct for height mismatch) model results with gridded observations. The other method compared observations at measurement sites directly with model results for grid cells containing the sites without doing any spatial interpolations of observations or model output. Statistical metrics varied between the two approaches. For example, the gridded method estimated a mean temperature bias of about $-1.2\text{ }^{\circ}\text{C}$ across all 9 episodes, whereas the direct-comparison method yielded a bias, for 7 of the episodes, of $-0.8\text{ }^{\circ}\text{C}$. However, the gridded technique produced a negative bias over elevated terrain that was an artifact of the methodology and contributed to the appearance of a bias that was essentially unverifiable. Thus, the difference in results between the two methods is not considered important, whereas a surface temperature bias of about $-1\text{ }^{\circ}\text{C}$ is considered to be quite good.

In other episode averaged comparisons, modeled surface wind speed was found to be biased high across episodes by roughly 0.8 to 1.1 m s^{-1} . Modeled surface mixing ratio was found to be biased low by an amount somewhere between 0.1 and 0.6 g kg^{-1} . Modeled surface wind direction was computed by both methods to have a bias, across episodes, within one degree of zero. Therefore, two methods both indicated that the meteorological modeling provided reasonably accurate surface-level reproductions of relevant parameters. Of course, larger biases and prediction errors were found when comparing model results and observations on a daily and an hourly basis.

Comparisons between modeled fields and observations aloft indicated that the maximum daily computed

mixing height over the fine grid was nearly always within ± 400 m of that estimated from upper air data. A couple episodes indicated some modest bias one way or the other. However, the spatial and temporal average for most episodes was typically within ± 200 m. A check of model conformity to upper air conditions for three of the episodes revealed that temperatures usually agreed within about 0.5 °C and wind speeds usually agreed within 1 m s⁻¹. This level of agreement was expected because of the influence of nudging.

An overview is provided of meteorological modeling performance statistics from over 20 modeling episodes other than SAMI. Regarding surface temperature, other studies have achieved results having biases in the -0.7 to 1.6 °C range. Most if not all of these studies relied on nudging to achieve such good results. The biases produced for the SAMI work are not that much different considering that no direct nudging of low-level temperature was done on the finest resolution grid. Likewise, mixing ratio bias for the non-SAMI episodes ranged between -2.0 and 0.8 g kg⁻¹, while SAMI episodes were between -0.6 and 0.0 g kg⁻¹. Wind speed root mean square error (RMSE) ranged between 1.6 and 3.2 m s⁻¹ for the non-SAMI studies, and SAMI RMSE was between 1.9 and 2.8 m s⁻¹. Finally, wind direction biases as large as 120 degrees occurred in non-SAMI episodes, while the largest for a SAMI episode was 103 degrees. These comparisons indicate that the SAMI modeling produced results that are at least as accurate as those for modeling done using other models, domains, and time periods.

One of the most important questions addressed in this report concerns whether the RAMS meteorological fields are adequate for their intended use in supporting the acid deposition modeling in SAMI. For the reasons discussed in Chapter 9, we are not able to answer this question definitively, yet a significant amount of information was developed in this study that supports our finding that the RAMS modeling results are suitable for use in the UAM-AERO acid deposition modeling although a number of important questions remain to be answered fully.

There is no simple way to answer definitively the question of whether the RAMS fields are adequate as input to the SAMI acid deposition model. There are no universally accepted performance benchmarks that, if passed, would allow one to declare unequivocally that the RAMS fields are appropriate for use. For complex atmospheric modeling problems like the ones being addressed by SAMI, it is quite doubtful that such a set of definitive performance criteria will ever be completely sufficient. The question of meteorological data set adequacy depends, at a minimum, upon the specific host emissions and air quality models and the nature of the modeling episodes being used. Meteorological fields that might be adequate for use in one situation may be quite deficient in another if the particular chemical and physical processes that must be simulated are different. Thus, quantitative statistical and graphical performance criteria, though helpful, are inherently insufficient in telling modelers and decision-makers whether meteorological fields are adequate for air quality modeling. In this study, we developed and then applied a multi-step evaluation process whereby the adequacy of the RAMS fields for use in the SAMI acid deposition modeling was evaluated.

In addition to comparing the SAMI results with a large range of previous meteorological model evaluation studies in the U.S., we also compared the RAMS evaluation results with a recently proposed set of meteorological model evaluation benchmarks based on the most recent model evaluation literature. While

these benchmarks are not aimed at assigning a passing or failing grade to a particular meteorological model application, they do help put the results into a useful context for decision-makers. Based on these and other analyses reported in Chapter 9, our overall conclusions regarding the adequacy of the RAMS modeling and the reliability of the meteorological fields supplied to the URM-AERO model are as follows:

- > The SAMI meteorological modeling activity clearly selected an appropriate regional prognostic model for use in the assessment;
- > The RAMS modeling was carried out in a logical, sound, well-documented manner that was consistent with good scientific principles and the procedures commonly used in the application of this sophisticated model;
- > The suite of evaluation procedures employed to test the RAMS model were comprehensive and reflected several different model testing perspectives;
- > The data base available to test the RAMS model was extremely limited, precluding a number of meaningful, stressful tests of the model to ascertain whether it suffers from internal, compensating errors; as the result, model testing was confined principally to an operational evaluation;
- > Generally, the RAMS performance for surface and aloft winds, temperatures, mixing ratios, and precipitation are consistent with contemporary modeling experience and with new proposed evaluation benchmarks;
- > In some cases, notably the under-prediction bias for surface temperature and over-prediction bias for surface wind speed, the RAMS model exhibits (for some episodes) features that could have an effect on the air quality model estimates; however, this has not been verified through sensitivity experiments with the URM-AERO modeling system to demonstrate that these biases are indeed important. In other cases, notably mixing ratio, the RAMS performance was much better than is typically encountered with modeling of this complexity; and
- > None of the performance testing results conducted have revealed flaws in RAMS performance of such a magnitude as to clearly indicate the presence of errors that would render the model inappropriate for use as input to regional air quality models.

We conclude that the RAMS meteorological fields may be used, with appropriate cautions, as input to the regional emissions and photochemical/aerosol models for each of the episodes selected for the SAMI assessment.

Description of Selected Acronyms

Acronym	Description
AG	Alpine Geophysics
AVHRR	Advanced Very High Resolution Radiometer
FDDA	Four-Dimensional Data Assimilation
GIT	Georgia Institute of Technology
GSM	Great Smoky Mountains National Park
MAPS	Model Performance Evaluation Analysis and Plotting Software
MM5	NCAR/PSU Mesoscale Model version 5
MPE	Model Performance Evaluation
NADP	National Atmospheric Deposition Program
NCAR	National Center for Atmospheric Research
NCEP	National Centers for Environmental Prediction
NDVI	Normalized Differential Vegetation Index
NOAA	National Oceanic and Atmospheric Administration
NWS	National Weather Service
PBL	Planetary Boundary Layer
PSU	The Pennsylvania State University
RAMS	Regional Atmospheric Modeling System
SAMI	Southern Appalachian Mountain Initiative
SST	Sea Surface Temperature
SNP	Shenandoah National Park
UAH	University of Alabama at Huntsville
URM	Urban-Regional Multiscale Model
UTC	Universal Time Coordinate (UTC - 5 hours = Eastern Standard Time)
TVA	Tennessee Valley Authority

1 INTRODUCTION

1.1 Overview

Computer-based modeling done as part of an integrated environmental impact assessment sponsored by the Southern Appalachian Mountains Initiative (SAMI) can be classified into four categories: (1) emissions, (2) meteorological, (3) air quality (atmospheric chemistry), and (4) environmental effects. Together this body of work represents an interdisciplinary approach for developing a comprehensive view of the relationships between anthropogenic emissions and the environment of the southern Appalachians as of the mid-1990s. In addition, SAMI is using its modeling system to forecast environmental changes expected to occur in response to alternative future emission scenarios. This report, prepared by contractors to SAMI and a member of the SAMI Atmospheric Modeling Subcommittee, describes the second modeling component that deals with the meteorological state of the atmosphere.

Meteorological modeling is necessary to provide certain required inputs to emissions modeling and to describe the state of the atmosphere in which a large number of chemical reactions determine air quality. Meteorology influences the transport and dispersion of pollutants, chemical reaction rates, and the natural (so-called “deposition”) processes that remove pollutants from the air. Therefore, meteorological modeling is a critical early step in the SAMI integrated assessment. The meteorological modeling done for SAMI represents a state-of-the-art analysis using a three-dimensional Eulerian (“grid”) model whose domain covers the continental United States. Airflow, air turbulence, temperature, water vapor, cloud liquid water and rain water content of the atmosphere were each computed to a depth of over 17 km through the atmosphere. This information in various forms was passed to the emissions and air quality models after completion of the meteorological simulations.

1.2 Episode Selection Criteria

Model simulations of the atmosphere, whether meteorological or chemical, make intensive use of computer resources. Even with today’s high-speed machines, modeling of more than a few weeks is usually cost- and time-prohibitive. Unfortunately, an assessment of air pollution impacts must examine pollutant levels over multiple seasons or years in order to provide useful estimates of long-term environmental effects. Therefore, SAMI elected to model air pollution using an episodic approach. In essence, this approach selects a subset of modeling days that have some known relationship to longer time periods of interest. After modeling is done the results can then be extrapolated to the longer periods. An unavoidable loss in accuracy occurs as a result. However, if modeling episodes are carefully selected then, in theory, the effect on accuracy can be quantified.

Before SAMI selected modeling episodes it hired a contractor to develop an episode characterization and selection scheme. This scheme is described in detail in section 4.1. The focus of the scheme was to characterize short periods (days or weeks) according to the level of pollutants observed during those periods. An observational data base was assembled for a period from 1991 through 1995. This data base included meteorological data and ground-level air quality data at selected target sites. The air quality data base components were hourly ozone mixing ratio, 24-hour average fine particle mass concentrations, and

weekly wet deposition totals for four cation/anion species, SO_4^{2-} , NO_3^- , Ca^{2+} and Mg^{2+} . Estimated weekly dry deposition totals were later examined to classify time periods for dry deposition, but these data were not part of the episode selection process. Time periods for each pollutant type were then classified and the ability of various days to represent entire classes was estimated based on a statistical analysis. Finally, various episodes were selected based on their overall ability to represent a full range of annual pollution conditions. SAMI selected nine episodes, a total of 69 days, for modeling. Details of the episode selection criteria are found in section 4.1.

1.3 Meteorological Model Evaluation

Model performance evaluation (MPE) is the process of testing a model's ability to estimate accurately observed atmospheric properties over a range of synoptic and geophysical conditions. When conducted thoughtfully and thoroughly, the process focuses and directs the continuing cycle of model development, data collection, model testing, diagnostic analysis, refinement, and re-testing. At times, however, this process has been foreshortened in order to "validate" the model with readily available data so that its operational or scientific use can be justified. Below, we briefly summarize the philosophy and objectives that govern the evaluation of the RAMS prognostic model for the SAMI application and then identify the specific evaluation procedures that we employed to calculate the model's performance relative to measurements. In Section 9.3 we present a formal process for judging the adequacy of the RAMS results.

1.3.1 The Importance of Meteorological Model Performance Evaluation

Historically, the practice of meteorological MPE consisted of comparing observed and predicted (actually, estimated) atmospheric state variables. The principal assessments included comparisons of two-dimensional fields of predicted and observed variables, temporal comparisons of differences between observations and estimates for individual monitoring sites, spatial comparisons of differences, as shown through residual maps, and a range of statistics, including regional and sub-regional average bias, root mean square error, and differences in area wide statistics (e.g., precipitation amounts) independent of time and location. The focus of all these types of comparisons have typically been within the planetary boundary layer (PBL) up to 850 millibars (mb) or so. A millibar is a unit of pressure often used in meteorology as a surrogate for height above the surface. Pressure decreases with altitude. The standard (average) pressure at sea level is taken to be 1013 mb.

No standard practice for judging meteorological model performance has evolved. While urban-scale photochemical air quality models have been accepted for use in regulatory control strategy assessments when average discrepancies (e.g., gross errors) for ozone are of the order of 35% or less, and inaccuracy or bias was "not large." (i.e., $\pm 5-15\%$ according to EPA definition), an analogous set of performance goals has yet to be adopted for meteorological models intended for air quality use (Seaman, 2000). Even when performance goals have been specified and achieved by air quality models, the models passing arbitrary performance criteria have often been found to contain significant flaws, typically in the form of internal compensating errors. Such errors can compromise the overall reliability of the modeling applications. Thus, requiring a prognostic meteorological model to pass similar ad hoc performance goals runs a similar risk.

A key limitation in meteorological model performance evaluation to date has been the generally inadequate level of stressfulness to which models have been subjected in testing. Three main outcomes of testing are possible: A model performs inadequately and is so judged, a model performs well and is so judged, or a model appears to perform adequately but is, in fact, significantly flawed. To ensure during testing that a model reveals any flaw(s), it must be adequately "stressed," that is, subjected to testing that is designed to reveal and even highlight or amplify inherent inadequacies. Because performance testing of prognostic meteorological models has not been sufficiently stressful, flawed models (actually models plus input data bases) containing internal compensating errors have occasionally been accepted for use. Recommendations for improvements to the meteorological MPE process have been proffered by several scientists (Tesche et al., 1990; Tesche, 1991a,b; 1994; Hanna, 1994; Seaman, 2000) motivated by a number of objectives, including improving the process, adequately stressing models, improving the quality of available data bases, standardizing the practice, and demystifying the practice through clearer communication.

Guidelines have been developed (Reynolds et al., 1994; Roth et al., 1998) for providing a sound context for model performance evaluation, establishing a common understanding of the process, and ensuring that evaluation efforts are properly formulated and reasonably complete. Elements of an "idea L model evaluation process" include: (a) evaluating the scientific formulation of the model through a thorough review process, (b) assessing the fidelity of the computer code to the scientific formulation, governing equations, and numerical solution process, (c) evaluating the predictive performance of individual process modules and preprocessor models (e.g., emissions and meteorological), (d) evaluating the predictive performance of the full model, (e) conducting sensitivity analyses, (f) carrying out corroborative analyses, (g) carrying out comparative modeling, and (h) implementing a quality assurance activity. Ideally, all of these activities should be carried out in accordance with the procedures prescribed in an application-specific MPE protocol.

Obviously, the effort suggested above is *considerably greater* than that customarily devoted to MPE for either meteorological or air quality models. However, integrated meteorological, emissions and air quality models are being viewed as essential tools in the development of emissions control plans. The costs of controls are sufficiently high that decision-makers as well as society in general will wish assurance that imposed controls will be effective in reducing air pollution levels. It is thus vital that the overall planning process includes sufficient time and resources for conducting thorough evaluations of model performance.

1.3.2 Evaluation Objectives

The objective of the RAMS performance evaluation was to assess the adequacy of the surface and aloft meteorological fields estimated by the model for the nine (9) episodes selected by SAMI. More specifically, we have attempted to assess the adequacy and reliability of the meteorological fields for input to the URM-1ATM regional photochemical model. Meteorological inputs required by URM-1ATM include hourly estimates of surface pressure and clouds; the three-dimensional distribution of winds, temperatures, and mixing ratio; and other physical parameters or diagnosed quantities such as turbulent mixing rates (i.e., eddy diffusivities) and planetary boundary layer heights. As described below, the RAMS evaluation centered on comparisons between surface and aloft meteorological measurements obtained principally from National Weather Service (NWS) reporting stations.

1.3.3 The Evaluation Process

As noted, the primary aim of the RAMS evaluation was to assess whether the simulated fields from the meteorological modeling systems may be relied upon to provide wind, temperature, mixing, moisture, and radiation inputs to URM-1ATM for a variety of adverse ozone, visibility and acid deposition periods in the eastern U.S. We use the term "modeling system" to refer to the RAMS model source code, its preprocessor and data preparation programs, the underlying data base, and the post-processor programs that map (i.e., interpolate) the simulated meteorological fields onto the air quality model grid meshes.

Ideally, a comprehensive evaluation of RAMS would include all of the steps identified previously: Such an intensive evaluation process is rarely, if ever, carried out due to time, resource and data base limitations. Nevertheless, it is useful to identify the *ideal* evaluation framework so that the results of the *actual* evaluation can be judged in the proper perspective. This also allows one to set realistic expectations for the reliability and robustness of the actual evaluation findings.

The RAMS modeling system is well-established with a rich development and refinement history spanning more than two decades (Pielke et al., 1992). The model has seen extensive use worldwide by many agencies, consultants, university scientists and research groups. Thus, the current version of the model as well as its predecessor versions have been extensively "peer-reviewed" and considerable algorithm development and module testing has been carried out with all of the important process components. Accordingly, the performance evaluation focused three steps in the ideal testing process; namely:

- > Evaluate the full modeling system's predictive performance;
- > Evaluate the direct meteorological output from the models as well as the mapped fields that processed into air quality model-ready inputs; and
- > Implement a quality assurance activity.

Performance testing of the RAMS model is divided into two general categories: operational and scientific. The *operational evaluation* refers to an assessment of a model's ability to estimate atmospheric observations independent of whether the actual process descriptions in the model are accurate (Tesche, 1991a,b). It is an examination of how well the model reproduces the observed meteorological fields in time and space consistent with the input needs of the air quality model. Here, the primary emphasis is on the model's ability to reproduce hourly surface wind speed, wind direction, temperature, and mixing ratio observations across the 12 km grid domain. The operational evaluation provides only limited information about whether the results are correct from a scientific perspective or whether they are the fortuitous product of compensating errors. Thus, a "successful" operational evaluation is a necessary but insufficient condition for achieving a sound, reliable performance testing exercise. An additional scientific evaluation is also needed.

The *scientific evaluation* attempts to elucidate the realism of the basic meteorological processes simulated by the model. This involves testing the model as an entire system (i.e., not merely focusing on surface wind

predictions) as well as its component parts. The scientific evaluation seeks to determine whether the model's behavior in the aggregate and in its component modules is consistent with prevailing theory, knowledge of physical processes, and observations. The main objective is to reveal the presence of bias and internal (compensating) errors in the model that, unless discovered and rectified, or at least quantified, may lead to erroneous or fundamentally incorrect technical or policy decisions. Typically, the scope of the scientific evaluation is limited by the availability of special meteorological observations (radar profiler winds, turbulence measurements, PBL heights, precipitation and radiation measurements, inert tracer diffusion experiments, and so on). Unfortunately little if any of this type of supplemental data collection was performed during the SAMI episodes. Thus, the scientific evaluation component in this study is quite limited, focusing on the models ability to reproduce daily precipitation amounts. Furthermore, due to the lack of adequate diagnostic information, where errors in the modeled precipitation fields arise, it is very difficult to assign a specific course.

1.3.4 Complementary Perspectives Brought to this Evaluation

One consequence of SAMI's selection of two different groups to perform the meteorological modeling elements of its study is that somewhat different perspectives are introduced into the model performance evaluation portion of the research. Generally speaking, the researchers at UAH examine model performance from a 'synoptic' or broad-scale perspective while scientists at AG emphasize the fidelity of model predictions in the vicinity of surface and aloft measurement sites within the planetary boundary layer. While there is definitely overlap between the two perspectives, the analytical procedures, statistical metrics and graphical tools employed by the two groups differ somewhat, reflecting their particular perspective and experience in prognostic model evaluation. Actually, these differences are a strength, leading to complementary and corroborating examinations of performance and producing insights into the model's operation that might not be as thoroughly examined via one approach alone. As a result, the results of the episodes evaluated by UAH (e.g., July 1995, May 1995, May 1993, March 1993, February 1994, and July 1991) are presented using the UAH-developed analysis software. In contrast, the MAPS evaluation software developed by AG was used in performance testing of the August 1993, June 1992, and April-May 1995 episodes. While the graphical presentation methods differ slightly, both have been used extensively and effectively in past evaluations reported broadly in the literature. Thus, readers should have minimal difficulty understanding each approach.

To integrate the UAH and AG evaluations with a common set of statistical and graphical tools, we have also re-evaluated seven of the episodes (four from UAH and three from AG) using certain of the MAPS statistical and graphical measures. Moreover, the UAH surface layer methodology was used to compute estimate mixing ratio, temperature, and wind speed and direction performance statistics for all nine of the SAMI episodes. Thus, the RAMS evaluation presented in this report features two complimentary perspectives from which the model testing is carried out together with two additional analyses that summarize most or all of the modeling episodes using common statistical and/or graphical tools. We feel this additional effort strengthens the overall evaluation of the model and far outweighs any inconvenience introduced by, say, different plotting methods in a common report.

1.3.5 Structure of Report

This report is organized as follows: Details of the meteorological model are described in section 2 and the application of the model is described in section 3. Section 4 outlines the episode selection process. The approach for the meteorological model performance evaluation is described in section 5. Results of the surface evaluation of the modeling are presented in section 6 and the evaluation of conditions aloft is presented in section 7. A comparison between SAMI modeling performance and that for other modeling exercises is presented in section 8. The report is summarized in section 9 together with an assessment of the suitability for the RAMS meteorological field as inputs to the URM-1ATM model.

2.0 THE METEOROLOGICAL MODEL

2.1 Overview of RAMS

The Regional Atmospheric Modeling System (RAMS) version 3a was the meteorological model used for the SAMI simulations. A description of the RAMS model and the modeling process is provided in the SAMI meteorological modeling protocol (see Appendix 4). The reader is referred to the protocol document for details not covered here.

RAMS is a three-dimensional primitive-equation model which has a sigma-z vertical coordinate and a choice of horizontal coordinates. For the SAMI simulations the horizontal coordinate system was an oblique stereographic map projection which yields map scale factors close to 1.0 if the map projection pole is chosen close to the center of the coarse grid domain. RAMS is a merger of a hydrostatic model originally developed at the University of Virginia (Pielke, 1974; Mahrer and Pielke, 1977; McNider and Pielke, 1981, 1984) and a non-hydrostatic model developed by Tripoli and Cotton (1982) at Colorado State University. RAMS was chosen as the meteorological model because of its previous successful simulations in the southeastern United States of circulations important in air pollution (e.g., Casey et al. 1995; Mueller et al. 1996) and because of the experience of the UAH contractor in using the model.

The July 1995 episode was the first simulation performed. This was followed by attempts at simulating the April 1994 episode. Examination of the results of these two simulations led to a series of changes to the RAMS system to improve performance in light of the SAMI requirements. The rest of the episodes were performed with essentially a fixed set of procedures and program codes. The inability to produce a realistic precipitation field for the April 1994 case led to it being replaced by the July 1991 episode.

2.2 RAMS Horizontal Grid Structure

Figure 2-1 shows the nested horizontal grid structure used for the July 1995 episode. The coarse, intermediate, and fine grids had grid cells of 48-, 24-, and 12-km, respectively. The next simulation attempted was the April 1994 episode and it revealed that the original grid structure would need to be changed because of unacceptable interactions between the eastern portions of the 12- and 24-km grids in high speed flows. The nested grid arrangement used for all the other episodes is shown in

Figure 2-2. The coarse, intermediate, and fine grids for this new grid setup had grid cells of 96-, 24-, and 12-km, respectively. The 96-km grid was chosen so that its borders were as far as possible from the other two grids and from natural boundaries such as the Rocky Mountains and land-ocean boundaries parallel with one or more grid edges.

SAMI RAMS Domain : Oblique Stereographic Projection

Grid 1 CLAT=37.800 CLON= -85.100 DX= 48.00 km DY= 48.00 km NX= 69 NY= 81
 Grid 2 CLAT=35.748 CLON= -80.045 DX= 24.00 km DY= 24.00 km NX= 70 NY= 88
 Grid 3 CLAT=35.651 CLON= -81.062 DX= 12.00 km DY= 12.00 km NX=102 NY= 68

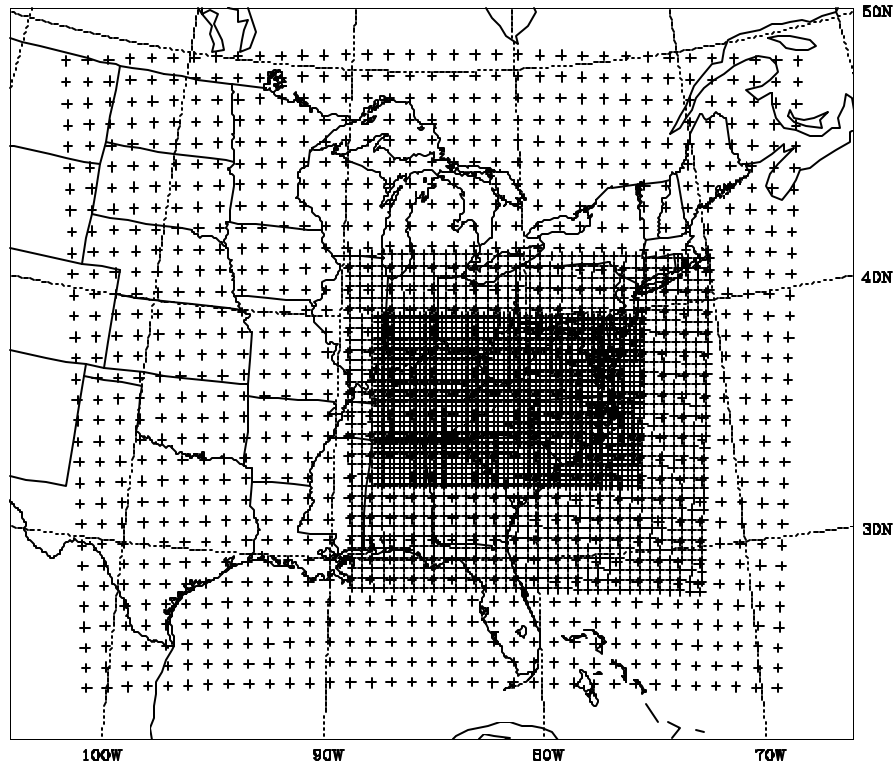


Figure 2-1. Nested grid system used for the July 1995 episode only. Only every other grid point is plotted for each of the grids by a “+”. “CLAT” and “CLON” in the top label refer to the central latitude and longitude, respectively, for each grid. “DX” and “DY” refer to the horizontal mesh size in km. “NX” and “NY” refer to the number of the grid points in the west-east and north-south directions, respectively.

SAMI RAMS Domain : Oblique Stereographic Projection

Grid 1 CLAT=37.000 CLON= -85.000 DX= 96.00 km DY= 96.00 km NX= 83 NY= 80
 Grid 2 CLAT=36.077 CLON= -81.259 DX= 24.00 km DY= 24.00 km NX=106 NY= 90
 Grid 3 CLAT=36.521 CLON= -81.641 DX= 12.00 km DY= 12.00 km NX=100 NY= 74

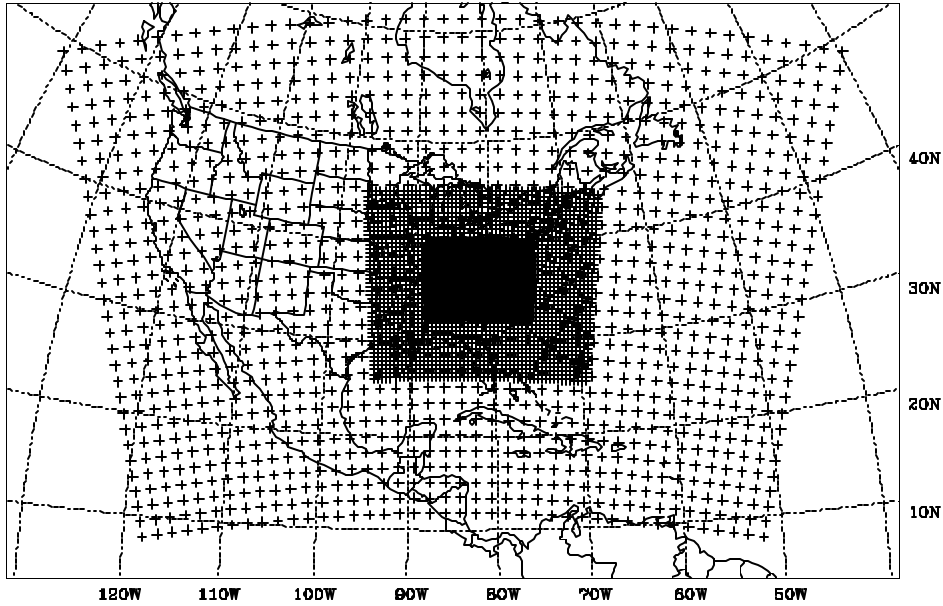


Figure 2-2. Nested grid system used for all the episodes after the July 1995 episode. Only every other grid point is plotted for each of the grids by a “+”. “CLAT” and “CLON” in the top label refer to the central latitude and longitude, respectively, for each grid. “DX” and “DY” refer to the horizontal mesh size in km. “NX” and “NY” refer to the number of the grid points in the west-east and north-south directions, respectively.

2.3 RAMS Vertical Grid Structure

RAMS employs a sigma-z vertical coordinate defined by

$$(2.1) \quad h_k = \frac{H (z_k - E)}{(H - E)},$$

where h_k is the sigma-z coordinate at level k , z_k is the actual height above mean sea level, H is a scale height at the top of the model domain where the sigma-z levels are horizontal, and E is the terrain height above mean sea level. RAMS has two vertical grids which are staggered with respect to each other. The first grid has only the vertical velocity defined on it and its first level is at the surface. The second grid with all the other variables has its first level below ground but has the same total number of levels. For the SAMI grid

35 vertical levels were chosen with H equal to 17.4 km. The SAMI grid is shown in Figure 2-3 for the second vertical grid with the exception that the first sigma-z level is plotted at the surface. The sigma-z surfaces follow the terrain surface in an approximate manner and are flat over areas where the terrain surface is uniform. In sigma-z coordinates, for either vertical grid, the first level above ground has a depth of 20 m.

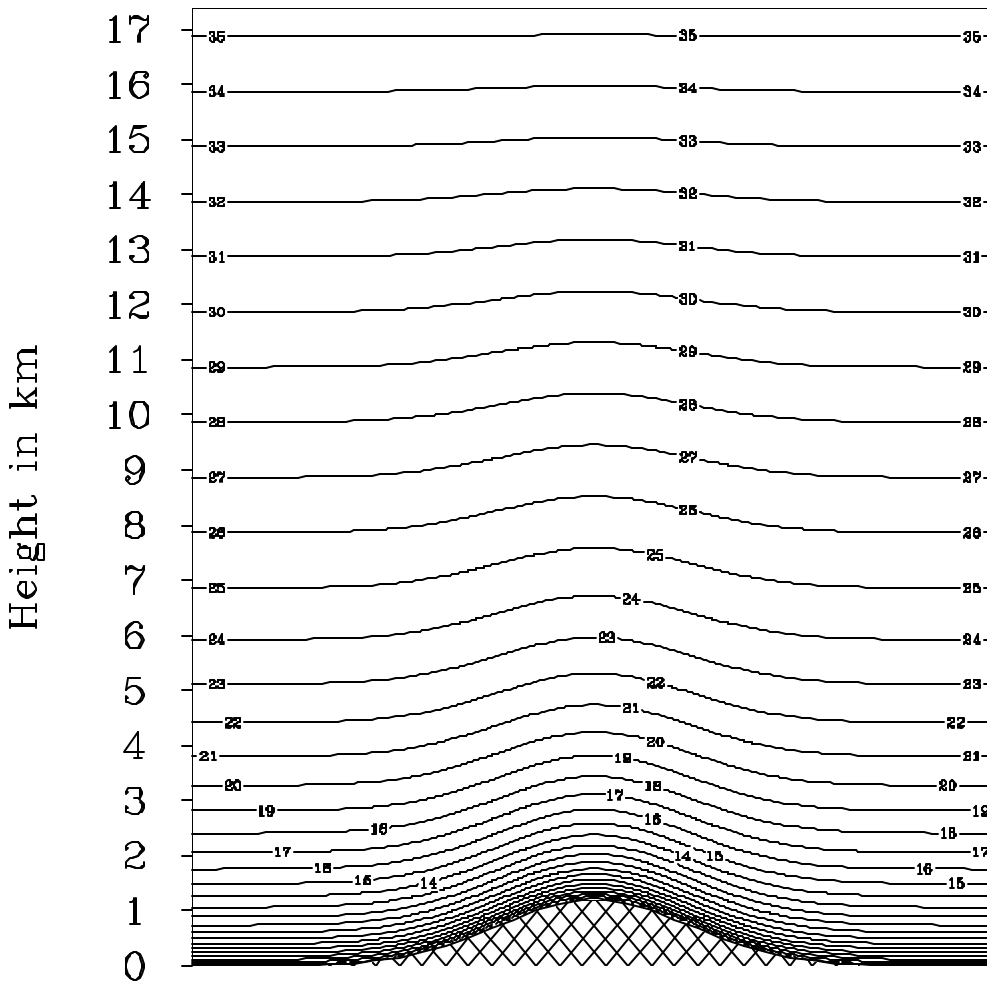


Figure 2-3. Sigma-z vertical coordinate system with 35 levels used for all episodes. Hypothetical mountain is shown with a maximum altitude of about 1.2 km which is about the maximum height of the actual terrain on the 12-km horizontal grid over the southern Appalachian Mountains.

2.4 RAMS Model Modifications

2.4.1 Surface Grid Files

The original scheme in RAMS calculates the surface fields of terrain, vegetation type, land percentage, and sea surface temperatures (SST) for each grid from data files which are part of the modeling system. The leaf area index (LAI) and vegetation fraction are calculated primarily through a single seasonal temperature. The soil type is also specified as a single type. The latter approach for the LAI, vegetation fraction, and soil type was used for the July 1995 episode. Initial simulations of the next episode (April 1994) revealed that the LAI and vegetation fraction fields would need to be defined in a better way. Soil type and vegetation fraction data were obtained from the Earth System Science Center (ESSC) of the Pennsylvania State University (<http://www.essc.psu.edu/>). The State Soil Geographic (STATSGO) data set provided 1-km resolution soil type data for the continental United States. The vegetation fraction data were derived from Advanced Very High Resolution Radiometer (AVHRR) satellite imagery using a normalized differential vegetation index (NDVI). These data had a spatial resolution of 1 km and were available as biweekly composites. NDVI data sets were chosen with beginning and ending times which best fit the SAMI episode. Another major data set was a CD-ROM collection from the International Satellite Land Surface Climatology Project (ISLSCP). This data set provided global 1° latitude-longitude resolution for leaf area index, soil type, and vegetation fraction data. The 1° soil type and vegetation fraction data provided coverage for those fields for the 96-km coarse grid which were not covered by the STATSGO and NDVI data. The 1° leaf area index data was interpolated to each of the nested SAMI grids. The ISLSCP soil type and vegetation fraction data were monthly averages from the year 1987 and were used by choosing the closest month for the SAMI episode being considered. Another major data set which will be discussed further in section 3.1 is the National Centers for Environmental Prediction/National Center for Atmospheric Research (NCEP/NCAR) reanalysis data (Kalnay et al. 1996). The reanalysis data was used to provide SST data rather than the RAMS monthly climatological values for all episodes. Original resolution of the reanalysis SST data is 1.875° longitude and approximately the same resolution by latitude. All the episodes after the July 1995 episode used these data sets to define the surface characteristics.

The soil moisture for the July 1995 episode was initialized by interpreting the reanalysis soil moisture values as a fraction of saturation and multiplying them times the RAMS saturation values. As discussed in section 6.1 there was a significant dry bias for boundary layer values of water vapor mixing ratio in the July 1995 simulation. The remaining episodes used a specified fraction of the reanalysis soil moisture for initializing the RAMS soil moisture values. The remaining episodes also used the surface nudging technique described in section 2.4.2.5 which reduces the impact of the soil moisture. In areas where the surface nudging is not done (primarily over mountainous areas) the primary influence of the soil moisture is the impact on the soil specific heat values.

Figure 2-4 illustrates the terrain field for the 12-km grid. The highest terrain had an altitude on the order of 1.1 km.

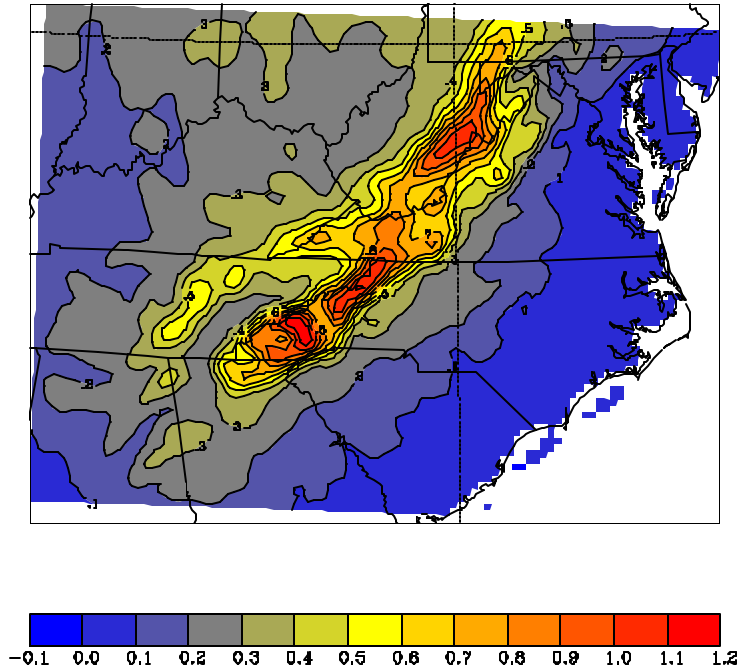


Figure 2-4. Terrain for the 12-km grid used for episodes after the July 1995 episode. The highest values are near 1.1 km over the West Virginia-Virginia and Carolinas-Tennessee borders.

2.4.2 Model Physics Changes

2.4.2.1 Microphysics

The complete RAMS microphysics suite of condensate regimes includes cloud water and six precipitation types: rain, pristine ice, snow, ice aggregates, graupel, and hail. A subset of these types was selected for the SAMI simulations because of time constraints and computer memory limitations. Only cloud water and rain precipitation water were activated for all episodes. In attempting to simulate the second episode (April 1994) it became apparent that several changes would be required in the microphysics with such a limited choice of condensate types. Unrealistic cloud water values at heights above 5 km led to changing the RAMS autoconversion of cloud water to a simple scheme as in Kessler (1969)

$$(1) \quad \frac{\partial r_c}{\partial t} = k_a [r_c - r_{crit}],$$

where r_c is the cloud water mixing ratio, r_{crit} is a threshold value, and k_a is a constant set to 10^{-3} s. When cloud water values are below the threshold value the autoconversion tendency is set to zero. The threshold value was determined by

$$(2) \quad r_{crit} = \min \left[0.10 r_{v,sat}, 0.5 \text{ g kg}^{-1} \right],$$

where $r_{v,sat}$ is the saturation water vapor mixing ratio. Equation (2) then sets the threshold value to the smallest of either 10% of the saturation water vapor mixing ratio or 0.50 g kg^{-1} .

Two other changes were made to accommodate the small selection of condensate types. One was to make the terminal velocity of rain a function of temperature. For temperatures above 0°C the default RAMS values were used. For temperatures below -20°C a value of 1 m s^{-1} was used to imitate the effects of small ice particles. For temperatures between the two limits a linear transition was used. The other change was to use the same temperature limits to make the collection efficiency a function of temperature. For temperatures above 0°C the efficiency was set to 1.0 and for temperatures below -20°C it was set to 0.50.

2.4.2.2 Kuo Convective Scheme

The only choice of a convective parameterization for this version of RAMS is a modified Kuo (1974) scheme with a simple downdraft. Initial simulations of the July 1995 episode revealed a need for some changes to the convective updraft calculations. The initial simulations revealed areas with unrealistically deep convection and also large areas of model convection were produced where none was observed. A simple entrainment model as originally proposed by Turner (1962) was introduced

$$(3) \quad \frac{1}{M} \frac{\partial M}{\partial z} = \frac{0.20}{R},$$

where M and R are the updraft mass and radius, respectively. The updraft radius was set to 1500 m as a typical value after Kain and Fritsch (1990). This change reduced the tendency for convection to be too deep in some areas. The default RAMS code allowed convection to occur in areas with large convective available potential energy (CAPE) but also with extremely large magnitudes of convective inhibition (CIN) (Colby, 1984), which in reality prevent convection from occurring. A CIN calculation was introduced into the Kuo scheme such that no convection was allowed to occur if the CIN was less than -20 J kg^{-1} regardless of the CAPE value. This change produced the needed results when compared with observations for initial simulations of the July 1995 episode.

The last change to the Kuo convective scheme allowed more flexibility in the maximum downdraft cooling at the surface. The original formulation set the surface cooling magnitude to the largest difference between the updraft and the environment with a limit of 2.5°C imposed. As an alternative the evaporation formula from Rutledge and Hobbs (1983) was used to calculate cooling rates beneath cloud base. This approach allowed more realistic variability for downdraft temperatures as a function of the relative humidity of the environment.

2.4.2.3 Radiation Calculations

Results from the July 1995 and April 1994 episodes revealed that clouds and precipitation were having too large of an impact on surface temperatures. In areas of precipitation this was characterized by surface temperatures being too cool during the daytime and to a lesser extent being too warm at night. One possible explanation for this is that cloud water values may be too large given the simple set of microphysics chosen for these simulations. No observations exist to verify cloud water values but the model values for all the simulations seemed reasonable even with the microphysics options chosen. The Stephens (1978) parameterization uses the vertical liquid water path (LWP) as a means to introduce condensate effects into the radiation calculations. The LWP for a given model layer is given by

$$(4) \quad LWP = f \rho r_t \Delta z,$$

where f is an arbitrary factor which will be discussed later, ρ is the air density, r_t is the total condensate mixing ratio including cloud and all types of precipitation, and Δz is the thickness of the model layer. To help with the problems discussed above, r_t was changed to include only cloud water and not precipitation water. In the original version there was no factor f but was introduced to reduce the LWP values. For the longwave calculations f was set to 10^{-2} while for the shortwave calculations it was set as a function of temperature. For temperatures greater than -5°C it was set to 0.50 and for temperatures less than -15°C it was set to 10^{-2} . For temperatures in between it was set as a linear transition between the two values. These changes helped with the temperature errors in areas of precipitation but did not remove them entirely.

In the original RAMS code the cloud fraction which is used in the radiation calculations is either one or zero. The Ek and Mahrt (1991) cloud fraction scheme was introduced as described by Mocko and Cotton (1995). This allowed cloud fractions in the unstable boundary layer to be a function of the horizontal mesh size, the surface moisture flux, and the standard deviation of the subgrid-scale vertical velocity. This change was made in an effort to improve the surface temperature performance of the model.

2.4.2.4 Nudging

The original nudging scheme in RAMS can be described as

$$(5) \quad \frac{\partial A_m}{\partial t} = W(A_{nd} - A_m),$$

where A_m is a given model variable, A_{nd} is the value being nudged towards, and W is a weight which is the inverse of a time scale which provides the magnitude of the desired nudging. The weight W is the maximum of two weighting schemes: one is a quadratic function of the horizontal distance from the nearest model grid edge, and the other is a linear function of height. The quadratic scheme can be described by

$$(6) \quad W_h = W_{\max} + (W_{\min} - W_{\max}) \frac{d^2}{d_m^2},$$

where d is the horizontal distance from the nearest model grid edge, d_m is the distance beyond which

$W_h = W_{\min}$, and the weights W_{\min} and W_{\max} are defined by the time scales as in (7). The distance d_m is represented by the RAMS variable NUDLAT.

$$(7) \quad \begin{cases} W_{\max} = 1/TNUDLAT \\ W_{\min} = 1/TNUDCENT \\ W_{top,max} = 1/TNUDTOP \end{cases}$$

The vertical scheme is described by (8) where z is the height of a given model grid point, z_t is the height of the top model level, z_b is a specified height which is the lowest height where the linear scheme is calculated, and $W_{top,max}$ is defined by a time scale as in (7). The height z_b is represented by the RAMS variable ZNUDTOP. The RAMS variables TNUDLAT, TNUDCENT, TNUDTOP, NUDLAT, and ZNUDTOP are specified in the RAMS file "RAMSIN."

$$(8) \quad W_z = W_{\min} \frac{z_t - z}{z_t - z_b} + W_{top,max} \frac{z - z_b}{z_t - z_b}$$

For heights below z_b the quadratic scheme is used to give W while for heights above z_b the maximum of the two schemes is used. In the original version of RAMS there is no provision for varying the RAMS variables TNUDLAT, TNUDCENT, TNUDTOP, NUDLAT, and ZNUDTOP across the nested grids. These were made variable for the SAMI episodes after the July 1995 episode and the values used are described in section 2.6. The values were chosen so that nudging was performed strongly on the coarse grid but then reduced sharply on the intermediate grid and with little or no nudging on the fine grid. The exception to this was near the model top where strong nudging was done on all grids to control noise production near the top boundary.

This original RAMS weighting scheme was modified for the SAMI simulations as in (9):

$$(9) \quad W_{adj} = W W_{pbl} W_{col}$$

where W_{adj} is the new adjusted weight and W_{pbl} and W_{col} are adjustments to the original RAMS weight W . The W_{pbl} adjustment is set to zero for the lowest 2 km in order to allow the model physics to perform fully without interference from the nudging fields which do not have the spatial and temporal resolution to be used there. The W_{col} was also used to turn off the nudging of moisture for lower levels where the nudging fields were less accurate with respect to the observed moisture.

The original RAMS model uses the Louis (1979) parameterization in determining the surface fluxes which eliminates the need for any iterative calculations to determine the Monin-Obukhov (1954) length. Beljaars and Holtslag (1991) provide evidence that the difference between the Louis (1979) approach and an exact calculation can be large in stable situations. Therefore, an efficient iterative approach which explicitly solves for the Monin-Obukhov length as a function of the surface Richardson number was implemented using the

general recommendations of Beljaars and Holtslag (1991). The transition of the surface fluxes to the free convection regime was implemented in a fashion similar to Beljaars (1994).

2.4.2.5 Surface Nudging

The July 1995 episode and attempts at simulating the April 1994 episode demonstrated the inability to specify soil moisture adequately to enable reasonable calculation of the surface heat and moisture fluxes by the model. This led to unacceptable errors in temperature and moisture in the planetary boundary layer (PBL) which could become quite large in the 10-day simulations required for SAMI. A scheme was developed which used observed analyses of near-surface temperature, moisture, and wind to improve the PBL performance of the model. The basics of the scheme are described by equations 10-14. They use a generic variable “A” which can represent temperature, water vapor mixing ratio, or wind speed. Using Monin-Obukhov (1954) similarity theory the vertical gradient of a variable “A” in the PBL surface layer is given by (10) (see e.g., Beljaars and Holtslag, 1991):

$$(10) \quad A_z - A_0 = \frac{A^*}{\nu_k} \left[\ln \frac{z}{z_r} - \Psi \left(\frac{z}{L} \right) + \Psi \left(\frac{z_r}{L} \right) \right] = A^* F ,$$

where the subscript z represents values at a specified level above the surface at height z (2 m for temperature, 10 m for winds), the subscript “0” represents surface values, A* is the similarity scaling parameter, ν_k is the von Karmen constant, z is an appropriate roughness length, Ψ is the integrated similarity function, and L is the Monin-Obukhov (1954) length. The right-hand side of (10) expresses the equation in a simple manner where the von-Karmen constant and the terms in the brackets have been relabeled as “F.”

$$(11) \quad A_{z,obs} - A_0 = \frac{A_{obs}^*}{\nu_k} \left[\ln \frac{z}{z_r} - \Psi \left(\frac{z}{L} \right) + \Psi \left(\frac{z_r}{L} \right) \right] = A_{obs}^* F$$

Equation (11) shows the same relationship but expressed for the observed value of A denoted by $A_{z,obs}$ with a corresponding scaling parameter A_{obs}^* . This is a correct statement if one assumes that the function “F” remains unchanged which is acceptable for the short time steps used in the model. Subtracting (11) from (10) gives equation (12) which expresses the difference between the observed and model similarity scaling parameter as a function of the difference between the observed and model values at height z.

$$(12) \quad \Delta A^* = A_{obs}^* - A^* = \frac{(A_{z,obs} - A_z)}{F}$$

The scaling parameter is then nudged toward a value in agreement with similarity theory by (13), where

Δt_s is a specified time scale (10 min for all episodes), and Δt_m is the model time step.

$$(13) \quad A_{new}^* = A^* + \frac{\Delta A^*}{\Delta t_s} \Delta t_m$$

The surface "skin" values of A are nudged in a similar manner based upon the difference between the observed and model values at height z as in (14).

$$(14) \quad A_{0,new} = A_0 + \frac{A_{z,obs} - A_z}{\Delta t_s} \Delta t_m$$

Test simulations showed that this technique improved near-surface values of temperature and moisture significantly but had little effect on winds. All three variables were nudged in this manner but the major impact was on the surface fluxes of heat and moisture. The near-surface analyses of the required observed values are obtained by a technique which is described in section 3.2. Figures 2-5 to 2-7 illustrate the regions where the surface nudging was performed on the 96-, 24-, and 12-km grids, respectively. The surface data used to create the observed surface analysis were only available for the United States and southern Canada. Surface nudging was not done in areas with no available data, areas over water, and areas exceeding specified terrain slope limits for each grid.

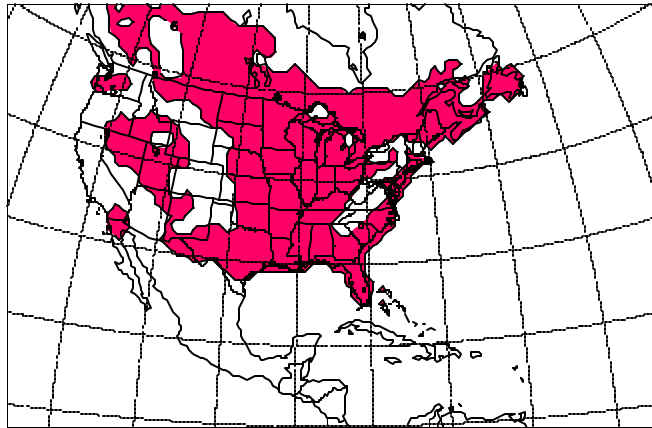


Figure 2-5. Colored areas denote where surface nudging was performed on the 96-km grid as described in the text. Non-colored regions are where surface nudging was not performed because of terrain slope, a water surface, or unavailability of data.

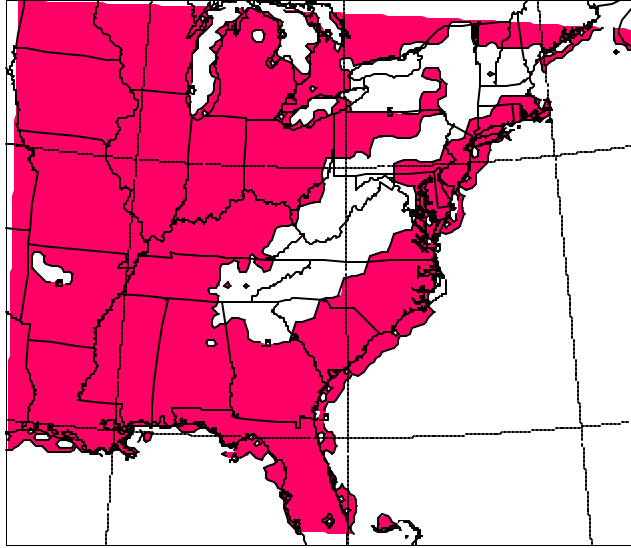


Figure 2-6. Colored areas denote where surface nudging was performed on the 24-km grid as described in the text. Non-colored regions are where surface nudging was not performed because of terrain slope, a water surface, or unavailability of data.

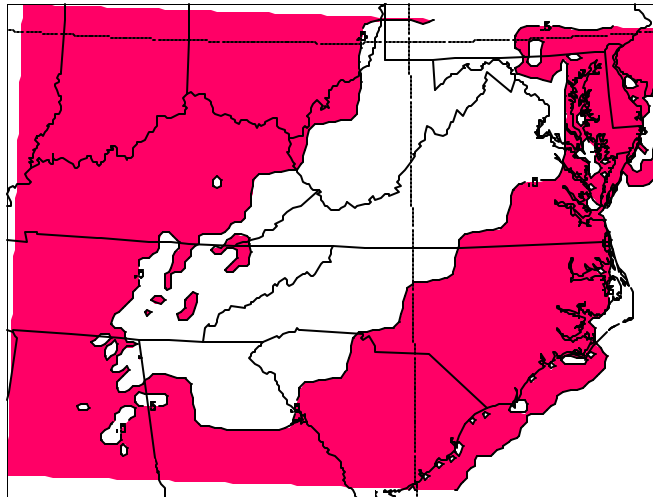


Figure 2-7. Colored areas denote where surface nudging was performed on the 12-km grid as described in the text. Non-colored regions are where surface nudging was not performed because of terrain slope, a water surface, or unavailability of data.

2.4.2.6 Surface Energy Budget

Initial simulations of the April 1994 episode revealed a strong cool bias of surface temperatures over vegetated areas. This led to changes in the radiation balance for the soil and vegetation canopy which considerably decreased the cool bias. The approach chosen was a simple version based on ideas taken primarily from Avissar and Mahrer (1988) but also some details from Sellers et al. 1986 and Yamazaki et al. 1992.

First the changes to the radiation balance for the soil surface will be discussed briefly. The transmissivity for both shortwave and longwave radiation for vegetation was calculated by

$$(15) \quad t_{veg} = \exp(-0.50 L),$$

where τ_{veg} is the vegetation transmissivity and L is the leaf area index. The net shortwave radiation for soil covered by vegetation is given by

$$(16) \quad R_{s,soil} = (1 - f_a \alpha_g) t_{veg} R_s,$$

where $R_{s,soil}$ is the shortwave radiation absorbed by the soil, R_s is the downward shortwave radiation just above the surface, α_g is the soil albedo, and f_a is an albedo reduction factor. The latter factor was set to 0.50 over mainly mountainous areas where the surface nudging is not done to help the remaining cool bias. The net shortwave radiation for bare soil is given by (16) with the vegetation transmissivity set to 1.0. The only other change made for the soil shortwave radiation was to set the albedo to a fixed value of 0.80 for areas with snow cover for the February 1994 episode. The contribution from the atmospheric downward longwave to soil covered by vegetation is given by

$$(17) \quad R_{L,soil} = \epsilon_v t_{veg} R_L,$$

where $R_{L,soil}$ is the longwave radiation absorbed by the soil, R_L is the downward longwave radiation just above the surface, and ϵ_v is the vegetation emissivity. The atmospheric longwave radiation for bare soil is given by (17) with the vegetation transmissivity and the vegetation emissivity set to 1.0. The longwave contribution from the vegetation to the soil surface is described by

$$(18) \quad R_{Lv,soil} = \epsilon_g^2 (1 - t_{veg}) (1 - \epsilon_v) \sigma T_g^4 + \epsilon_g \epsilon_v (1 - t_{veg}) \sigma T_v^4 - \epsilon_g \sigma T_g^4,$$

(a)
(b)
(c)

where $R_{Lv,soil}$ is the longwave radiation emitted by the vegetation and absorbed by the soil, ϵ_g is the soil emissivity, T_g is the soil skin temperature, T_v is the bulk canopy vegetation temperature, and σ is the Stefan-Boltzmann constant. In (18) term (a) represents the radiation initially emitted from the soil and reflected back to the surface, term (b) represents the radiation emitted from the vegetation to the surface, and term

(c) represents the emission from the soil surface itself. For soil with no vegetation terms (a) and (b) are zero.

Total shortwave radiation absorbed by the vegetation, $R_{s,veg}$, is given by (19) where α_v is the vegetation albedo. Term (a) in (19) is the portion of the downward solar radiation which is directly absorbed while term (b) is that portion which is absorbed after one reflection from the ground.

$$(19) \quad R_{s,veg} = \underbrace{(1 - t_{veg} - f_a a_v)}_{(a)} R_s + \underbrace{f_a a_g t_{veg}}_{(b)} R_s$$

The atmospheric longwave radiation absorbed by the vegetation, $R_{L,veg}$ is given by (20). The remaining components of the vegetation longwave balance are given by (21) where term (a) represents the absorption of some of the longwave radiation emitted by the vegetation initially and then reflected from the soil surface, and term (b) represents the emission of longwave radiation from both sides of the vegetation canopy.

$$(20) \quad R_{L,veg} = e_v (1 - t_{veg}) R_L$$

$$(21) \quad R_{Lv,veg} = \underbrace{e_v^2 (1 - t_{veg}) (1 - e_g)}_{(a)} \sigma T_v^4 - 2 \underbrace{e_v (1 - t_{veg})}_{(b)} \sigma T_v^4$$

The bulk specific heat for the vegetation canopy was changed to the formulation suggested by Sellers et al. 1986

$$(22) \quad c_{pv} = 0.20 c_{ww} LAI \text{ ,}$$

where c_{pv} is the vegetation specific heat, c_{ww} is the specific heat for liquid water, and LAI is the leaf area index.

2.4.2.7 Alternate Convective Parameterization

Initial simulations of the July 1991 episode (chosen to replace the April 1994 episode) showed poor precipitation performance using the Kuo convective parameterization. An alternate scheme was used only for this episode. It consists of a plume model for the convective updraft and downdraft and a mass balance approach to determine the environmental subsidence. A closure scheme is then used for weighting the contributions from the updraft, downdraft, and environment to the grid-scale tendencies of temperature and moisture.

The updraft plume model follows the Kain and Fritsch (1990) approach for calculating the entrainment of environmental air into the updraft. The level chosen for starting the updraft parcel is the one with the largest

CAPE greater than 50 J kg^{-1} with a CIN greater than -20 J kg^{-1} and with a positive grid-scale vertical velocity. The initial updraft radius is taken as the largest of the following: a radius which is a function of the bulk Richardson number, a radius based on the planetary boundary layer (PBL) mass flux, and a radius which is a function of the depth of the PBL. The updraft calculations also include the following: 1) a simple form of Kessler (1969) microphysics; 2) the effects of water loading, friction, and perturbation pressure on the vertical velocity; 3) freezing of condensate water; and 4) the updraft radius is calculated by a mass conservation approach.

The downdraft calculations also use a plume model and are done after the updraft calculations. The initial and highest starting level for the downdraft calculations is the level of the minimum saturated equivalent potential temperature (LFS). Downdrafts are attempted starting at this level and at consecutively lower levels down to the updraft condensation level (LCL). The acceptable downdraft is the first one which reaches the ground or if none reach the ground the one with the deepest thickness. The initial downdraft starting radius is set to the average updraft radius between the LFS and LCL heights. The downdraft plume model includes the effects of water loading, ice melting, friction, entrainment, and the evaporation of precipitation. The downdraft is fed by a steady-state calculation of precipitation from the updraft. This initial downdraft calculation is then modified to achieve a rain-cooled pool of air below cloud base. The total mass of the cool pool is calculated from the initial downdraft values of vertical velocity and radius at cloud base and a time scale required to build the updraft above cloud base, which for this discussion is denoted by τ_u . The initial downdraft radius profile between the levels LFS and LCL is then adjusted by iteration to provide a time required to build the complete cool pool which is close to the time scale τ_u .

The last major set of calculations involve the determination of an environmental radius, R_e , which controls the magnitude of the environmental subsidence and provides a means to weight the updraft, downdraft, and environmental contributions to the total tendencies. The radius R_e is chosen as the largest of the following: the radius of PBL air required to build the updraft, the surface cool pool radius, the maximum updraft radius, and a radius based on the mean wind speed over the updraft depth and a time scale based on the mean Brunt-Vaisala frequency over the upper half of the updraft. The environmental heating and moistening rates are determined by the vertical gradients of temperature and moisture multiplied by an environmental vertical velocity, W_e . The velocity W_e is calculated from a mass flux conservation approach which allows environmental subsidence to complete the mass balance from the residual of the updraft and downdraft mass fluxes. The final step in determining the grid-scale tendencies is an area weighting of the updraft, downdraft, and environmental tendencies.

2.4.2.8 Changes in Other Physical Parameterizations

The diffusivity of water vapor was changed to a formulation which included the effects of pressure following the formula given by Pruppacher and Klett (1980). The thermal conductivity of dry air was also changed to a formula given by Pruppacher and Klett (1980). The saturation vapor pressure formulation after the July 1995 episode was changed to the absolute norm of the eighth order scheme described by Flatau et al. (1992) to accommodate a broader range of possible temperatures.

A summary of the changes described in this section across the episodes is given in Table 2-1.

Table 2-1 Summary of main changes to the RAMS modeling system across all episodes.

Modification Type	EPISODES								
	July 1995	May 1993	May 1995	Mar 1993	Feb 1994	July 1991	Aug 1993	June 1992	April 1995
Surface Grid Definition	no	yes	yes	yes	yes	yes	yes	yes	yes
Microphysics	no	yes	yes	yes	yes	yes	yes	yes	yes
Kuo Convective Scheme	yes	yes	yes	yes	yes	yes	yes	yes	yes
Radiation Calculations	yes	yes	yes	yes	yes	yes	yes	yes	yes
Nudging	yes	yes	yes	yes	yes	yes	yes	yes	yes
Surface Layer Calculations	yes	yes	yes	yes	yes	yes	yes	yes	yes
Surface Nudging	no	yes	yes	yes	yes	yes	yes	yes	yes
Surface Radiation Budget	no	yes	yes	yes	yes	yes	yes	yes	yes
Alternate Convective Parameterization	no	no	no	no	no	yes	no	no	no
Water Vapor Diffusivity Change	yes	yes	yes	yes	yes	yes	yes	yes	yes
Thermal Conductivity Change	yes	yes	yes	yes	yes	yes	yes	yes	yes
Saturation Water Vapor Change	no	yes	yes	yes	yes	yes	yes	yes	yes

2.5 Other Differences with Respect to Meteorological Modeling Protocol

This section summarizes departures from the meteorological modeling protocol (see Appendix 4) that were not described previously. The protocol mentioned the possibility of performing 4-km simulations. Time constraints did not allow for this. A cumulus parameterization (Kuo scheme for all episodes except the July 1991 episode; alternate scheme for the July 1991 episode) was used on all grids whereas the protocol indicated the possibility of not using a cumulus parameterization on the 12-km grid. Without using a cumulus parameterization on the 12-km grid it would have been difficult to achieve any significant precipitation for the warm-season cases. Time constraints did not allow for the comparison of model cloud fields with satellite data. A comparison with the Pennsylvania State University - National Center for Atmospheric Research (PSU-NCAR) mesoscale model, version 5, (MM5) was performed for the April 1994 episode. Neither MM5 or RAMS was capable of a realistic precipitation forecast over the Appalachians so that episode was replaced by the July 1991 episode. Time constraints also prevented the calculation of Lagrangian particle model trajectories as mentioned in the protocol.

2.6 RAMSIN Selections

The file which provides the choices for various RAMS model options is called the RAMSIN file. Table 2-2 gives a summary of the main RAMSIN variables which are either not a function of the nested grid or which were constant across the grids. Unless stated otherwise the values mentioned were used for all the episodes. The variable ITMDIFF controls the type of time differencing used and was set to 3 which uses leapfrog time differencing for the velocity components and pressure and uses forward time differencing for all other variables. The variable NONHYD was set to 1 which activated the nonhydrostatic mode. The frequency at which the radiation tendencies were updated is controlled by the variable RADFRQ and was set to 1200 s. The frequency at which the convective tendencies were updated is controlled by the variable CONFRQ and was set to 1200 s for all the episodes except the July 1991 case where it was set to 1800 s. The basic diffusion scheme is controlled by the IDIFFK variable and it was set to 1. This choice makes the horizontal diffusion a function of the gradients of the horizontal wind components; the horizontal grid size; and the variables CSX, XKHKM, and AKMIN. It also makes the vertical diffusion calculated by a turbulent kinetic energy scheme according to Mellor and Yamada (1982). The variable CSX was set to 0.3 and XKHKM was set to 1.0 for all grids and simulations except the July 1995 episode where it was to 3.0. The horizontal momentum diffusion coefficients for variables other than momentum are obtained by multiplying the horizontal momentum diffusion coefficients by the factor XKHKM. If a simulation remains stable then in general one desires to use a minimum amount of diffusion and therefore XKHKM was reduced for the other episodes. The variable AKMIN sets a minimum value for the diffusion and is in a later table. The variable NLEVEL controls the degree to which water in its various phases effects several calculations. Setting NLEVEL=3 allows the maximum influence. The variables IRAIN, IPRIS, ISNOW, IAGGR, IGRAUP, and IHAIL control the activation of the following condensate regimes, respectively: rain, pristine ice, snow, ice aggregates, graupel, and hail. Only rain was considered in the SAMI simulations so it was the only one with a non-zero value. The variable ISWRTP was set to 1 which activated the Chen and Cotton (1983) shortwave radiation parameterization which includes the effects of clouds. The variable ILWRTP was set to 1 which activated the Chen and Cotton (1983) longwave radiation parameterization that also includes the effects of clouds.

Table 2-2 Summary of main RAMSIN variables which are either not a function of the nested grid or which were constant across the grids.	
RAMSIN Variable Name	Value
ITMDIFF	3
NONHYD	1
RADFRQ	1200 s
CONFRQ	1200 s (July 91 used 1800 s)
IDIFFK	1 (all grids)
CSX	0.3
XKHKM	1.0 (all grids) (July 95 used 3.0 for all grids)
NLEVEL	3
IRAIN	1
IPRIS	0
ISNOW	0
IAGGR	0
IGRAUP	0
IHAIL	0

ISWRTYP	1
ILWRTYP	1

Table 2-3 Summary of main RAMSIN variables which are a function of the nested grid for the July 1995 episode.

RAMSIN Variable Name	48-km grid	24-km grid	12-km grid
TIMESTEP	80	40	20
TNUDLAT	3,600 s	3,600 s	3,600 s
TNUDCENT	10,800 s	10,800 s	10,800 s
TNUDTOP	600 s	600 s	600 s
ZNUDTOP	12 km	12 km	12 km
NUDLAT	15	15	15
AKMIN	1.5	1.5	1.5

Table 2-3 gives a summary of the main RAMSIN variables which are a function of the nested grid for the July 1995 episode. As discussed earlier the nudging time scales were held constant across the grids for this episode. The AKMIN parameter was also held constant at 1.5 across all the grids.

Table 2-4 gives a summary of the main RAMSIN variables which are a function of the nested grid for all the other episodes. The nudging time scales below a height of 12 km varied in the following manner: for the 96-km grid the time scale increased from 1 h at the outer boundary to 3 h at the 15th row/column inward, for the 24-km grid the time scale increased from 3 h at the outer boundary to 24 h at the 19th row/column inward, and for the 12-km grid the time scale was held constant at 24 h which essentially amounts to little or nudging. The top nudging time scale was held constant at a value of 10 min across all the grids. The AKMIN diffusion parameter increased from 0.5 for the 96-km grid to 1.0 for the 12-km grid.

Table 2-4 Summary of main RAMSIN variables which are a function of the nested grid for all episodes other than the July 1995 episode.

RAMSIN Variable Name	96- km grid	24-km grid	12-km grid
TIMESTEP	120 s	60 s	30 s
TNUDLAT	3,600 s	10,800 s	86,400 s
TNUDCENT	10,800 s	86,400 s	86,400 s
TNUDTOP	600 s	600 s	600 s
ZNUDTOP	12 km	12 km	12 km
NUDLAT	15	19	19
AKMIN	0.5	0.8	1.0

3.0 OVERVIEW OF RAMS SIMULATION PROCESS

3.1 NCEP/NCAR Reanalysis Data

Figure 3-1 provides a description of the major data sets and programs which are required for a SAMI RAMS simulation. In section 2.4.1 the various data sets used to define surface conditions were discussed. Here the discussion will focus on the sources and preparation of the atmospheric data for the RAMS model.

The only source for atmospheric three-dimensional variables was the NCEP/NCAR reanalysis data (Kalnay et al. 1996) (<http://dss.ucar.edu/pub/reanalysis/>). The reanalysis data set is the result of a large effort to analyze global data back to 1957 with a fixed state-of-the-art analysis/forecast system. Part of the effort was a comprehensive quality control scheme that screened all observations used by the system. Therefore, no further checks of this kind were made for the SAMI simulations. The reanalysis data variables are a mixture of model and observations, with observations dominating in those areas where data is more plentiful. Reanalysis fields are classified as A-D according to the following: A) variables which are dominated by observations (e.g., upper-air temperatures and winds); B) variables which are affected by observations but also are significantly influenced by the model (e.g., upper-air humidity and surface temperature); C) variables which are only model dependent; and D) variables which are only climatological values. The nudging scheme described in section 2.4.2.4 used the class A variables of the upper-air winds, temperatures, and pressure and the class B variable of the water vapor specific humidity. Nudging with respect to the specific humidity was the strongest over the coarse grid and was essentially zero for the fine grid (12-km) except for levels above 13 km. The latter choice was made in light of the early simulations of the April 1994 episode which attempted to nudge strongly toward the reanalysis values above the PBL on all grids and produced model values of clouds and precipitation which were too small.

3.2 Preparation of RAMS Input and Nudging Files

In Figure 3-1 the surface grid definitions files and the NCAR/NCEP reanalysis data are input into the RWGRIB program which transforms the reanalysis data to the RAMS grid and makes other adjustments to make the data compatible with the RAMS model. Details of this procedure are given in the SAMI meteorological modeling protocol (see Appendix 4). The bulk of the computation time at this step is the adjustment of the divergent component of the horizontal wind to insure a near-zero vertical velocity at the model top. The output from RWGRIB is composed of three-dimensional fields of horizontal wind components, water vapor mixing ratio, potential temperature, and a scaled pressure (the Exner function) every 6 h for the episode period for the coarse grid. The first RWGRIB file output is used by RAMS to initialize all the nested grids whereas all the other times are used for nudging as described in this section and in section 2.4.2.4. RWGRIB files for the 24- and 12-km grids are obtained by interpolation done by the RAMS model internally.

An independent run of RWGRIB uses the hourly surface observations obtained from NCAR to create analyses on the coarse grid of the near-surface values of temperature, water vapor, and wind speed. The NCAR data set used for this was DS472.0 which is the hourly airways surface data (<http://dss.ucar.edu/datasets/ds472.0/>). Again details of this procedure are given in the SAMI

meteorological modeling protocol (see Appendix 4) but the basic method is a Barnes (1973) analysis scheme as implemented by Koch et al. (1983). These analyses are used in two ways. The first is the surface nudging scheme described in section 2.4.2.5. The required surface nudging fields on the 24-km and 12-km grids were obtained by bilinear interpolation from the 96-km analysis. The second is to verify the model coarse grid results and will be used in section 6 for the various episodes. Limited quality control was performed on this data. Each station variable was compared against its neighboring station values and not included in the analysis if it exceeded specified criteria.

Once the initial, nudging, and surface analysis fields are produced by RWGRIB a RAMS model simulation can be started. After completion of a RAMS simulation the relevant data are sent to the Air Quality Modeling phase.

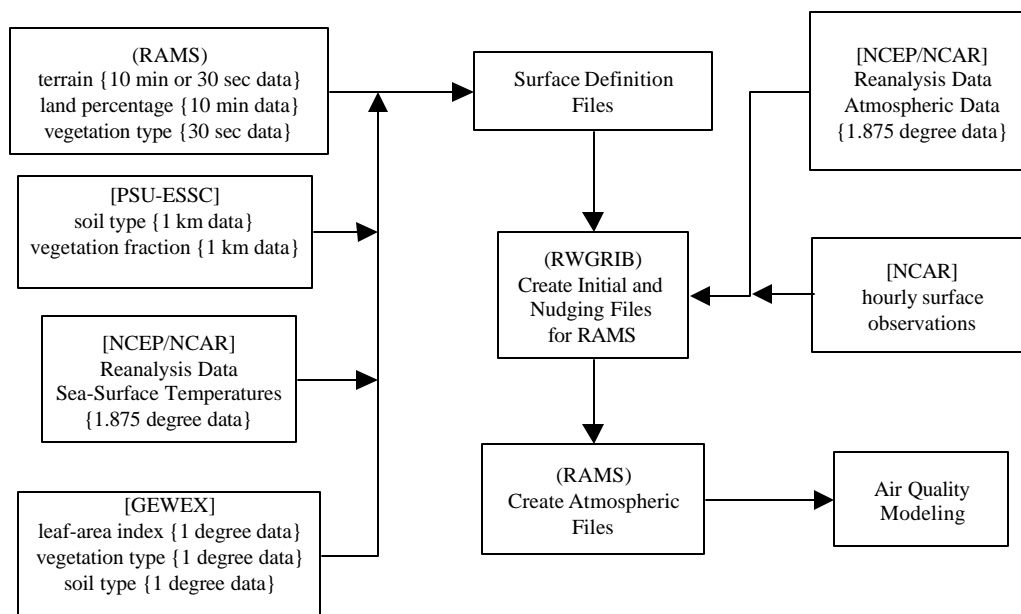


Figure 3-1. Flow diagram of major data sets and programs for a RAMS simulation for a SAMI episode. Names inside [] represent data sources, names inside () represent computer programs, and names inside { } represent the horizontal resolution of the original data source. See the text for additional details.

4.0 THE SAMI MODELING EPISODES

4.1 SAMI Episode Selection

This section provides an overview of the episode selection process. Additional details are described in Appendices 1 and 2. SAMI's integrated assessment is focusing on the impacts of ozone, visibility, and acid deposition on the natural resources in the Southern Appalachian mountains. The impacts of these pollutants are generally measured on an annual or seasonal time scale. Therefore, model predicted changes in pollutants need to be estimated on an annual and/or seasonal basis.

Ideally, several years of meteorology would be modeled to simulate the variability in meteorological influences on air quality over a long time period. A presumably robust response to future control strategies could be predicted by examining the average predicted change in annual and/or seasonal air quality metrics derived from modeling multiple years.

Due to the ambitious SAMI goal of modeling multiple pollutants in a "one atmosphere" approach, SAMI chose to use a sophisticated 3 dimensional Eulerian air quality model (the Urban-Regional Multi-scale model) to simultaneously model ozone, visibility, and acid deposition. The Urban-Regional Multiscale model (URM-1ATM) treats gaseous, aerosol, and precipitation chemistry. Computer limitations (even with the fastest modern CPUs available) forced SAMI to limit the number of potential modeling days to approximately 50-100.

Therefore, it became necessary to model a number of discreet episodes in order to approximate a full year or season. The challenge was to determine how to model the seasonal and/or annual metrics for 3 pollutants for the SAMI area with a limited set of modeling days. A contractor, SAI, Inc., developed software to aid in the selection of the SAMI episodes.

The objective of the episode selection process was to identify multi-day episodes that could represent the range of effects of emissions controls on air quality values. An attempt was made to optimize the selection process across seasonal ozone, annual visibility, and annual acid deposition, for two Class I areas: Great Smoky Mountains National Park (GSM) and Shenandoah National Park (SNP). These two Parks were used to represent all of the Class I areas in the SAMI region. Optimizing across two Class I areas (rather than a larger number) greatly simplified the episode selection process. GSM and SNP were chosen because they contained the most complete ambient data sets, they are spatially representative of the southern and northern portion of the SAMI domain respectively, and they are the most visited Class I areas in the SAMI region.

Historical ambient air quality and meteorological data from the 1991-1995 time period were used to classify each day using the Classification and Regression Tree analysis software (CART) (Brieman, 1984). More details on the use of CART and the development of the episode selection software can be found in SAI's episode selection documentation (Deuel, 1998).

In the analysis, each pollutant was represented by a daily or weekly ambient air quality value. Ozone was represented by the daily W_{126} cumulative exposure index defined as

$$W_{126} = \sum [O_3] f_w [O_3] ,$$

where $[O_3]$ is the one hour average ozone mixing ratio and f_w is a weighting function of $[O_3]$. The sum in the equation is done over all hours during April-October to compute a seasonal index. For classification purposes, a daily W_{126} (the sum being done over all hours in a single day) was calculated for each day during the ozone season in the 1991-1995 ozone data base.

Visibility was represented by the 24-hour average sum of sulfate, nitrate, organic carbon, and soil fine mass¹. The mass measurements were from the IMPROVE monitoring network. Acid deposition was represented by the weekly sum of wet deposition of sulfate, nitrate, calcium, and magnesium as measured by the NADP monitoring network.

The daily (and weekly for acid deposition) observed air quality information was divided into 4 or 5 “classes” before being input into CART. The classes were defined from low to high observed air quality values with Class 1 being the lowest (or cleanest) and Class 4 or 5 being the highest (or dirtiest). The ozone and acid deposition classifications were Class 1, 2, 3, and 4 defined as the cleanest 70%, 20%, 7%, and 3% of days (weeks) respectively. The visibility classification was Class 1, 2, 3, 4, and 5 defined as the cleanest 30%, 20%, 20%, 17%, and 3% of days respectively.

Air quality data were combined with observed meteorological data within CART to allow days to be segregated into “bins”. Bins represent similar patterns of meteorology within similar ranges of observed air quality values. CART was run for each pollutant for both Class I areas creating six sets of bins.

The following air quality and meteorological data was used as CART input:

Table 4-1. Air Quality Variables (used only for ozone)	
1.	Maximum observed ozone concentration in the Baltimore/Washington area
2.	Maximum observed ozone concentration in the region between the GSM and SNP
3.	Maximum observed ozone concentration in the Knoxville/Chattanooga area
4.	Maximum observed ozone concentration in the Atlanta area
5.	Previous day’s maximum observed ozone concentration in the Baltimore/Washington area
6.	Previous day’s maximum observed ozone concentration in the region between the GSM and SNP

1. The CART analysis was run for both annual visibility and “summer” visibility (June, July, and August). During the episode selection process SAMI decided to limit the visibility analysis to calculation of the annual average only. Therefore, all episode selection results presented in this document are for the annual average. It is possible to use the selected episode days to recalculate the summer average visibility using the episode selection software. But the errors associated with the summer average visibility would be relatively large since only 4 out of 9 episodes occur during the summer.

7. Previous day's maximum observed ozone concentration in the Knoxville/Chattanooga area
8. Previous day's maximum observed ozone concentration in the Atlanta area

Table 4-2. Surface Meteorological Variables for Ozone and Visibility
1. Average surface wind direction from 0000-0700 LST. The measured values were used for the averaging, and the final vector direction was cast into one of five bins, one representing calm and four centered on N, S, E, and W.
2. Ibid., but from 0800-1500 LST
3. Ibid., but from 1600-2300 LST
4. Average surface wind speed from 0000 to 2300 LST
5. Cumulative surface precipitation measured from 0000-2300 LST.
6. Average solar radiation from 0800-1500 LST
7. Average dew point temperature depression ² from 0000-2300 LST (Look Rock ³ only)
8. Average relative humidity from 0000-2300 LST (Big Meadows ⁴ only)
9. Maximum surface temperature
10. Minimum surface temperature

Table 4-3. Surface Meteorological Variables for Acid Deposition
1. Cumulative surface precipitation measured from 1200 LST on day one of the measurement period to 1200 LST on day eight of the measurement period
2. eight-dimensional array variable indicating whether precipitation occurred for each day of the measurement period (this variable will consist of a series of ones and zeros, with one indicating that precipitation occurred, for example, 11001101)
3. Average (over days and time) solar radiation from 0800-1100 LST
4. Ibid., but from 1200-2300 LST
5. Average (over days and time) dew point temperature depression from 0000-1100 LST (Look Rock only)
6. Average (over days and time) dew point temperature depression from 1200-2300 LST (Look Rock only)
7. Average (over days and time) relative humidity from 0000-1100 LST (Big Meadows only)
8. Average (over days and time) relative humidity from 1200-2300 LST (Big Meadows only)
9. Average (over days) maximum surface temperature (treated as pm for averaging)
10. Average (over days) minimum surface temperature (treated as am for averaging)

2. Dew point depression is defined as the difference between the ambient temperature and the dew point temperature (a measure of the moisture content of the air). A large dew point depression indicates that the air is relatively dry; a small dew point depression indicates that the air is relatively moist.

3. Look Rock data is from Great Smokies

4. Big Meadows data is from Shenandoah

Table 4-4. Upper Air Meteorological Variables for Ozone and Visibility
1. Wind direction bin at the 850 mb pressure level from the morning sounding for each individual site. Wind directions were cast into five bins, one representing calm and four centered on N, S, E, and W.
2. Ibid., but from the afternoon sounding
3. wind speed at the 850 mb pressure level, from the morning sounding, for each individual site
4. Ibid., but from the afternoon sounding
5. Average height of the morning 850 mb pressure level over all sites
6. Ibid., but from the afternoon sounding
7. Average temperature at the 850 mb pressure level, from the morning sounding over all sites
8. Ibid., but from the afternoon sounding
9. Same variables as above, but for the 700 mb pressure level

Table 4-5. Upper Air Meteorological Variables for Acid Deposition
1. Same upper air variables as for ozone and visibility except the morning and afternoon sounding variables were averaged over a seven day period

CART defines the best way to sort the days within each pollutant class, given observed meteorological and air quality variables, to explain the variation in observed air quality data. The following number of bins were identified by CART:

Table 4-6. Summary of CART bins	Shenandoah	Great Smokies
Seasonal Ozone	32	32
Annual Visibility	29	26
Annual Acid Deposition	12	19

4.1.2 Important Meteorological and Air Quality Variables

For each pollutant and for each park, certain variables were important in distinguishing between bins. For ozone at GSM, the most important variables were relative humidity, morning wind speed at 850 mb at Greensboro, evening 700 mb height at Athens, and maximum observed ozone between GSM and SNP.

For ozone at SNP, the most important variables were relative humidity, evening 700 mb temperature at Huntington, incoming solar radiation, average surface wind speed, and maximum observed ozone between SNP and GSM and in the Baltimore/Washington area.

For annual visibility at GSM, the most important variables were maximum surface temperature, morning 700 mb wind speed at Athens, morning 700mb wind direction at Nashville, 700mb

temperature at Nashville, precipitation at GSM, morning 850 mb wind speed at Athens, and evening 850 mb height at Greensboro.

For annual visibility at SNP, the most important variables were minimum and maximum surface temperature, morning 700 mb temperature at Dulles, precipitation at SNP, morning 700 mb wind speed at Huntington, and morning 700 mb height at Greensboro.

For acid (wet) deposition at GSM, the most important variables were precipitation at GSM, average maximum temperature, solar radiation, 700 mb height at Greensboro, and dew point temperature.

For acid (wet) deposition at SNP, the most important variables were precipitation at SNP, morning 700 mb wind direction at Greensboro, evening 850 mb wind speed at Dulles, and the number of days of measurable precipitation (during the 8 day period).

4.1.3 CART Performance

The accuracy of the CART process can be examined by looking at the number of “misclassified days” in each class for each pollutant and Class I area. The episode days are identified as a Class 1, 2, 3, 4, or 5 day so that all of the Class 1 days should be sorted into Class 1 bins at the end of the CART process and each of the Class 2 days should be sorted into Class 2 bins, etc. Days that are classified into the wrong bin (based on their observed air quality value) are termed misclassified days. A large number of misclassified days may indicate that more independent variables were needed in order to differentiate between days. It may also indicate that the relationship between the observed air quality value and the observed meteorology may be weak.

The CART results indicate that the number of misclassified ozone and acid deposition days (weeks) are relatively small. The number of misclassified visibility days is much larger. This is likely due to the difference in the definition of the visibility classes as compared to the other pollutants. The software had a particularly difficult time distinguishing the Class 1, 2, and 3 visibility days from each other. Performance for the Class 4 and 5 days was much better.

Details of the classification statistics and a more complete description of the meteorological variables that were important in the classification can be found in the SAI report (SAI, 1998).

4.1.4 Episode Selection Software

The outputs from the CART software analysis became the basis of the episode selection. CART sorted all of the days into classes and bins (by pollutant and air quality ‘Class I’ area). At this point, some combination of days could be selected to represent the seasonal and annual air quality metrics. The class definitions could be used to ensure that a variety of air quality values were selected and the bin definitions could be used to ensure that a variety of meteorological regimes were represented. But it would be nearly impossible to hand select days for each pollutant and Class I area in an effort to replicate each of the annual and seasonal metrics.

Therefore, software was developed to aid in the selection of episode days. The software automatically selects a set of days given certain user defined inputs. The software attempts to optimize across the pollutants and Class I areas in an effort to minimize the errors associated with using a set of episode days to represent annual or seasonal air quality metrics.

4.1.5 Episode Software “Theory”

The following is the basic theory behind the episode selection software. Each bin contains a certain number of days and each day has an observed air quality value. Therefore, if you add up the value of all the days for all bins for each pollutant/Class I area, it should equal the annual or seasonal metric. Additionally, if you multiply the mean value of the population in each bin by the number of days in each bin and then sum the total, you will arrive at the same annual or seasonal metric.

This calculation provides a basis for the episode selection. If a single day was selected from each CART bin and that day had a value exactly equal to the mean value of the bin, then the annual or seasonal metric could easily be replicated (assuming the number of days in each bin is known). Additionally, this would ensure that each meteorological/air quality regime would be represented by at least one episode day.

Table 4-7 shows a simple mathematical example. Let’s assume that for a single pollutant at a single Class I area there are 2 classes and 2 bins in each class. There are a total of 40 observation days with a total annual metric of 210. The “weight” of each bin is calculated as the number of days times the observed daily values in the bin. If an episode day was selected from Class 1, bin 1 and that day had a value of 3, then the value could be multiplied by the number of days in the bin to get a total weight of 21. This represents 10% of the total annual weight. So in this case, the single episode day would represent 10% of the annual metric. Note that this takes into account both the magnitude of the ambient value and the frequency of occurrence. If one day was selected from each of the 4 bins and each day had a value exactly equal to the mean of each bin, then the annual metric could be exactly recalculated. Of course, in most cases, selected episode days will not have a value exactly equal to the mean value of the bin. This is a potential source of “error” in the episode selection process.

Class	Bin Number	Days	Mean Value	Weight (days X mean)	% of Annual Weight
Class 1	Bin 1	7	3	21	10.0
	Bin 2	13	8	104	49.5
Class 2	Bin 1	15	2	30	14.3
	Bin 2	5	11	55	26.2
Total		40		210	100%

The above example assumes that at least one episode day is chosen from each bin. Unfortunately, this was not possible in the SAMI episode selection process. There are a total of 150 bins between the 3 pollutants and 2 Parks. There are too many bins to be able to select a single day from each one. Additionally, the collection frequency of the ambient air quality data adds to the difficulty of episode selection. The ambient ozone data is available on a daily basis. But the IMPROVE visibility data are only collected on

Wednesdays and Saturdays. This means that even if a Wednesday and Saturday were selected from the same week, all of the days in between need to be modeled to form a continuous episode. Modeling a full week only yields two valid visibility days. The acid deposition data are collected as a total weekly sample. Modeling a single acid deposition “day” actually means modeling an entire 8 day period (Tuesday-Tuesday). Also, it was recommended by SAI to exclude “misclassified” days from consideration as episode days. This also made it more difficult to string together continuous episode periods. With all of these factors, modeling at least a single day from each bin may have entailed modeling as many as 300-400 actual modeling days.

Since the approximate number of modeling days needed to be limited to ~50-100 days, sacrifices had to be made in selecting episode days. Not all bins could be represented. This was taken into account when the episode software was designed. The software established rules for selecting bins and also contained scaling factors to account for errors and biases introduced by not representing all episode bins and/or classes and by not selecting misclassified days.

4.1.6 Episode Software Rules

If episode days were not selected from all bins and/or classes then the order in which days were selected becomes important. There needs to be a way to select from the “most important” bins first. Also, since the episode selection was optimized across the 3 pollutants and 2 parks, a pollutant order and a park order needed to be established.

The “importance” of the bins was established by using the previously defined “weight” of each bin (weight is equal to the number of days times the ambient value). Within each park for each pollutant, the bins were ordered by their total weight. This ensures that days with a high frequency of occurrence and/or a high magnitude are selected first. In theory, the bins that are not used in the episode selection should be bins with low weights that contribute a relatively small portion of the annual and/or seasonal metrics. This episode selection rule was hardwired into the software.

Another selection rule was that a day/week had to be selected for each park/metric combination prior to a second day being selected for any park/metric combination. There were 3 metrics and 2 parks, so six days/weeks would be selected before each park/metric combination was repeated. The order of the park/metric selection is chosen by the user in the episode selection input file.

4.1.7 Episode Selection Error Terms

All days must be modeled in order to represent an entire five-year data period without introducing non-model errors or biases. However, this scope of modeling was not possible. Therefore, an attempt was made to minimize non-model errors caused by modeling only a subset of days.

There is variability within each pollutant class identified by CART. Non-model error occurs in part because most days chosen to represent a class of days do not contribute to the seasonal or annual metric for a given pollutant category in a manner identical to all days in a class. The exception is the unlikely occurrence of a

day on which the pollutant metric (for example, W_{126}) equals the average daily metric across all days in its class. The extent to which a subset of days fails to replicate conditions across all days is one component of non-model error associated with episodic modeling.

4.1.8 Biased (Unscaled) Error

Another component of non-model error is due to the inability of the episodic days that are selected to represent all CART class bins. Within the episode software, the error associated with not selecting days from all bins is termed “biased error” or “unscaled error”. This error term is based on the amount of weight represented by the selected episode days. The biased error is equal to the amount of weight that is not represented by the selected episode days.⁵ Since not selecting all bins always results in an underestimate of annual/seasonal weight, the biased error term is always negative. For example, the biased error for ozone at Shenandoah is -16.6%. This means that the selected episode days represent 83.4% of the total seasonal ozone weight. In the SAMI episode

$$A_r = \frac{1}{S} \left[\frac{N}{\sum_{\substack{k \text{ a class not} \\ \text{represented}}} P_k} \sum_{k=1}^{n_{class}} \left\{ \left(\frac{\sum_{j=1}^{b_k} P_j}{\sum_{l_k} P_{l_k}} \right) \left[\sum_{l_k} \left(\frac{WA_{l_k}}{WP_{l_k}} \right) \left(\frac{n_{l_k}}{m_{l_k}} \right) \sum_{j=1}^{m_{l_k}} a_{jl_k} \right] \right\} \right]$$

selection the biased errors ranged from -16.6% to -55.2%. **In all cases, the primary goal in the episode selection was to minimize the biased errors for all pollutants and parks.**

4.1.9 Distance (Scaled) Error

The episode selection software attempts to minimize the error in day selection by creating several “scaling factors” which try to account for unrepresented bins, classes and misclassified days. The complete equation to calculate the annual and/or seasonal metrics is equation 4-1 in the episode software documentation. The documentation also contains a complete description of equation 4-1.

where:

- A_r is the value of the metric due to all selected, representative days
- S is the number of seasons or years included in the data set
- N is the total number of days included in the data set
- P_j is the number of days in bin j ($P_j = n_j$ if the user specifies that all days can be used to represent

5. The biased error is also affected by how close the selected days are to the mean value of their respective bins. The difference between the mean and the selected day(s) is part of the unbiased error calculation. Errors associated with selected days with values higher than the bin mean can be canceled out by days with values lower than the bin mean.

the bin; when only properly classified days are used, they may differ).

n_{class} is the number of distinct values of the classification variable

b_k is the number of bins with predicted value k of the classification variable

WA_j is the weight for bin j using all days in bin j

WP_j is the weight for bin j using only the properly classified days, or all days, in bin j , depending on the user's specification

l_k runs over all bins with the classification value k , from which a representative day was chosen

n_j is the number of properly classified days, or all days, in bin j , depending on the user's specification

m_j is the number of representative days chosen from bin j

a_{jk} is the observation-based value of the metric for representative day j in bin k

Within equation 4-1 are several scaling factors which attempt to reduce the error associated with not selecting all bins. There are three general scaling factors:

The WA/WP portion of the equation is a scaling factor to account for misclassified days. In the episode selection, SAMI chose to allow the selection of only properly classified days as episode days. The scaling factor accounts for the number of unused misclassified days.

The P_j/P_1 portion of the equation is a scaling factor to account for unselected bins within each class. It is assumed that all bins within a class have a similar mean value. Therefore, the weight of the selected bins is used to approximate the weight from the unselected bins. There is some uncertainty in this assumption since the mean values between bins in the same class can differ (although not by a large amount).

The N/P_k portion of the equation is a scaling factor to account for classes not selected. This would only be used if no bins within a class were selected⁶. The factor uses the values of the days selected to account for the bins and classes that were not selected. There is a large amount of uncertainty in this assumption. For example, the values of a Class 1 day should not be used to approximate values from a Class 4 bin. If the missing class is a high or low class, it is probably a poor assumption to adjust the values based on bins from other classes (it may be reasonable to scale for Class 2 based on Class 1 or 3 days.)

Equation 4-1 performs the scaling of the results and calculates a final "distance" or "scaled" error. In most cases this error term is < 10%. But since the scaled error has a number of assumptions built into it, the unscaled error was used as the primary judgment of episode selection error. The scaled error was used as a secondary measure.

Using equation 4-1, the episode selection software outputs all of the information necessary to recalculate the annual and/or seasonal metrics from the selected episode days.

⁶ In testing of the software, it was found that the largest source of error (creating a large scaling factor) was not selecting at least one bin from each class for each pollutant. It was made a priority to always choose at least one day for each class. This was accomplished for all pollutants except dry deposition.

4.1.10 Reproducing the Annual and Seasonal Metrics

Selecting the episode days to be modeled was an iterative process that took more than a year to complete. This process occurred in parallel with the early stages of the actual modeling. In the end, nine episodes were selected to represent the range of conditions for ozone, visibility and acid deposition at Great Smoky Mountains and Shenandoah National Parks. Details of the selection process are described in Appendix 2.

The episode selection software tool that was a critical component in the selection process outputs the necessary information to reproduce the annual and seasonal metrics from the selected episode days⁷. The following series of tables contain the scaling factors and other information needed to recreate the annual totals for acid deposition and visibility and the seasonal total for ozone.

The following is an explanation of the variables used to reconstruct the annual/seasonal metrics:

Table 4-8. Variable definitions	
Date	Date of the first day of each acid deposition week or the actual episode days for ozone and visibility.
	The CART bin classification for each day/week
1/S*N/P(j)	1 divided by the number of years (or seasons) of air quality data used
Class	The class that each day/week was assigned to.
B (Class)	A scaling factor which accounts for bins and/or classes not selected. A separate “B” scaling factor is applied to all selected days within the same class.
WA/WP	A scaling factor which accounts for misclassified days within a bin. A separate WA/WP scaling factor is applied to all selected days within the same bin.
n(j)/m(j)	The number of days in the bin. n(j) is the number of days in the bin selected. This number is divided by the number of days selected from the same bin (m(j)). For example, if 2 days from the same bin are selected, then each day will be weighted by half of the number of days in the bin. This avoids double counting the weights.
Deposition/ PM2.5/ W126	The observed ambient value of wet deposition, dry deposition, PM2.5, or ozone on the selected day/week. The units are kg/ha/week, ug/m3, ng/m3, and W126, respectively.
Contribution (absolute)	This is the absolute contribution to the annual or seasonal total. This value is calculated by the formula: [1/S*N/P(j)] * [B(Class)] * [WA/WP] * [n(j)/m(j)] * [Deposition/PM2.5/W126]. The absolute contribution is weighted by both the ambient concentrations and the frequency of occurrence. The absolute contribution attributable to each episode day represents a portion of the annual or seasonal metric.
Contribution (%)	This is the same as the absolute contribution except normalized to 100%. The percent contribution of each day/week represents the percentage that each day/week contributes to the annual or seasonal total. For example, an ozone day with a contribution percentage of 4.2% means that the observed W126 on that day represents 4.2% of the seasonal total W126. (It does not represent 4.2% of the days in a season.)

⁷ The episode software only calculates the metrics for GSM and SNP. Interpolation methods need to be applied to calculate the metrics for the other SAMI class 1 areas. Different methods will be used for each pollutant.

Table 4-9. Episodic days selected for GSM wet acid deposition modeling

Date	Bin	1/S*N/P(j)	Class	B(Class)	WA/WP	n(j)/m(j)	Deposition (kg/ha/week)	Contribution (absolute)	Contribution (%)
910723	19	0.2	4	1.6	1	5	5.49	8.78	23.2
920623	15	0.2	2	2.023	1.122	17	0.89	6.87	18.1
930323	4	0.2	2	2.023	1.186	8	1.13	4.34	11.4
930511	12	0.2	3	1.846	1.268	4	1.64	3.07	8.1
930803	12	0.2	3	1.846	1.268	4	1.89	3.54	9.3
940208	4	0.2	2	2.023	1.186	8	1.17	4.49	11.8
950425	7	0.2	1	1.136	1.081	25	0.69	4.24	11.2
950523	1	0.2	1	1.136	1.093	61	0.17	2.58	6.8
Total								37.90	100.0

Table 4-10. Episodic days selected for SNP wet acid deposition modeling

Date	Bin	1/S*N/P(j)	Class	B(Class)	WA/WP	n(j)/m(j)	Deposition (kg/ha/week)	Contribution (absolute)	Contribution (%)
910723	12	0.2	4	1.286	1.13	2.5	5.12	3.72	13.1
920623	1	0.2	1	1.474	1	38	0.21	2.35	8.3
930323	6	0.2	3	1.286	1.403	14	1.97	9.95	35.0
930511	12	0.2	4	1.286	1.13	2.5	2.84	2.06	7.3
940208	8	0.2	2	1.186	1.619	4.5	1.24	2.14	7.5
950425	3	0.2	2	1.186	1.541	11	1.02	4.10	14.4
950523	8	0.2	2	1.186	1.619	4.5	1.41	2.44	8.6
950711	1	0.2	1	1.474	1	38	0.15	1.68	5.9
Total								28.45	100.0

Table 4-11. Episodic days used for GSM dry acid deposition modeling

Date	Bin	1/S*N/P(j)	Class	B(Class)	WA/WP	n(j)/m(j)	Deposition (ug/m3)	Contribution (absolute)	Contribution (%)
910723	16	0.2	1	1.314	1.019	19.75	3.62	19.1	10.8
920623	16	0.2	1	1.314	1.019	19.75	7.16	37.9	21.3
930323	7	0.2	1	1.314	1.068	12	6.73	22.7	12.8
930511	5	0.2	2	5.667	1	2	9.65	21.9	12.3
930803	16	0.2	1	1.314	1.019	19.75	6.02	31.8	17.9
940208	7	0.2	1	1.314	1.068	12	3.41	11.5	6.5
950523	16	0.2	1	1.314	1.019	19.75	6.17	32.6	18.4
950711	21	0.2	2	5.667	1.135	6	8.14	62.8	35.4
Total								177.5	100.0

Table 4-12. Episodic days used for SNP dry acid deposition modeling

Date	Bin	1/S*N/P(j)	Class	B(Class)	WA/WP	n(j)/m(j)	Deposition (ug/m3)	Contribution (absolute)	Contribution (%)
910723	17	0.2	1	1.171	1.273	19	8.97	50.8	12.7
930323	17	0.2	1	1.171	1.273	19	9.58	54.3	13.6
930803	17	0.2	1	1.171	1.273	19	13.55	76.8	19.2
940208	11	0.2	1	1.171	1.087	18	13.42	61.5	15.4
950425	17	0.2	1	1.171	1.273	19	6.31	35.7	9.0
950523	17	0.2	1	1.171	1.273	19	7.49	42.4	10.6
950711	17	0.2	1	1.171	1.273	19	13.68	77.5	19.4
Total								399.0	100.0

Table 4-13. Episodic days selected for GSM visibility modeling

Date	Bin	1/S*N/P(j)	Class	B(Class)	WA/WP	n(j)/m(j)	PM 2.5 (ng/m3)	Contribution (absolute)	Contribution (%)
910727	22	0.2	5	1.667	1.031	3.5	26605	32007.8	3.6
910731	18	0.2	5	1.667	1	1	31824	10610.1	1.2
920624	16	0.2	4	1.383	1.404	9	20918	73110.9	8.3
930324	7	0.2	2	1.223	1.872	50	8223	188262.0	21.3
930327	1	0.2	1	1.263	2.743	13	4505	40578.6	4.6
930515	15	0.2	3	1.311	1.445	16	15464	93743.8	10.6
930804	17	0.2	3	1.311	1.521	10	10029	39996.3	4.5
930807	17	0.2	3	1.311	1.521	10	9338	37240.5	4.2
930811	16	0.2	4	1.383	1.404	9	19024	66491.1	7.5
940209	9	0.2	1	1.263	1.904	27	3919	50890.8	5.7
950426	4	0.2	2	1.223	1.156	11	6538	20335.4	2.3
950429	6	0.2	3	1.311	1.894	16	9766	77597.8	8.8
950527	16	0.2	4	1.383	1.404	9	17516	61220.5	6.9
950712	16	0.2	4	1.383	1.404	9	17785	62160.7	7.0
950715	22	0.2	5	1.667	1.031	3.5	25882	31138.0	3.5
Total								885384.1	100.0

Table 4-14. Episodic days selected for SNP visibility modeling

Date	Bin	1/S*N/P(j)	Class	B(Class)	WA/WP	n(j)/m(j)	PM 2.5 (ng/m3)	Contribution (absolute)	Contribution (%)
910724	29	0.2	4	1.215	1.157	8	16610	37359.3	3.7
910731	24	0.2	4	1.215	1.613	6	23289	54770.0	5.5
920624	25	0.2	4	1.215	1	3.5	16664	14172.7	1.4
920627	25	0.2	4	1.215	1	3.5	18077	15374.5	1.5
930324	9	0.2	2	1.467	1	5	5580	8185.9	0.8
930331	12	0.2	1	1.9	2.805	18	3892	74672.7	7.5
930512	13	0.2	4	1.215	1.609	7	23834	65231.5	6.5
930515	14	0.2	3	1.49	1.246	13	9576	46223.4	4.6
930804	27	0.2	3	1.49	1.414	7.5	13994	44225.1	4.4
930807	13	0.2	4	1.215	1.609	7	16282	44562.4	4.5
930811	23	0.2	4	1.215	1.392	5	18647	31537.3	3.2
940209	12	0.2	1	1.9	2.805	18	3715	71276.7	7.1
950426	1	0.2	2	1.467	1.736	21.333	5548	60283.5	6.0
950429	1	0.2	2	1.467	1.736	21.333	9031	98129.1	9.8
950503	1	0.2	2	1.467	1.736	21.333	6745	73289.8	7.3
950524	29	0.2	4	1.215	1.157	8	16746	37665.2	3.8
950527	7	0.2	3	1.49	1.174	10	11944	41786.3	4.2
950712	20	0.2	5	1	1.568	7	26001	57077.4	5.7
950715	20	0.2	5	1	1.568	7	38917	85430.6	8.5
950719	27	0.2	3	1.49	1.414	7.5	12226	38637.7	3.9
Total								999891.1	100.0

4-15. Episodic days selected for GSM ozone modeling

Date	Bin	1/S*N/P(j)	Class	B(Class)	WA/WP	n(j)/m(j)	W126 (ppb)	Contribution (absolute)	Contribution (%)
910726	23	0.2	3	1.747	1.056	8	871.8	2573.3	3.8
910727	7	0.2	2	1.217	1.207	5.333	499.3	782.3	1.1
910728	3	0.2	1	1	1.349	30	243.4	1970.1	2.9
910731	7	0.2	2	1.217	1.207	5.333	620.7	972.5	1.4
920624	16	0.2	4	1.178	1.081	9	1396.5	3201.0	4.7
920626	21	0.2	1	1	1.263	23	83.3	484.0	0.7
920628	25	0.2	3	1.747	1.473	5	763.8	1965.5	2.9
930511	10	0.2	2	1.217	1.162	6	638.3	1083.2	1.6
930513	1	0.2	1	1	1.138	94.8	89	1920.3	2.8
930515	5	0.2	2	1.217	1.623	15.75	488.6	3040.0	4.4
930516	10	0.2	2	1.217	1.162	6	551.9	936.6	1.4
930517	13	0.2	2	1.217	1.442	3	703.6	740.9	1.1
930805	5	0.2	2	1.217	1.623	15.75	385.8	2400.4	3.5
930806	1	0.2	1	1	1.138	94.8	104.2	2248.3	3.3
930807	3	0.2	1	1	1.349	30	290.8	2353.7	3.4
930808	2	0.2	2	1.217	1.882	7	558.2	1789.9	2.6
930809	7	0.2	2	1.217	1.207	5.333	549.6	861.1	1.3
930811	5	0.2	2	1.217	1.623	15.75	568.5	3537.1	5.2
950426	5	0.2	2	1.217	1.623	15.75	540.6	3363.5	4.9
950429	12	0.2	3	1.747	1.49	2.5	807.6	1051.1	1.5
950501	1	0.2	1	1	1.138	94.8	168.6	3637.8	5.3
950502	1	0.2	1	1	1.138	94.8	78.5	1693.8	2.5
950503	2	0.2	2	1.217	1.882	7	548.4	1758.5	2.6
950524	25	0.2	3	1.747	1.473	5	820.4	2111.2	3.1
950525	12	0.2	3	1.747	1.49	2.5	771.7	1004.4	1.5
950526	29	0.2	3	1.747	1.438	1.5	767.1	578.1	0.8
950527	2	0.2	2	1.217	1.882	7	658.4	2111.2	3.1
950529	1	0.2	1	1	1.138	94.8	87.9	1896.6	2.8
950711	30	0.2	3	1.747	1	3	1017	1066.0	1.6
950712	25	0.2	3	1.747	1.473	5	874.6	2250.6	3.3
950713	25	0.2	3	1.747	1.473	5	1086.4	2795.7	4.1
950714	31	0.2	4	1.178	1.281	10.5	1351.1	4281.6	6.3
950715	29	0.2	3	1.747	1.438	1.5	1012.2	762.9	1.1
950717	32	0.2	3	1.747	1.327	4	824.2	1528.6	2.2
950719	31	0.2	4	1.178	1.281	10.5	1161.2	3679.8	5.4
Total								68431.2	100.0

Table 4-16. Episodic days selected for SNP ozone modeling

Date	Bin	1/S*N/P(j)	Class	B(Class)	WA/WP	n(j)/m(j)	W126 (ppb)	Contribution (absolute)	Contribution (%)
910723	29	0.2	3	1.425	1.174	1	1143.1	382.5	0.6
910726	18	0.2	2	1.191	1.688	5.818	658.9	1541.4	2.3
910728	18	0.2	2	1.191	1.688	5.818	737.8	1725.9	2.6
910730	1	0.2	1	1	1.089	52.875	62.8	723.2	1.1
910731	18	0.2	2	1.191	1.688	5.818	638.5	1493.6	2.3
920624	18	0.2	2	1.191	1.688	5.818	391.5	915.8	1.4
920625	4	0.2	1	1	1.134	53	224.5	2698.6	4.1
920626	18	0.2	2	1.191	1.688	5.818	547	1279.6	1.9
920628	18	0.2	2	1.191	1.688	5.818	449	1050.4	1.6
920629	22	0.2	3	1.425	1.323	12	1022.1	4624.7	7.0
930511	29	0.2	3	1.425	1.174	1	1019.6	341.1	0.5
930512	10	0.2	3	1.425	1.497	9.333	958.4	3816.2	5.8
930513	1	0.2	1	1	1.089	52.875	72.4	833.8	1.3
930805	4	0.2	1	1	1.134	53	70.4	846.2	1.3
930806	1	0.2	1	1	1.089	52.875	89.8	1034.2	1.6
930809	18	0.2	2	1.191	1.688	5.818	745.4	1743.7	2.6
930810	18	0.2	2	1.191	1.688	5.818	567.9	1328.5	2.0
930811	18	0.2	2	1.191	1.688	5.818	549.3	1285.0	1.9
950427	6	0.2	4	1.205	1.477	2	1167.8	831.4	1.3
950428	2	0.2	1	1	1.452	37	250.6	2692.6	4.1
950429	3	0.2	2	1.191	1.356	23	428.7	3184.8	4.8
950501	1	0.2	1	1	1.089	52.875	65.8	757.8	1.1
950502	1	0.2	1	1	1.089	52.875	85.6	985.8	1.5
950503	1	0.2	1	1	1.089	52.875	140.6	1619.2	2.4
950524	10	0.2	3	1.425	1.497	9.333	1121.6	4466.1	6.7
950525	18	0.2	2	1.191	1.688	5.818	620	1450.4	2.2
950528	1	0.2	1	1	1.089	52.875	72	829.2	1.3
950529	1	0.2	1	1	1.089	52.875	58.1	669.1	1.0
950711	10	0.2	3	1.425	1.497	9.333	935.8	3726.2	5.6
950712	27	0.2	3	1.425	1.554	3	901.7	1198.1	1.8
950713	26	0.2	4	1.205	1.013	5	1162.6	1419.1	2.1
950714	30	0.2	4	1.205	1.108	13	1456.6	5056.4	7.6
950715	28	0.2	4	1.205	1.181	7	1334.7	2659.2	4.0
950717	23	0.2	2	1.191	1.379	12	527.3	2078.5	3.1
950718	18	0.2	2	1.191	1.688	5.818	430.6	1007.3	1.5
950719	15	0.2	2	1.191	1.577	19	545.2	3891.2	5.9
Total								66186.7	100.0

4.2 The 11-19 July 1995 Episode

The synoptic discussion for each episode will have four basic elements. These are the following: discussion of why the episode was chosen (expanded discussion of this is available in section 4), discussion of the

departure of the 500-mb geopotential height from a longer term mean, discussion of the main upper-air and surface weather features during the episode, and a discussion of the main features of the meteograms of the NWS sites closest to the Great Smoky National Park (GSM) and the Shenandoah National Park (SNP). The 500-mb geopotential height anomaly plots were obtained from the National Oceanic and Atmospheric Administration - Cooperative Institute for Research in Environmental Sciences (NOAA-CIRES) Climate Diagnostics Center web page (www.cdc.noaa.gov/HistData). The episode synoptic discussion utilized the NOAA publication *Daily Weather Maps*. Because of the importance of the Class I areas in GSM and SNP, meteograms of the closest NWS sites to these locations were included. For GSM it was Knoxville, Tennessee (about 22 km from the center of GSM), and for SNP it was Charlottesville, Virginia (about 44 km from the center of SNP). Because of missing data problems at Charlottesville, the alternate sites of Staunton, Virginia and Martinsburg, West Virginia (49 and 105 km from the center of SNP, respectively) were also used.

The July 1995 episode was Class 1 for acid deposition at SNP. The episode contained one Class 5 visibility day and one Class 4 visibility day at GSM, and two Class 5 and one Class 3 visibility days at SNP. For ozone at GSM there were five Class 3 days and two Class 4 days. For ozone at SNP there were three Class 2 days, two Class 3 days, and three Class 4 days. Overall, this episode experienced periods of low visibility and high ozone. Apart from SAMI it is well known for a relatively short but intense heat wave which claimed around 800 lives across the country (Changnon et al. 1996; Kunkel et al. 1996)

The anomaly field (showing departures from a 15-year mean) for the 500-mb geopotential height for this episode is shown in Figure 4-1. Heights were on average 30-45 m above the long-term mean over portions of Midwest. This resulted in surface high pressure over the same area for much of the period which contributed to the heat wave. The 500-mb ridge intensified and moved eastward from the Nebraska-Kansas area on 10 July to northern Illinois by 14 July. During this period most precipitation occurred on the periphery of the ridge over the Great Lakes and coastal areas of the Atlantic and Gulf coasts. Temperatures warmed during this period so that by 14 July a large portion of the Midwest had maximum temperatures 35°C or higher. For the period 15-20 July the 500-mb ridge slowly weakened and moved southward taking up a position generally from Texas to Georgia. At the same time a cold front moved slowly southeastward from the northern Great Plains and became stationary across the South by the end of the period. This brought cooler and less humid air to much of the eastern United States along with scattered precipitation.

Figures 4-2 and 4-3 contain time series of observations for Knoxville, while Figures 4-4 and 4-5 show the same for Staunton, Virginia. The Charlottesville, Virginia site had large segments of missing data for this episode. Maximum temperatures at Knoxville warm to near 35°C on 15 July and then slowly decline thereafter due to an increase in cloud cover from scattered afternoon convection and the frontal passage on 18 July. The frontal passage is clearly indicated by the drop in the dew point temperatures and the mixing ratios. The relative humidity showed the typical maxima near saturation in the mornings and minima in the afternoons in the range of 45-55 %. Six-hour precipitation amounts were only on the order of 1 mm and were recorded on 16 July and 17 July but the associated cooling can be seen in the transient dips on the temperature curves for the same times. Wind speeds at Knoxville were generally below 3-4 m s⁻¹ with the maximum value of 6 m s⁻¹ on 15 July. Winds were generally calm at night. With the upper-air ridge and

surface high pressure to the west for most of the period wind directions were generally west to northwest. The same plots for Staunton in Figures 4-4 and 4-5 show similar patterns except no precipitation was recorded and the dew point temperature and mixing ratio showed more variability.

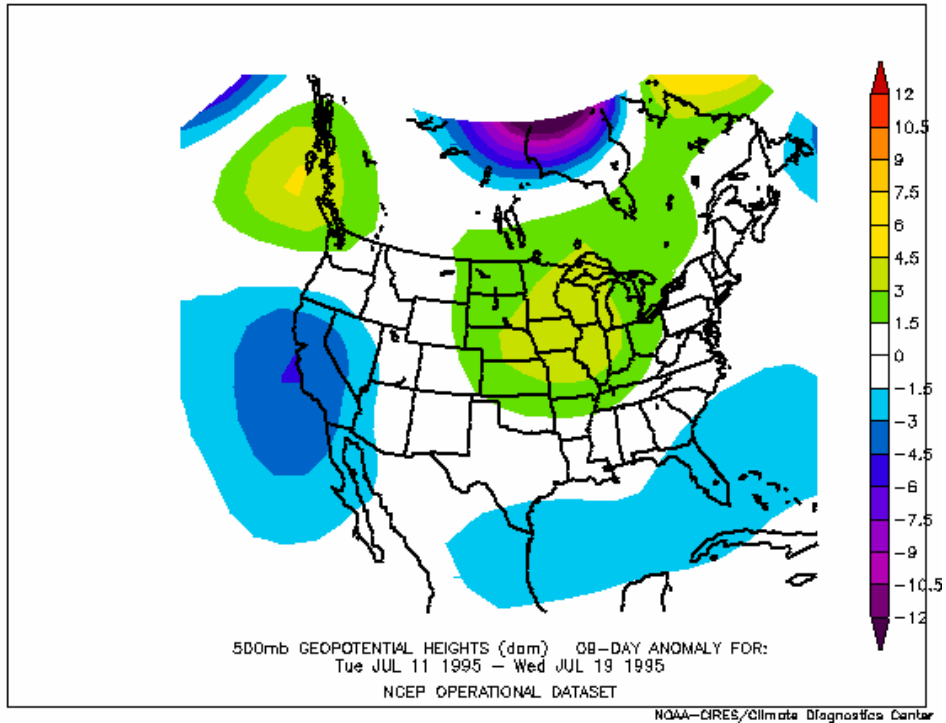


Figure 4-1. Anomaly field for the 500-mb geopotential heights created by taking the mean value for the period 0000 UTC July 11 – 1200 UTC July 19 1995 and subtracting from it the 15-year mean for the same period. Units are in decameters (dam). Image obtained from NOAA-CIRES CDC.

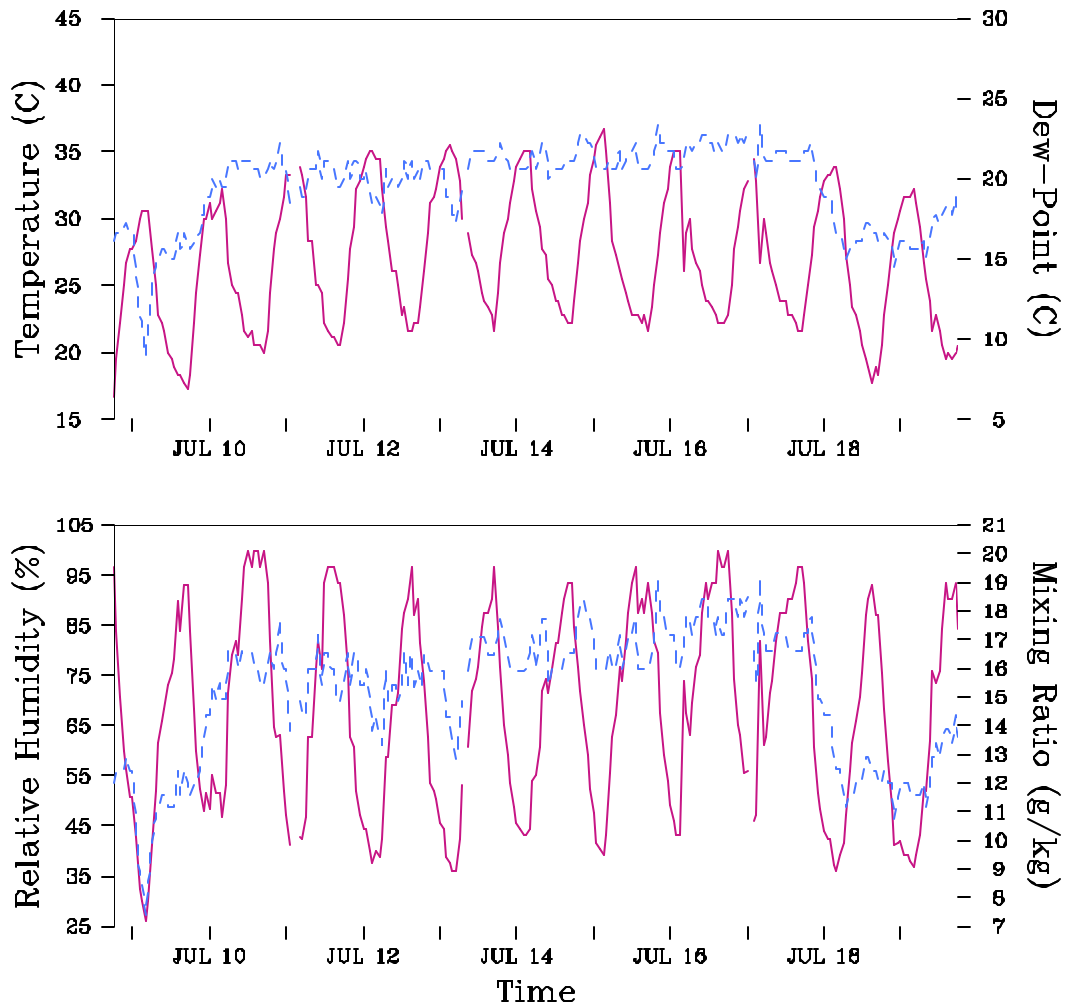


Figure 42. Top Panel: Hourly observed temperatures ($^{\circ}\text{C}$) at 2 m (solid curve) and dewpoint temperatures ($^{\circ}\text{C}$) at 2 m (dashed curve) at Knoxville, Tennessee from 9 July 1995 1200 UTC to 20 July 1995 1200 UTC. Temperatures are with respect to the left vertical axis while the dewpoint temperatures are with respect to the right vertical axis. The tick marks on the horizontal axis are at 1800 UTC each day but are only labeled every other day. Bottom Panel: Hourly observed relative humidities (per cent) at 2 m (solid curve) and mixing ratios (g kg^{-1}) at 2 m (dashed curve) at Knoxville, Tennessee from 9 July 1995 1200 UTC to 20 July 1995 1200 UTC. Relative humidities are with respect to the left vertical axis while the mixing ratios are with respect to the right vertical axis. The tick marks on the horizontal axis are marked in the same way as for the top panel.

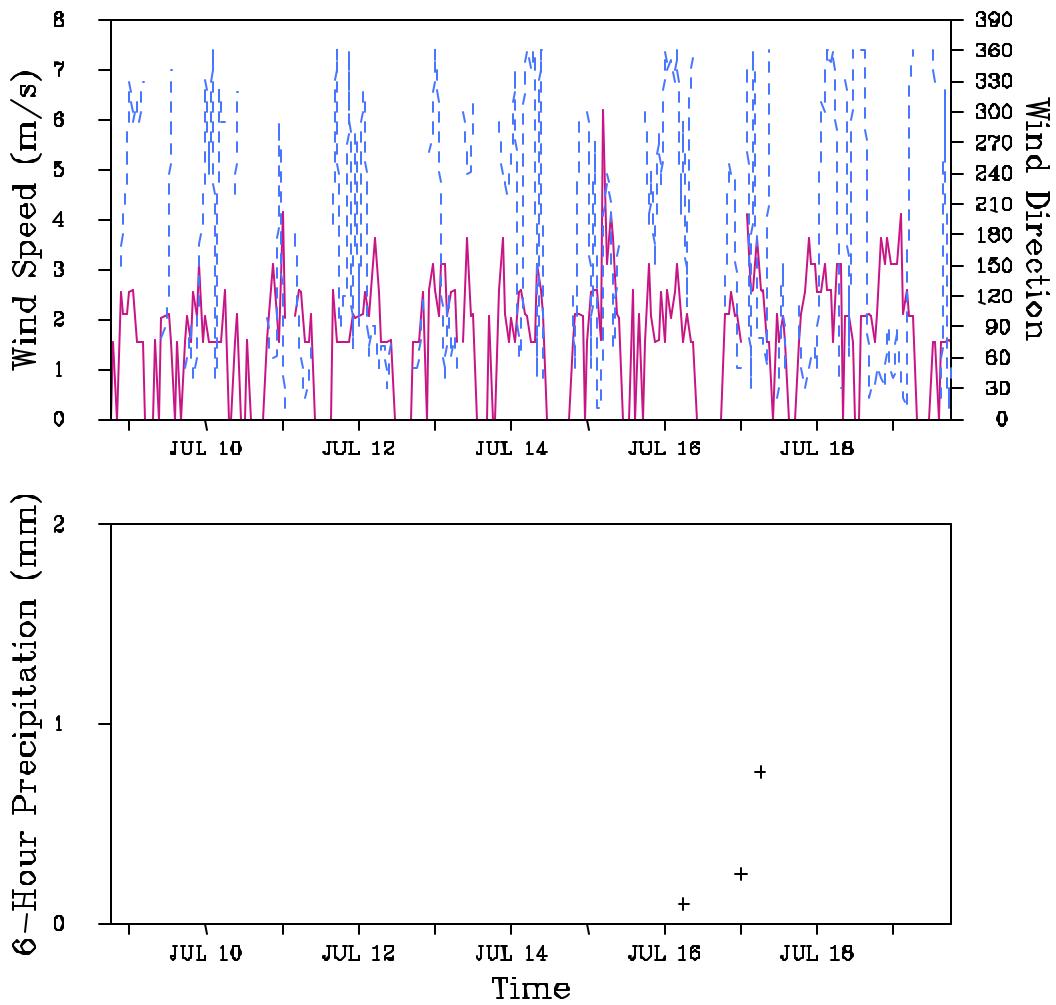


Figure 4-3. Top Panel: Hourly observed wind speeds (m s^{-1}) at 10 m (solid curve) and wind directions (degrees) at 10 m (dashed curve) at Knoxville, Tennessee from 9 July 1995 1200 UTC to 20 July 1995 1200 UTC. Wind speeds are with respect to the left vertical axis while the wind directions are with respect to the right vertical axis. The tick marks on the horizontal axis are at 1800 UTC each day but are only labeled every other day. Bottom Panel Six-hourly observed precipitation amounts (mm) at Knoxville, Tennessee from 9 July 1995 1200 UTC to 20 July 1995 1200 UTC. The tick marks on the horizontal axis are marked in the same way as for the top panel.

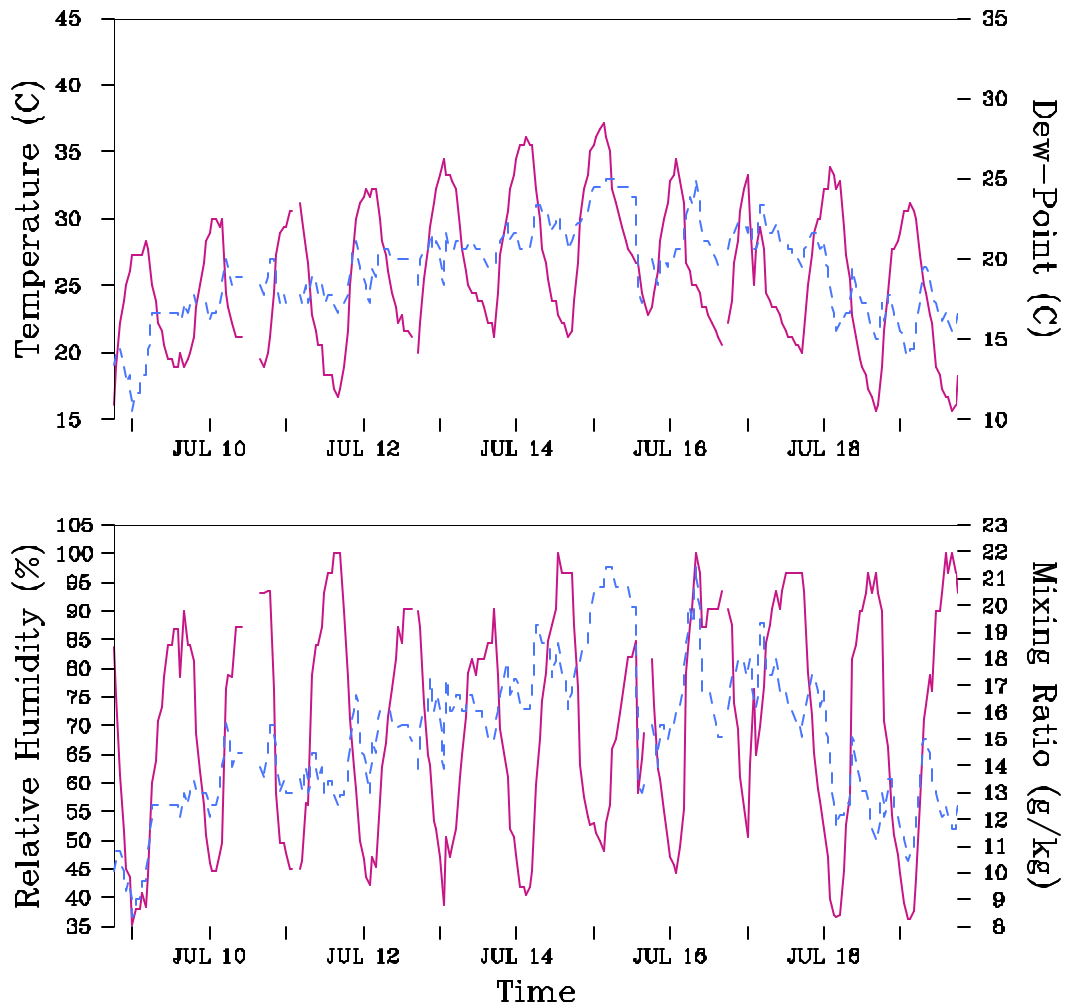


Figure 4.4. Top Panel: Hourly observed temperatures ($^{\circ}\text{C}$) at 2 m (solid curve) and dewpoint temperatures ($^{\circ}\text{C}$) at 2 m (dashed curve) at Staunton, Virginia from 9 July 1995 1200 UTC to 20 July 1995 1200 UTC. Temperatures are with respect to the left vertical axis while the dewpoint temperatures are with respect to the right vertical axis. The tick marks on the horizontal axis are at 1800 UTC each day but are only labeled every other day. Bottom Panel: Hourly observed relative humidities (per cent) at 2 m (solid curve) and mixing ratios (g kg^{-1}) at 2 m (dashed curve) at Staunton, Virginia from 9 July 1995 1200 UTC to 20 July 1995 1200 UTC. Relative humidities are with respect to the left vertical axis while the mixing ratios are with respect to the right vertical axis. The tick marks on the horizontal axis are marked in the same way as for the

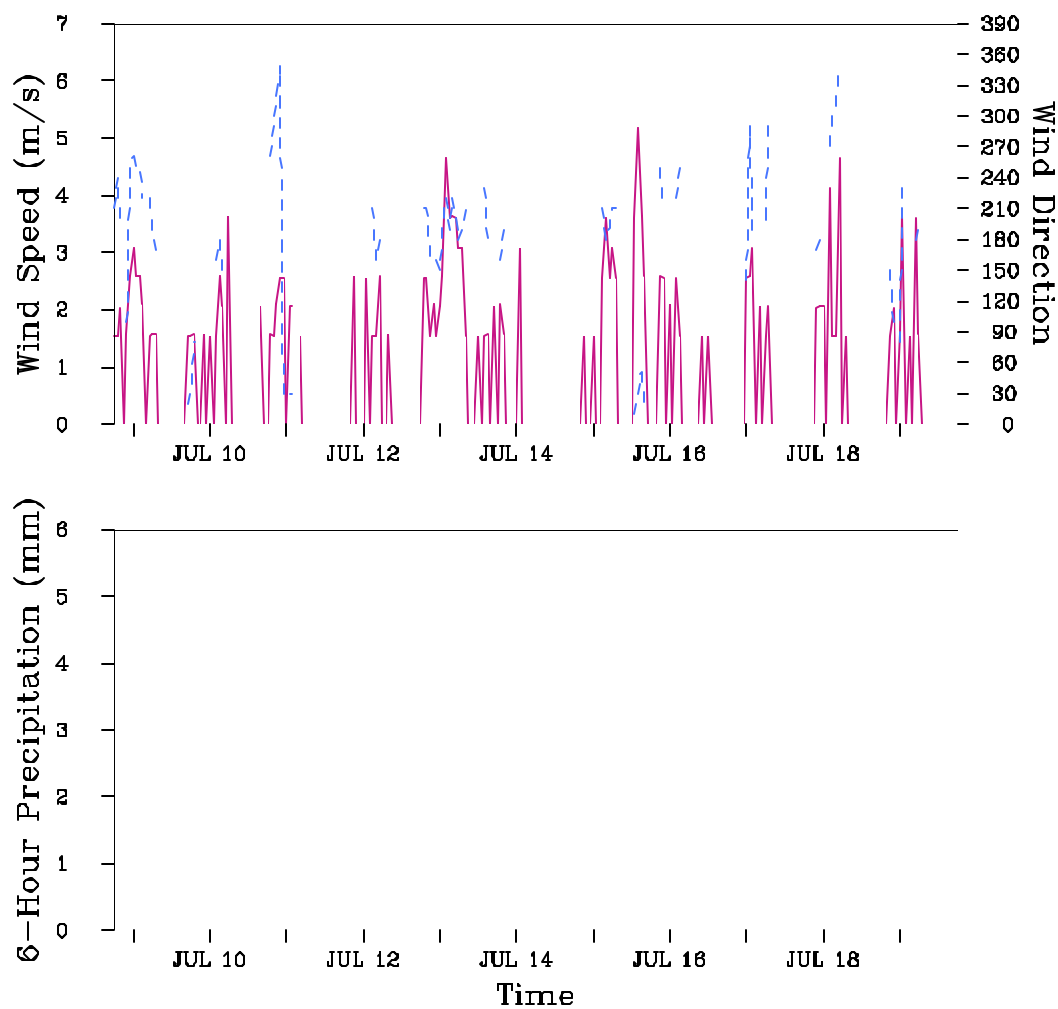


Figure 4-5. Top Panel: Hourly observed wind speeds (m s^{-1}) at 10 m (solid curve) and wind directions (degrees) at 10 m (dashed curve) at Staunton, Virginia from 9 July 1995 1200 UTC to 20 July 1995 1200 UTC. Wind speeds are with respect to the left vertical axis while the wind directions are with respect to the right vertical axis. The tick marks on the horizontal axis are at 1800 UTC each day but are only labeled every other day. Bottom Panel Six-hourly observed precipitation amounts (mm) at Staunton, Virginia from 9 July 1995 1200 UTC to 20 July 1995 1200 UTC. The tick marks on the horizontal axis are marked in the same way as for the top panel.

4.3 The 9-18 May 1993 Episode

The May 1993 episode was categorized as Class 3 for GSM and Class 4 for SNP for the metric of acidic deposition. For visibility there was one Class 3 day at GSM and one Class 3 and Class 4 days at SNP. For ozone at GSM there was one Class 1 day and four Class 2 days. For ozone at SNP there was one Class 1 day and two Class 3 days. This episode was similar to the May 1995 episode in that it was chosen for a broad range of conditions including moderate to high acidic deposition, moderate ranges of visibility, and mainly low levels of ozone.

The anomaly field for the 500-mb geopotential height for this episode is shown in Figure 4-6. It shows an area of above normal heights over western Canada and the western United States. Two areas of below normal heights were observed: one over the southern Great Plains and another over southeastern Canada. The two below normal areas are reflections of two closed upper-level low circulations which controlled much of the weather over the eastern United States for this episode. The episode started on 9 May with an upper-level trough over the Rocky Mountains and a ridge from the Great Lakes to Florida. The associated surface features included a frontal system from North Dakota to Texas and a high pressure ridge covering the eastern third of the United States. For the period 10-12 May an upper-level closed low remained over parts of Oklahoma, Kansas, Missouri, and Arkansas along with its surface low pressure center. A slow-moving cold front or trough from this surface low moved across parts of the southern Gulf of Mexico coastal states during this period. At times another frontal system extended northward or northeastward from this same surface low to the Great Lakes or New England. By 13 May the upper-level cutoff low had opened and moved to the Southeast. A new upper-level closed low was developing southeast of Hudson Bay. One frontal system extended from Oklahoma northeastward to the mid-Atlantic while another was located across southern Canada. For the period 14-16 May the intense upper-level low south of Hudson Bay created fast zonal flow for the northern United States. In response the southern Canadian frontal system moved south and by 16 May was located from the mid-Atlantic westward to a weak surface low over the Ohio Valley and then west to Texas and then northward as a stationary front over the Rocky Mountains. This same frontal system was quasi-stationary for the period 17-18 May with several waves moving along it.

Figures 4-7 and 4-8 show the time series of observations for Knoxville, Tennessee while Figures 4-9 and 4-10 show the same for Martinsburg, West Virginia. Martinsburg was chosen as the nearest NWS site to SNP in place of Staunton and Charlottesville, Virginia which both had large periods of missing data.

Knoxville maximum temperatures at the beginning of the episode were near 26°C and then declined to near 22°C on the afternoon of 13 May in response to the clouds and precipitation from the closed upper-level system in the Southern Plains moving eastward. For the rest of the episode, maximum temperatures increased slowly once again to near 26°C. Dew point temperatures followed a similar pattern, starting near 20°C and decreased to 10°C on 14 May, and then increased to 20°C by 18 May. The corresponding 2-m mixing ratios started at 15 g kg⁻¹ on 9 May, decreased to near 8 g kg⁻¹ on 14 May, and then slowly increased back to 15 g kg⁻¹ by 18 May. The 100% relative humidity values suggest morning fog which was confirmed by surface observations. The highest wind speeds were near 6 m s⁻¹ on the afternoons of 12 and 16 May. Otherwise afternoon wind speeds were generally 2-4 m s⁻¹. Nighttime wind speeds were light or calm. Wind directions covered a broad range but were typically southwest to northwest. Measured 6-h precipitation fell on 12-13 May with amounts of 2-18 mm and with amounts under 1 mm during 16-18 May.

For Martinsburg similar patterns were observed except that maximum temperatures made less of a recovery after the middle of the episode. Dew point and mixing ratio values were also smaller than Knoxville in general, and especially for late in the episode with Martinsburg being north of a stationary front. Wind speeds were somewhat faster and precipitation amounts were smaller. On 13 May 6-h values up to 6 mm

were observed while lighter amounts of near 2 mm were observed on 16 May.

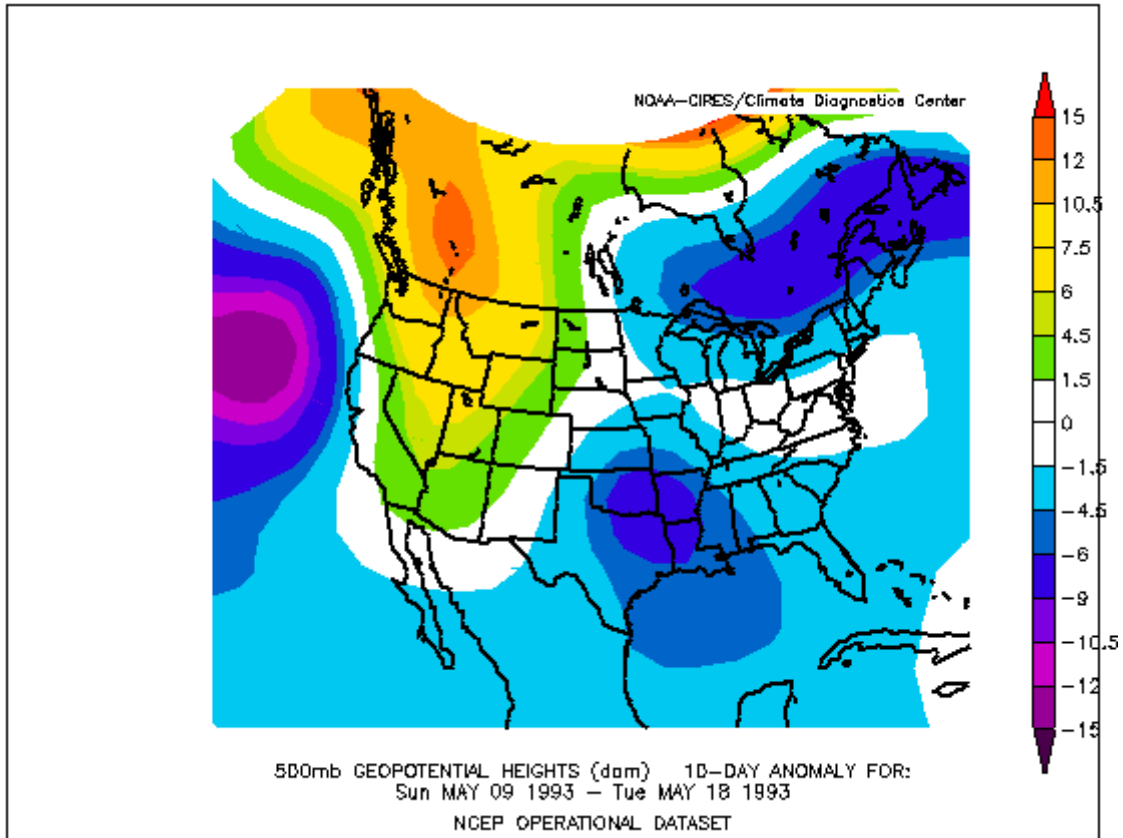


Figure 4-6. Anomaly field for the 500-mb geopotential heights created by taking the mean value for the period 0000 UTC 09 May - 1200 UTC 18 May 1993 and subtracting from it the 15-year mean for the same period. Units are in decameters (dam). Image obtained from NOAA-CIRES CDC.

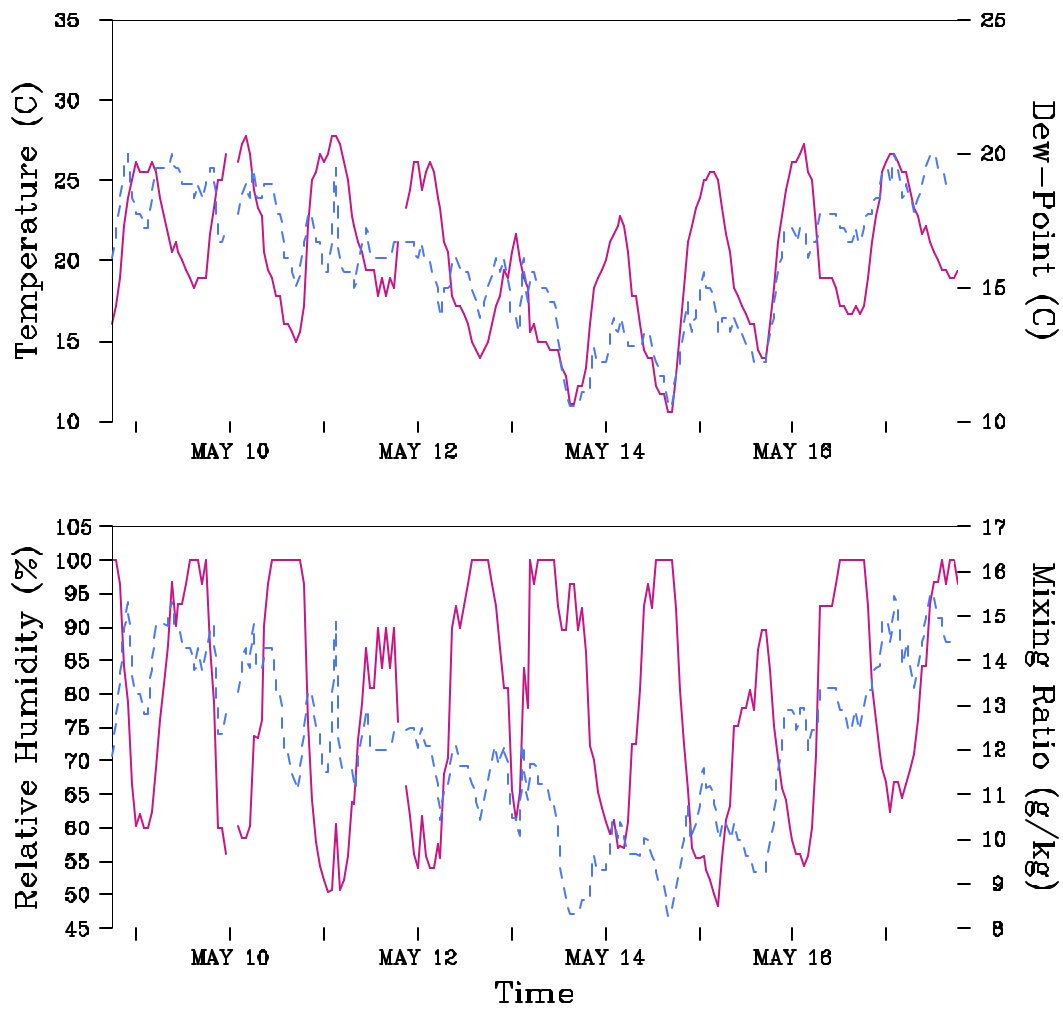


Figure 47. Top Panel: Hourly observed temperatures ($^{\circ}\text{C}$) at 2 m (solid curve) and dewpoint temperatures ($^{\circ}\text{C}$) at 2 m (dashed curve) at Knoxville, Tennessee from 1200 UTC 09 May 1993 to 1200 UTC 18 May 1993. Temperatures are with respect to the left vertical axis while the dewpoint temperatures are with respect to the right vertical axis. The tick marks on the horizontal axis are at 1800 UTC each day but are only labeled every other day. Bottom Panel: Hourly observed relative humidities (per cent) at 2 m (solid curve) and mixing ratios (g kg^{-1}) at 2 m (dashed curve) at Knoxville, Tennessee from 1200 UTC 09 May 1993 to 1200 UTC 18 May 1993. Relative humidities are with respect to the left vertical axis while the mixing ratios are with respect to the right vertical axis. The tick marks on the horizontal axis are marked in the same way as for the top panel.

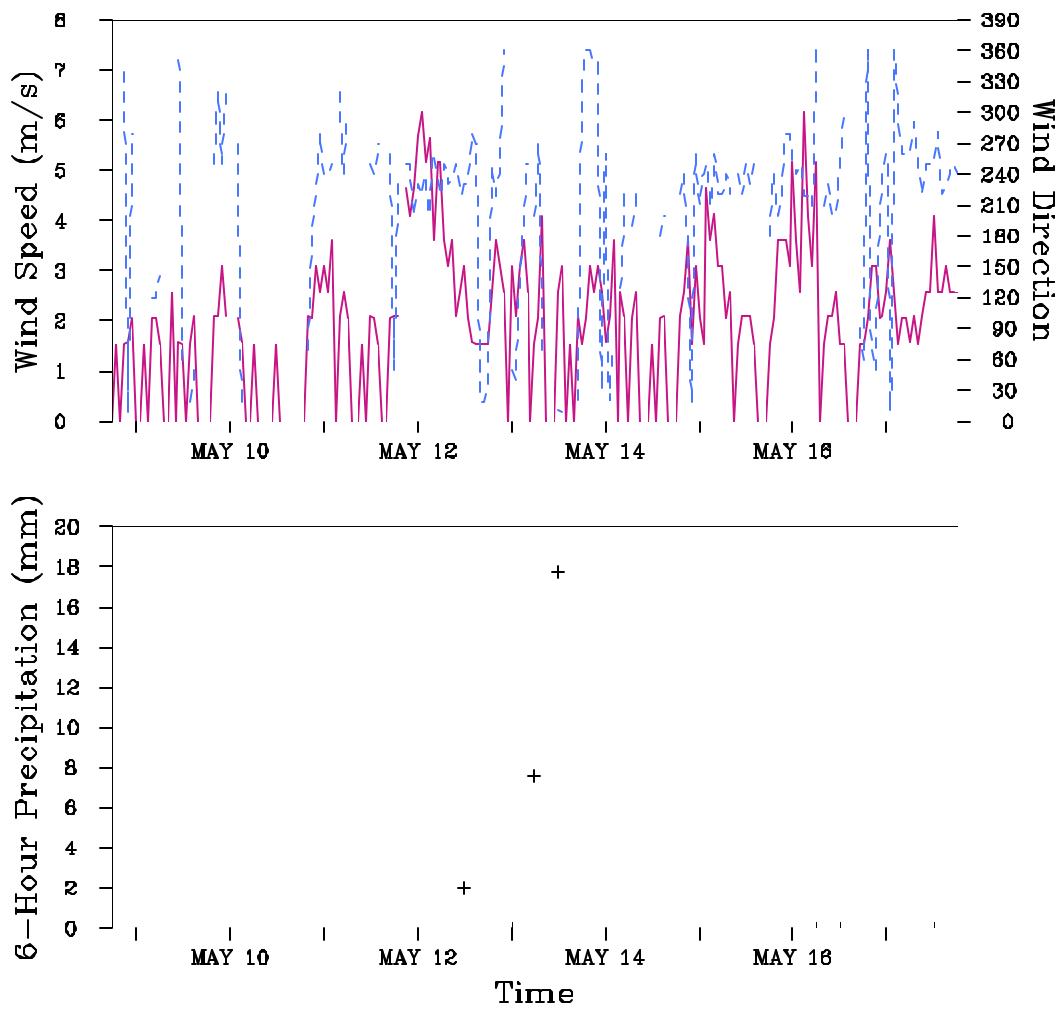


Figure 4-8. Top Panel: Hourly observed wind speeds (m s^{-1}) at 10 m (solid curve) and wind directions (degrees) at 10 m (dashed curve) at Knoxville, Tennessee from 1200 UTC 09 May 1993 to 1200 UTC 18 May 1993. Wind speeds are with respect to the left vertical axis while the wind directions are with respect to the right vertical axis. The tick marks on the horizontal axis are at 1800 UTC each day but are only labeled every other day. Bottom Panel: Six-hourly observed precipitation amounts (mm) at Knoxville, Tennessee from 1200 UTC 09 May 1993 to 1200 UTC 18 May 1993. The tick marks on the horizontal axis are marked in the same way as for the top panel.

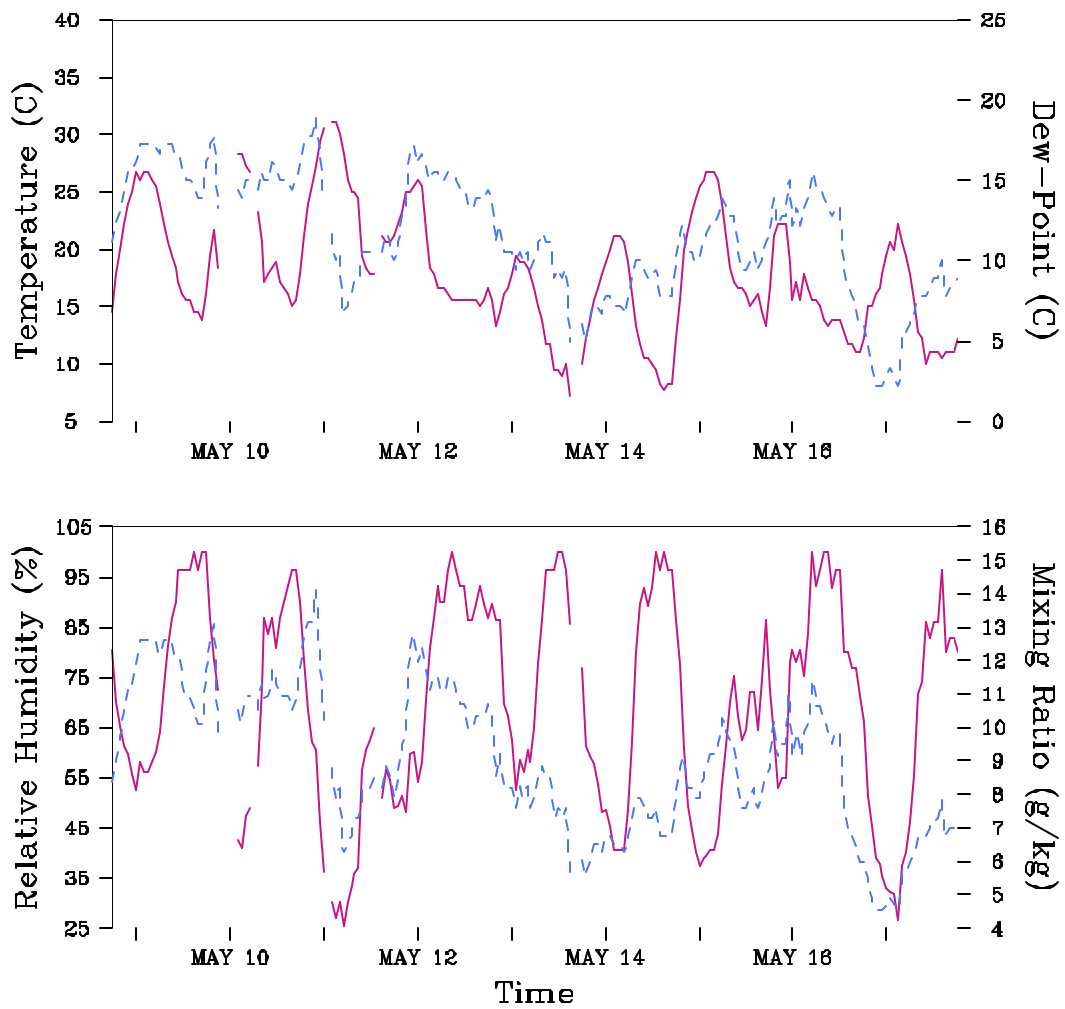


Figure 4-9. Top Panel: Hourly observed temperatures ($^{\circ}\text{C}$) at 2 m (solid curve) and dewpoint temperatures ($^{\circ}\text{C}$) at 2 m (dashed curve) at Martinsburg, West Virginia from 1200 UTC 09 May 1993 to 1200 UTC 18 May 1993. Temperatures are with respect to the left vertical axis while the dewpoint temperatures are with respect to the right vertical axis. The tick marks on the horizontal axis are at 1800 UTC each day but are only labeled every other day. Bottom Panel Hourly observed relative humidities (per cent) at 2 m (solid curve) and mixing ratios (g kg^{-1}) at 2 m (dashed curve) at Martinsburg, West Virginia from 1200 UTC 09 May 1993 to 1200 UTC 18 May 1993. Relative humidities are with respect to the left vertical axis while the mixing ratios are with respect to the right vertical axis. The tick marks on the horizontal axis are marked in the same way as for the top panel.

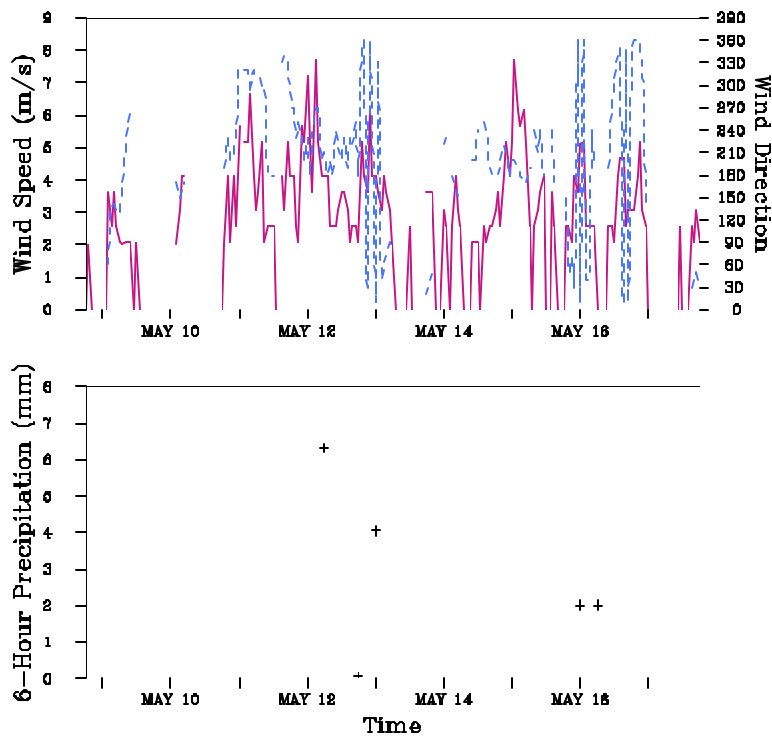


Figure 4-10. Top Panel: Hourly observed wind speeds (m s^{-1}) at 10 m (solid curve) and wind directions (degrees) at 10 m (dashed curve) at Martinsburg, West Virginia from 1200 UTC 09 May 1993 to 1200 UTC 18 May 1993. Wind speeds are with respect to the left vertical axis while the wind directions are with respect to the right vertical axis. The tick marks on the horizontal axis are at 1800 UTC each day but are only labeled every other day. Bottom Panel: Six-hourly observed precipitation amounts (mm) at Martinsburg, West Virginia from 1200 UTC 09 May 1993 to 1200 UTC 18 May 1993. The tick marks on the horizontal axis are marked in the same way as for the top panel.

4.4 The 21 March - 1 April 1993 Episode

The March 1993 episode was categorized as Class 2 for GSM and Class 3 for SNP for the metric of acidic deposition. For visibility there was one Class 1 and one Class 2 days for both GSM and SNP. This episode was outside the normal ozone season and ozone classes were not defined. The episode was chosen for low to moderate acidic deposition and high to moderate ranges of visibility.

The anomaly field for the 500-mb geopotential height for this episode is shown in Figure 4-11. A large area of above normal heights with values up to 150 m above normal existed over southern Canada and the northern United States whereas an area with below normal heights with a smaller magnitude existed over the southeastern United States. This anomaly pattern was the result of two closed upper-level systems during the episode generally located over the central United States and an active subtropical jet stream across the southern United States. The episode began on 21 March with mainly zonal upper-level flow across the extreme northern United States and with a trough extending from the northern Rocky Mountains southwestward to Arizona. Surface features included a ridge of high pressure from southern Ontario southward to the Ohio River Valley. East of this ridge a low and associated fronts were moving across the

eastern United States while another low pressure center and associated fronts were located over the central and southern Rocky Mountains. By 23 March the western upper-level trough moved east and developed a closed low over Iowa. In conjunction with this the western frontal system had also moved east to the Ohio River Valley with a cold front southward to the Gulf of Mexico and a warm front across the southern Appalachians. For the period 24-25 March the Ohio Valley surface system moved off the mid-Atlantic coast with the southern portion remaining as a stationary front along the Gulf coast. High pressure built over the Great Lakes and New England. The closed upper-level low moved little with a position essentially over Illinois. For 26-27 March the upper-level low slowly moved to Georgia as a new upper-level trough moved into the Southwest. A new surface system developed along the Gulf Coast stationary front and was located over Georgia on 27 March. During 28-30 March the eastern upper-level low and its associated surface system moved northward along the east coast and eventually offshore while the new western upper-level trough moved inland to a position near Texas by 30 March. This latter upper-level system was also associated with a developing surface system over the southern Great Plains. For the remainder of the episode for the period of 31 March to 1 April the new upper level trough intensified and became a closed low over Illinois by 1 April. The associated surface low deepened and became a major storm moving from Oklahoma to Ohio and pulling first a warm front and then a cold front across most of the southern portion of the immediate SAMI region. This system produced precipitation at both GSM and SNP but with the heavier amounts at GSM.

Figures 4-12 and 4-13 show the time series of observations for Knoxville, Tennessee while Figures 4-14 and 4-15 show the same for Martinsburg, West Virginia. Martinsburg was chosen as the nearest NWS site to SNP in place of Staunton and Charlottesville, Virginia which both again had large periods of time with missing data. Maximum temperatures at Knoxville increased to near 22°C on 25 March and then decreased to 14-17°C for the period 26-28 March. This was in association with the frontal system moving up the East coast which brought light precipitation and northerly flow. Maximum temperatures increased to 20-23°C for the remainder of the episode in advance of the last strong storm system. Dew point temperatures at Knoxville were in the range of +2 to +15°C during the same period. Mixing ratio values were in the range of 4 to 11 g kg⁻¹. Wind speeds at 10 m were generally under 5 m s⁻¹ except for 31 March and later when speeds reached 7 m s⁻¹ in advance of the last storm system. Wind directions were highly variable with the multiple storm systems. Three precipitation periods were delineated by the 6-h observed precipitation amounts. For the periods 22-23 March and 26-28 March amounts were under 10 mm. The third precipitation event had amounts up to near 30 mm. Conditions at Martinsburg were similar except for the following: temperatures and mixing ratios were smaller, wind speeds were generally higher, and precipitation amounts were smaller.

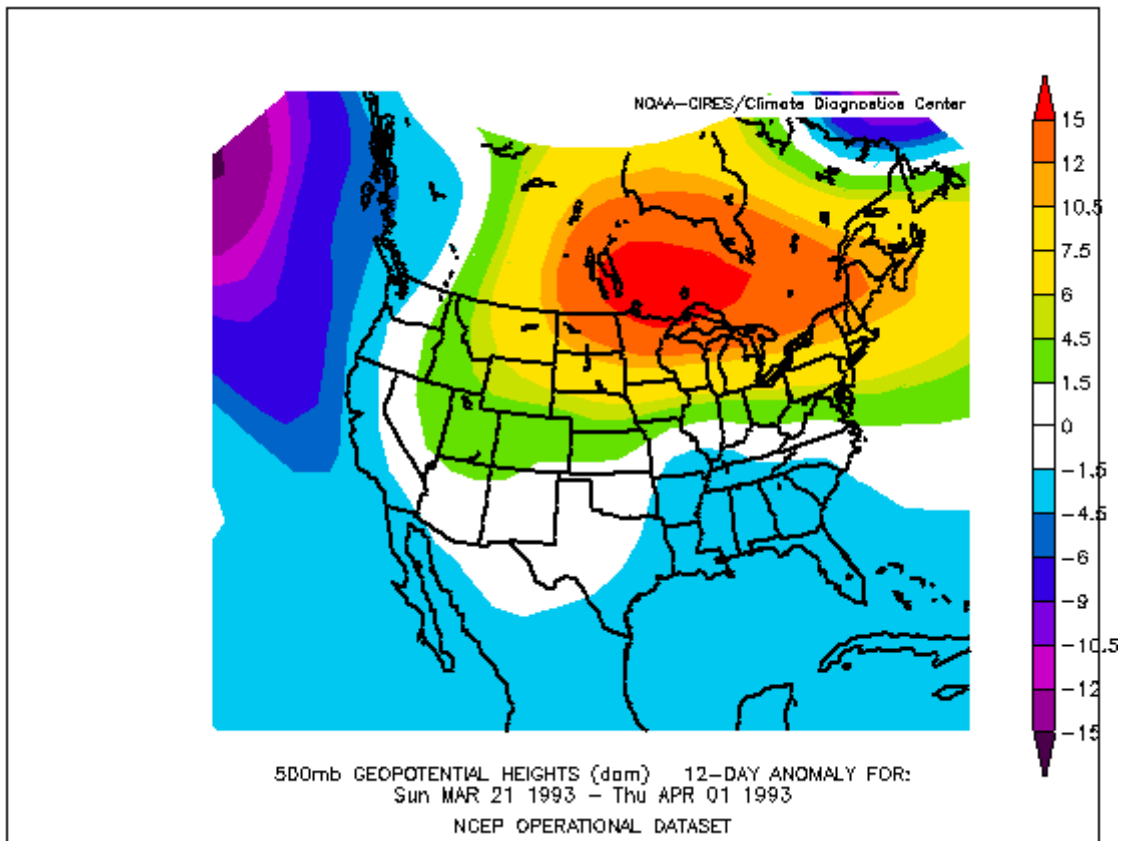


Figure 4-11. Anomaly field for the 500-mb geopotential heights created by taking the mean value for the period 0000 UTC 21 March - 1200 UTC 1 April 1993 and subtracting from it the 15-year mean for the same period. Units are in decameters (dam). Image obtained from NOAA-CIRES CDC.

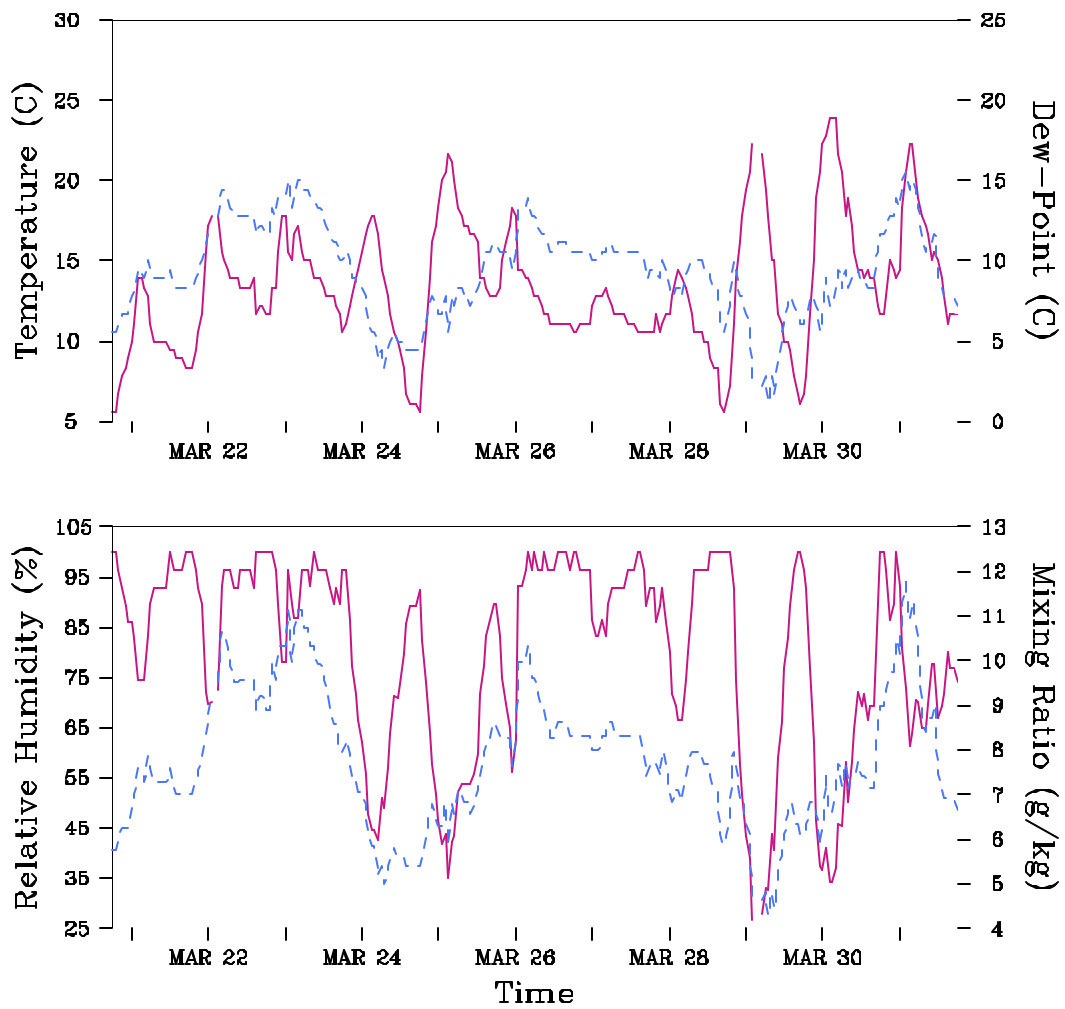


Figure 412. Top Panel: Hourly observed temperatures ($^{\circ}\text{C}$) at 2 m (solid curve) and dewpoint temperatures ($^{\circ}\text{C}$) at 2 m (dashed curve) at Knoxville, Tennessee from 1200 UTC 21 March 1993 to 1200 UTC 1 April 1993. Temperatures are with respect to the left vertical axis while the dewpoint temperatures are with respect to the right vertical axis. The tick marks on the horizontal axis are at 1800 UTC each day but are only labeled every other day. Bottom Panel Hourly observed relative humidities (per cent) at 2 m (solid curve) and mixing ratios (g kg^{-1}) at 2 m (dashed curve) at Knoxville, Tennessee from 1200 UTC 21 March 1993 to 1200 UTC 1 April 1993. Relative humidities are with respect to the left vertical axis while the mixing ratios are with respect to the right vertical axis. The tick marks on the horizontal axis are marked in the same way as for the top panel.

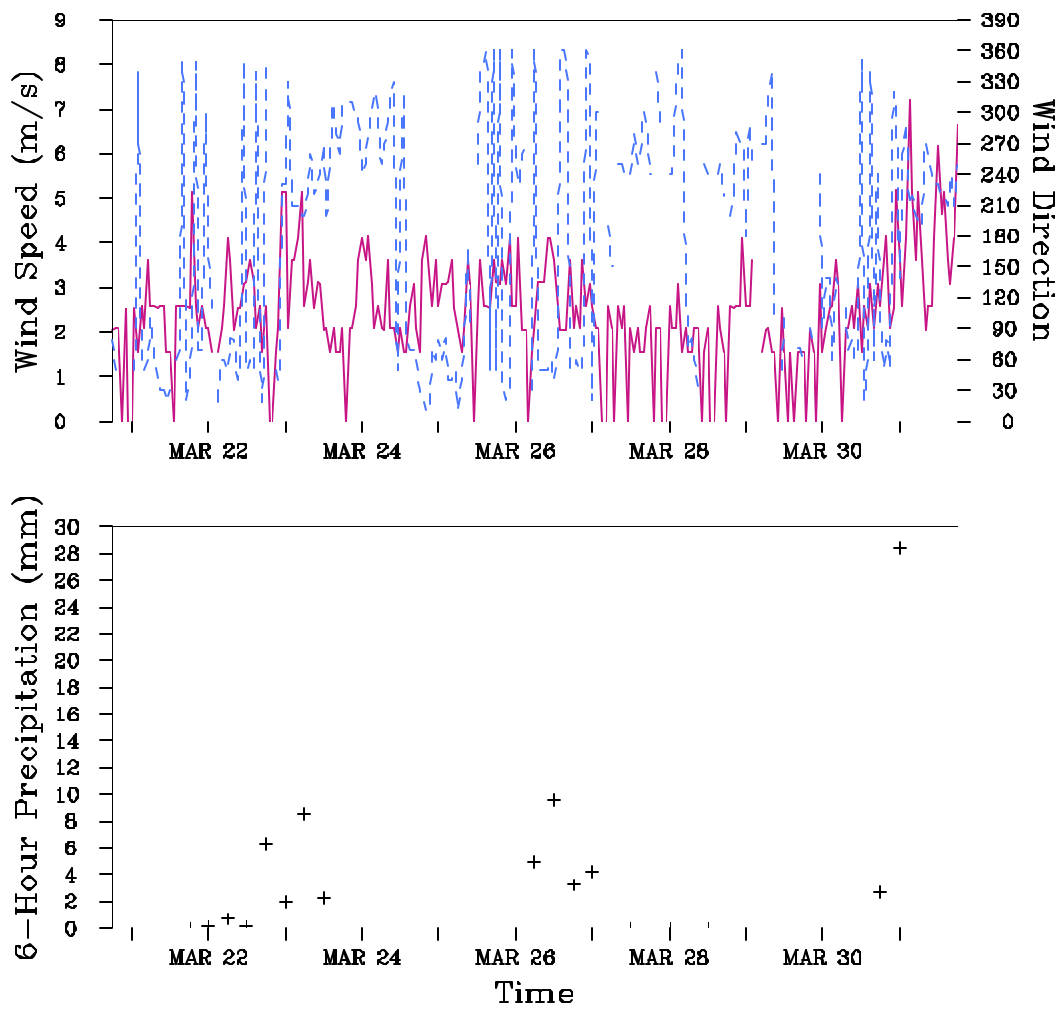


Figure 4-13. Top Panel: Hourly observed wind speeds (m s^{-1}) at 10 m (solid curve) and wind directions (degrees) at 10 m (dashed curve) at Knoxville, Tennessee from 1200 UTC 21 March 1993 to 1200 UTC 1 April 1993. Wind speeds are with respect to the left vertical axis while the wind directions are with respect to the right vertical axis. The tick marks on the horizontal axis are at 1800 UTC each day but are only labeled every other day. Bottom Panel Six-hourly observed precipitation amounts (mm) at Knoxville, Tennessee from 1200 UTC 21 March 1993 to 1200 UTC 1 April 1993. The tick marks on the horizontal axis are marked in the same way as for the top panel.

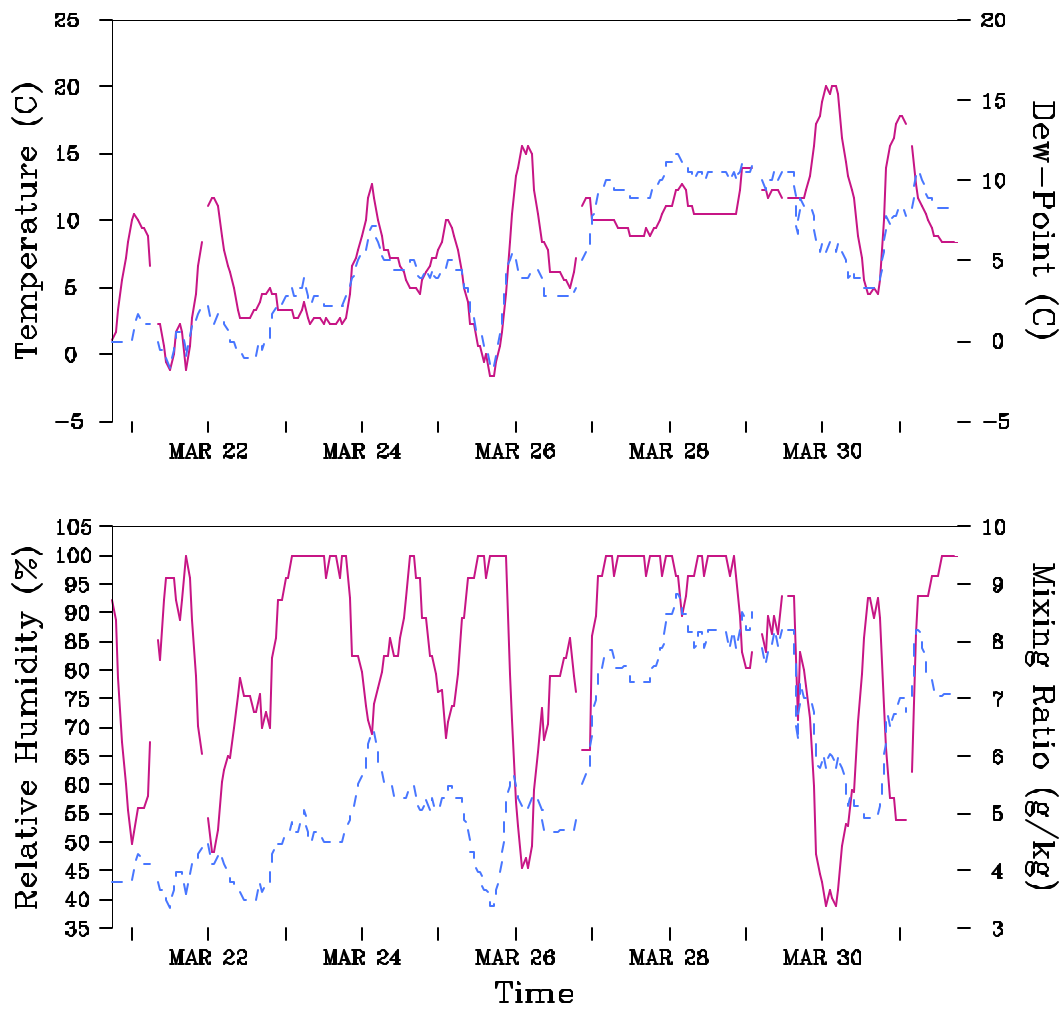


Figure 414. Top Panel: Hourly observed temperatures ($^{\circ}\text{C}$) at 2 m (solid curve) and dewpoint temperatures ($^{\circ}\text{C}$) at 2 m (dashed curve) at Martinsburg, West Virginia from 1200 UTC 21 March 1993 to 1200 UTC 1 April 1993. Temperatures are with respect to the left vertical axis while the dewpoint temperatures are with respect to the right vertical axis. The tick marks on the horizontal axis are at 1800 UTC each day but are only labeled every other day. Bottom Panel: Hourly observed relative humidities (per cent) at 2 m (solid curve) and mixing ratios (g kg^{-1}) at 2 m (dashed curve) at Martinsburg, West Virginia from 1200 UTC 21 March 1993 to 1200 UTC 1 April 1993. Relative humidities are with respect to the left vertical axis while the mixing ratios are with respect to the right vertical axis. The tick marks on the horizontal axis are marked in the same way as for the top panel.

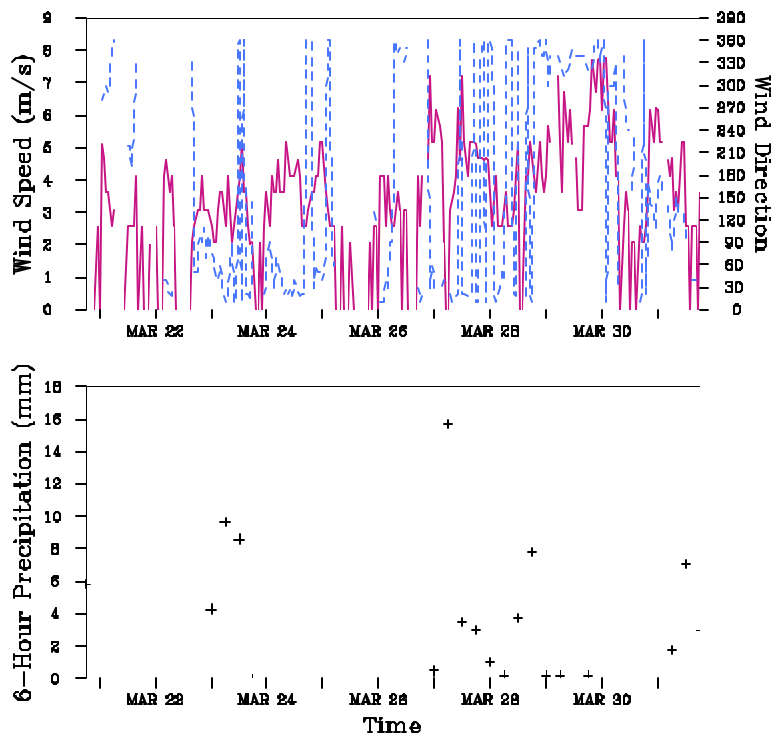


Figure 4-15. Top Panel: Hourly observed wind speeds (m s^{-1}) at 10 m (solid curve) and wind directions (degrees) at 10 m (dashed curve) at Martinsburg, West Virginia from 1200 UTC 21 March 1993 to 1200 UTC 1 April 1993. Wind speeds are with respect to the left vertical axis while the wind directions are with respect to the right vertical axis. The tick marks on the horizontal axis are at 1800 UTC each day but are only labeled every other day. Bottom Panel: Six-hourly observed precipitation amounts (mm) at Martinsburg, West Virginia from 1200 UTC 21 March 1993 to 1200 UTC 1 April 1993. The tick marks on the horizontal axis are marked in the same way as for the top panel.

4.5 The 6-14 February 1994 Episode

The February 1994 episode was categorized as Class 2 for GSM and for SNP for the metric of acidic deposition. For visibility there was one Class 1 day for both GSM and SNP. This episode was outside the normal ozone season and was chosen for moderate acidic deposition and high visibility.

The anomaly field for the 500-mb geopotential height for this episode is shown in Figure 4-16. A large area of below normal heights extended from most of southern Canada southwestward across the Great Lakes and then most of the western United States. Above normal heights were observed over the Southeast. The 500-mb heights which were above normal over the Southeast are somewhat misleading in that a major incursion of Arctic air occurred during the period 9-11 February for the eastern half of the United States and was accompanied by a major ice storm from Texas to Ohio. The episode began on 6 February with an intense upper-level closed low over Hudson Bay and broad cyclonic flow over much of the United States. At the surface there was one frontal system across the northern United States from the Rocky Mountains eastward to New England and another one across the Gulf Coast states. A surface high of 1044 mb was

over Alberta and would be the source of the Arctic air for later in the period. During 7-10 February the Canadian high pressure moved south and east and brought much below normal temperatures to most of the eastern United States. By 10 February the upper-level flow had become more zonal across the northern-half of the United States and with a sharp trough over Texas and New Mexico. A southern frontal system on 6 February dissipated while a northern one in advance of Arctic air moved south and east. By 10 February the Arctic front was located from Georgia southwestward to the Gulf of Mexico. A large area of overrunning freezing precipitation developed in back of the front and was the first phase of an ice storm for much of the Southeast. During the period 10-11 February the upper-level trough over Texas moved eastward and in conjunction a weak wave developed on the southern frontal system bringing more winter precipitation to much of the Southeast. By 12 February the Arctic air had retreated to New England with a large area of Pacific high pressure building over the western United States behind a developing frontal system across the Great Plains. The upper-level flow was characterized by a trough from the northern Plains southwestward to Arizona. For the period 13-14 February the Plains frontal system moved eastward off the Atlantic coast and was followed by high pressure over much of the Southeast. Another Arctic front moved across New England. By 14 February the upper-level flow had become zonal over much of the United States except over New England where the flow was influenced by a closed low over southern Quebec.

Figures 4-17 and 4-18 show the time series of observations for Knoxville, Tennessee while Figures 4-19 and 4-20 show the same for Martinsburg, West Virginia. Martinsburg was chosen as the nearest NWS site to SNP in place of Staunton and Charlottesville, Virginia which both again had large periods of time with missing data. The highest maximum temperature at Knoxville was near 20°C on 8 February followed by a drop of about 20°C with the passage of the Arctic front on 9 February. Temperatures only slowly recovered to 5°C on 12 February before another frontal passage on 13 February reduced temperatures to near -5°C at the end of the episode. Dew point temperatures were in the range of -5 to 15°C with the mixing ratios of 2-11 g kg⁻¹. The almost continuous relative humidity above 95% during the period 9-12 February coincide with the major period of frozen precipitation. The highest 10-m wind speeds were in advance of the Arctic front on February 9 with values near 10 m s⁻¹. Otherwise wind speeds were typically in the range of 3-5 m s⁻¹. The wind direction was dominated by northerly to northeasterly flow except for the period 11-13 February when winds were generally westerly. The main precipitation event of 9-11 February had 6-h amounts up to 44 mm. Conditions at Martinsburg were similar except for the following: 1) temperatures were colder, 2) dew point temperatures and mixing ratios were smaller, 3) the highest wind speeds were at the end of the episode during the period 12-13 February, and 4) 6-h precipitation amounts were less than or equal to 8 mm and were more scattered across the episode.

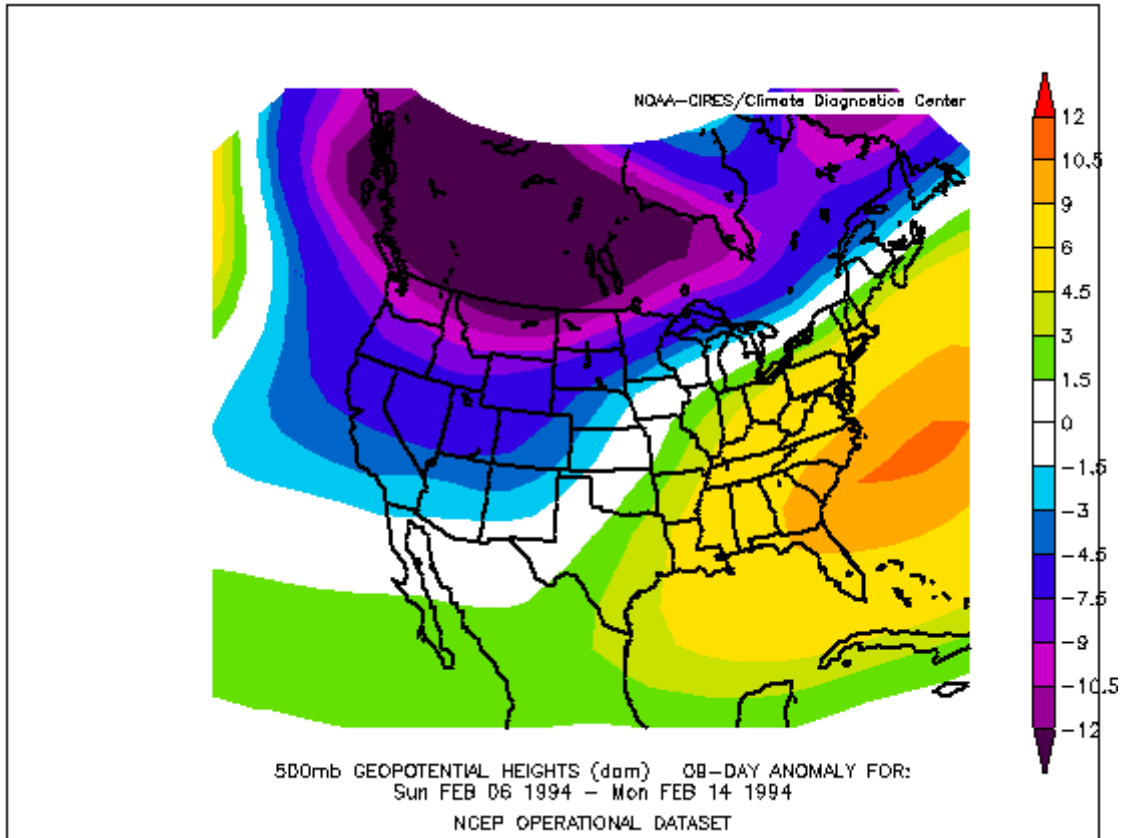


Figure 4-16. Anomaly field for the 500-mb geopotential heights created by taking the mean value for the period 0000 UTC 6 February - 1200 UTC 14 February 1994 and subtracting from it the 15-year mean for the same period. Units are in decameters (dam). Image obtained from NOAA-CIRES CDC.

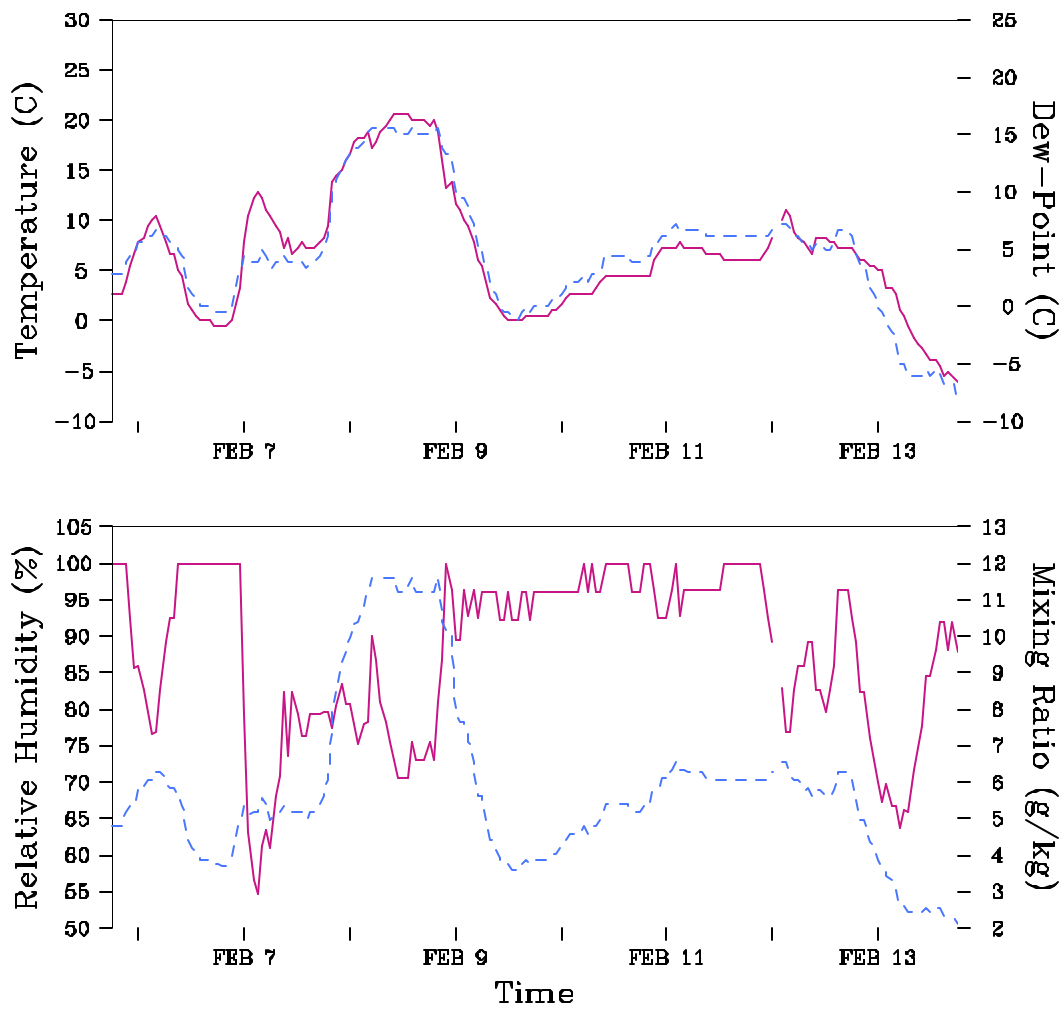


Figure 417. Top Panel: Hourly observed temperatures ($^{\circ}\text{C}$) at 2 m (solid curve) and dewpoint temperatures ($^{\circ}\text{C}$) at 2 m (dashed curve) at Knoxville, Tennessee from 1200 UTC 6 February 1994 to 1200 UTC 14 February 1994. Temperatures are with respect to the left vertical axis while the dewpoint temperatures are with respect to the right vertical axis. The tick marks on the horizontal axis are at 1800 UTC each day but are only labeled every other day. Bottom Panel Hourly observed relative humidities (per cent) at 2 m (solid curve) and mixing ratios (g kg^{-1}) at 2 m (dashed curve) at Knoxville, Tennessee 1200 UTC 6 February 1994 to 1200 UTC 14 February 1994. Relative humidities are with respect to the left vertical axis while the mixing ratios are with respect to the right vertical axis. The tick marks on the horizontal axis are marked in the same way as for the top panel

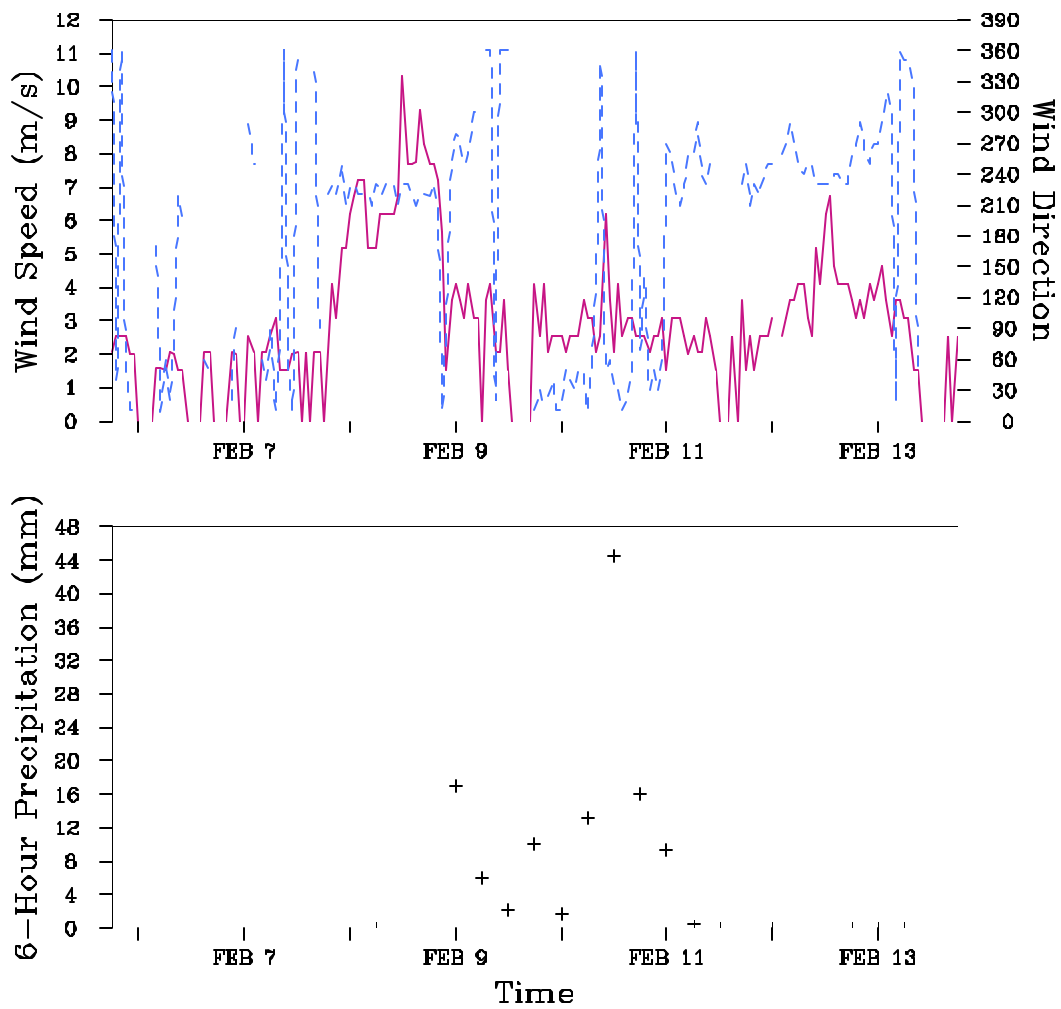


Figure 4-18. Top Panel: Hourly observed wind speeds (m s^{-1}) at 10 m (solid curve) and wind directions (degrees) at 10 m (dashed curve) at Knoxville, Tennessee from 1200 UTC 6 February 1994 to 1200 UTC 14 February 1994. Wind speeds are with respect to the left vertical axis while the wind directions are with respect to the right vertical axis. The tick marks on the horizontal axis are at 1800 UTC each day but are only labeled every other day. Bottom Panel Six-hourly observed precipitation amounts (mm) at Knoxville, Tennessee from 1200 UTC 6 February 1994 to 1200 UTC 14 February 1994. The tick marks on the horizontal axis are marked in the same way as for the top panel.

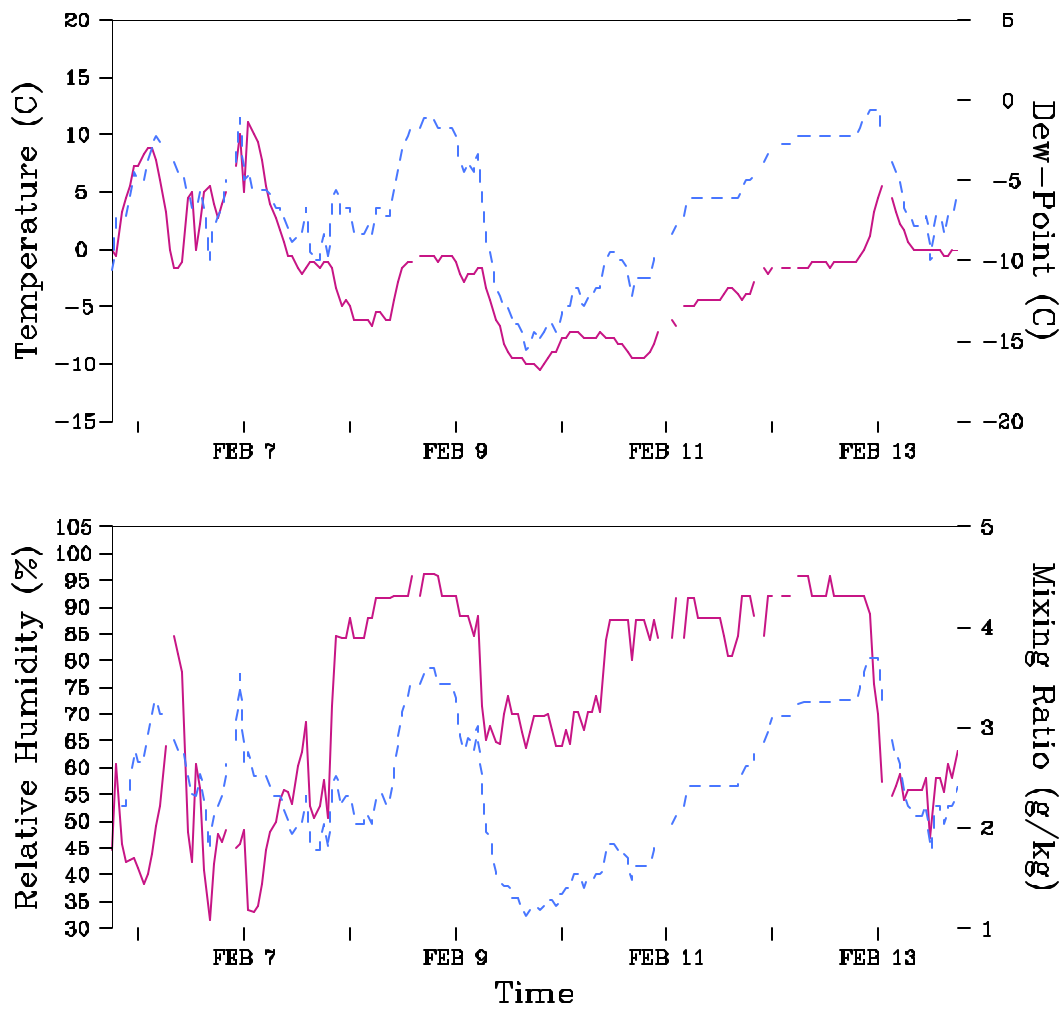


Figure 419. Top Panel: Hourly observed temperatures (°C) at 2 m (solid curve) and dewpoint temperatures (°C) at 2 m (dashed curve) at Martinsburg, West Virginia from 1200 UTC 6 February 1994 to 1200 UTC 14 February 1994. Temperatures are with respect to the left vertical axis while the dewpoint temperatures are with respect to the right vertical axis. The tick marks on the horizontal axis are at 1800 UTC each day but are only labeled every other day. Bottom Panel: Hourly observed relative humidities (per cent) at 2 m (solid curve) and mixing ratios (g kg⁻¹) at 2 m (dashed curve) at Martinsburg, West Virginia from 1200 UTC 6 February 1994 to 1200 UTC 14 February 1994. Relative humidities are with respect to the left vertical axis while the mixing ratios are with respect to the right vertical axis. The tick marks on the horizontal axis are marked in the same way as for the top panel.

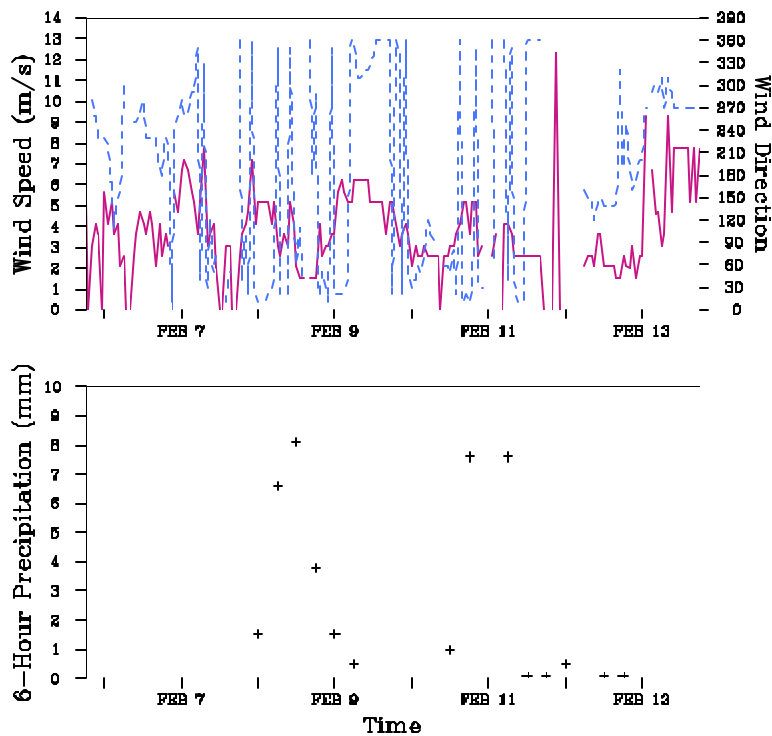


Figure 4-20. Hourly observed wind speeds (m s^{-1}) at 10 m (solid curve) and wind directions (degrees) at 10 m (dashed curve) at Martinsburg, West Virginia from 1200 UTC 6 February 1994 to 1200 UTC 14 February 1994. Wind speeds are with respect to the left vertical axis while the wind directions are with respect to the right vertical axis. The tick marks on the horizontal axis are at 1800 UTC each day but are only labeled every other day. Bottom Panel Six-hourly observed precipitation amounts (mm) at Martinsburg, West Virginia from 1200 UTC 6 February 1994 to 1200 UTC 14 February 1994. The tick marks on the horizontal axis are marked in the same way as for the top panel.

4.6 The 21 July - 1 August 1991 Episode

The July 1991 episode was chosen to replace an April 1994 episode for which attempts to simulate realistic precipitation amounts had failed. The July 1991 episode was Class 4 for acidic deposition at both GSM and SNP. For visibility there were two Class 5 days at GSM and two Class 4 days at SNP. A broad range of ozone conditions were represented at both parks with Classes 1-3. This episode represents high acidic deposition, low visibility, and low to moderate ozone at both GSM and SNP.

The anomaly field for the 500-mb geopotential height for this episode is shown in Figure 4-21. The main feature affecting this episode was the area of below normal heights south of Hudson Bay to the Great Lakes area. This was the result of an upper-level closed low in that region for much of the episode. Several short waves rotated around this circulation and their associated surface fronts traveled southeastward across the Midwest and Southeast and then stalled over parts of the Southeast. This resulted in an active and very wet pattern for areas along and east of the Appalachians with locally heavy rains and flooding. The episode began on 21 July with an upper-level closed low northeast of Hudson Bay and a trough extending southward to the Great Lakes. Another Canadian trough was located over western Canada. At the

surface high pressure was located over the Great Lakes and over the Southeast with a frontal system across the northern United States. During 22-25 July the closed upper-level low remained in the vicinity of Hudson Bay and the northern frontal system slowly moved southeastward and by 25 July it was a stationary front extending from Texas to Kentucky to Maryland. During this time several minor waves moved along the front. The remainder of the episode experienced another frontal system moving southeastward from the northern Plains which once again became stationary over the Southeast in about the same position. Both fronts produced showers and thunderstorms along and south of their positions.

Figures 4-22 and 4-23 show the time series of observations for Knoxville, Tennessee while Figures 4-23 and 4-24 show the same for Martinsburg, West Virginia. Martinsburg was chosen as the nearest NWS site to SNP in place of Staunton and Charlottesville, Virginia which both again had large periods of time with missing data. Maximum temperatures at the beginning of the episode, from 21-23 July at Knoxville, were near 34°C and then decreased to near 29-30°C for the rest of the episode with increased afternoon clouds and showers. Dew point temperatures ranged from 18-22°C with the related mixing ratios in the range of 14-19 g kg⁻¹. Afternoon wind speeds were typically 3-5 m s⁻¹ with generally light or calm winds at night. Wind directions were highly variable across the episode. The 6-h precipitation amounts were as large as 13 mm with precipitation being recorded on 24, 26, and 28 July. Conditions at Martinsburg were similar except for the following: 1) lower temperatures and mixing ratios, 2) higher wind speeds, and 3) lower precipitation amounts. As will be seen when the 12-km model results are discussed (in section 6.6.2), the Tennessee Valley Authority rain gauge network indicated that much heavier precipitation occurred in the mountains than either Knoxville or Martinsburg recorded.

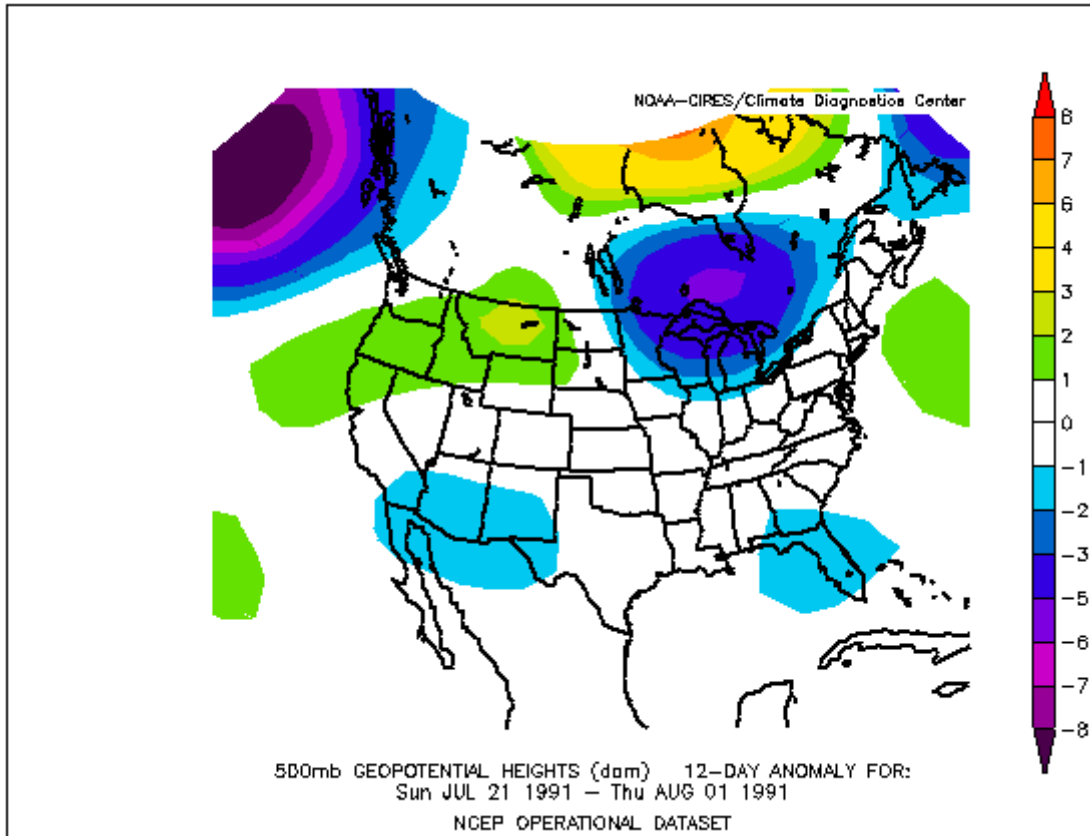


Figure 4-21. Anomaly field for the 500-mb geopotential heights created by taking the mean value for the period 0000 UTC 21 July - 1200 UTC 1 August 1991 and subtracting from it the 15-year mean for the same period. Units are in decameters (dam). Image obtained from NOAA-CIRES CDC.

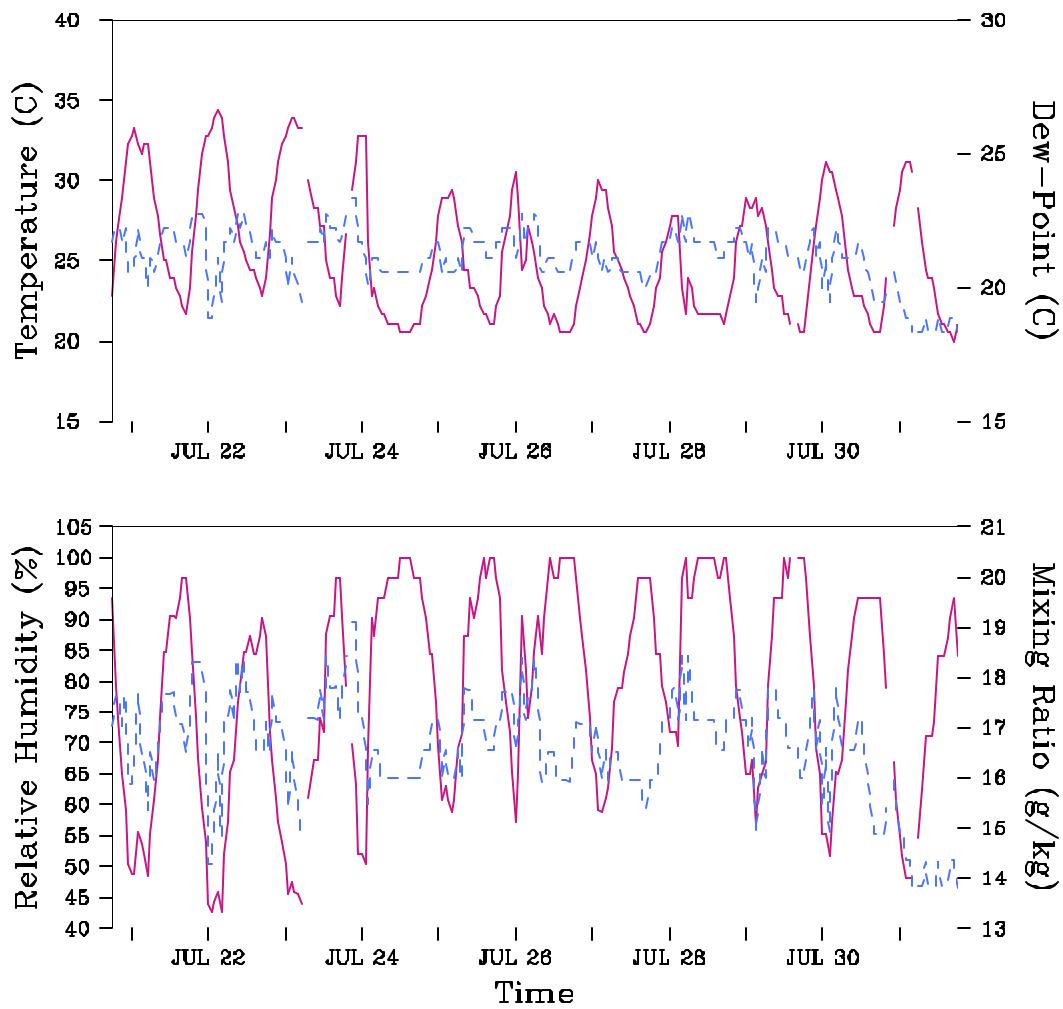


Figure 422. Top Panel: Hourly observed temperatures ($^{\circ}\text{C}$) at 2 m (solid curve) and dewpoint temperatures ($^{\circ}\text{C}$) at 2 m (dashed curve) at Knoxville, Tennessee from 1200 UTC 21 July 1991 to 1200 UTC 1 August 1991. Temperatures are with respect to the left vertical axis while the dewpoint temperatures are with respect to the right vertical axis. The tick marks on the horizontal axis are at 1800 UTC each day but are only labeled every other day. Bottom Panel: Hourly observed relative humidities (per cent) at 2m (solid curve) and mixing ratios (g kg^{-1}) at 2 m (dashed curve) at Knoxville, Tennessee from 1200 UTC 21 July 1991 to 1200 UTC 1 August 1991. Relative humidities are with respect to the left vertical axis while the mixing ratios are with respect to the right vertical axis. The tick marks on the horizontal axis are marked in the same way as for the top panel.

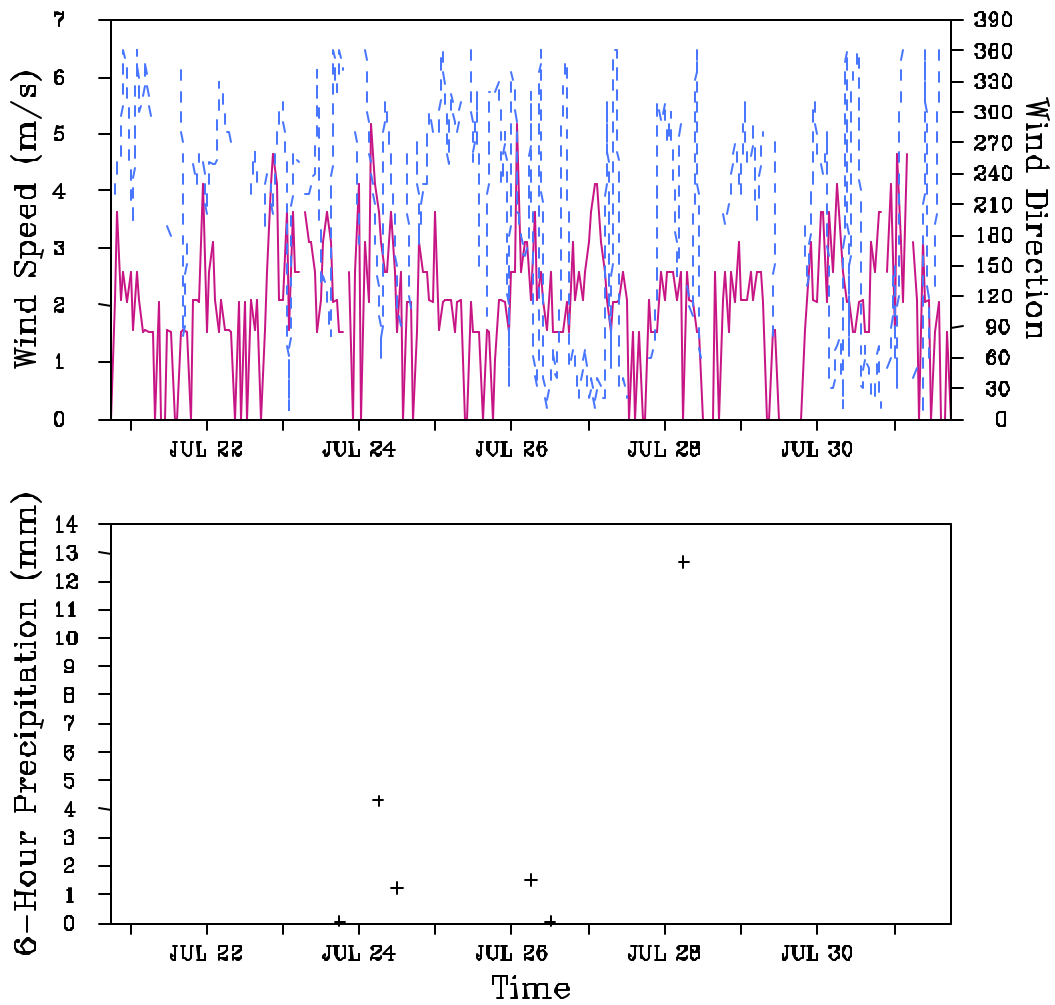


Figure 4-23. Top Panel: Hourly observed wind speeds (m s^{-1}) at 10 m (solid curve) and wind directions (degrees) at 10 m (dashed curve) at Knoxville, Tennessee from 1200 UTC 21 July 1991 to 1200 UTC 1 August 1991. Wind speeds are with respect to the left vertical axis while the wind directions are with respect to the right vertical axis. The tick marks on the horizontal axis are at 1800 UTC each day but are only labeled every other day. Bottom Panel Six-hourly observed precipitation amounts (mm) at Knoxville, Tennessee from 1200 UTC 21 July 1991 to 1200 UTC 1 August 1991. The tick marks on the horizontal axis are marked in the same way as for the top panel.

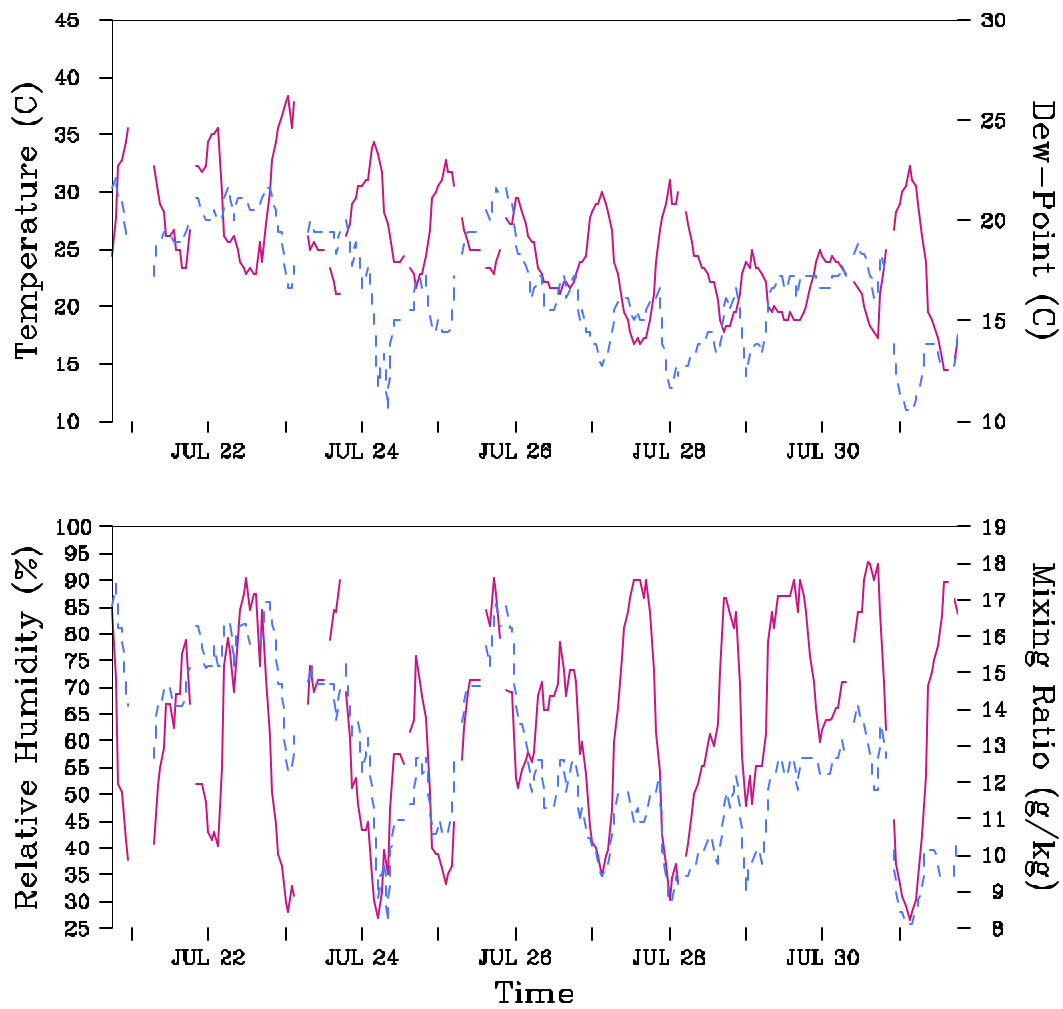


Figure 4-24. Top Panel: Hourly observed temperatures ($^{\circ}\text{C}$) at 2 m (solid curve) and dewpoint temperatures ($^{\circ}\text{C}$) at 2 m (dashed curve) at Martinsburg, West Virginia from 1200 UTC 21 July 1991 to 1200 UTC 1 August 1991. Temperatures are with respect to the left vertical axis while the dewpoint temperatures are with respect to the right vertical axis. The tick marks on the horizontal axis are at 1800 UTC each day but are only labeled every other day. Bottom Panel: Hourly observed relative humidities (per cent) at 2 m (solid curve) and mixing ratios (g kg^{-1}) at 2 m (dashed curve) at Martinsburg, West Virginia from 1200 UTC 21 July 1991 to 1200 UTC 1 August 1991. Relative humidities are with respect to the left vertical axis while the mixing ratios are with respect to the right vertical axis. The tick marks on the horizontal axis are marked in the same way as for the top panel.

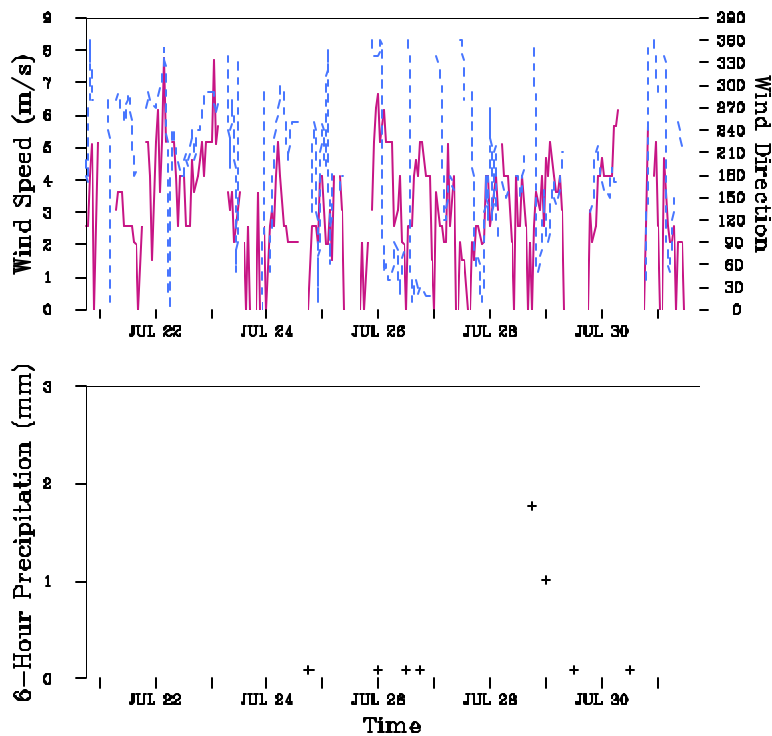


Figure 4-25. Top Panel: Hourly observed wind speeds (m s^{-1}) at 10 m (solid curve) and wind directions (degrees) at 10 m (dashed curve) at Martinsburg, West Virginia from 1200 UTC 21 July 1991 to 1200 UTC 1 August 1991. Wind speeds are with respect to the left vertical axis while the wind directions are with respect to the right vertical axis. The tick marks on the horizontal axis are at 1800 UTC each day but are only labeled every other day. Bottom Panel: Six-hourly observed precipitation amounts (mm) at Martinsburg, West Virginia from 1200 UTC 21 July 1991 to 1200 UTC 1 August 1991. The tick marks on the horizontal axis are marked in the same way as for the top panel.

4.7 The 3-12 August 1993 Episode

The 3-12 August 1993 episode contained one Class 3 day for acid deposition at GSM. Also at GSM, the episode contained two Class 3 visibility days and one Class 4 visibility day. At SNP, there was one Class 3 and two Class 4 visibility days during the episode. For ozone at GSM there were two Class 1 and four Class 2 days while at SNP there was one Class 1 and three Class 2 days. Thus, this episode was chosen for periods of moderately low visibility and high ozone.

The anomaly field for the 500-mb geopotential height for this episode is shown in Figure 4-26. Heights were about average over the southeastern U.S. and about 20 to 30 m below the long-term mean over portions of upper Midwest.

Figures 4-27 and 4-28 show the time series of observations for Knoxville. Maximum daily temperatures at Knoxville were in the 29°C to 33°C range during the episode with the minimum occurring during the middle of the period. The relative humidity showed the typical maxima near saturation in the mornings and minima in the afternoon in the range of 40-65 %. Precipitation occurred on several days of the episode.

The greatest six-hour precipitation amounts occurred on 5 August (27 mm) and 13 August (23 mm) with lesser amounts (2mm to 17 mm) being recorded during other 6-hr periods on the same or other days. Wind speeds at Knoxville were generally in the 1.5 m s^{-1} to 4 m s^{-1} range although occasionally winds did reach as high as 7 m s^{-1} . Winds were generally calm at night. At Knoxville, winds were generally westerly for the first three days of the episode, becoming northerly for the 6th through 9th and then southeasterly through southwesterly through the remainder of the period.

The meteorological times series at Martinsburg, WV are shown in Figures 4-29 and 4-30. At Martinsburg maximum daily temperatures were in the 26° C to 32° C range. As at Knoxville, the minimum occurred during the middle of the period. Relative humidity showed the typical maxima near saturation in the mornings and minima in the afternoon in the range of 35-55 %. Precipitation occurred on a few days at Martinsburg during the episode. The greatest six-hour precipitation amounts occurred on 7 August (19 mm) with lesser amounts (2mm to 16 mm) recorded during other 6-hr periods on the same or other days. Wind speeds were generally in the 2.5 m s^{-1} to 5 m s^{-1} range although occasionally winds did reach as high as 8 m s^{-1} . Winds were generally calm at night. Wind directions were generally variable at Martinsburg during the episode and missing data occurred for many hours.

4.8 The 22-29 June 1992 Episode

The 22-29 June 1992 episode contained one Class 2 day for acid deposition at GSM and one Class 1 acid deposition day at SNP. The episode contained one Class 4 visibility day at GSM while SNP had two Class 4 days. For ozone at GSM there was one Class 3 and one Class 4 days while at SNP there were three Class 3 days, one Class 1 day and one Class 3 day as well.

The anomaly field for the 500-mb geopotential height for this episode is shown in Figure 4-31. Heights were systematically lower than average over the eastern U.S. during the June 1992 episode. Over the southeastern U.S., the geopotential heights were typically 30 to 60 m or more lower than the long-term mean. The greatest depression was in the upper Midwest where the means were as much as 150 m lower than normal.

Figures 4-32 and 4-33 show the time series of observations for Knoxville. Maximum daily temperatures at Knoxville were in the 24° C to 31° C range during the episode with the maxima occurring during the middle and at the very end of the period. Relative humidity showed maxima near saturation on about half of the mornings and minima in the afternoon in the range of 40-65%. Light precipitation (i.e., less than 1 mm) occurred on three days of the episode. Wind speeds at Knoxville were generally in the 1.5 m s^{-1} to 5 m s^{-1} range although occasionally winds did reach as high as 7 m s^{-1} . Winds were generally calm at night. At Knoxville, winds were generally westerly for the first three days of the episode, becoming northerly for the remainder of the period.

The meteorological times series at Martinsburg, WV are shown in Figures 4-34 and 4-35. At Martinsburg maximum daily temperatures climbed steadily throughout the episode from 22° C to 30° C . Nighttime lows were around 12° C . The relative humidity showed the typical maxima near saturation in the mornings and minima in the afternoon in the range of 35-55 %. Light precipitation occurred on a couple of days at

Martinsburg during the episode. The greatest six-hour precipitation amounts occurred on 25 June (6 mm) with 3mm recorded on 24 June. Wind speeds at Knoxville were generally in the 2 m s^{-1} to 6 m s^{-1} range although occasionally winds did reach as high as 7 m s^{-1} to 8 m s^{-1} . Winds were calm at night. Wind directions were generally westerly at Martinsburg for the first half of the episode, becoming northerly on the 26th through 28th and then becoming southerly on the 29th. Missing data were reported for many hours.

4.9 The 24 April – 3 May 1995 Episode

The 24 April – 3 May 1995 episode contained one Class 1 day for acid deposition at GSM and one Class 2 acid deposition day at SNP. AT GSM, the episode contained one visibility day in each of Classes 2, 3, and 4. At SNP, there were three Class 2 visibility days during the episode. For ozone at GSM there was one Class 1, two Class 2, and one Class 1 days while at SNP there were three Class 1, one Class 2, and one Class 4 days.

The anomaly field for the 500-mb geopotential height for this episode is shown in Figure 4-36. Heights were about 25 m to 75 m below the long-term mean over the southeastern U.S. with larger depressions from normal over the upper Midwest.

Figures 4-37 and 4-38 show the time series of observations for Knoxville. Maximum daily temperatures at Knoxville were in the 16° C to 24° C range during the episode with the maximum occurring during the middle of the period (i.e., 29 April). Relative humidity showed the typical maxima near saturation in the mornings and minima in the afternoon in the approximate range of 30-80 %. Precipitation occurred on several days of the episode. The greatest six-hour precipitation amounts occurred on a few days during the period. On 1 May, the highest 6-hr precipitation total was 17 mm with 9 mm in the subsequent 6-hr period. Trace amounts ($< 2\text{mm}$) were reported on a couple of other days. Wind speeds at Knoxville were generally in the 1.5 m s^{-1} to 5 m s^{-1} range although occasionally winds did reach as high as 8 m s^{-1} . Winds were generally calm at night. The wind directions at Knoxville generally westerly for the first four days of the episode, becoming southerly by 1 May and then veering to the west for much of the remainder of the period.

The meteorological times series at Staunton, VA are shown in Figures 4-39 and 4-40. At Staunton, maximum daily temperatures were in the 18° C to 24° C range. The minimum temperature occurred on 27 April. Relative humidity showed the typical maxima near saturation in the mornings and minima in the afternoon in the range of 30-55%. No precipitation was measured at Staunton during the episode. Wind speeds were generally in the 1.5 m s^{-1} to 5 m s^{-1} range although occasionally winds did reach as high as 8 m s^{-1} . Winds were generally calm at night. West to southwesterly wind directions were measured at Staunton during the first few days of the episode, becoming northeast easterly for the remainder of the period. There were many hours for which wind direction data were missing at Staunton.

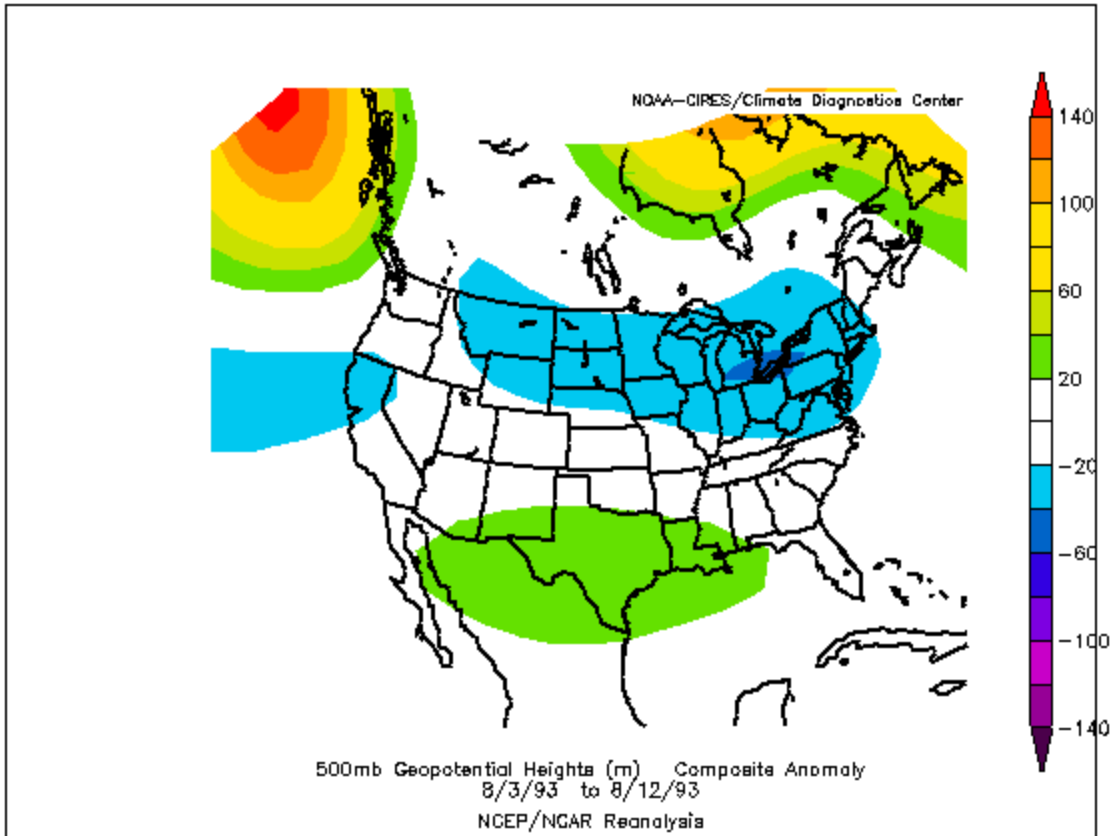


Figure 4-26. Anomaly Field for the 500-mb Geopotential Heights Created by Taking the Mean Value for the Period 0000 UTC 3 August – 1200 UTC 12 August 1993 and Subtracting From it the 15-Year Mean for the Same Period. Units are in Meters.

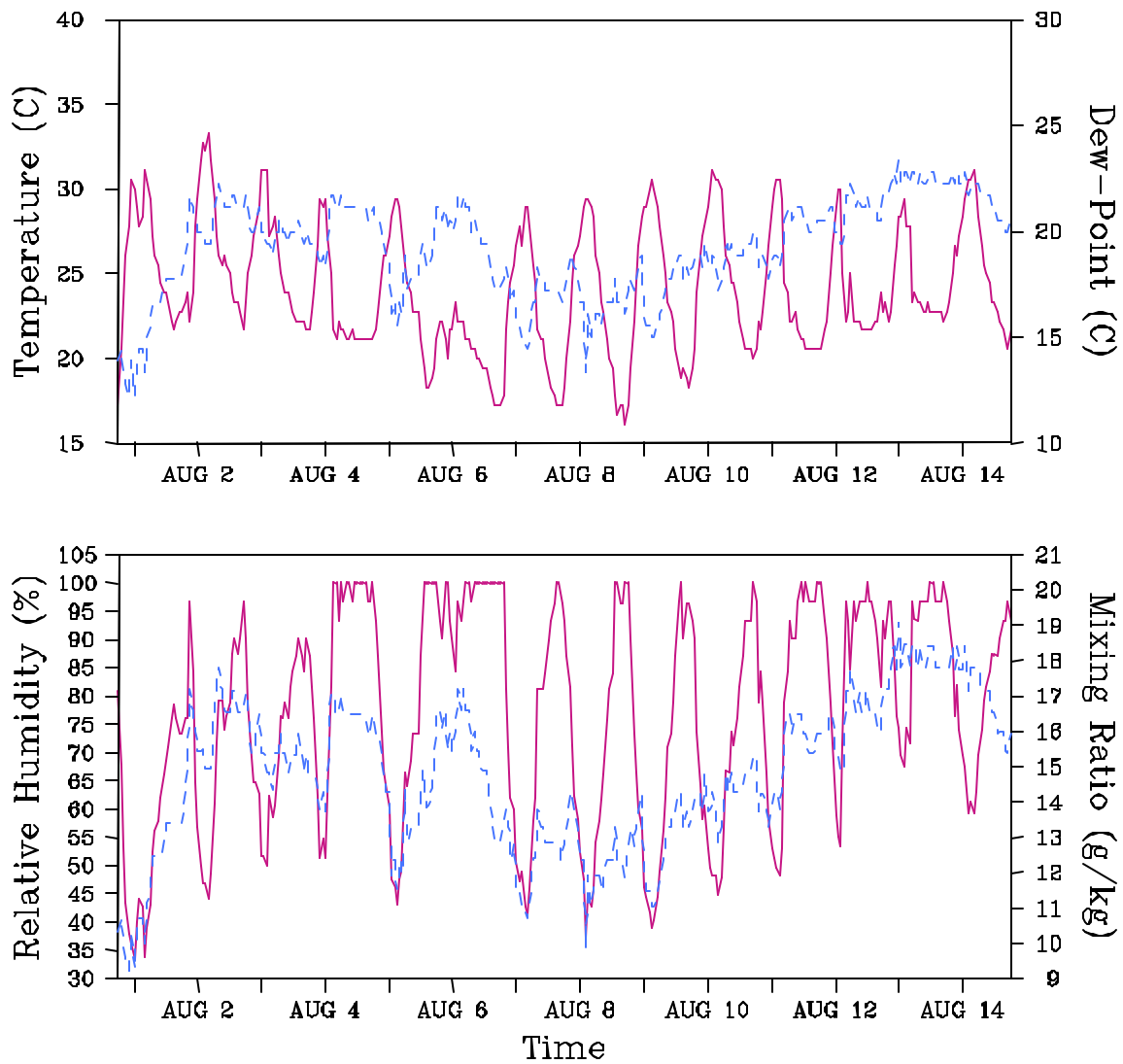


Figure 4-27. *Top Panel:* Hourly Observed Temperatures ($^{\circ}\text{C}$) at 2 m (solid curve) and Dewpoint Temperatures ($^{\circ}\text{C}$) at 2 m (dashed curve) at Knoxville, Tennessee From 3 August 1993 1200 UTC to 12 August 1993 1200 UTC. *Bottom Panel:* Hourly Observed Relative Humidities (%) at 2 m (solid curve) and Mixing Ratios (gm kg^{-1}) at 2 m (dashed curve) at Knoxville, Tennessee From 3 August 1993 1200 UTC to 12 August 1993 1200 UTC.

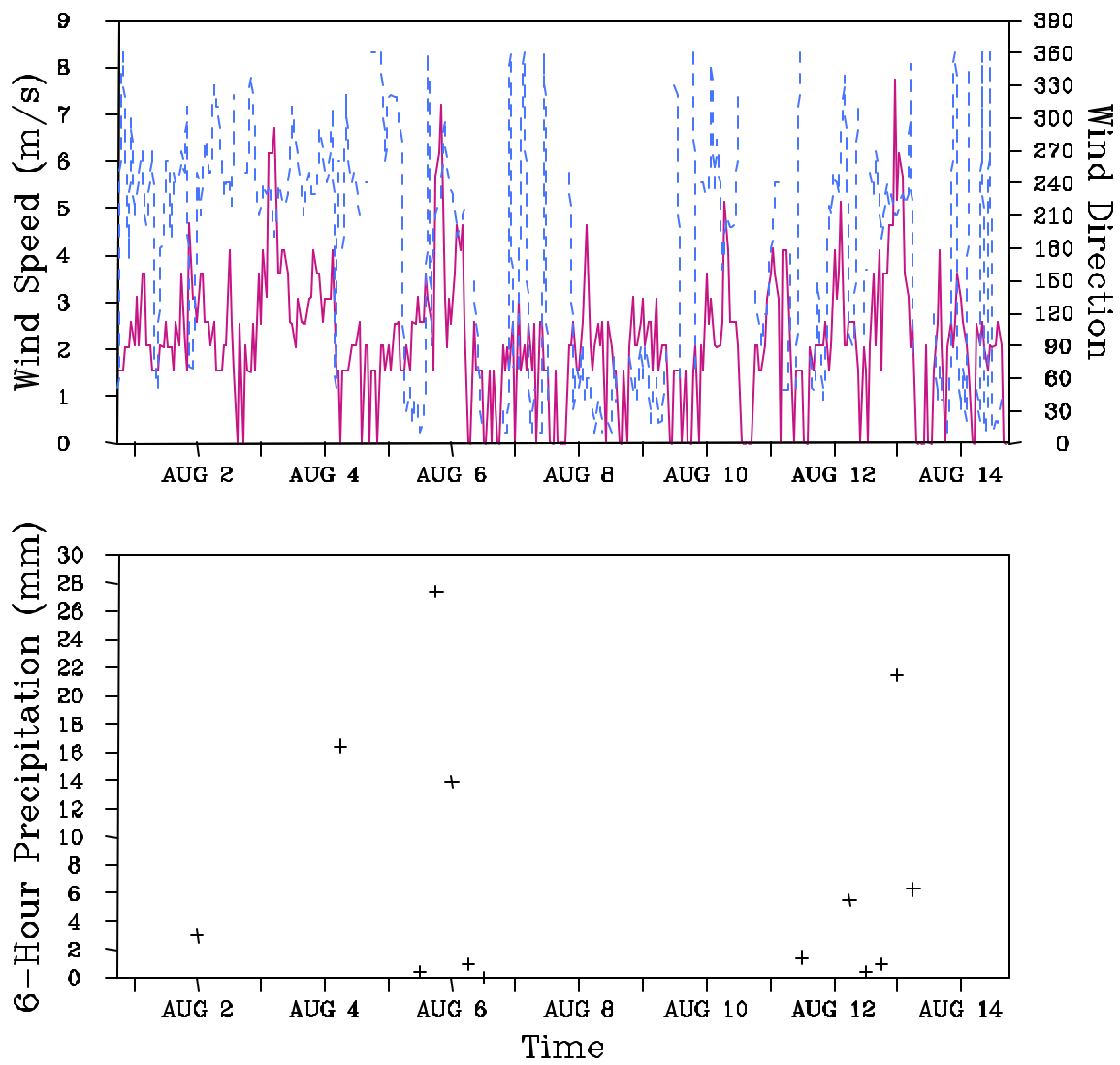


Figure 4-28. *Top Panel:* Hourly Observed Wind Speeds (m s^{-1}) at 10 m (solid curve) and Wind Directions (degrees) at 10 m (dashed curve) at Knoxville, Tennessee from 3 August 1993 1200 UTC to 12 August 1993 1200 UTC. *Bottom Panel:* Six-Hourly Observed Precipitation Amounts (mm) at Knoxville, Tennessee From 3 August 1993 1200 UTC to 12 August 1993 1200 UTC.

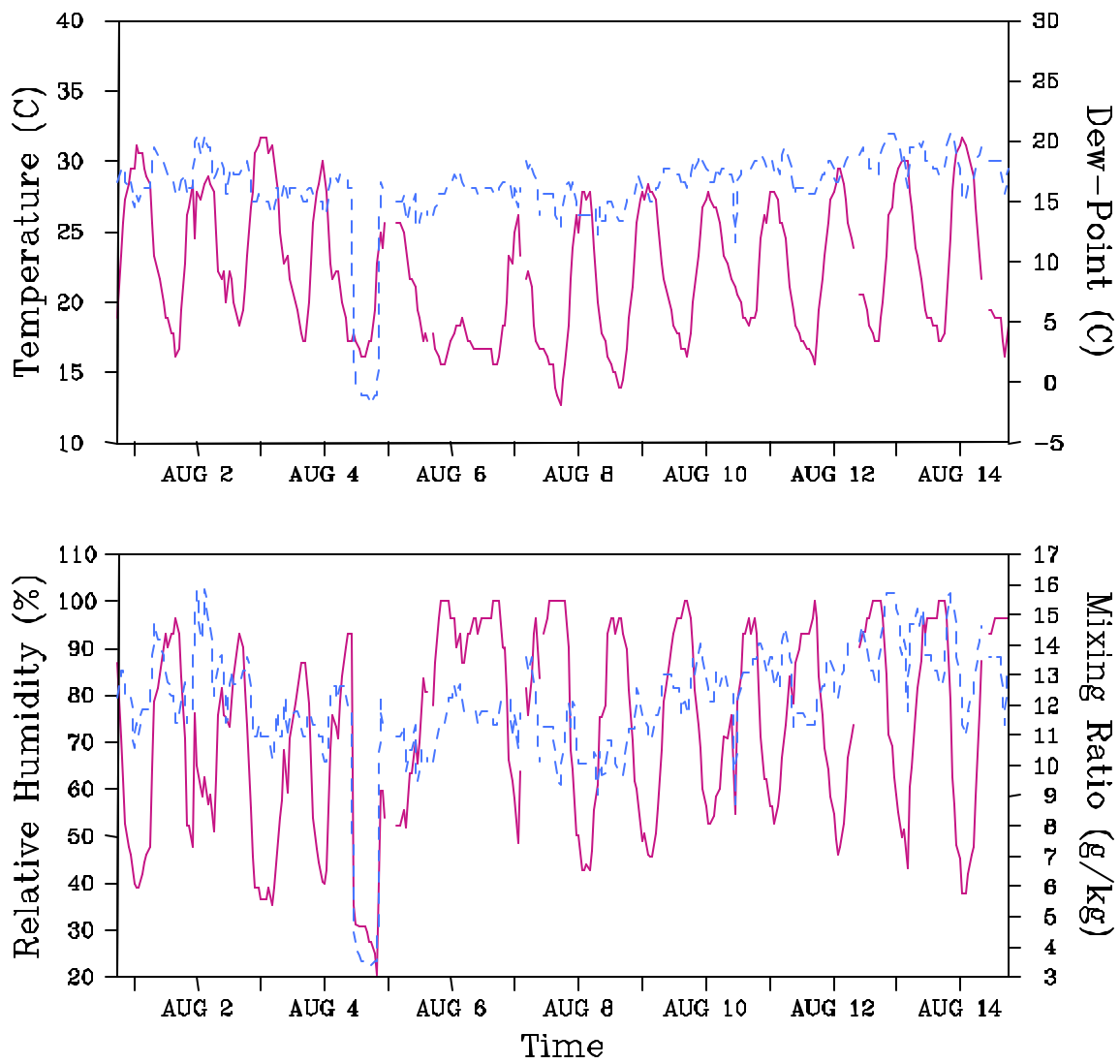


Figure 429. *Top Panel:* Hourly Observed Temperatures ($^{\circ}\text{C}$) at 2 m (solid curve) and Dewpoint Temperatures ($^{\circ}\text{C}$) at 2 m (dashed curve) at Martinsburg, West Virginia From 3 August 1993 1200 UTC to 12 August 1993 1200 UTC. *Bottom Panel:* Hourly Observed Relative Humidities (%) at 2 m (solid curve) and Mixing Ratios (gm kg^{-1}) at 2 m (dashed curve) at Martinsburg, West Virginia From 3 August 1993 1200 UTC to 12 August 1993 1200 UTC.

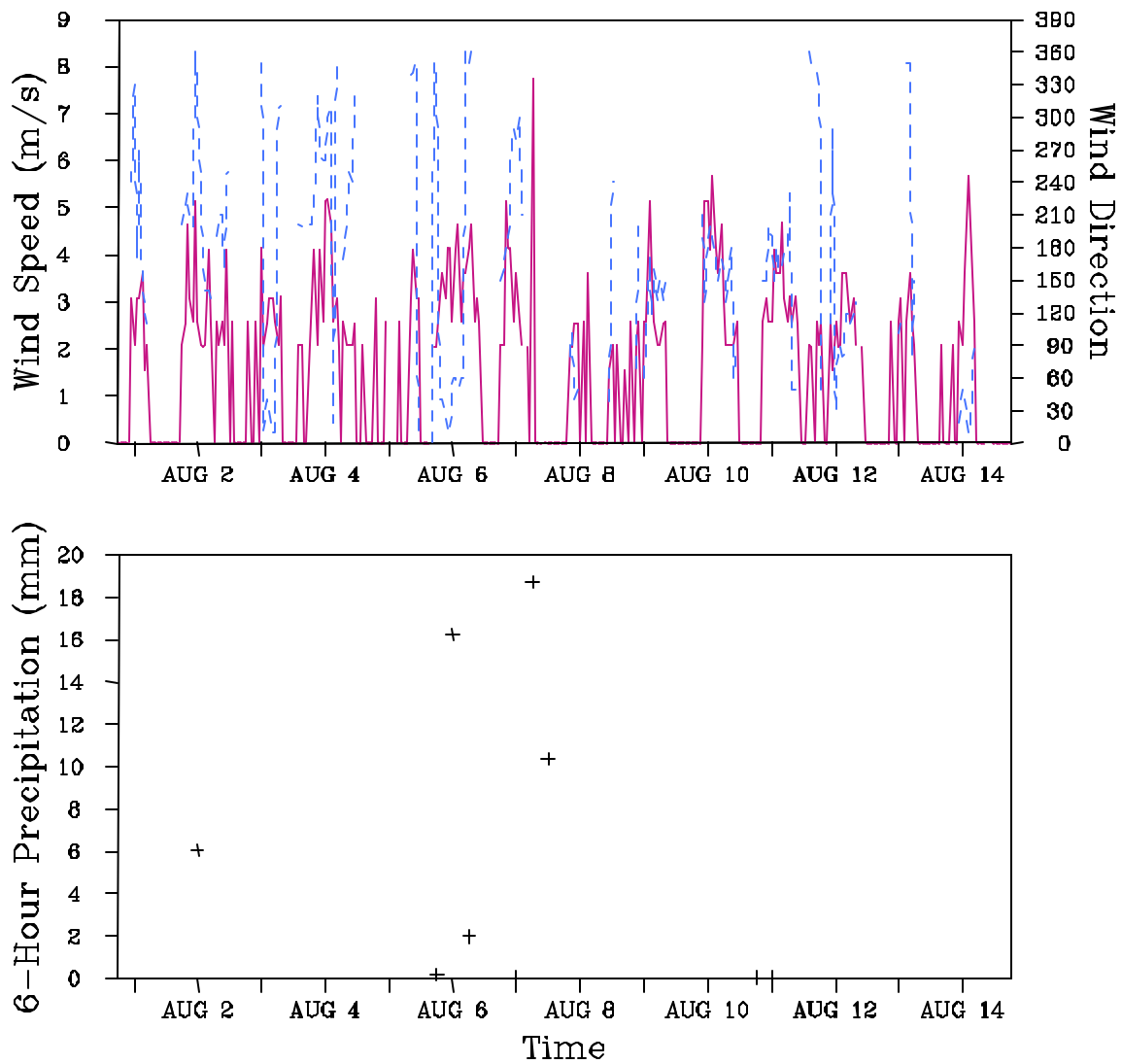


Figure 4-30. *Top Panel:* Hourly Observed Wind Speeds (m s^{-1}) at 10 m (solid curve) and Wind Directions (degrees) at 10 m (dashed curve) at Martinsburg, West Virginia From 3 August 1993 1200 UTC to 12 August 1993 1200 UTC. *Bottom Panel:* Six-Hourly Observed Precipitation Amounts (mm) at Martinsburg, West Virginia from 3 August 1993 1200 UTC to 12 August 1993 1200 UTC.

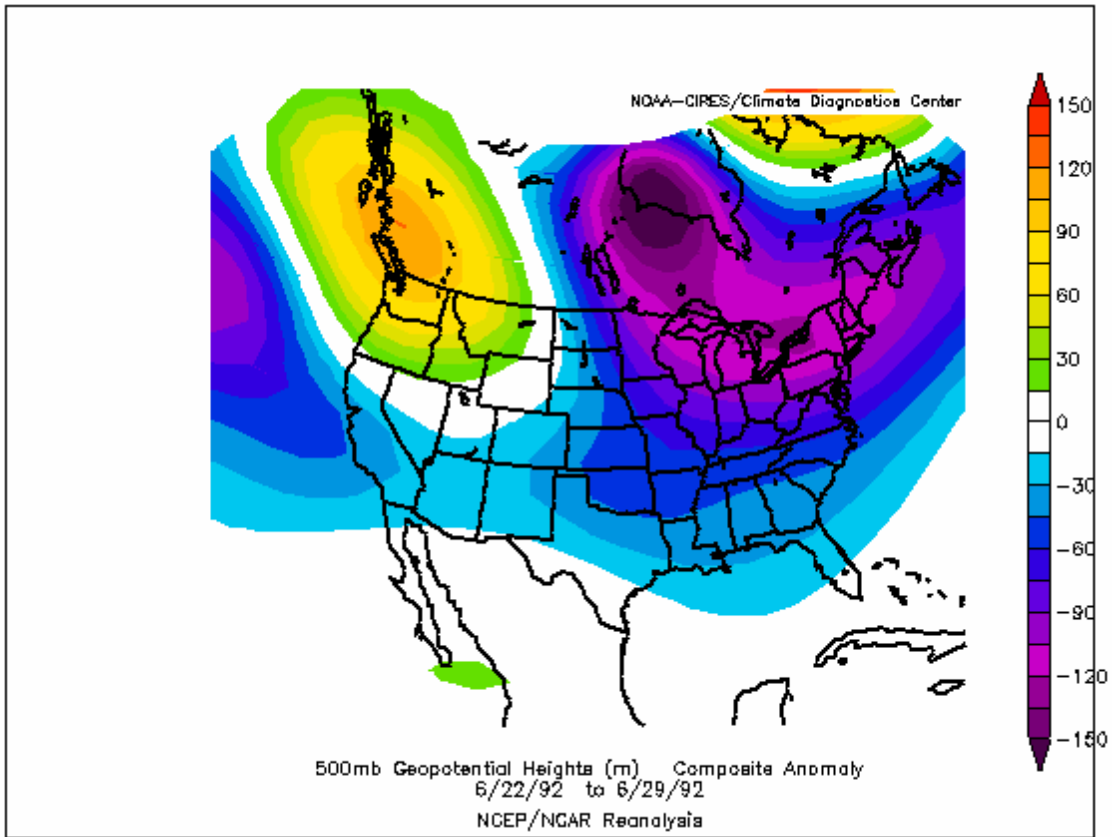


Figure 4-31. Anomaly Field for the 500-mb Geopotential Heights Created by Taking the Mean Value for the Period 0000 UTC 22 June – 1200 UTC 29 June 1992 and Subtracting From it the 15-Year Mean for the Same Period. Units are in Meters.

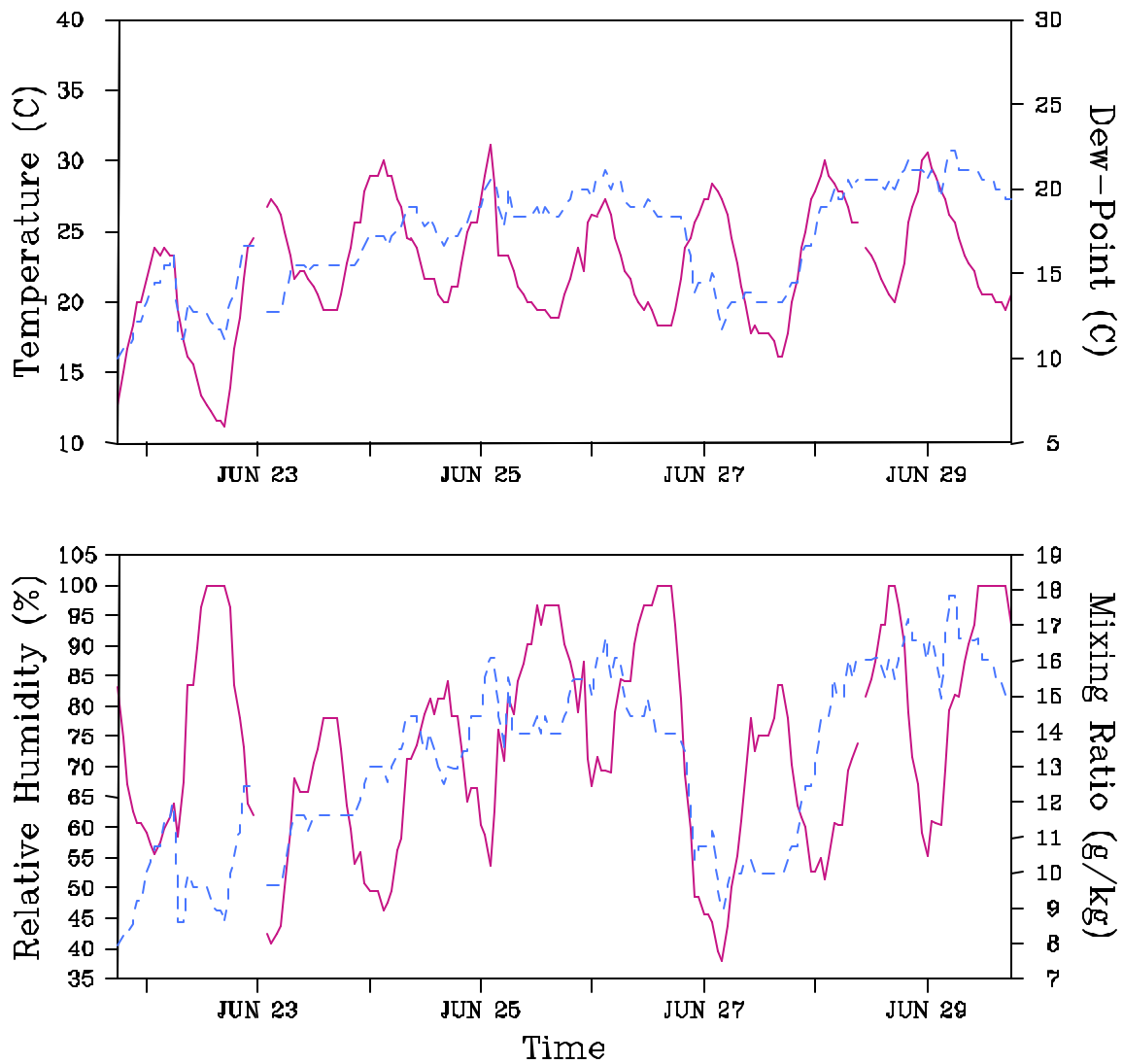


Figure 4-32. *Top Panel:* Hourly Observed Temperatures ($^{\circ}\text{C}$) at 2 m (solid curve) and Dewpoint Temperatures ($^{\circ}\text{C}$) at 2 m (dashed curve) at Knoxville, Tennessee From 22 June 1992 1200 UTC to 29 June 1992 1200 UTC. *Bottom Panel:* Hourly Observed Relative Humidities (%) at 2 m (solid curve) and Mixing Ratios (gm kg^{-1}) at 2 m (dashed curve) at Knoxville, Tennessee From 22 June 1992 1200 UTC to 29 June 1992 1200 UTC.

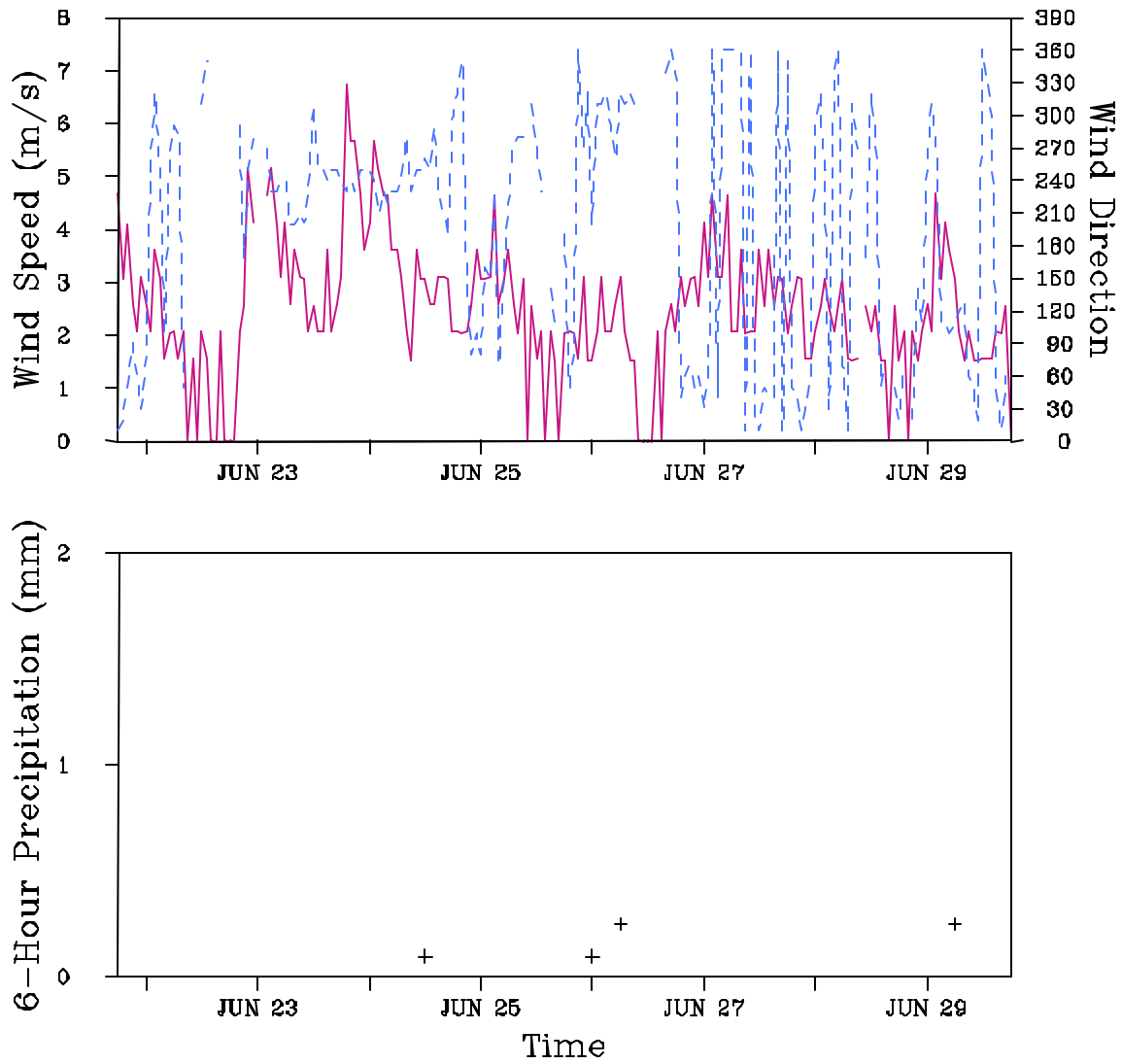


Figure 4-33. *Top Panel:* Hourly Observed Wind Speeds (m s^{-1}) at 10 m (solid curve) and Wind Directions (degrees) at 10 m (dashed curve) at Knoxville, Tennessee from 22 June 1992 1200 UTC to 29 June 1992 1200 UTC. *Bottom Panel:* Six-Hourly Observed Precipitation Amounts (mm) at Knoxville, Tennessee From 22 June 1992 1200 UTC to 29 June 1992 1200 UTC.

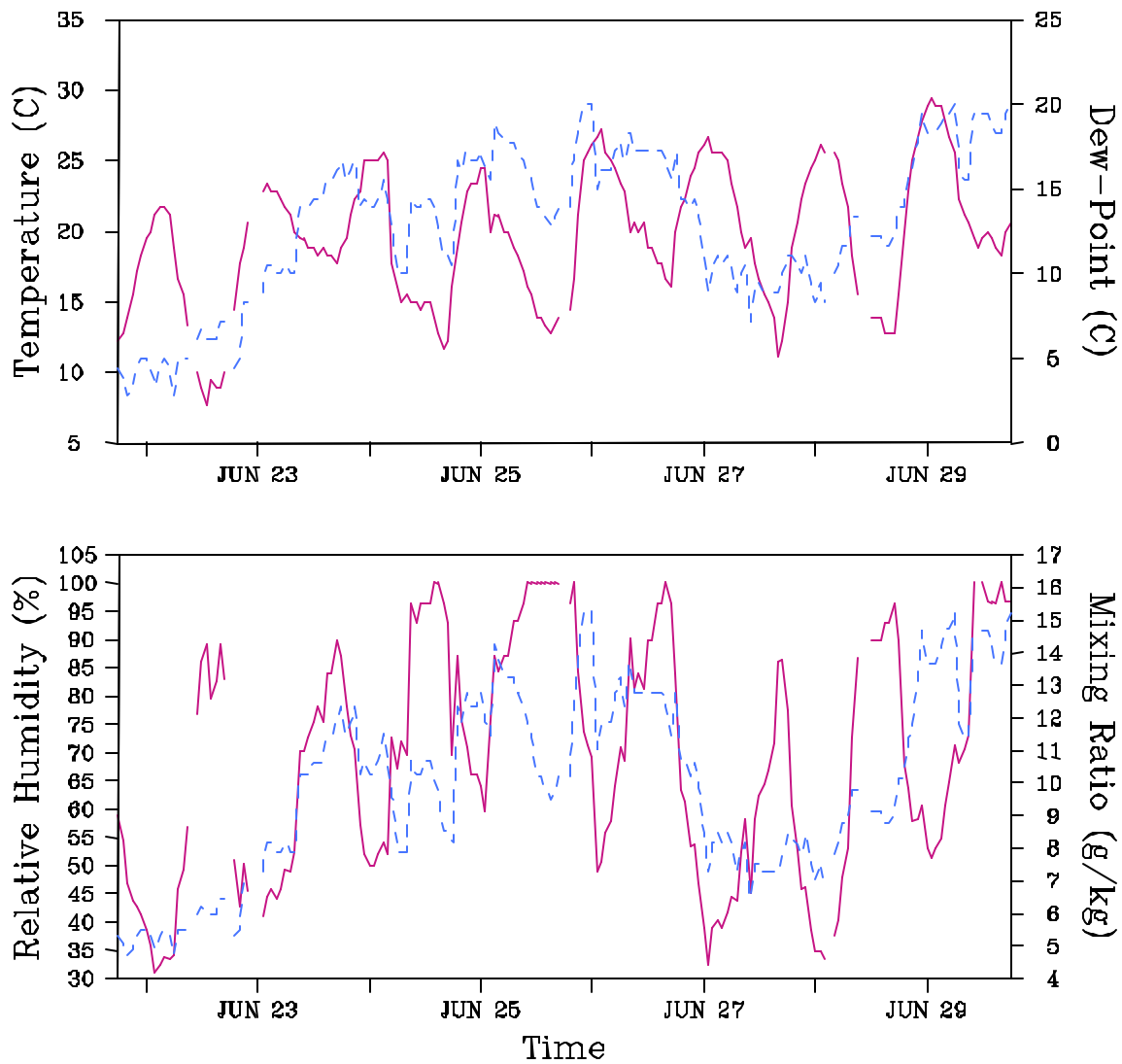


Figure 434. *Top Panel:* Hourly Observed Temperatures ($^{\circ}\text{C}$) at 2 m (solid curve) and Dewpoint Temperatures ($^{\circ}\text{C}$) at 2 m (dashed curve) at Martinsburg, West Virginia From 22 June 1992 1200 UTC to 29 June 1992 1200 UTC. *Bottom Panel:* Hourly Observed Relative Humidities (%) at 2 m (solid curve) and Mixing Ratios (gm kg^{-1}) at 2 m (dashed curve) at Martinsburg, West Virginia From 22 June 1992 1200 UTC to 29 June 1992 1200 UTC.

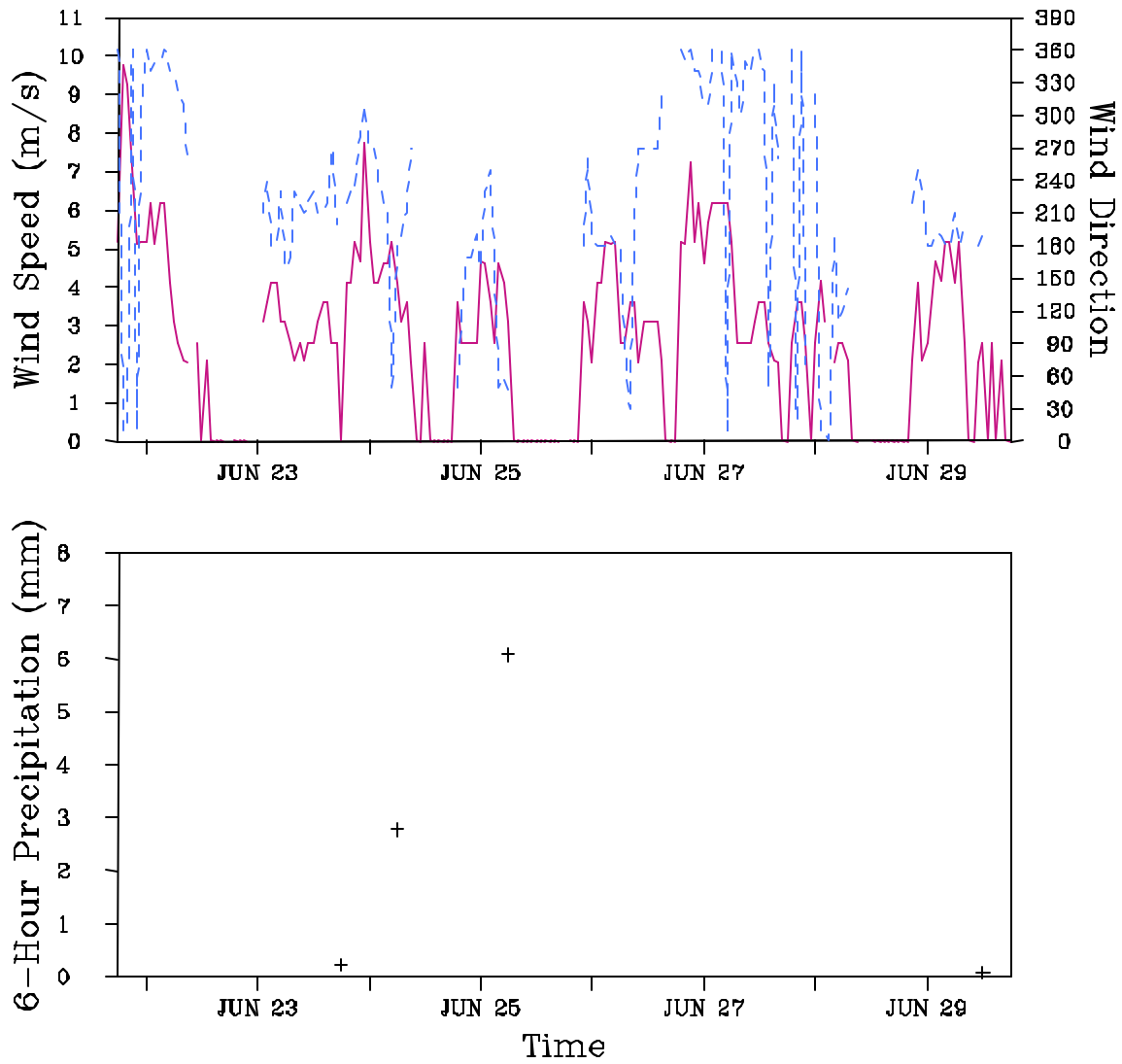


Figure 4-35. Top Panel: Hourly Observed Wind Speeds (m s^{-1}) at 10 m (solid curve) and Wind Directions (degrees) at 10 m (dashed curve) at Martinsburg, West Virginia From 22 June 1992 1200 UTC to 29 June 1992 1200 UTC. **Bottom Panel:** Six-Hourly Observed Precipitation Amounts (mm) at Martinsburg, West Virginia from 22 June 1992 1200 UTC to 29 June 1992 1200 UTC.

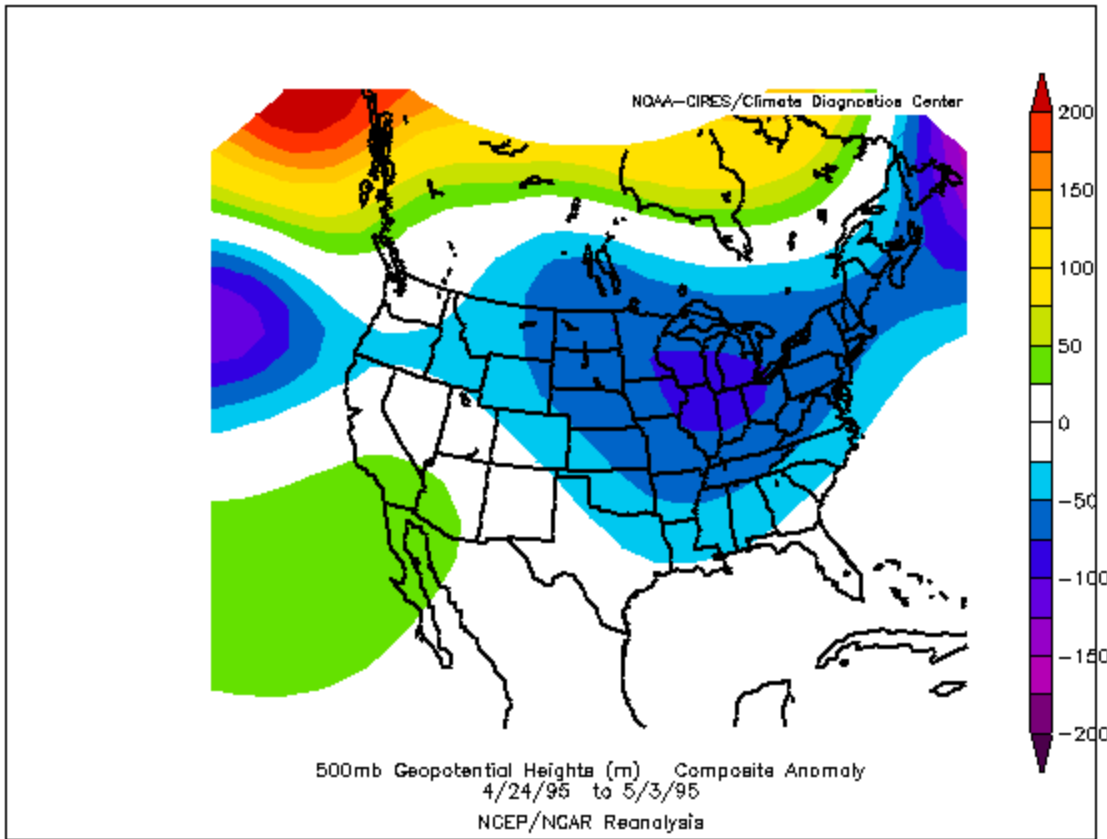


Figure 4-36. Anomaly Field for the 500-mb Geopotential Heights Created by Taking the Mean Value for the Period 0000 UTC 24 April – 1200 UTC 3 May 1995 and Subtracting From it the 15-Year Mean for the Same Period. Units are in Meters.

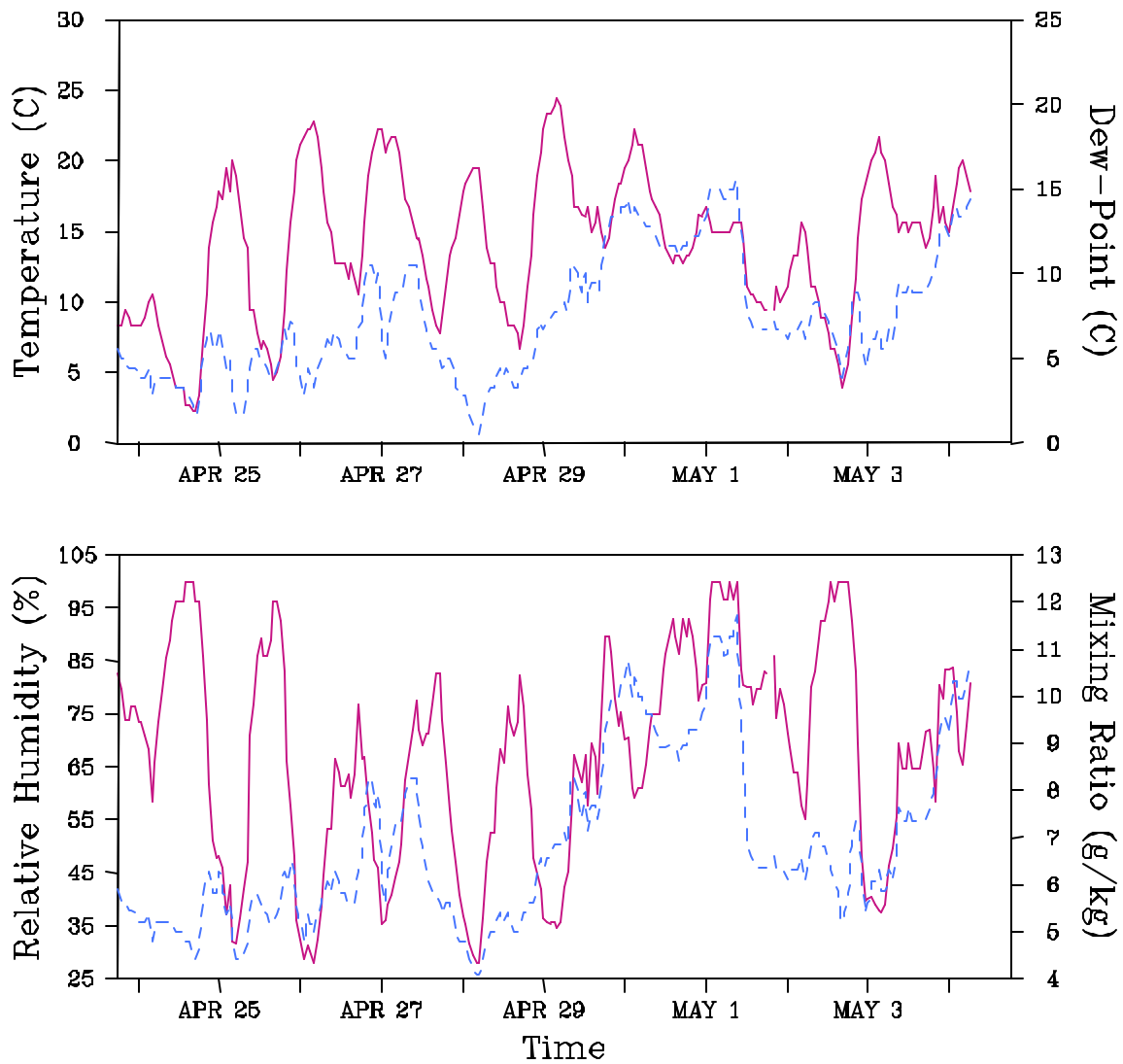


Figure 4-37. Top Panel: Hourly Observed Temperatures ($^{\circ}\text{C}$) at 2 m (solid curve) and Dewpoint Temperatures ($^{\circ}\text{C}$) at 2 m (dashed curve) at Knoxville, Tennessee from 24 April 1995 1200 UTC to 3 May 1995 1200 UTC. **Bottom Panel:** Hourly Observed Relative Humidities (%) at 2 m (solid curve) and Mixing Ratios (gm kg^{-1}) at 2 m (dashed curve) at Knoxville, Tennessee From 24 April 1995 1200 UTC to 3 May 1995 1200 UTC.

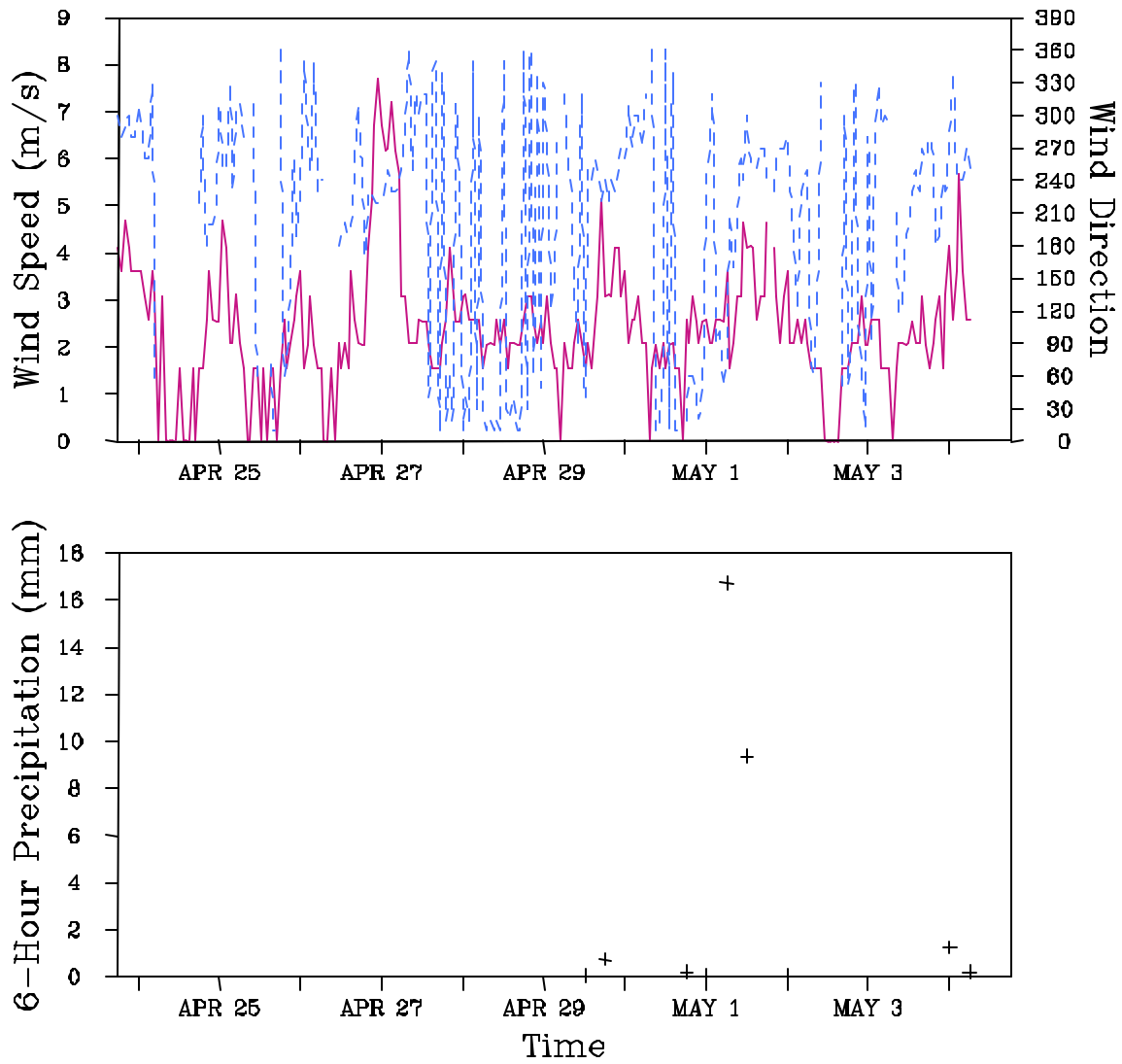


Figure 4-38. Top Panel: Hourly Observed Wind Speeds (m s^{-1}) at 10 m (solid curve) and Wind Directions (degrees) at 10 m (dashed curve) at Knoxville, Tennessee from 24 April 1995 1200 UTC to 3 May 1995 1200 UTC. **Bottom Panel:** Six-Hourly Observed Precipitation Amounts (mm) at Knoxville, Tennessee From 24 April 1993 1200 UTC to 3 May 1995 1200 UTC.

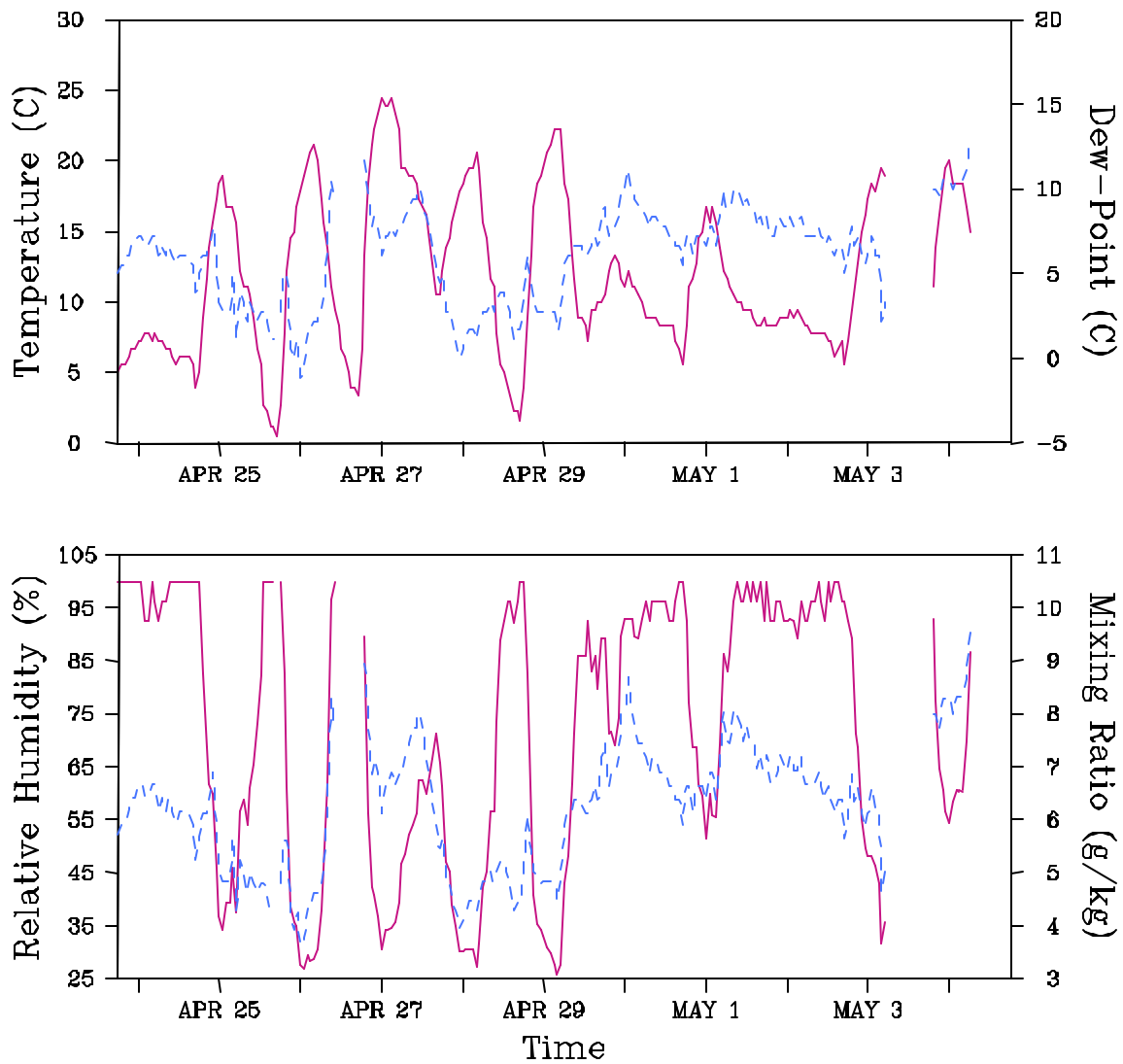


Figure 439. Top Panel: Hourly Observed Temperatures ($^{\circ}\text{C}$) at 2 m (solid curve) and Dewpoint Temperatures ($^{\circ}\text{C}$) at 2 m (dashed curve) at Staunton, Virginia From 24 April 1995 1200 UTC to 3 May 1995 1200 UTC. **Bottom Panel:** Hourly Observed Relative Humidities (%) at 2 m (solid curve) and Mixing Ratios (gm kg^{-1}) at 2 m (dashed curve) at Staunton, Virginia From 24 April 1995 1200 UTC to 3 May 1995 1200 UTC.

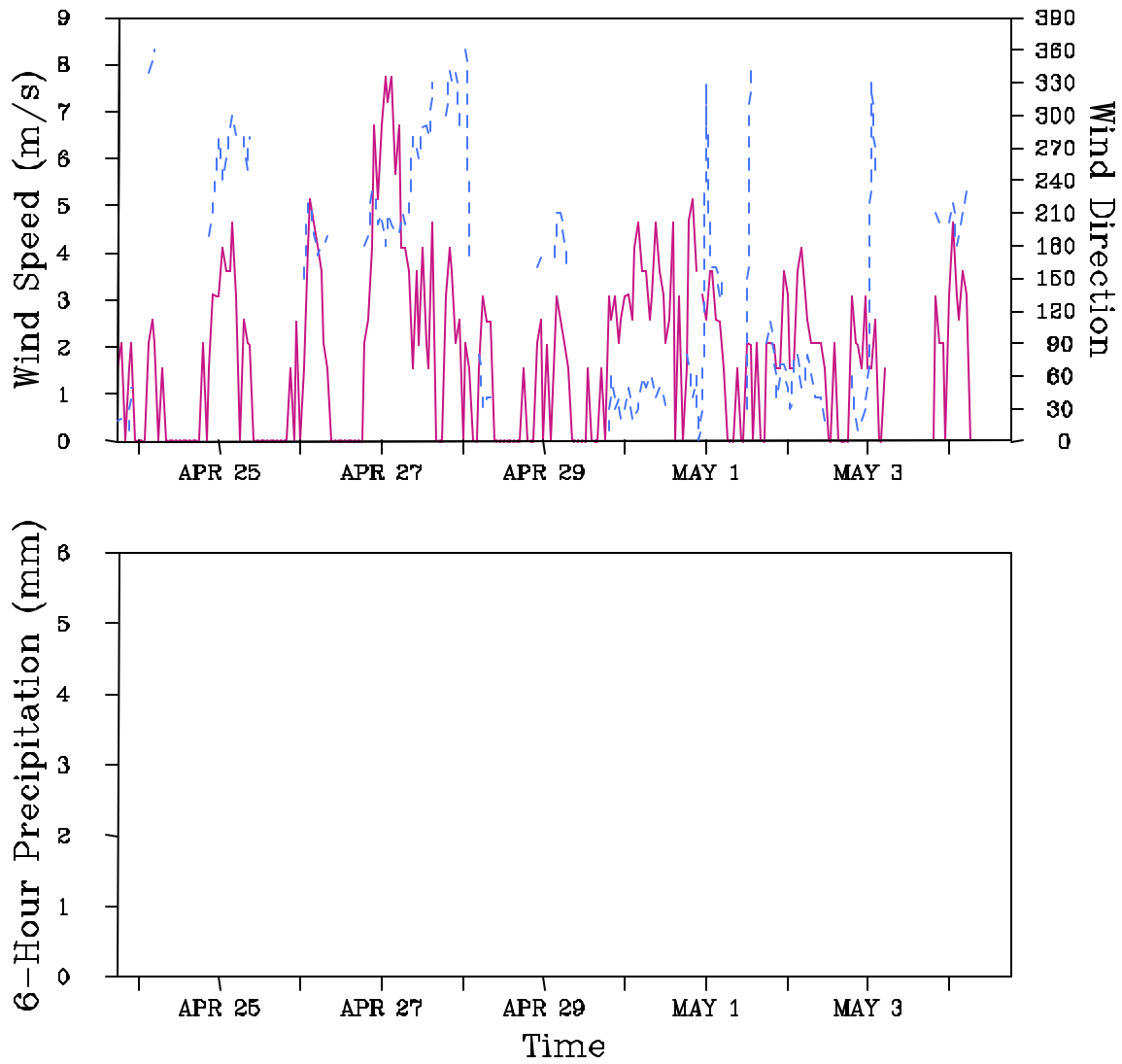


Figure 4-40. Top Panel: Hourly Observed Wind Speeds (m s^{-1}) at 10 m (solid curve) and Wind Directions (degrees) at 10 m (dashed curve) at Staunton, Virginia from 24 April 1995 1200 UTC to 3 May 1995 1200 UTC. **Bottom Panel:** Six-Hourly Observed Precipitation Amounts (mm) at Staunton, Virginia from 24 April 1995 1200 UTC to 3 May 1995 1200 UTC.

4.10 The 22-30 May 1995 Episode

The May 1995 episode was categorized as a Class 1 for GSP and Class 2 for SNP for the metric of acidic deposition. For visibility there was one Class 4 day at GSM and one Class 3 and one Class 4 days at SNP. For ozone both Parks registered Class 1, Class 2, and Class 3 days. For GSP the number of days (in parentheses) for each class was: Class 1 (1), Class 2 (1), and Class 3 (3). For SNP the number of days (in parentheses) for each class was: Class 1 (2), Class 2 (1), and Class 3 (1). So overall this episode was chosen for a broad range of conditions which can briefly be summarized as low to moderate acidic deposition, moderate ranges of visibility, and low to moderately high levels of ozone.

The anomaly field for the 500-mb geopotential height for this episode is shown in Fig 4-41. It reveals below normal heights for much of the western and central United States and above normal heights for much of the eastern and southeastern United States. The boundary between these two areas represented an active frontal area with several storm systems with the strongest being during the period 27-30 May. The surface low with the latter system tracked from Kansas on 27 May to northeast of Maine on 30 May. This system produced an unusual F4 tornado in Great Barrington, Massachusetts (*Storm Data*). During the time of 22-26 May the surface pattern was predominated by a quasi-stationary front which extended generally from Texas northeastward to New England. By 26 May the eastern portions of this front had moved south such that the frontal position was located from Texas to Virginia. Several waves which moved along this front brought considerable precipitation to the central and northern United States. Very little precipitation fell across the immediate SAMI region during this period where surface high pressure dominated. The episode ended with the strong storm system mentioned earlier which pulled the stationary front back north as a warm front across the entire SAMI region during 28-29 May followed by a cold frontal passage during 29-30 May.

Figures 4-42 and 4-43 show the time series of observations for Knoxville, while Figures 4-44 and 4-45 show the same for Staunton, Virginia. The Charlottesville, Virginia site again had large segments of missing data for this episode. Knoxville experienced a slow warming trend for 22-27 May with maximum temperatures increasing from near 25°C to near 30°C on 27 May. Maximum temperatures decreased for 28-29 May in response to increased clouds and precipitation related to the strong system moving across the northern United States. Dew point temperatures showed a similar trend, increasing from near 12°C on May 22 to 22°C on 27 May followed by fairly constant values until a decrease on the morning of 30 May with a cold frontal passage. The related mixing ratios increased from 10 g kg⁻¹ on May 22 to near 17 g kg⁻¹ on 27 May followed by a slight decrease until the cold frontal passage on 30 May when values decreased to near 11 g kg⁻¹. On several mornings the relative humidity was at 100% which probably meant fog was observed. Winds were typically light or calm at night with afternoon maximum speeds generally of 3-5 m s⁻¹ and from directions of 180-270° in response to the surface high pressure for most of the week. Precipitation was only observed on 27-28 May with 6-h amounts ranging up to 12 mm. Staunton experienced similar conditions with the following exceptions. Temperatures were cooler in general with the lowest maximum temperatures near 17°C recorded during 27-28 May when Knoxville was the warmest for the episode. This was the result of being north of the stationary front much of the time. Afternoon maximum wind speeds were higher than Knoxville, being in the range of 4-7 m s⁻¹. No precipitation was recorded at Staunton for the entire episode.

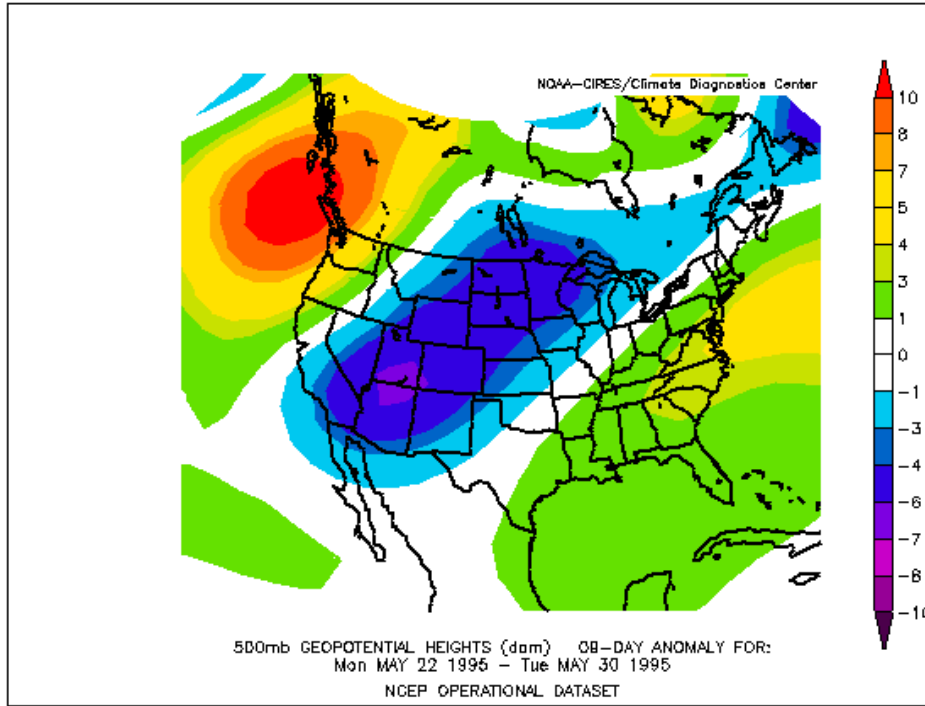


Figure 4-41. Anomaly field for the 500-mb geopotential heights created by taking the mean value for the period 0000 UTC 22 May - 1200 UTC 30 May 1995 and subtracting from it the 15-year mean for the same period. Units are in decameters (dam). Image obtained from NOAA-CIRES CDC.

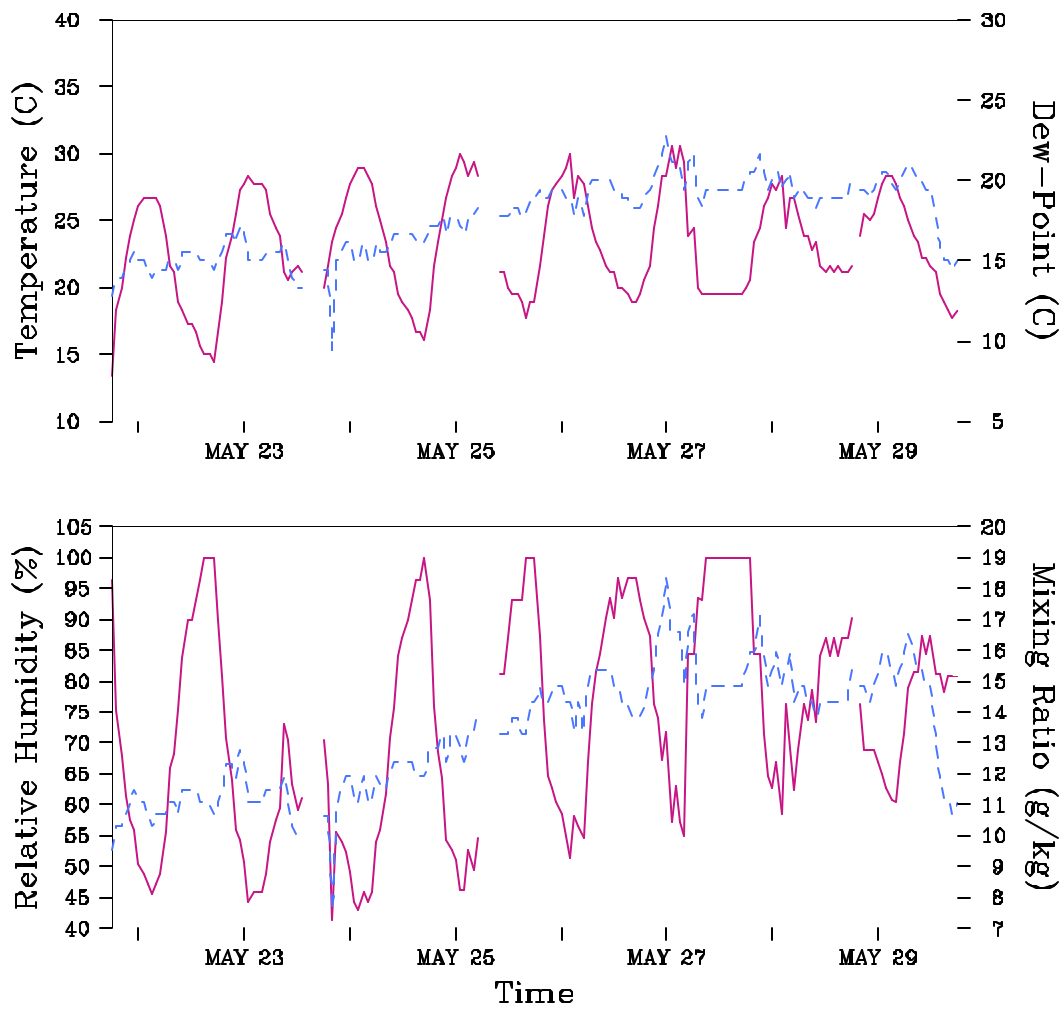


Figure 442. Top Panel: Hourly observed temperatures ($^{\circ}\text{C}$) at 2 m (solid curve) and dewpoint temperatures ($^{\circ}\text{C}$) at 2 m (dashed curve) at Knoxville, Tennessee from 1200 UTC 22 May 1995 to 1200 UTC 30 May 1995. Temperatures are with respect to the left vertical axis while the dewpoint temperatures are with respect to the right vertical axis. The tick marks on the horizontal axis are at 1800 UTC each day but are only labeled every other day. **Bottom Panel** Hourly observed relative humidities (per cent) at 2 m (solid curve) and mixing ratios (g kg^{-1}) at 2 m (dashed curve) at Knoxville, Tennessee from 1200 UTC 22 May 1995 to 1200 UTC 30 May 1995. Relative humidities are with respect to the left vertical axis while the mixing ratios are with respect to the right vertical axis. The tick marks on the horizontal axis are marked in the same way as for the top panel.

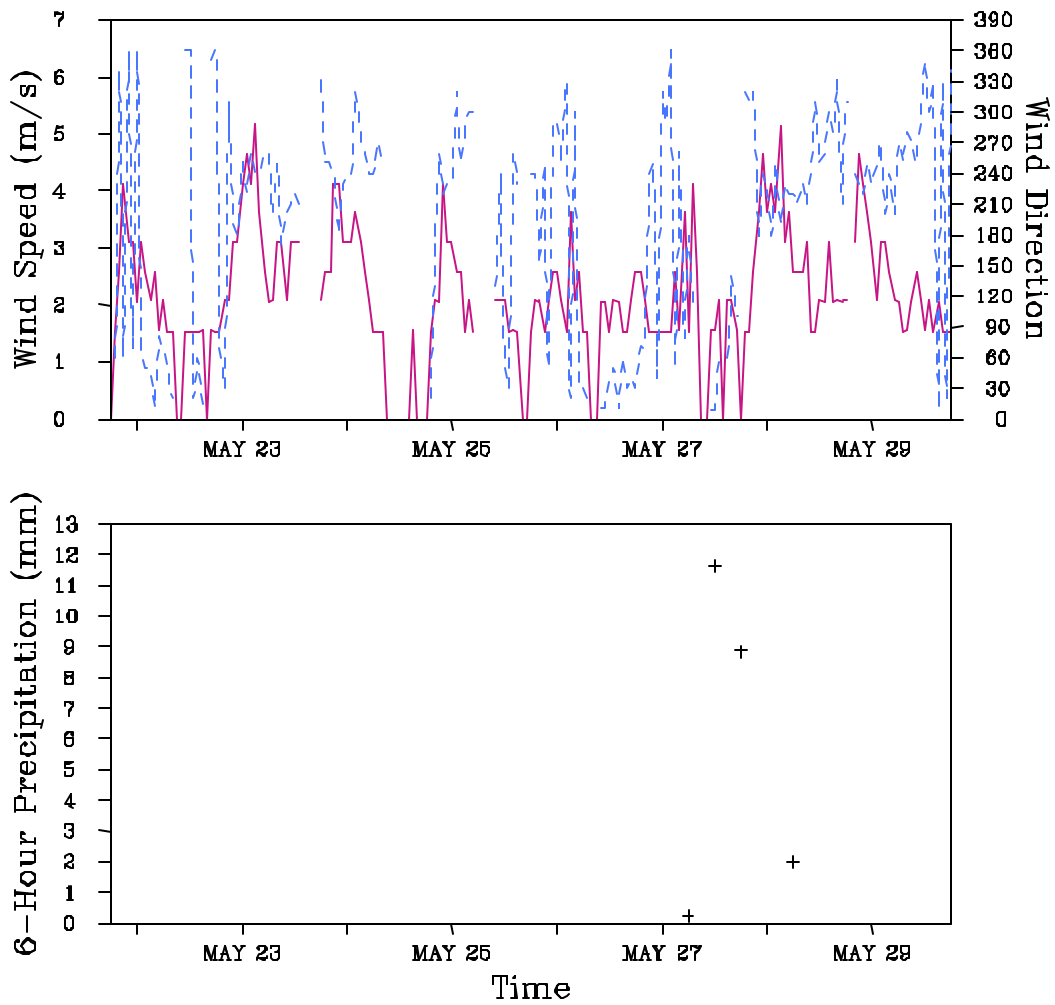


Figure 4-43. Top Panel: Hourly observed wind speeds (m s^{-1}) at 10 m (solid curve) and wind directions (degrees) at 10 m (dashed curve) at Knoxville, Tennessee from 1200 UTC 22 May 1995 to 1200 UTC 30 May 1995. Wind speeds are with respect to the left vertical axis while the wind directions are with respect to the right vertical axis. The tick marks on the horizontal axis are at 1800 UTC each day but are only labeled every other day. **Bottom Panel** Six-hourly observed precipitation amounts (mm) at Knoxville, Tennessee from 1200 UTC 22 May 1995 to 1200 UTC 30 May 1995. The tick marks on the horizontal axis are marked in the same way as for the top panel.

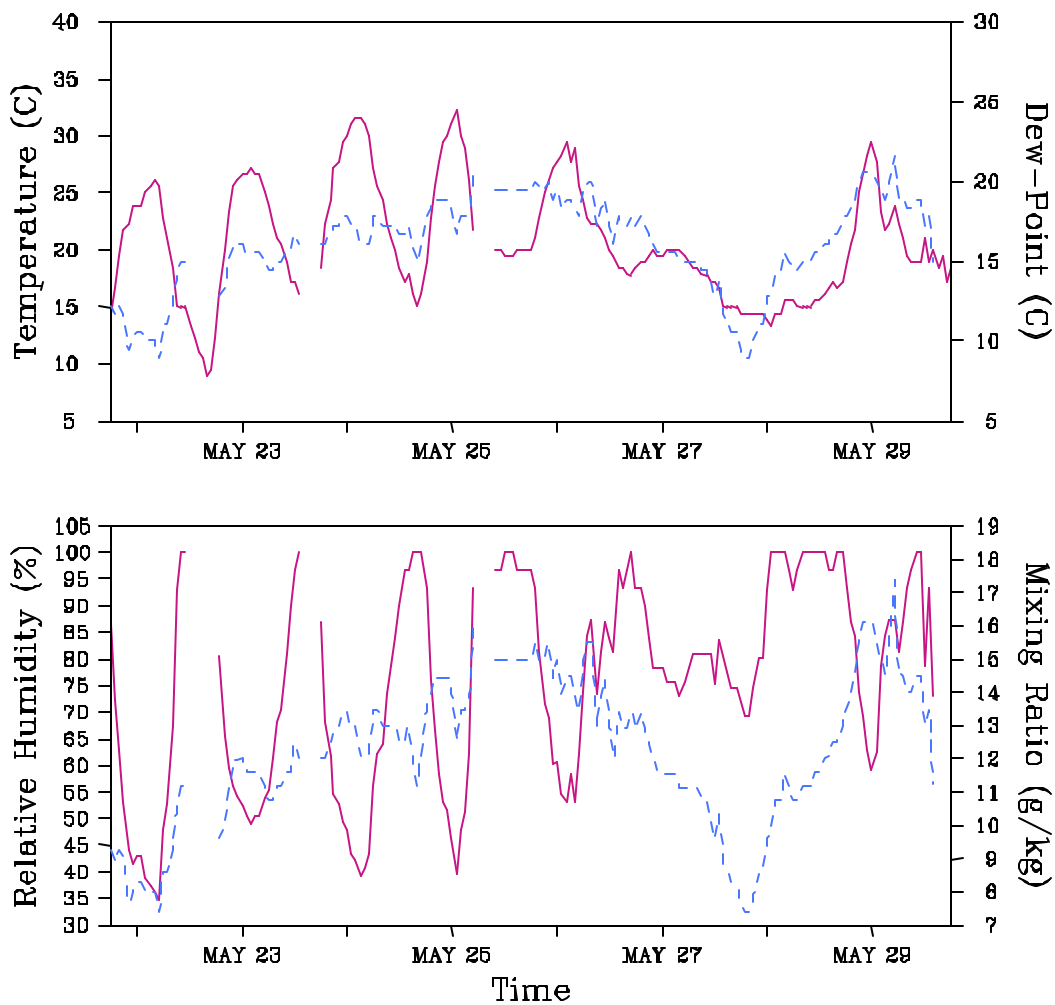


Figure 444. Top Panel: Hourly observed temperatures ($^{\circ}\text{C}$) at 2 m (solid curve) and dewpoint temperatures ($^{\circ}\text{C}$) at 2 m (dashed curve) at Staunton, Virginia from 1200 UTC 22 May 1995 to 1200 UTC 30 May 1995. Temperatures are with respect to the left vertical axis while the dewpoint temperatures are with respect to the right vertical axis. The tick marks on the horizontal axis are at 1800 UTC each day but are only labeled every other day. **Bottom Panel** Hourly observed relative humidities (per cent) at 2 m (solid curve) and mixing ratios (g kg^{-1}) at 2 m (dashed curve) at Staunton, Virginia from 1200 UTC 22 May 1995 to 1200 UTC 30 May 1995. Relative humidities are with respect to the left vertical axis while the mixing ratios are with respect to the right vertical axis. The tick marks on the horizontal axis are marked in the same way as for the top panel.

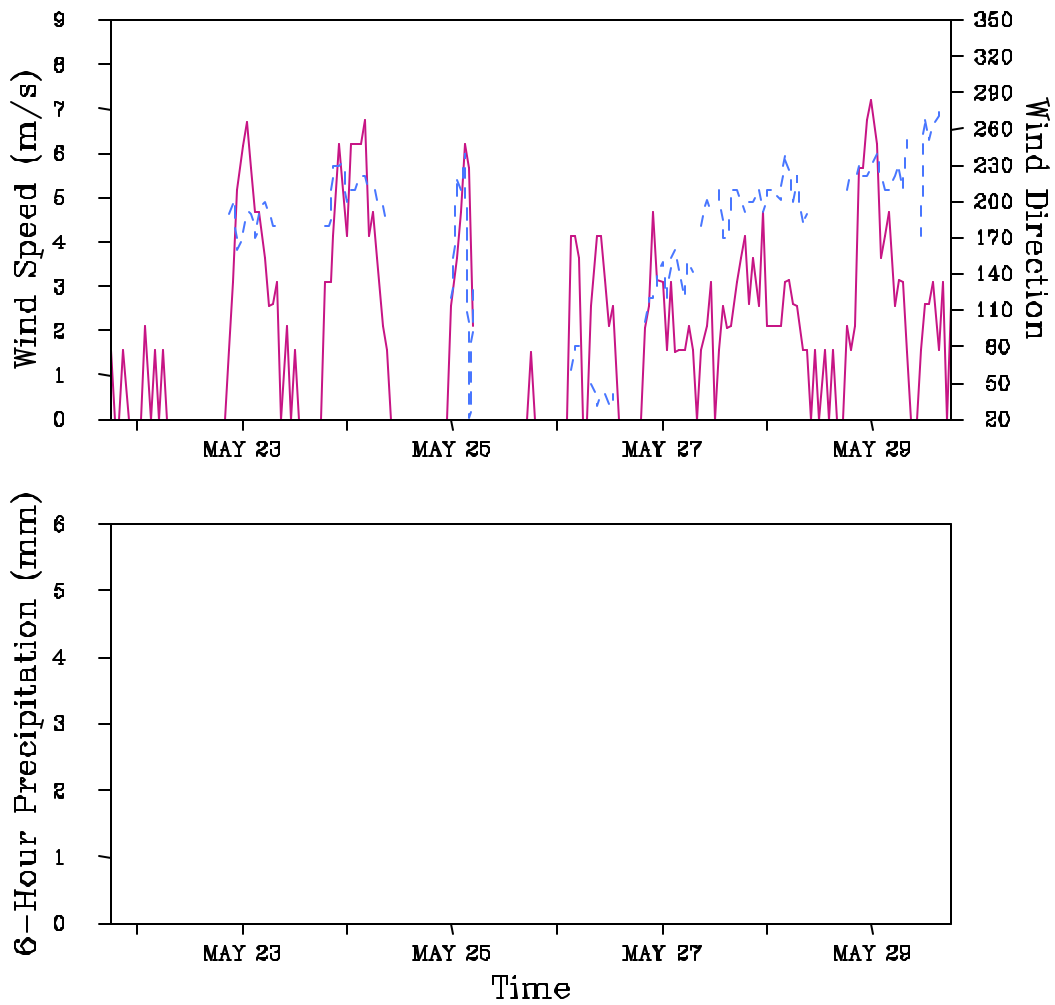


Figure 4-45. Top Panel: Hourly observed wind speeds (m s^{-1}) at 10 m (solid curve) and wind directions (degrees) at 10 m (dashed curve) at Staunton, Virginia from 1200 UTC 22 May 1995 to 1200 UTC 30 May 1995. Wind speeds are with respect to the left vertical axis while the wind directions are with respect to the right vertical axis. The tick marks on the horizontal axis are at 1800 UTC each day but are only labeled every other day. **Bottom Panel** Six-hourly observed precipitation amounts (mm) at Staunton, Virginia from 1200 UTC 22 May 1995 to 1200 UTC 30 May 1995. The tick marks on the horizontal axis are marked in the same way as for the top panel.

5.0 TECHNICAL APPROACH TO THE MODEL PERFORMANCE EVALUATION

5.1 Components of the RAMS Evaluation

The goal of the RAMS model evaluation is to assess whether and to what extent confidence may be placed in the modeling system to provide meteorological variables such as wind, temperature, moisture, cloud, and precipitation inputs to the SAMI URM-1ATM air quality model. The term "modeling system" refers both to the core RAMS model code as well as its various preprocessor and data preparation programs, and the supporting data bases used to exercise the model. The main objective of the evaluation is to reveal the presence of bias and internal, compensating errors in the model that, unless discovered and rectified, or at least quantified, may lead to erroneous or fundamentally incorrect decisions based on air quality model usage. If the evaluation is sufficiently rigorous and no significant errors or causes for concern are identified, then there is justification for declaring the model suitable for use in its intended purpose, i.e, supporting regional acid deposition and visibility modeling.

The present evaluation of the RAMS model consists of two components. The *operational evaluation* entails an assessment of the model's ability to estimate correctly key meteorological variables including surface wind, temperature, and mixing ratios largely independent of whether the actual process descriptions in the model are accurate. The operational evaluation essentially tests whether the predicted meteorological fields used as inputs URM-1ATM are reasonable, consistent and agree adequately with available observations. In this study, the operational evaluation focuses on the RAMS' ability to reproduce hourly surface wind speed, wind direction, temperature, and mixing ratio observations across the SAMI modeling domain. Tables 5-1 and 5-2 identify the full set of statistical measures and graphical displays that have been produced the SAMI RAMS simulations. (Only for the July '95 and July '91 episodes was a more limited set of evaluation statistics/displays developed).

Ideally, the *scientific evaluation* addresses the realism of the meteorological processes simulated by the model through testing the model as an entire system (i.e., not merely focusing on surface wind predictions) as well as its component parts. The scientific evaluation seeks to determine whether the model's behavior, in the aggregate and in its component modules, is consistent with prevailing theory, knowledge of physical processes, and observations. Ideally, the scientific evaluation consists of a series of diagnostic and mechanistic tests aimed at: (a) examining the existence of compensatory errors, (b) determining the causes of failure of a flawed model, (c) stressing a model to ensure failure if indeed the model is flawed, (d) provide additional insight into model performance beyond that supplied through routine, operational evaluation procedures. Unfortunately, a detailed scientific evaluation of the RAMS model was not possible with the SAMI data sets due to the absence of the specific measurements needed to test the process modules (e.g., soil moisture, Reynolds stress measurements, and so on). However, we can provide a limited scientific evaluation through comparisons of the modeled and observed liquid precipitation fields. However, where discrepancies exist, there is insufficient data to allow a definitive diagnosis of the potential causes.

5.2 Data Supporting Model Evaluation

Hourly surface observations were obtained from NCAR to support an evaluation of RAMS near-surface

temperature, water vapor, and wind speed fields. The specific NCAR data set used for this purpose was DS472.0 which is the hourly airways surface data. The primary data set available for comparing model performance aloft was the NCEP/NCAR reanalysis data files. The reanalysis data set is the result of a large effort to reanalyze global data back to 1957 with a fixed state-of-the-art analysis/forecast system. The reanalysis data variables are a mixture of model and observations, with observations dominating in those areas where data is more plentiful. The reanalysis data were processed as described in section 3.2 and in the SAMI meteorological modeling protocol (Norris and Doty, 1998).

5.3 Statistical and Graphical Evaluation Tools

The operational evaluation includes the calculation and analysis of several statistical measures of model performance and the plotting of specific graphical displays to elucidate the basic performance of the model in simulating atmospheric variables. These specific statistical measures are defined below. These procedures have been employed extensively in other prognostic model performance testing (see, for example, Steyn and McKendry, 1988; Ulrickson and Mass, 1990; Hanna, 1994; Tesche and McNally, 1993, 1996; McNally and Tesche, 1996a,b, 1998; Seaman and Stauffer, 1996; Seaman et al., 1997; Tesche et al., 2000). These analysis procedures are incorporated into the Model Performance Evaluation, Analysis, and Plotting Software (MAPS) system (McNally and Tesche, 1994) which also includes a variety of other statistical and graphical testing methods for photochemical and meteorological models.

5.3.1 Mean and Global Statistics

Several statistical measures are calculated as part of the meteorological model evaluation. In the definitions below, the variable F represents a model-estimated or derived quantity, e.g., wind speed, wind direction, PBL height, mixing ratio, precipitation amount, or temperature. The subscripts e and o correspond to model-estimated and observed (i.e., measured) quantities, respectively. The subscript i refers to the ninth hour of the day.

Mean Estimation (M_e). The mean model estimate is given by:

$$M_e = \frac{I}{N} \sum_{i=1}^N \Phi_{ei}$$

where N is the product of the number of simulation hours and the number of ground-level monitoring locations providing hourly-averaged observational data. F_{ei} represents the model-estimate at hour i .

Mean Observation (M_o). The mean observation is given by:

$$M_o = \frac{I}{N} \sum_{i=1}^N \Phi_{oi}$$

Here, F_{oi} represents the observations at hour i .

Average Wind Direction. Because wind direction has a crossover point between 0 degrees and 360 degrees, standard linear statistical methods cannot be used to calculate the mean or standard deviation. The

method proposed by Yamartino (1984) performs well in estimating the wind direction standard deviation. Specifically, this quantity is calculated by:

$$s_a = \arcsin (\mathbf{b}) [1 + 0.1547 \mathbf{b}^3]$$

where:

$$\mathbf{b} = \left[1.0 - \left[(\overline{\sin \alpha})^2 + (\overline{\cos \alpha})^2 \right] \right]^{1/2}$$

Here, α is the measured hourly or instantaneous wind direction value.

5.3.2 Difference Statistics

Residual (d_i). For quantities that are continuous in space and time (i.e., wind speed, temperature, pressure, PBL height, species concentrations) difference statistics provide considerable insight into the model's performance, temporally and spatially. Difference statistics are based on the definition of a residual quantity. A mixing ratio residual, for example, is defined as:

$$d_i = c_e(x_i, t) - c_o(x_i, t)$$

where d_i is the i -th residual based on the difference between model-estimated (c_e) and observed (c_o) mixing ratio at location x and time i . In the definitions that follow, we shall use the letter c to denote any continuous atmospheric variable (e.g., temperature, precipitation amount, PBL height).

Standard Deviation of Residual Distribution (SD_r). The standard deviation of the residual distribution is given by:

$$SD_r = \left(\frac{1}{N-1} \sum_{i=1}^N (d_i - \text{MBE})^2 \right)^{0.5}$$

where the residual is defined as:

$$d_i = c_e(x_i, t) - c_o(x_i, t)$$

and MBE is the first moment, i.e., the mean bias error, defined shortly. This statistic describes the "dispersion" or spread of the residual distribution about the estimate of the mean. The standard deviation is calculated using all estimation-observation pairs above the cutoff level. The second moment of the residual distribution is the variance, the square of the standard deviation. Since the standard deviation has the same units of measure as the variable (e.g., meters/sec for wind), it is used here as the metric for dispersion. The standard deviation and variance measure the average "spread" of the residuals, independent of any systematic bias in the estimates. No direct information is provided concerning sub-regional errors or about

large discrepancies occurring within portions of the diurnal cycle although in principle these, too, could be estimated.

Mean Bias Error (MBE). The mean bias error is given by:

$$MBE = \frac{I}{N} \sum_{i=1}^N (c_e(x_i, t) - c_o(x_i, t))$$

where N equals the number of hourly estimate-observation pairs drawn from all valid monitoring station data on the simulation day of interest.

Mean Normalized Bias Error (MNBE). The mean normalized bias error, often just called the bias, is given by:

$$MNBE = \frac{I}{N} \sum_{i=1}^N \frac{(c_e(x_i, t) - c_o(x_i, t))}{c_o(x_i, t)} \times 100 \%$$

Mathematically, the bias is derived from the average signed deviation of the mixing ratio (or temperature) residuals and is calculated using all pairs of estimates and observations above the cutoff level.

Mean Absolute Gross Error (MAGE). The mean gross error is calculated in two ways, similar to the bias. The mean absolute gross error is given by:

$$MAGE = \frac{I}{N} \sum_{i=1}^N |c_e(x_i, t) - c_o(x_i, t)|$$

Mean Absolute Normalized Gross Error (MANGE). The mean absolute normalized gross error (or simply ‘gross error’) is:

$$MANGE = \frac{I}{N} \sum_{i=1}^N \frac{|c_e(x_i, t) - c_o(x_i, t)|}{c_o(x_i, t)} \times 100 \%$$

The gross error quantifies the mean absolute deviation of the residuals. It indicates the average unsigned discrepancy between hourly estimates and observations and is calculated for all pairs. Gross error is a robust measure of overall model performance and provides a useful basis for comparison among model simulations across different model grids or episodes. Unless calculated for specific locations or time intervals, gross error estimates provide no direct information about sub-regional errors or about large discrepancies occurring within portions of the diurnal cycle.

Root Mean Square Error (RMSE). The root mean square error is given by:

$$RMSE = \left[\frac{I}{N} \sum_{i=1}^N |\Phi_{ei} - \Phi_{oi}|^2 \right]^{1/2}$$

The RMSE, as with the gross error, is a good overall measure of model performance. However, since large errors are weighted heavily, large errors in a small subregion may produce large a RMSE even though the errors may be small elsewhere.

Systematic Root Mean Square Error (RMSE_s). A measure of the model's linear (or systematic) bias may be estimated from the systematic root mean square error given by:

$$RMSE_s = \left[\frac{I}{N} \sum_{i=1}^N |\hat{\Phi}_{ei} - \Phi_{oi}|^2 \right]^{1/2}$$

Unsystematic Root Mean Square Error (RMSE_u). A measure of the model's unsystematic bias is given by the unsystematic root mean square error, that is:

$$RMSE_u = \left[\frac{I}{N} \sum_{i=1}^N |\Phi_{ei} - \hat{\Phi}_{ei}|^2 \right]^{1/2}$$

The unsystematic difference is a measure of how much of the discrepancy between estimates and observations is due to random processes or influences outside the legitimate range of the model.

A "good" model will provide low values of the root mean square error, RMSE, explaining most of the variation in the observations. The systematic error, RMSE_s, should approach zero and the unsystematic error RMSE_u should approach RMSE since:

$$RMSE^2 = (RMSE_s)^2 + (RMSE_u)^2$$

It is important that RMSE, RMSE_s, and RMSE_u are all analyzed. For example, if only RMSE is estimated (and it appears acceptable) it could consist largely of the systematic component. This bias might be removed, thereby reducing the bias transferred to the photochemical model. On the other hand, if the RMSE consists largely of the unsystematic component (RMSE_u), this indicates further error reduction may require model refinement and/or data acquisition. It also provides error bars that may used with the inputs in subsequent sensitivity analyses.

5.3.3 Skill Measures

Index of Agreement (I). Following Willmont (1981), the index of agreement is given by:

$$I = 1 - \left[\frac{N (RMSE)^2}{\sum_{i=1}^N (|\Phi_{ei} - M_o| + |\Phi_{oi} - M_o|)^2} \right]$$

This metric condenses all the differences between model estimates and observations into one statistical quantity. It is the ratio of the cumulative difference between the model estimates and the corresponding observations to the sum of two differences: between the estimates and observed mean and the observations and the observed mean. Viewed from another perspective, the index of agreement is a measure of how well the model estimates departure from the observed mean matches, case by case, the observations' departure from the observed mean. Thus, the correspondence between estimated and observed values across the domain at a given time may be quantified in a single metric and displayed as a time series. The index of agreement has a theoretical range of 0 to 1, the latter score suggesting perfect agreement.

RMS Skill Error (Skill_e). The root mean square error skill ratio is defined as:

$$Skill_E = \frac{RMSE_u}{SD_o}$$

Variance Skill Ratio (Skill_{var}). The variance ratio skill is given by:

$$Skill_{var} = \frac{SD_e}{SD_o}$$

5.3.4 Graphical Tools

Many features of meteorological model simulations are best analyzed through graphical means. In addition to revealing important qualitative relationships, graphical displays also supply quantitative information. The main graphical displays used to analyze the performance results include:

- > The temporal correlation between estimates and observations;
- > The spatial distribution of estimated fields;
- > The correlation among hourly pairs of estimates, observations and residuals;
- > The variation in bias and error estimates as functions of time and space;
- > The degree of mismatch between volume-averaged model estimates and point measurements;
and
- > Log p/Skew-T plots of wind, temperature and mixing ratio.

These plotting methods are exemplified in the many recent prognostic meteorological model evaluation studies (see, for example, Seaman, 2000; Tesche, et al., 2000).

Table 5-1. Statistical Measures and Graphical Displays Used in the Operational Evaluation of RAMS Surface Meteorological Variables

Statistical Measure	Graphical Display
<i>Surface Winds (ms⁻¹)</i>	
Vector mean observed wind speed	Vector mean modeled and observed wind speeds as a function of time
Vector mean predicted wind speed	Scalar mean modeled and observed wind speeds as a function of time
Scalar mean observed wind speed	Modeled and observed mean wind directions as a function of time
Scalar mean predicted wind speed	Modeled and observed standard deviations in wind speed as a function of time
Mean observed wind direction	RMSE, RMSE _s , and RMSE _u errors as a function of time
Mean predicted wind direction	Index of Agreement as a function of time
Standard deviation of observed wind speeds	Surface wind vector plots of modeled and observed winds every 3-hrs
Standard deviation of predicted wind speeds	
Standard deviation of observed wind directions	
Standard deviation of predicted wind directions	
Total RMSE error in wind speeds	
Systematic RMSE error in wind speeds	
Unsystematic RMSE error in wind speeds	
Index of Agreement (I) in wind speeds	
SKILL _E skill scores for surface wind speeds	
SKILL _{var} skill scores for surface wind speeds	
<i>Surface Temperatures (°C)</i>	
Maximum region-wide observed surface temperature	Normalized bias in surface temperature estimates as a function of time
Maximum region-wide predicted surface temperature	Normalized error in surface temperature estimated as a function of time
Normalized bias in hourly surface temperature	Scatter plot of hourly observed and modeled surface temperatures
Mean bias in hourly surface temperature	Scatter Plot of daily maximum observed and modeled surface temperatures
Normalized gross error in hourly surface temperature	Standard deviation of modeled and observed surface temperatures as a function of time
Mean gross error in hourly surface temperature	Spatial mean of hourly modeled and observed surface temperatures as a function of time
Average accuracy of daily maximum temperature estimates over all stations	Isopleths of hourly ground level temperatures every 3-hr
Variance in hourly temperature estimates	Time series of modeled and observed hourly temperatures as selected stations
<i>Surface Mixing Ratio (gm/Kg)</i>	
Maximum region-wide observed mixing ratio	Normalized bias in surface mixing ratio estimates as a function of time
Maximum region-wide predicted mixing ratio	Normalized error in surface mixing ratio estimates as a function of time
Normalized bias in hourly mixing ratio	Scatter Plot of hourly observed and modeled surface mixing ratios
Mean bias in hourly mixing ratio	Scatter Plot of daily maximum observed and modeled surface mixing ratios
Normalized gross error in hourly mixing ratio	Standard deviation of modeled and observed surface mixing ratios as a function of time
Mean gross error in hourly mixing ratio	Spatial mean of hourly modeled and observed surface mixing ratios as a function of time
Average accuracy of daily maximum mixing ratio	Isopleths of hourly ground level mixing ratios every 3-hr
Variance in hourly mixing ratio estimates	Time series of modeled and observed hourly mixing ratios at selected stations

Table 5-2. Statistical Measures and Graphical Displays Used in the RAMS Operational Evaluation of Aloft Meteorological Variables

Statistical Measure	Graphical Display
<i>Aloft Winds (ms⁻¹)</i>	
Vertically averaged mean observed wind speed aloft for each sounding	Vertical profiles of modeled and observed horizontal winds at each sounding location
Vector averaged mean predicted wind speed aloft for each sounding	
Vertically averaged mean observed wind direction aloft for each sounding	
Vertically averaged mean predicted wind direction aloft for each sounding	
<i>Aloft Temperatures (°C)</i>	
Vertically averaged mean temperature observations aloft for each sounding	Vertical profiles of modeled and observed temperatures at each sounding location
Vertically averaged mean temperature predictions aloft for each sounding	
<i>Aloft Mixing Ratio (gm/Kg)</i>	
Vertically averaged mean mixing ratio observations aloft for each sounding	Vertical profiles of modeled and observed mixing ratios at each sounding location
Vertically averaged mean mixing ratio predictions aloft for each sounding	

6.0 EVALUATION OF SURFACE METEOROLOGICAL FIELDS

There is a variety of methods that can be used to evaluate the performance of meteorological modeling. Besides the statistical measures described in section 5, there are different ways of manipulating both model results and observations for direct comparison between them. Therefore, it is not surprising, with two groups doing the meteorological simulations for SAMI, that each shared some common evaluation elements while also having preferences for somewhat different approaches. This section describes the performance evaluations for each episode. Similarities and differences in techniques are highlighted, where appropriate. Note that differences in techniques are more a matter of preference than correctness. Each technique requires some assumptions that influence the outcome. It is possible, by using a variety of approaches, to look at model performance from different viewpoints and gain a clearer understanding of the results.

Both sets of modeling episodes were evaluated by focusing primarily on model performance for the 12-km grid. In addition, both approaches computed bias, relative error, root mean square error, and index of agreement for temperature, wind speed and direction, water vapor mixing ratio and precipitation. Both approaches also examined model performance using measurements made near the surface (section 6) and aloft (section 7).

Methodological differences were mainly due to the emphasis on analyzing a variety of residual measures (i.e. differences between predictions and observations at discrete monitoring locations) for the April 1995, June 1992 and August 1993 episodes (the so-called Alpine Geophysics, or AG, episodes), while for the other (so-called University of Alabama in Huntsville, or UAH) episodes more emphasis was placed on the computation of spatial biases and comparisons between the model and measurements for two ground stations near GSM and SNP. In addition, surface statistical results for the AG episodes were computed by comparing model results for the lowest level directly with surface observations. Surface observations were not measured at the exact same heights above ground as the corresponding model level, so some differences between model and observation are caused by the height difference. For the UAH episodes the model-to-observation comparisons were done by vertically interpolating, using similarity theory, model parameters to match the measurement heights. This reduces bias for these comparisons in many situations, but can also introduce bias under certain conditions. Likewise, the computation of spatial differences in modeled fields done for the UAH episodes provides a picture of model performance that is easy to understand, but it is complicated by the fact that observations must be spatially interpolated for comparison with model results across all portions of the grid. The AG method for spatial comparison is more straightforward and does not rely on spatial interpolation assumptions, but results are somewhat more difficult to visualize. Therefore, no “perfect” system for model evaluation exists, but the techniques used by UAH and AG are complementary and comprehensive. *Section 8 provides an analysis of RAMS performance across all SAMI modeling episodes using a common set of performance metrics.*

However, one important aspect of the meteorological modeling that was not assessed was the simulation of cloud cover. Clouds play important roles in controlling the surface energy balance, vertical long- and short-wave radiation fluxes (the latter influencing photochemical reaction rates), precipitation formation and heterogeneous chemical reactions. Although no formal attempt was made to determine the success of cloud modeling, a simple comparison was made between cloud cover observations at two NWS sites near the

GSM (Knoxville and Asheville) and cloud cover as expressed in the URM-1ATM by cloud information passed to it from RAMS. This comparison, done for the April 1995 and June 1992 episodes, revealed that the cloud cover (expressed as fractional cloud cover) in URM-1ATM was far less than observed. There is insufficient information to draw conclusions, but it should be noted that, for episodes experiencing extensive cloud cover, an underestimation bias could contribute to biases in simulated near-surface air temperature (underestimates at night and overestimates during the day), wind speed, wind direction, and even to some extent water vapor mixing ratio. In addition, insufficient clouds would likely lead to an under-representation of heterogeneous chemical processes such as the aqueous phase oxidation of sulfur dioxide to sulfate in cloud water.

6.1 11-19 July 1995 Episode Results

Verification of the UAH episodes was done with respect to the eastern portions of the coarse grid (48-km for the July 1995 episode, 96-km for all the rest) and the 12-km grid. Unless otherwise noted the entire simulation was used, including the so-called "ramp-up days". The verification tools for the coarse grid were horizontal plots of the bias and the root mean square error (RMSE) statistics for temperature and water vapor mixing ratio at 2 m, and for wind direction and wind speed at 10 m. Horizontal plots were also presented of the total model and observed precipitation on the coarse grid. The bias and RMSE are defined by 6.1-6.4

$$(6.1) \quad BIAS = \frac{1}{n} \sum_{i=1}^n (A_m - A_c),$$

$$(6.2) \quad BIAS = \frac{100}{n} \sum_{i=1}^n \left(\frac{A_m - A_c}{A_c} \right)$$

$$(6.3) \quad RMSE = \frac{1}{n} \sqrt{\sum_{i=1}^n (A_m - A_c)^2},$$

$$(6.4) \quad RMSE = \frac{100}{n} \sqrt{\sum_{i=1}^n \left(\frac{A_m - A_c}{A_c} \right)^2},$$

where n is the number of comparison times, A_m is the model value of the variable "A", and A_c is the comparison value for the same variable. Equations (6.2) and (6.4) express the bias and RMSE, respectively, as a percentage of the comparison values. Unless otherwise noted, all hours of an episode will comprise the number of comparison times. For the coarse grid the comparison values are obtained by using a Barnes (1973) analysis (as discussed in section 3.2) of NWS hourly observations which gives an observed analysis on the same grid as the model coarse grid. One important note must be made about such an observed analysis: it is not an accurate indication of actual conditions in high terrain areas because the

observations are almost entirely made from locations outside the mountainous areas. For example, if the model is performing correctly in situations where the temperatures are decreasing with height, then there will be a cool "bias" over high terrain areas. For the 12-km verifications the model values are bi-linearly interpolated to an observation site (usually Knoxville, Tennessee or Charlottesville, Virginia) and the comparison values are the actual reported station values.

Two other verification tools were used for precipitation. One was to interpolate the model 12-km 24-hour precipitation amounts to rain gauge positions at GSM and SNP. The other used the 12-km 6-hour model precipitation amounts interpolated to all available NWS sites within the 12-km domain. These values are then used to calculate rainfall statistics as described by McBride and Ebert (2000) and Schaeffer (1990) which all use the contingency table categories shown in Table 6-1. The categories of correct no-rain forecasts, false alarms, misses, and hits are denoted by Z, F, M, and H, respectively.

Table 6-1. Contingency table categories used for comparing 12-km 6-hour model precipitation with 6-hour observed values at National Weather Service site locations. Terminology taken from McBride and Ebert (2000)		
	Predicted	
Observed	No Rain	Rain
No Rain	Z	F
Rain	M	H

$$(6.5) \quad PBIAS = \frac{F + H}{M + H}$$

$$(6.6) \quad POD = \frac{H}{M + H}$$

$$(6.7) \quad FAR = \frac{F}{F + H}$$

$$(6.8) \quad ANR = \frac{Z}{Z + F}$$

$$(6.9) \quad HK = POD + ANR - 1$$

$$(6.10) \quad ET = \frac{HZ - MF}{(M + F)(H + M + F + Z) + (HZ - MF)}$$

Each of the precipitation statistics will be calculated for thresholds of 0.2, 2, 5, 10, 15, 25, 35, 50, and 75 mm with respect to the observed 6-hour amounts. The precipitation bias (PBIAS) as defined by (6.5) is the total number of model forecasts of precipitation divided by the total number of observed precipitation events. The precipitation probability of detection (POD) given by (6.6) is the total number of correct model

forecasts of precipitation divided by the total number of observed precipitation events. The precipitation false alarm ratio (FAR) defined by (6.7) is the total number of times of model predictions of precipitation when there was none observed divided by the total number of model forecasts of precipitation. The accuracy for non-rain events (ANR) given by (6.8) is the total number of correct model forecasts of no precipitation divided by the total number of observed no precipitation events. The Hanssen-Kuipers score (HK) described by (6.9) is a composite of the POD and ANR and has a range of ± 1 . Schaeffer (1990) originally introduced a modified critical success index which has become known as the equitable threat score (ET) and is defined by (6.10). It has a range of +1.0 to -1/3. The correct way to verify model grid precipitation forecasts with observations is to have observations of enough density to create an observed analysis on the same grid mesh as the model. That was outside the scope of this report so model values are essentially being compared against point measurements. Apart from model precipitation errors this implies that the model will have a low bias on larger observed thresholds which will be especially true when the precipitation is predominately convective in nature.

6.1.1 48-km Results

Figure 6-1 shows the bias and RMSE of temperatures at 2-m for the 48-km grid using hourly data for the entire episode. The immediate SAMI region away from the Appalachian mountains generally had bias values of $\pm 1^\circ\text{C}$ but with a warm bias of $+2^\circ\text{C}$ and higher over the Ohio valley and northwestward to the northern Plains and southward to the Gulf coast. The RMSE for temperature was generally 3°C or less in most places. In Figure 6-2 the bias and RMSE of the water vapor mixing ratio at 2-m are expressed as a percentage of the observed values. A definite dry bias is observed with a large area of the eastern United States having values of 5-15 % below observed values. This was mainly due to the difficulties of specifying the RAMS soil moisture which was discussed in section 2.4.1. The water vapor bias patterns explain much of the temperature bias. Where the near-surface mixing ratio is too dry are the same areas with a warm bias and conversely. An example of the latter is over central Georgia where temperatures were cooler than observed and the surface moisture was too wet. The RMSE values for the mixing ratio were generally in the range of 10-20 % of the observed values. GIT was able to use this episode in the Air Quality Modeling phase by utilizing a boundary layer correction file for the water vapor mixing ratios. This did not change the model precipitation or the cloud water values but did improve the water vapor values in the lowest layers. The wind speed bias and RMSE at the level of 10 m in Figure 6-3 show bias values generally in the $\pm 0.5 \text{ m s}^{-1}$ range and RMSE values around 1 m s^{-1} . The large bias values over Maine in Figure 6-3 may be due to boundary problems or some other reason. The wind direction bias in Figure 6-4 is generally in the range of ± 10 degrees, while the wind direction RMSE approaches 90° over a large area of the Southeast. One reason for this is that in light wind conditions such as this episode the observed winds are dominated by local terrain effects which can not be duplicated on model grids even at the 12-km resolution. The comparison of the total model precipitation with the total observed for the episode is given by Figure 6-5 which confirms the dry bias observed in the near-surface mixing ratio values. The most extreme dryness in model precipitation was observed over the Kansas-Missouri area and over the Gulf Coast.

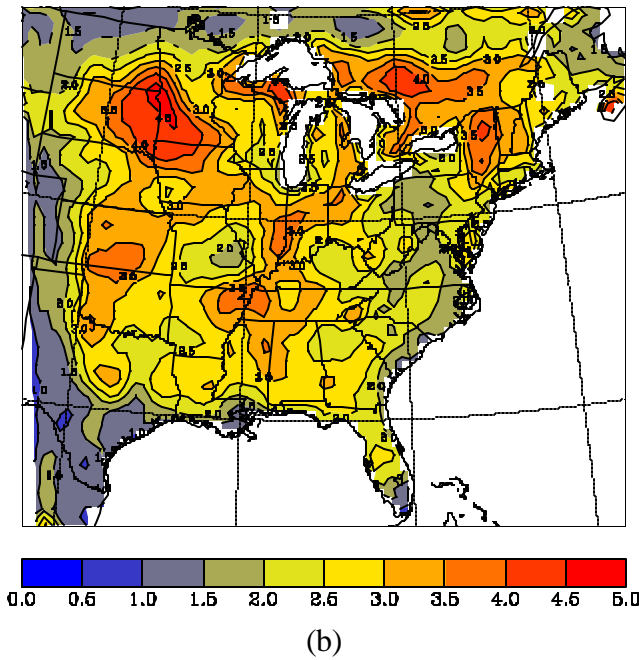
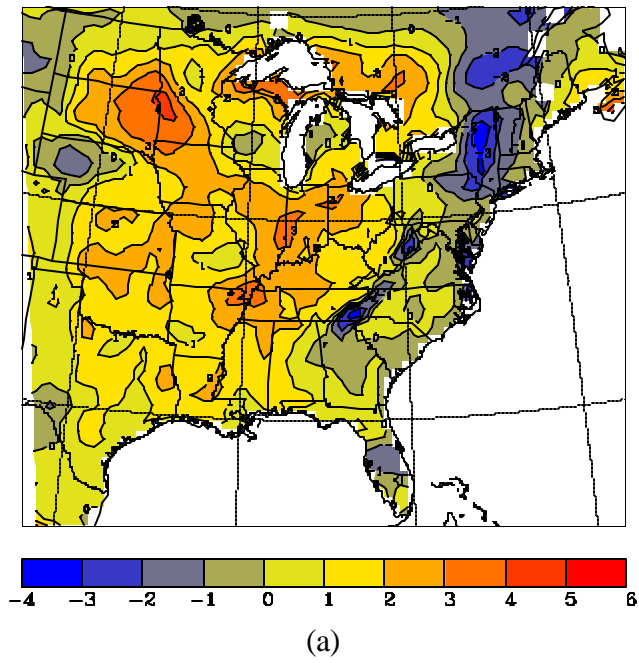
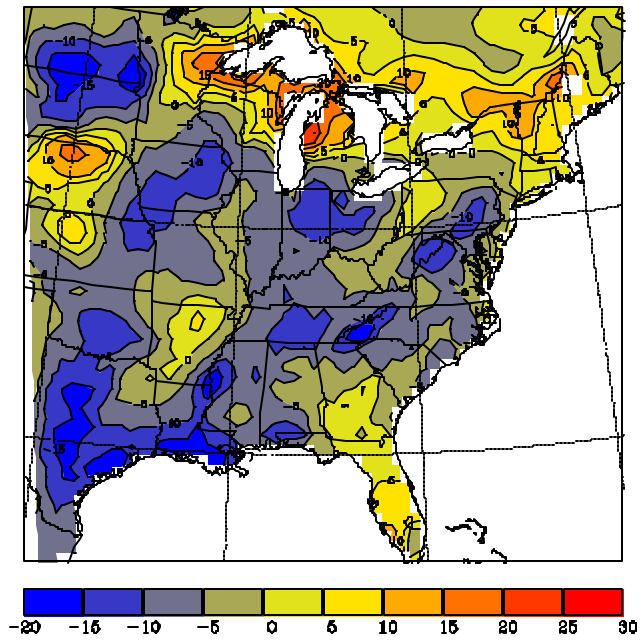
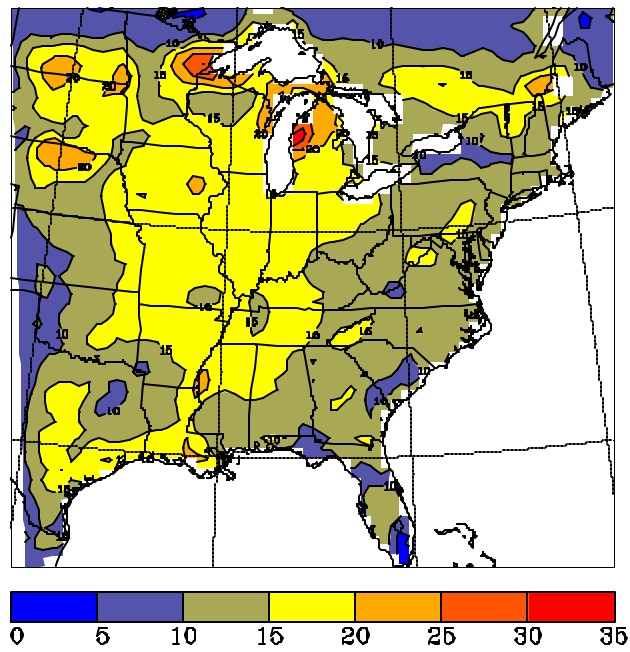


Figure 6-1. (a) Bias of the model minus the observed temperature at 2 m in degrees Celsius for the July 1995 episode for the 48-km grid. (b) Root mean square error (RMSE) of the same field for the same time and grid.

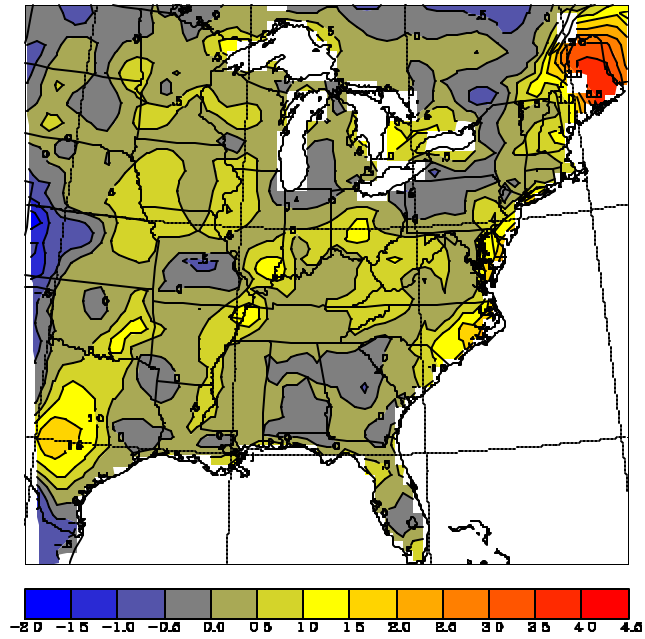


(a)

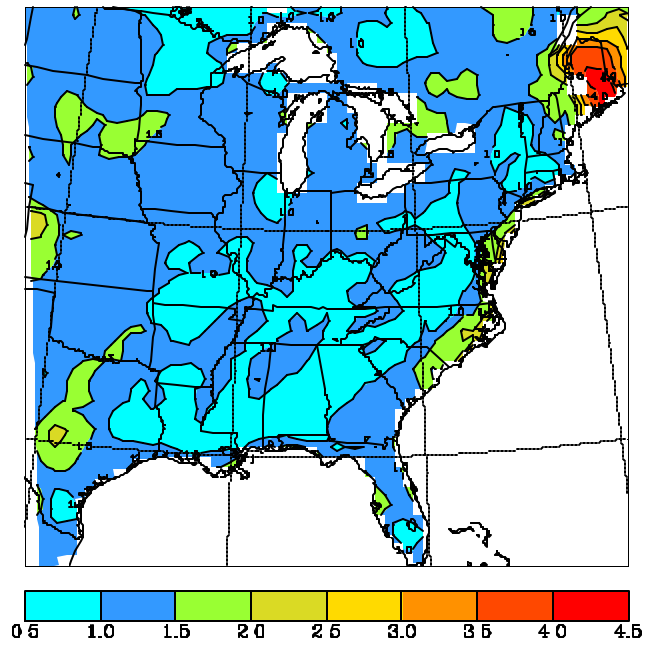


(b)

Figure 6-2. (a) Bias of the model minus the observed water vapor mixing ratio at 2 for the July 1995 episode for the 48-km grid. (b) Root mean square error (RMSE) of the same field for the same time and grid. The bias and RMSE are expressed as a percentage of the observed value.

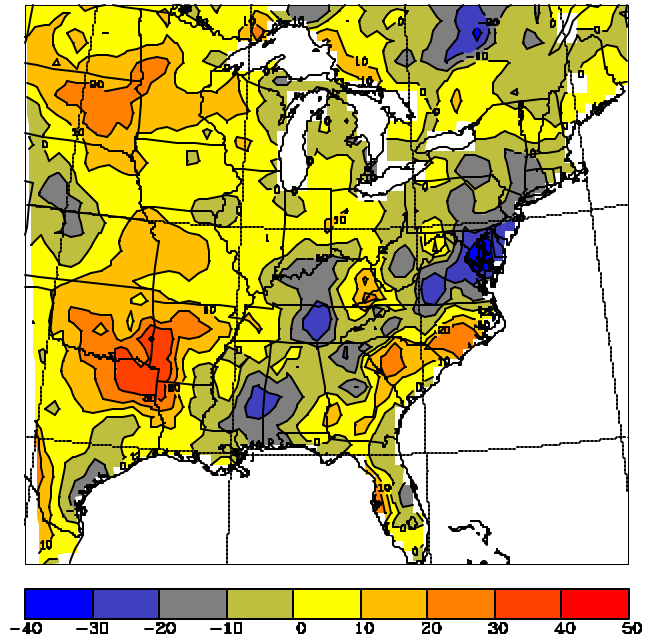


(a)

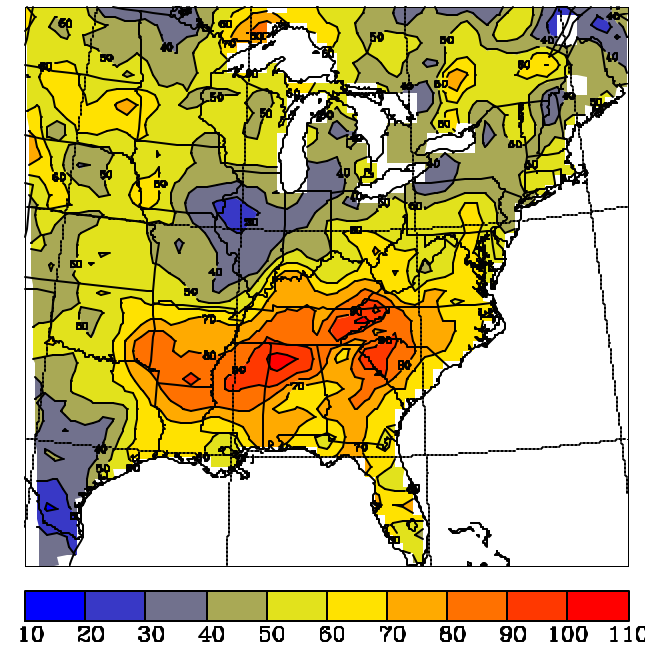


(b)

Figure 6-3. (a) Bias of the model minus the observed wind speed at 10 m in m s^{-1} for the July 1995 episode for the 48-km grid. (b) Root mean square error (RMSE) of the same field for the same time and grid.

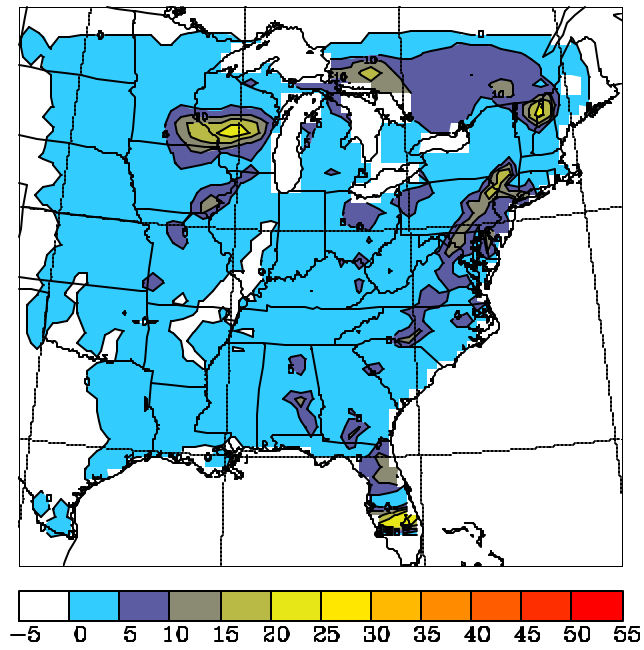


(a)

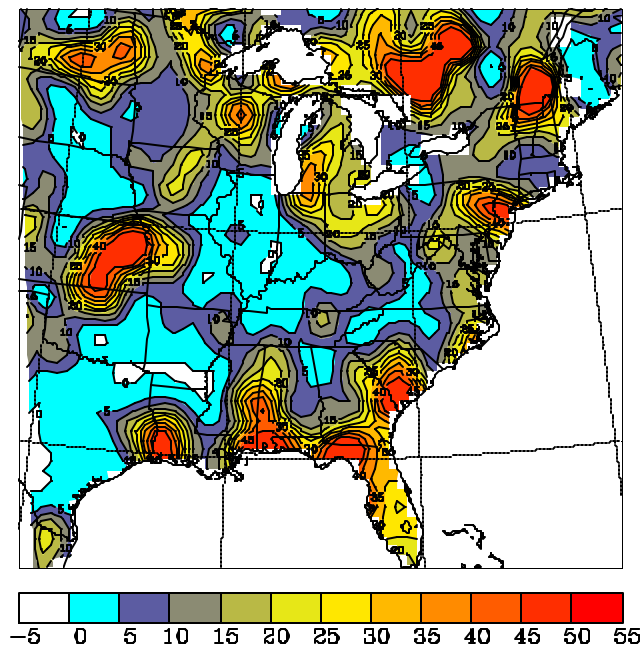


(b)

Figure 6-4. (a) Bias of the model minus the observed wind direction at 10 m in degrees for the July 1995 episode for the 48-km grid. (b) Root mean square error (RMSE) of the same field for the same time and grid.



(a)



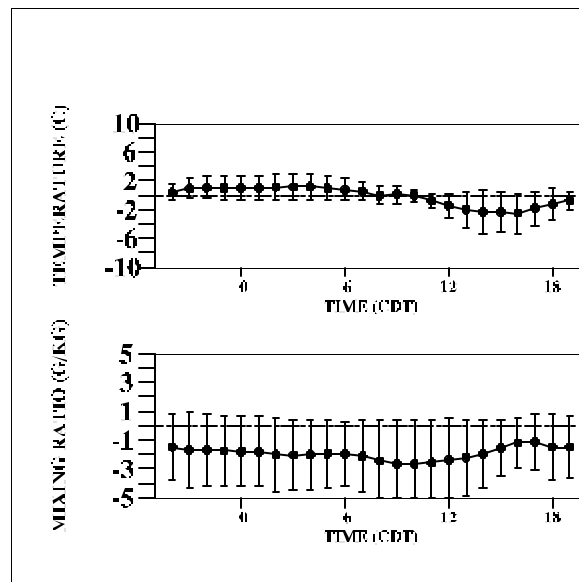
(b)

Figure 6.5. (a) Model precipitation in mm for the entire July 1995 episode for the 48-km grid. (b) Analysis of observed total precipitation for the same period for the 48-km grid. Analyzed values in excess of 50 mm have been truncated to 50 mm.

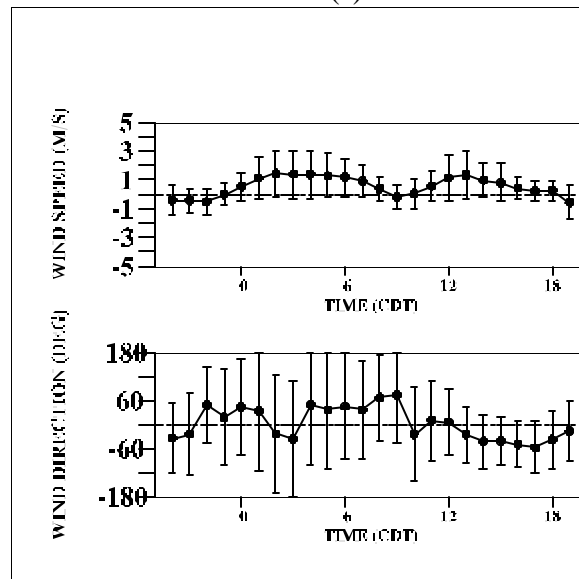
6.1.2 12-km Results

Figure 6-6 shows the bias and RMSE for the near-surface variables for Knoxville, Tennessee for the July 1995 episode for the 12-km grid. Nighttime temperatures at 2 m had a bias on the order of $+1^{\circ}\text{C}$ and a minimum cool bias of about -2°C in the afternoon. RMSE values were near 2°C at night and approached 3°C in the afternoon. The mixing ratio at 2 m had a dry bias at all hours of around -1 to -2 g kg^{-1} and RMSE values of around 2 g kg^{-1} . The wind speed bias at 10 m was generally positive with the largest values of $+1$ to $+2\text{ m s}^{-1}$ occurring after midnight and around noon. RMSE values for wind speed were largest at night with values around 2 m s^{-1} . The wind direction bias at 10 m had less of an overall pattern with values of ± 60 degrees and with perhaps a consistent negative bias in the afternoon hours. RMSE values for the wind direction were largest at night with values approaching 180 degrees. Some of these large values are reflective of very light or calm wind conditions. Figure 6-7 shows the same variables for Staunton, Virginia which was used in place of Charlottesville, Virginia because of large segments of missing data. The overall patterns were very similar to Knoxville with the exception of smaller wind speed RMSE at 10 m.

Table 6-2 compares the 24-h 12-km precipitation with the daily rain gauge values at GSM and SNP. Model values were reasonable at the Elkmont and Big Meadows sites but the model missed the large values at the Look Rock site at GSM. Table 6-3 gives the rainfall statistics for all the NWS sites within the 12-km domain for the entire episode. The dry bias is clearly evident with all measures of skill having poor values for thresholds of 5 mm and above.

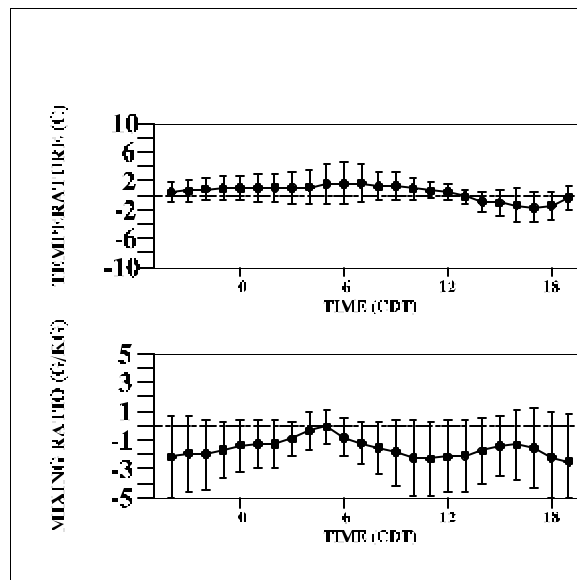


(a)

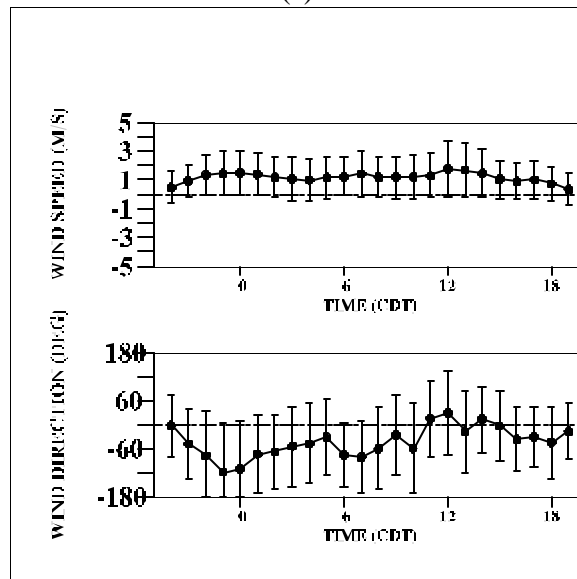


(b)

Figure 6-6. Diurnal time series of bias (solid dots) and root mean square error (vertical bars with horizontal hash marks) for the model minus the station observation for Knoxville, Tennessee for the period 1200 UTC 9 July - 1200 UTC 20 July 1995. Model values are obtained by horizontal interpolation of the hourly 12-km gridpoint values to the observation site. Time (CDT) is plotted on the horizontal axis. (a) Top plot is for temperature at 2 m in °C while the bottom plot is for water vapor mixing ratio at 2 m in g kg^{-1} . (b) Top plot is for wind speed at 10 m in m s^{-1} while the bottom plot is for wind direction at 10 m in degrees.



(a)



(b)

Figure 6-7. Diurnal time series of bias (solid dots) and root mean square error (vertical bars with horizontal hash marks) for the model minus the station observation for Staunton, Virginia for the period 1200 UTC 9 July - 1200 UTC 20 July 1995. Model values are obtained by horizontal interpolation of the hourly 12-km gridpoint values to the observation site. Time (CDT) is plotted on the horizontal axis. (a) Top plot is for temperature at 2 m in $^{\circ}\text{C}$ while the bottom plot is for water vapor mixing ratio at 2 m in g kg^{-1} . (b) Top plot is for wind speed at 10 m in m s^{-1} while the bottom plot is for wind direction at 10 m in degrees.

Table 6-2. Midnight to midnight 24-h precipitation values in inches for the period 11-19 July 1995. The Look Rock site is within the Great Smoky Mountain National Park while the Big Meadows site is within the Shenandoah National Park. Model values at the two observation sites were obtained by linear horizontal interpolation of the 12-km gridpoint data.

Day	Look Rock Observed	Look Rock Model	Elkmont Observed	Elkmont Model	Big Meadows Observed	Big Meadows Model
11	0.00	0.00	0.00	0.00	0.00	0.00
12	0.00	0.00	0.00	0.00	0.00	0.00
13	0.00	0.00	0.00	0.00	0.00	0.00
14	0.02	0.00	0.00	0.00	0.00	0.00
15	0.21	0.01	0.00	0.00	0.00	0.00
16	0.92	0.04	0.01	0.03	0.00	0.00
17	1.00	0.10	0.02	0.08	0.12	0.06
18	0.00	0.03	0.00	0.02	0.00	0.04
19	0.00	0.01	0.00	0.00	0.00	0.06
TOTAL	2.15	0.19	0.03	0.13	0.12	0.16

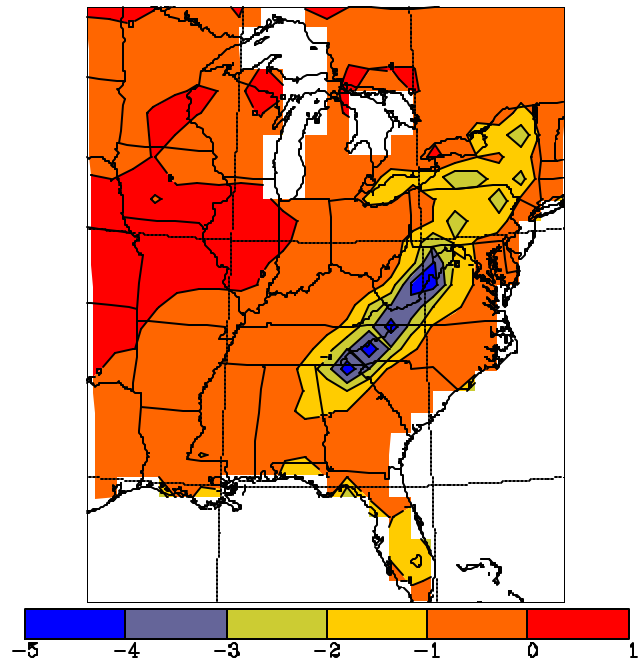
Table 6-3. Rainfall statistics for various thresholds for 6-hour model precipitation from the 12-km grid compared against 6-hour observed values at all National Weather Service sites within the 12-km grid for the July 1995 episode. Statistic abbreviations and definitions are described in the text. Categories with -99 are those where model data did not exist for a calculation. The row labeled "OBS EVENTS" is the sum of all non-zero precipitation 6-hour events across all observation sites for each threshold.

STATISTIC	THRESHOLD (mm)								
	0.2	2	5	10	15	25	35	50	75
BIAS	1.9802	0.2018	0.0247	0	0	0	0	0	-99
POD	0.2129	0.0263	0	0	0	0	0	0	-99
FAR	0.8925	0.8696	1	-99	-99	-99	-99	-99	-99
ANR	0.9303	0.9962	0.9996	1	1	1	1	1	1
HK	0.1432	0.0225	-0.0004	0	0	0	0	0	-99
ET	0.05	0.02	-0.00	0.00	0.00	0.00	0.00	0.00	-99
OBS EVENTS	202	114	81	48	32	19	7	3	0

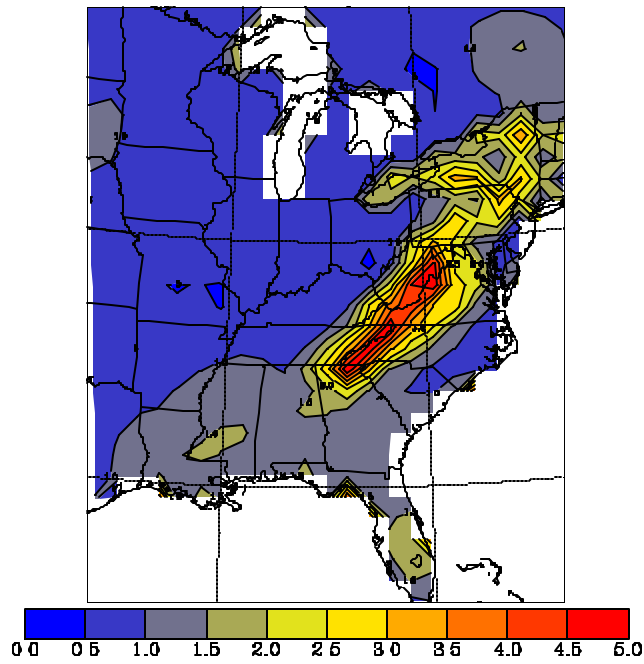
6.2 22-30 May 1995 Episode Results

6.2.1 96-km Results

Figure 6-8 shows the bias and RMSE of 2-m temperatures for the 96-km grid using hourly data for the entire episode. This episode was the first to use the surface nudging technique as described in Section 2.4.2.5. As a result the bias values outside of the immediate SAMI region were $\pm 1^{\circ}\text{C}$ with values approaching -4°C over the higher terrain of the Appalachians. The latter feature was an indication of the model decreasing temperatures with height in areas where the observed analysis was dominated by lower-level observations. RMSE values were generally $0.5\text{-}1.5^{\circ}\text{C}$ in the nudged areas and approached 4.5°C over the higher terrain of the Appalachians. In Figure 6-9 the bias and RMSE of the 2-m water vapor mixing ratio are expressed as a percentage of the observed values. Bias and RMSE values were generally within 2% of the observed values outside of the immediate SAMI region except near the coastlines of the Great Lakes, the Atlantic, and the Gulf of Mexico where the observed analysis is probably inadequate. The 10-m wind speed bias in Figure 6-10 shows errors of $\pm 0.5\text{ m s}^{-1}$ over most of the southeastern United States with larger values over the Great Lakes region and southeastern Canada. The 10-m wind speed RMSE showed a similar pattern with values near 1 m s^{-1} over most of the southeastern United States and with larger values elsewhere. Figure 6-11 shows 10-m wind direction biases generally of $\pm 20^{\circ}$ with the largest magnitudes in the coastal areas of the mid-Atlantic and New England and the central Great Plains. The RMSE wind direction values over the southeastern United States were generally in the range of $40\text{-}60^{\circ}$. This is the result of the Southeast being dominated by surface high pressure and light wind conditions for much of the episode. The model and analyzed observed precipitation for the entire episode for the 96-km grid are presented in Figure 6-12. The model simulation reproduced the large areas of precipitation quite well but over-predicted precipitation in a west-east band extending from Iowa eastward to Pennsylvania.

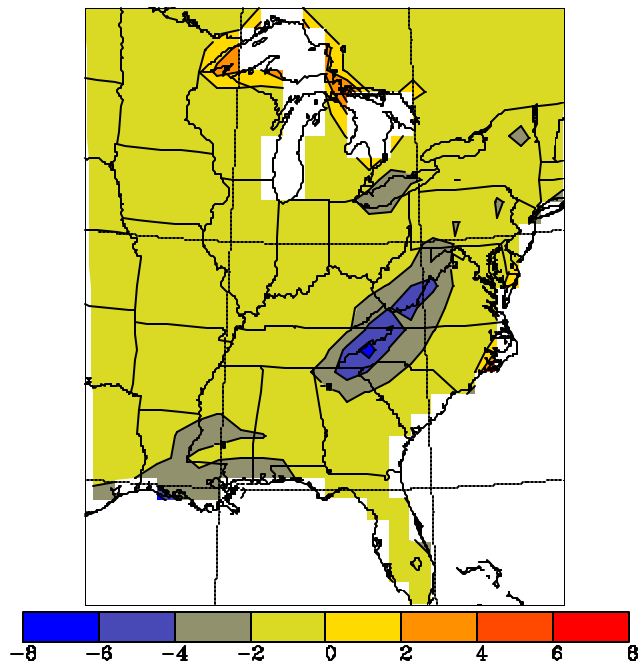


(a)

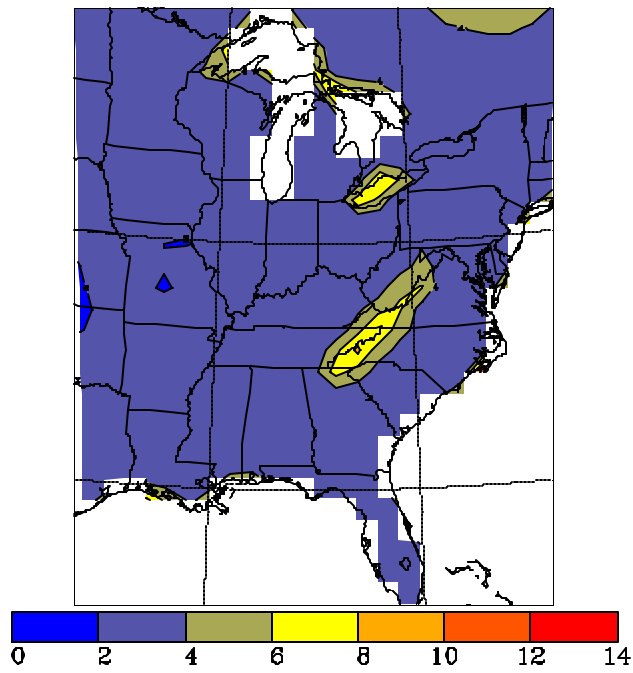


(b)

Figure 6-8. (a) Bias of the model minus the observed temperature at 2 m in degrees Celsius for the May 1995 episode for the 96-km grid. (b) Root mean square error (RMSE) of the same field for the same time and grid.

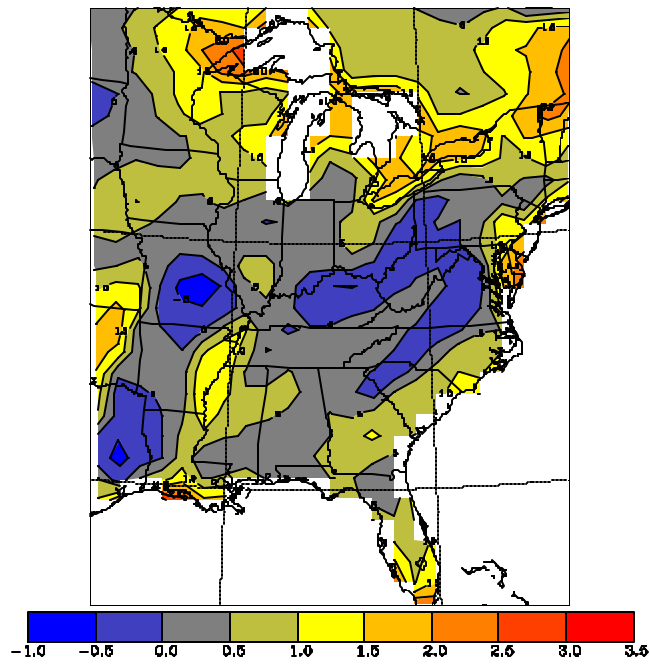


(a)

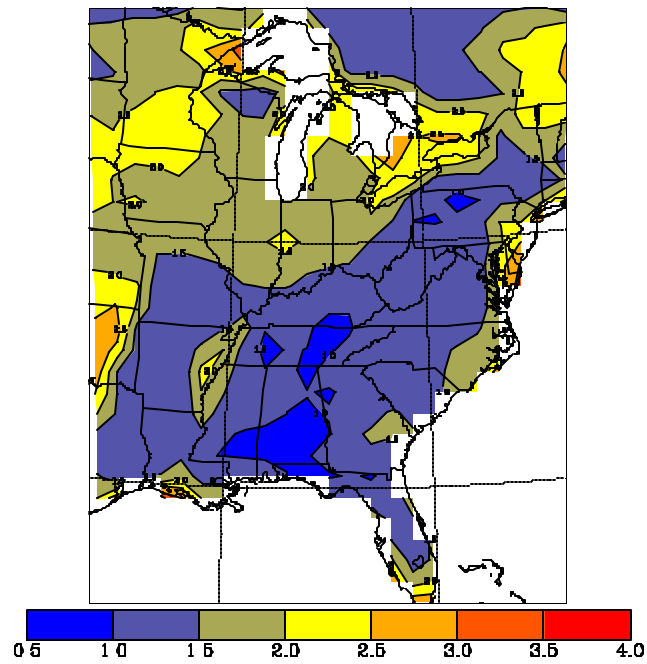


(b)

Figure 6-9. (a) Bias of the model minus the observed water vapor mixing ratio at 2 m for the May 1995 episode for the 96-km grid. (b) Root mean square error (RMSE) of the same field for the same time and grid. The bias and RMSE are expressed as a percentage of the observed value.

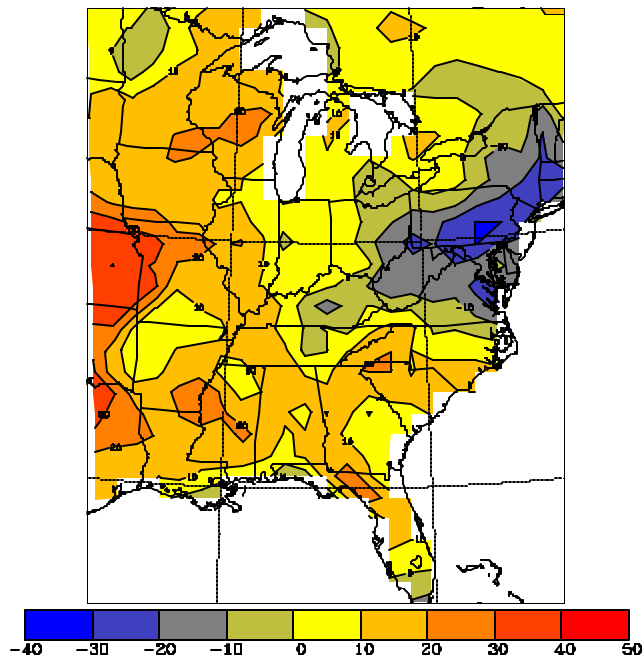


(a)

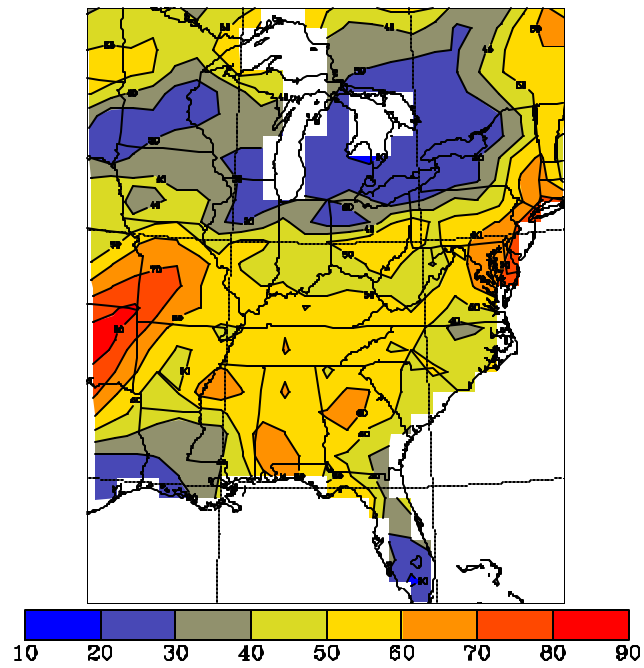


(b)

Figure 6-10. (a) Bias of the model minus the observed wind speed at 10 m in m s^{-1} for the May 1995 episode for the 96-km grid. (b) Root mean square error (RMSE) of the same field for the same time and grid.

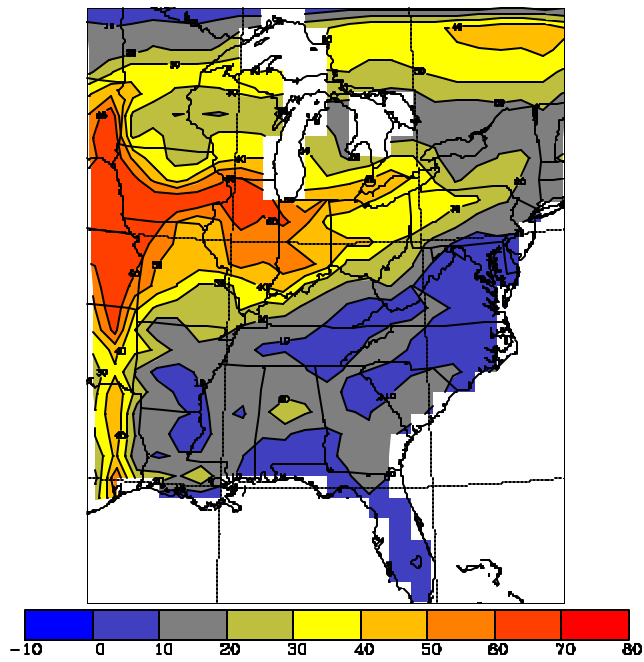


(a)

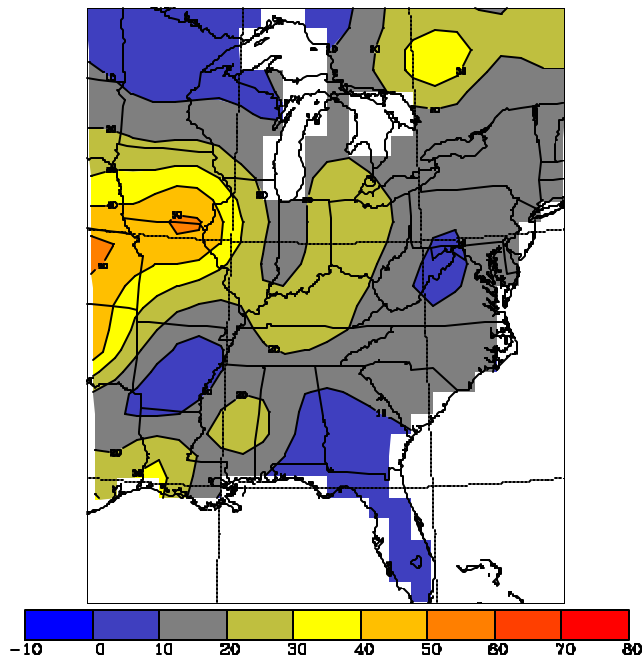


(b)

Figure 6-11. (a) Bias of the model minus the observed wind direction at 10 m in degrees for the May 1995 episode for the 96-km grid. (b) Root mean square error (RMSE) of the same field for the same time and grid.



(a)



(b)

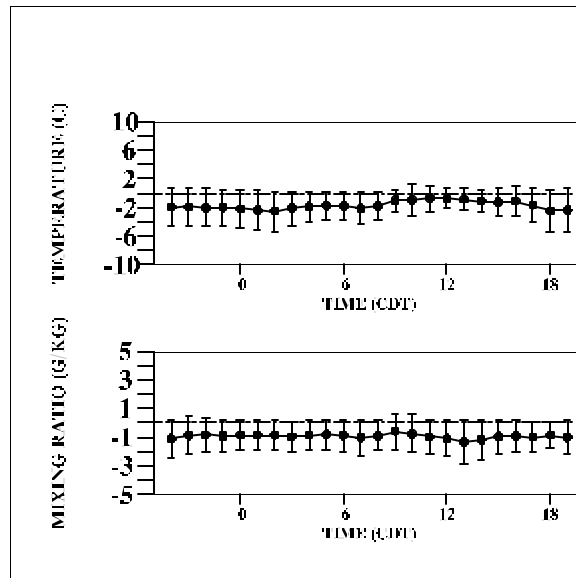
Figure 6-12. (a) Model precipitation in mm for the entire May 1995 episode for the 96-km grid. (b) Analysis of observed total precipitation for the same period for the 96-km grid. Analyzed values in excess of 70 mm have been truncated to 70 mm.

6.2.2 12-km Results

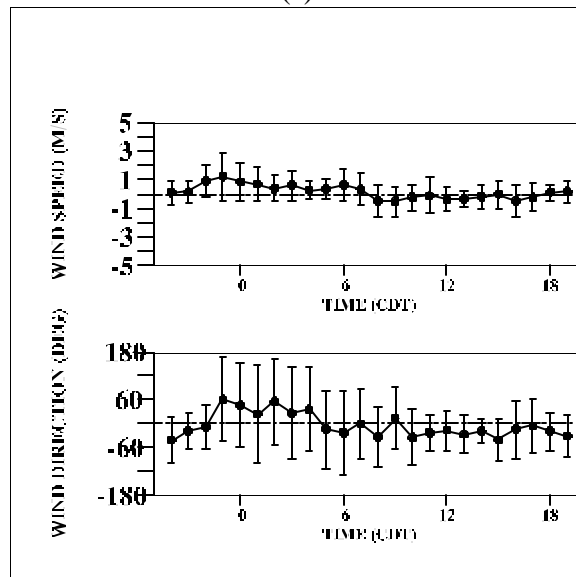
Figure 6-13 shows the bias and RMSE for the near-surface variables for Knoxville, Tennessee for the May 1995 episode for the 12-km grid. For the 2-m temperatures a generally consistent bias of -2°C was evident across the daily period and with RMSE values of $2\text{-}4^{\circ}\text{C}$. A consistent bias was observed as well with the 2-m mixing ratio of -1 g kg^{-1} and with RMSE values of $1\text{-}2\text{ g kg}^{-1}$. The 10-m wind speed bias was near $\pm 0.5\text{ m s}^{-1}$ during the daytime and with a positive values at night which approached 1.5 m s^{-1} . The RMSE values for the wind speed were generally in the range of $1\text{-}2\text{ m s}^{-1}$ across the day. The wind direction bias and RMSE were the largest during the night with magnitudes of 60° and larger. Daytime values of the same quantities were generally less than 60° . The same plots for Staunton, Virginia in Figure 6-14 show similar patterns but with larger values for the bias and RMSE for the temperature and mixing ratio.

Table 6-4 compares the interpolated 12-km daily precipitation with selected rain gauge sites at GSM and SNP. The model episode totals at Look Rock and Elkmont of about 11 and 9 mm, respectively, compared well with the observed values at the same respective sites of 4 and 17 mm. At Big Meadows the model episode total of $\sim 3\text{ mm}$ is much smaller than the observed value of near 52 mm. The observed analyses at 96-km does not show any precipitation of this magnitude so this may have been a more local precipitation event which the model did not simulate.

Table 6-5 gives the rainfall statistics for all the NWS sites within the 12-km domain for the entire episode. The "OBS EVENTS" row indicates that nearly all the 6-h observed amounts were 15 mm or less. Most of the heavy precipitation for this episode was outside of the 12-km domain. The bias values show over-prediction for the thresholds of 2 mm and less and under-prediction of the thresholds of 5 mm and higher. The false alarm ratios were 0.80 or higher for all the thresholds. Inspection of the model and observed 6-h precipitation amounts for the 96-km grid (not shown) indicate a tendency for the model to over-predict the area of light precipitation which explains part of the false alarm ratio patterns.

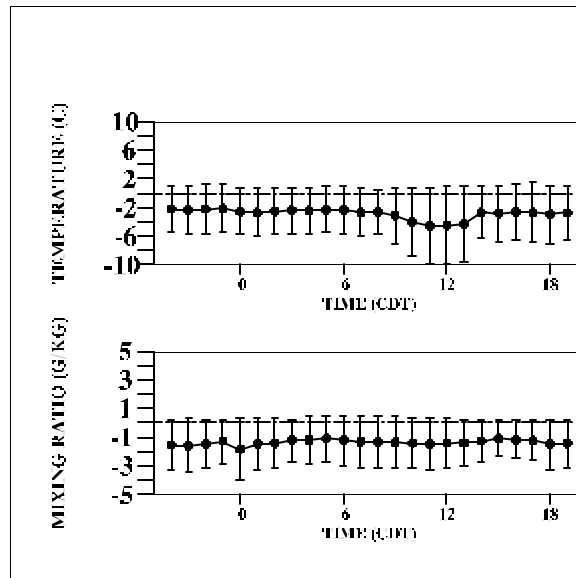


(a)

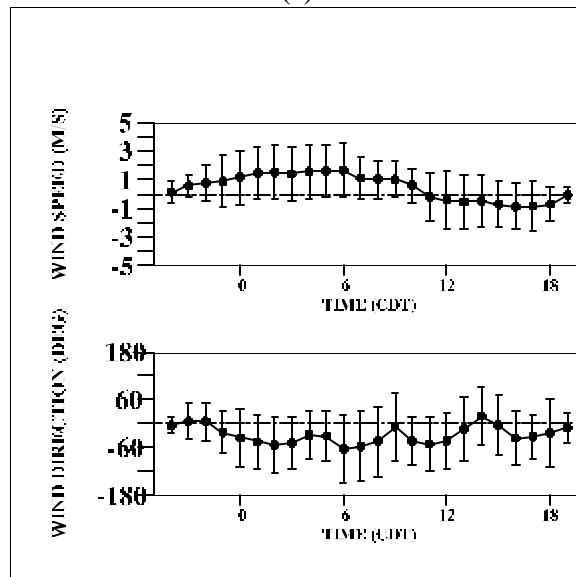


(b)

Figure 6-13. Diurnal time series of bias (solid dots) and root mean square error (vertical bars with horizontal hash marks) for the model minus the station observation for Knoxville, Tennessee for the period 1200 UTC 22 May 1995 to 1200 UTC 30 May 1995. Model values are obtained by horizontal interpolation of the hourly 12-km gridpoint values to the observation site. Time (CDT) is plotted on the horizontal axis. (a) Top plot is for temperature at 2 m in $^{\circ}\text{C}$ while the bottom plot is for water vapor mixing ratio at 2 m in g kg^{-1} . (b) Top plot is for wind speed at 10 m in m s^{-1} while the bottom plot is for wind direction at 10 m in degrees.



(a)



(b)

Figure 6-14. Diurnal time series of bias (solid dots) and root mean square error (vertical bars with horizontal hash marks) for the model minus the station observation for Staunton, Virginia for the period 1200 UTC 22 May 1995 to 1200 UTC 30 May 1995. Model values are obtained by horizontal interpolation of the hourly 12-km gridpoint values to the observation site. Time (CDT) is plotted on the horizontal axis. (a) Top plot is for temperature at 2 m in °C while the bottom plot is for water vapor mixing ratio at 2 m in g kg^{-1} . (b) Top plot is for wind speed at 10 m in m s^{-1} while the bottom plot is for wind direction at 10 m in degrees.

Table 6-4. Midnight to midnight 24-h precipitation values in mm for the period 24-29 May 1995. The Look Rock and Elkmont sites are within the Great Smoky Mountain National Park while the Big Meadows site is within the Shenandoah National Park. Model values at the observation sites were obtained by linear horizontal interpolation of the 12-km gridpoint data.

Day	Look Rock Observed	Look Rock Model	Elkmont Observed	Elkmont Model	Big Meadows Observed	Big Meadows Model
24	0.00	0.00	0.00	0.00	0.00	0.00
25	0.00	2.90	0.00	1.79	44.50	0.80
26	0.00	1.79	0.00	3.63	0.00	1.29
27	0.80	3.88	8.40	1.73	0.00	0.04
28	1.30	0.09	8.40	0.27	6.90	0.98
29	1.50	2.00	0.00	1.81	0.50	0.02
TOTAL	3.60	10.66	16.80	9.23	51.90	3.13

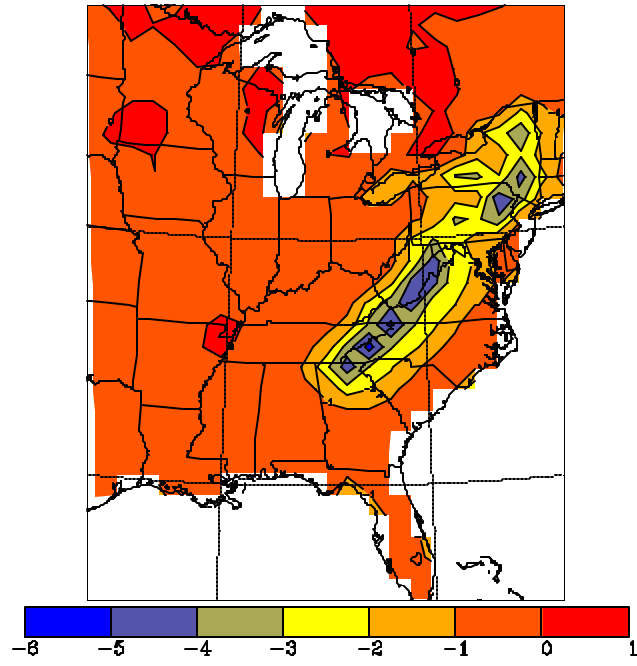
Table 6-5. Rainfall statistics for various thresholds for 6-hour model precipitation from the 12-km grid compared against 6-hour observed values at all National Weather Service sites within the 12-km grid for the May 1995 episode. Statistic abbreviations and definitions are described in the text. Categories with -99 are those where model data did not exist for a calculation. The row labeled "OBS EVENTS" is the sum of all non-zero precipitation 6-hour events across all observation sites for each threshold.

STATISTIC	THRESHOLD (mm)								
	0.2	2	5	10	15	25	35	50	75
BIAS	3.11	1.38	0.56	0.54	0.42	0.25	0.00	0.00	-99.0
POD	0.59	0.23	0.09	0.02	0.00	0.00	0.00	0.00	-99.0
FAR	0.81	0.84	0.84	0.96	1.00	1.00	-99.0	-99.0	-99.0
ANR	0.77	0.94	0.99	0.99	1.00	1.00	1.00	1.00	1.00
HK	0.37	0.17	0.08	0.02	-0.00	-0.00	0.00	0.00	-99.0
ET	0.10	0.08	0.05	0.01	-0.00	-0.00	0.00	0.00	-99
OBS EVENTS	311	176	110	46	19	4	1	1	0

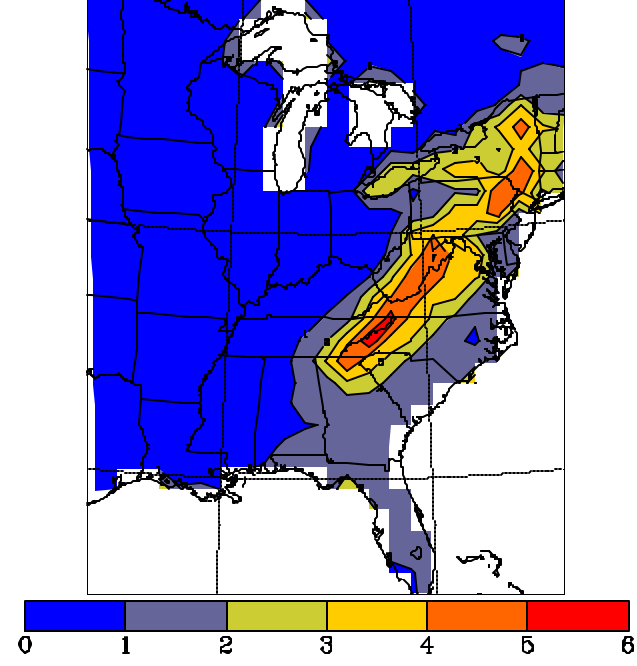
6.3 9-18 May 1993 Episode Results

6.3.1 96-km Results

Figure 6-15 shows the bias and RMSE of 2-m temperatures for the 96-km grid using hourly data for the entire episode. Again, because of the surface nudging technique the bias outside of the immediate SAMI region and higher terrain was $\pm 1^{\circ}\text{C}$. Bias values as large as -5°C were observed over parts of the Appalachians. As mentioned in other episodes the negative bias over higher terrain is an indication of the model being cooler as it should be than the observed analysis which was dominated by sites not in high terrain. The cool bias in lower terrain areas where surface nudging was not performed is, among other things, the result of the inability to specify soil moisture adequately. The RMSE values showed a similar pattern with values of 1°C outside of the immediate SAMI region and values as high as 5°C in higher terrain areas. In Figure 6-16 the bias and RMSE of the 2-m water vapor mixing ratio are expressed as a percentage of the observed values. Bias and RMSE values were generally within 2% of the observed values outside of the immediate SAMI region except near the coastlines of the Great Lakes. The 10-m wind speed bias in Figure 6-17 was generally in the range of $\pm 0.50\text{ m s}^{-1}$ but with values as large as $+2.5\text{ m s}^{-1}$ in southeastern Canada. RMSE values were generally under 2 m s^{-1} over most of the eastern United States. The 10-m wind direction bias in Figure 6-18 was generally in the range ± 10 degrees but with values as large as $+20$ degrees over two regions: one over parts of Oklahoma, Kansas, Arkansas, and Mississippi, and the other over Iowa. RMSE values were generally in a range of 20-50 degrees except for a west-east band of near 60 degrees from eastern Oklahoma northeastward to the Mid-Atlantic. This was coincident with the frontal position which was in that vicinity for much of the week. Winds are typically light near a stationary front and therefore are more difficult to model. The total model and observed precipitation on the 96-km grid are shown in Figure 6-19. The large-scale patterns were reasonably simulated by the model but precipitation was over-predicted along the Ohio River Valley across parts of southern Illinois, Indiana and Ohio and northern Kentucky.



(a)



(b)

Figure 6-15. (a) Bias of the model minus the observed temperature at 2 m in degrees Celsius for the May 1993 episode for the 96-km grid. (b) Root mean square error (RMSE) of the same field for the same time and grid.

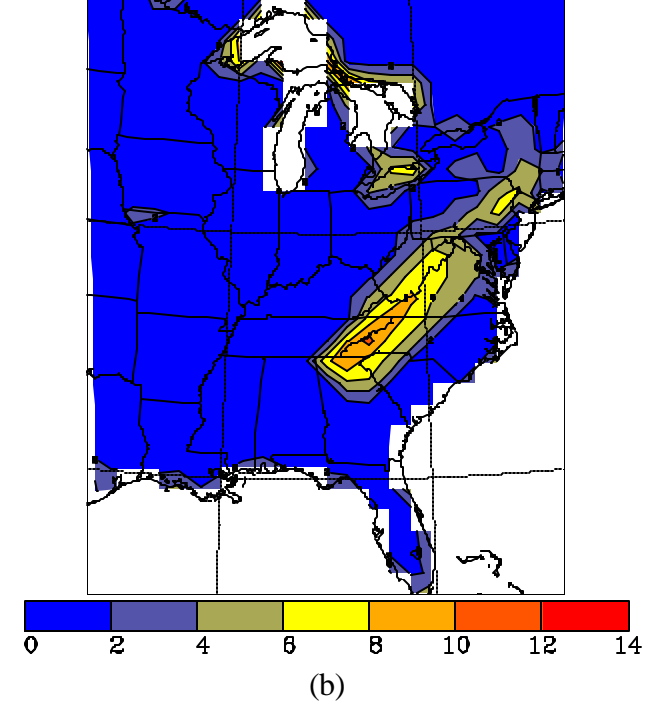
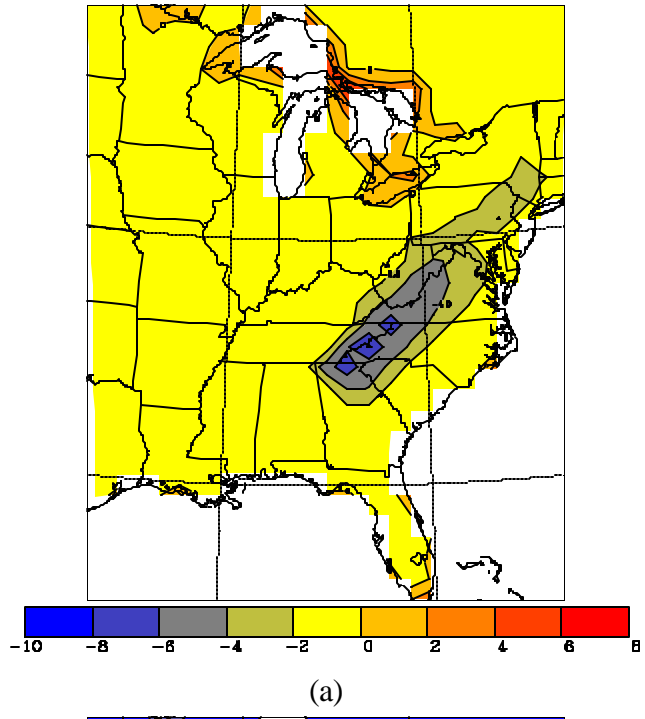
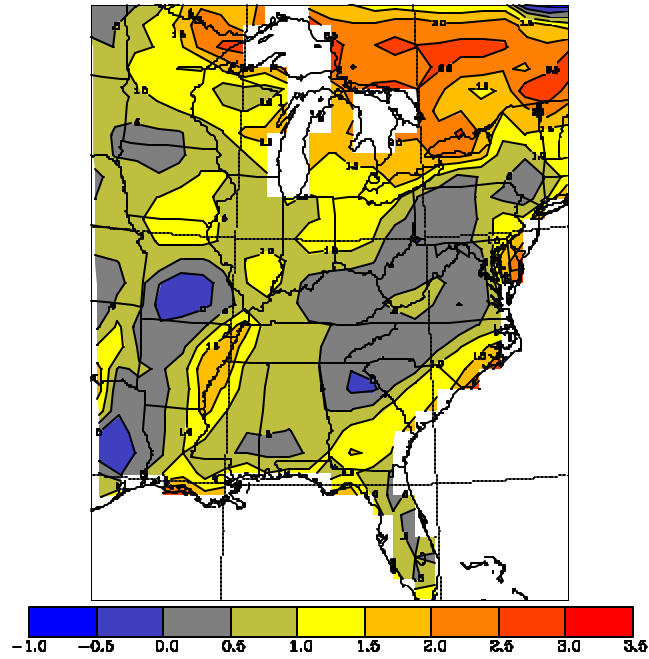
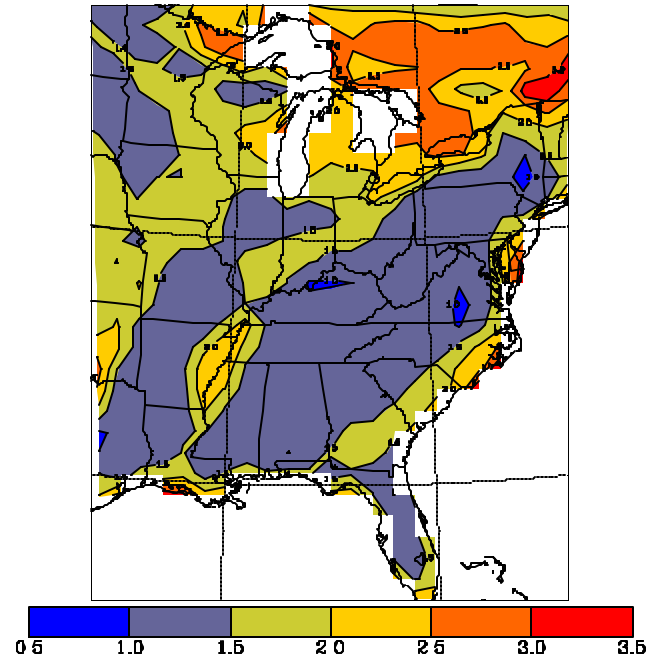


Figure 6-16. (a) Bias of the model minus the observed water vapor mixing ratio at 2 m for the May 1993 episode for the 96-km grid. (b) Root mean square error (RMSE) of the same field for the same time and grid. The bias and RMSE are expressed as a percentage of the observed value.

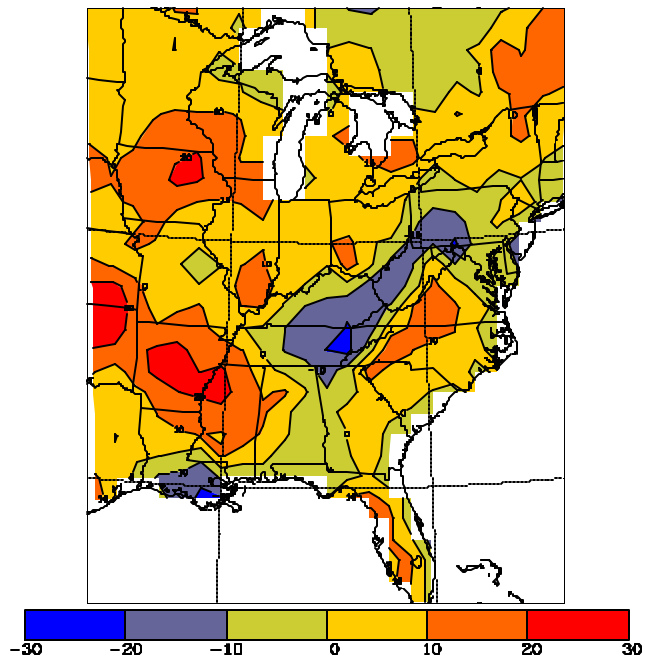


(a)

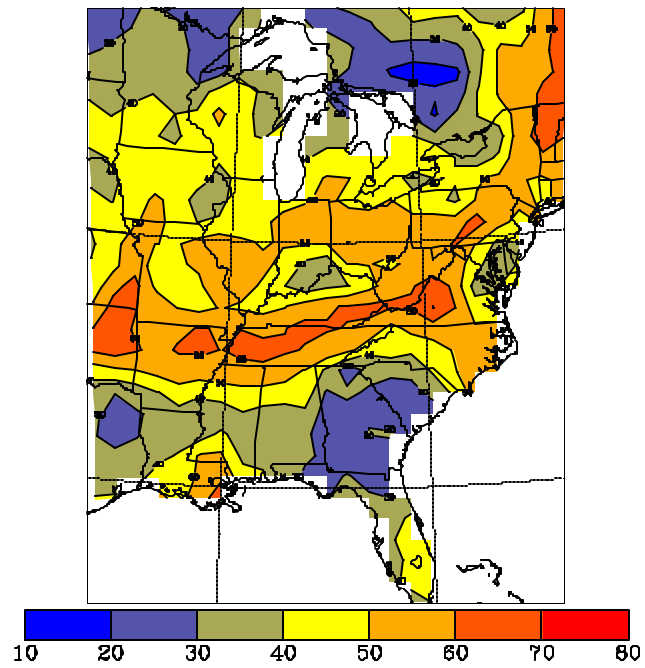


(b)

Figure 6-17. (a) Bias of the model minus the observed wind speed at 10 m in m s^{-1} for the May 1993 episode for the 96-km grid. (b) Root mean square error (RMSE) of the same field for the same time and grid.

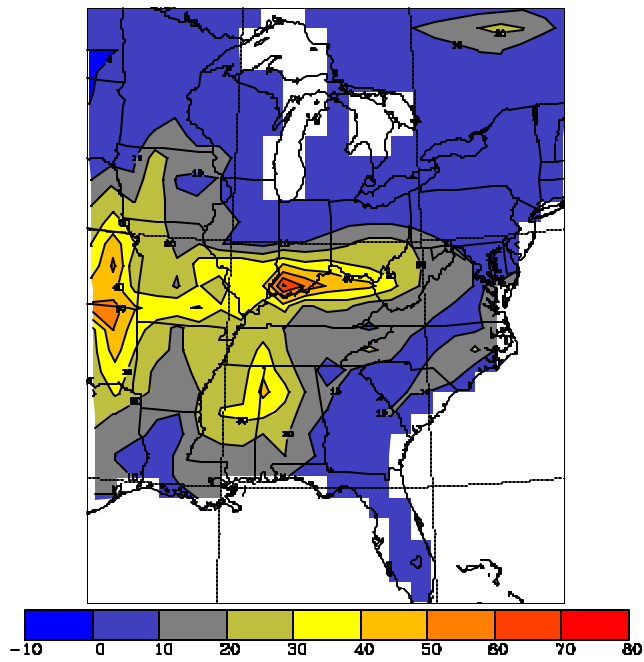


(a)

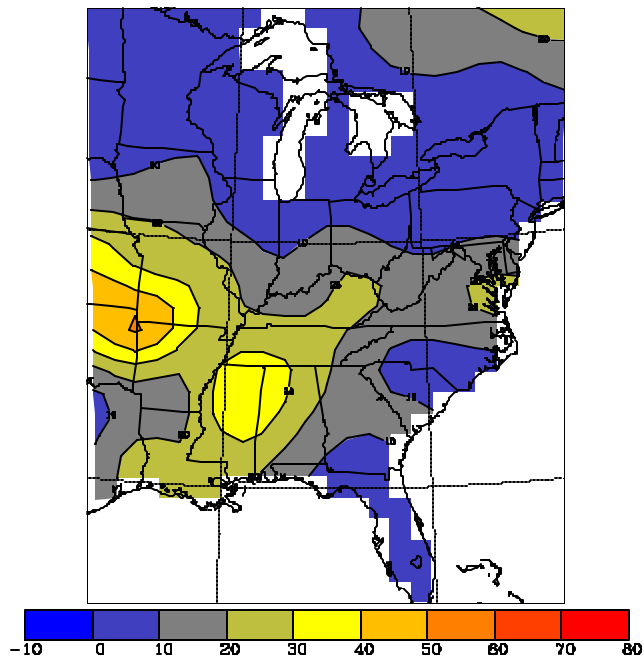


(b)

Figure 6-18. (a) Bias of the model minus the observed wind direction at 10 m in degrees for the May 1993 episode for the 96-km grid. (b) Root mean square error (RMSE) of the same field for the same time and grid.



(a)



(b)

Figure 6-19. (a) Model precipitation in mm for the entire May 1993 episode for the 96-km grid. (b) Analysis of observed total precipitation for the same period for the 96-km grid. Analyzed values in excess of 70 mm have been truncated to 70 mm.

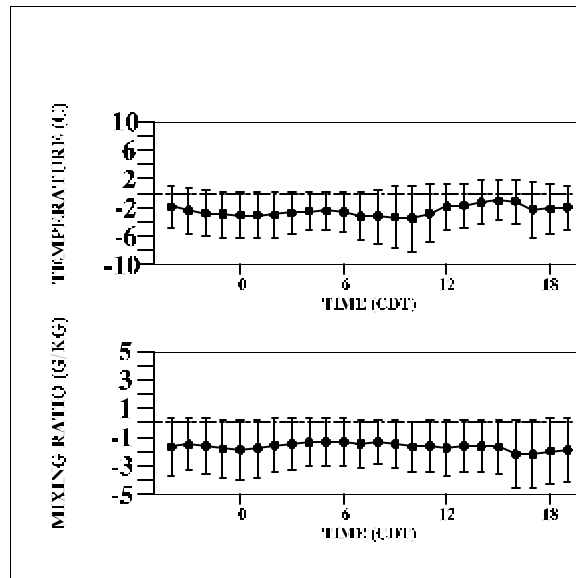
6.3.2 12-km Results

Figure 6-20 shows the bias and RMSE for the near-surface variables for Knoxville, Tennessee for the May 1993 episode for the 12-km grid. A fairly consistent bias of near -2°C was observed with RMSE values generally from $2\text{-}6^{\circ}\text{C}$. A dry bias of about 2 g kg^{-1} existed across the hours with RMSE values approaching 3 g kg^{-1} at times. Wind speed biases were on the order of $+1\text{ m s}^{-1}$ at night but near zero in the afternoon with RMSE values of $1\text{-}2\text{ m s}^{-1}$. Wind direction biases had no clear diurnal pattern with values generally in the range of ± 30 degrees. RMSE values were as large as 120 degrees with the largest values at night when winds are light or calm.

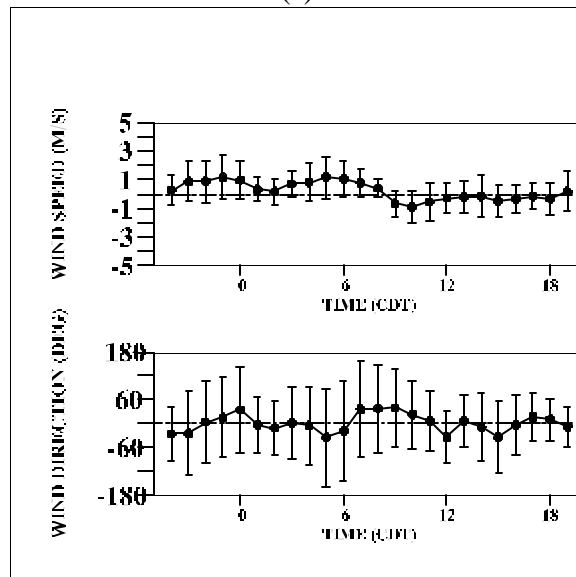
The results for Martinsburg, West Virginia in Figure 6-21 show overall different patterns. Temperature biases were negative at night and decreased to about -3°C in the early morning hours but were near zero for the afternoon. RMSE were as large as 5°C in the early afternoon. The mixing ratio bias was near zero for all hours and RMSE values were generally 2 g kg^{-1} or less. Wind speed biases were in the range of $\pm 1\text{ m s}^{-1}$ with a negative bias at night and a positive bias during the day. RMSE values for wind speed were 2 m s^{-1} or less. Wind direction biases were the largest around noon with values of $+60$ to $+90$ degrees. At other times the wind direction values were in the range of ± 30 degrees. RMSE values also were the largest in the afternoon with values around 90 degrees.

Table 6-6 compares the interpolated 12-km daily precipitation with selected rain gauge sites at GSM and SNP. The model episode totals at Look Rock and Elkmont of about 12 and 17 mm, respectively, were smaller than the observed values at the same respective sites of 24 and 34 mm. At Big Meadows the model episode total near 11 mm was also smaller than the observed value of near 36 mm.

Table 6-7 gives the rainfall statistics for all the NWS sites within the 12-km domain for the entire episode. The "OBS EVENTS" row indicates that nearly all the 6-h observed amounts were 15 mm or less. The bias values show over-prediction for the thresholds of 2 mm and less and under-prediction of the thresholds of 5 mm and higher. The false alarm ratios were 0.72 or higher for all the thresholds.

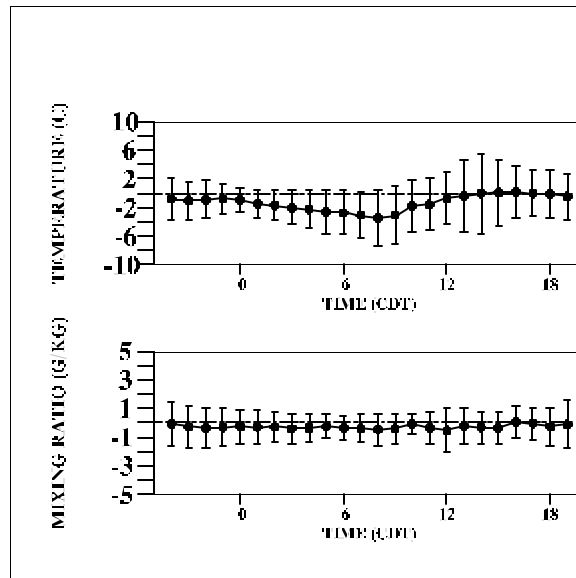


(a)

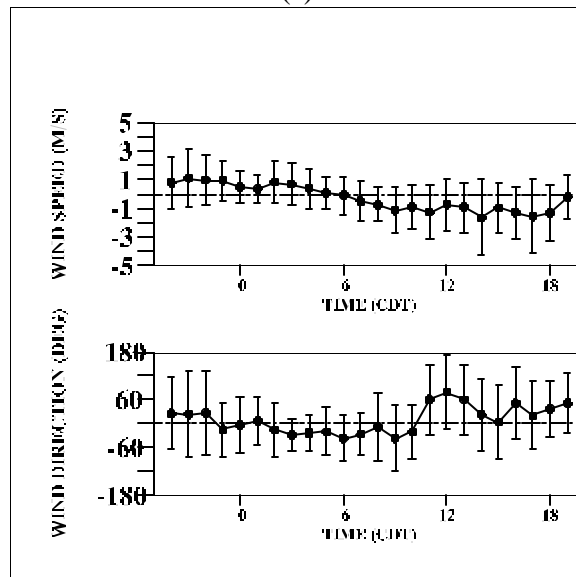


(b)

Figure 6-20. Diurnal time series of bias (solid dots) and root mean square error (vertical bars with horizontal hash marks) for the model minus the station observation for Knoxville, Tennessee for the period 1200 UTC 09 May 1993 to 1200 UTC 19 May 1993. Model values are obtained by horizontal interpolation of the hourly 12-km gridpoint values to the observation site. Time (CDT) is plotted on the horizontal axis. (a) Top plot is for temperature at 2 m in $^{\circ}\text{C}$ while the bottom plot is for water vapor mixing ratio at 2 m in g kg^{-1} . (b) Top plot is for wind speed at 10 m in m s^{-1} while the bottom plot is for wind direction at 10 m in degrees.



(a)



(b)

Figure 6-21. Diurnal time series of bias (solid dots) and root mean square error (vertical bars with horizontal hash marks) for the model minus the station observation for Martinsburg, West Virginia for the period 1200 UTC 09 May 1993 to 1200 UTC 19 May 1993. Model values are obtained by horizontal interpolation of the hourly 12-km gridpoint values to the observation site. Time (CDT) is plotted on the horizontal axis. (a) Top plot is for temperature at 2 m in $^{\circ}\text{C}$ while the bottom plot is for water vapor mixing ratio at 2 m in g kg^{-1} . (b) Top plot is for wind speed at 10 m in m s^{-1} while the bottom plot is for wind direction at 10 m in degrees.

Table 6-6. Midnight to midnight 24-h precipitation values in mm for the period 10-17 May 1993. The Look Rock and Elkmont sites are within the Great Smoky Mountain National Park while the Big Meadows site is within the Shenandoah National Park. Model values at the two observation sites were obtained by linear horizontal interpolation of the 12-km gridpoint data.

Day	Look Rock Observed	Look Rock Model	Elkmont Observed	Elkmont Model	Big Meadows Observed	Big Meadows Model
10	0.0	1.9	0.0	2.6	0.0	1.4
11	2.5	2.7	0.0	2.3	0.5	0.9
12	0.0	2.7	0.0	2.3	10.9	1.8
13	14.0	1.3	29.2	8.1	2.5	3.7
14	0.0	0.8	5.1	0.5	0.0	0.0
15	7.4	0.0	0.0	0.0	0.0	0.0
16	0.0	0.2	0.0	0.0	21.8	3.3
17	0.0	2.6	0.0	1.6	0.0	0.0
Total	23.9	12.2	34.3	17.4	35.7	11.1

Table 6-7. Rainfall statistics for various thresholds for 6-hour model precipitation from the 12-km grid compared against 6-hour observed values at all National Weather Service sites within the 12-km grid for the May 1993 episode. Statistic abbreviations and definitions are described in the text. Categories with -99 are those where model data did not exist for a calculation. The row labeled "OBS EVENTS" is the sum of all non-zero precipitation 6-hour events across all observation sites for each threshold.

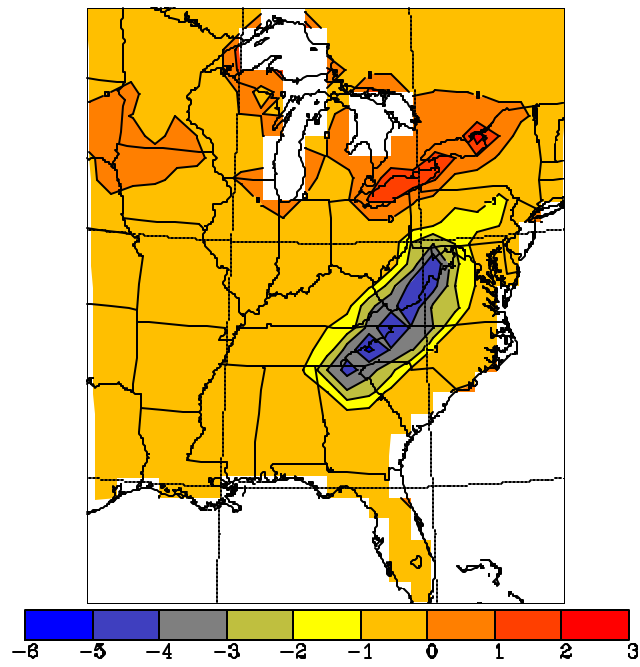
STATISTIC	THRESHOLD (mm)								
	0.2	2	5	10	15	25	35	50	75
BIAS	2.86	1.21	0.72	0.42	0.26	0.00	0.00	-99	-99
POD	0.66	0.33	0.18	0.06	0.00	0.00	0.00	-99	-99
FAR	0.77	0.72	0.75	0.86	1.00	-99	-99	-99	-99
ANR	0.80	0.96	0.99	1.00	1.00	1.00	1.00	1.00	1.00
HK	0.46	0.29	0.17	0.05	-0.00	0.00	0.00	-99	-99
ET	0.14	0.15	0.11	0.04	-0.00	0.00	0.00	-99	-99
OBS EVENTS	364	210	111	52	27	11	2	0	0

6.4 21 March to 1 April 1993 Episode Results

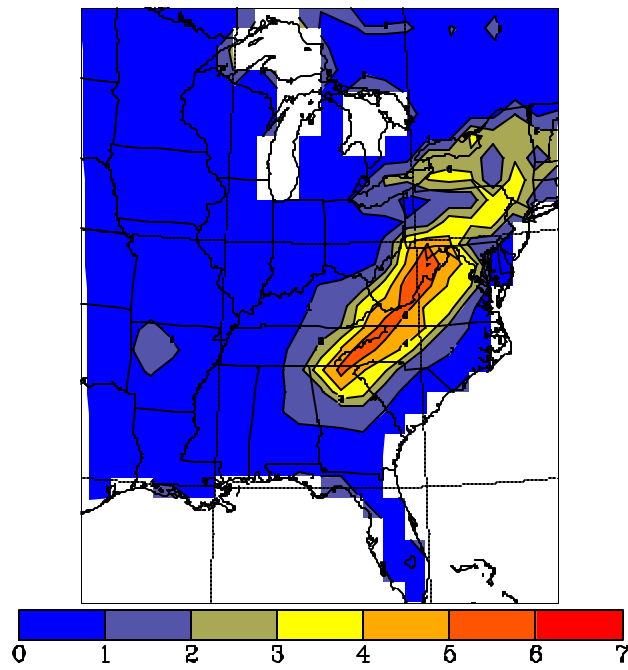
6.4.1 96-km Results

Figure 6-22 shows the bias and RMSE of the 2-m temperatures for the 96-km grid using hourly data for the entire episode. Again as the result of the surface nudging technique bias values were in the range of $\pm 1^\circ\text{C}$ outside of the immediate SAMI region. Bias values approached -5°C over the higher terrain of the southern Appalachians. Consistent with other episodes, the observed analysis used in calculating the bias is based on observations which are almost entirely outside of the higher terrain of the Appalachians. As a result when temperatures on average are decreasing with height one would expect the model to be cooler than the "observed analysis" over mountainous areas. RMSE values were usually 1°C or less with higher values approaching 5°C over parts of the Appalachians. In Figure 6-23 the bias and RMSE of the 2-m water vapor mixing ratio are expressed as a percentage of the observed values. Bias and RMSE values were generally within a range of $\pm 5\%$ outside of the immediate SAMI region and areas close to the Great Lakes.

Bias values over the southern Appalachians were in the range of -5 to -10%. The RMSE values were generally under 5% outside the immediate SAMI region and were in the range of 5 to 15 % over the Appalachians. The 10-m wind speed bias in Figure 6-24 showed most of the eastern United States with values of +0.5 to +1.5 m s⁻¹. RMSE values for wind speed were generally under 2 m s⁻¹. The 10-m wind direction bias in Figure 6-25 shows values generally in the range of +5 to +20 degrees. The RMSE values for wind direction were the largest in a southwest to northeast corridor from Louisiana to New England with largest values being near 70 degrees over the Appalachians in western Pennsylvania. The total model and observed precipitation for the episode are given in Figure 6-26. The model simulated the large-scale patterns in a reasonable manner with a possible over-prediction of precipitation across western portions of the Carolinas and Virginia.

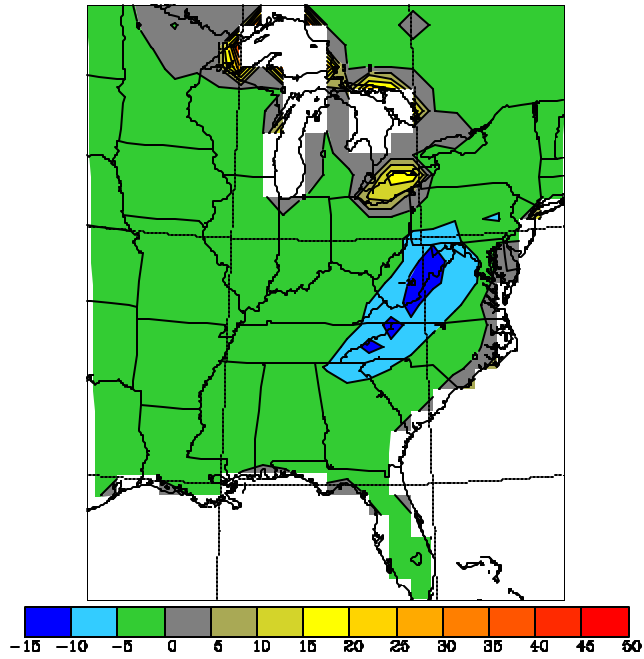


(a)

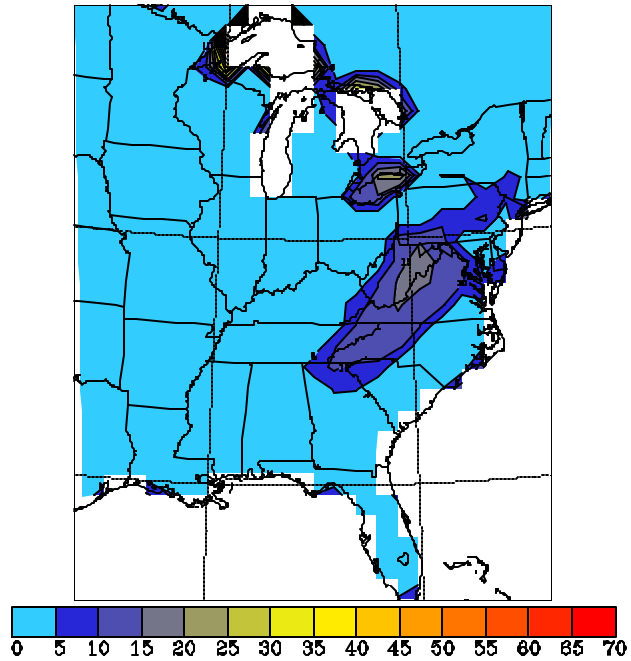


(b)

Figure 6-22. (a) Bias of the model minus the observed temperature at 2 m in degrees Celsius for the March 1993 episode for the 96-km grid. (b) Root mean square error (RMSE) of the same field for the same time and grid.

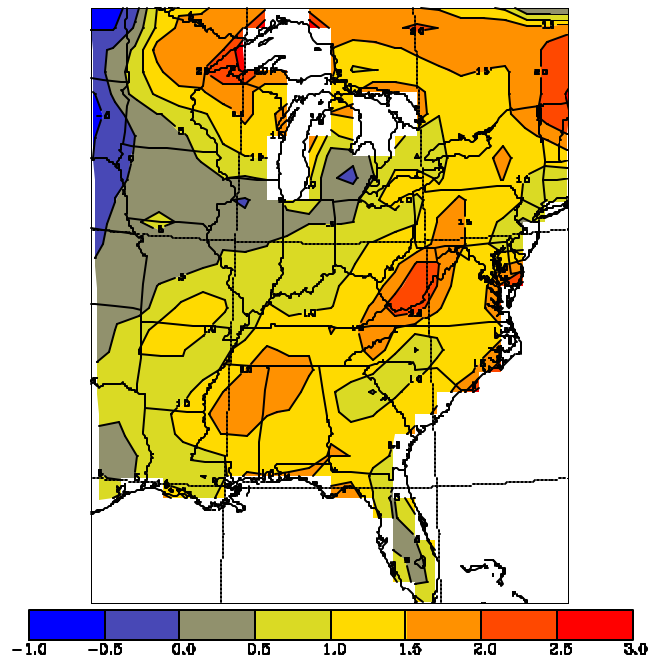


(a)

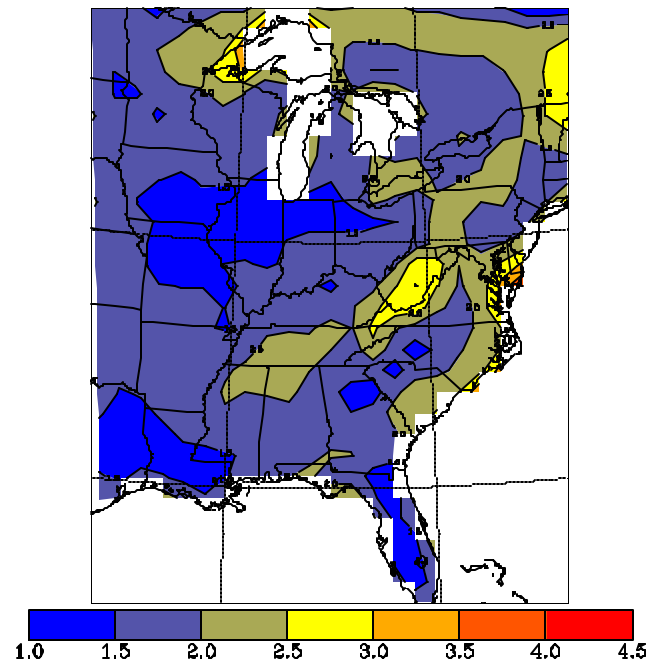


(b)

Figure 6-23. (a) Bias of the model minus the observed water vapor mixing ratio at 2 m for the March 1993 episode for the 96-km grid. (b) Root mean square error (RMSE) of the same field for the same time and grid. The bias and RMSE are expressed as a percentage of the observed value.

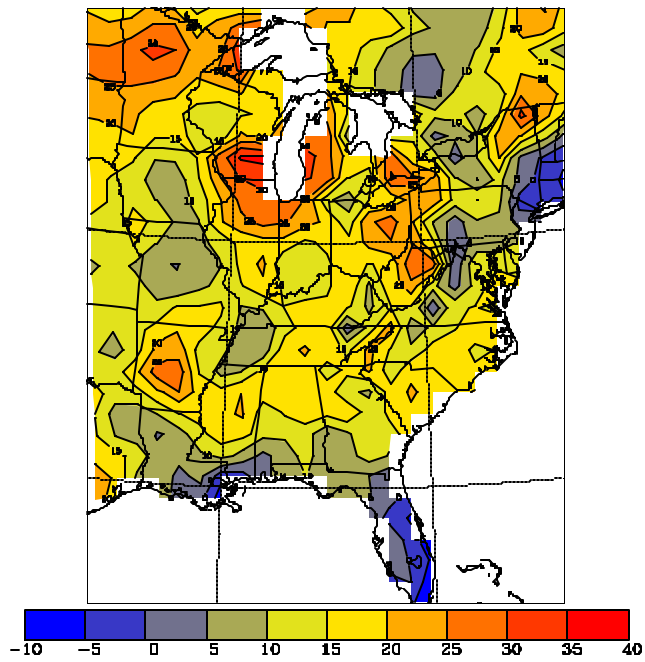


(a)

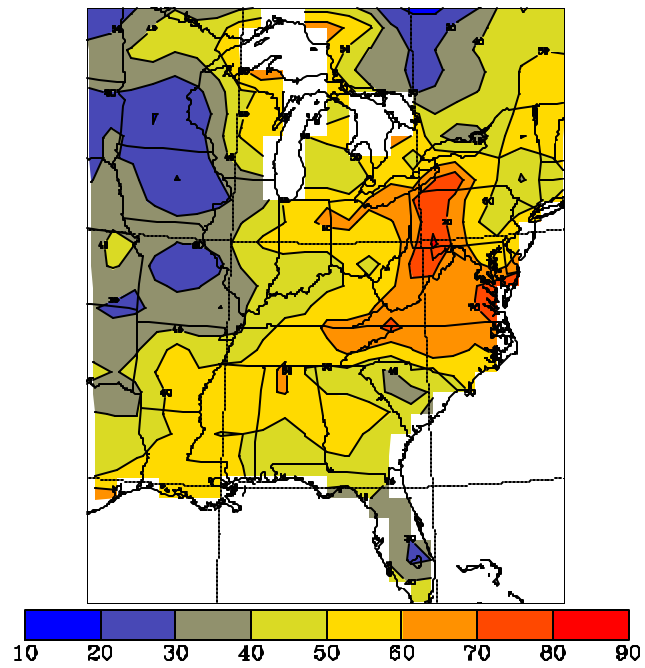


(b)

Figure 6-24. (a) Bias of the model minus the observed wind speed at 10 m in m s^{-1} for the March 1993 episode for the 96-km grid. (b) Root mean square error (RMSE) of the same field for the same time and grid.

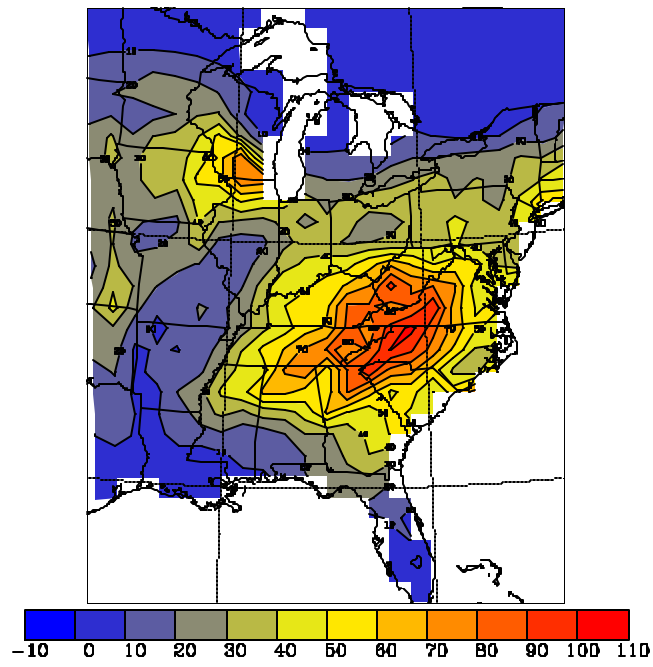


(a)

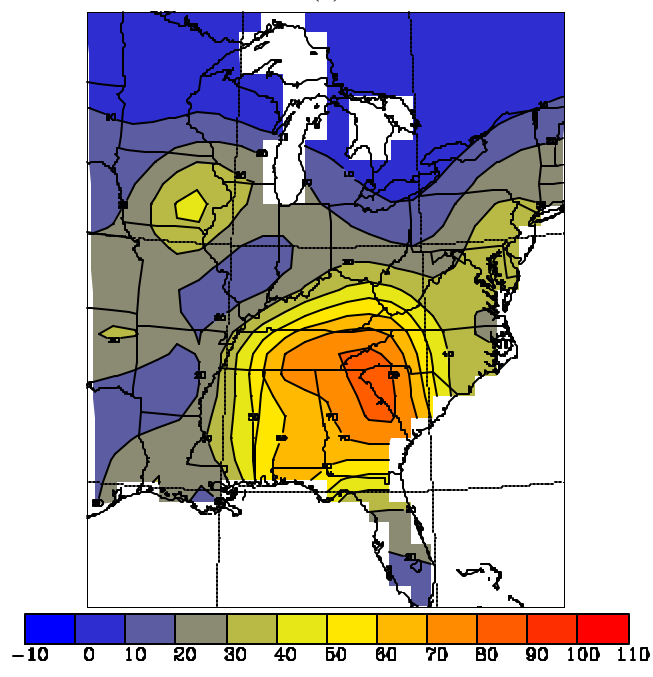


(b)

Figure 6-25. (a) Bias of the model minus the observed wind direction at 10 m in degrees for the March 1993 episode for the 96-km grid. (b) Root mean square error (RMSE) of the same field for the same time and grid.



(a)



(b)

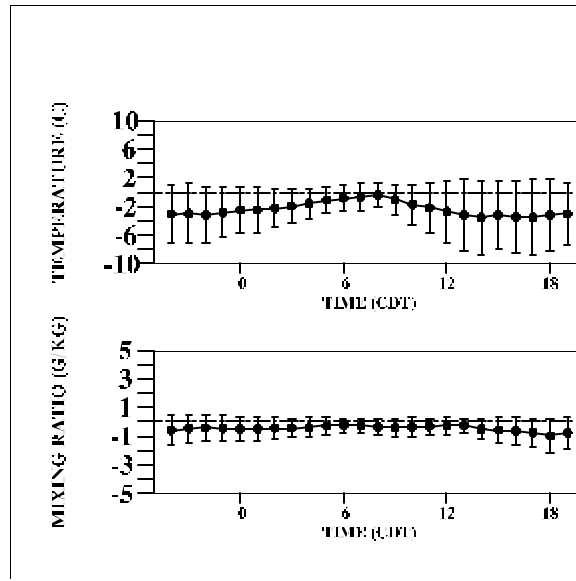
Figure 6-26. (a) Model precipitation in mm for the entire March 1993 episode for the 96-km grid. (b) Analysis of observed total precipitation for the same period for the 96-km grid.

6.4.2 12-km Results

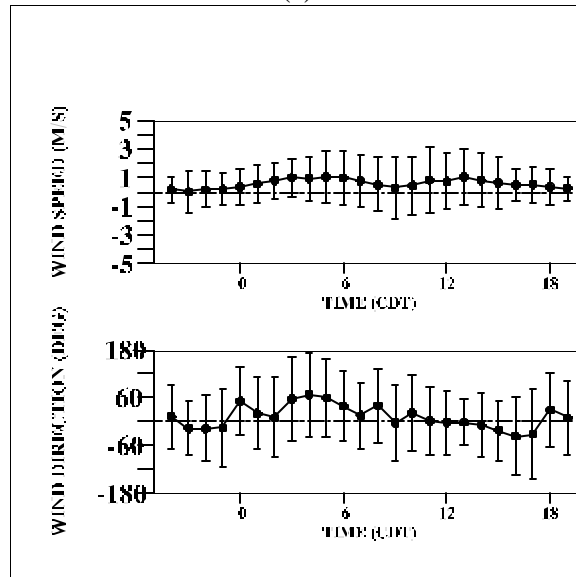
Figure 6-27 shows the bias and RMSE for the near-surface variables for Knoxville, Tennessee for the March 1993 episode for the 12-km grid. A bias of -2 to -4°C for the 2-m temperature was evident for most hours except early in the daytime when values were close to zero. RMSE values for the 2-m temperature were 6°C or less. Mixing ratio biases at 2 m were fairly consistent, being in the range of -0.5 to -1 g kg⁻¹. RMSE for the mixing ratio were 1 g kg⁻¹ or less. The wind speed bias at 10 m was usually in the range of +0.50 to +1 m s⁻¹ with RMSE values as large as 2 m s⁻¹. Wind direction biases were usually in the range of ±30 degrees with RMSE values as large as 90 degrees. The same plots for Martinsburg, West Virginia in Figure 6-28 were similar except for larger RMSE values for temperature.

Table 6-8 compares the interpolated 12-km daily precipitation with selected rain gauge sites at GSM and SNP. The model over-predicted total precipitation at Look Rock and Elkmont and under-predicted total precipitation at Big Meadows.

Table 6-9 gives the rainfall statistics for all the NWS sites within the 12-km domain for the entire episode. The "OBS EVENTS" row indicates that nearly all the 6-h observed amounts were 25 mm or less. The bias values indicate some skill for thresholds of 10 mm and below.

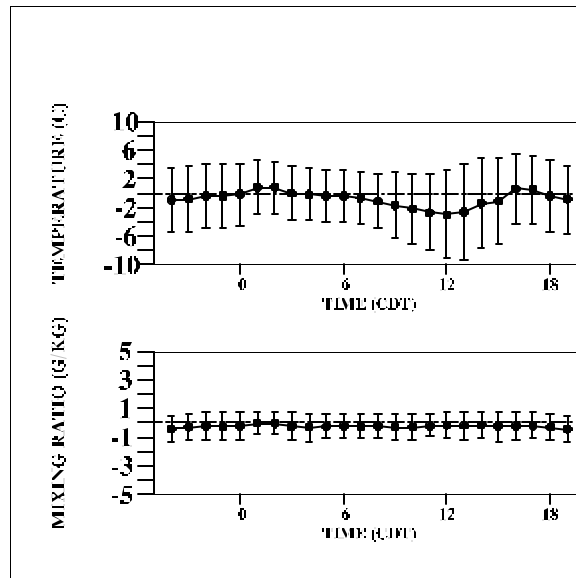


(a)

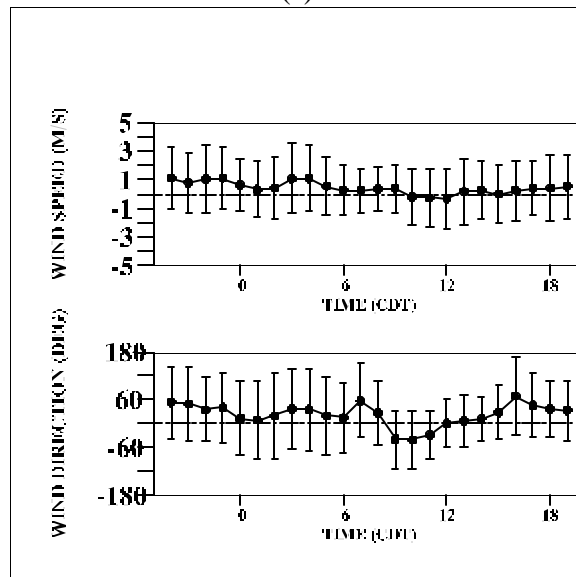


(b)

Figure 6-27. Diurnal time series of bias (solid dots) and root mean square error (vertical bars with horizontal hash marks) for the model minus the station observation for Knoxville, Tennessee for the period 1200 UTC 21 March 1993 to 1200 UTC 1 April 1993. Model values are obtained by horizontal interpolation of the hourly 12-km gridpoint values to the observation site. Time (CDT) is plotted on the horizontal axis. (a) Top plot is for temperature at 2 m in °C while the bottom plot is for water vapor mixing ratio at 2 m in g kg^{-1} . (b) Top plot is for wind speed at 10 m in m s^{-1} while the bottom plot is for wind direction at 10 m in degrees.



(a)



(b)

Figure 6-28. Diurnal time series of bias (solid dots) and root mean square error (vertical bars with horizontal hash marks) for the model minus the station observation for Martinsburg, West Virginia from 1200 UTC 21 March 1993 to 1200 UTC 1 April 1993. Model values are obtained by horizontal interpolation of the hourly 12-km gridpoint values to the observation site. Time (CDT) is plotted on the horizontal axis. (a) Top plot is for temperature at 2 m in °C while the bottom plot is for water vapor mixing ratio at 2 m in g kg^{-1} . (b) Top plot is for wind speed at 10 m in m s^{-1} while the bottom plot is for wind direction at 10 m in degrees.

Table 6-8. Midnight to midnight 24-h precipitation values in inches for the period 23-31 March 1993. The Look Rock and Elkmont sites are within the Great Smoky Mountain National Park while the Big Meadows site is within the Shenandoah National Park. Model values at the two observation sites were obtained by linear horizontal interpolation of the 12-km gridpoint data.

Day	Look Rock Observed	Look Rock Model	Elkmont Observed	Elkmont Model	Big Meadows Observed	Big Meadows Model
23	18.03	10.90	25.90	19.40	6.40	13.20
24	1.00	1.40	0.50	2.50	4.80	5.00
25	0.00	12.90	0.50	13.90	0.00	0.40
26	14.20	17.70	10.20	20.70	0.00	0.30
27	12.40	6.60	15.20	8.60	30.70	27.30
28	3.60	5.70	1.80	6.30	6.90	3.00
29	0.00	0.00	0.00	0.00	18.80	0.00
30	0.00	0.00	0.00	0.00	0.80	0.00
31	6.90	17.2	1.30	14.80	6.40	8.10
TOTAL	56.13	72.40	55.40	86.20	74.80	57.30

Table 6-9. Rainfall statistics for various thresholds for 6-hour model precipitation from the 12-km grid compared against 6-hour observed values at all National Weather Service sites within the 12-km grid for the March 1993 episode. Statistic abbreviations and definitions are described in the text. Categories with -99 are those where model data did not exist for a calculation. The row labeled "OBS EVENTS" is the sum of all non-zero precipitation 6-hour events across all observation sites for each threshold.

STATISTIC	THRESHOLD (mm)								
	0.2	2	5	10	15	25	35	50	75
BIAS	1.92	1.35	1.21	0.91	0.60	0.16	0.00	0.00	-99
POD	0.72	0.49	0.29	0.10	0.03	0.00	0.00	0.00	-99
FAR	0.63	0.64	0.76	0.89	0.94	1.00	-99	-99	-99
ANR	0.72	0.90	0.94	0.97	0.99	1.00	1.00	1.00	1.00
HK	0.44	0.38	0.24	0.08	0.03	-0.00	0.00	0.00	-99
ET	0.19	0.20	0.12	0.04	0.02	-0.00	0.00	0.00	-99
OBS EVENTS	1030	577	314	162	87	32	8	1	0

6.5 6-14 February 1994 Episode Results

6.5.1 96-km Results

Figure 6-29 shows the bias and RMSE of the 2-m temperatures for the 96-km grid using hourly data for the entire episode. Bias values were mainly in the range of $\pm 1^\circ\text{C}$ in all areas. The typical "cool bias" over the higher terrain in the Appalachians observed in other episodes is not evident here. This is possibly because of the nature of strong shallow Arctic air masses where a strong inversion exists most of the time such that temperatures increase rather than decrease with height near the surface. RMSE values for the 2-m temperature were generally 1°C or less outside of the immediate SAMI region but were as large as 5°C over the Appalachians and near the Great Lakes. Figure 6-30 shows the bias and RMSE of the 2-m water vapor mixing ratio expressed as a percentage of the observed values. Bias values were generally in the range of $\pm 2\%$ away from coastal areas and the Great Lakes. RMSE values were usually below 4% except

again for coastal areas and the Great Lakes. Reasons for the higher values for the bias and RMSE in the coastal areas and the Great Lakes include the following: 1) the observations used to create the observed analysis may not provide the required resolution in those areas, and 2) for the Great Lakes it was outside the scope of this project to acquire actual water temperatures and ice coverage which both effect the surface evaporation and, therefore, the 2-m water vapor mixing ratios. The 10-m wind speed bias and RMSE in Figure 6-31 both show in general values of $+2.5 \text{ m s}^{-1}$ or less. The 10-m wind direction bias in Figure 6-32 shows values generally in the range of -5 to +25 degrees, with the largest values being over the Appalachians, New York, and parts of Illinois, Missouri, and Iowa. The large differences over the Appalachians are indeterminate because of the lack of observations. The wind direction RMSE values were typically 40-60 degrees but as large as 90 degrees in some locations. The total model and observed precipitation are given in Figure 6-33. The model reproduced the large-scale patterns well with the possible exception of over-predicting precipitation over the southern Appalachians.

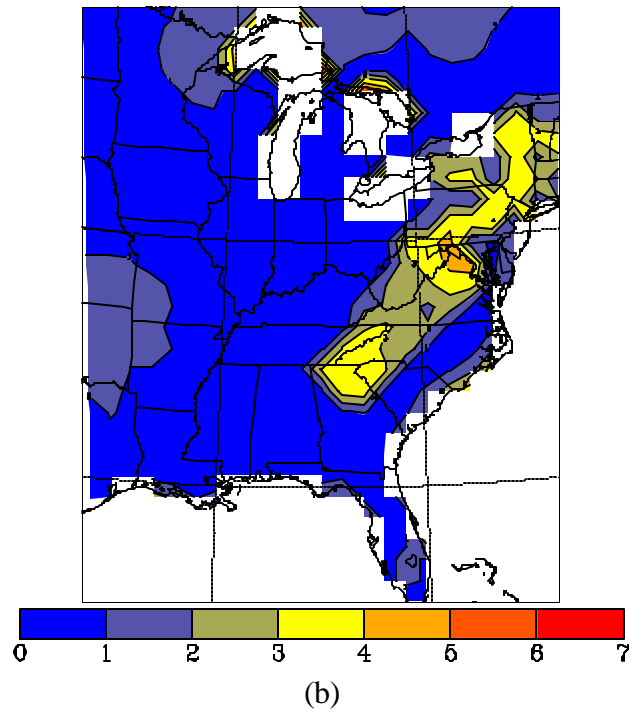
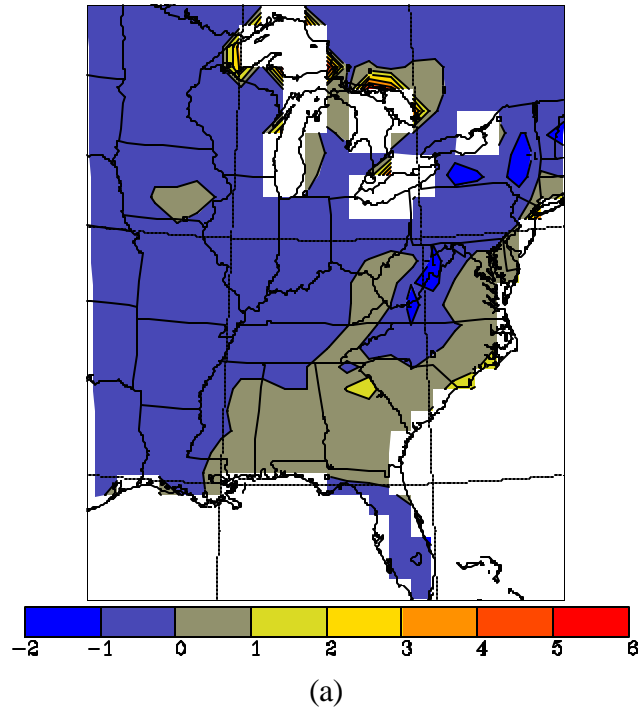
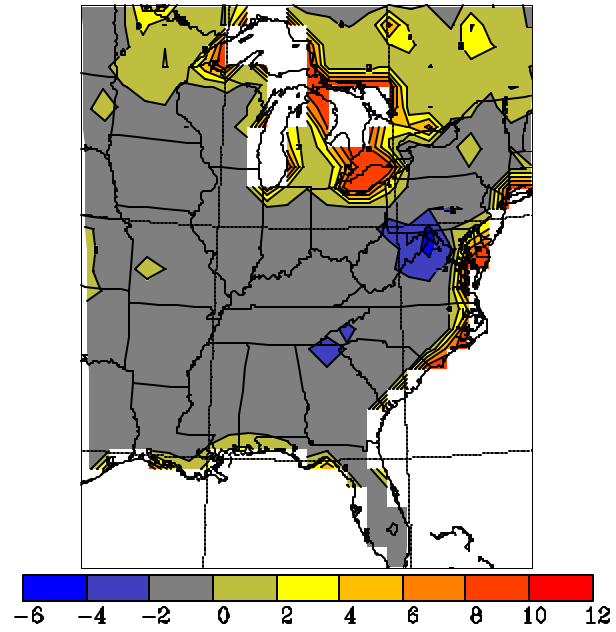
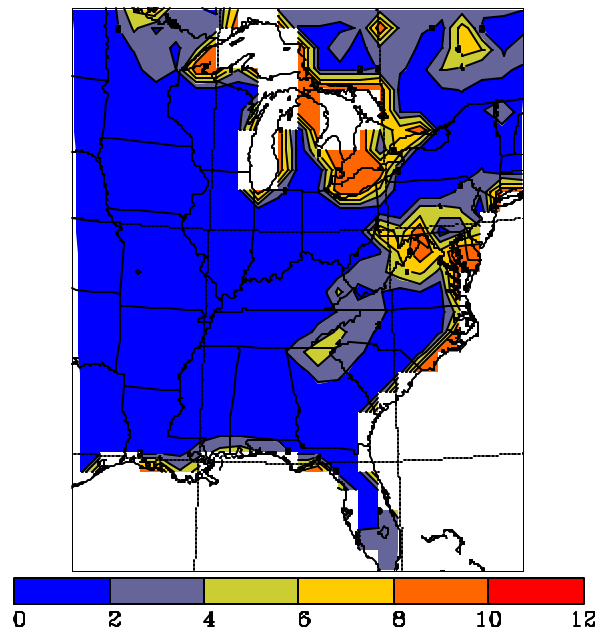


Figure 6-29. (a) Bias of the model minus the observed temperature at 2 m in degrees Celsius for the February 1994 episode for the 96-km grid. (b) Root mean square error (RMSE) of the same field for the same time and grid.

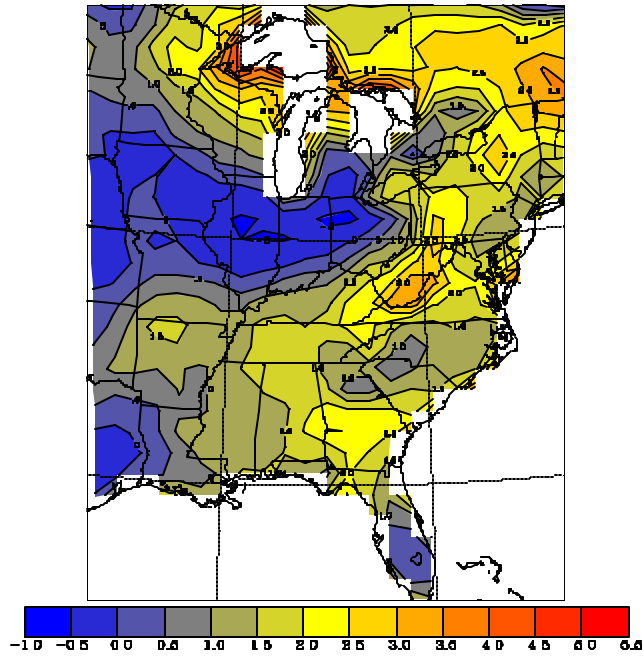


(a)

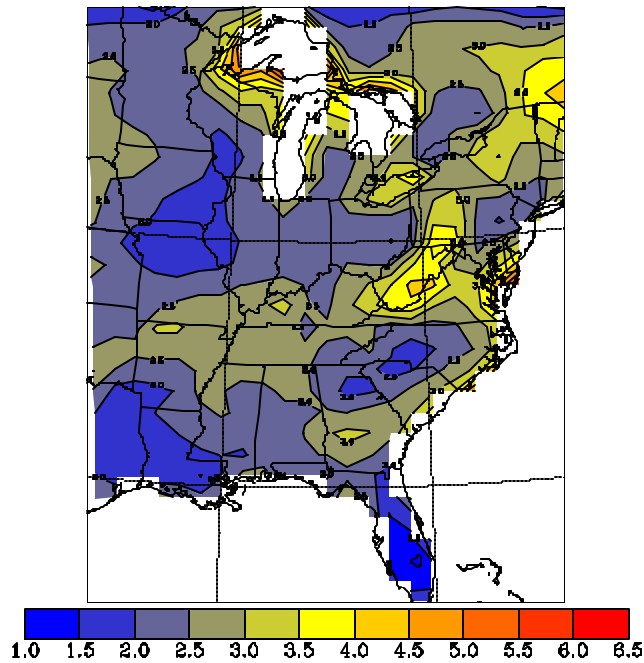


(b)

Figure 6-30. (a) Bias of the model minus the observed water vapor mixing ratio at 2 m for the February 1994 episode for the 96-km grid. (b) Root mean square error (RMSE) of the same field for the same time and grid. The bias and RMSE are expressed as a percentage of the observed value. Values in excess of 10% have been truncated to 10%

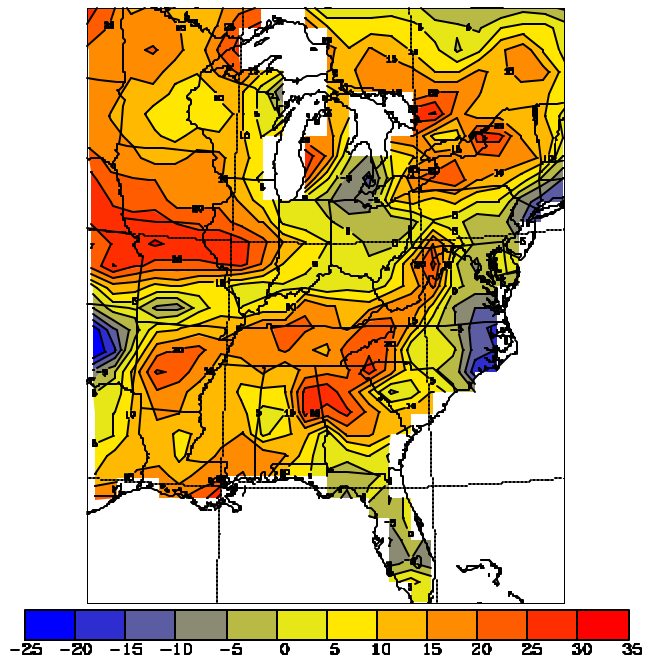


(a)

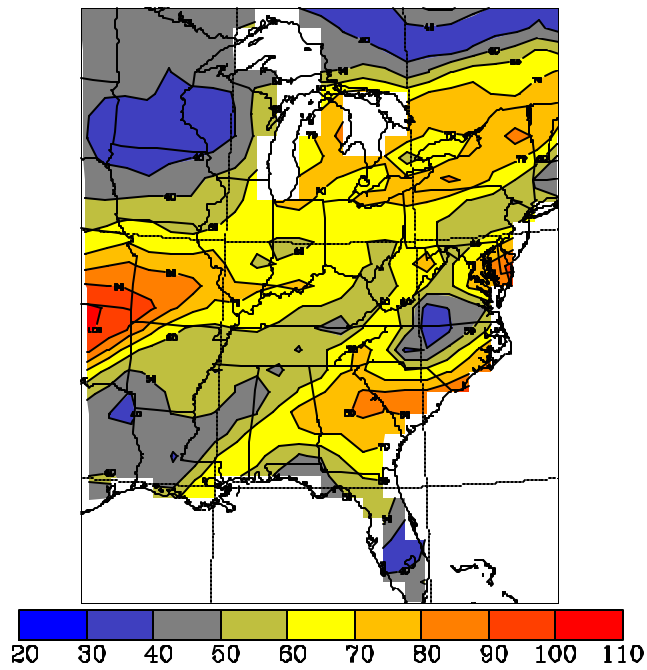


(b)

Figure 6-31. (a) Bias of the model minus the observed wind speed at 10 m in m s^{-1} for the February 1994 episode for the 96-km grid. (b) Root mean square error (RMSE) of the same field for the same time and grid.

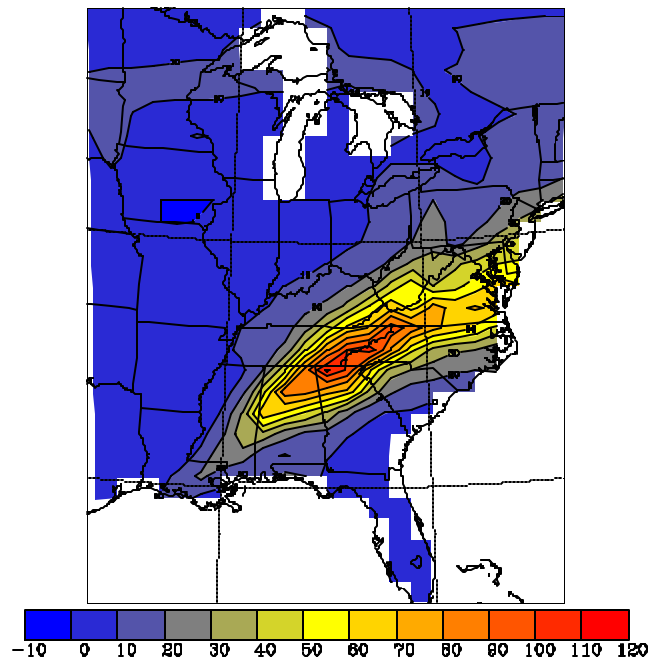


(a)

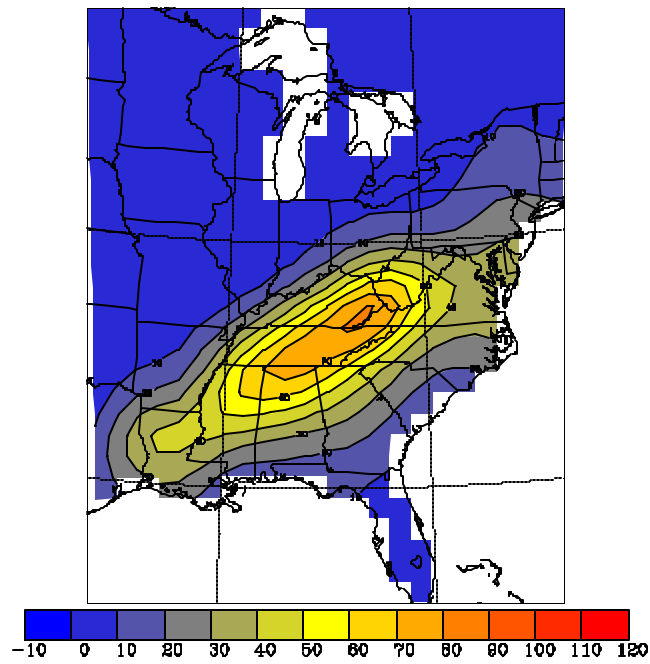


(b)

Figure 6-32. (a) Bias of the model minus the observed wind direction at 10 m in degrees for the February 1994 episode for the 96-km grid. (b) Root mean square error (RMSE) of the same field for the same time and grid.



(a)



(b)

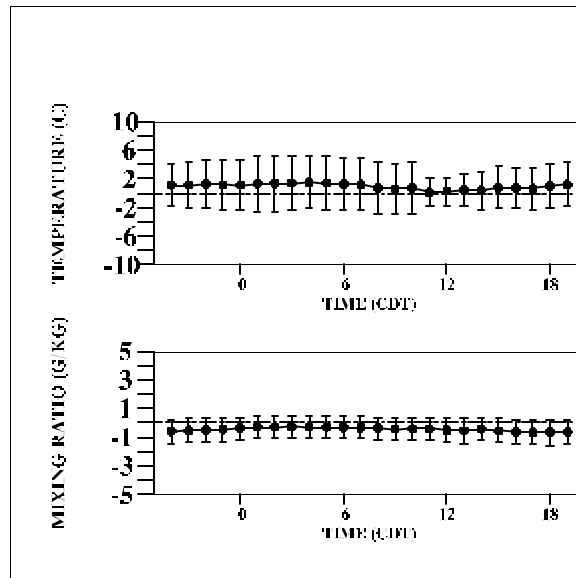
Figure 6-33. (a) Model precipitation in mm for the entire February 1994 episode for the 96-km grid. (b) Analysis of observed total precipitation for the same period for the 96-km grid.

6.5.2 12-km Results

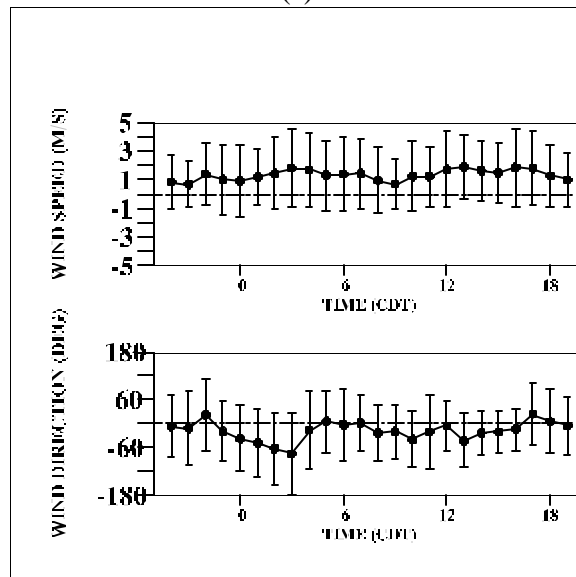
Figure 6-34 shows the bias and RMSE for the near-surface variables for Knoxville, Tennessee for the February 1994 episode for the 12-km grid. Temperatures at 2 m showed a fairly consistent warm bias of about $+1^{\circ}\text{C}$ with RMSE values of $2\text{-}4^{\circ}\text{C}$. The 2-m water vapor mixing ratio showed a consistent dry bias of about -0.50 g kg^{-1} with RMSE values of 1 g kg^{-1} or less. The 10-m wind speed revealed a fairly uniform bias of $1\text{-}2\text{ m s}^{-1}$ with RMSE values of 3 m s^{-1} or less. The wind direction bias had no clear pattern with values of -60 to $+30$ degrees and with RMSE values as large as 90 degrees. The patterns for Martinsburg, West Virginia in Figure 6-35 were very similar except for a temperature bias closer to zero.

Table 6-10 compares the interpolated 12-km daily precipitation with selected rain gauge sites at GSM and SNP. The model under-predicted total precipitation by about 12 mm at Look Rock and over-predicted by about 23 mm at Elkmont. The comparison at Big Meadows was good with the model under-predicting the total precipitation by about 4 mm. Comparisons for each day were also quite reasonable.

Table 6-11 gives the rainfall statistics for all the NWS sites within the 12-km domain for the entire episode. The "OBS EVENTS" row indicates that nearly all the 6-h observed amounts were 25 mm or less. The bias values indicate some skill for thresholds of 10 mm and below. The overall patterns of the bias (BIAS), false alarm ratio (FAR), and accuracy of no rain (ANR) indicate a tendency for the model to develop large-scale precipitation patterns correctly, but to over-predict the amounts and area of smaller precipitation amounts and the timing and location of heavier amounts.

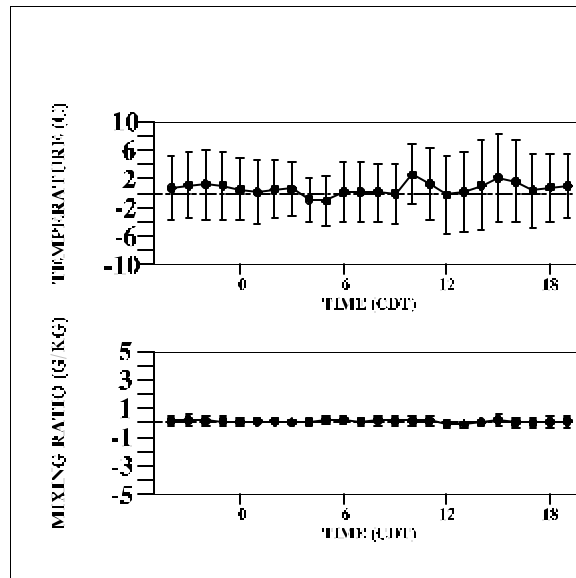


(a)

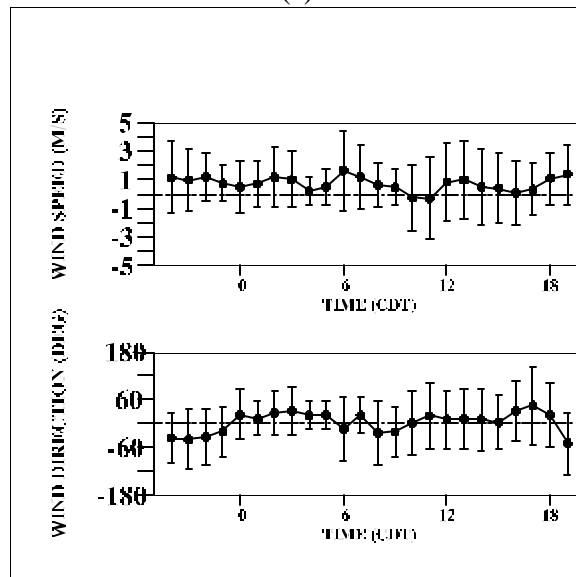


(b)

Figure 6-34. Diurnal time series of bias (solid dots) and root mean square error (vertical bars with horizontal hash marks) for the model minus the station observation for Knoxville, Tennessee for the 1200 UTC 6 February 1994 to 1200 UTC 14 February 1994. Model values are obtained by horizontal interpolation of the hourly 12-km gridpoint values to the observation site. Time (CDT) is plotted on the horizontal axis. (a) Top plot is for temperature at 2 m in °C while the bottom plot is for water vapor mixing ratio at 2 m in g kg^{-1} . (b) Top plot is for wind speed at 10 m in m s^{-1} while the bottom plot is for wind direction at 10 m in degrees.



(a)



(b)

Figure 6-35. Diurnal time series of bias (solid dots) and root mean square error (vertical bars with horizontal hash marks) for the model minus the station observation for Martinsburg, West Virginia for the period 1200 UTC 6 February 1994 to 1200 UTC 14 February 1994. Model values are obtained by horizontal interpolation of the hourly 12-km gridpoint values to the observation site. Time (CDT) is plotted on the horizontal axis. (a) Top plot is for temperature at 2 m in $^{\circ}\text{C}$ while the bottom plot is for water vapor mixing ratio at 2 m in g kg^{-1} . (b) Top plot is for wind speed at 10 m in m s^{-1} while the bottom plot is for wind direction at 10 m in degrees.

Table 6-10. Midnight to midnight 24-h precipitation values in mm for the period 8-13 February 1994. The Look Rock and Elkmont sites are within the Great Smoky Mountain National Park while the Big Meadows site is within the Shenandoah National Park. Model values at the two observation sites were obtained by linear horizontal interpolation of the 12-km gridpoint data.

Day	Look Rock Observed	Look Rock Model	Elkmont Observed	Elkmont Model	Big Meadows Observed	Big Meadows Model
8	0.80	1.30	2.00	3.20	6.40	0.60
9	24.90	21.90	24.10	26.40	10.90	0.10
10	52.80	40.00	33.80	47.50	6.90	5.00
11	30.20	33.40	28.70	33.80	17.80	34.00
12	0.30	0.00	0.00	0.00	1.30	0.10
13	1.00	1.60	1.30	2.10	1.50	1.10
Total	110.0	98.20	89.90	113.00	44.80	40.90

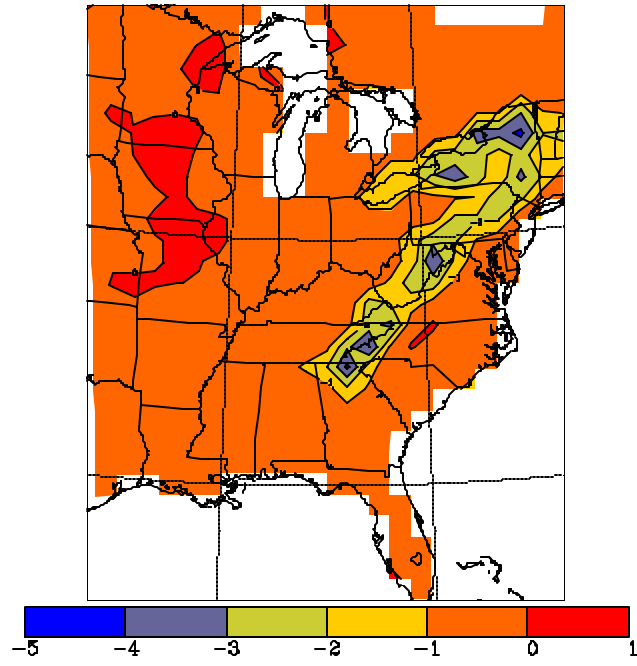
Table 6-11. Rainfall statistics for various thresholds for 6-hour model precipitation from the 12-km grid compared against 6-hour observed values at all National Weather Service sites within the 12-km grid for the February 1994 episode. Statistic abbreviations and definitions are described in the text. Categories with -99 are those where model data did not exist for a calculation. The row labeled "OBS EVENTS" is the sum of all non-zero precipitation 6-hour events across all observation sites for each threshold.

STATISTIC	THRESHOLD (mm)								
	0.2	2	5	10	15	25	35	50	75
BIAS	1.57	1.08	0.89	1.09	0.75	0.32	0.14	0.0	-99
POD	0.76	0.56	0.38	0.29	0.16	0.05	0.00	0.00	-99
FAR	0.52	0.48	0.57	0.73	0.78	0.83	1.00	-99	-99
ANR	0.79	0.93	0.96	0.98	0.99	1.00	1.00	1.00	1.00
HK	0.55	0.49	0.34	0.27	0.15	0.05	-0.00	0.00	-99
ET	0.30	0.31	0.22	0.15	0.10	0.04	-0.00	0.00	-99
OBS EVENTS	790	473	304	116	61	19	7	1	0

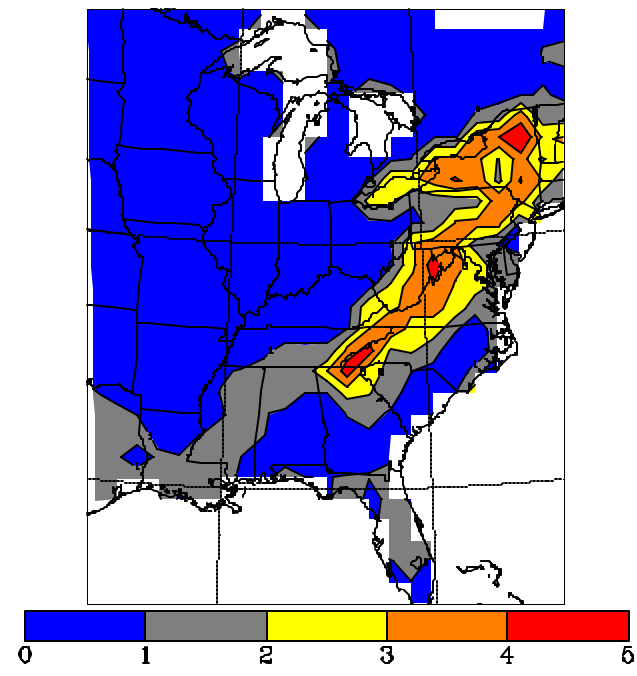
6.6 21 July - 1 August 1991 Episode Results

6.6.1 96-km Results

Figure 6-36 shows the bias and RMSE of the 2-m temperatures for the 96-km grid using hourly data for the entire episode. Again as the result of the surface nudging technique bias values were mainly in the range of $\pm 1^\circ\text{C}$ in all areas outside of the immediate SAMI region. Bias values approached -4°C over the higher terrain of the Appalachians. The RMSE values followed a similar pattern with values 1°C or less outside of the immediate SAMI region but with values up to 4°C over higher terrain. Again, as mentioned before, the larger magnitude of the bias and RMSE values over the higher terrain of the Appalachians is partially the result of the observed analysis being dominated by observations not located in high terrain areas. For those areas outside of the highest terrain but still in the area where nudging was not performed with regard to temperature the larger errors are the result, among other things, of the inability to specify soil moisture correctly. The bias and RMSE of the 2-m water vapor mixing ratio in Figure 6-37 show that most areas had bias values in the range of -2 to -4% of the observed values. RMSE values followed a similar pattern with values generally 2% or less outside the Appalachians and up to 12% in the higher terrain areas. The 10-m wind speed bias in Figure 6-38 was generally in the range of $\pm 0.5\text{ m s}^{-1}$ but with values approaching $+3\text{ m s}^{-1}$ near the Atlantic coast. RMSE values followed a similar pattern with most areas having values of 1 m s^{-1} or less but values as high as 5 m s^{-1} on the Carolina coasts. The larger errors near the Atlantic coast could be the result of model winds which were too strong or insufficient data used for the observed analysis to define the coastal winds adequately. The 10-m wind direction bias in Figure 6-39 showed values in most areas of ± 10 degrees but with higher values in parts of the Mississippi Valley and along the East coast. RMSE values followed a similar pattern with values typically at 60 degrees or less but with values as large as 100 degrees over parts of Virginia and North Carolina. The area with largest wind direction errors was inland from the area with larger wind speed errors. Comparison with the mean observed wind speed at 10 m (not shown) indicates that much of the area with the largest RMSE wind direction errors occurred in regions with mean wind speeds of 2 m s^{-1} or less. As indicated before, the wind direction in light wind regimes is dependent on local terrain which could not be duplicated at the resolutions used for this project. The total model and observed precipitation are shown in Figure 6-40. The model simulated the overall precipitation patterns well but overestimated precipitation amounts compared to the observed analysis. The model precipitation is discussed more fully in Section 6.6.2 for the 12-km results.



(a)



(b)

Figure 6-36. (a) Bias of the model minus the observed temperature at 2 m in degrees Celsius for the July 1991 episode for the 96-km grid. (b) Root mean square error (RMSE) of the same field for the same time and grid.

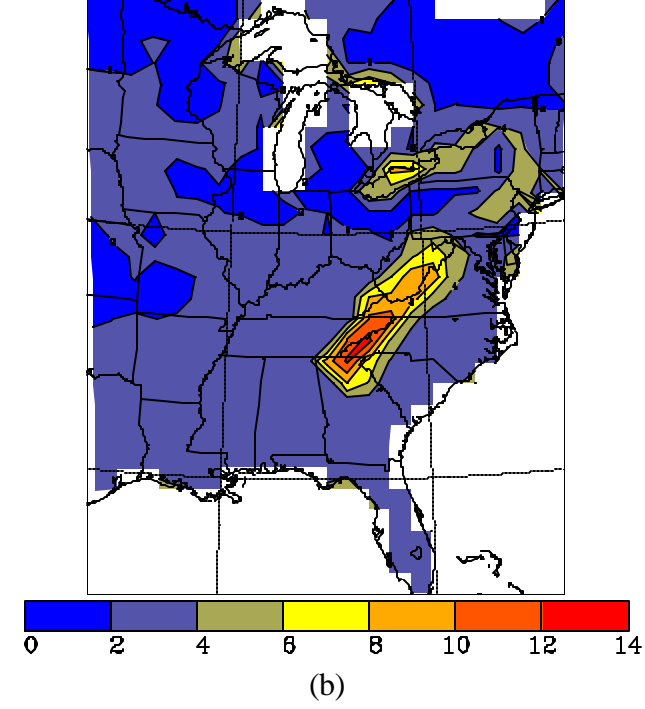
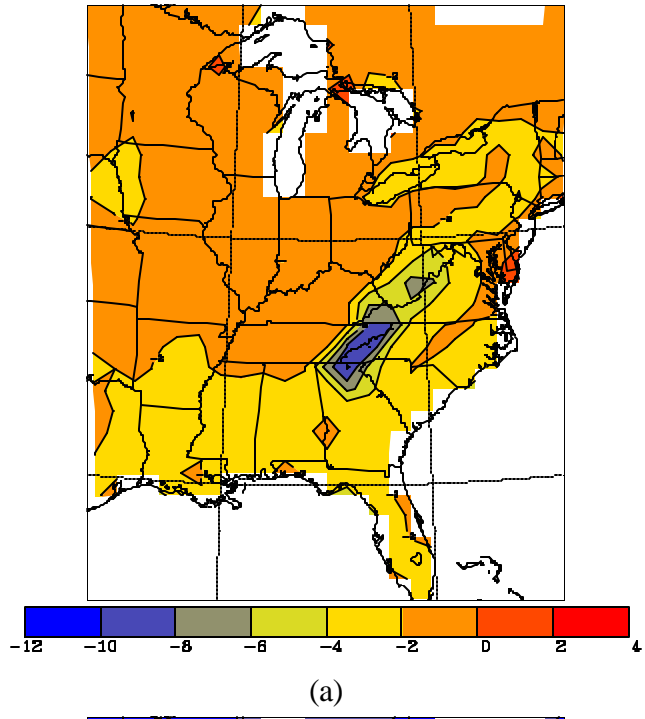
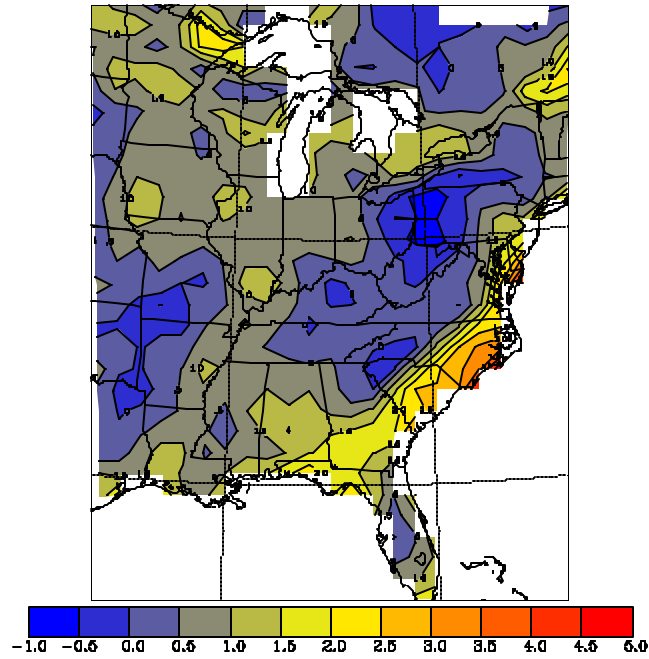
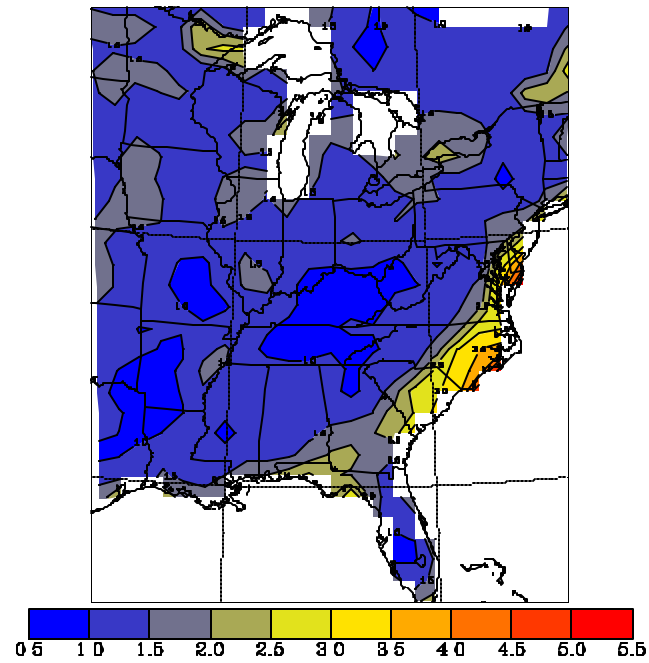


Figure 6-37. (a) Bias of the model minus the observed water vapor mixing ratio at 2 m for the July 1991 episode for the 96-km grid. (b) Root mean square error (RMSE) of the same field for the same time and grid. The bias and RMSE are expressed as a percentage of the observed value.

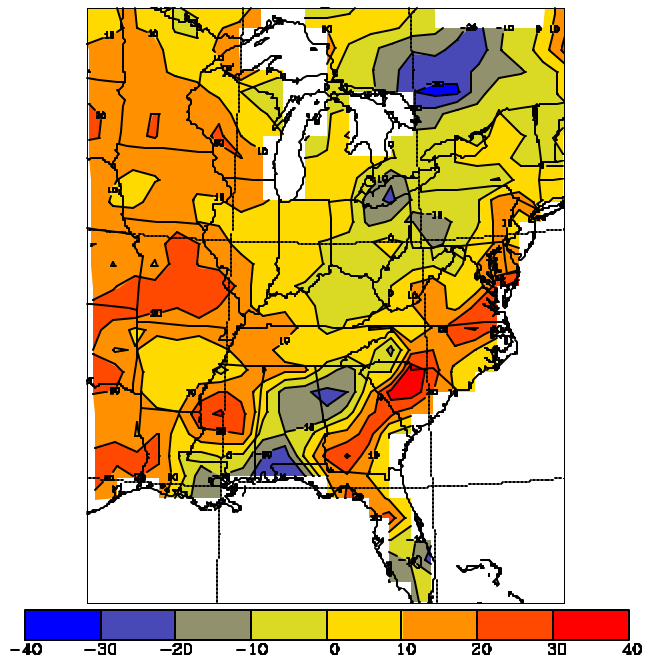


(a)

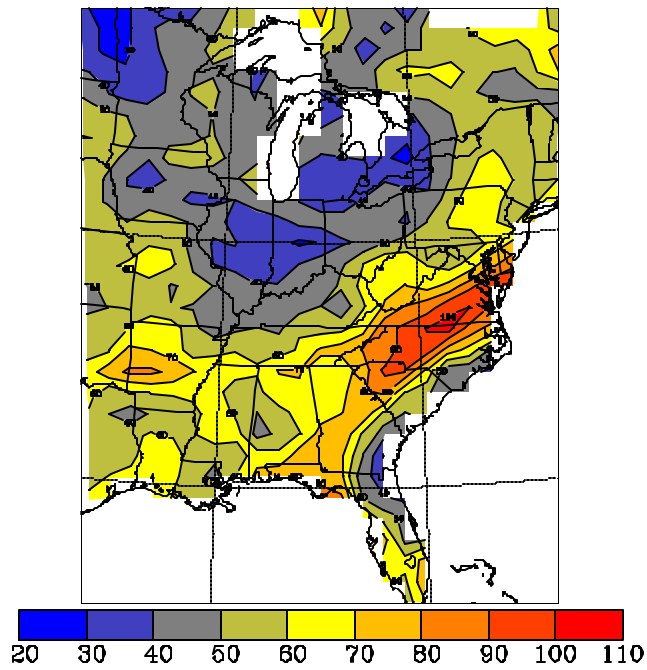


(b)

Figure 6-38. (a) Bias of the model minus the observed wind speed at 10 m in m s^{-1} for the July 1991 episode for the 96-km grid. (b) Root mean square error (RMSE) of the same field for the same time and grid.

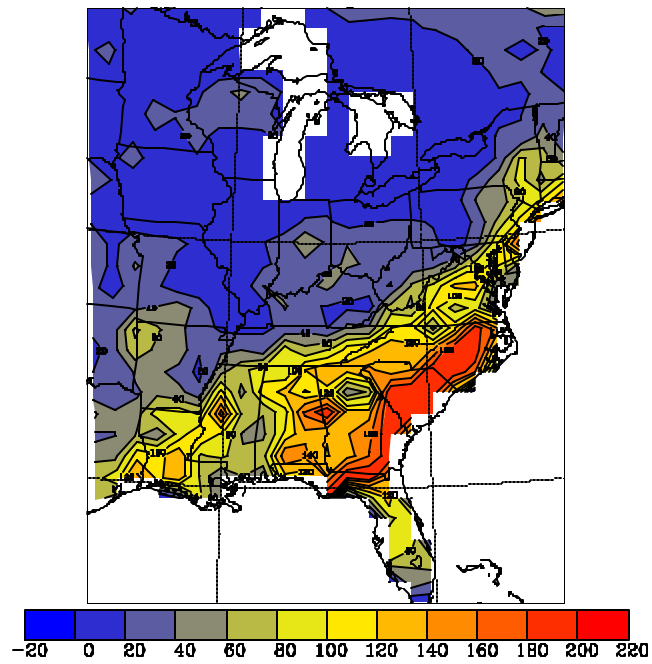


(a)

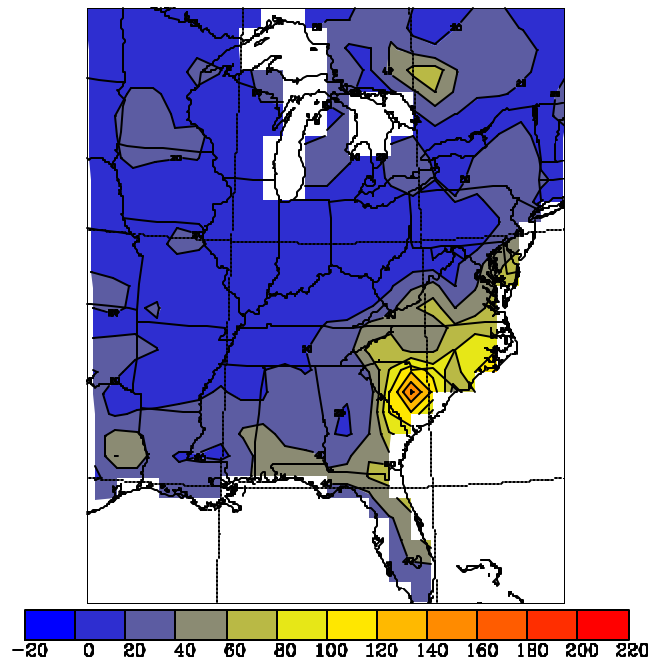


(b)

Figure 6-39. (a) Bias of the model minus the observed wind direction at 10 m in degrees for the July 1991 episode for the 96-km grid. (b) Root mean square error (RMSE) of the same field for the same time and grid.



(a)



(b)

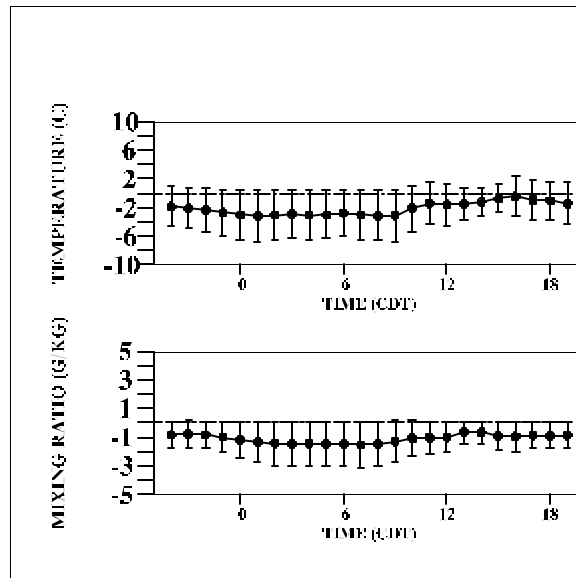
Figure 6-40. (a) Model precipitation in mm for the entire July 1991 episode for the 96-km grid. (b) Analysis of observed total precipitation for the same period for the 96-km grid. Values in excess of 200 mm have been truncated to 200 mm.

6.6.2 12-km Results

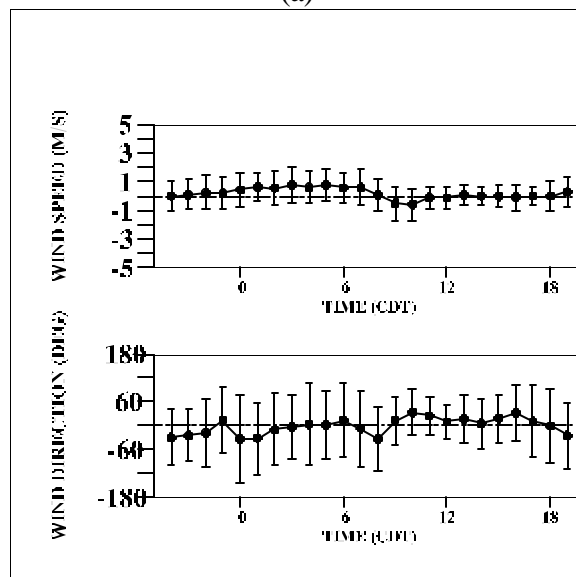
Figure 6-41 shows the bias and RMSE for the near-surface variables for Knoxville, Tennessee for the July 1991 episode for the 12-km grid. A bias of -2 to -4°C for the 2-m temperature was evident for the nighttime hours and a bias of -1 to -2°C during the daytime with RMSE values being the largest at night with values up to 4°C. A consistent dry bias of -1 to -2 g kg⁻¹ was observed with RMSE values up to 2 g kg⁻¹. A positive wind speed bias of about 0.50 m s⁻¹ was observed at night but with a bias near zero during the daytime. RMSE values for the wind speed were 1 m s⁻¹ or less. The wind direction bias had no clear pattern and was typically in the range of ±30 degrees with RMSE values up to 90 degrees. The patterns for the Martinsburg, West Virginia location in Figure 6-42 were similar with the following exceptions: 1) a moist bias up to 2 g kg⁻¹ during the daytime, and 2) a positive wind speed bias at night as large as 1 m s⁻¹ and a negative wind speed bias during the day as large as -2 m s⁻¹.

Figure 6-43 shows the total model precipitation for the 12-km grid plus the total observed precipitation observed from the Tennessee Valley Authority network analyzed to portions of the 12-km grid. The 12-km model precipitation is reasonable over the northern and southern sections of the Tennessee-North Carolina border but overestimates precipitation over central portions of the latter area where the model had in excess of 200 mm but observations showed only values around 80 mm. The model did duplicate the observed values in excess of 200 mm over the steeply sloped terrain over extreme western South Carolina. The model area with amounts in excess of 200 mm over parts of Virginia and the Carolinas was probably overdone (as will be seen by the rainfall statistics later in this section) but locally very heavy rainfall was reported in these areas in the publication *Storm Data* with amounts of 100-150 mm.

Daily rain gauge data were not available for this episode for the Look Rock, Elkmont, and Big Meadows sites at GSM and SNP. Table 6-12 gives the rainfall statistics for all the NWS sites within the 12-km domain for the entire episode. The "OBS EVENTS" row indicates that the 6-h observed amounts covered all the threshold values. The bias statistic indicates that amounts 10 mm and under were modeled with a high bias. Again the combination of high values for the analysis of no-rain (ANR) and false alarm ratio (FAR) statistics indicate the model's tendency to get large-scale patterns of precipitation correct but to over-predict the mesoscale coverage of precipitation.

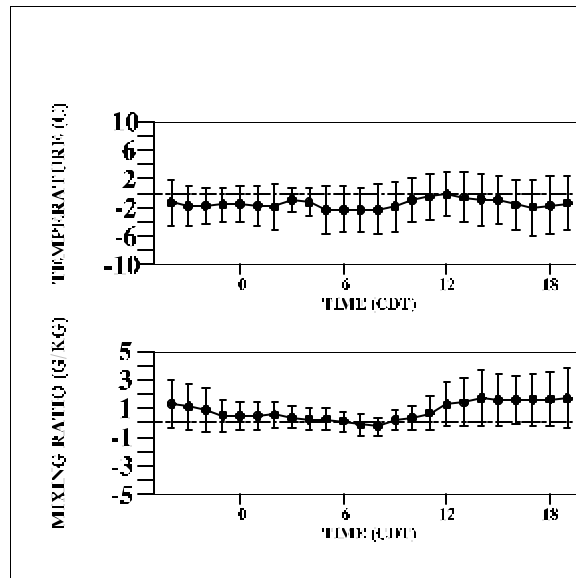


(a)

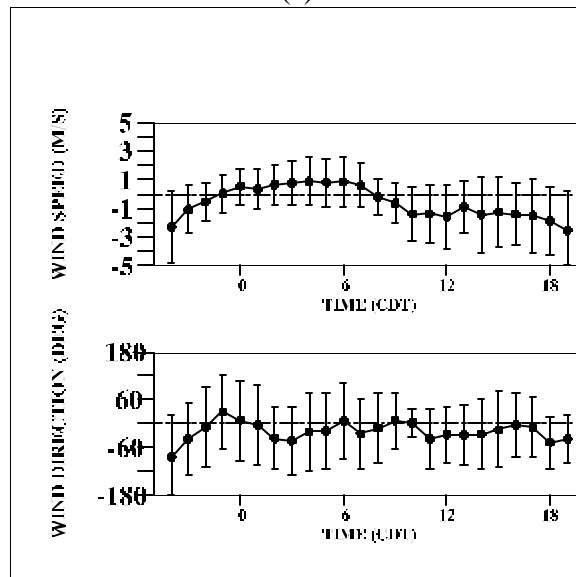


(b)

Figure 6-41. Diurnal time series of bias (solid dots) and root mean square error (vertical bars with horizontal hash marks) for the model minus the station observation for Knoxville, Tennessee for the period 1200 UTC 21 July 1991 to 1200 UTC 1 August 1991. Model values are obtained by horizontal interpolation of the hourly 12-km gridpoint values to the observation site. Time (CDT) is plotted on the horizontal axis. (a) Top plot is for temperature at 2 m in $^{\circ}\text{C}$ while the bottom plot is for water vapor mixing ratio at 2 m in g kg^{-1} . (b) Top plot is for wind speed at 10 m in m s^{-1} while the bottom plot is for wind direction at 10 m in degrees.



(a)



(b)

Figure 6-42. Diurnal time series of bias (solid dots) and root mean square error (vertical bars with horizontal hash marks) for the model minus the station observation for Martinsburg, West Virginia for the period 1200 UTC 21 July 1991 to 1200 UTC 1 August 1991. Model values are obtained by horizontal interpolation of the hourly 12-km gridpoint values to the observation site. Time (CDT) is plotted on the horizontal axis. (a) Top plot is for temperature at 2 m in $^{\circ}\text{C}$ while the bottom plot is for water vapor mixing ratio at 2 m in g kg^{-1} . (b) Top plot is for wind speed at 10 m in m s^{-1} while the bottom plot is for wind direction at 10 m in degrees.

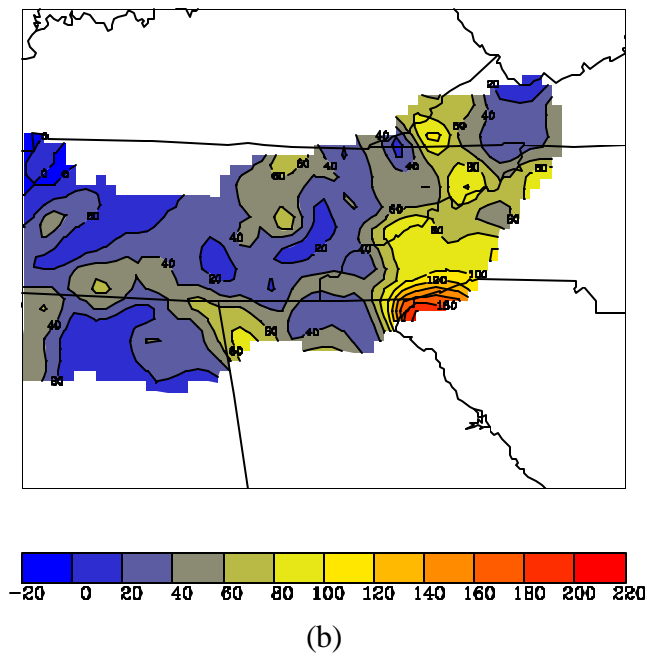
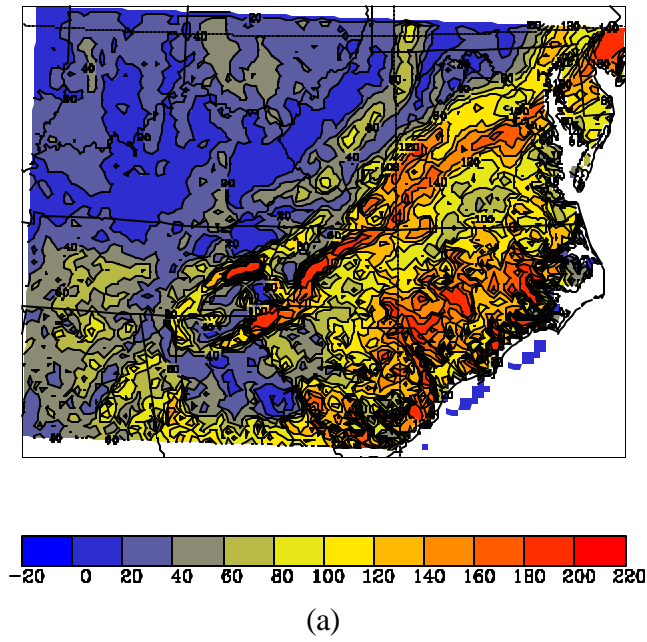


Figure 6-43. (a) Model precipitation in mm for the entire July 1991 episode for the 12-km grid. (b) Analysis of observed total precipitation for the same period for the 12-km grid using the Tennessee Valley Authority raingauge network. For both plots values in excess of 200 mm have been truncated to 200 mm.

Table 6-12. Rainfall statistics for various thresholds for 6-hour model precipitation from the 12-km grid compared against 6-hour observed values at all National Weather Service sites within the 12-km grid for the July 1991 episode. Statistic abbreviations and definitions are described in the text. Categories with -99 are those where model data did not exist for a calculation. The row labeled "OBS EVENTS" is the sum of all non-zero precipitation 6-hour events across all observation sites for each threshold.

STATISTIC	THRESHOLD (mm)								
	0.2	2	5	10	15	25	35	50	75
BIAS	2.75	2.59	2.06	1.46	0.82	0.48	0.38	0.42	0.33
POD	0.53	0.34	0.22	0.11	0.05	0.00	0.00	0.00	0.00
FAR	0.81	0.87	0.90	0.92	0.94	1.00	1.00	1.00	1.00
ANR	0.70	0.84	0.91	0.96	0.99	1.00	1.00	1.00	1.00
HK	0.23	0.18	0.13	0.08	0.03	-0.00	-0.00	-0.00	-0.00
ET	0.07	0.05	0.04	0.03	0.02	-0.00	-0.00	-0.00	-0.00
OBS EVENTS	577	335	222	127	85	46	29	12	3

6.7 3-12 August 1993 Episode Results

6.7.1 Surface Temperatures

6.7.1.1 Statistical Measures of Near-Surface Temperatures

Table 6-7.1 presents statistical summaries of the modeled and observed near-surface temperatures on the 12 km and 24 km grids for the 10 modeling days. (In the following analyses we focus on the 12 km results; the 24 km results are presented for completeness.) The daily *maximum* temperatures during the August episode began at 36.7°C on the 3rd and dropped to a low of 31.7°C on the 7th. Thereafter, a warming trend ensued with the daily maximum temperature rising up to 34.4°C on the 10th. As indicated in Table 6-7.1, RAMS did a good job of reproducing the daily maximum temperatures on each day. The episode-averages of the daily maximum observed and predicted temperatures were 33.6°C and 34.8°C, respectively, for a 3.6% discrepancy. Also from Table 6-7.1, the mean bias in predicted *hourly* surface temperatures across the 12 km domain ranges from -0.7°C to 0.1°C. On average across the August 1993 episode, the mean bias in surface temperature prediction for the RAMS models is -0.4°C. The average gross errors in surface temperature predictions for the 10 days were 1.6°C.

6.7.1.2 Spatial Mean Surface Temperatures

Figures 6-44 and 6-45 present the spatial mean near-surface temperatures and mean normalized bias in hourly temperatures across the 12 km and 24 km domains as a function of time of day. Considering first the spatial mean temperature plot (Figure 6-44), we see that RAMS tends to follow the hourly mean temperature measurements fairly well except for a few hours around the time of the daily maximum temperature. At this time, the spatial mean RAMS temperature prediction ‘clips’ the afternoon peaks by a one to two degrees C. RAMS also exhibits a slight temperature overestimation at night. This very high degree of temporal correlation in the spatial mean time series is not normally seen in prognostic model evaluations.

The exact cause(s) for the negative daytime (underestimation) and positive nighttime (overestimation) biases are difficult to isolate. Because the near surface predictions from RAMS are taken from grid layer 1 (approximate height of 13 m) one might expect RAMS nighttime estimates to be slightly warmer than the measurements (at 2 m) which are influenced by nocturnal radiational cooling at the ground. At midday, the RAMS predictions would be expected to be slightly lower than the measurements during this super-adiabatic period, all other factors being equal.

6.7.1.3 Mean Normalized Bias in Surface Temperatures

In Figure 6-45, the mean normalized bias in RAMS’ estimates of hourly near-surface temperature predictions on the 12 km grid are fairly small throughout the episode. Typically, RAMS tends to slightly overestimate (~ 3%-5%) hourly temperatures in the morning hours and under predict (~2%-4%) later in the day. These periods of under and overestimation of near-surface temperatures, revealed in the hourly bias

time series plots, are ‘masked’ through the computation of daily average bias statistics (see Table 6-7.1) because of the cancellation of positive and negative biases within the diurnal cycle.

6.7.1.4 Surface Temperature Fields

Hourly averaged ground-level temperature fields for the 12 km domain are shown in Figure 6-46 for four representative hours on 3 August 1993. In the figures, the bold numerals represent the measured temperatures in degrees C. Evident in the figures is the cooler air temperatures over the high terrain of the Appalachian mountains and the warmer areas in coastal environments, particularly during the afternoon periods.

6.7.2 Surface Wind Speed and Direction

6.7.2.1 Statistical Measures of Near-Surface Wind Speed and Direction

Table 6-7.2 presents a variety of statistical measures of RAMS model performance for the winds during the 3-12 August 1993 episode. To begin, the table lists the daily mean observed and modeled surface wind speed for the 10 days during the episode. On the 12 km grid, RAMS estimates mean wind speeds (2.66 m s^{-1}) that are on average more than twice the magnitude of the episode mean observations (1.11 m s^{-1}). RAMS overestimates the daily average observed wind speed on each day. Over the entire episode, RAMS over-predicts surface wind speeds by 140%. However, it should be noted that on half the days, the average observed wind speed across the 12 km domain is less than 1 m s^{-1} . Part of this over-prediction is expected because the height of the first RAMS grid layer ($\sim 20 \text{ m}$) exceeds that of standard anemometer height (10 m). Since wind speeds typically increase rapidly with height within the lowest portion of the boundary layer, the modeled winds in layer 1 should be systematically higher than the measurements.

Modeled wind directions show fairly good agreement with the observations on most days of the August episode. Across the full 10-day period the mean modeled (178.9 degrees) and observed surface wind directions (203.5 degrees) differ by only 25 degrees. From day-to-day, the difference between daily average and observed wind direction varies from 4 to 107 degrees. The daily average index of agreement parameter for MM5 modeling ranges between 0.64 and 0.84 with a 10-day mean of 0.75. These results are consistent with those achieved with the MM5 results for summertime ozone episode applications. Table 6-7.2 also lists the systematic and unsystematic components of the RMSE errors. For all days the systematic component is larger than the unsystematic component suggesting that more of the RMSE errors are due to systematic biases that might be reduced through further refinement of model algorithms and/or application procedures. One factor contributing to the systematic RMSE is the difference in height above ground between the lowest RAMS level and standard instrument heights.

6.7.2.2 Vector Mean Wind Speeds

Figures 6-47 through 6-48 present various surface wind speed and wind direction summary plots for the 3-12 August 1993 episode. To begin, Figure 6-47 gives the vector mean modeled wind speed (the solid line)

and the vector mean observed wind speed (the dashed line) for the RAMS model over the 12 km domain. The plot shows that RAMS systematically overestimates the observed mean wind speeds for every day of the episode. For many of the days the vector mean winds on both the 12 km and 24 km grids possess temporal variability similar to that exhibited in the measurements event though the predicted values are systematically biased high. On many of the days, the model represents the afternoon wind speed increase fairly well notwithstanding the over-prediction.

6.7.2.3 Mean Wind Direction

Figure 6-48 presents the hourly variation in modeled versus observed surface wind directions over the 10 days. Generally, there is very good agreement with the exception of 8 August and early on the 9th when the model predicts winds that are 100 degrees or more out of phase with the observations. Overall, however, the agreement with mean wind direction is very good.

6.7.2.4 Root Mean Square Error in Wind Speeds

The RMSE errors and index of agreement are shown in Figures 6-49 and 6-50, respectively. In Figure 6-49, three lines are plotted. The dotted line depicts the unsystematic component of the RMSE (i.e., $RMSE_U$) while the dashed line (the middle line) corresponds to the systematic component ($RMSE_S$). The total RMSE error is given by the solid line, always the topmost line in the figure. The episode average values of the unsystematic, systematic, and total RMSE errors are 1.28 m s^{-1} , 1.72 m s^{-1} and 2.18 m s^{-1} , respectively. Examination of Figure 6-49 reveals that there does not appear to be any significant error growth throughout the simulation with the exception of 7-8 August when the errors are somewhat larger than for the rest of the episode days. Also, the fact that most of the RAMS RMSE error is from the systematic component (model physics- related) is graphically evident in the figure.

6.7.2.5 Index of Agreement in Surface Wind Speeds

The index of agreement (I_a) results for the August 1993 episode (Figure 6-50) are quite consistent with results in other MM5 and RAMS performance evaluations conducted elsewhere in the U.S. The RAMS results exhibits typical hourly variation in the agreement index parameter. The index is lowest during the morning period when wind speeds are lowest and the directions are more variable. In the afternoon when speeds are greater, the index increases. The mean value of I_a over the entire episode is 0.75.

6.7.2.6 Ground-Level Wind Fields

Figures 6-51 presents afternoon RAMS surface wind field comparisons over the 12 km domains on four different days during the August 1993 episode. The bold red vectors in the plots correspond to the observed surface winds; lighter black vectors correspond to modeled winds. While there are obviously some locations where the modeled and observed winds do not agree well, for the most part both the RAMS modeled winds do a reasonable job of replicating the observed values.

6.7.3 Mixing Ratios

6.7.3.1 Statistical Measures of Near-Surface Mixing Ratios

Statistical results from the operational evaluation of near surface specific humidity (or mixing ratios) are listed in Table 6-7.3 for the August 1993 episode for the 12 km and 24 km grids. Across the 12 km domain the agreement between the episode mean daily maximum observed (20.1 g/Kg) and modeled (17.2 g/Kg) mixing ratios is fairly good. RAMS systematically underestimates the maximum ratio on each day by 2 to 3 g/Kg. The mean bias and error in mixing ratios are also quite good, with 10-day mean values of -0.6 g/Kg and 1.1 g/Kg respectively. These results suggest that the model is doing a fairly good job of reproducing the daily maximum and hourly specific humidity across the 12 km domain.

6.7.3.2 Spatial Mean Surface Mixing Ratios

Figure 6-52 presents the spatial mean surface mixing ratios for the August 1993 episode. At both 12 km and 24 km scales, the model does a very good job of estimating the spatial trends in specific humidity across the entire episode. The slight tendency to underestimate mixing ratio is evident in the plots. A portion of this underestimation may be attributed to the vertical mismatch between the height of the mixing ratio measurement and the first RAMS grid level from which the predicted mixing ratio is derived.

6.7.3.3 Bias in Surface Mixing Ratios

The systematic underestimation of near-surface mixing ratio is again seen in the normalized bias time series for the 12 km and 24 km grid domains shown in Figure 6-55. The largest biases in mixing ratio tend to occur during the nighttime hours. At midday, the mixing ratio bias estimates are close to zero on most days. No apparent diurnal performance problems are evident in the mixing ratio results.

6.7.3.4 Surface Mixing Ratio Fields

Figure 6-54 presents examples of ground-level mixing ratio fields across the 12 km domain at two time periods (0300 and 1500 EST) on 7 August. These plots are fairly typical of the entire set of mixing ratio fields for the August 1993 episode. No strong gradients in mixing ratios are evident in these or the other hourly fields for this episode and there is generally good agreement between the predicted humidity and those observed at the various monitoring stations (represented by the numerals in the figures).

6.7.4 Precipitation

6.7.4.1 Statistical Measures of Total Daily Precipitation

Rain occurred on 8 of the 10 days of the August 1993 episode as indicated in Table 6-47. The maximum observed total daily precipitation at any rain gauge varied between 9.0 mm and 119 mm with an episode mean of 50 mm. RAMS predicted a range of rainfall of 11.5 mm to 102.7 mm with an episode mean of

40.3 mm. The mean observed and predicted precipitation across all rain gauges was 5.3 mm and 6.7 mm, yielding an overall discrepancy of 26% which represents excellent agreement for a mesoscale prognostic model. The bias in daily rainfall predictions ranges from -0.30 mm to 10.38 mm with an episode mean of 1.9 mm. Only on 5 August did the model experience significant difficulty reproducing the daily rainfall totals. The daily gross errors in rainfall ranged between 0.41 mm and 13.91 mm with an episode mean of 5.8 mm. Overall, the model did an excellent job of simulating the daily and episode average rainfall totals.

6.7.4.2 Temporal Distribution of Total Daily Rainfall Across All Sites

Figure 6-55 presents time series plots of the daily precipitation totals derived from the measured and predicted values averaged across all reporting stations in the 12 km and 24 km domains. With the exception of the modest over-prediction on 5 August, the day-to-day rainfall predictions match the observations very closely in this comparison. We believe, however, that the excellent agreement suggested in the daily total spatial time series plot (Figure 6-55) paints too optimistic a picture of the model's replication of the precipitation fields for this episode. The following graphical tools indicate that there are in fact some larger differences between daily average prediction and observation.

6.7.4.3 Spatial Distribution of Daily Total Measured and Observed Rainfall

One of the challenging problems in evaluating meteorological model precipitation predictions is devising a scheme for comparing point rainfall measurements with spatially distributed (i.e., gridded) model predictions. In Figure 6-56 we make this comparison by presenting in the top panel the gridded daily precipitation totals (in mm) across the 12 km domain for 7 August 1993. In the bottom panel, we present the daily total measurements (also in mm) utilizing the same color coding scheme. Comparing the predicted and observed rainfall totals on 7 August, we see that there is a broad band of predicted precipitation (> 25 mm) across Tennessee and central Kentucky extending to the east coast. Such a broad swath of precipitation is not evident in the monitors although there are many areas where large voids in the measurement network exist. From Table 6-7.4 we note that on the 7th, there was a 4.34 mm over-prediction bias in the model which might explain a portion of the apparent discrepancy between the modeled field and observed values in the 12 km grid results.

6.7.4.4 Correlation of Daily Maximum Rainfall Across All Sites

Figure 6-57 presents a scatter plot of predicted and observed daily total precipitation on 7 August 1993. Comparison of this plot with the spatial time series plot in Figure 6-55 clearly underscores the need for use of multiple statistical and graphical tools when evaluating the performance of complex atmospheric models. While the spatial time series plot in Figure 6-55 suggests very good model performance based on averages across all monitoring stations, the Scatter Plot in Figure 6-57 reveals that this seemingly good agreement comes as the result of cancellation of model over- and under-predictions at the numerous individual monitors. Indeed, visual inspection of the Scatter Plot suggests little if any correlation between the various reporting sites. Thus, while RAMS appears to do a credible job of estimating the total precipitation across the 12 km domain on each day during the August 1993 episode, the spatial distribution of rainfall events exhibits much less skill.

Table 6-7.1. RAMS Model Evaluation Results for the 3-12 August 1993 SAMI Episode – Surface Temperatures (deg C). (a) 12 Km Grid											
Performance Attribute	3 Aug Day 215	4 Aug Day 216	5 Aug Day 217	6 Aug Day 218	7 Aug Day 219	8 Aug Day 220	9 Aug Day 221	10 Aug Day 222	11 Aug Day 223	12 Aug Day 224	Mean Value
Max Observed Temp.	36.7	33.9	33.9	35.0	31.7	32.2	32.8	34.4	33.3	31.7	33.6
Max. Predicted Temperature	35.0	31.7	34.1	32.4	33.4	36.0	37.1	37.5	37.7	33.2	34.8
Mean Bias (deg C)	-0.4	-0.7	-0.4	-0.5	-0.5	0.1	-0.3	-0.7	-0.7	0.5	-0.4
Gross Error (deg C)	1.9	1.9	1.3	1.6	1.6	1.5	1.7	1.7	1.7	1.3	1.6

Table 6-7.1. RAMS Model Evaluation Results for the 3-12 August 1993 SAMI Episode – Surface Temperatures (deg C). (b) 24 Km Grid											
Performance Attribute	3 Aug Day 215	4 Aug Day 216	5 Aug Day 217	6 Aug Day 218	7 Aug Day 219	8 Aug Day 220	9 Aug Day 221	10 Aug Day 222	11 Aug Day 223	12 Aug Day 224	Mean Value
Max Observed Temperature	37.2	37.2	36.1	36.7	37.2	36.7	36.7	37.2	37.2	36.1	36.8
Max Predicted Temperature	33.5	38.6	36.2	34.6	35.1	35.4	36.8	35.6	36.9	34.8	35.8
Mean Bias (deg C)	-0.7	-0.7	-0.6	-0.6	-0.5	-0.2	-0.4	-0.7	-0.8	0.2	-0.5
Gross Error (deg C)	2.0	2.0	1.8	1.9	1.7	1.7	1.8	1.8	1.9	1.4	1.8

Performance Attribute	3 Aug Day 215	4 Aug Day 216	5 Aug Day 217	6 Aug Day 218	7 Aug Day 219	8 Aug Day 220	9 Aug Day 221	10 Aug Day 222	11 Aug Day 223	12 Aug Day 224	Mean Value
Mean Observed Wind Speed	2.05	2.02	1.01	0.96	0.74	0.53	1.13	1.16	0.89	0.65	1.11
Mean Predicted Wind Speed	3.98	3.92	2.92	2.58	2.76	0.93	1.59	2.19	2.62	3.12	2.66
Observed Standard Deviation	1.91	1.88	1.79	2.38	1.94	1.57	1.58	1.84	1.70	1.38	1.80
Predicted Standard Deviation	1.74	1.25	1.39	3.07	2.31	1.61	1.73	2.06	1.61	1.17	1.79
RMSE	2.37	2.21	1.92	2.56	2.54	1.73	1.78	1.96	2.10	2.58	2.18
RMSE _S	1.96	1.84	1.60	1.84	1.91	1.36	1.31	1.51	1.60	2.31	1.72
RMSE _U	1.30	1.20	1.05	1.76	1.66	1.02	1.15	1.22	1.33	1.12	1.28
Index of Agreement, I	0.73	0.70	0.79	0.84	0.79	0.77	0.70	0.78	0.74	0.64	0.75
Skill _E	0.73	0.67	0.62	0.78	0.90	0.66	0.79	0.72	0.84	0.82	0.75
Skill _{VAR}	0.98	0.68	0.81	1.30	1.23	1.06	1.18	1.17	0.97	0.85	1.02
Mean Observed Wind Direction (°)	225.7	250.3	299.0	184.8	283.8	82.3	76.2	110.2	128.7	147.8	178.9
Mean Predicted Wind Direction (°)	229.4	231.9	258.5	210.0	267.3	188.9	121.5	150.7	181.1	195.5	203.5

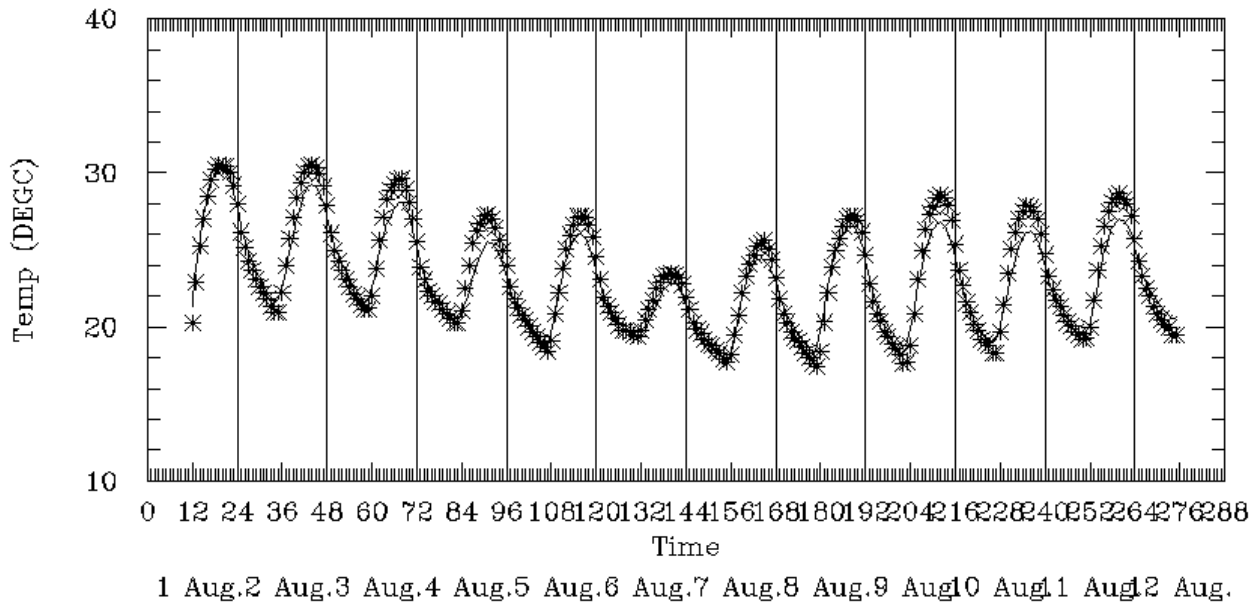
Performance Attribute	3 Aug Day 215	4 Aug Day 216	5 Aug Day 217	6 Aug Day 218	7 Aug Day 219	8 Aug Day 220	9 Aug Day 221	10 Aug Day 222	11 Aug Day 223	12 Aug Day 224	Mean Value
Mean Observed Wind Speed	1.99	1.67	1.09	0.57	0.24	0.78	1.27	1.24	1.08	0.90	1.08
Mean Predicted Wind Speed	3.91	3.27	2.56	1.65	0.72	1.61	2.36	2.65	2.65	2.96	2.43
Observed Standard Deviation	2.21	2.31	2.12	2.33	2.03	1.91	2.13	2.15	2.00	1.53	2.07
Predicted Standard Deviation	2.37	2.25	1.99	2.85	2.94	2.11	2.30	2.37	2.13	1.93	2.32
RMSE	2.71	2.50	2.21	2.42	2.64	2.00	2.10	2.29	2.39	2.84	2.41
RMSE _S	1.74	1.93	1.78	1.62	1.57	1.27	1.24	1.53	1.68	2.30	1.67
RMSE _U	0.83	1.54	1.28	1.76	2.10	1.51	1.63	1.65	1.69	1.63	1.56
Index of Agreement, I	0.73	0.76	0.79	0.85	0.82	0.81	0.82	0.80	0.76	0.63	0.78
Skill _E	0.83	0.67	0.63	0.79	1.10	0.85	0.79	0.79	0.86	1.07	0.84
Skill _{VAR}	1.11	0.99	0.97	1.26	1.52	1.19	1.11	1.13	1.28	1.27	1.18
Mean Observed Wind Direction (°)	235.4	258.8	271.0	231.9	169.2	150.3	153.9	154.4	183.6	148.8	195.7
Mean Predicted Wind Direction (°)	227.5	235.0	243.4	218.2	239.0	188.9	180.3	189.5	192.2	188.6	210.3

Table 6-7.3. RAMS model evaluation results for the 3-12 August 1993 SAMI episode – surface mixing ratios (gm/kg). (a) 12 Km Grid											
Performance Attribute	3 Aug Day 215	4 Aug Day 216	5 Aug Day 217	6 Aug Day 218	7 Aug Day 219	8 Aug Day 220	9 Aug Day 221	10 Aug Day 222	11 Aug Day 223	12 Aug Day 224	Mean Value
Maximum Observed Mixing Ratio	21.8	21.0	19.7	20.6	20.5	20.3	19.6	18.3	18.2	20.8	20.1
Maximum Predicted Mixing Ratio	18.4	17.7	17.4	17.3	17.4	16.9	16.8	15.7	16.8	17.2	17.2
Mean Bias (gm/Kg)	-0.8	-0.6	-0.4	-0.5	-0.4	-0.6	-0.8	-0.7	-0.5	-0.3	-0.6
Gross Error (gm/Kg)	1.4	1.1	1.0	1.1	1.0	1.0	1.2	1.1	1.2	1.0	1.1

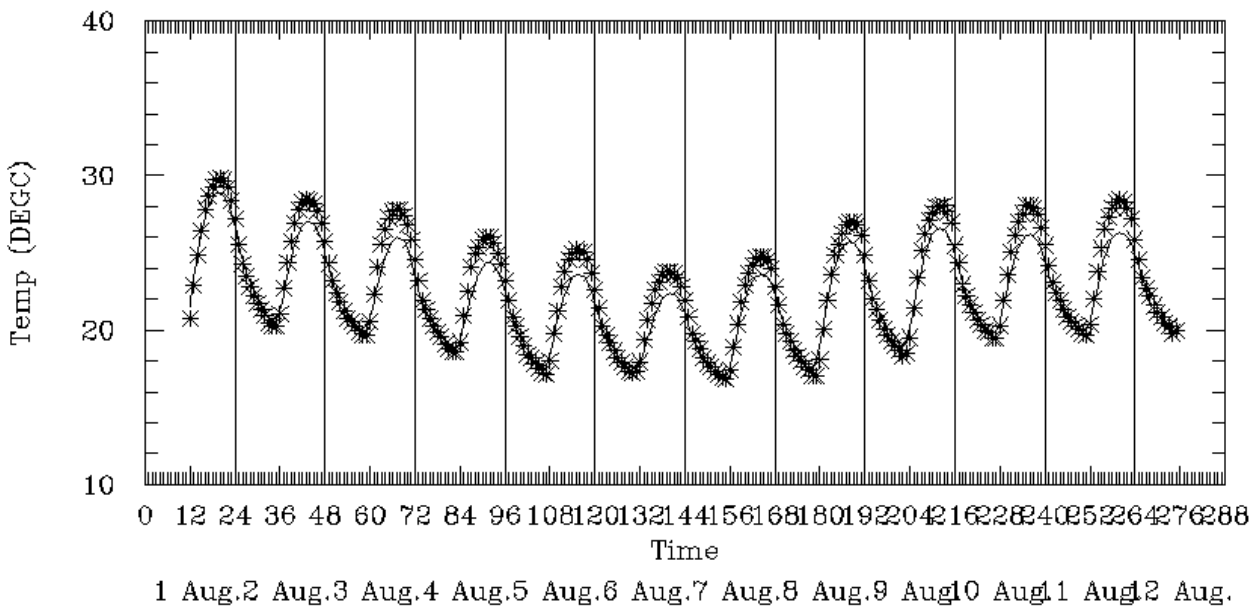
Table 6-7.3. RAMS model evaluation results for the 3-12 August 1993 SAMI episode – surface mixing ratios (gm/kg). (b) 24 Km Grid											
Performance Attribute	3 Aug Day 215	4 Aug Day 216	5 Aug Day 217	6 Aug Day 218	7 Aug Day 219	8 Aug Day 220	9 Aug Day 221	10 Aug Day 222	11 Aug Day 223	12 Aug Day 224	Mean Value
Maximum Observed Mixing Ratio	24.2	24.0	24.0	24.1	24.1	24.0	23.3	22.0	22.8	22.9	23.5
Maximum Predicted Mixing Ratio	19.2	18.4	18.4	18.3	18.7	18.3	18.5	18.6	19.3	19.7	18.7
Mean Bias (gm/Kg)	-0.5	-0.4	-0.3	-0.3	-0.4	-0.5	-0.6	-0.5	-0.5	-0.1	-0.4
Gross Error (gm/Kg)	1.2	1.1	1.0	1.0	1.0	1.1	1.2	1.2	1.2	1.2	1.1

Table 6-7.4. RAMS model evaluation results for the 3-12 August 1993 SAMI episode – daily total precipitation (mm). (a) 12 Km Grid											
Performance Attribute	3 Aug Day 215	4 Aug Day 216	5 Aug Day 217	6 Aug Day 218	7 Aug Day 219	8 Aug Day 220	9 Aug Day 221	10 Aug Day 222	11 Aug Day 223	12 Aug Day 224	Mean Value
Maximum Observed Precipitation	34.0	52.0	85.0	26.0	119.0	52.0	32.0	9.0	--	--	50.0
Maximum Predicted Precipitation	11.5	37.6	51.6	26.1	102.7	22.9	40.0	30.0	--	--	40.3
Mean Observed Precipitation	1.5	4.9	4.8	1.2	25.6	3.5	0.9	0.1	--	--	5.3
Mean Predicted Precipitation	2.4	3.3	14.7	2.5	27.7	2.4	0.6	0.3	--	--	6.7
Mean Bias (mm)	0.93	-1.27	10.38	1.33	4.34	-0.81	-0.30	0.23	--	--	1.9
Gross Error (mm)	2.89	6.44	13.91	3.00	16.4	2.35	1.30	0.41	--	--	5.8

Table 6-7.4. RAMS model evaluation results for the 3-12 August 1993 SAMI episode – daily total precipitation (mm). (b) 24 Km Grid											
Performance Attribute	3 Aug Day 215	4 Aug Day 216	5 Aug Day 217	6 Aug Day 218	7 Aug Day 219	8 Aug Day 220	9 Aug Day 221	10 Aug Day 222	11 Aug Day 223	12 Aug Day 224	Mean Value
Maximum Observed Precipitation	67.0	52.0	85.0	67.0	119.0	67.0	47.0	74.0	--	--	72.3
Maximum Predicted Precipitation	13.3	31.4	49.3	46.7	97.5	30.0	32.2	24.6	--	--	40.6
Mean Observed Precipitation	1.8	3.6	4.1	1.9	18.3	3.6	1.1	0.9	--	--	4.4
Mean Predicted Precipitation	1.8	2.7	9.4	2.6	18.5	2.1	0.5	0.5	--	--	4.8
Mean Bias (mm)	0.03	-0.65	5.92	0.67	2.04	-1.36	-0.58	-0.38	--	--	0.7
Gross Error (mm)	2.67	4.94	9.96	3.24	12.34	2.91	1.40	1.20	--	--	4.8

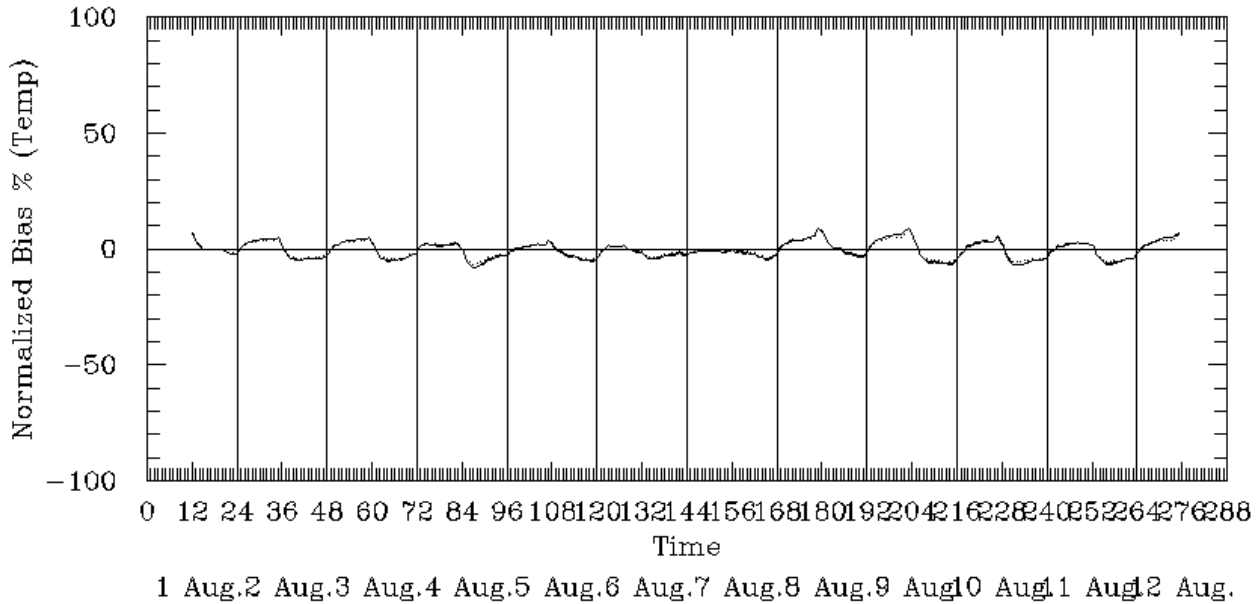


(a) 12 Km Grid

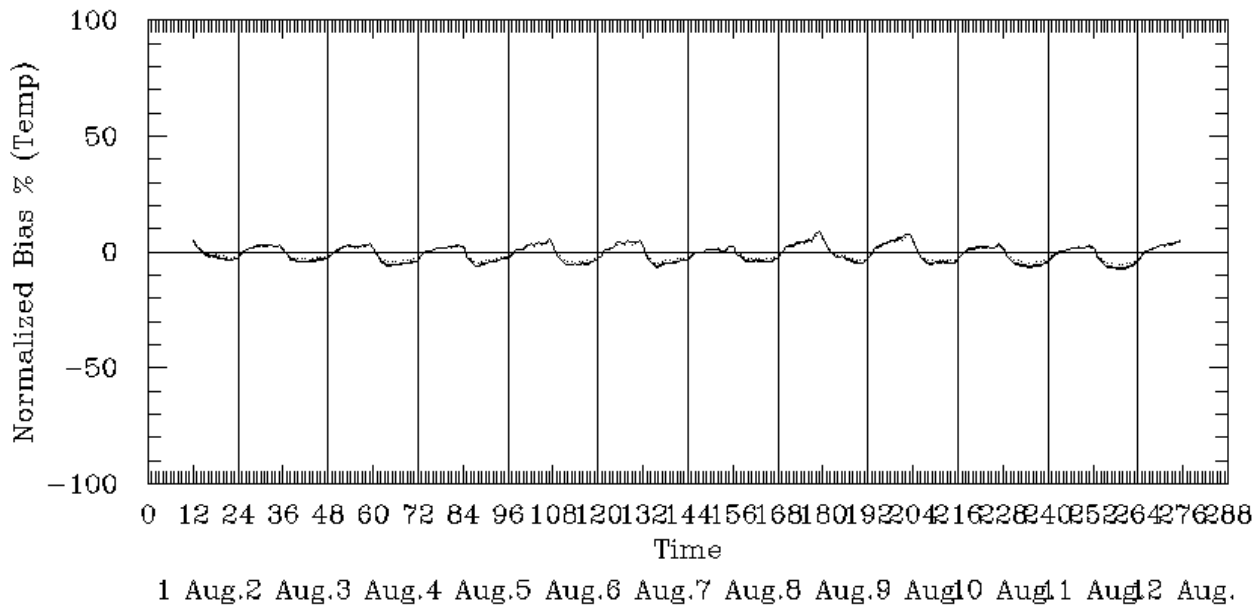


(b) 24 Km Grid

Figure 6-44. Spatial Mean Ground-Level Temperatures for the 3-12 August 1993 Episode.

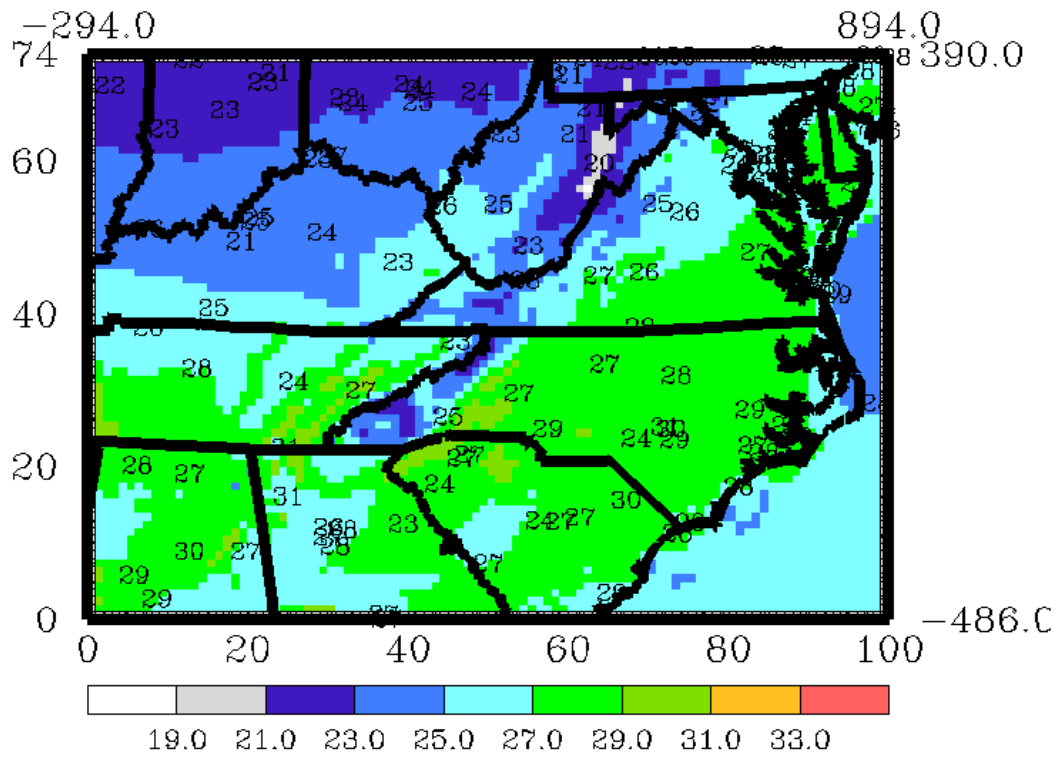


(a) 12 Km Grid

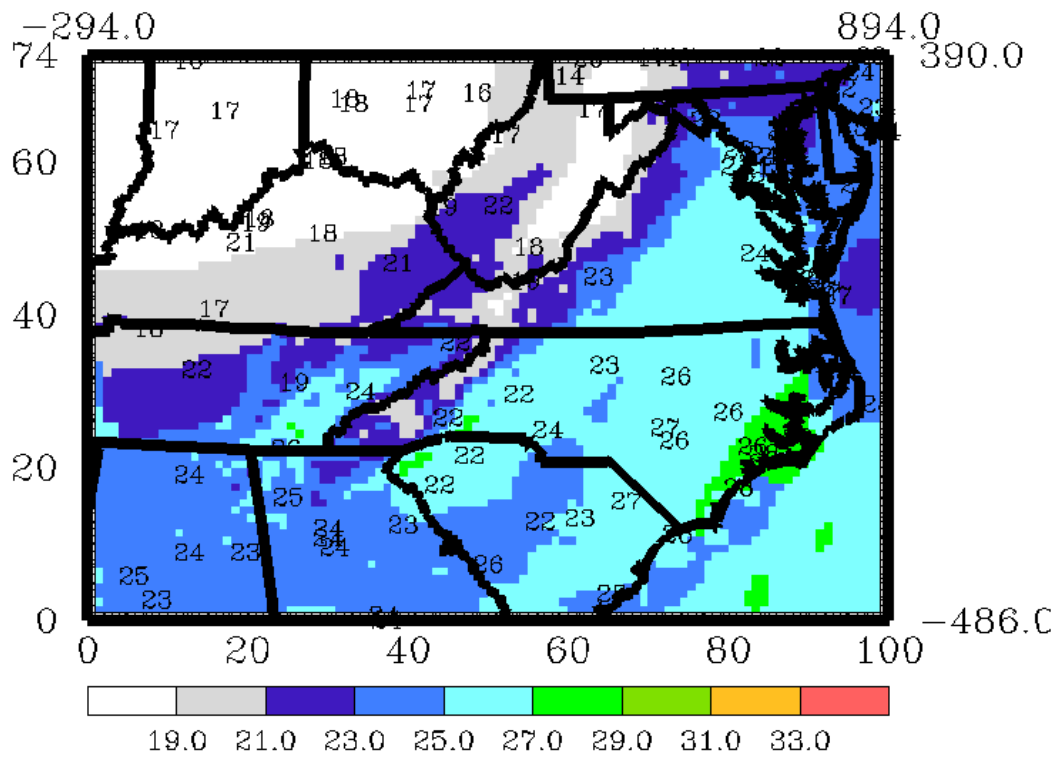


(b) 24 Km Grid

Figure 6-45. Mean Normalized Bias in Ground-Level Temperatures for the 3-12 August 1993 Episode.

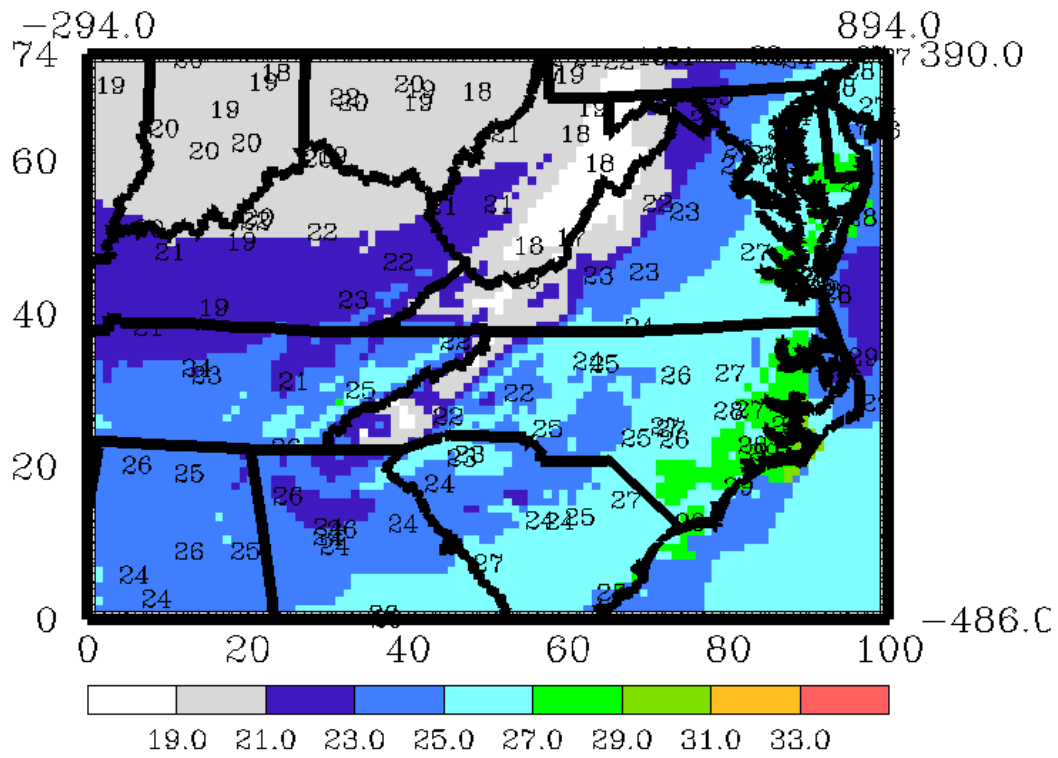


(a) 0100 UTC (2100 EST)

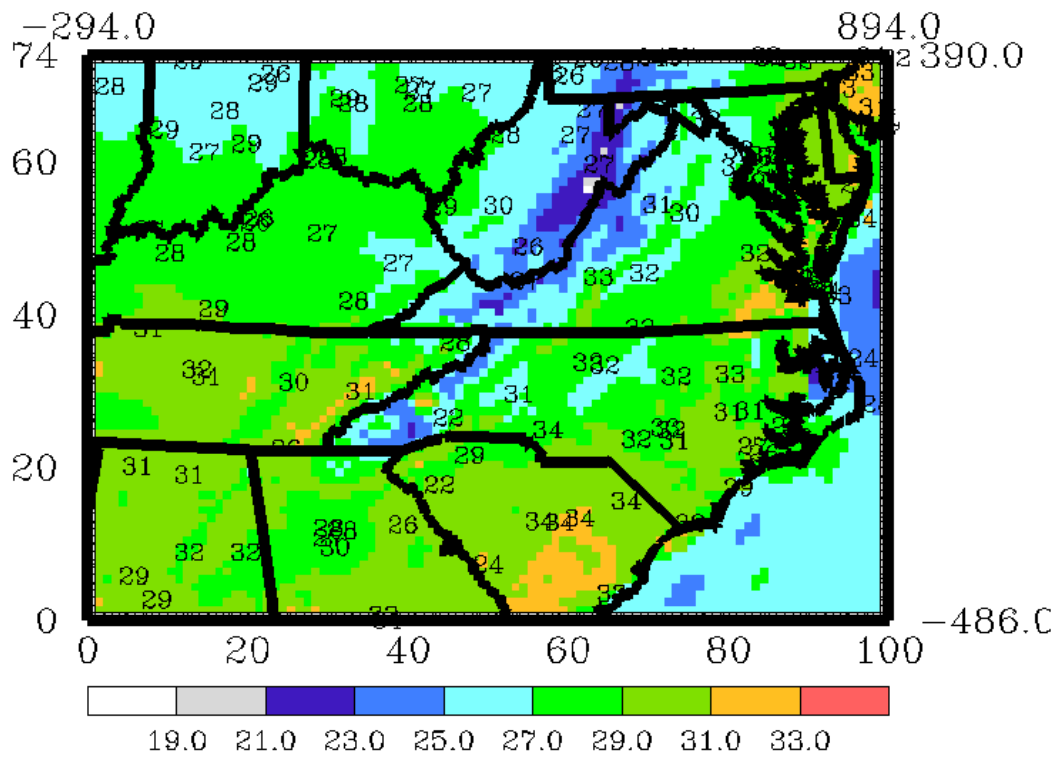


(b) 0700 UTC (0300 EST)

Figure 6-46. Ground-Level Temperature Fields for 3 August 1993.

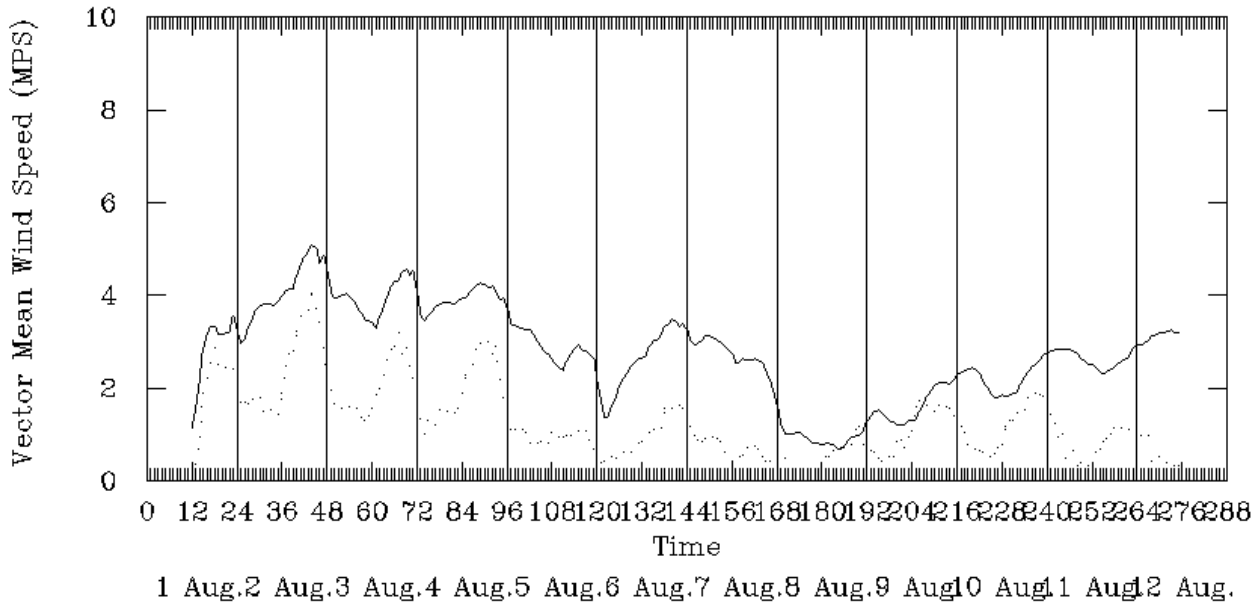


(c) 1300 UTC (0900 EST)

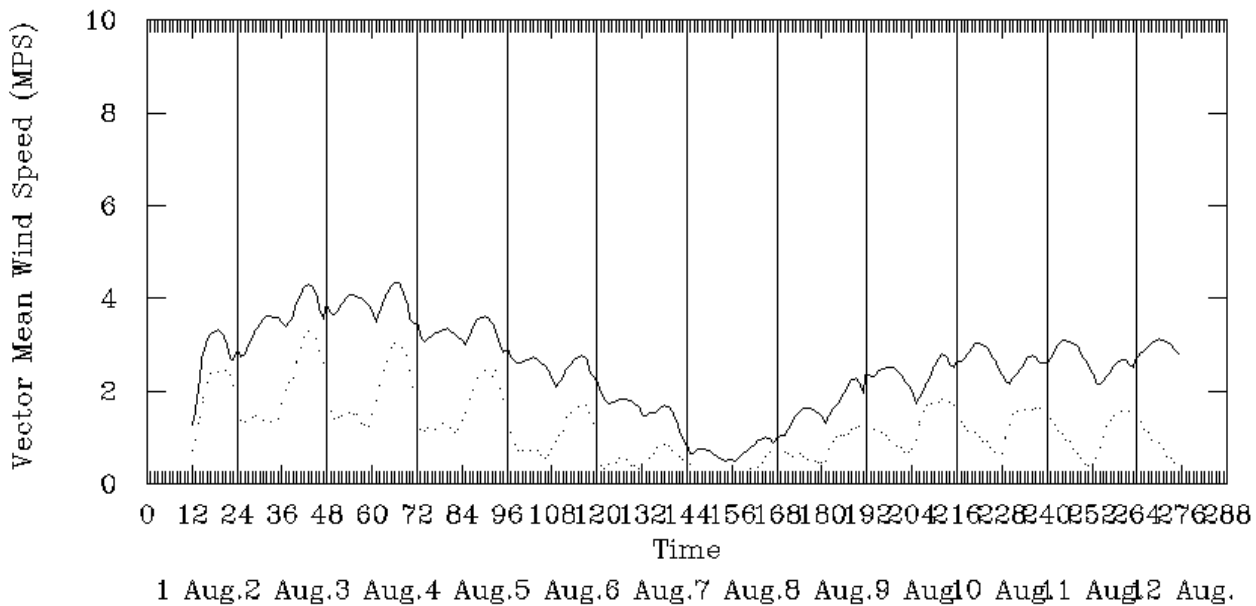


(d) 1900 UTC (1500 EST)

Figure 6-46. Concluded.

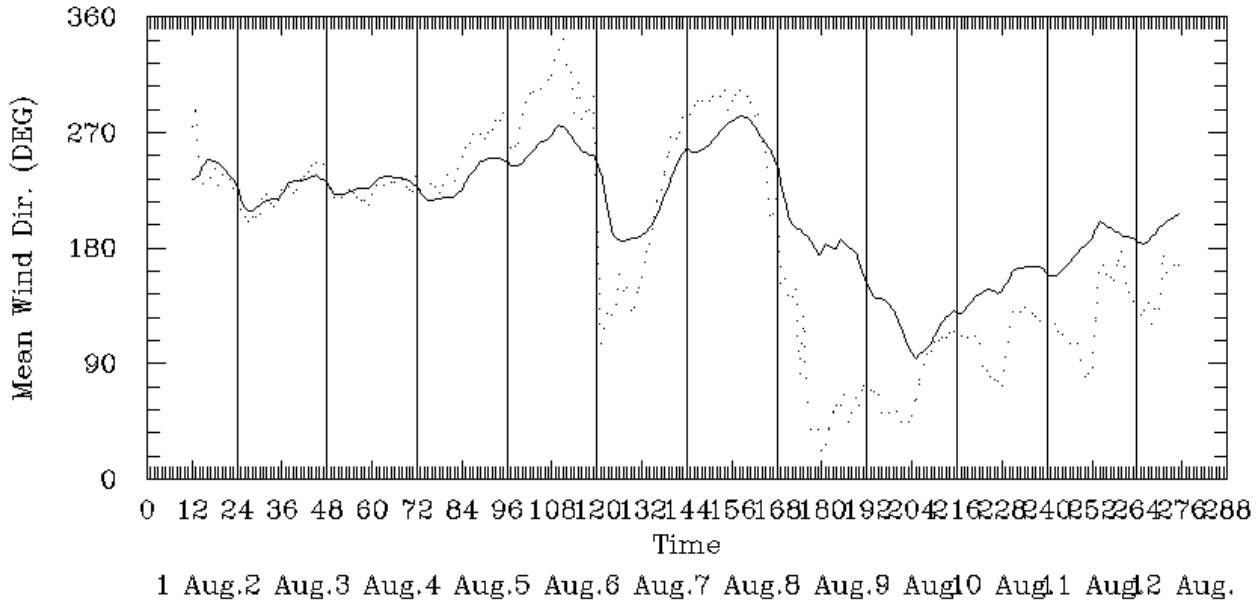


(a) 12 Km Grid

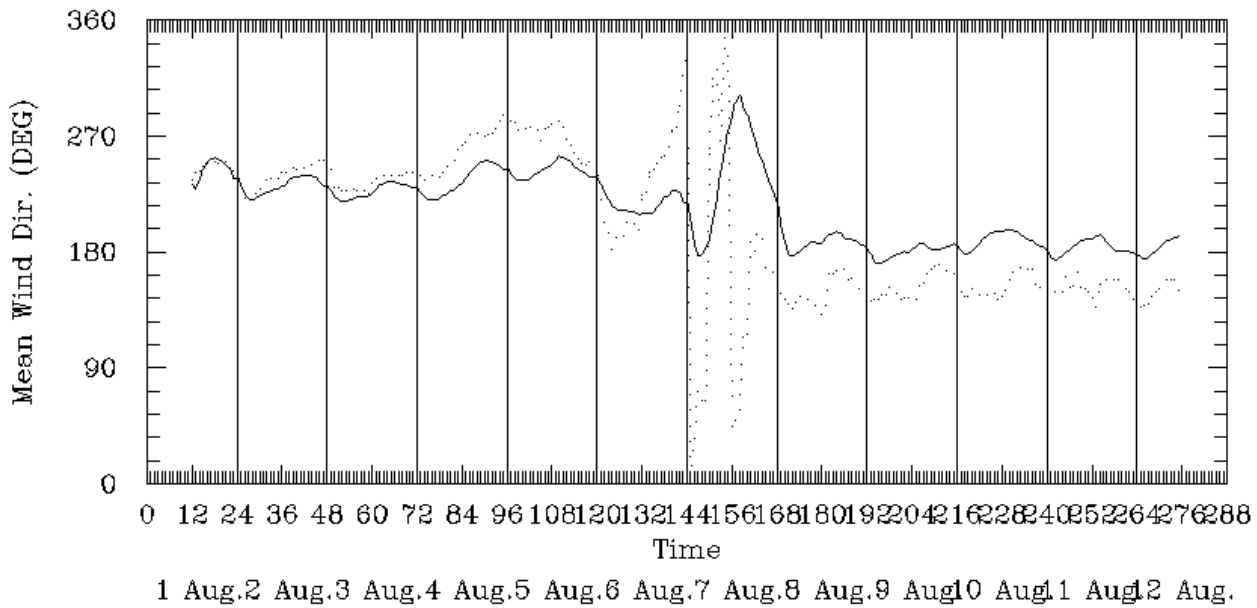


(b) 24 Km Grid

Figure 6-47. Vector Mean Wind Speed for the 3-12 August 1993 Episode.

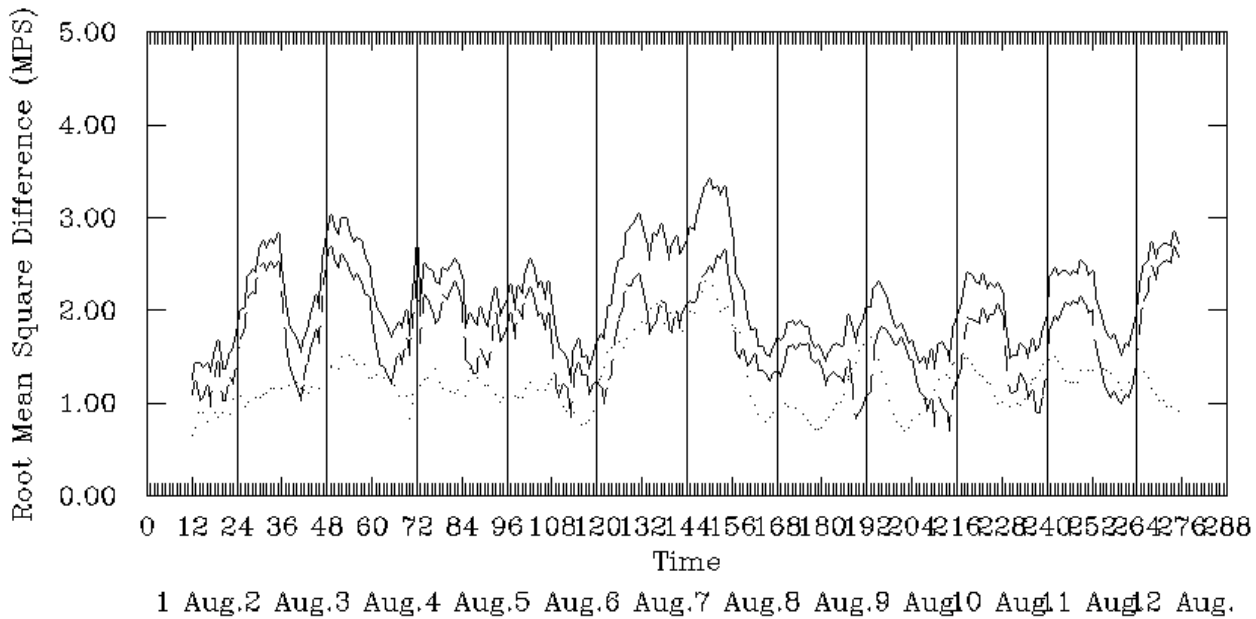


(a) 12 Km Grid

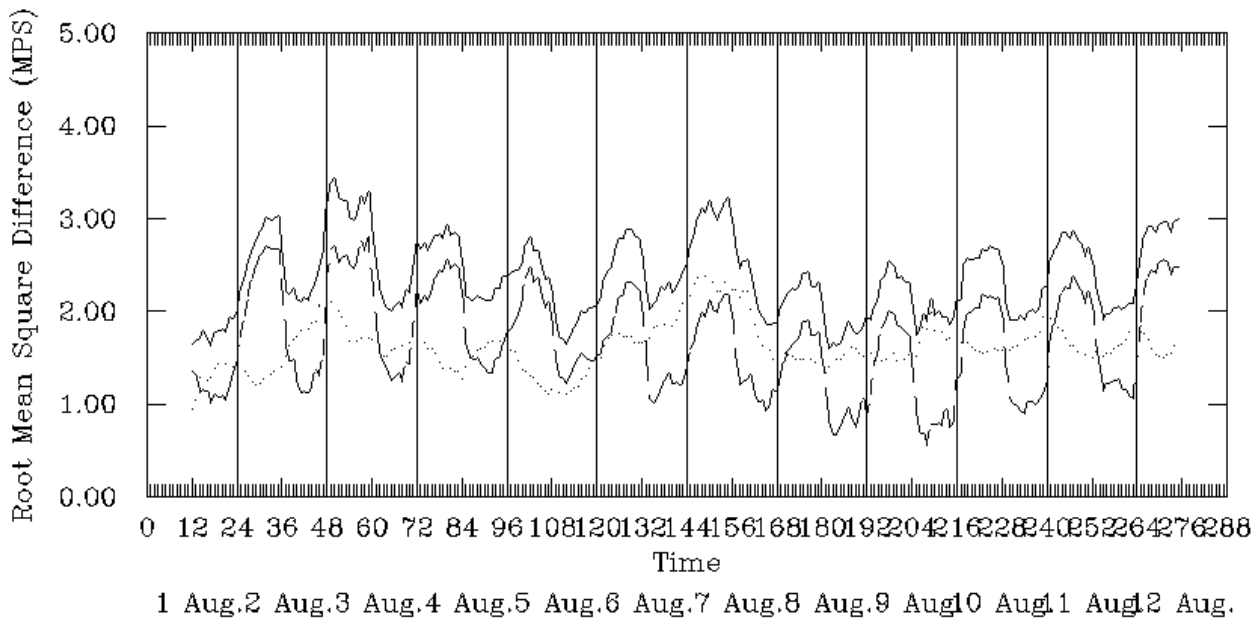


(b) 24 Km Grid

Figure 6-48. Mean Wind Direction for the 3-12 August 1993 Episode.

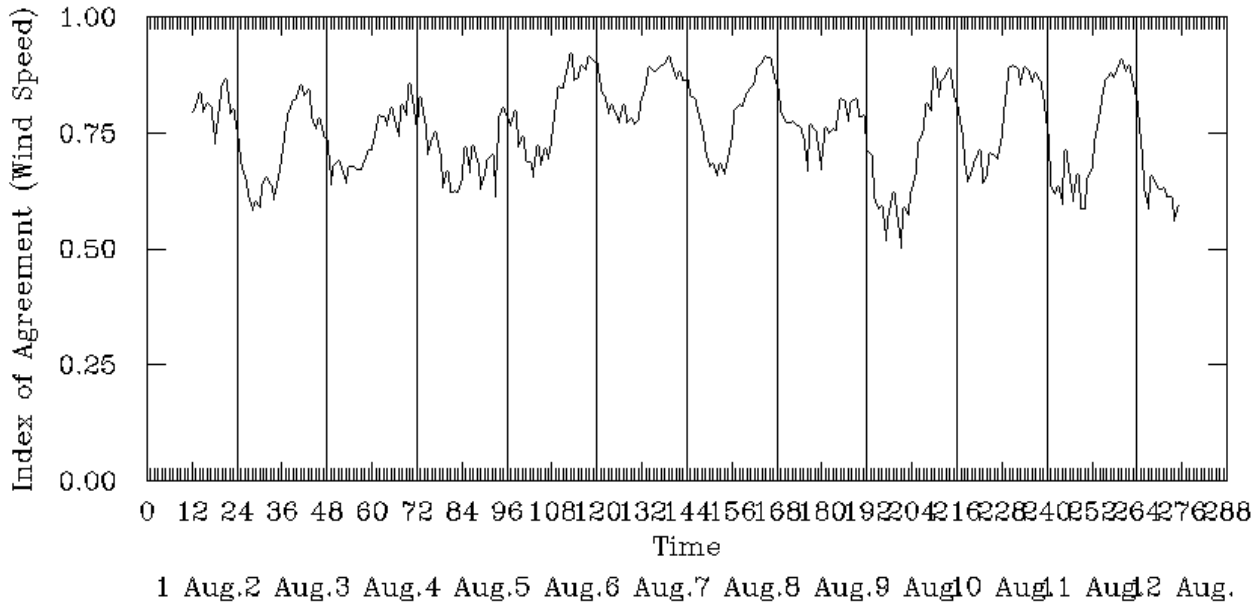


(a) 12 Km Grid

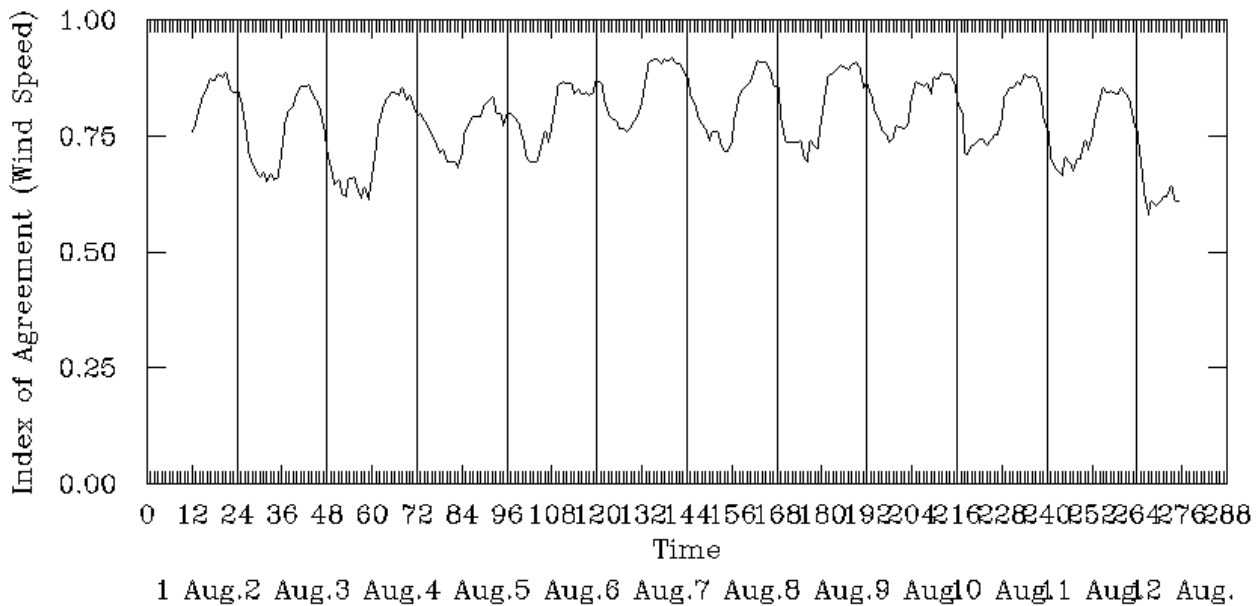


(b) 24 Km Grid

Figure 6-49. Root Mean Square Error in Ground-Level Wind Speeds for the 3-12 August 1993 Episode.

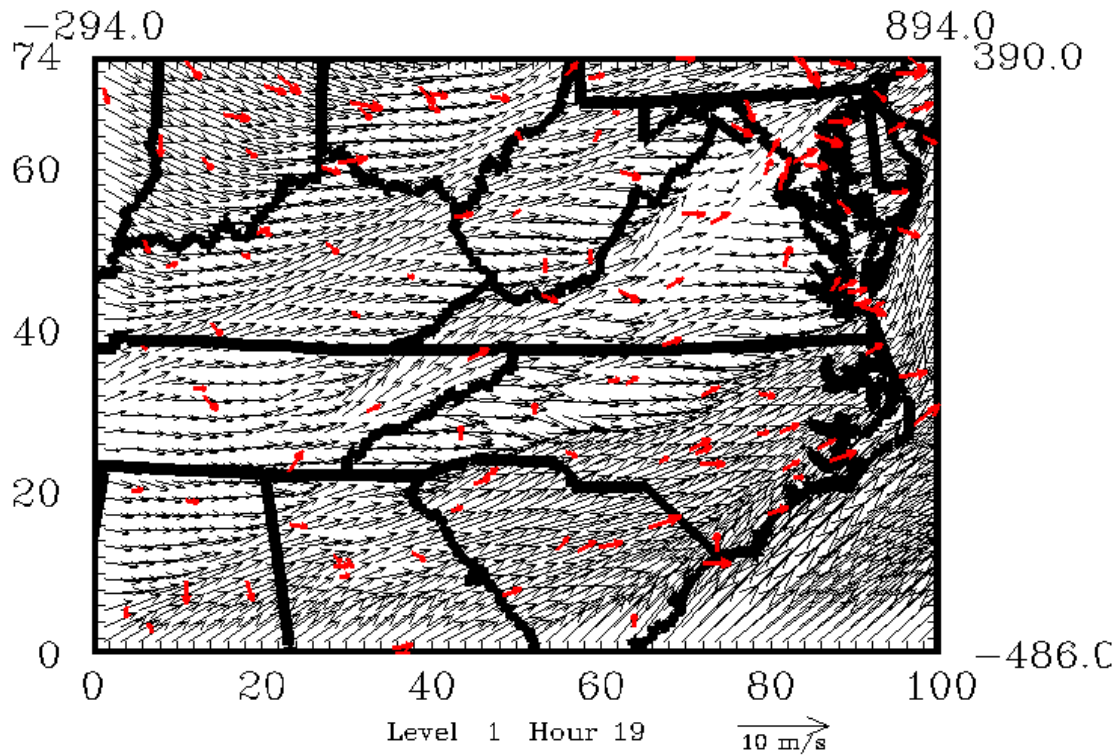


(a) 12 Km Grid

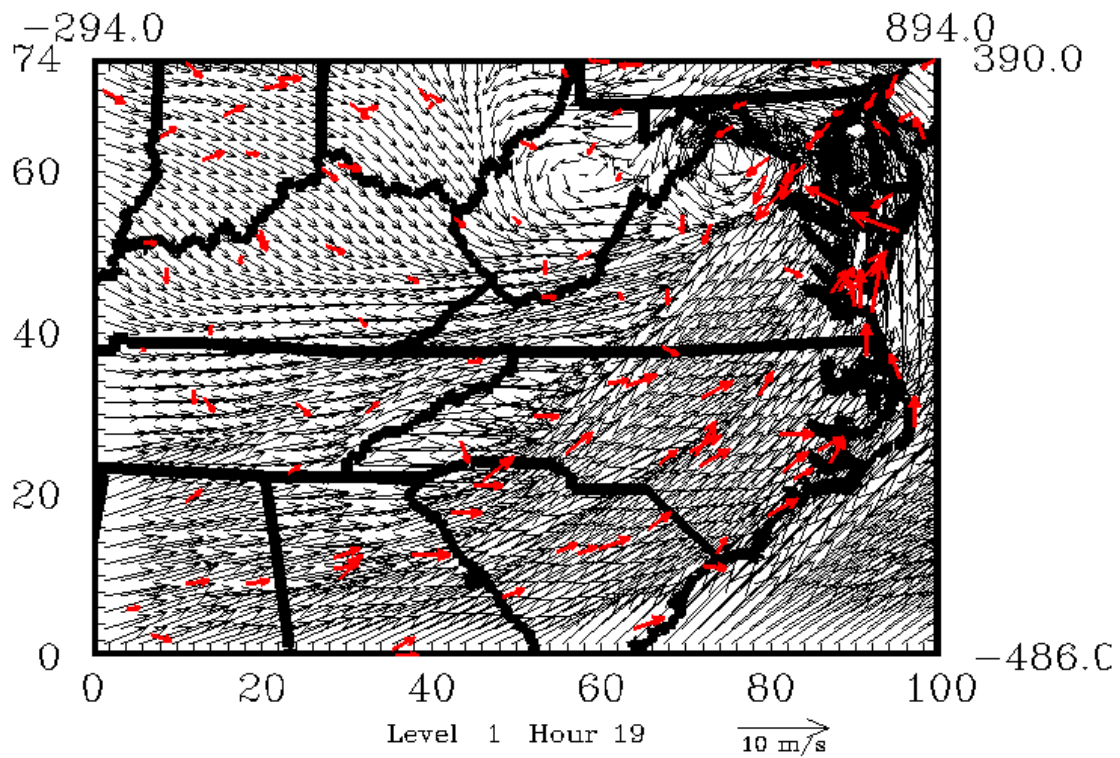


(b) 24 Km Grid

Figure 6-50. Index of Agreement in Surface Wind Speed for the 3-12 August 1993 Episode.

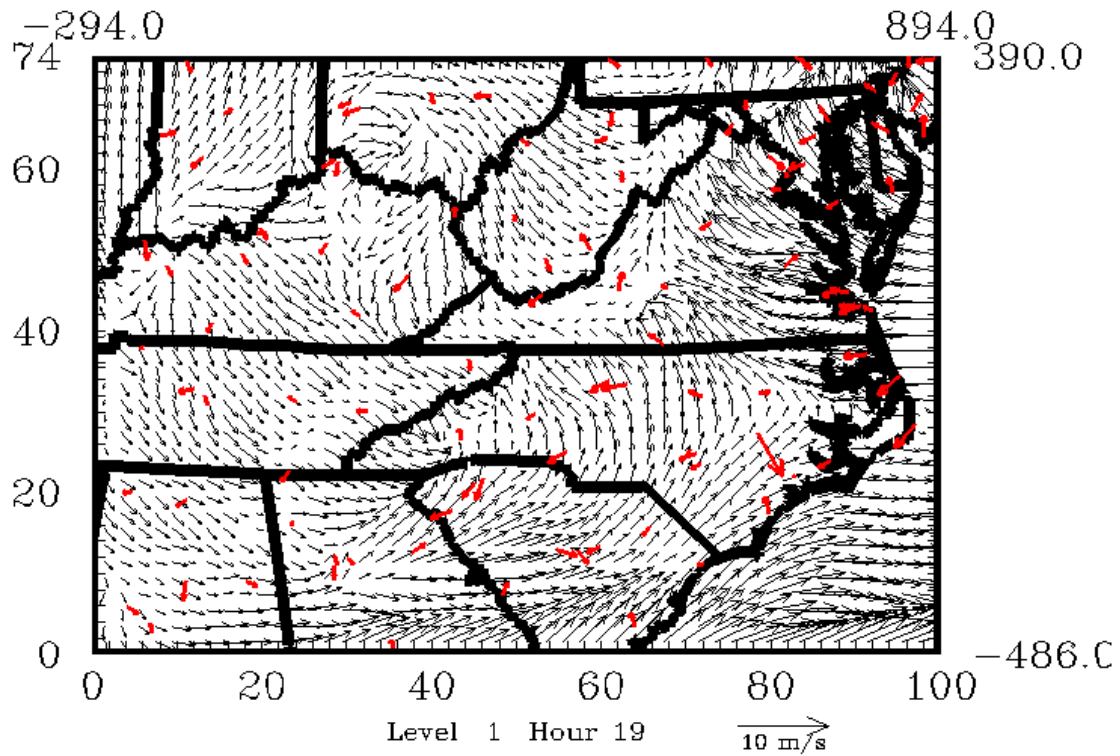


(a) 4 August 1993, 1900 UTC (1500 EST)

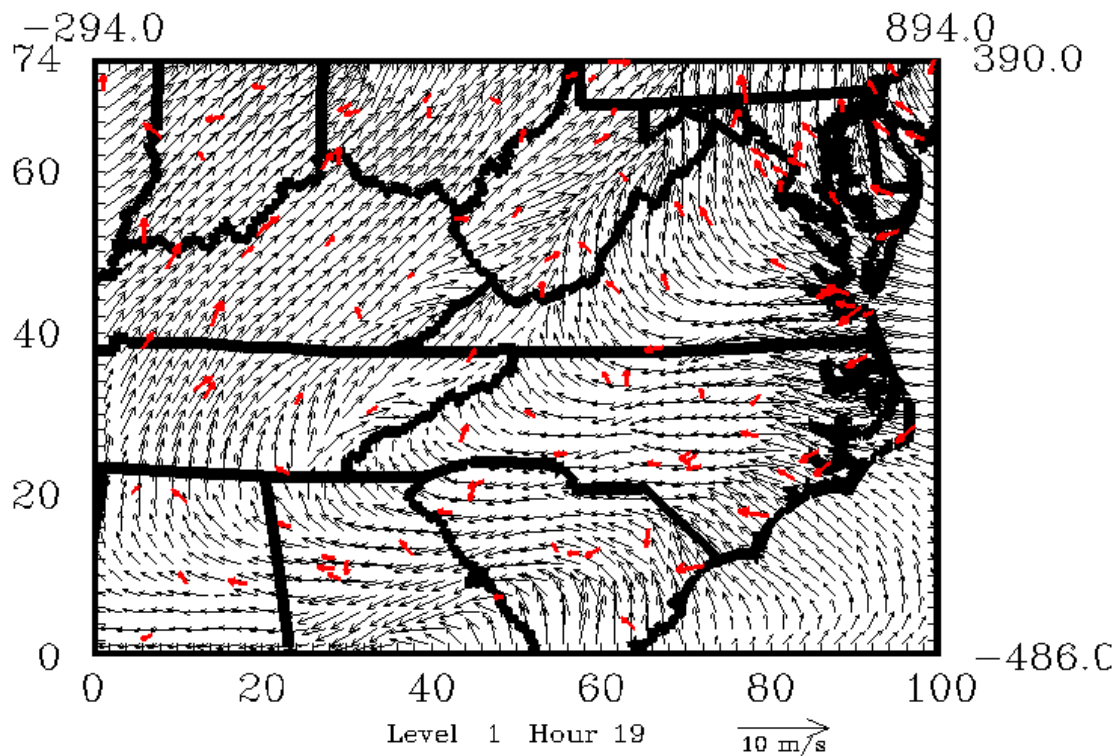


(b) 6 August 1993, 1900 UTC (1500 EST)

Figure 6-51. Ground-Level Wind Fields for the 3-12 August 1993 Episode.

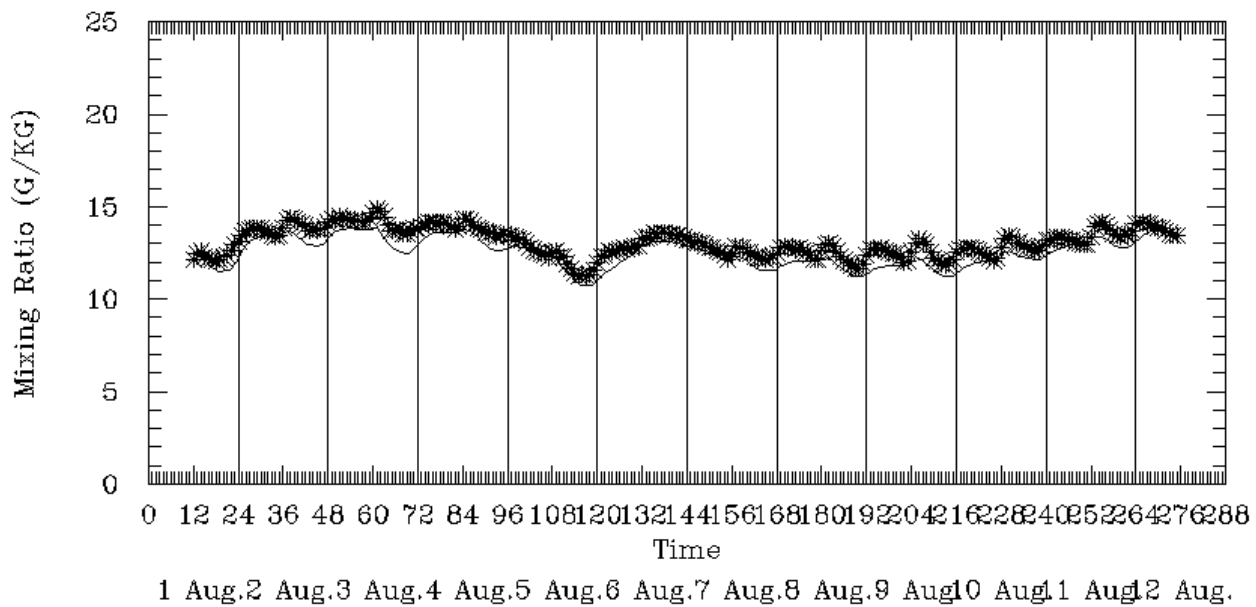


(c) 8 August 1993, 1900 UTC (1500 EST)

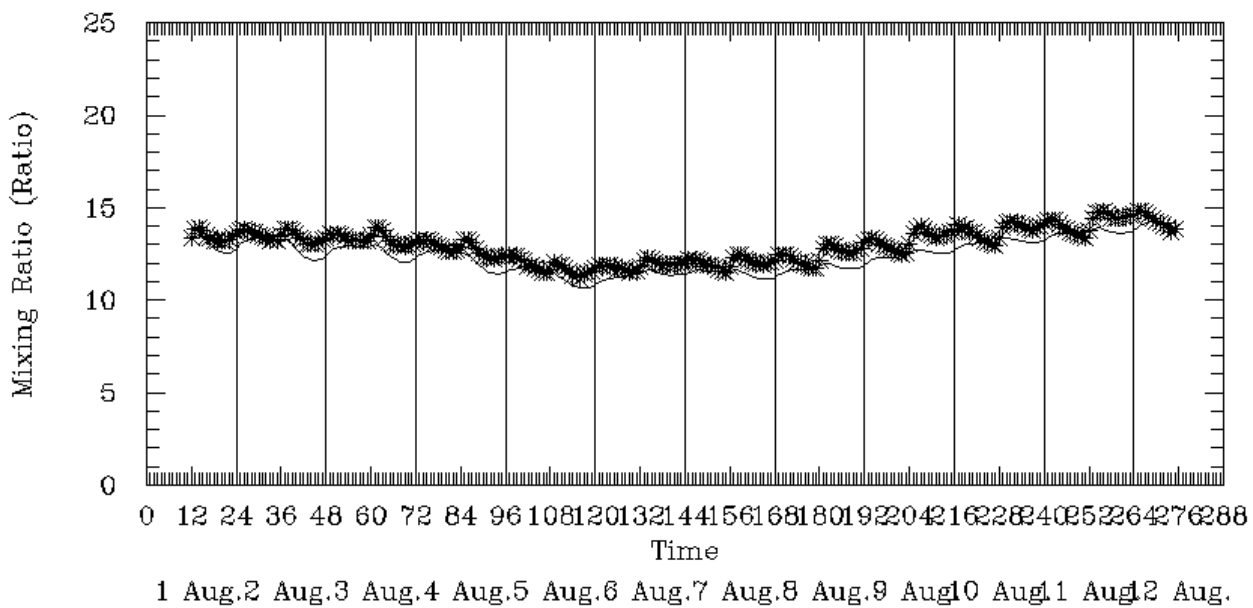


(d) 10 August 1993, 1900 UTC (1500 EST)

Figure 6-51. Concluded.

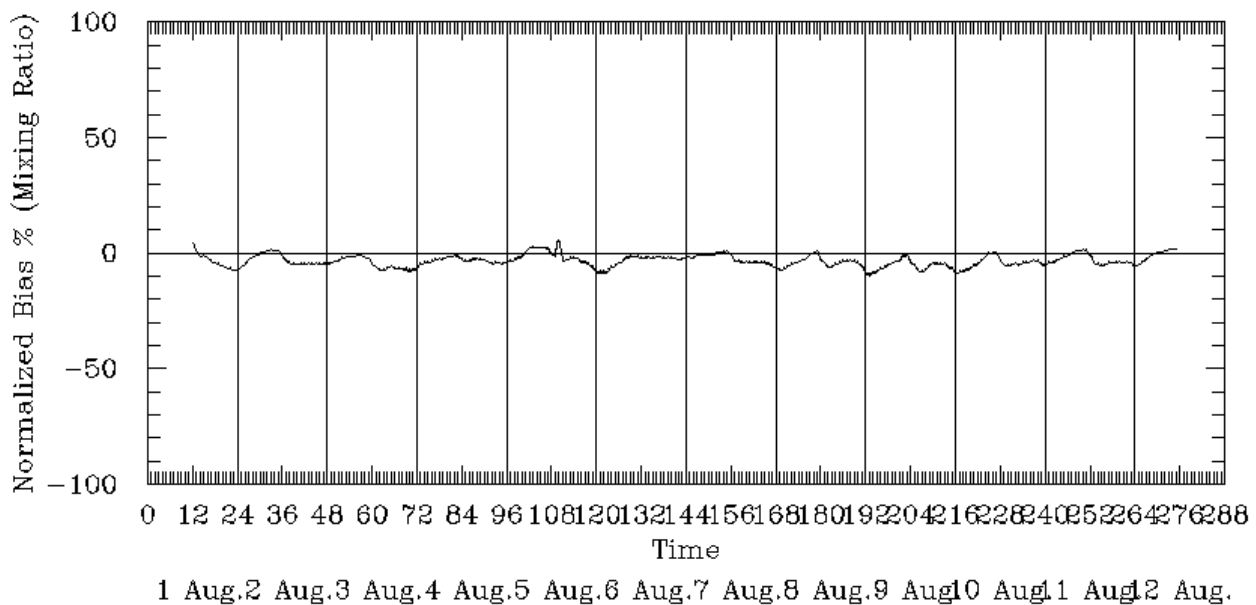


(a) 12 Km Grid

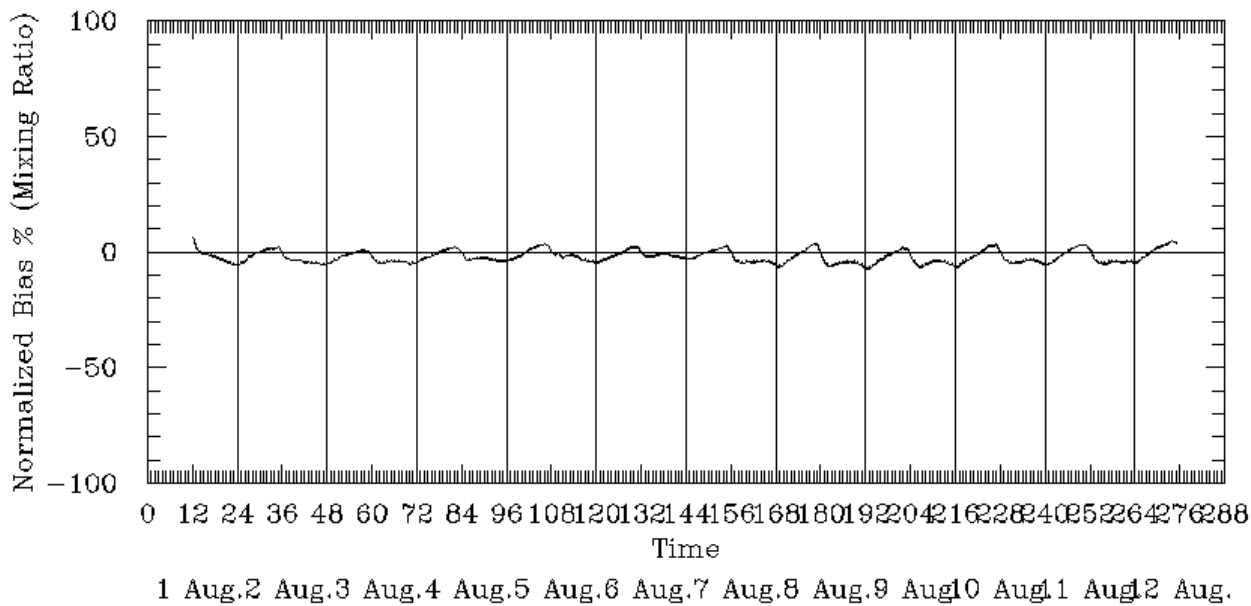


(b) 24 Km Grid

Figure 6-52. Spatial Mean Ground-Level Mixing Ratios for the 3-12 August 1993 Episode.

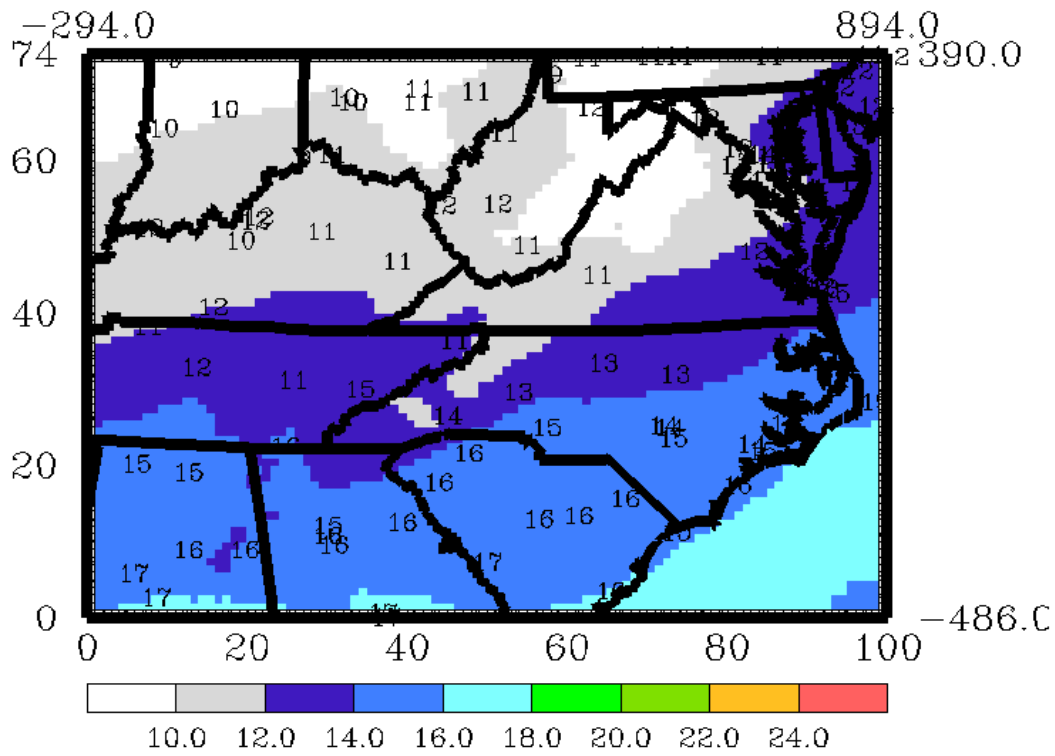


(a) 12 Km Grid

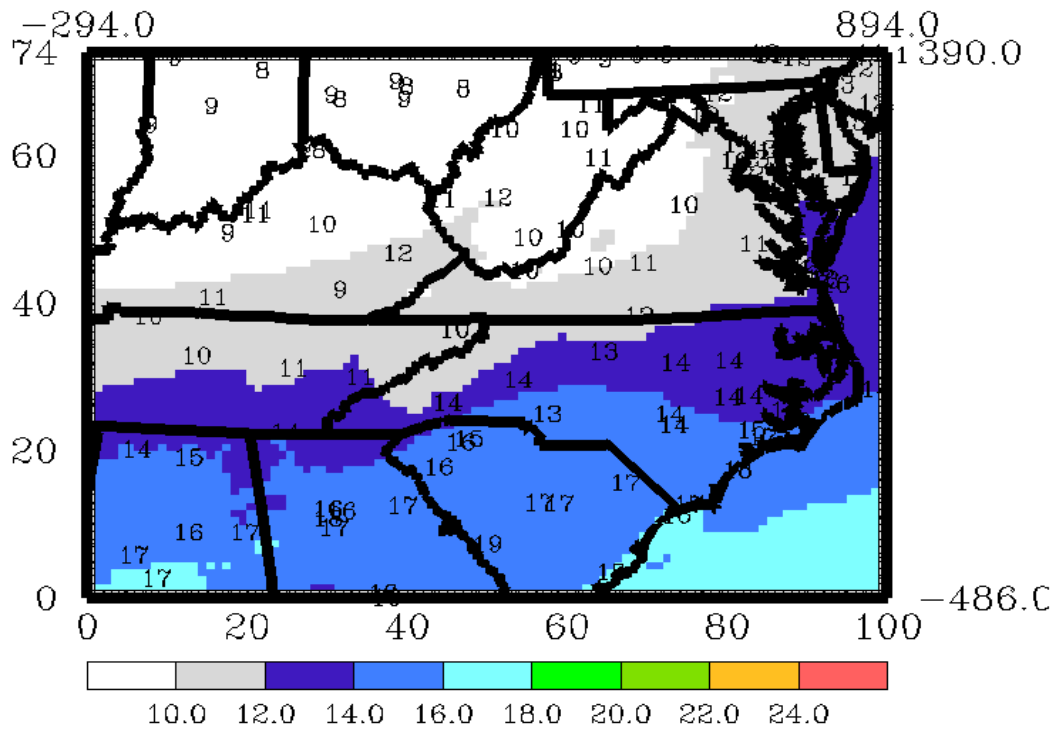


(b) 24 Km Grid

Figure 6-53. Mean Normalized Bias in Ground-Level Mixing Ratios for the 3-12 August 1993 Episode.

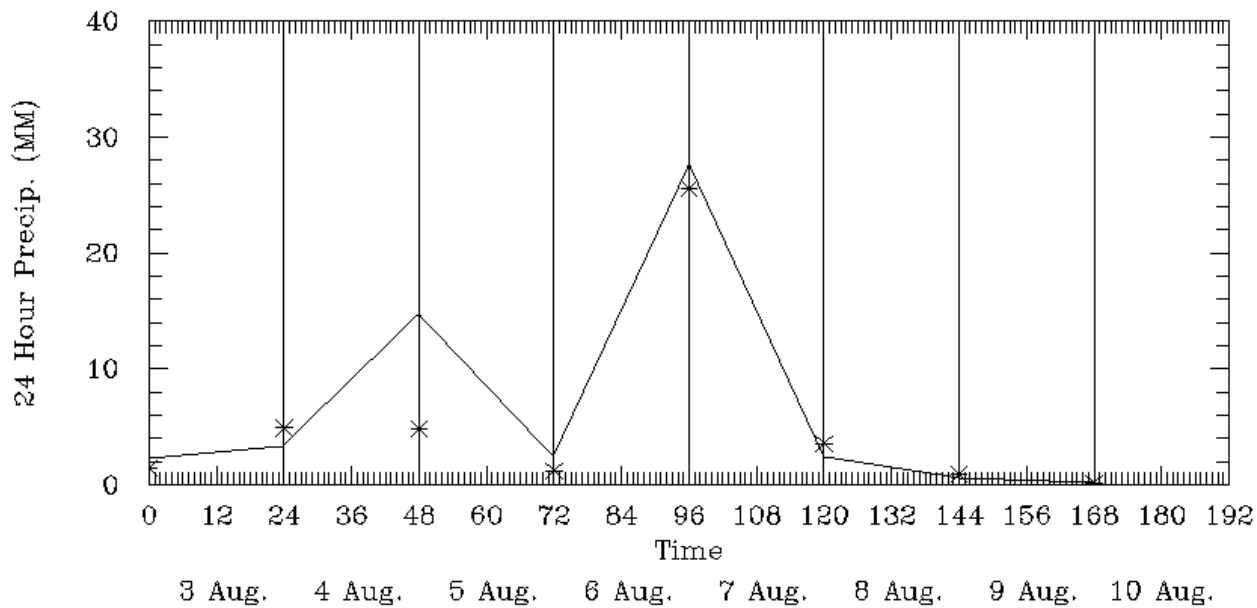


(a) 0700 UTC (0300 EST)

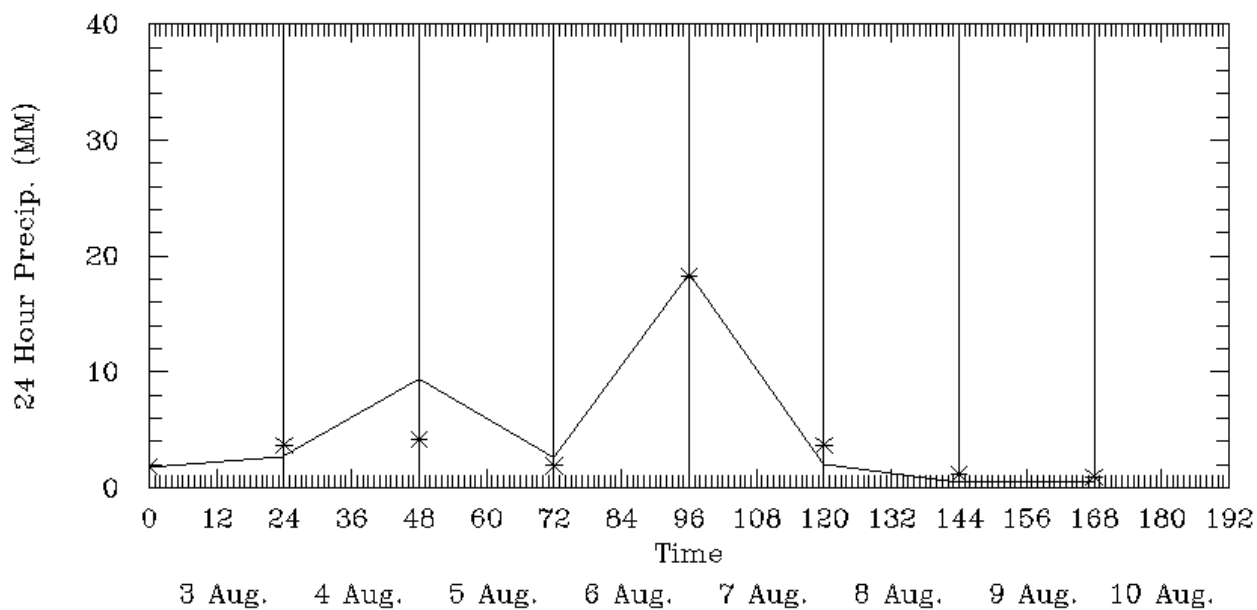


(b) 1900 UTC (1500 EST)

Figure 6-54. Ground-Level Mixing Ratio Fields for 7 August 1993.

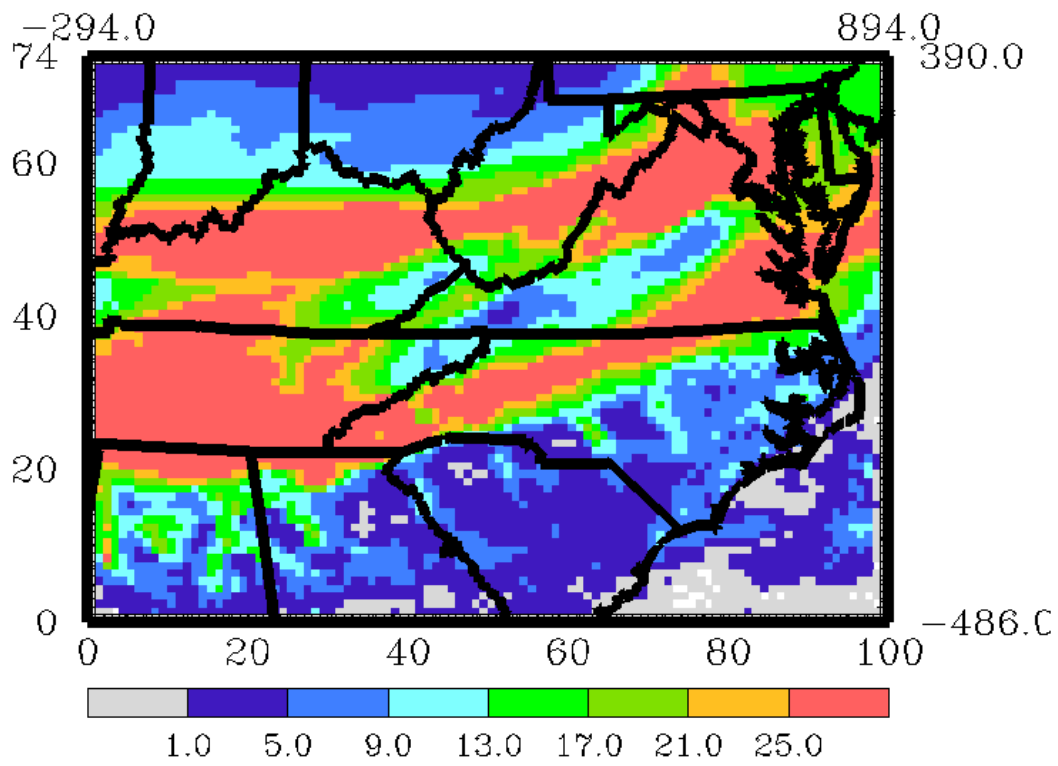


(a) 12 Km Grid

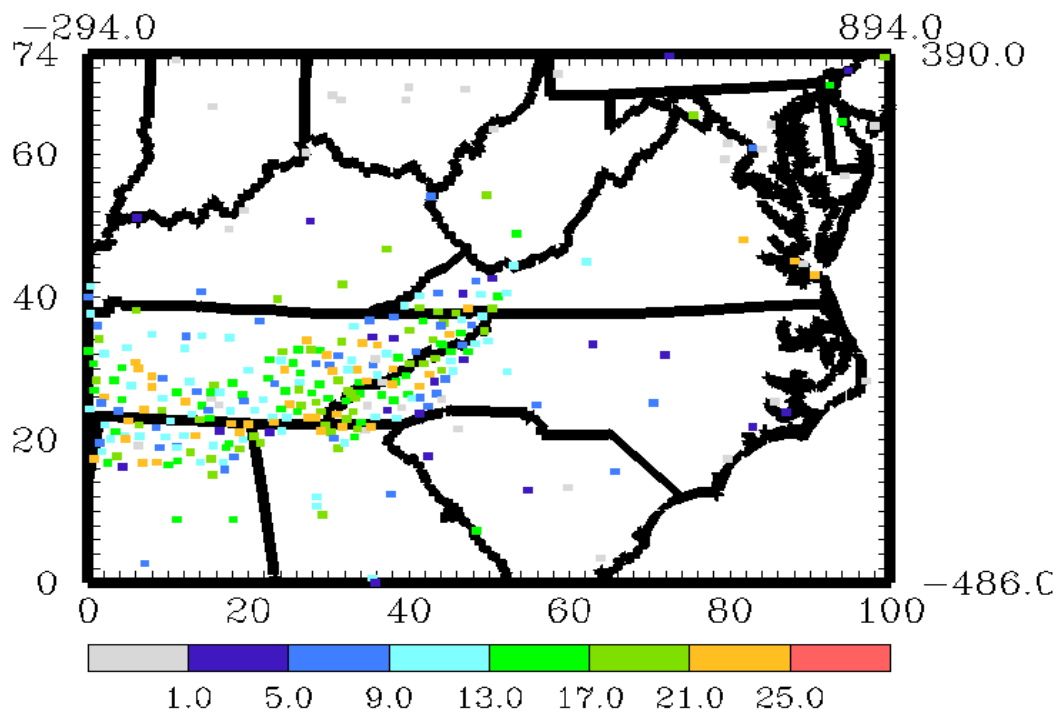


(b) 24 Km Grid

Figure 6-55. Spatial Mean Daily Precipitation (mm) for the 3-12 August 1993 Episode.

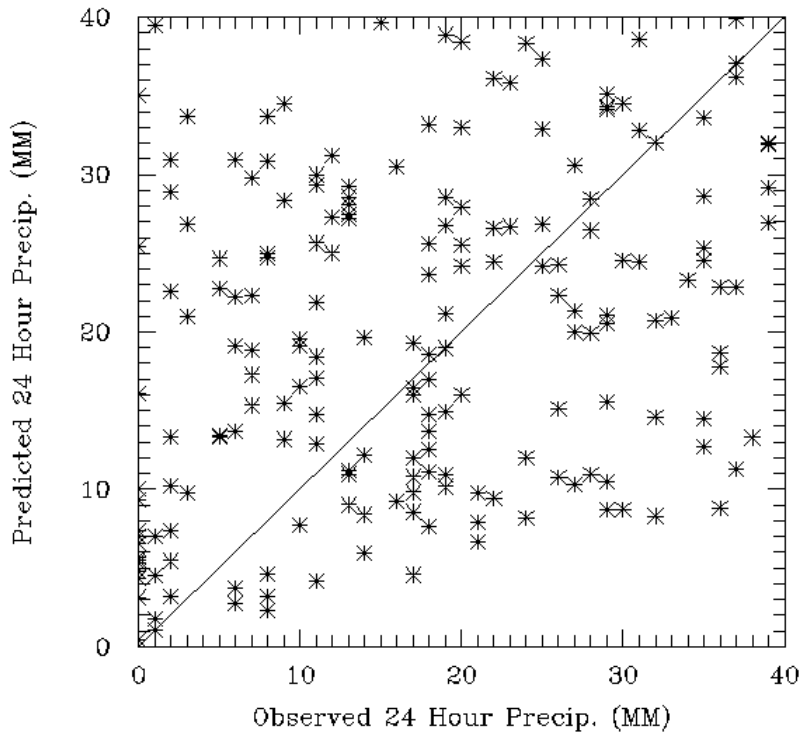


(a) Predicted Precipitation (mm)

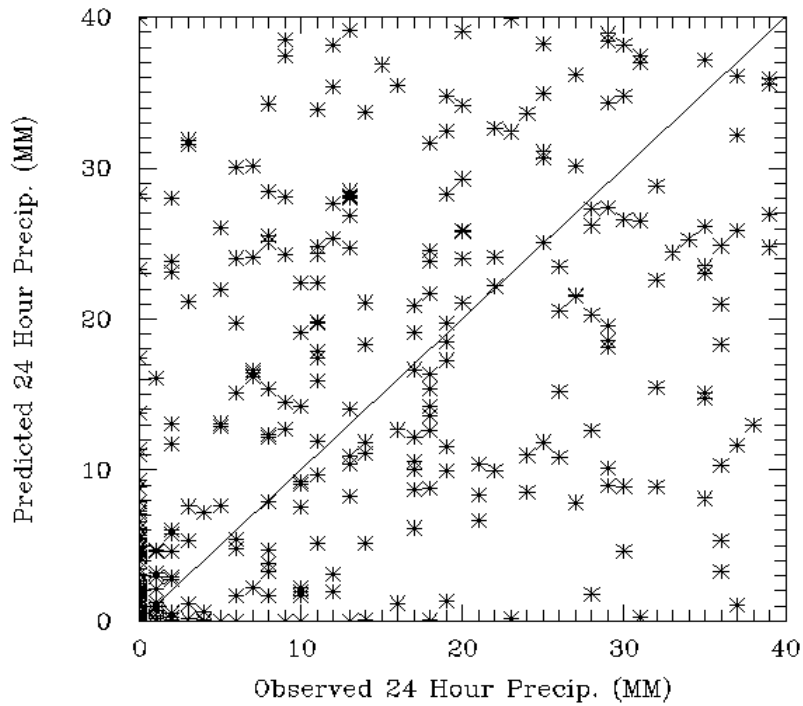


(b) Measured Precipitation (mm)

Figure 6-56. Daily Precipitation Fields for 7 August 1993.



(a) 12 Km Grid



(b) 24 Km Grid

Figure 6-57. Scatter Plot of Daily Maximum Rainfall (mm) for 7 August 1993.

6.8 22-29 June 1992 Episode Results

6.8.1 Surface Temperatures

6.8.1.1 Statistical Measures of Near-Surface Temperatures

Table 6-8 gives the statistical results for predicted and observed near-surface temperatures for the eight modeling days of the 22-29 June 1992 episode. The daily maximum temperatures during the June episode began at 27.8°C on the 22nd and increased to a high of 36.1°C on the 26th, whereupon a cooling trend ensued with the maximum temperatures dropping down to 32.2°C on the 28th. As indicated in Table 6-8, RAMS did a very job of reproducing the daily maximum temperatures on each day with the exception of 26 June where the peak was underestimated by 3.4°C. The episode-averages of the daily maximum observed and predicted temperatures were 32.7°C and 32.8°C, respectively, for a 0.3% discrepancy. Also from Table 6-8, the mean bias in predicted hourly surface temperatures across the 12 km domain ranges from -1.7°C to -0.2°C. On average across the June 1992 episode, the mean bias in RAMS surface temperature prediction -1.1°C. The average gross errors in surface temperature predictions for the 8 days were 1.8°C.

6.8.1.2 Spatial Mean Surface Temperatures

Figures 6-58 and 6-59 show the spatial mean near-surface temperatures and mean normalized bias in hourly temperatures as a function of time of day. From the spatial mean temperature plot (Figure 6-58), RAMS generally follows the hourly mean temperature measurements fairly well. However, the model systematically underestimates the afternoon spatial mean peak values on each day and this discrepancy appears to worsen as the episode ensues. By the 29th, the mean under-prediction at midday is roughly 6°C. Recall from Table 6-8.1 that the model reproduced the domain-wide maximum temperature on this day to within 0.3°C. In addition to this systematic tendency to underestimate the average high temperatures across the monitoring network, the model also tends to underestimate the nighttime lows by a degree or so, at least on the 12 km grid. The under-prediction of the afternoon peaks is more pronounced than the August episode where RAMS clipped the afternoon peaks by a one to two degrees C. The temporal correlation shown in the spatial mean time series (Figure 6-58.) is more typical of that normally seen in prognostic model evaluations compared with the August 1993 episode results (Figure 6-44). As with the August episode, the cause of daytime underestimation biases is difficult to identify unambiguously but we attribute part of this discrepancy to the difference in heights between measurement and layer 1 model predictions.

6.8.1.3 Mean Normalized Bias in Surface Temperatures

In Figure 6-59, the mean normalized bias in RAMS estimates of hourly near-surface temperature predictions on the 12 km grid are fairly small throughout the episode although they are slightly larger than those in the August episode (Figure 6-45). For the June episode RAMS tends to slightly underestimate (~5% to 10%) hourly temperatures in the morning hours and on a couple of days to over predict (~2%-3%) midday. The sustained periods of underestimation of near-surface temperatures shown in the hourly bias

time series plots are corroborated by the systematic under-prediction biases for each day listed in Table 6-58.

6.8.1.4 Surface Temperature Fields

Hourly averaged ground-level temperature fields for the 12 km domain are shown in Figure 6-60 for four representative hours on 25 June 1992. On this day, the general afternoon warming trend in the southern states is evident.

6.8.2 Surface Wind Speed and Direction

6.8.2.1 Statistical Measures of Near-Surface Wind Speed and Direction

Table 6-8.2 presents a variety of statistical measures of RAMS model performance for the winds during the 22-29 June 1992 episode. On the 12 km grid, RAMS estimates mean wind speeds (2.55 m s^{-1}) that are on average 66% greater than the magnitude of the episode mean observations (1.54 m s^{-1}). RAMS overestimates the daily average observed wind speed on all but one day (28 June). Mean wind speeds for the June episode are higher than those encountered in the August 1993 period discussed previously. Part of the over-prediction in surface wind speed is due to the difference between the heights of the surface wind measurements and the height of the first RAMS grid layer.

Modeled wind directions show reasonable agreement with the observations on most days. Across the 8-day episode, the mean modeled (229.7 degrees) and observed surface wind directions (250.3 degrees) differ by only 21 degrees. From day-to-day, the difference between daily average and observed wind direction varies from 10 to 150 degrees. On the day with the largest wind discrepancy (28 June), a front moved through the region.

The daily average index of agreement parameter for the MM5 model ranges between 0.66 and 0.89 with an 8-day mean of 0.75. These results are consistent with those achieved in the August 1993 episode and with other prognostic model applications (see Chapter 8). Table 6-8.2 also lists the systematic and unsystematic components of the RMSE errors. For all but the first and last days in the episode the systematic component is larger than the unsystematic component suggesting that more of the RMSE errors are due to systematic biases that might be reduced through further refinement of model algorithms and/or application procedures. The episode average RMSE error is 1.89 ms^{-1} .

6.8.2.2 Vector Mean Wind Speeds

Figures 6-61 through 6-62 present various surface wind speed and wind direction summary plots for the 22-29 June 1992 episode. The vector mean modeled wind speed (Figure 6-61) is systematically overestimated compared to the observed mean wind speeds for every day of the June episode and this overestimation tendency is quite similar to that encountered in the August episode (Figure 6-47). For many of the June episode days the vector mean winds on both the 12 km and 24 km grids possess temporal variability similar to that exhibited in the measurements even though the predicted values are systematically

biased high. On some of the days, the model represents the afternoon wind speed increase fairly well notwithstanding the over-prediction.

6.8.2.3 Mean Wind Direction

Figure 6-62 presents the hourly variation in modeled versus observed surface wind directions over the eight June modeling days. As with the August episode, there is generally very good agreement with the exception of 28 June and early on the 29th when the model predicts winds that are about 80 to 90 degrees more southerly than the observations. Overall, however, the agreement with hourly mean wind direction across the various monitoring sites is quite good.

6.8.2.4 Root Mean Square Error in Wind Speeds

The RMSE errors and index of agreement are shown in Figures 6-63 and 6-64, respectively. The episode average values of the unsystematic, systematic, and total RMSE errors are 1.24 m s^{-1} , 1.38 m s^{-1} and 1.89 m s^{-1} , respectively. These results are an improvement over the August 1993 episode. From Figure 6-63 there does not appear to be any significant error growth throughout the latter two thirds of the simulation. Slight error growth occurs during the first three days of the episode when the errors are somewhat larger than for the rest of the episode days. That the preponderance of the RAMS RMSE error is from the systematic component (model physics- related) is graphically evident in Figure 6-63.

6.8.2.5 Index of Agreement in Surface Wind Speeds

The index of agreement results for the June 1992 episode (Figure 6-64) are quite consistent with other prognostic model evaluations. For this episode, RAMS exhibits typical hourly variation in the agreement index parameter with the lowest values occurring during the morning period when wind speeds are lowest and the directions are more variable. In the afternoon when speeds are greater, the index increases. The mean value of the index of agreement varies diurnally throughout the episode; the mean over the whole period is 0.75

6.8.2.6 Ground-Level Wind Fields

Figures 6-65 presents afternoon RAMS surface wind field comparisons over the 12 km domains on four different days during the June 1992 episode. Generally, the RAMS modeled winds on these days are in reasonable agreement with the observed values. In examining the full set of hourly surface wind plots for this (and the August 1993) episode, we did not find instances where there were substantial discrepancies in the predicted versus observed surface wind fields, which would have raised concerns about the fidelity of the modeling.

6.8.3 Mixing Ratios

6.8.3.1 Statistical Measures of Near-Surface Mixing Ratios

Statistical results for near surface mixing ratios are listed in Table 6-60 for the June 1992 episode. Across the 12 km domain the agreement between the episode mean daily maximum observed (19.3 g/Kg) and modeled (16.8 g/Kg) mixing ratios is fairly good. RAMS systematically underestimates the maximum ratio on each day except 22 June by 2 to 4 g/Kg. The mean bias and error in mixing ratios are also quite good,

with 8-day mean values of -0.3 g/Kg and 1.0 g/Kg respectively. As with the August 1993 episode, these results suggest that RAMS is doing a fairly good job of reproducing the daily maximum and hourly specific humidity across the 12 km domain.

6.8.3.2 Spatial Mean Surface Mixing Ratios

Figure 6-66 is a spatial mean surface mixing ratio plot for the June 1992. RAMS does an excellent job at both 12 km and 24 km scales in estimating the mean trend in specific humidity across the entire episode. As with the August 1993 episode, there is a slight tendency to underestimate mixing ratio.

6.8.3.3 Bias in Surface Mixing Ratios

The minor underestimation of near-surface mixing ratio is also apparent in the normalized bias time series for the 12 km and 24 km grid domains shown in Figure 6-67. The largest biases in mixing ratio tend to occur at night or late in the afternoon or evening. At midday, the mixing ratio bias estimates tend to change from positive to negative during the first five days of the episode. No significant diurnal performance problems are evident in the mixing ratio results.

6.8.3.4 Surface Mixing Ratio Fields

Figure 6-68 presents examples of ground-level mixing ratio fields across the 12 km domain at two time periods (0300 and 1500 EST) on 26 June 1992. These plots are typical of the mixing ratio fields for the June episode. Similar to the August 1993 episode, no strong gradients in mixing ratios are evident in these or the other hourly fields. There is generally good agreement between the predicted and observed mixing ratios at the various monitoring stations.

6.8.4 Precipitation

6.8.4.1 Statistical Measures of Total Daily Precipitation

Rain occurred on 5 of the 8 days during the June 1992 episode (see Table 6-8.4). The maximum daily precipitation at any rain gauge varied between 4.0 mm and 122 mm with an episode mean of 53.8 mm. RAMS predicted a range of daily maximum rainfall totals from 9.0 mm to 110.5 mm with an episode mean of 41.7 mm. The mean observed and predicted precipitation across all rain gauges was 2.9 mm and 3.9 mm, yielding an overall discrepancy of 35% which constitutes good agreement for a mesoscale model. The bias in daily rainfall predictions ranges from -0.60 mm to 4.82 mm with an episode mean of 0.9 mm. Only on 27 June did the model experience significant difficulty reproducing the daily rainfall totals as evidenced by bias and error scores of 4.82 mm and 11.57 mm, respectively. The daily gross errors in rainfall ranged between 0.23 mm and 11.57 mm with an episode mean of 4.0 mm. Overall, the model did a good job of simulating the daily and episode average rainfall totals when averaged across all monitoring stations.

6.8.4.2 Temporal Distribution of Total Daily Rainfall Across All Sites

Figure 6-69 presents time series plots of the daily precipitation totals derived from the measured and predicted values averaged across all reporting stations in the 12 km and 24 km domains. With the exception of the 50% over-prediction on 27 June (see Table 6-8.4), the day-to-day rainfall predictions match the observations very closely in this comparison. However, as with the August 1993 episode, the very good agreement seen in the daily total spatial time series plot (Figure 6-69) masks much larger errors when the model's skill at individual monitoring stations on specific days is concerned (see below).

6.8.4.3 Spatial Distribution of Daily Total Measured and Observed Rainfall

Figure 6-70 compares the gridded daily precipitation predictions (in mm) across the 12 km domain for 27 June 1992 while the bottom panel presents the daily total measurements (also in mm). On 27 June 1992, RAMS predicts bands of predicted precipitation (>25 mm) across portions of northern Alabama, Tennessee and southeastern Kentucky, western Virginia and south Carolina. Data from the sparse rain gauge network does not show such high rainfall amounts in the same areas as predicted. On the 27th, (see Table 6-8.4) the model did overestimate the domain-wide precipitation by 50% so this may explain in part why there are few monitors that are associated with precipitation above 25 mm (i.e., colored red).

6.8.4.4 Correlation of Daily Maximum Rainfall Across All Sites

Figure 6-71 presents a Scatter Plot of predicted and observed daily total precipitation on 27 June 1992. While the spatial time series plot in Figure 6-69 suggests good model performance (based on averages across all monitoring stations), the Scatter Plot reveals that this good agreement derives from cancellation of over- and under-predictions at the various rain gauges. The Scatter Plot suggests poor correlation between prediction and observation at the individual reporting sites. Thus, as with the August 1993 episode, RAMS does a credible job of estimating the total precipitation when averaged across the monitoring network on each episode day but the model's ability to predict the exact rainfall amounts paired in time and space with specific monitors is generally poor.

Table 6-8. RAMS Model Evaluation Results for the 22-29 June 1992 SAMI Episode – Surface Temperatures (deg C).									
Performance Attribute	22 June Day 174	23 June Day 175	24 June Day 176	25 June Day 177	26 June Day 178	27 June Day 179	28 June Day 180	29 June Day 181	Mean Value
Maximum Observed Temperature	27.8	31.1	33.3	35.0	36.1	32.8	32.2	33.3	32.7
Maximum Predicted Temperature	30.2	31.5	33.4	33.4	32.7	33.8	34.0	33.0	32.8
Mean Bias (deg C)	-0.2	-0.7	-1.2	-1.1	-1.1	-1.6	-1.1	-1.7	-1.1
Gross Error (deg C)	1.4	1.6	1.8	1.9	2.0	1.9	1.8	2.3	1.8

Table 6-8. RAMS Model Evaluation Results for the 22-29 June 1992 SAMI Episode – Surface Temperatures (deg C). (b) 24 Km Grid									
Performance Attribute	22 June Day 174	23 June Day 175	24 June Day 176	25 June Day 177	26 June Day 178	27 June Day 179	28 June Day 180	29 June Day 181	Mean Value
Maximum Observed Temperature	38.9	34.4	36.1	36.1	36.1	36.7	37.8	35.6	36.5
Maximum Predicted Temperature	32.1	33.2	34.5	33.8	32.3	31.5	32.0	33.8	32.9
Mean Bias (deg C)	-0.2	-0.7	-0.7	-1.0	-1.0	-1.1	-1.2	-1.3	-0.9
Gross Error (deg C)	1.5	1.7	1.7	1.9	2.0	1.9	2.0	2.3	1.9

Table 6-8. RAMS Model Evaluation Results for the 22-29 June 1992 Episode – Surface Wind Speeds (meters/sec). (a) 12 Km Grid									
Performance Attribute	22 June Day 174	23 June Day 175	24 June Day 176	25 June Day 177	26 June Day 178	27 June Day 179	28 June Day 180	29 June Day 181	Mean Value
Mean Observed Wind Speed	1.92	1.33	2.55	1.66	0.78	1.67	1.31	1.07	1.54
Mean Predicted Wind Speed	2.01	2.54	4.27	3.62	2.68	2.06	1.14	2.06	2.55
Observed Standard Deviation	2.47	1.65	1.91	1.87	2.04	1.84	1.73	1.61	1.89
Predicted Standard Deviation	2.17	1.57	1.48	1.25	1.56	1.47	1.44	1.52	1.56
RMSE	1.52	1.89	2.38	2.12	2.08	1.70	1.61	1.84	1.89
RMSE _S	0.77	1.49	1.86	1.72	1.61	1.36	1.33	0.91	1.38

Table 6-8. RAMS Model Evaluation Results for the 22-29 June 1992 Episode – Surface Wind Speeds (meters/sec). (a) 12 Km Grid									
Performance Attribute	22 June Day 174	23 June Day 175	24 June Day 176	25 June Day 177	26 June Day 178	27 June Day 179	28 June Day 180	29 June Day 181	Mean Value
Index of Agreement, I	0.89	0.74	0.66	0.74	0.81	0.69	0.68	0.79	0.75
Skill _E	0.52	0.71	0.79	0.68	0.70	0.55	0.52	0.78	0.66
Skill _{VAR}	0.88	1.01	0.79	0.69	0.79	0.81	0.84	0.91	0.84
Mean Observed Wind Direction (°)	303.1	187.3	210.8	242.5	227.7	312.1	27.3	131.5	250.3
Mean Predicted Wind Direction (°)	248.2	222.3	221.0	224.3	224.5	235.4	237.0	224.5	229.7

Table 6-8. RAMS Model Evaluation Results for the 22-29 June 1992 Episode – Surface Wind Speeds (meters/sec). (a) 12 Km Grid. (b) 24 Km Grid									
Performance Attribute	22 June Day 174	23 June Day 175	24 June Day 176	25 June Day 177	26 June Day 178	27 June Day 179	28 June Day 180	29 June Day 181	Mean Value
Mean Observed Wind Speed	1.33	0.97	1.38	1.30	0.83	0.91	0.57	1.10	1.05
Mean Predicted Wind Speed	2.15	2.41	2.88	2.95	1.84	1.61	1.92	2.65	2.30
Observed Standard Deviation	2.97	2.35	2.33	2.19	2.34	2.26	2.21	2.15	2.35
Predicted Standard Deviation	2.81	2.65	2.42	2.07	2.50	2.21	2.39	2.21	2.41
RMSE	1.88	2.21	2.46	2.21	2.30	1.95	2.14	2.20	2.17
RMSE _S	0.80	1.42	1.62	1.56	1.50	1.40	1.37	1.55	1.40
RMSE _U	1.69	1.67	1.81	1.54	1.72	1.35	1.60	1.53	1.61
Index of Agreement, I	0.92	0.86	0.79	0.80	0.83	0.84	0.86	0.81	0.84
Skill _E	0.57	0.75	0.79	0.75	0.77	0.63	0.74	0.74	0.72
Skill _{VAR}	0.95	1.17	1.05	0.96	1.11	1.10	1.12	1.08	1.07
Mean Observed Wind Direction (°)	299.5	231.4	216.2	243.6	277.3	316.5	245.1	182.4	251.5
Mean Predicted Wind Direction (°)	269.6	243.8	233.2	232.4	235.0	241.5	240.2	235.1	241.4

Table 6-8. RAMS Model Evaluation Results for the 22-29 June 1992 SAMI Episode – Surface Mixing Ratios (gm/Kg).									
(a) 12 Km Grid									
Performance Attribute	22 June Day 174	23 June Day 175	24 June Day 176	25 June Day 177	26 June Day 178	27 June Day 179	28 June Day 180	29 June Day 181	Mean Value
Maximum Observed Mixing Ratio	12.6	17.9	19.9	21.3	20.7	19.2	19.3	23.4	19.3
Maximum Predicted Mixing Ratio	15.9	16.1	16.4	16.8	17.9	17.4	17.3	16.7	16.8
Mean Bias (gm/Kg)	-0.3	-0.2	-0.2	0.4	-0.3	-0.5	-0.3	-0.5	-0.3
Gross Error (gm/Kg)	0.7	0.9	1.1	1.0	1.1	1.0	1.0	1.2	1.0

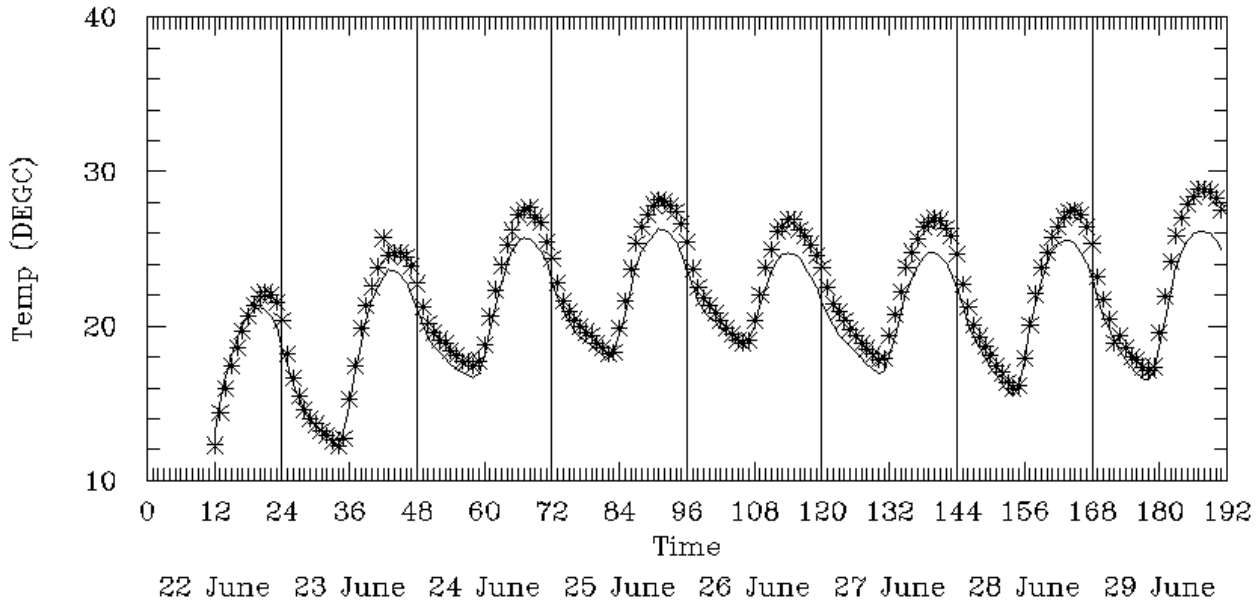
Table 6-8. RAMS Model Evaluation Results for the 22-29 June 1992 SAMI Episode – Surface Mixing Ratios (gm/Kg).									
(a) 12 Km Grid. (b) 24 Km Grid									
Performance Attribute	22 June Day 174	23 June Day 175	24 June Day 176	25 June Day 177	26 June Day 178	27 June Day 179	28 June Day 180	29 June Day 181	Mean Value
Maximum Observed Mixing Ratio	21.9	24.3	21.3	22.7	21.9	24.5	22.1	23.4	22.8
Maximum Predicted Mixing Ratio	19.8	19.4	19.3	19.3	19.0	19.1	19.2	20.4	19.4
Mean Bias (gm/Kg)	-0.2	-0.1	-0.2	-0.2	-0.1	-0.3	-0.2	-0.3	-0.2
Gross Error (gm/Kg)	0.7	0.9	1.0	1.0	1.0	0.9	0.9	1.1	0.9

Table 6-8. RAMS Model Evaluation Results for the 22-29 June 1992 SAMI Episode – Daily Total Precipitation (mm).
(a) 12 Km Grid

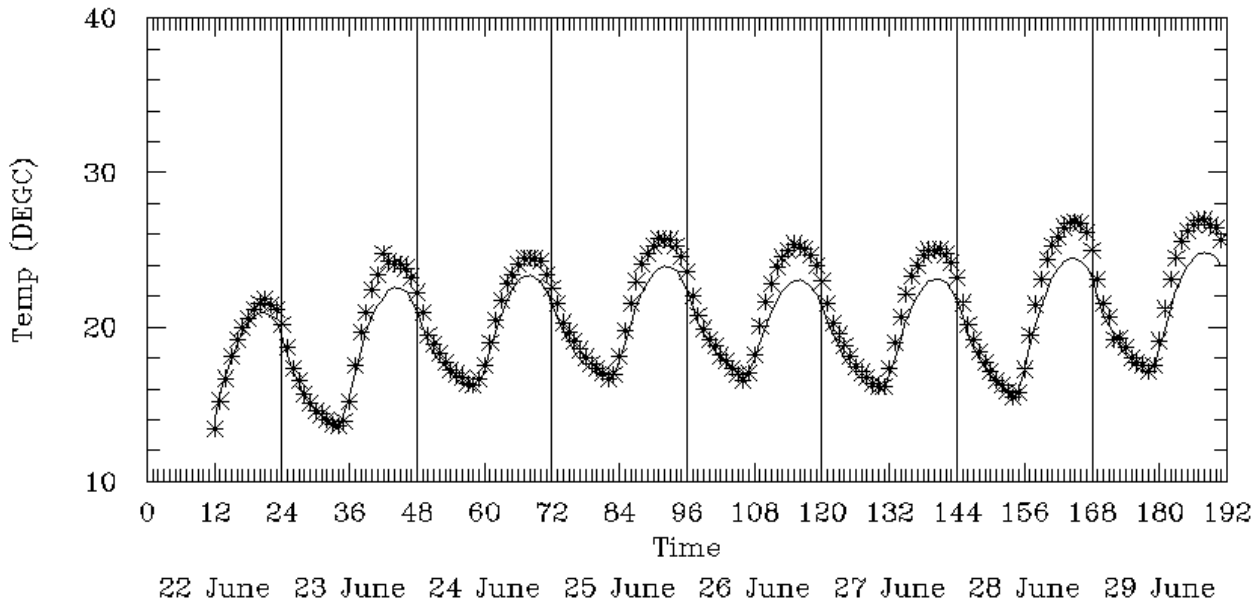
Performance Attribute	22 June Day 174	23 June Day 175	24 June Day 176	25 June Day 177	26 June Day 178	27 June Day 179	28 June Day 180	29 June Day 181	Mean Value
Maximum Observed Precipitation	--	--	4.0	27.0	48.0	122.0	68.0	--	53.8
Maximum Predicted Precipitation	--	--	9.0	20.8	34.0	110.5	34.1	--	41.7
Mean Observed Precipitation			0.0	0.8	3.5	8.9	1.4		2.9
Mean Predicted Precipitation			0.6	1.9	3.1	13.4	0.7		3.9
Mean Bias (mm)	--	--	-0.17	1.06	-0.60	4.82	-0.60	--	0.9
Gross Error (mm)	--	--	0.23	1.95	4.46	11.57	1.71	--	4.0

Table 6-8. RAMS Model Evaluation Results for the 22-29 June 1992 SAMI Episode – Daily Total Precipitation (mm). (b) 24 Km Grid

Performance Attribute	22 June Day 174	23 June Day 175	24 June Day 176	25 June Day 177	26 June Day 178	27 June Day 179	28 June Day 180	29 June Day 181	Mean Value
Maximum Observed Precipitation	--	--	14.0	35.0	98.0	122.0	68.0	--	67.4
Maximum Predicted Precipitation	--	--	10.1	65.1	56.3	101.0	125.9	--	71.7
Mean Observed Precipitation			0.2	1.8	3.2	7.0	1.8		2.8
Mean Predicted Precipitation			0.8	1.9	2.7	9.6	0.7		3.1
Mean Bias (mm)	--	--	0.18	0.00	-0.65	3.09	-0.91	--	0.3
Gross Error (mm)	--	--	0.42	2.41	4.12	9.01	2.12	--	3.6

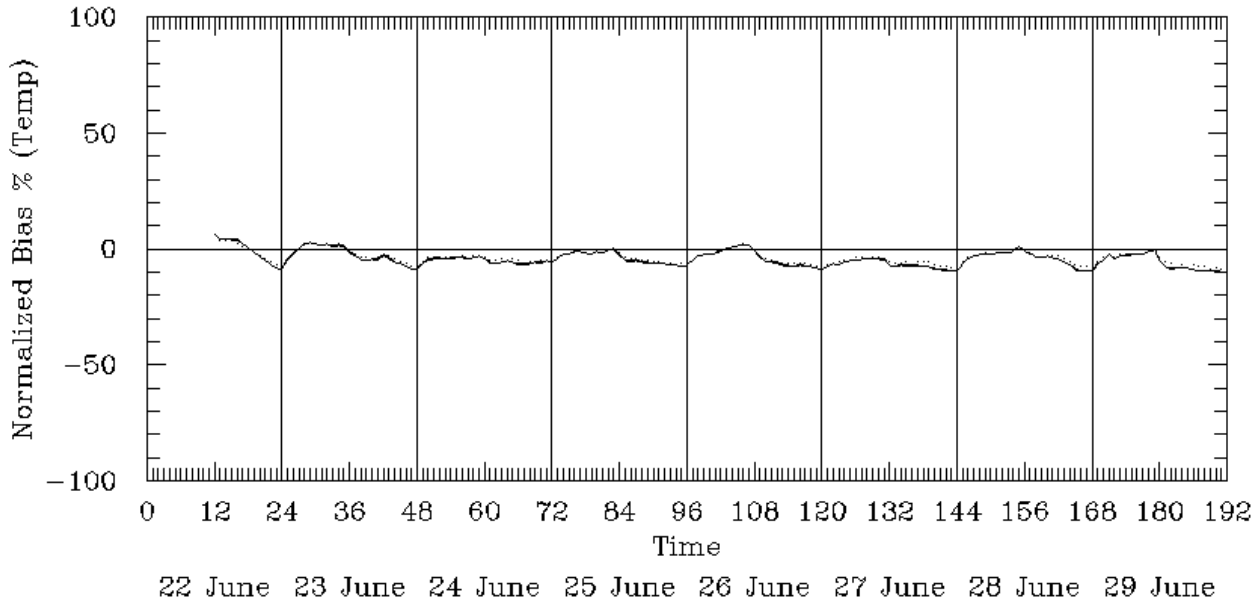


(a) 12 Km Grid

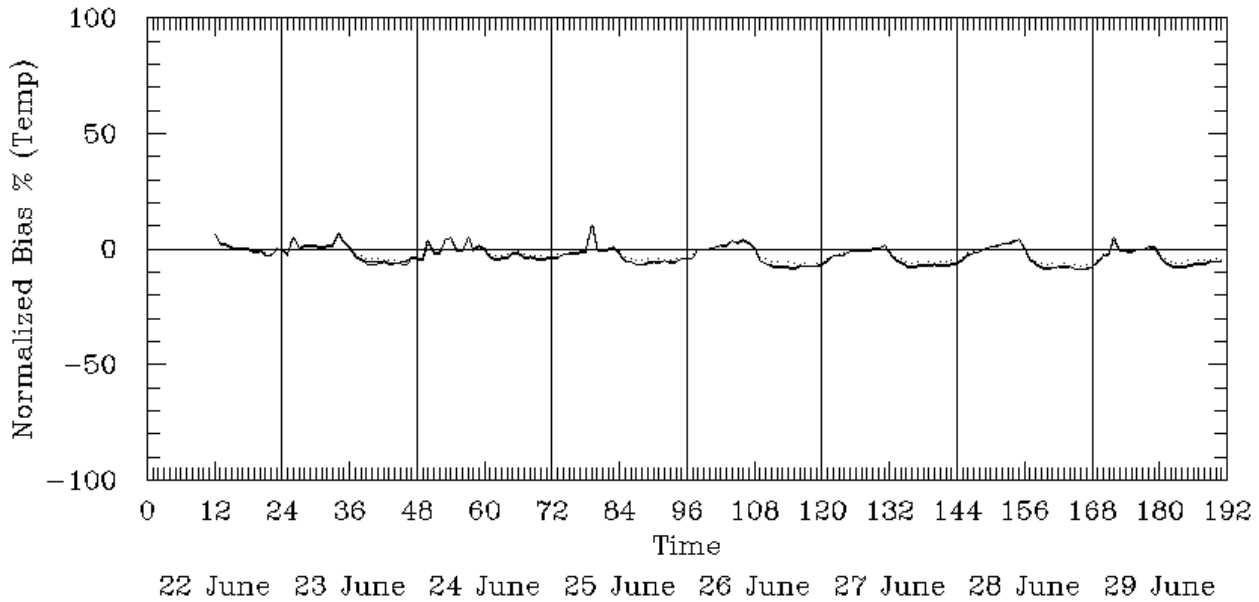


(b) 24 Km Grid

Figure 6-58. Spatial Mean Ground-Level Temperatures for the 22-29 June 1992.

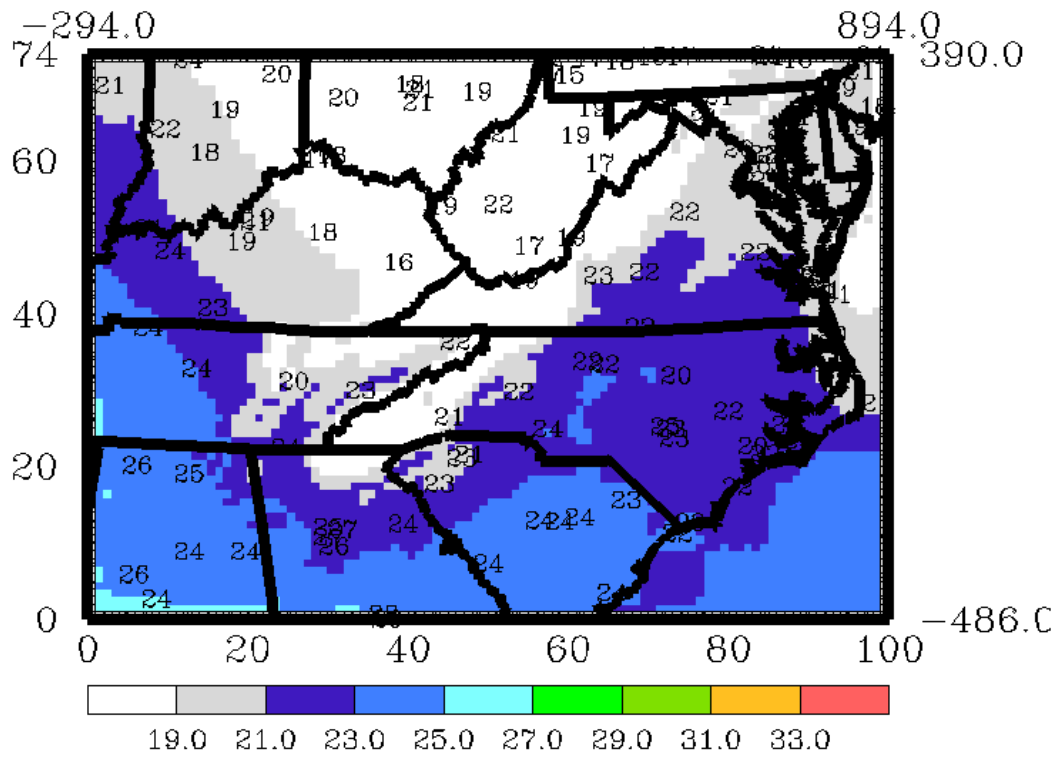


(a) 12 Km Grid

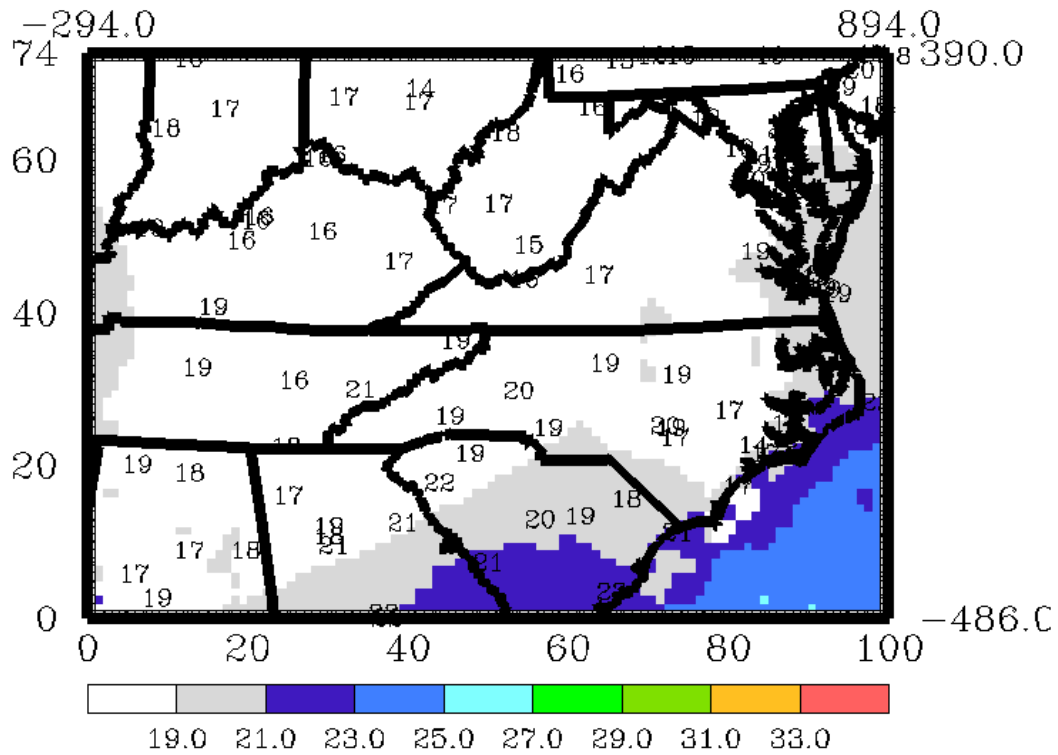


(b) 24 Km Grid

Figure 6-59. Mean Normalized Bias in Ground-Level Temperatures for the 22-29 June 1992 Episode.

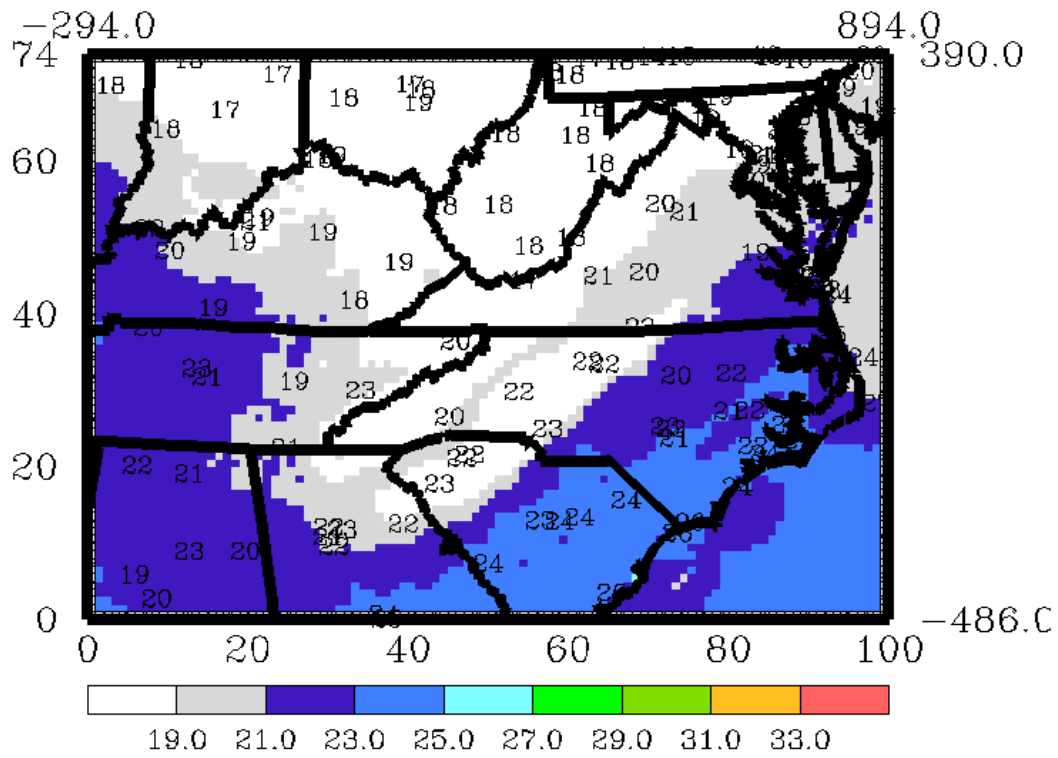


(a) 0100 UTC (2100 EST)

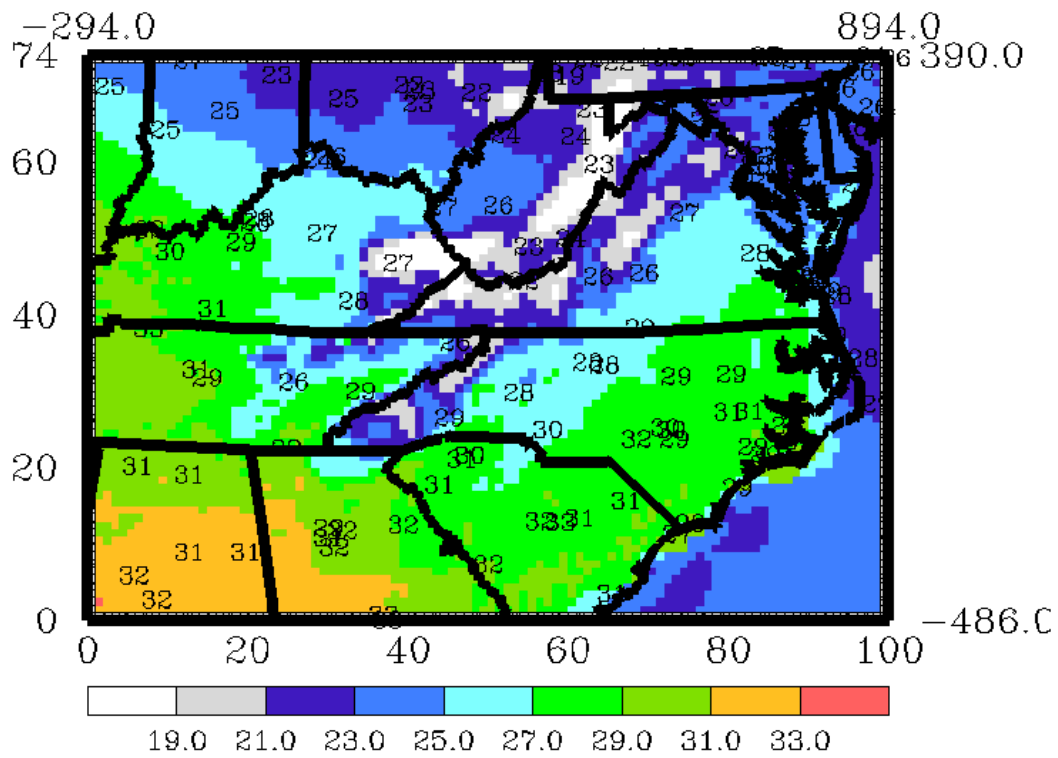


(b) 0700 UTC (0300 EST)

Figure 6-60. Ground-Level Temperature Fields for 25 June 1992.

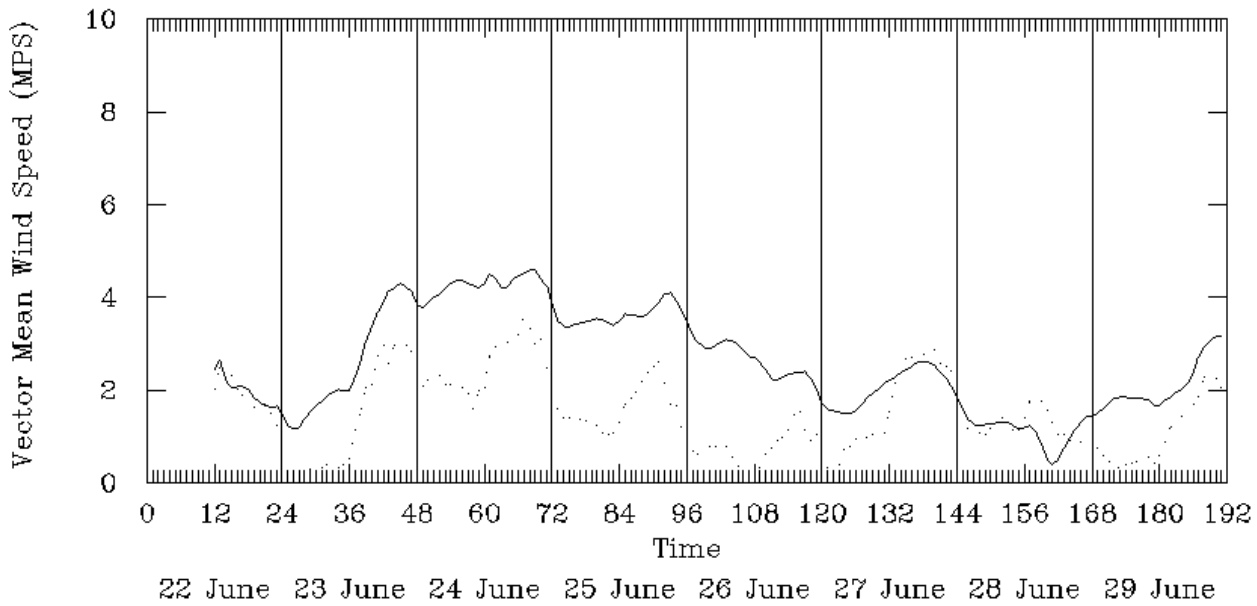


(c) 1300 UTC (0900 EST)

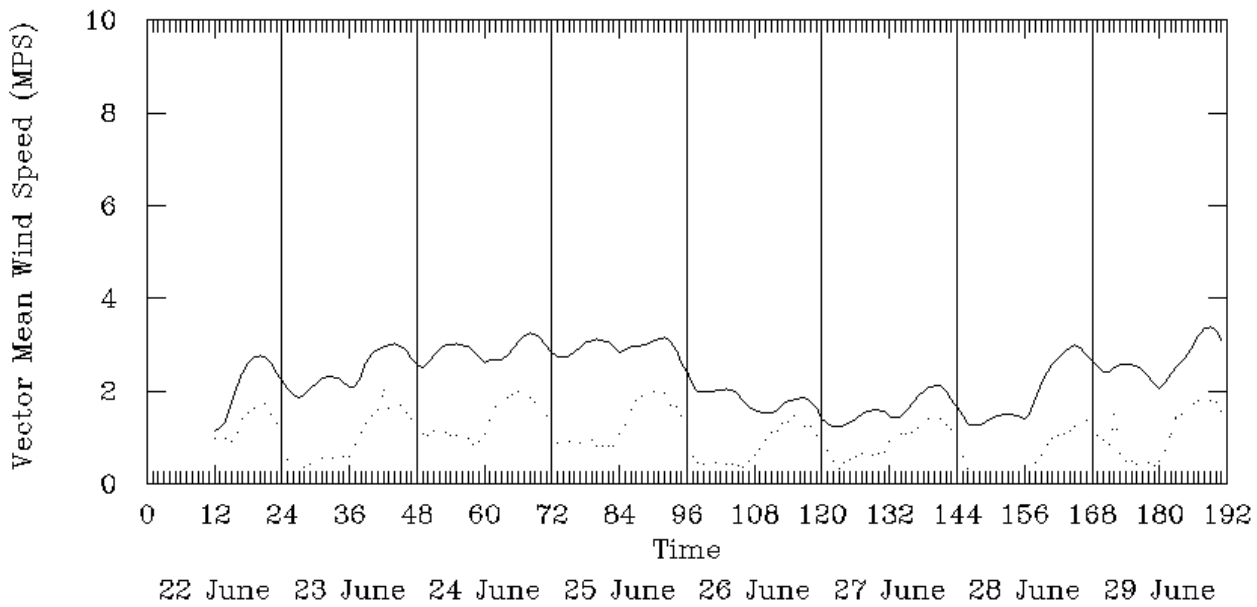


(d) 1900 UTC (1500 EST)

Figure 6-60. Concluded.

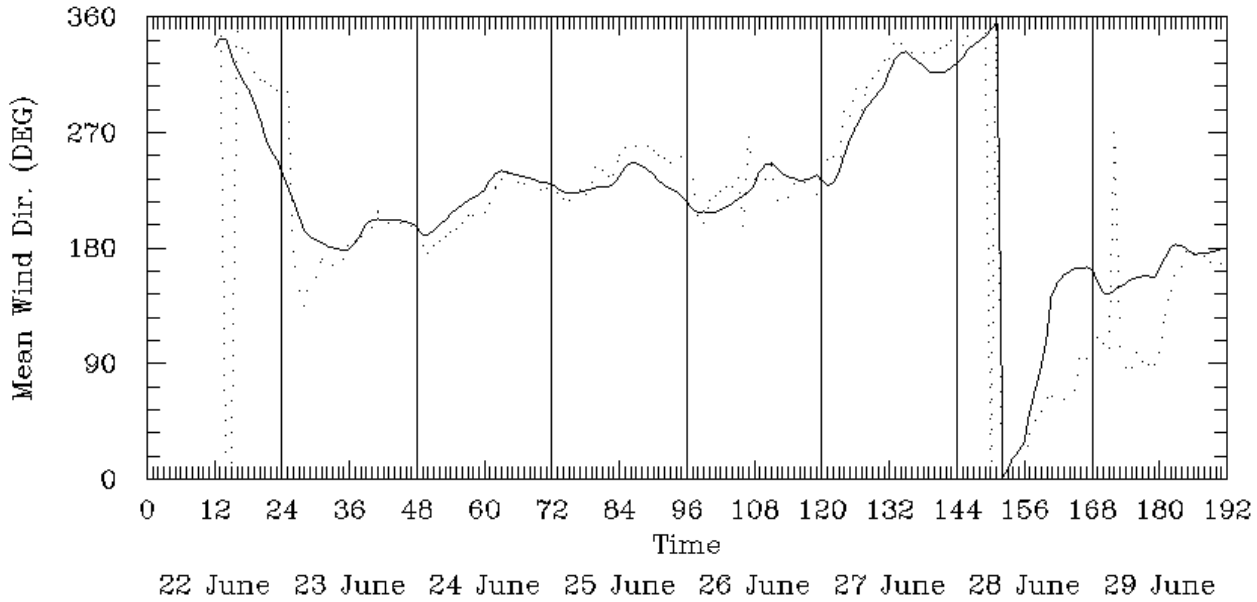


(a) 12 Km Grid

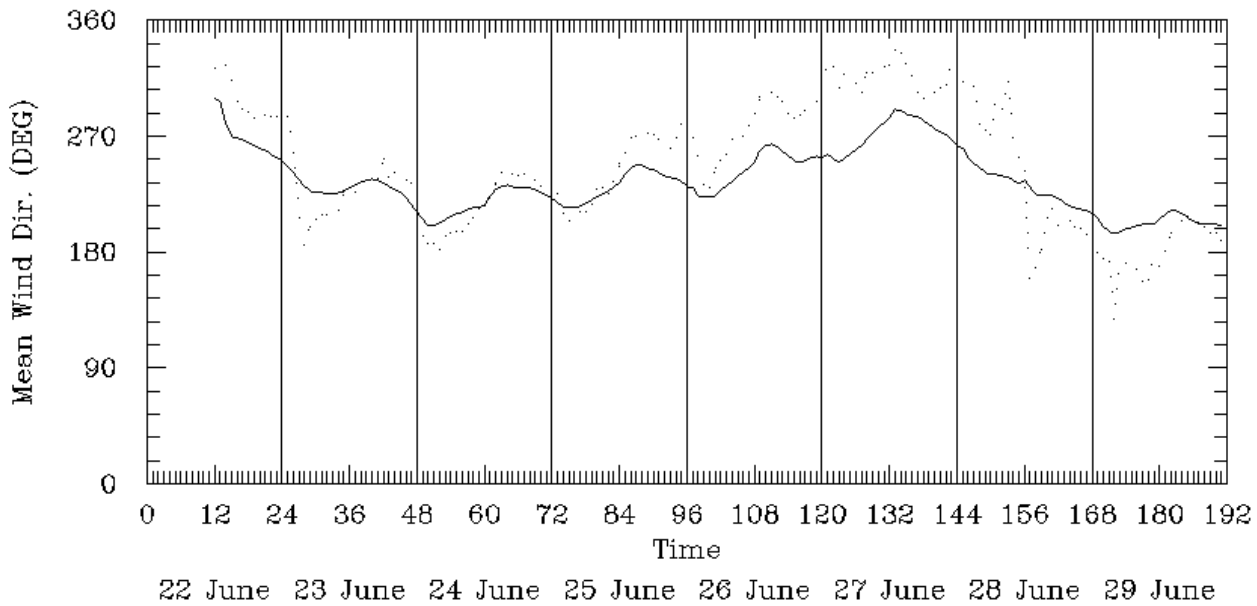


(b) 24 Km Grid

Figure 6-61. Vector Mean Wind Speed for the 22-29 June 1992 Episode.

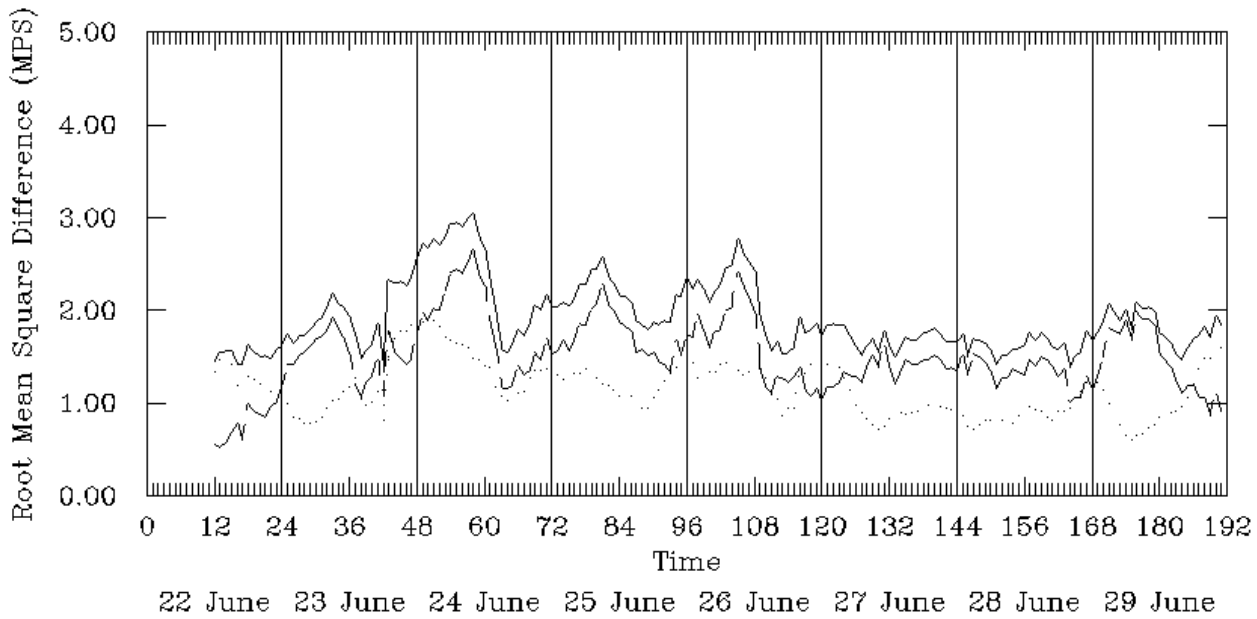


(a) 12 Km Grid

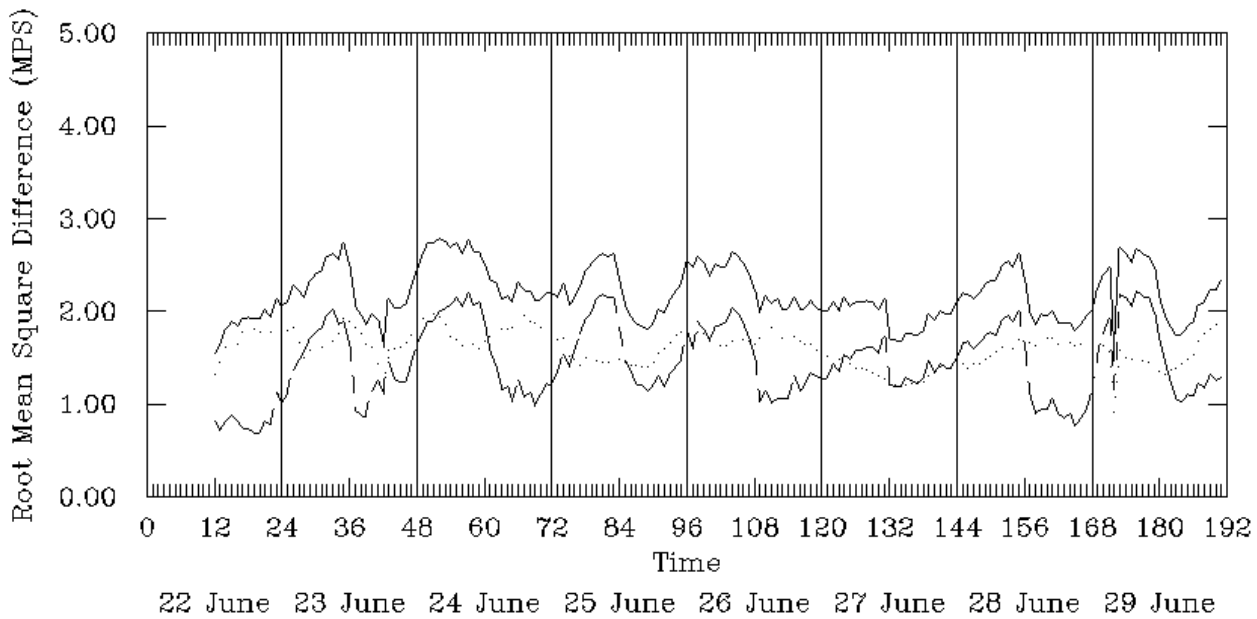


(b) 24 Km Grid

Figure 6-62. Mean Wind Direction for the 22-29 June 1992 Episode.

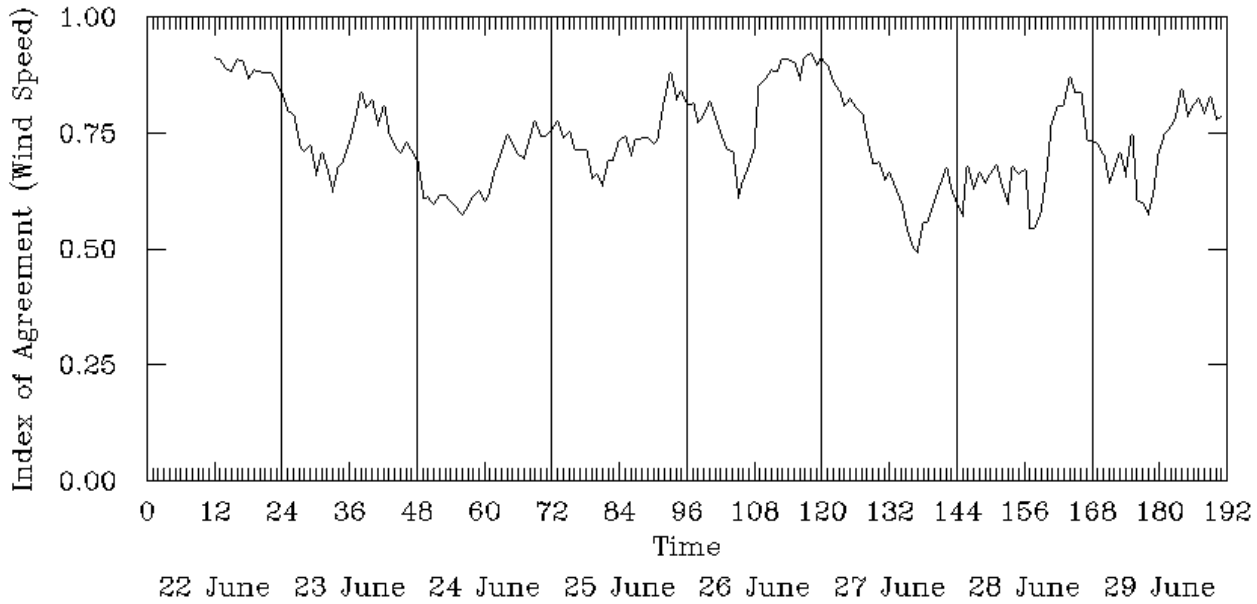


(a) 12 Km Grid

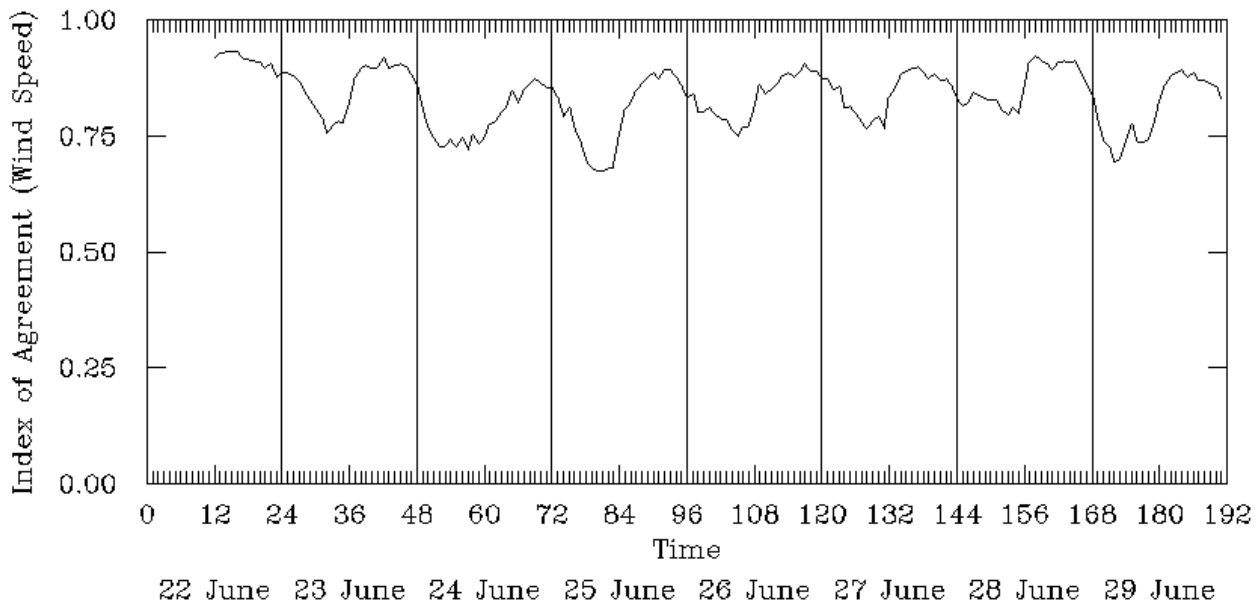


(b) 24 Km Grid

Figure 6-63. Root Mean Square Error in Ground-Level Wind Speeds for the 22-29 June 1992 Episode.

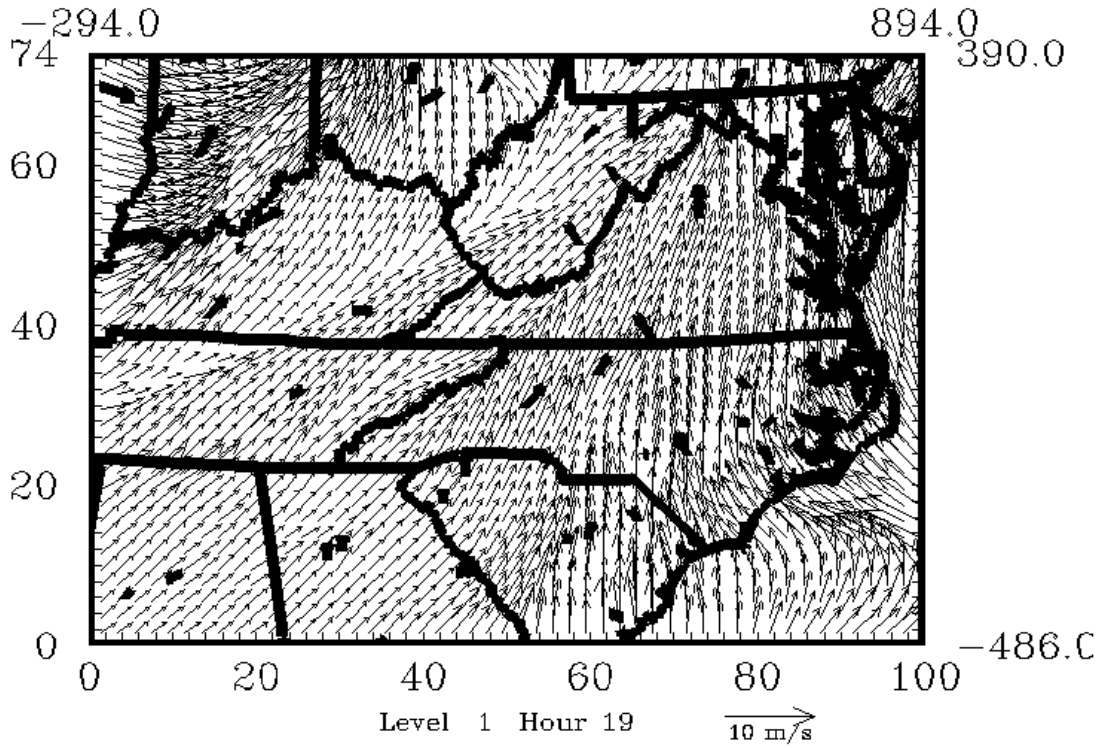


(a) 12 Km Grid

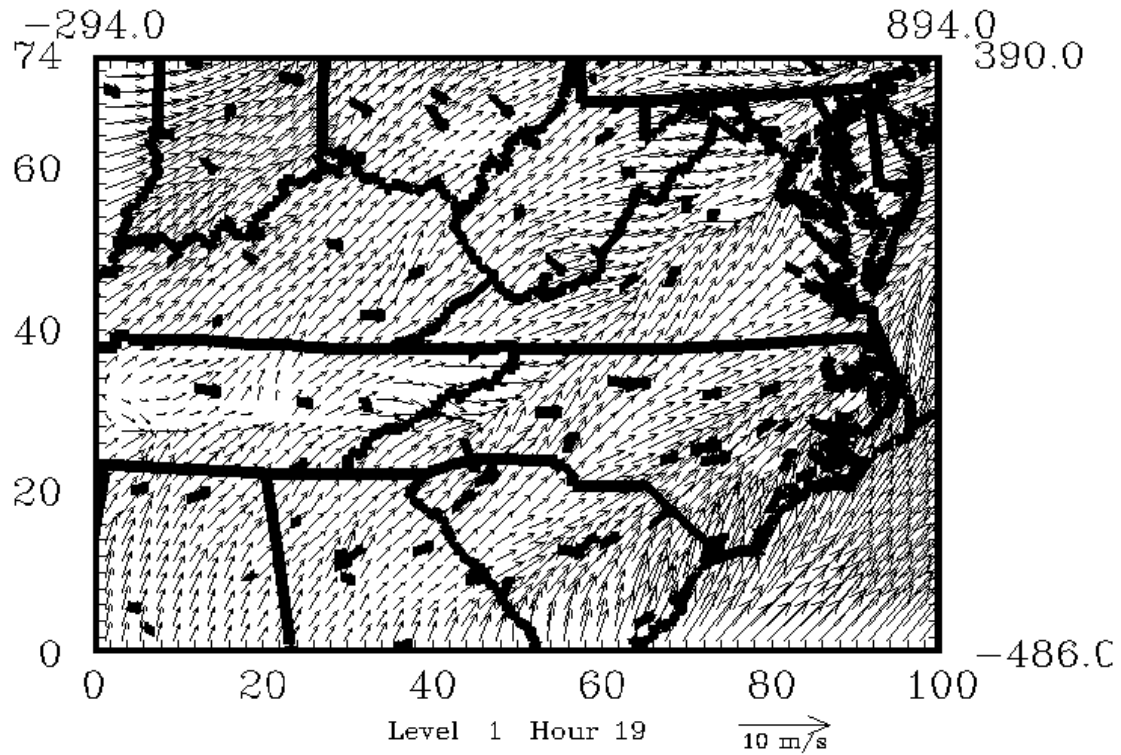


(b) 24 Km Grid

Figure 6-64. Index of Agreement in Surface Wind Speed for the 22-29 June 1992 Episode.



(a) 23 June 1992, 1900 UTC (1500 EST)



(b) 25 June 1992, 1900 UTC (1500 EST)

Figure 6-65. Ground-Level Wind Fields for the 22-29 June 1992 Episode.

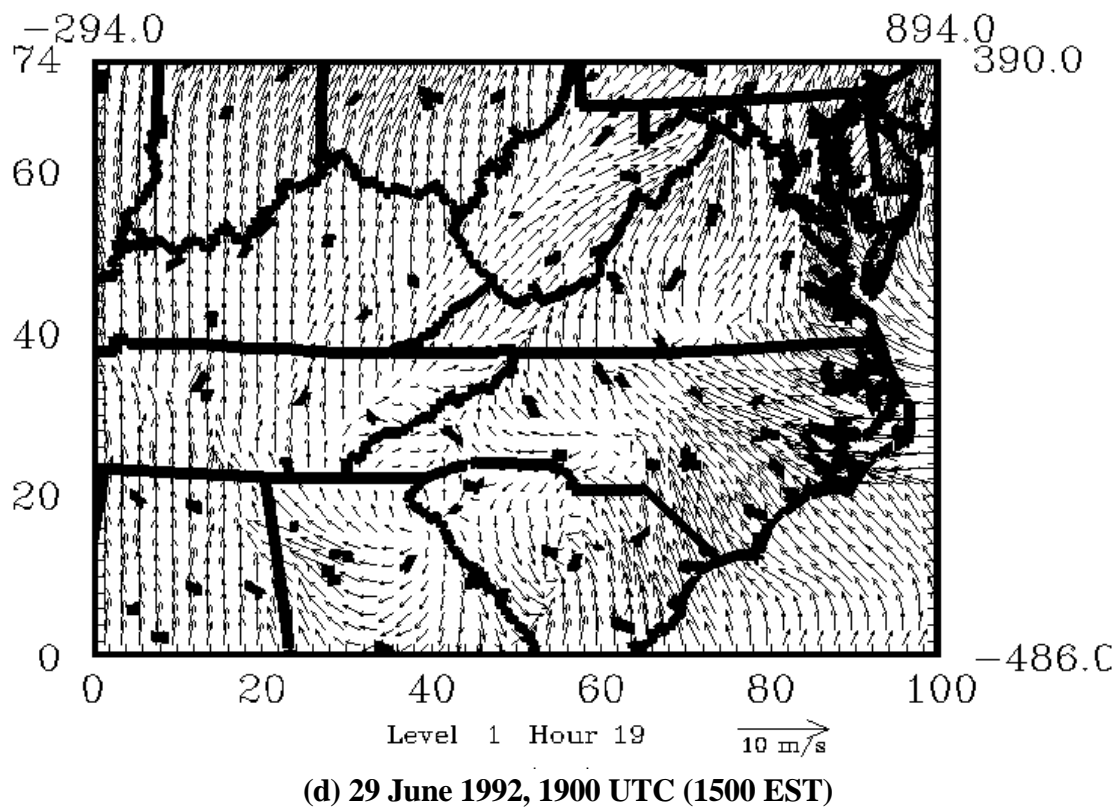
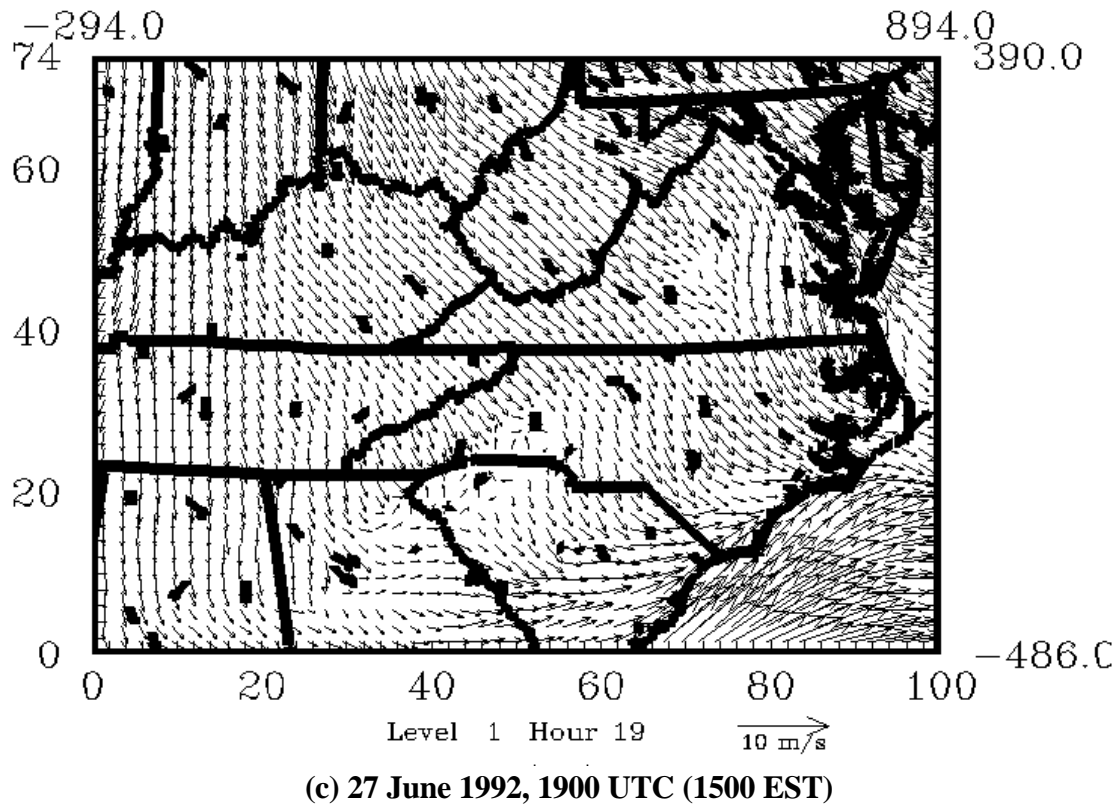
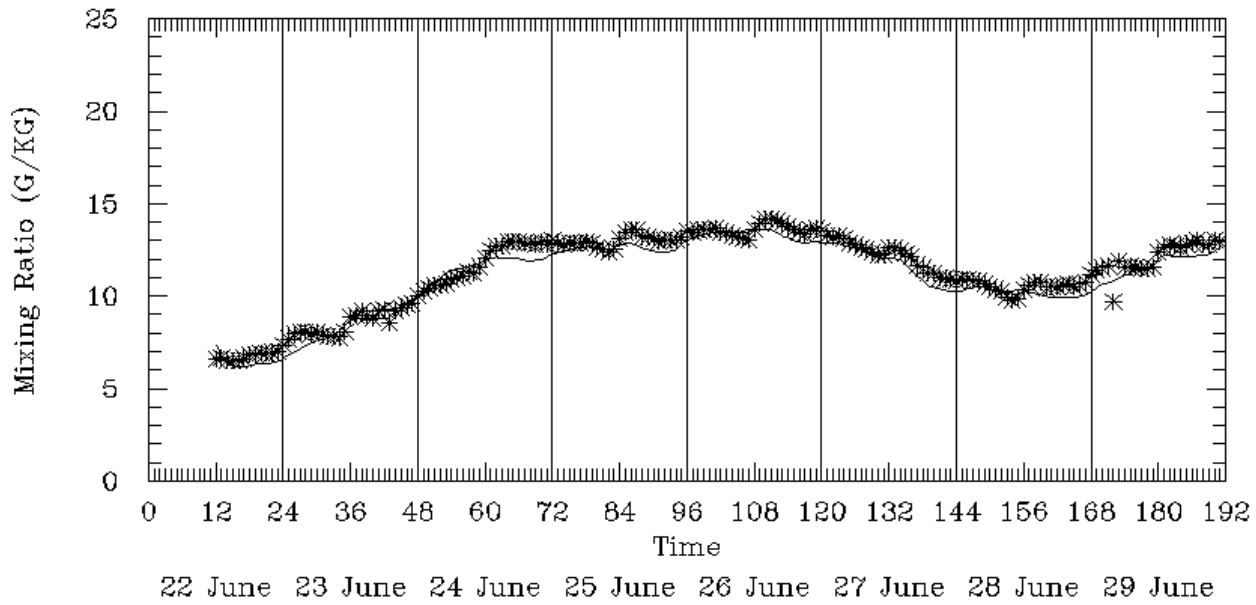
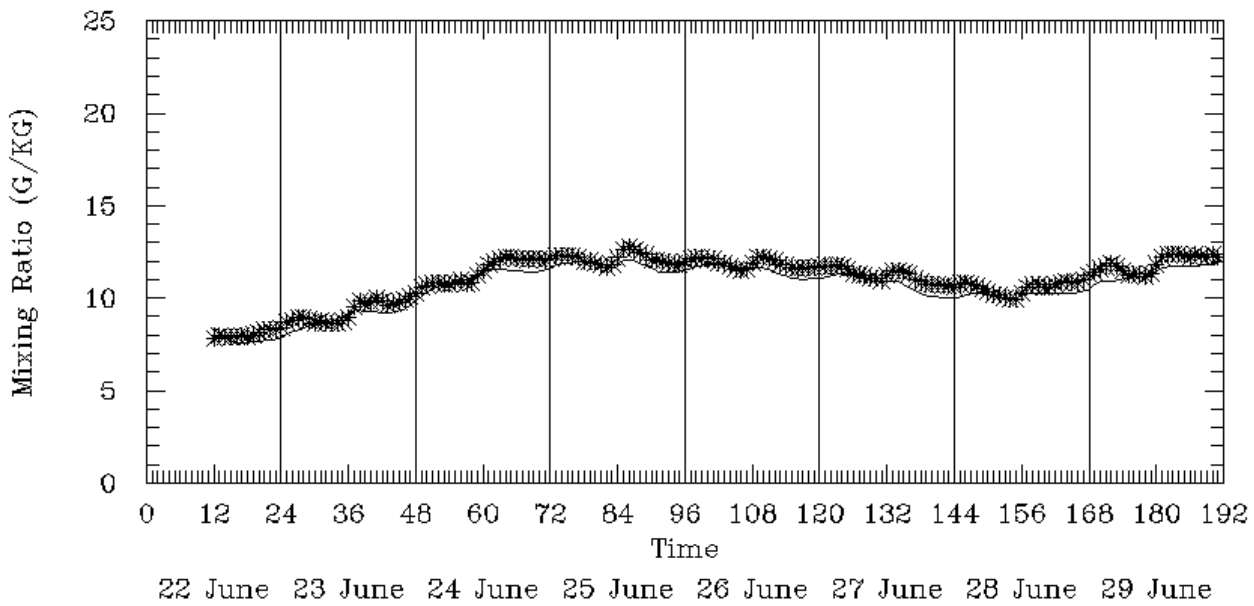


Figure 6-65. Concluded.

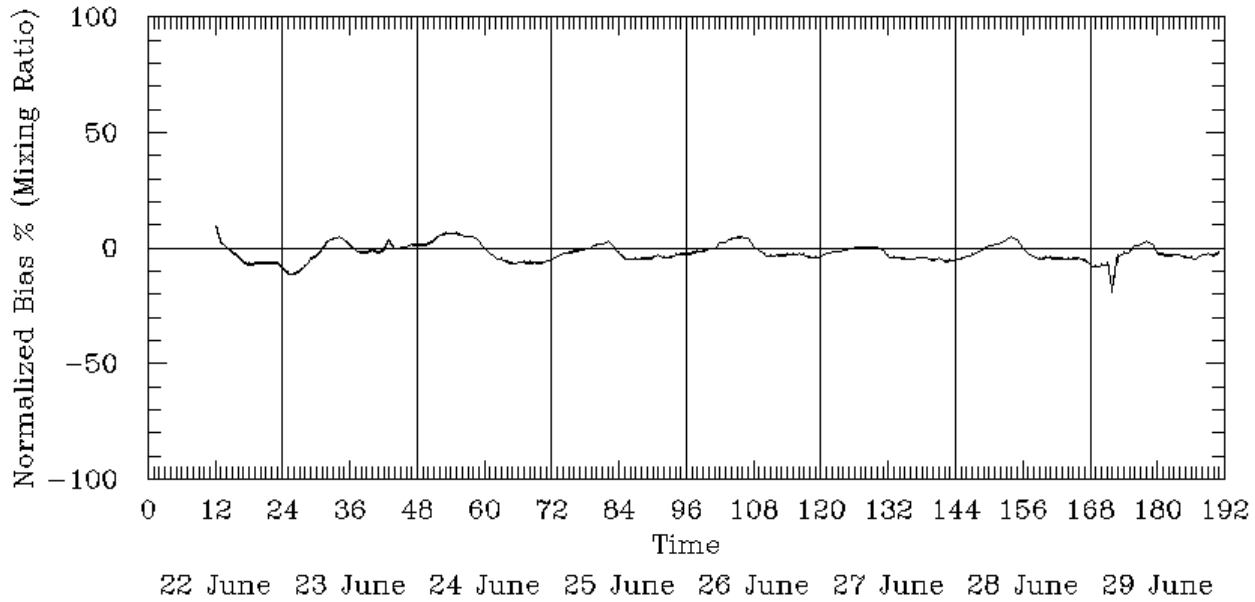


(a) 12 Km Grid

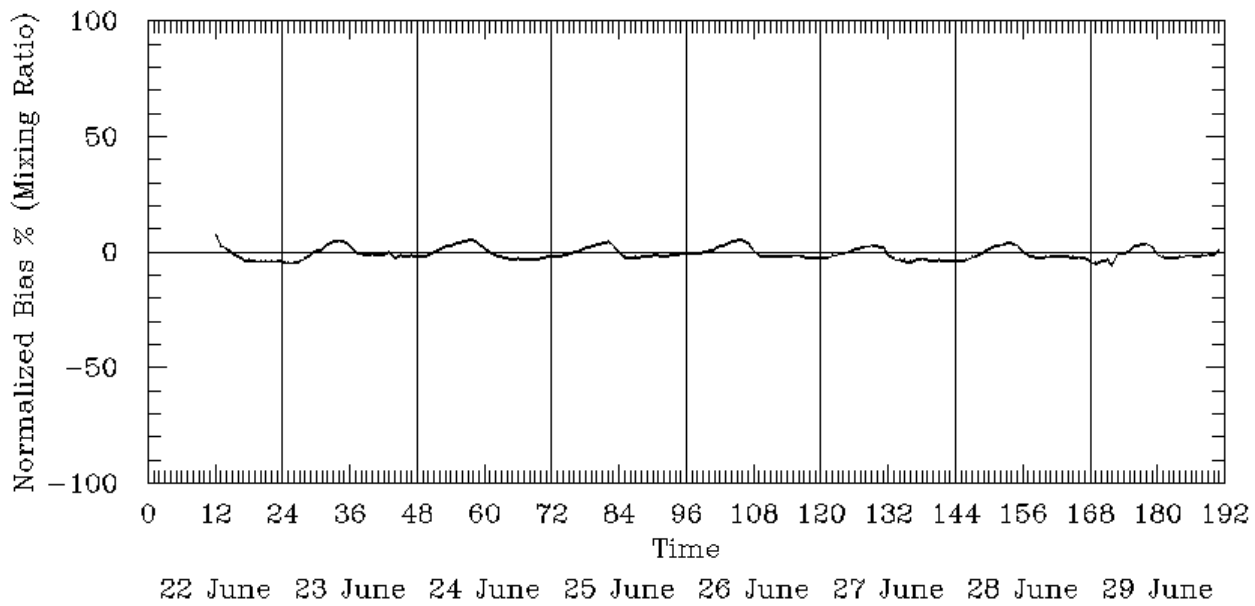


(b) 24 Km Grid

Figure 6-66. Spatial Mean Ground-Level Mixing Ratios for the 22-29 June 1992 Episode.

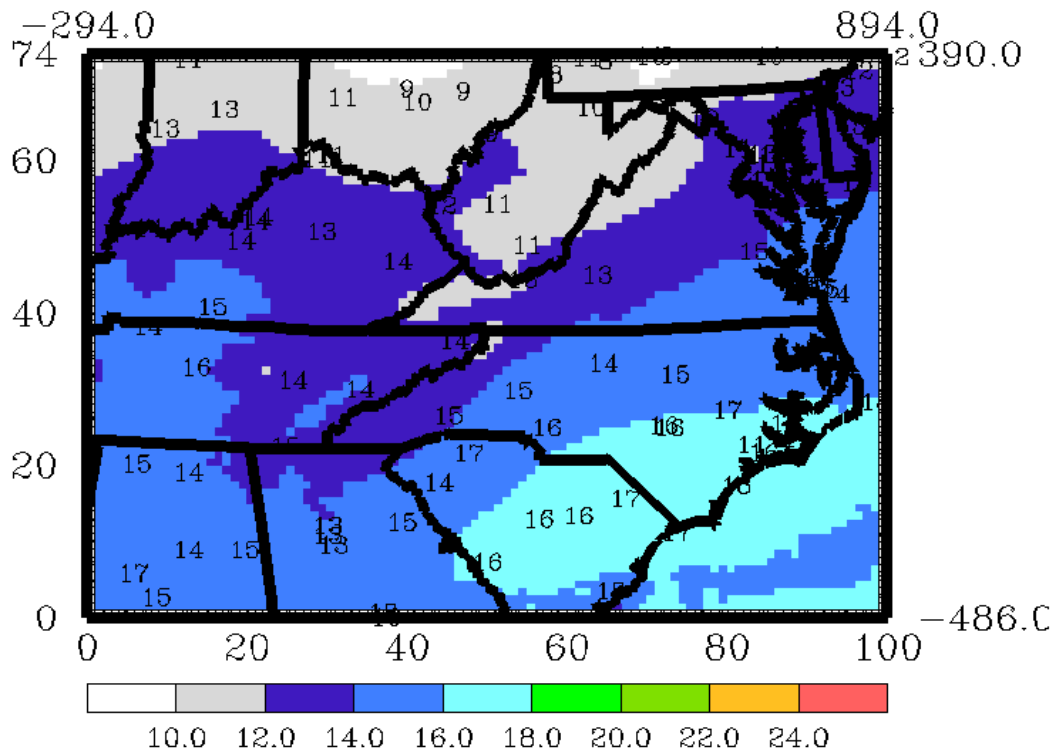


(a) 12 Km Grid

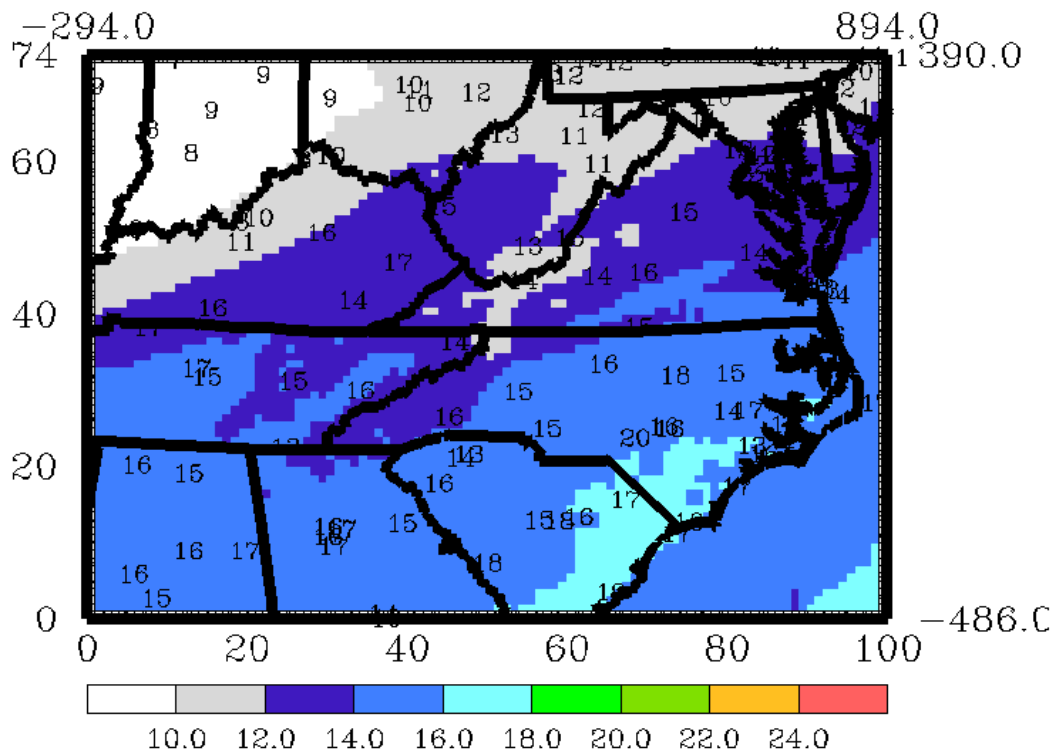


(b) 24 Km Grid

Figure 6-67. Mean Normalized Bias in Ground-Level Mixing Ratios for the 22-29 June 1992 Episode.

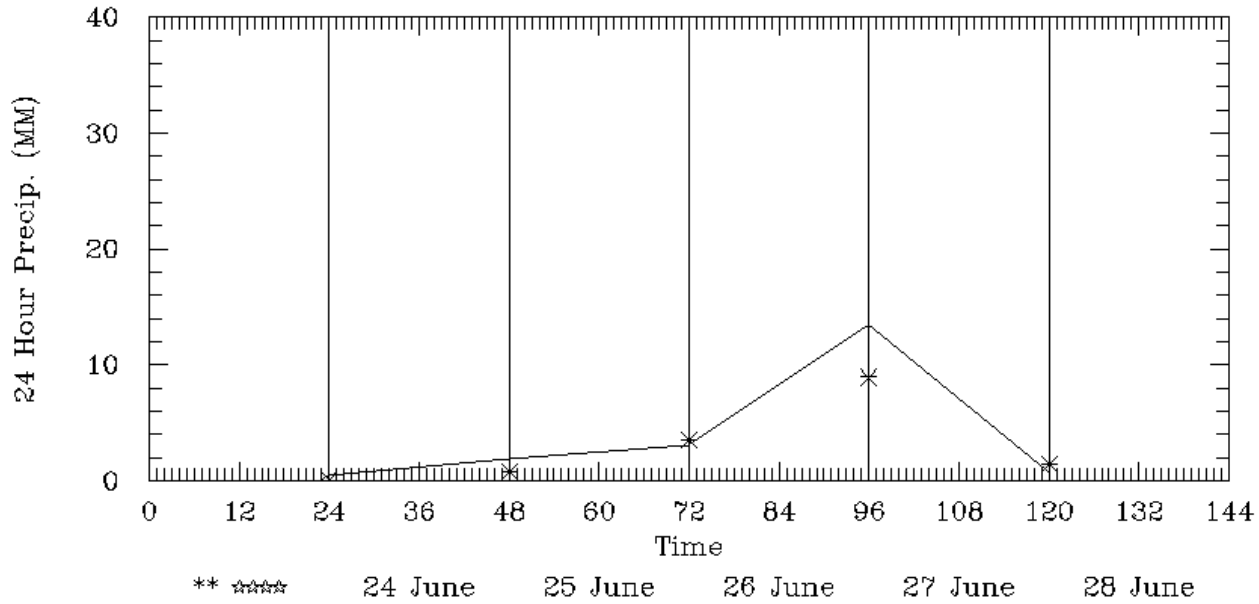


(a) 0700 UTC (0300 EST)

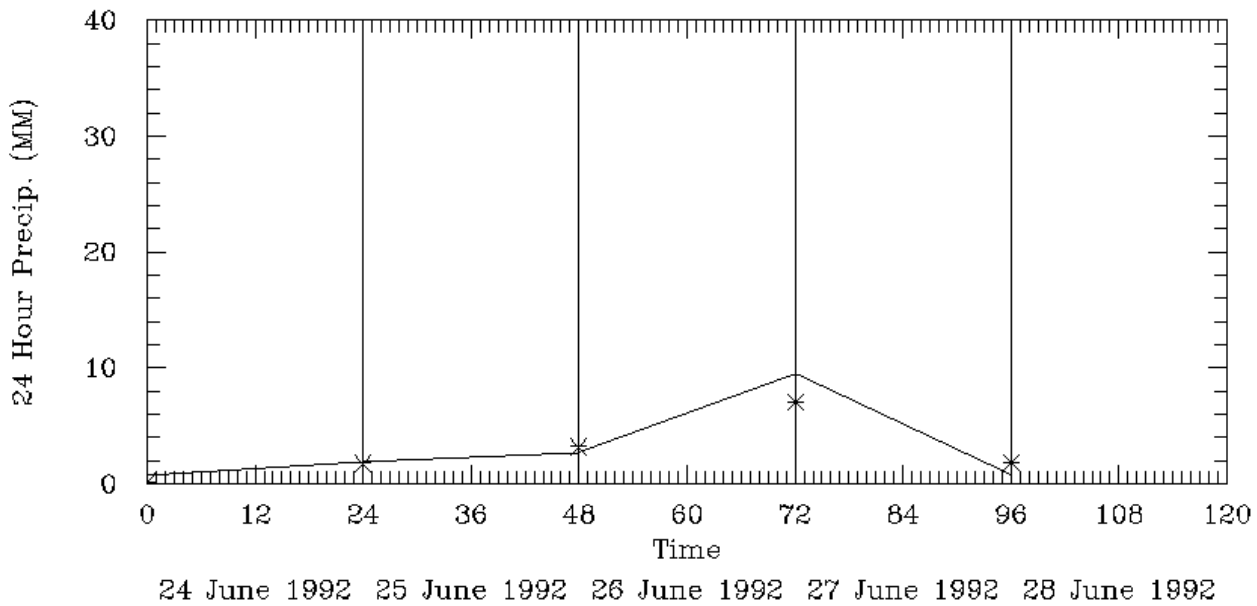


(b) 1900 UTC (1500 EST)

Figure 6-68. Ground-Level Mixing Ratio Fields for 26 June 1992.

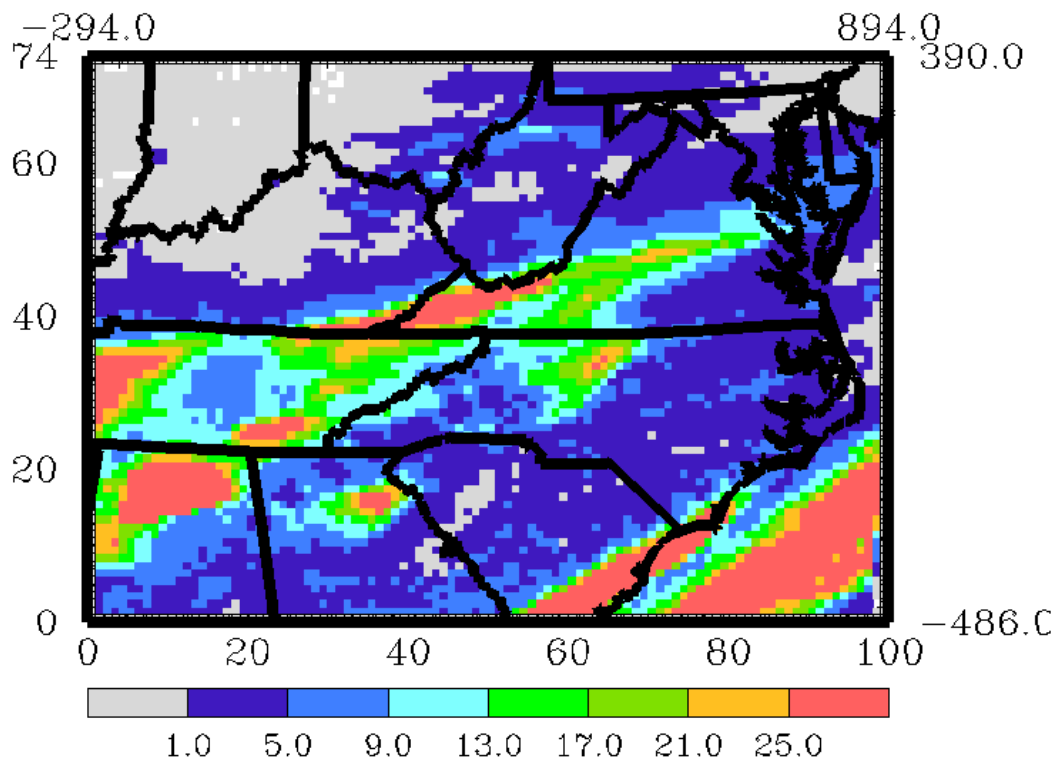


(a) 12 Km Grid

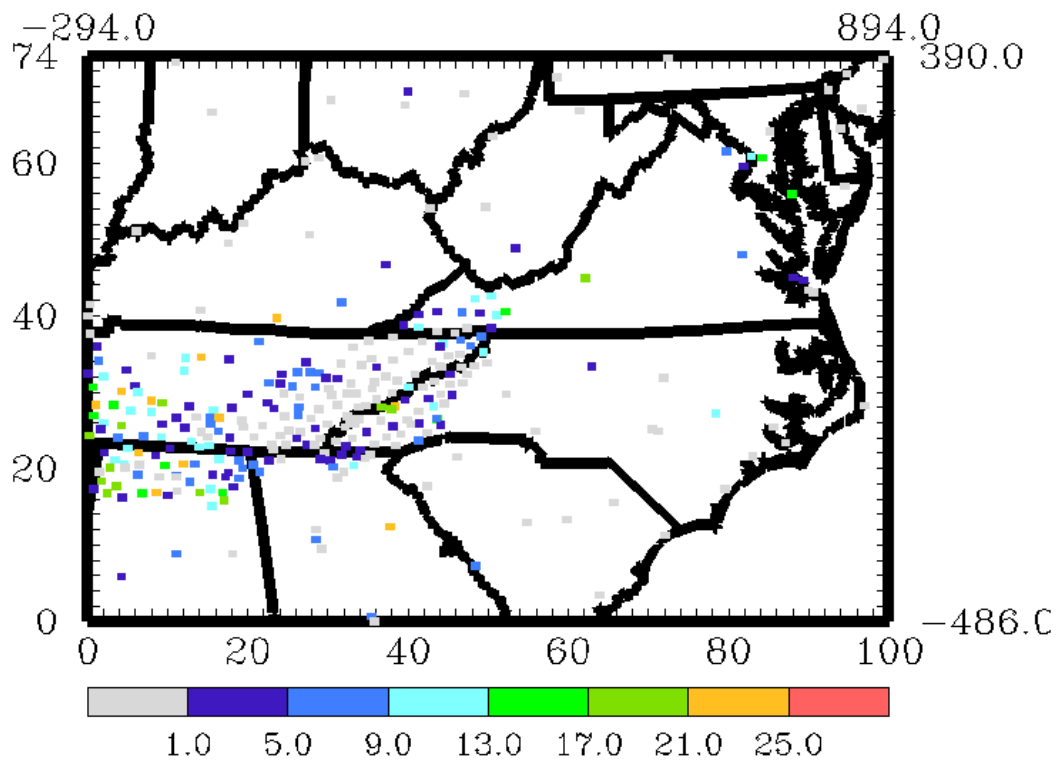


(b) 24 Km Grid

Figure 6-69. Spatial Mean Daily Precipitation (mm) for the 22-29 June 1992 Episode.

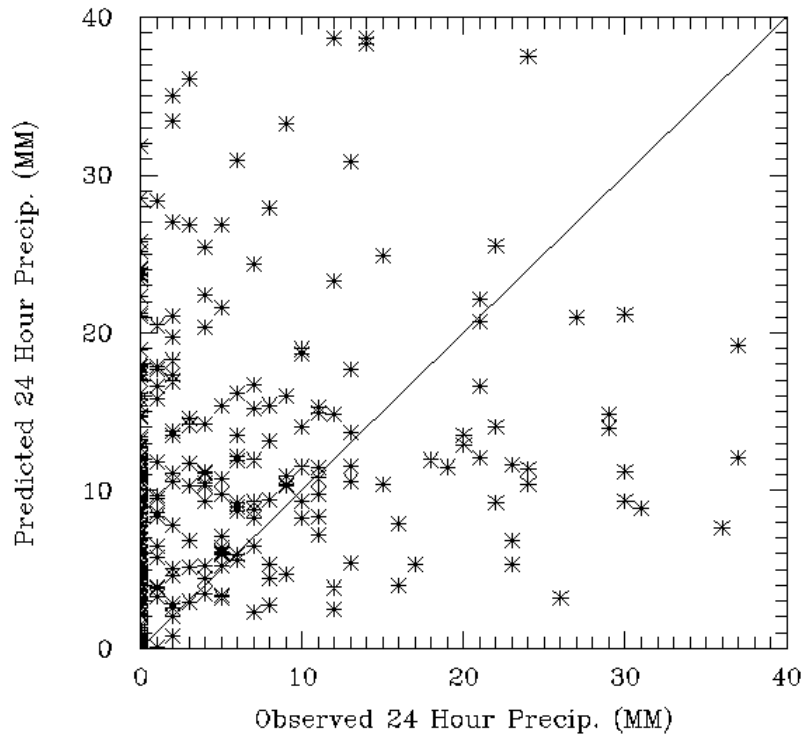


(a) Predicted Precipitation (mm)

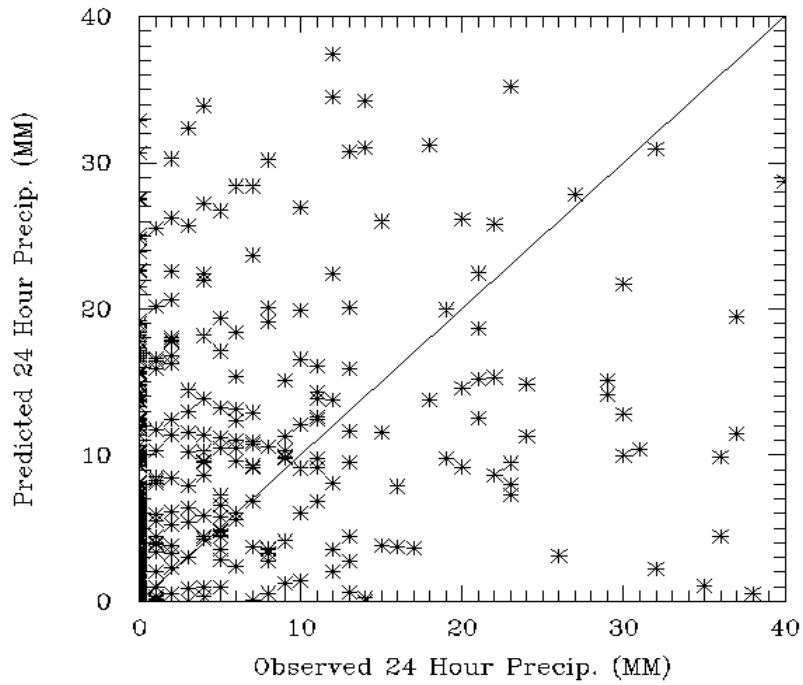


(b) Measured Precipitation (mm)

Figure 6-70. Daily Precipitation Fields for 27 June 1992.



(a) 12 Km Grid



(b) 24 Km Grid

Figure 6-71. Scatter Plot of Daily Maximum Rainfall (mm) for 27 June 1992.

6.9 24 April – 3 May 1995 Episode Results

6.9.1 Surface Temperatures

6.9.1.1 Statistical Measures of Near-Surface Temperatures

Table 6-72 presents the statistics for predicted and observed near-surface temperatures for the ten modeling days of the 24 April – 3 May 1995 SAMI episode. The daily maximum temperatures during the episode began at 22.8°C on the 24th and increased to a high of 31.1°C on the 30th. Later, a strong cooling trend developed and the maximum daily temperatures dropped down to 23.3°C by 3 May. RAMS did a very job of reproducing the daily maximum temperatures on each day. The episode-averages of the daily maximum observed and predicted temperatures were 26.9°C and 26.6°C, respectively, for a 1.1% discrepancy. Also from Table 6-9, the mean bias in predicted hourly surface temperatures across the 12 km domain ranges from -1.9°C to 0.7°C. On average across the episode, the mean bias in surface temperature prediction -0.8°C. The average gross errors in surface temperature predictions for the 10 days were 1.8°C, the same as the June 1992 episode.

6.9.1.2 Spatial Mean Surface Temperatures

Figures 6-72 and 6-73 depict time series plots of the spatial mean surface temperatures and normalized bias in hourly temperatures. From the spatial mean temperature plot (Figure 6-72), RAMS follows the hourly mean temperatures fairly well but, as with the August 1993 and June 1992 episodes, the model systematically underestimates the afternoon peaks in the latter part of April, but does a good job on the 1st and 2nd of May. These discrepancies at midday are typically on the order of 2 to 3°C. The under-prediction of the afternoon peaks is more pronounced than the August 1993 episode but about the same as the June 1992 episode.

6.9.1.3 Mean Normalized Bias in Surface Temperatures

In Figure 6-73, the mean normalized bias in RAMS' estimates of hourly near-surface temperature predictions on the 12 km grid is quite large on the first three days of the episode but begins to diminish and level out as the episode ensues. The hourly temperature biases for the April-May episode are significantly larger than those for the August and June episodes. RAMS tends to underestimate (~ 10% to 15%) hourly temperatures in the afternoon and evening hours and during the morning as well on several days. The sustained periods of underestimation of near-surface temperatures shown in the hourly bias time series plots are corroborated by the systematic under-prediction biases for most days listed in Table 6-9.1.

6.9.1.4 Surface Temperature Fields

Hourly averaged ground-level temperature fields for the 12 km domain are shown in Figure 6-74 for four representative hours on 29 April 1995. On this day, lower temperatures are evident in regions of elevated terrain compared to the coastal and interior sections of the Midwest.

6.9.2 Surface Wind Speed and Direction

6.9.2.1 Statistical Measures of Near-Surface Wind Speed and Direction

Statistical measures of model performance for the winds during the 24 April-3 May 1995 episode are listed in Table 6-9. On the 12 km grid, RAMS estimates mean wind speeds (2.98 m s^{-1}) that are on average 60% greater than the magnitude of the episode mean observations (1.86 m s^{-1}). RAMS overestimates the daily average observed wind speeds during this episode by about the same amount as the June 1992 episode. Mean wind speeds are also higher than those encountered in the August 1993 period.

Modeled wind directions show reasonable agreement with the observations on the first five days of the episode and fairly poor agreement on the last five days. Across the 10-day episode, the mean modeled (257.0 degrees) and observed surface wind directions (261.4 degrees) differ by only 4 degrees. From day-to-day, however, the discrepancies between daily average and observed wind direction varies from 2 to 158 degrees. On the 29th through the 3rd of May, the mean (absolute) discrepancy between daily averaged modeled and observed wind direction is 131 degrees. During the latter half of the episode a weak front moved through the eastern U.S. producing rain and unsettled weather, contributing in part to the generally poorer model performance for daily averaged wind direction.

The daily average index of agreement parameter for the MM5 model ranges between 0.72 and 0.88 with a 10-day mean of 0.81. These results are better than those achieved with the August 1993 and June 1992 episodes. Table 6-8.2 also lists the systematic and unsystematic components of the RMSE errors. For all but 1 May, the systematic component is larger than the unsystematic component. The episode average RMSE error is 1.84 m s^{-1} , nearly identical to the June 1992 episode.

6.9.2.2 Vector Mean Wind Speeds

Figures 6-75 through 6-78 present various surface wind speed and wind direction summary plots for the April-May 1995 episode. As with the August and June episodes, the vector mean modeled wind speed (Figure 6-75) is systematically overestimated compared to the observed mean wind speeds for every day of the episode except 1 May. This overestimation tendency bears several similarities to that encountered in the August 1993 and June 1992 episodes (see Figures 6-47 and 6-61). On several of the days, the model represents the afternoon wind speed increase fairly well notwithstanding the over-prediction.

6.9.2.3 Mean Wind Direction

Figure 6-76 presents the hourly variation in modeled versus observed surface wind directions over the ten April-May modeling days. There is generally good agreement for the first five days, but beginning with 29 April, the model's wind direction predictions begin to diverge significantly from the observations.

6.9.2.4 Root Mean Square Error in Wind Speeds

The RMSE errors and index of agreement are shown in Figures 6-77 and 6-78, respectively. The episode average values of the unsystematic, systematic, and total RMSE errors are 1.46 m s^{-1} , 1.84 m s^{-1} and 2.35 m s^{-1} , respectively. These results are poorer than the August 1993 and June 1992 episodes. From Figure 6-77 there does not appear to be any significant error growth during the simulation but the RMSE errors are greater than the June and August episodes. The systematic component (model physics-related) of the RMSE error is clearly the larger contributor to the total RMSE error in this episode as shown graphically in Figure 6-77.

6.9.2.5 Index of Agreement in Surface Wind Speeds

The index of agreement results for the April-May 1995 episode (Figure 6-78) are quite good. This is somewhat surprising given the poorer wind direction and RMSE error performance of the model for this episode relative to the August 1993 and June 1992 periods. For this episode, RAMS exhibits typical hourly variation in the agreement index parameter with the lowest values occurring during the morning period. In the afternoon when speeds are greater, the index increases. The mean value of the index of agreement varies diurnally throughout the episode; the mean over the whole period is 0.81, an improvement over the 0.75 figure obtained with the August and June episodes.

6.9.2.6 Ground-Level Wind Fields

Figure 6-79 presents afternoon RAMS surface wind field comparisons over the 12 km domain on four different days during the April-May 1995 episode. The modeled winds on these days are in reasonable agreement with the observed values. When examining the full set of hourly surface wind plots for the episode we did not find instances where there were major regional discrepancies in the predicted versus observed surface wind fields.

6.9.3 Mixing Ratios

6.9.3.1 Statistical Measures of Near-Surface Mixing Ratios

Statistical results for near surface mixing ratios are listed in Table 6-9 for the June 1992 episode. Across the 12 km domain the agreement between the episode mean daily maximum observed (13.1 g/Kg) and modeled (13.5 g/Kg) mixing ratios is quite good. RAMS slightly underestimates the maximum ratio on most days. The mean bias and error in mixing ratios are also quite good, with 10-day mean values of -0.1 g/Kg and 0.7 g/Kg respectively. As with the August 1993 and June 1992 episodes, these results indicate that RAMS does a fairly good job of reproducing the daily maximum and hourly specific humidity across the 12 km domain.

6.9.3.2 Spatial Mean Surface Mixing Ratios

Figure 6-80 is a spatial mean surface mixing ratio plot for the April-May 1995 episode. The agreement between prediction and observation is excellent at both 12 km and 24 km scales. Except on the night of 29 April, there is no discernable tendency in this plot to underestimate mixing ratio.

6.9.3.3 Bias in Surface Mixing Ratios

The minor underestimation of hourly mixing ratio is evident in the normalized bias time series shown in Figure 6-81. The largest biases in mixing ratio tend to occur at night or in the early morning hours although on 1 and 2 May there is a tendency to overestimate during the middle of the day. No significant diurnal performance problems are evident in the mixing ratio results.

6.9.3.4 Surface Mixing Ratio Fields

Figure 6-82 presents examples of ground-level mixing ratio fields across the 12 km domain at two time periods (0300 and 1500 EST) on 30 April 1995. These plots show fairly low humidity and weak spatial gradients in the fields, predominantly in a latitudinal direction. There is generally good agreement between the predicted and observed mixing ratios at the various monitoring stations.

6.9.4 Precipitation

6.9.4.1 Statistical Measures of Total Daily Precipitation

Rain occurred on 8 of the 10 days during the 24 April – 3 May 1995 episode (see Table 6-9). The maximum daily precipitation at any rain gauge varied between 3 mm and 48 mm with an episode mean of 21 mm. RAMS predicted a range of daily maximum rainfall totals from 2.0 mm to 38.6 mm with an episode mean of 20.1 mm. The mean observed and predicted precipitation across all rain gauges was 2.5 mm and 4.1 mm, yielding an overall discrepancy of 64% which constitutes fair agreement. RAMS' performance in predicting rainfall for this episode is poorer than for the August 1993 and July 1992 episodes.

The bias in daily rainfall prediction ranges from –5.95 mm to 10.23 mm with an episode mean of 1.5 mm. On May 1st and 2nd, RAMS over-predicted the mean daily rainfall amounts by 10.5 mm and 5.9 mm, respectively. The daily gross errors in rainfall ranged between 0.02 mm and 10.63 mm with an episode mean of 3.5 mm. Overall, the model did a fair job of simulating the daily and episode average rainfall totals when averaged across all monitoring stations.

6.9.4.2 Temporal Distribution of Total Daily Rainfall Across All Sites

Figure 6-83 presents time series plots of the daily precipitation totals derived from the measured and predicted values averaged across all reporting stations in the 12 km and 24 km domains. With the exception of the significant over-prediction on 1 May and 2 May (see Table 6-9), the day-to-day rainfall predictions match the observations closely in this comparison.

6.9.4.3 Spatial Distribution of Daily Total Measured and Observed Rainfall

Figure 6-84 compares the gridded daily precipitation predictions (in mm) across the 12 km domain for 2 May 1995 while the bottom panel presents the daily total measurements (also in mm). On 2 May, RAMS predicts bands of moderate precipitation (> 21 mm) across central Tennessee, southeastern Kentucky, and

northern Alabama. Data from the rain gauge network corroborates the general features of this predicted distribution but the network is far too sparse to make definitive spatial comparisons.

6.9.4.4 Correlation of Daily Maximum Rainfall Across All Sites

Figure 6-85 presents a Scatter Plot of predicted and observed daily total precipitation on 2 May 1995. While the spatial time series plots in Figure 6-83 suggests fair model performance based on averages across all monitoring stations, the scatter plots again reveal that this agreement derives from cancellation of over- and under-predictions at the various rain gauges. The Scatter Plot suggests generally poor correlation between prediction and observation at the individual reporting sites. Thus, as with the August 1993 and June 1992 episodes, RAMS does a credible job of estimating the total precipitation when averaged across the monitoring network on each episode day but the model's ability to predict the exact rainfall amounts paired in time and space with specific monitors is generally poor.

Table 6-9. RAMS Model Evaluation Results for the 24 April – 3 May 1995 SAMI Episode – Surface Temperatures (deg C). (a) 12 Km Grid											
Performance Attribute	24 Apr Day 114	25 Apr Day 115	26 Apr Day 116	27 Apr Day 117	28 Apr Day 118	29 Apr Day 119	30 Apr Day 120	1 May Day 121	2 May Day 122	3 May Day 123	Mean Value
Maximum Observed Temperature	22.8	23.9	26.1	27.2	28.3	28.8	31.1	30.0	27.2	23.3	26.9
Maximum Predicted Temperature	24.4	25.8	24.8	26.0	28.4	27.8	29.0	29.2	26.7	24.0	26.6
Mean Bias (deg C)	0.7	-0.7	-0.5	-1.1	-1.9	-1.8	-1.2	-0.5	0.0	-1.3	-0.8
Gross Error (deg C)	1.8	1.5	1.6	1.9	2.3	2.3	2.0	1.4	1.5	1.9	1.8

Table 6-9. RAMS Model Evaluation Results for the 24 April – 3 May 1995 SAMI Episode – Surface Temperatures (deg C). (b) 24 Km Grid											
Performance Attribute	24 Apr Day 114	25 Apr Day 115	26 Apr Day 116	27 Apr Day 117	28 Apr Day 118	29 Apr Day 119	30 Apr Day 120	1 May Day 121	2 May Day 122	3 May Day 123	Mean Value
Maximum Observed Temperature	33.9	29.4	28.3	31.1	31.1	37.8	32.2	34.4	32.2	32.2	32.3
Maximum Predicted Temperature	29.8	27.5	28.0	28.4	29.3	29.5	30.4	31.4	29.9	30.5	29.5
Mean Bias (deg C)	-0.5	-0.7	-0.6	-0.7	-1.0	-0.9	-0.5	-0.6	-0.7	-1.0	-0.7
Gross Error (deg C)	1.8	1.7	1.7	1.8	1.8	1.9	1.7	1.6	1.8	2.0	1.8

Table 6-9. RAMS Model Evaluation Results for the 24 April – 3 May 1995 Episode – Surface Wind Speeds (meters/sec). (a) 12 Km Grid											
Performance Attribute	24 Apr Day 114	25 Apr Day 115	26 Apr Day 116	27 Apr Day 117	28 Apr Day 118	29 Apr Day 119	30 Apr Day 120	1 May Day 121	2 May Day 122	3 May Day 123	Mean Value
Mean Observed Wind Speed	2.53	2.41	1.22	2.91	2.36	0.91	0.83	2.28	1.83	1.36	1.86
Mean Predicted Wind Speed	2.46	3.77	3.52	5.55	3.77	1.48	2.89	1.55	2.25	2.58	2.98
Observed Standard Deviation	2.67	2.06	2.22	2.42	2.37	2.18	2.58	2.41	3.40	1.88	2.42
Predicted Standard Deviation	3.22	2.00	2.00	2.43	2.69	2.37	2.99	3.12	4.27	2.29	2.73
RMSE	2.15	2.18	2.24	3.09	2.46	2.13	2.71	1.95	2.26	2.31	2.35
RMSE _S	1.53	1.66	1.73	2.73	1.94	1.75	2.07	1.21	2.08	1.68	1.84
RMSE _U	1.49	1.38	1.31	1.40	1.45	1.15	1.70	1.51	1.63	1.57	1.46
Index of Agreement, I	0.83	0.74	0.82	0.72	0.78	0.81	0.82	0.82	0.88	0.76	0.81
Skill _E	0.56	0.68	0.60	0.62	0.63	0.54	0.70	0.63	0.49	0.92	0.64
Skill _{VAR}	1.20	1.01	0.95	0.99	1.15	1.16	1.18	1.31	1.25	1.27	1.15
Mean Observed Wind Direction (°)	346.6	292.5	237.0	199.5	287.8	26.2	106.6	35.1	12.0	351.1	261.4
Mean Predicted Wind Direction (°)	318.3	290.2	260.6	240.2	250.2	246.7	235.0	237.4	240.0	250.9	257.0

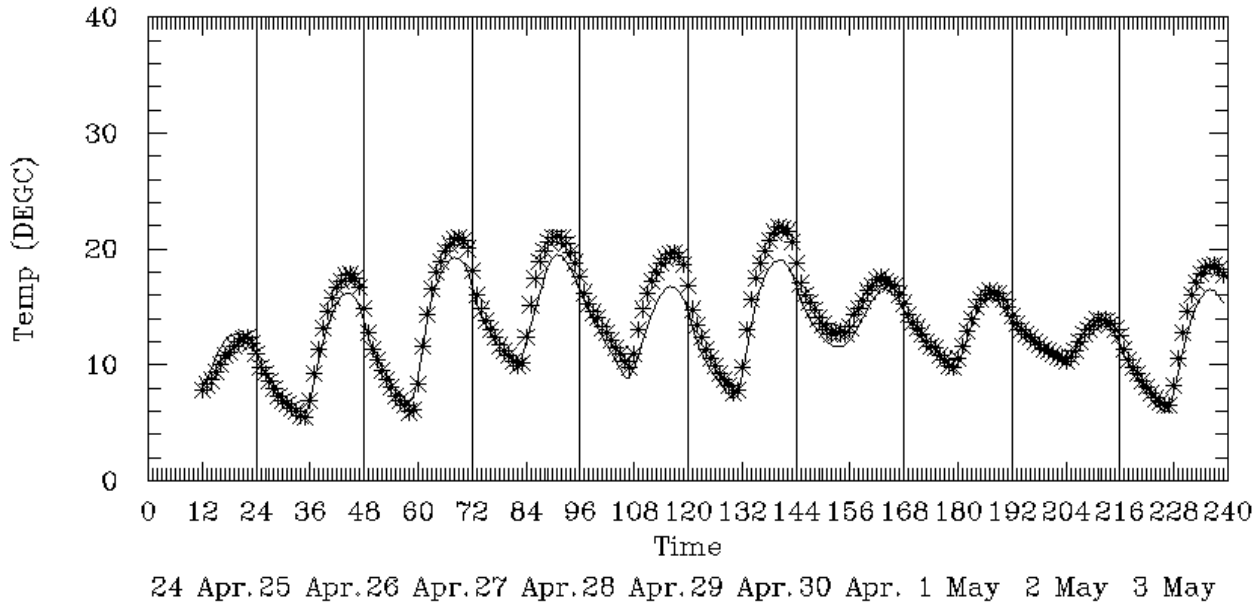
Table 6-9. RAMS Model Evaluation Results for the 24 April – 3 May 1995 Episode – Surface Wind Speeds (meters/sec). (b) 24 Km Grid											
Performance Attribute	24 Apr Day 114	25 Apr Day 115	26 Apr Day 116	27 Apr Day 117	28 Apr Day 118	29 Apr Day 119	30 Apr Day 120	1 May Day 121	2 May Day 122	3 May Day 123	Mean Value
Mean Observed Wind Speed	2.0	1.53	0.97	1.20	1.51	0.48	1.23	1.86	1.40	0.76	1.29
Mean Predicted Wind Speed	2.13	2.70	3.19	3.18	2.81	1.52	0.92	1.51	1.42	1.24	2.06
Observed Standard Deviation	3.17	2.58	2.98	3.38	2.99	2.62	2.50	2.76	2.97	2.31	2.83
Predicted Standard Deviation	2.97	2.70	3.41	3.77	3.54	3.09	3.09	3.55	3.59	3.17	3.29
RMSE	2.04	2.38	2.83	3.00	2.67	2.36	2.42	2.47	2.38	2.54	2.51
RMSE _S	1.32	1.83	2.13	2.22	1.67	1.80	1.69	1.45	1.40	1.59	1.71
RMSE _U	1.55	1.49	1.83	1.91	2.04	1.49	1.67	1.97	1.90	1.96	1.78
Index of Agreement, I	0.88	0.81	0.86	0.88	0.86	0.89	0.82	0.83	0.88	0.83	0.85
Skill _E	0.49	0.60	0.64	0.57	0.70	0.58	0.68	0.73	0.64	0.90	0.65
Skill _{VAR}	0.94	1.09	1.18	1.14	1.20	1.21	1.28	1.32	1.21	1.45	1.20
Mean Observed Wind Direction (°)	328.5	291.7	202.6	228.0	273.0	56.4	62.0	40.8	7.2	44.4	261.9
Mean Predicted Wind Direction (°)	303.7	285.2	254.4	241.2	243.8	237.4	225.4	221.3	229.7	233.2	247.5

Table 6-9. RAMS Model Evaluation Results for the 24 April – 3 May 1995 SAMI Episode – Surface Mixing Ratios (gm/Kg). (a) 12 Km Grid											
Performance Attribute	24 Apr Day 114	25 Apr Day 115	26 Apr Day 116	27 Apr Day 117	28 Apr Day 118	29 Apr Day 119	30 Apr Day 120	1 May Day 121	2 May Day 122	3 May Day 123	Mean Value
Maximum Observed Mixing Ratio	15.7	9.9	9.8	13.0	13.6	13.5	16.0	14.6	15.2	9.7	13.1
Maximum Predicted Mixing Ratio	15.5	13.8	8.6	12.8	13.2	12.3	13.5	14.5	15.5	15.0	13.5
Mean Bias (gm/Kg)	0.1	-0.3	-0.4	0.3	-0.2	-0.5	-0.1	0.2	0.1	-0.4	-0.1
Gross Error (gm/Kg)	0.8	0.5	0.6	0.8	0.7	0.7	0.9	0.8	0.8	0.6	0.7

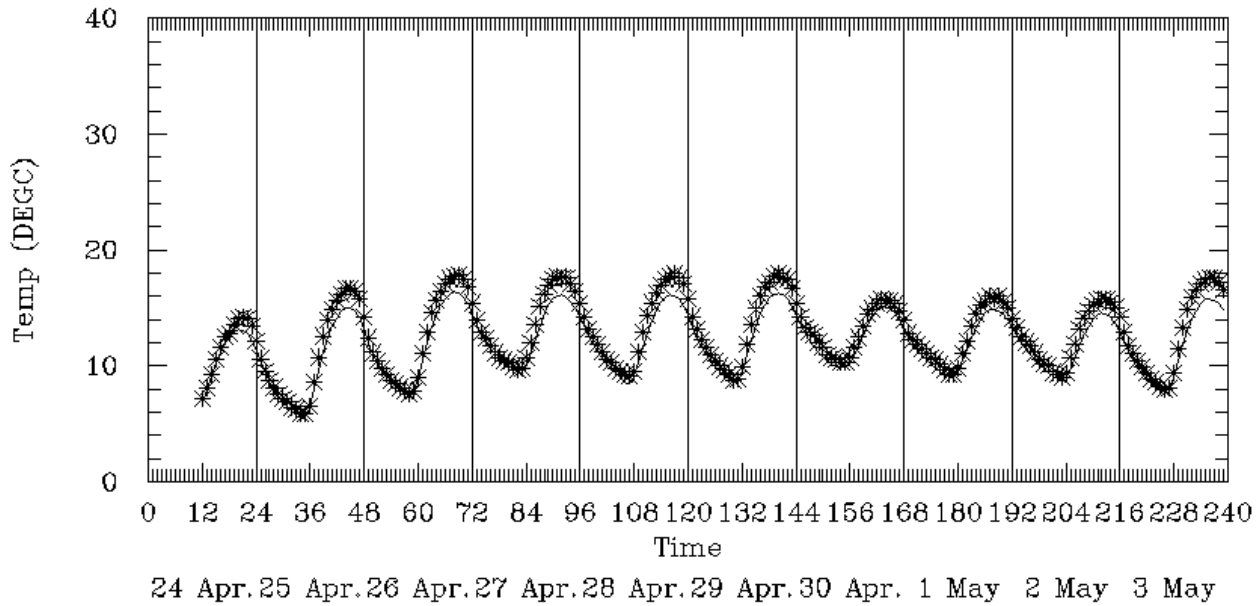
Table 6-9. RAMS Model Evaluation Results for the 24 April – 3 May 1995 SAMI Episode – Surface Mixing Ratios (gm/Kg). (b) 24 Km Grid											
Performance Attribute	24 Apr Day 114	25 Apr Day 115	26 Apr Day 116	27 Apr Day 117	28 Apr Day 118	29 Apr Day 119	30 Apr Day 120	1 May Day 121	2 May Day 122	3 May Day 123	Mean Value
Maximum Observed Mixing Ratio	19.9	18.0	16.6	17.9	17.3	16.7	18.5	19.9	18.6	18.6	18.2
Maximum Predicted Mixing Ratio	17.2	17.1	16.8	16.8	15.8	15.4	16.3	17.4	17.0	17.7	16.8
Mean Bias (gm/Kg)	-0.1	-0.2	-0.1	0.2	-0.1	0.0	0.1	0.2	0.2	-0.1	0.0
Gross Error (gm/Kg)	0.6	0.6	0.6	0.8	0.7	0.8	0.8	0.7	0.7	0.6	0.7

Table 6-9. RAMS Model Evaluation Results for the 24 April – 3 May 1995 SAMI Episode – Daily Total Precipitation (mm). (a) 12 Km Grid											
Performance Attribute	24 Apr Day 114	25 Apr Day 115	26 Apr Day 116	27 Apr Day 117	28 Apr Day 118	29 Apr Day 119	30 Apr Day 120	1 May Day 121	2 May Day 122	3 May Day 123	Mean Value
Maximum Observed Precipitation	--	--	10.0	3.0	37.0	3.0	7.0	27.0	33.0	48.0	21.0
Maximum Predicted Precipitation	--	--	2.0	7.2	12.9	9.7	26.6	38.6	28.5	35.3	20.1
Mean Observed Precipitation	--	--	0.1	0.0	0.2	0.0	0.0	3.2	7.6	8.5	2.5
Mean Predicted Precipitation	--	--	0.1	0.0	2.0	0.2	0.5	13.7	13.5	2.8	4.1
Mean Bias (mm)	--	--	-0.07	-0.01	1.50	0.20	0.29	10.23	5.71	-5.95	1.5
Gross Error (mm)	--	--	0.14	0.02	1.75	0.22	0.34	10.63	7.96	6.50	3.5

Table 6-9. RAMS Model Evaluation Results for the 24 April – 3 May 1995 SAMI Episode – Daily Total Precipitation (mm). (b) 24 Km Grid											
Performance Attribute	24 Apr Day 114	25 Apr Day 115	26 Apr Day 116	27 Apr Day 117	28 Apr Day 118	29 Apr Day 119	30 Apr Day 120	1 May Day 121	2 May Day 122	3 May Day 123	Mean Value
Maximum Observed Precipitation	--	--	10.0	53.0	41.0	24.0	197.0	27.0	45.0	48.0	55.6
Maximum Predicted Precipitation	--	--	17.8	27.3	32.8	25.3	43.6	37.1	40.6	34.3	32.4
Mean Observed Precipitation	--	--	0.2	1.1	1.2	0.4	1.3	2.9	6.3	5.7	2.4
Mean Predicted Precipitation	--	--	0.2	0.8	2.4	0.6	1.7	9.1	10.2	2.2	3.4
Mean Bias (mm)	--	--	-0.10	-0.40	0.97	0.02	-0.14	6.58	3.88	-3.64	0.9
Gross Error (mm)	--	--	0.32	0.77	2.50	0.46	1.71	7.42	6.37	4.64	3.0

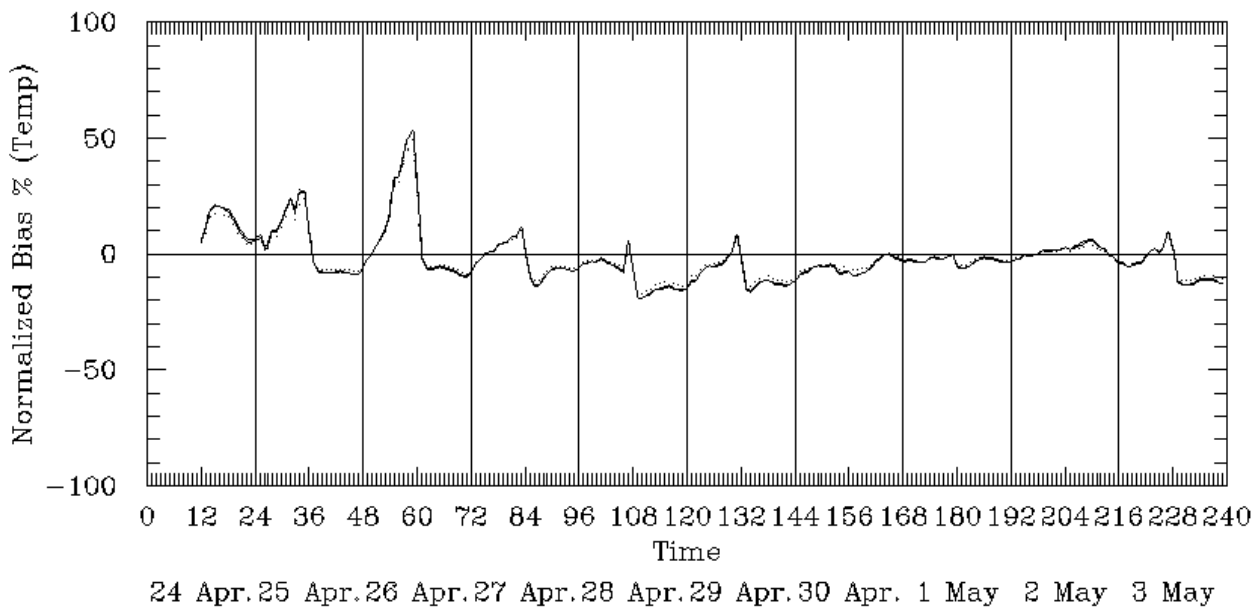


(a) 12 Km Grid



(b) 24 Km Grid

Figure 6-72. Spatial Mean Ground-Level Temperatures for the 24 April – 3 May 1995 Episode.



(a) 12 Km Grid

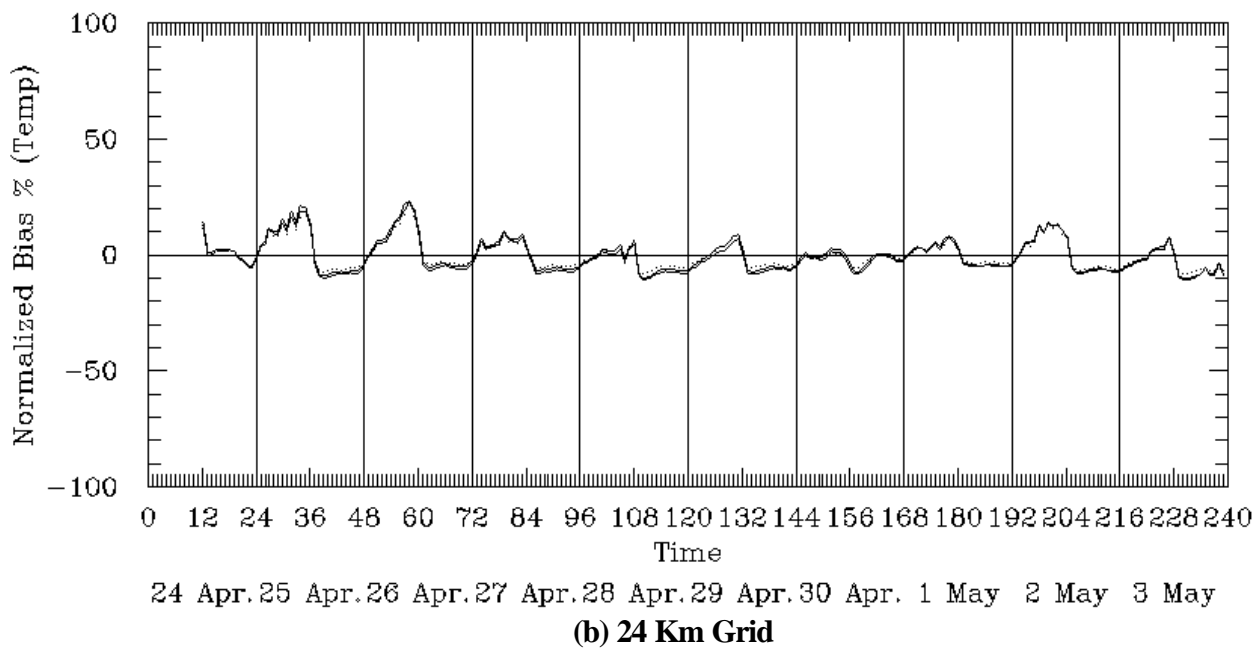
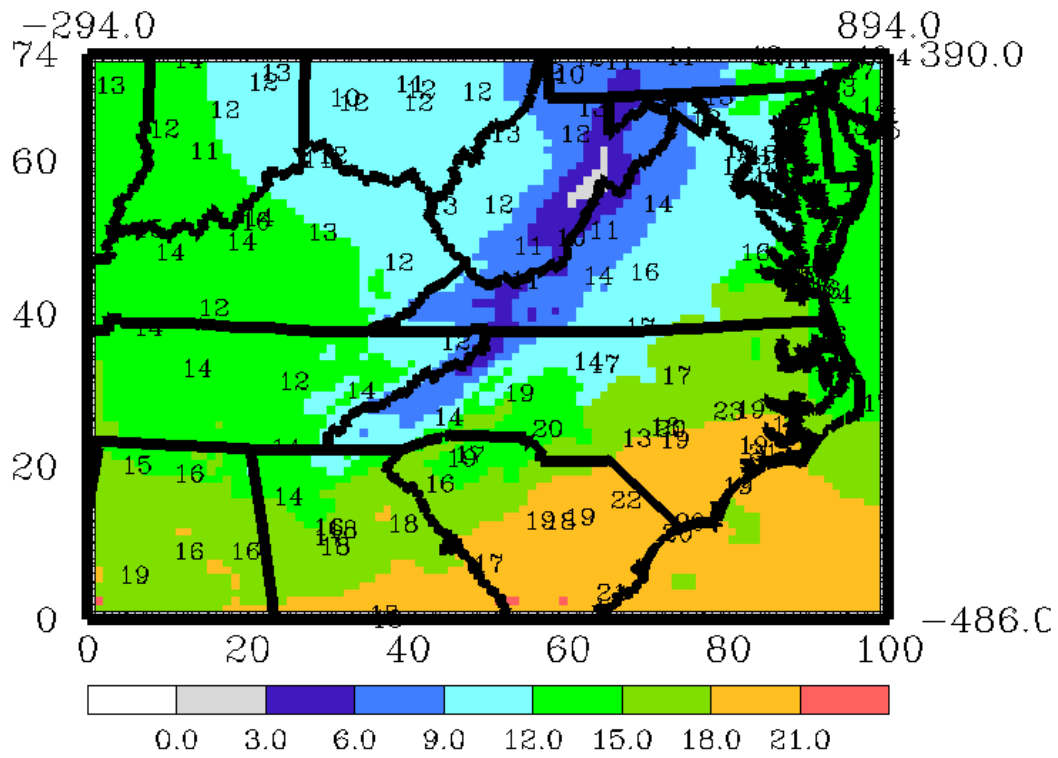
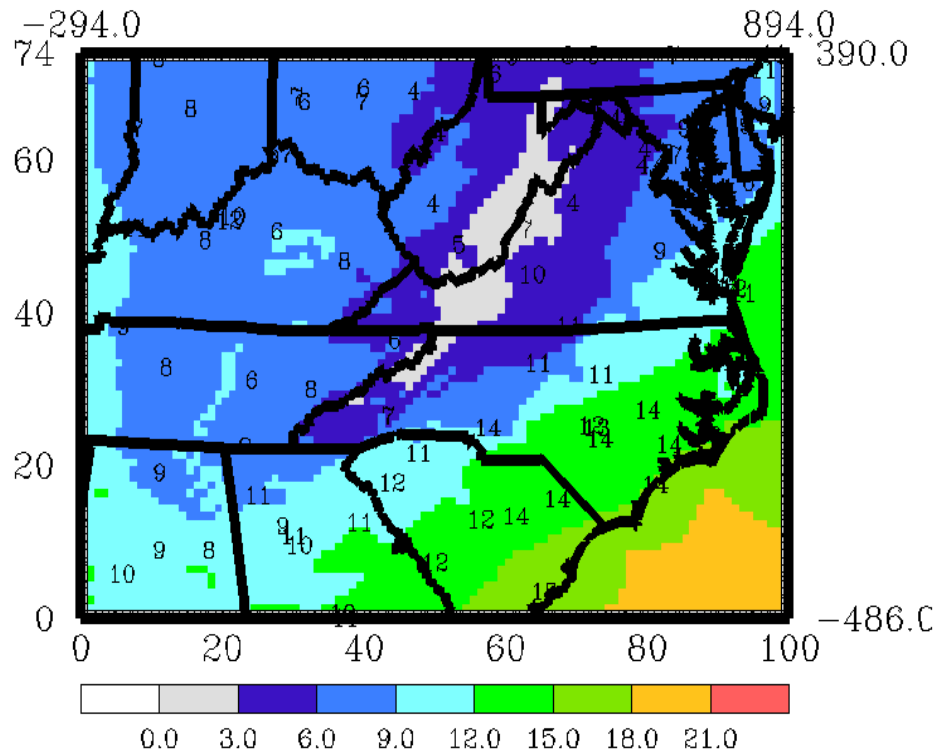


Figure 6-73. Mean Normalized Bias in Ground-Level Temperatures for the 24 April – 3 May 1995 Episode.

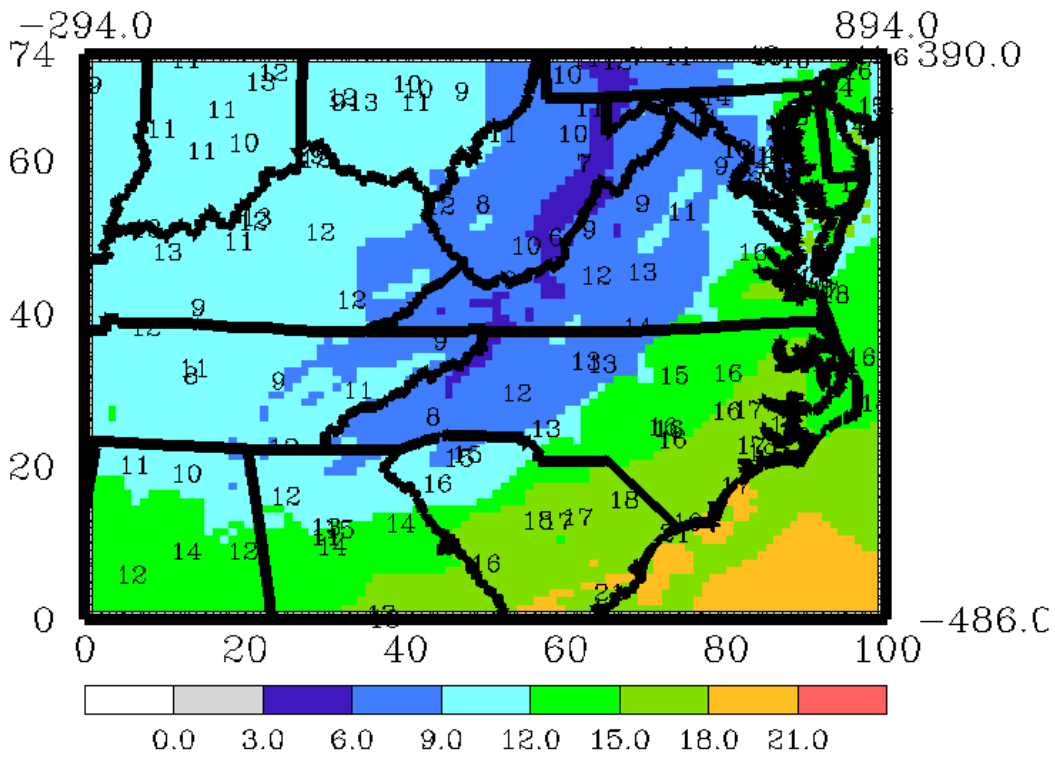


(a) 0100 UTC (2100 EST)

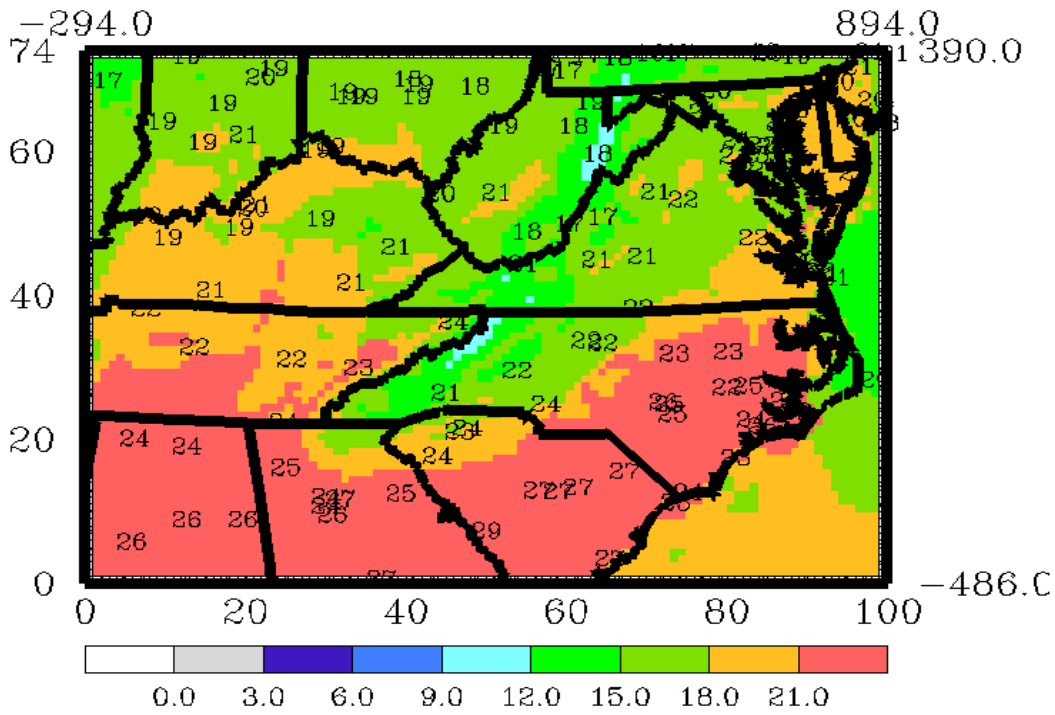


(b) 0700 UTC (0300 EST)

Figure 6-74. Ground-Level Temperature Fields for 29 April 1995.

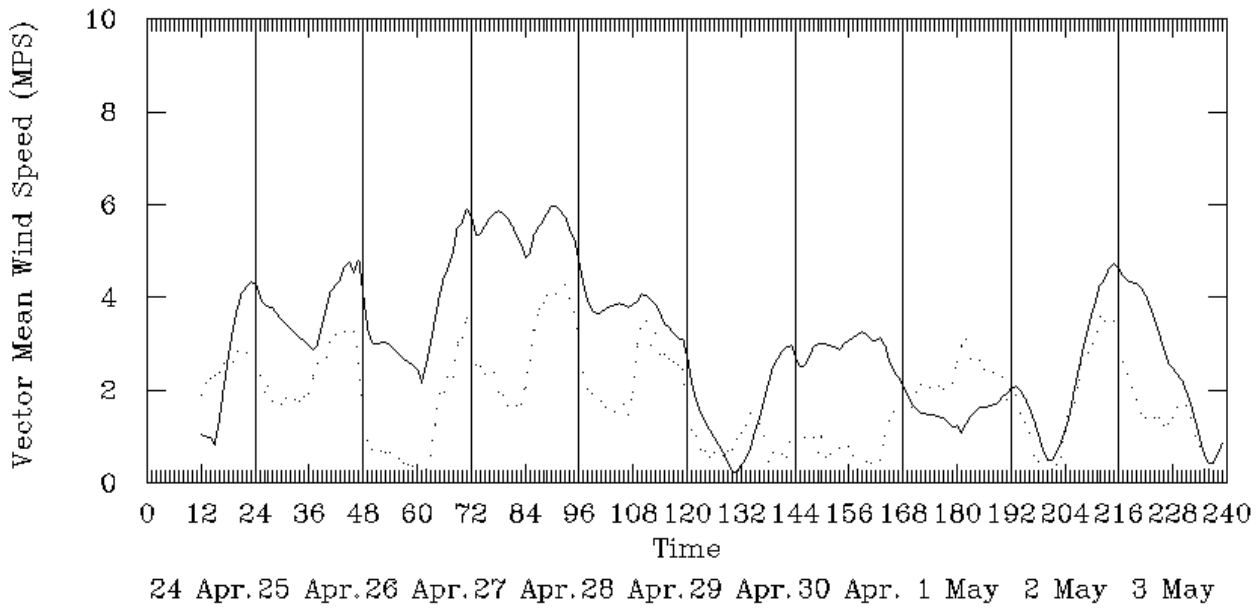


(c) 1300 UTC (0900 EST)

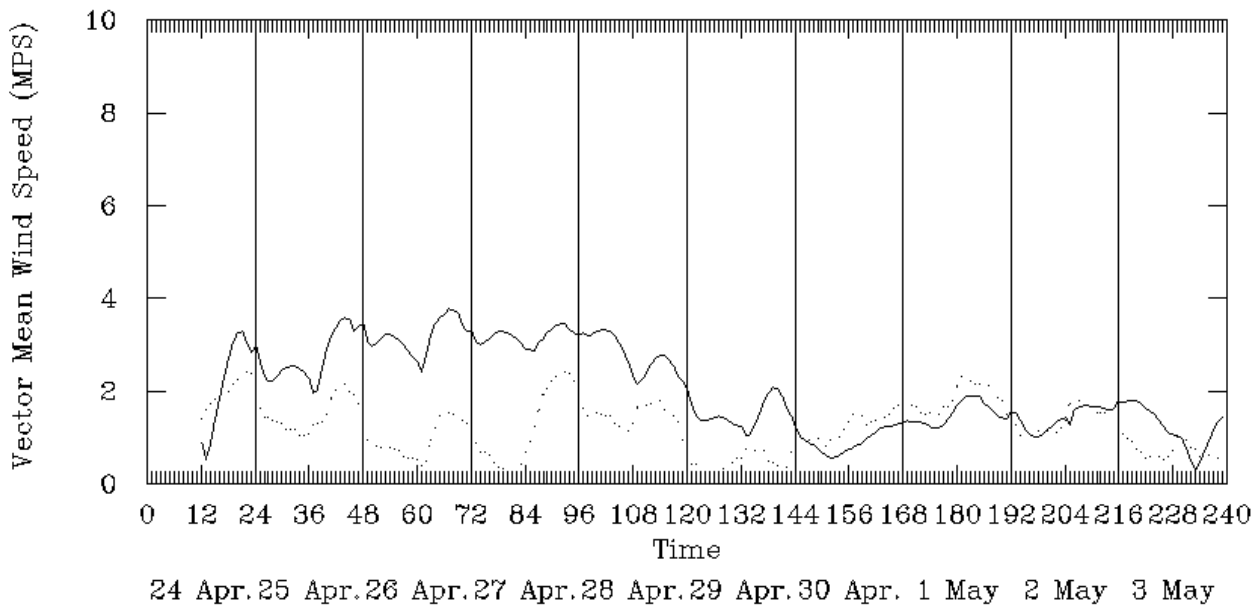


(d) 1900 UTC (1500 EST)

Figure 6-74. Concluded.

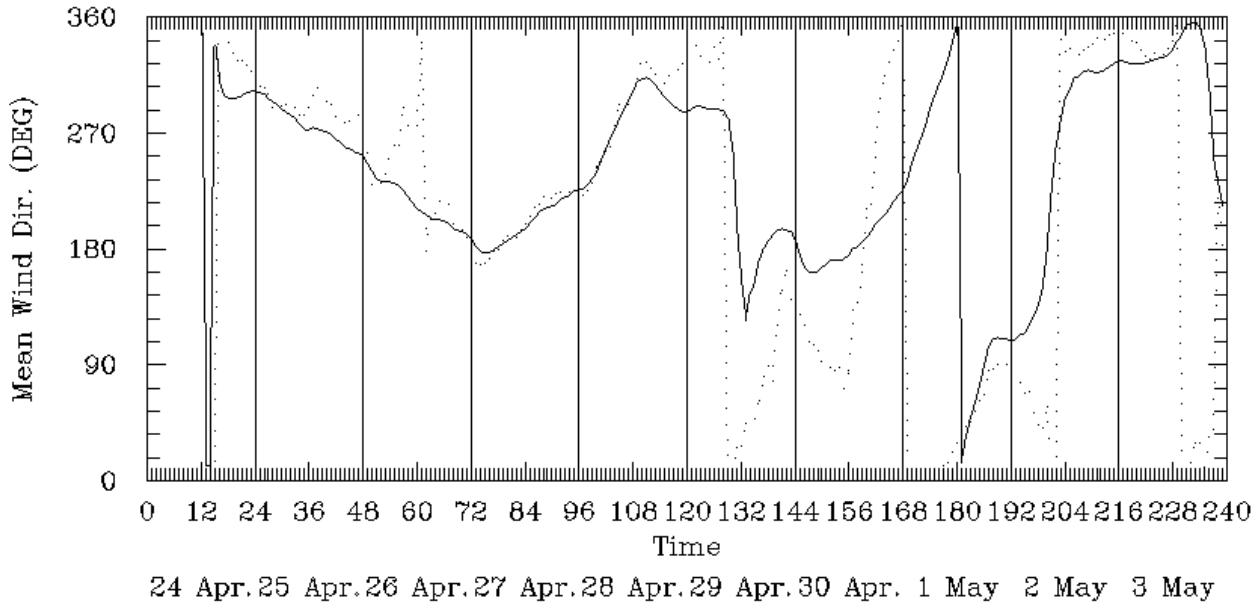


(a) 12 Km Grid

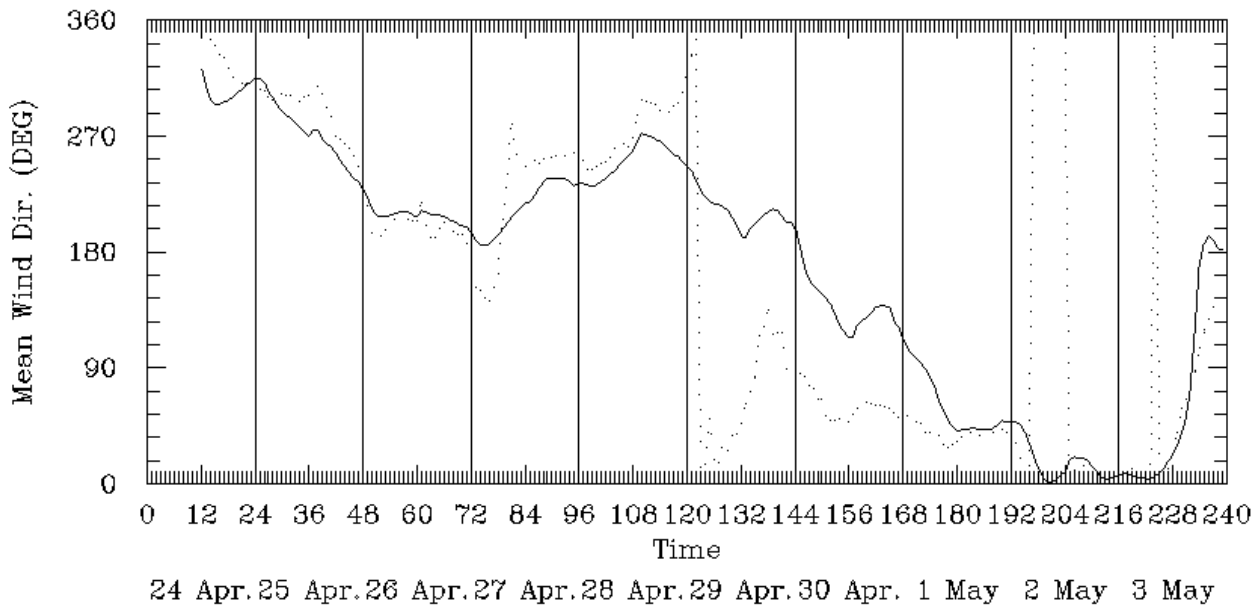


(b) 24 Km Grid

Figure 6-75. Vector Mean Wind Speed for the 24 April – 3 May 1995 Episode.

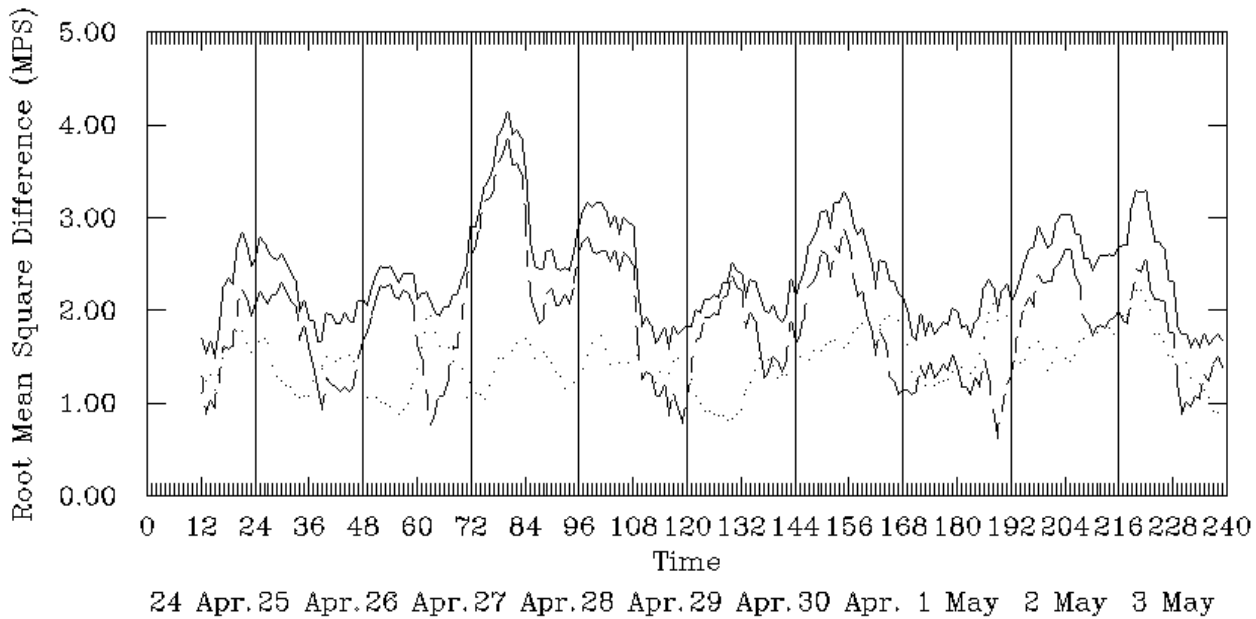


(a) 12 Km Grid

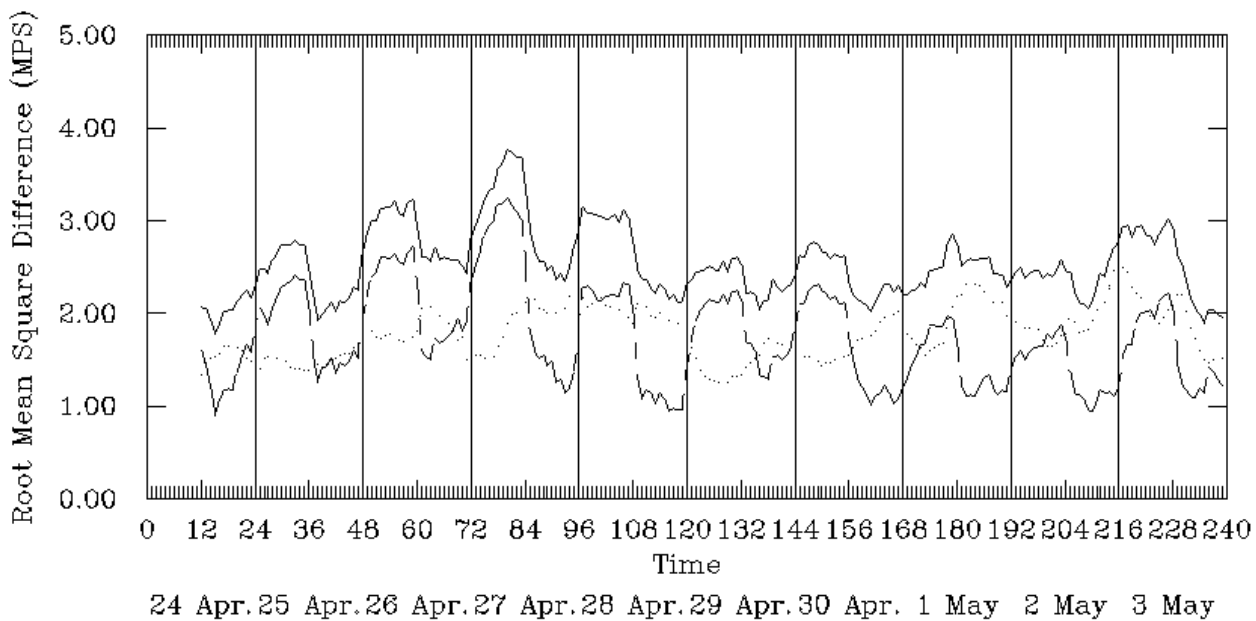


(b) 24 Km Grid

Figure 6-76. Mean Wind Direction for the 24 April – 3 May 1995 Episode.

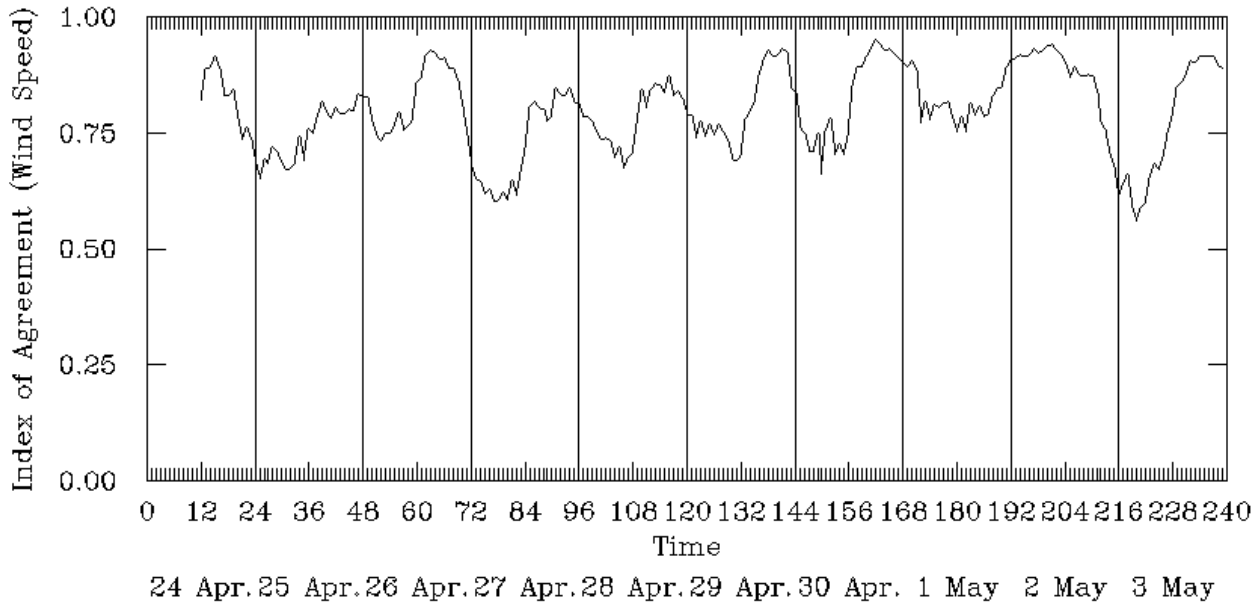


(a) 12 Km Grid

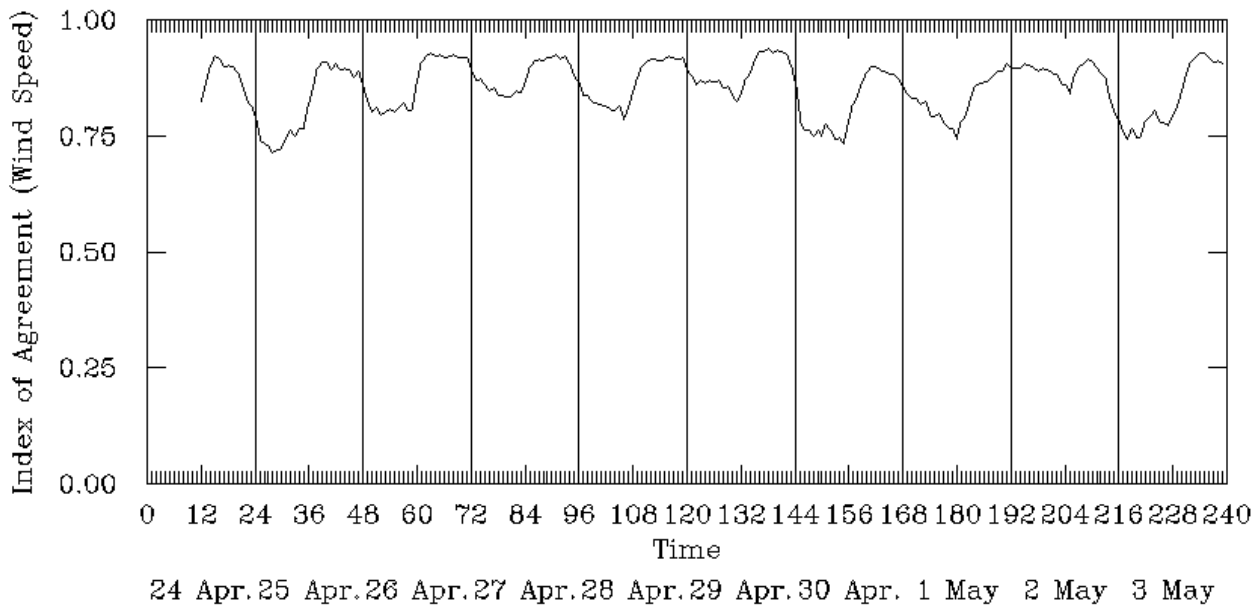


(b) 24 Km Grid

Figure 6-77. Root Mean Square Error in Ground-Level Wind Speeds for the 24 April – 3 May 1995 Episode.

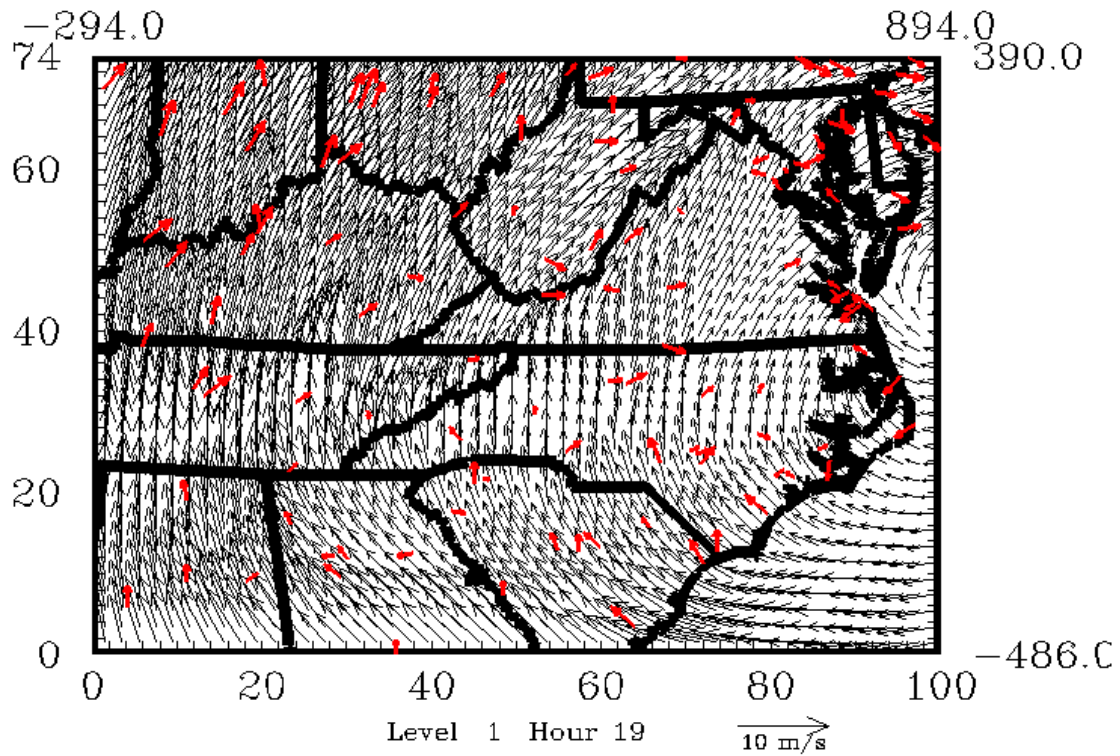


(a) 12 Km Grid

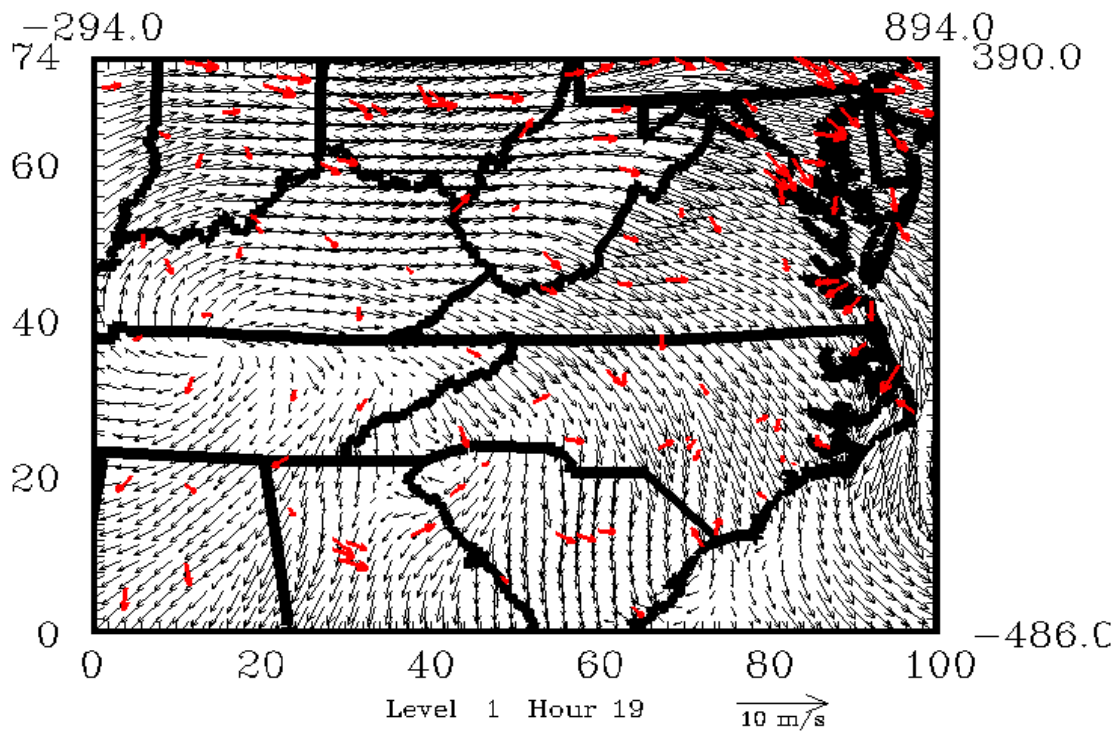


(b) 24 Km Grid

Figure 6-78. Index of Agreement in Surface Wind Speed for the 24 April – 3 May 1995 Episode.

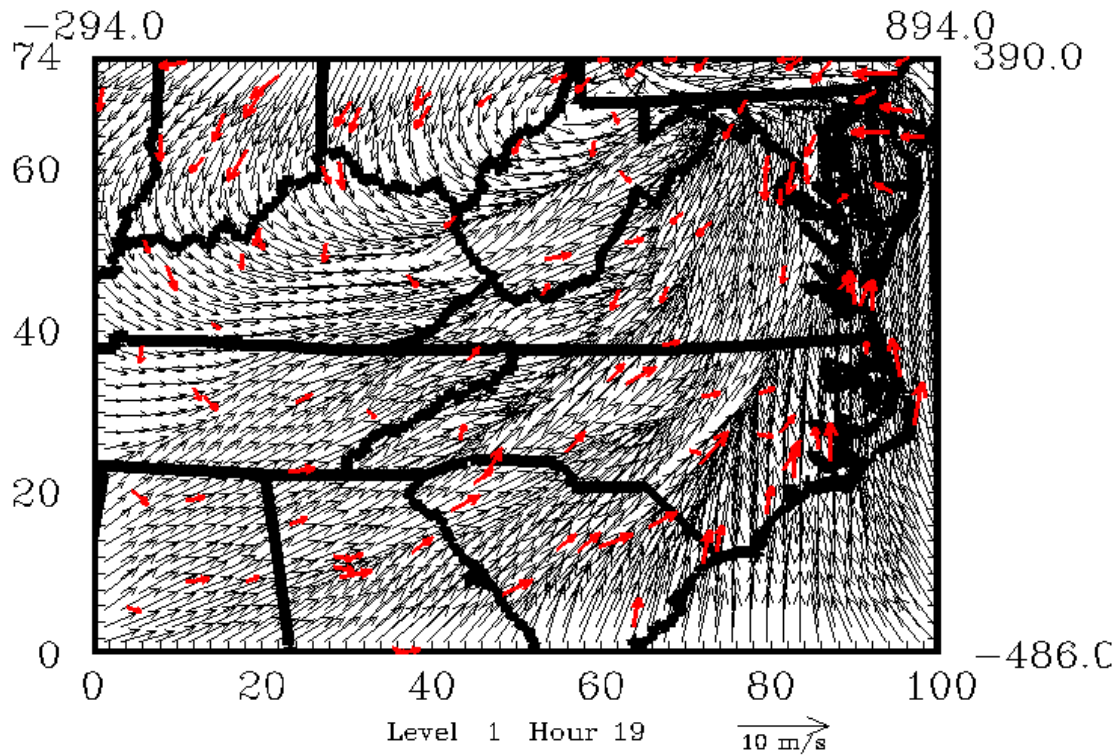


(a) 26 April 1995, 1900 UTC (1500 EST)

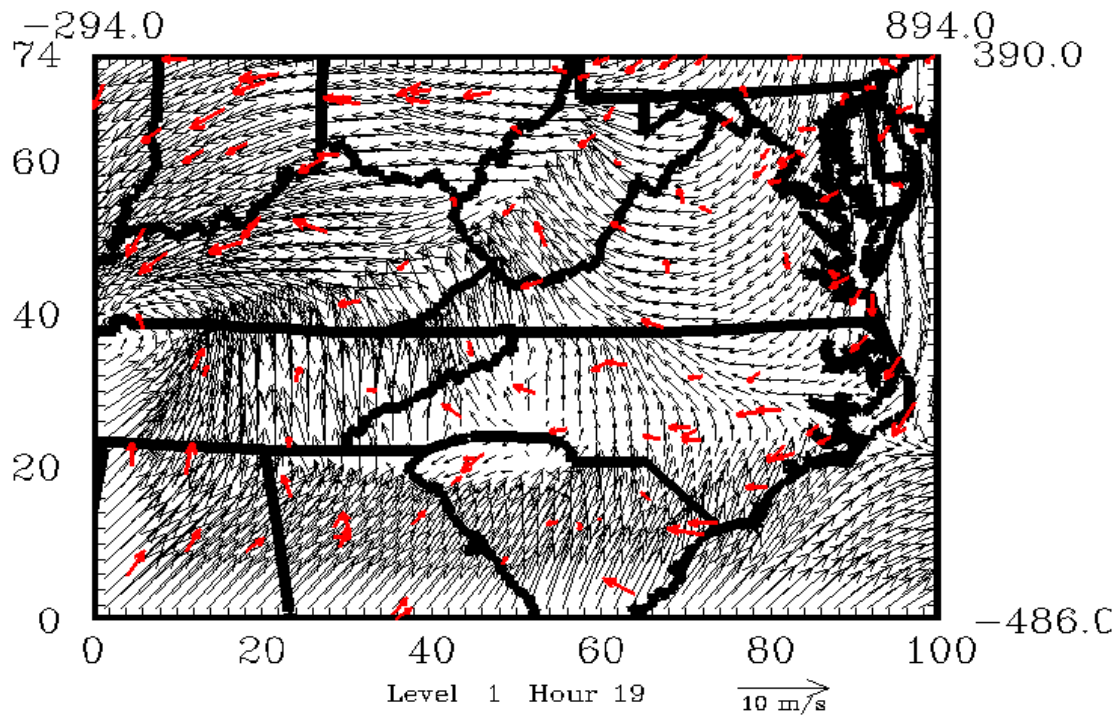


(b) 28 April 1995, 1900 UTC (1500 EST)

Figure 6-79. Ground-Level Wind Fields for the 24 April – 3 May 1995 Episode.

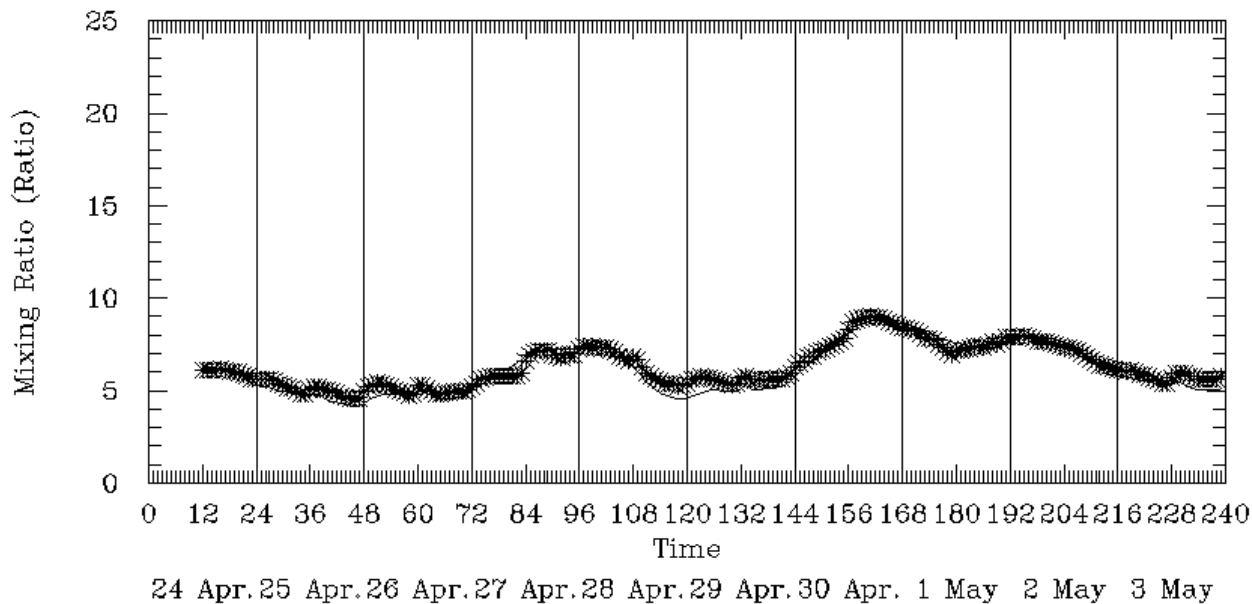


(c) 30 April 1995, 1900 UTC (1500 EST)

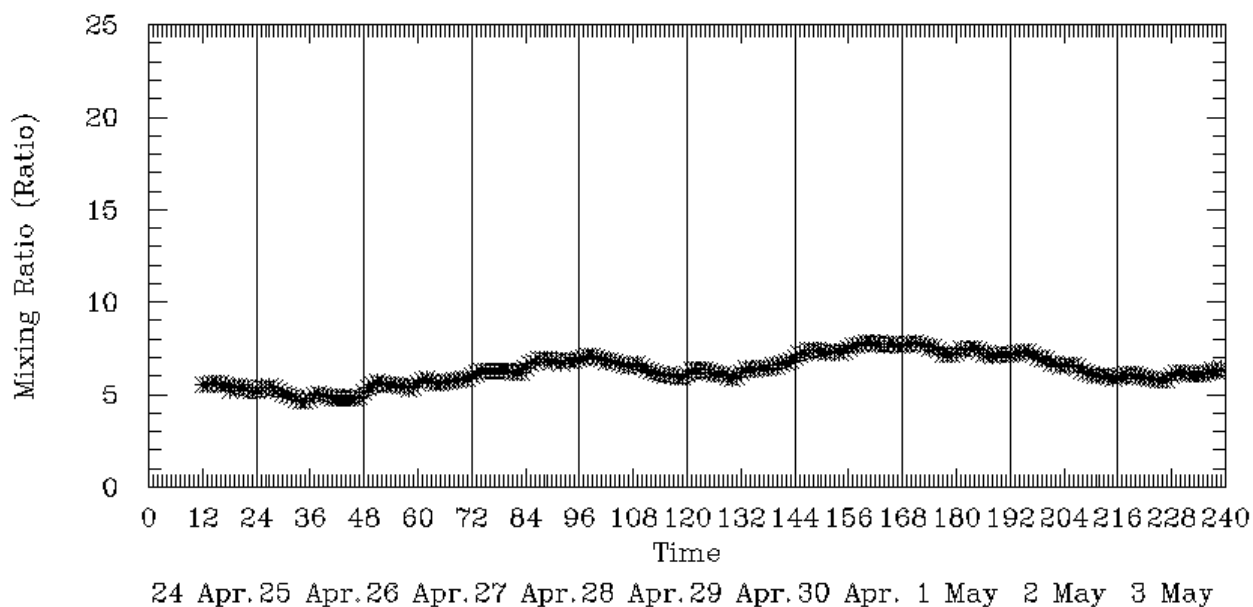


(d) 1 May 1995, 1900 UTC (EST)

Figure 6-79. Concluded.

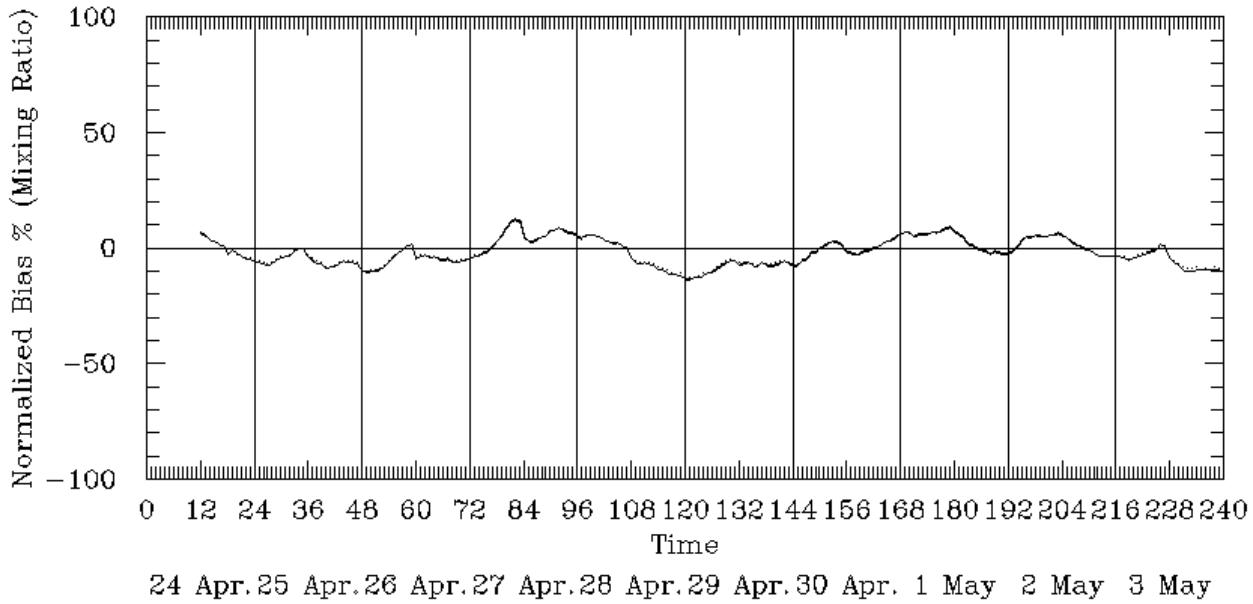


(a) 12 Km Grid

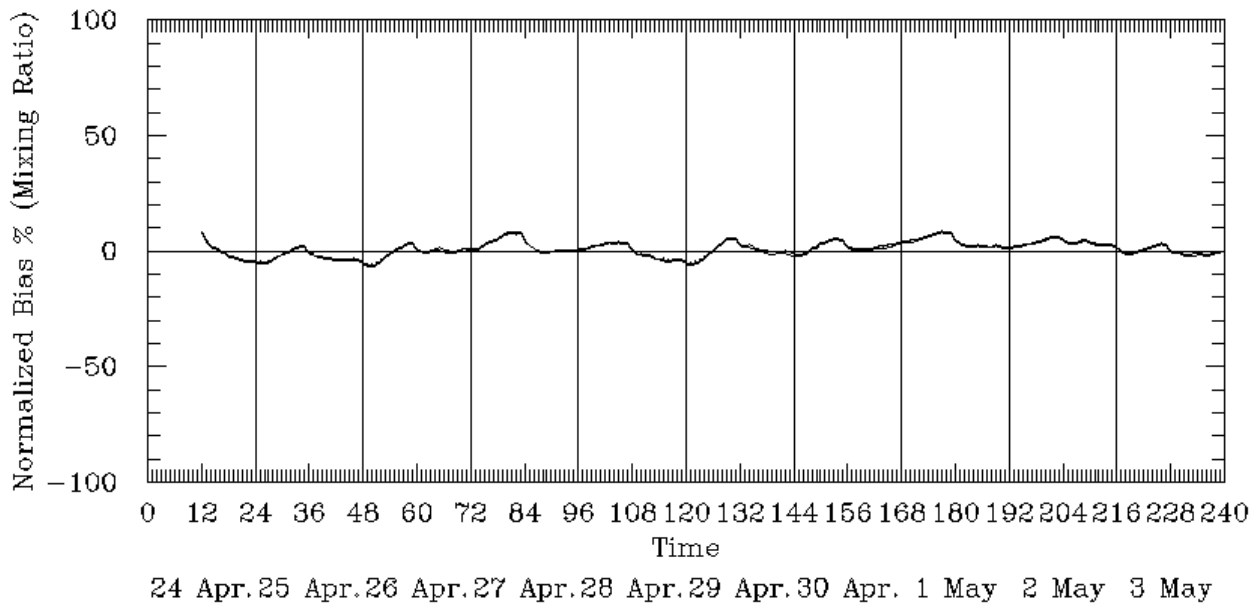


(b) 24 Km Grid

Figure 6-80. Spatial Mean Ground-Level Mixing Ratios for the 24 April – 3 May 1995 Episode.

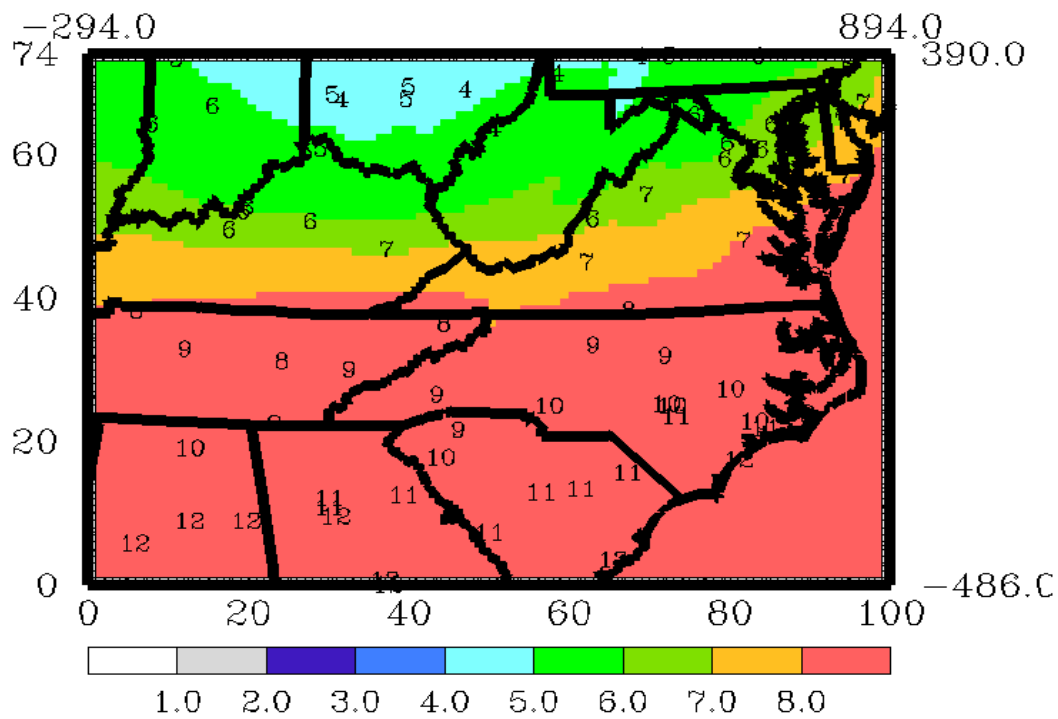


(a) 12 Km Grid

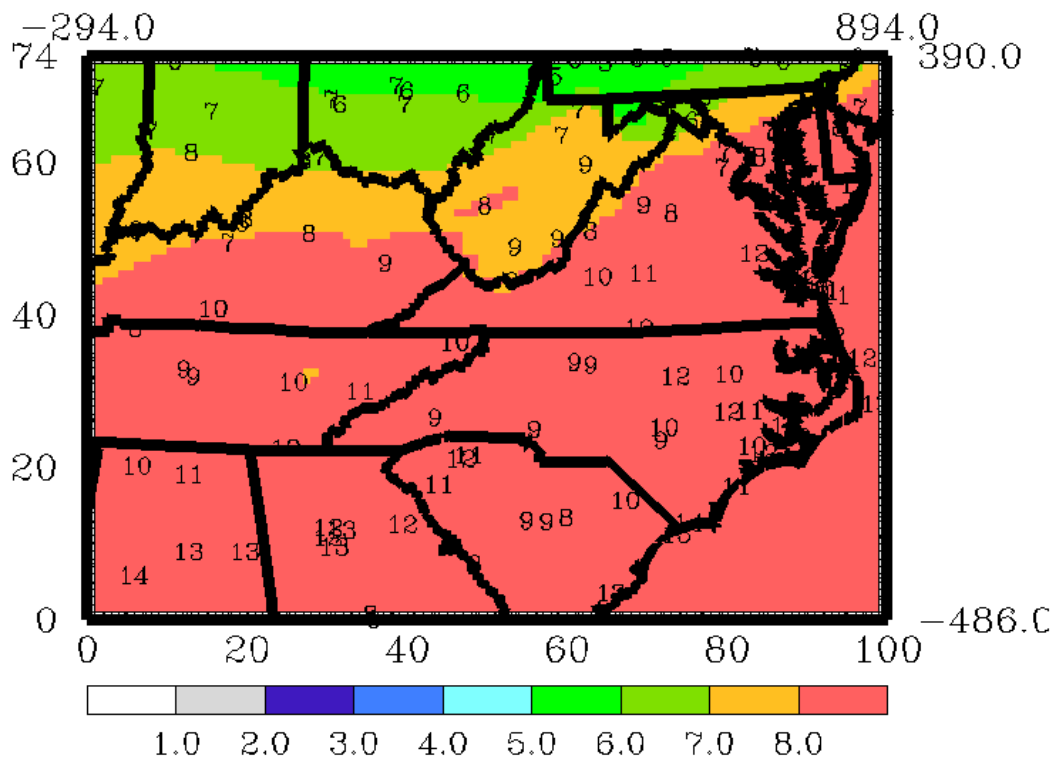


(b) 24 Km Grid

Figure 6-81. Mean Normalized Bias in Ground-Level Mixing Ratios for the 24 April – 3 May 1995 Episode.

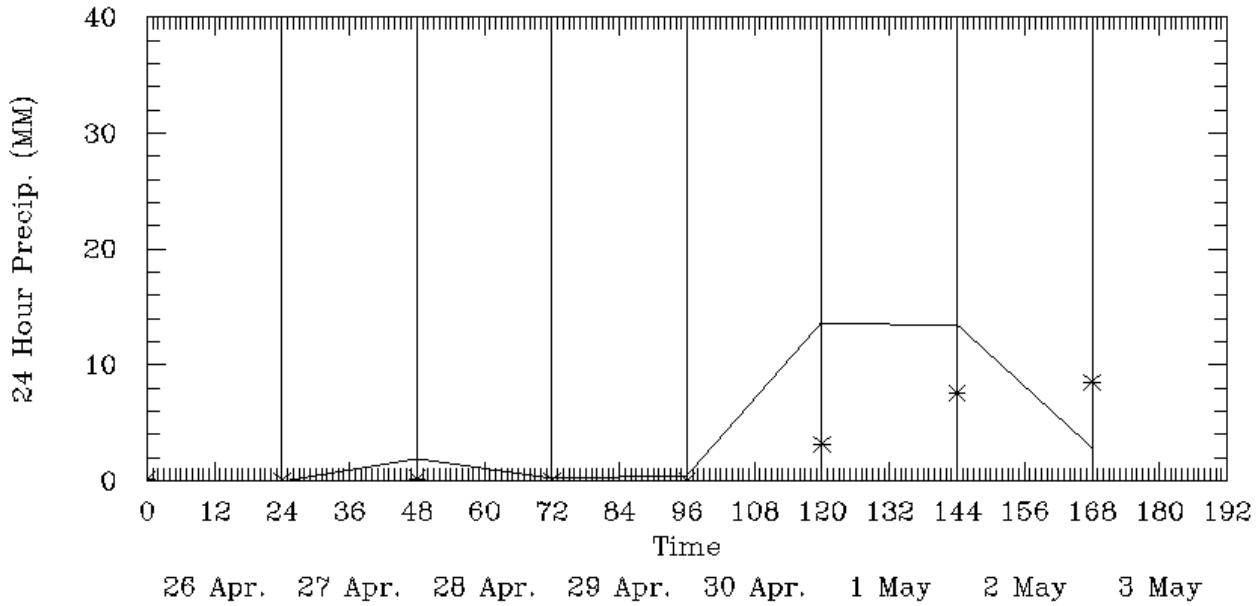


(a) 0700 UTC (0300 EST)

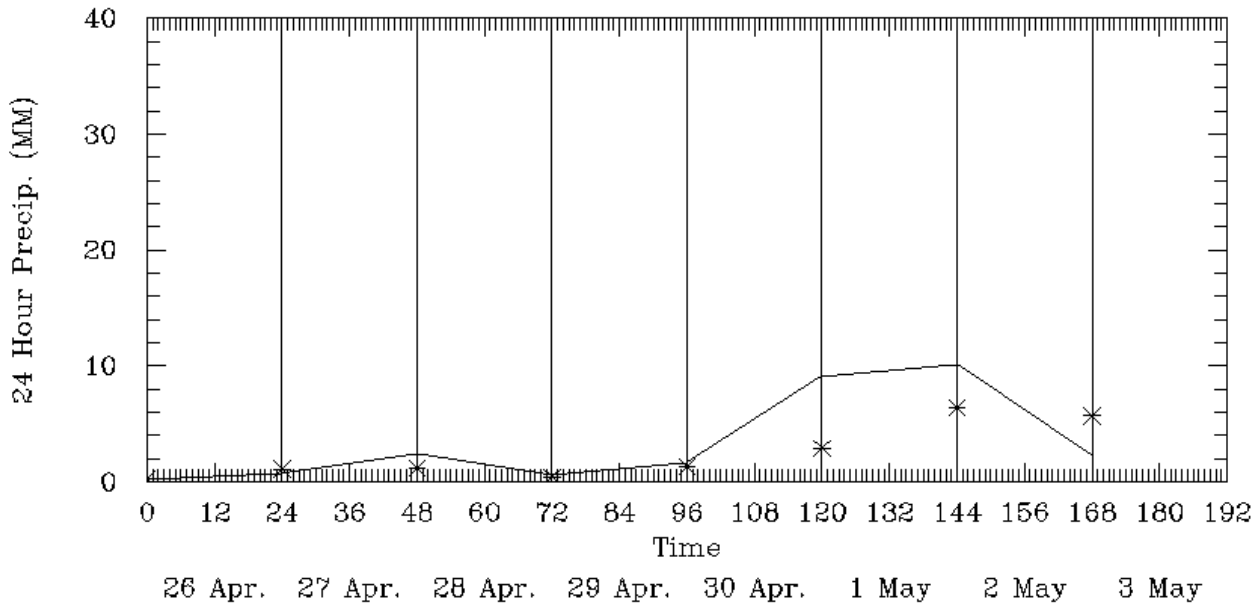


(b) 1900 UTC (1500 EST)

Figure 6-82. Ground-Level Mixing Ratio Fields for 30 April 1995.



(a) 12 Km Grid



(b) 24 Km Grid

Figure 6-83. Spatial Mean Daily Precipitation (mm) for the 24 April –3 May 1995 Episode.

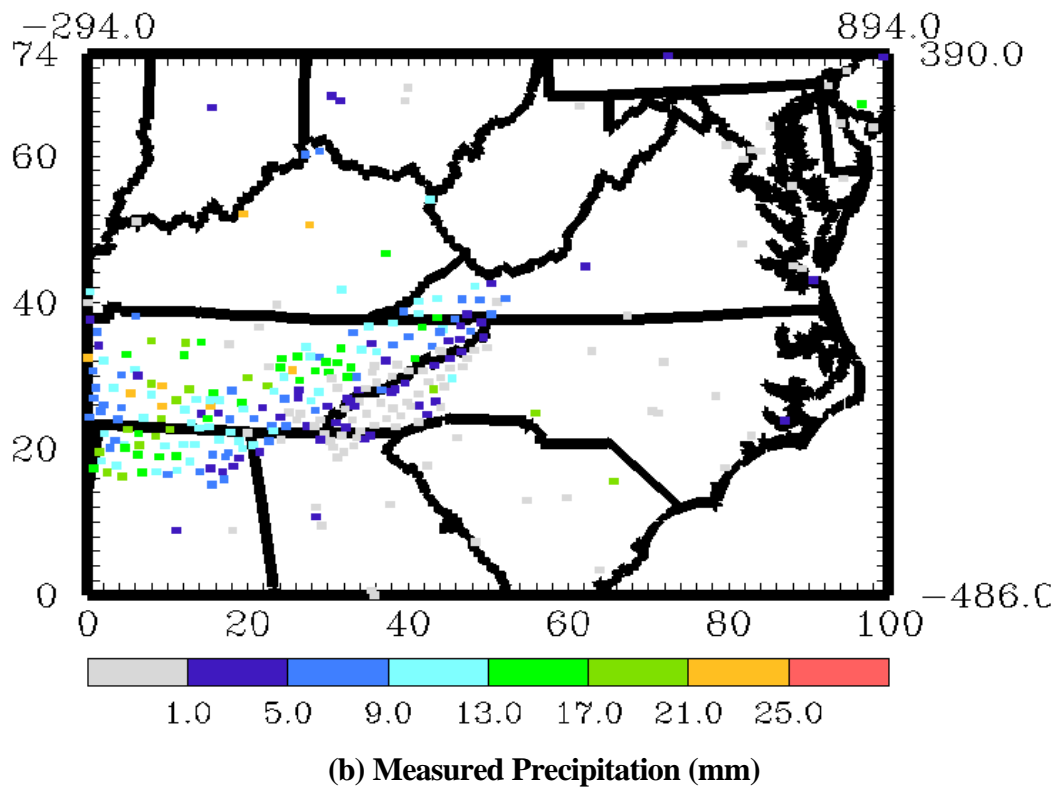
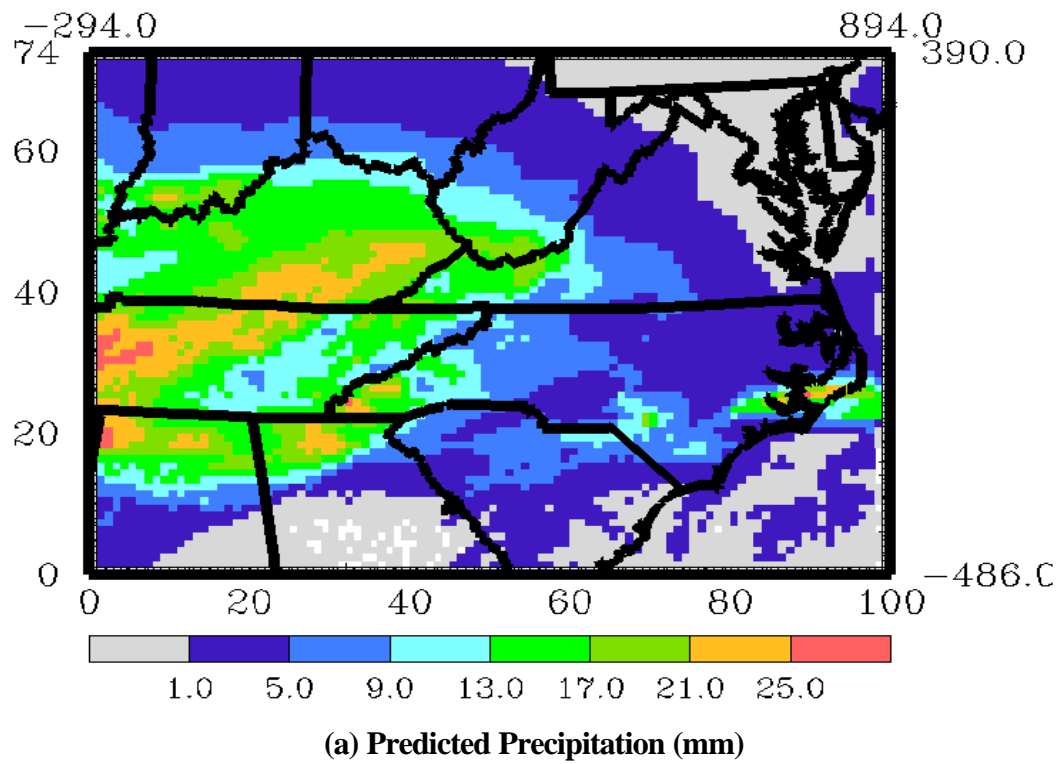
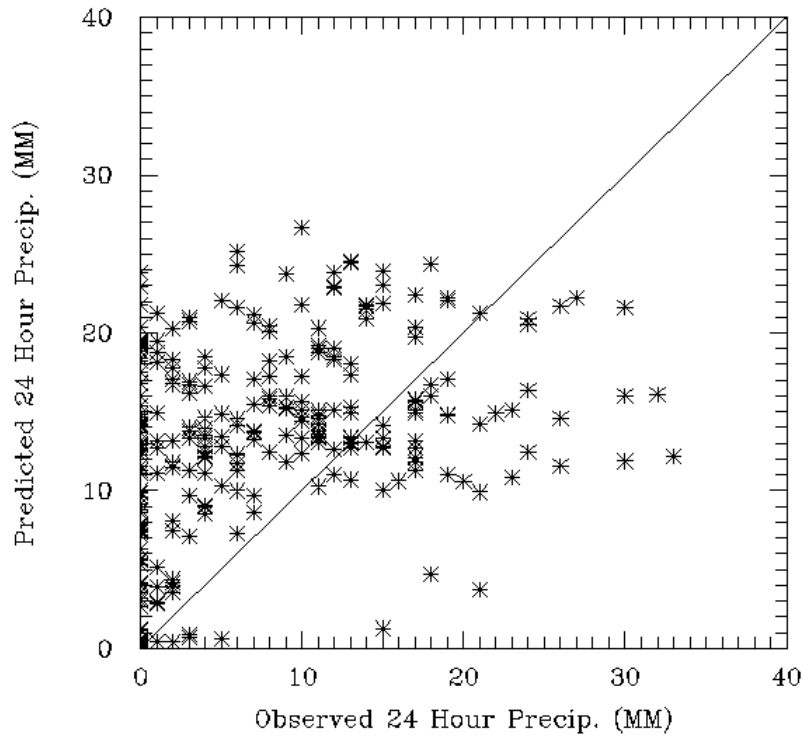
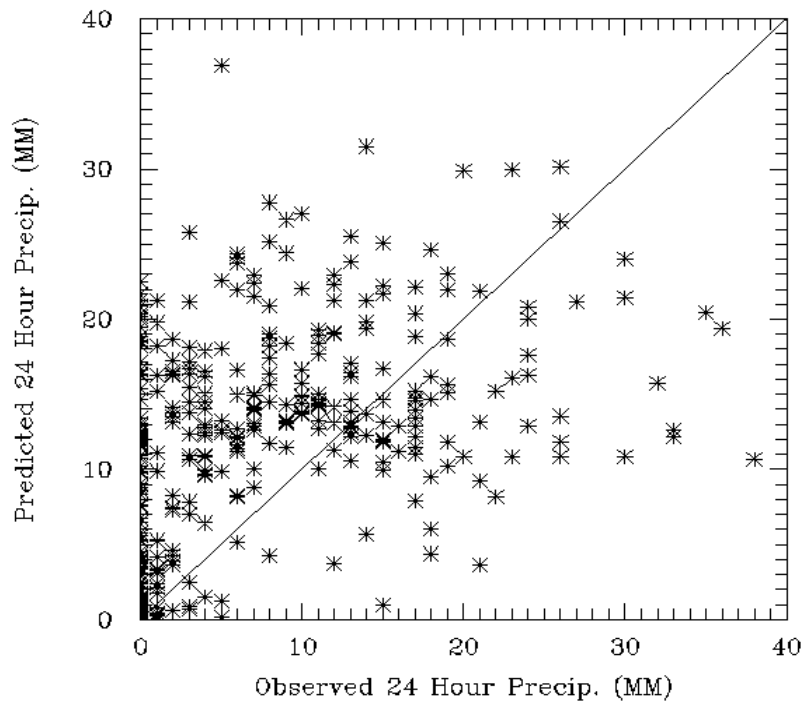


Figure 6-84. Daily Precipitation Fields for 2 May 1995.



(a) 12 Km Grid



(b) 24 Km Grid

Figure 6-85. Scatter Plot of Daily Maximum Rainfall (mm) for 2 May 1995.

7.0 EVALUATION OF ALOFT METEOROLOGICAL FIELDS

The NCEP/NCAR reanalysis data (Kalnay et al. 1996) was processed as described in section 3.2 and in the SAMI meteorological modeling protocol (see Appendix 4) for use in the RAMS model. For each episode coarse grid upper-air model results are compared with the 6-h reanalysis fields. The primary metrics are the bias and RMSE of the model minus the reanalysis at 850 mb for temperature, mixing ratio, and wind speed. Three issues need to be remembered for these comparisons: 1) the reanalysis data have an original longitudinal resolution of 1.875° (corresponds to about 165 km at 37° north latitude) and the RAMS model is capable of resolving scales smaller than this even on the coarse grid; 2) no nudging was performed below 2 km above the surface so the 850-mb fields are less constrained by the nudging towards the reanalysis fields, and 3) winds and temperatures are strongly constrained by upper-air observations over the United States and to a lesser extent the water vapor mixing ratios as discussed in section 3.1. Because of these issues not all differences between the model and the reanalysis data can be attributed to model error. Another comparison made here is between the model and observed afternoon mixing heights for the coarse grid. This comparison is an important one because of its implications for the air quality modeling phase but also a difficult one because of the nature of mixing heights. In the RAMS model the mixing height is not a prognostic variable. It was diagnosed from the vertical profile of the vertical exchange coefficient (K_h) for heat at each grid point. In most cases the mixing height was set at the height where K_h dropped below a value of $1 \text{ m}^2 \text{ s}^{-2}$. More involved procedures were used when there were multiple maxima in the K_h profile. Likewise an estimate of an observed mixing height has to be diagnosed from other quantities. The procedure chosen for this report was to take the average of two estimates of the observed mixing height. Both used the reanalysis data as a proxy for rawinsonde data and one used observed analyses of temperature. One estimate was to take the height where the dry-adiabat with the maximum hourly temperature at 2 m between 1800-000 UTC intersected the potential temperature profile at 1200 UTC of the same day. The second estimate diagnosed the mixing height at 0000 UTC by locating an inversion with specified criteria. The actual comparison at each grid point is then the difference between the average model mixing height between 1800-0000 UTC and the observed mixing height (as just described) for the same time. This difference was then averaged over all days of the episode. This type of difference should give a broad representation of the model performance for afternoon mixing heights for the coarse grid. An exception to this procedure was for the February 1994 case, where the model mixing heights were averaged only for the period 1800-2200 UTC and the 0000 UTC inversion-derived mixing height was not used as part of the estimate of the observed height. These changes were made for this episode given the earlier sunset times for this case.

This section also presents a brief evaluation of MM5 and RAMS model performance in simulating the upper level horizontal winds and temperatures for the 26-28 June 1991 and 17-19 July 1991 episodes. Due to data and resource constraints, this evaluation was limited to a brief comparison of daily averaged winds and temperatures which are vertically integrated from the surface to the top of the meteorological model domains. Thus, this analysis is at best a summary indication of the coarser performance characteristics of the two models in reproducing the vertical wind and thermodynamic structures of the two episodes.

7.1 11-19 July 1995 Episode

Figure 7-1 shows the bias and RMSE of the 850-mb temperature in °C for the July 1995 episode. Bias values were generally in the 0-1°C range from the Ohio Valley northwestward to the northern Plains and 0 to -2°C range everywhere else. RMSE values were generally 1-1.5°C except over New England where higher values were observed. The 850-mb mixing ratio patterns in Figure 7-2 can be explained in part by the surface temperature biases described in section 6.1 and the mixing height differences shown in Figure 7-4. The warm bias of surface temperatures in Figure 6-1 from the northern Plains southeastward to Ohio and then southward to the Gulf coast correspond well to a high bias of model mixing heights in the same areas of 200-400 m. Although the mixed layer values of mixing ratio in these same areas were generally too dry compared to surface observations, the fact that the model mixing heights were apparently too high implies the usual sharp transition to lower mixing ratios above the PBL was also elevated. This probably explains the positive bias in mixing ratio of +2 g kg⁻¹ and higher over parts of the Ohio and the mid-Mississippi valleys. The RMSE of mixing ratio in Figure 7-2 had almost the same pattern and magnitude as the bias. The bias of the 850-mb wind speeds in Figure 7-3 shows general negative values of 0 to -1 m s⁻¹ over the Southeast, the northern Plains, and the eastern Great Lakes area and 0 to +0.50 m s⁻¹ elsewhere. The same high bias seen in other surface and 850-mb fields is seen in the 850-mb wind speed over parts of New England. RMSE values of the wind speed at 850 mb were mostly in the 1-2 m s⁻¹ range.

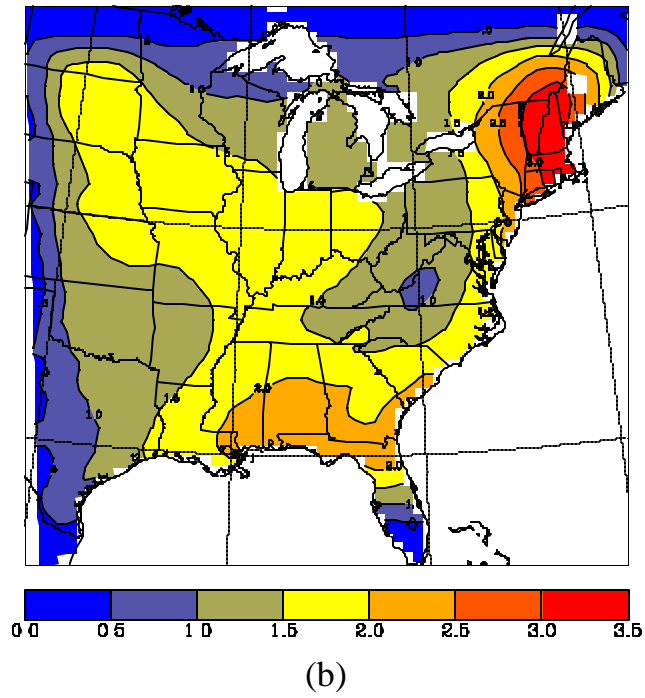
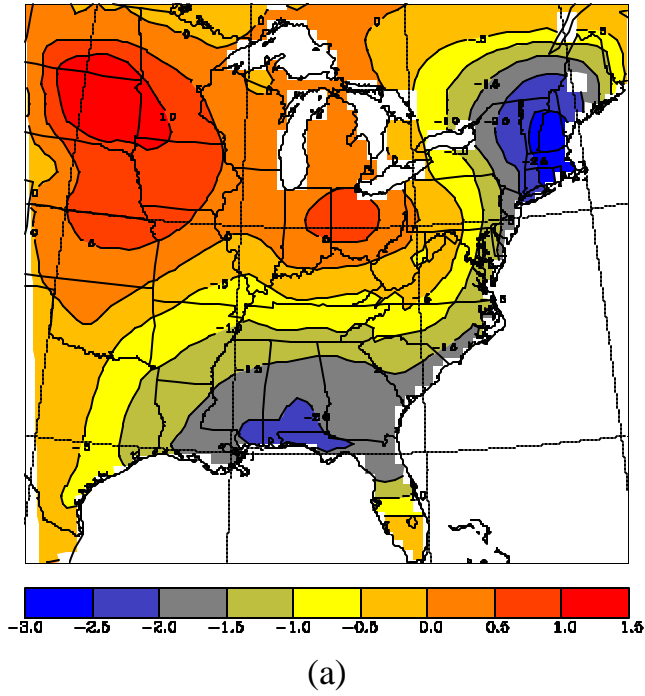
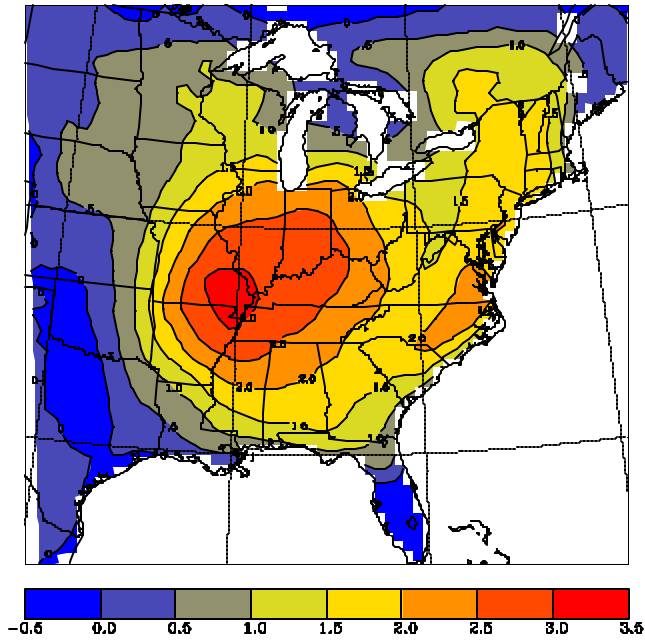
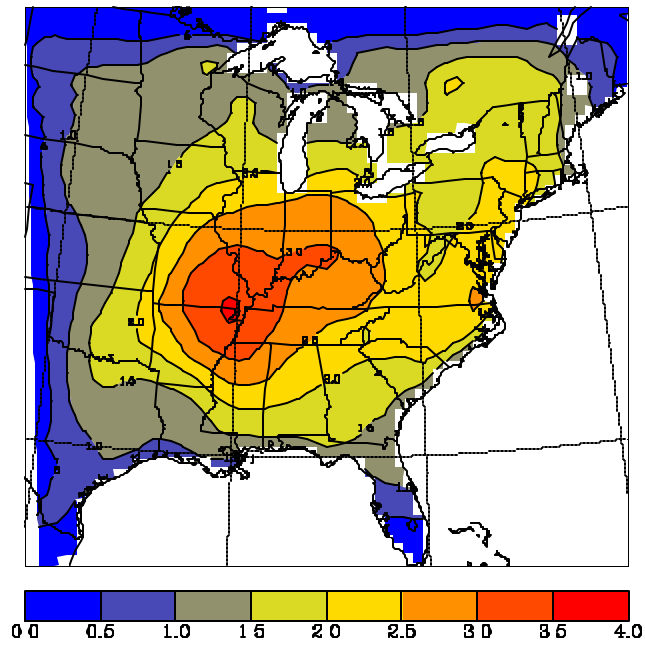


Figure 7-1. (a) Bias of the model minus the NCAR/NCEP reanalysis temperature at 850 mb in degrees C for the July 1995 episode for the 48-km grid. (b) Root mean square error (RMSE) of the same field for the same time and grid.



(a)



(b)

Figure 7-2. (a) Bias of the model minus the NCAR/NCEP reanalysis water vapor mixing ratio at 850 mb in g kg^{-1} for the July 1995 episode for the 48-km grid. (b) Root mean square error (RMSE) of the same field for the same time and grid.

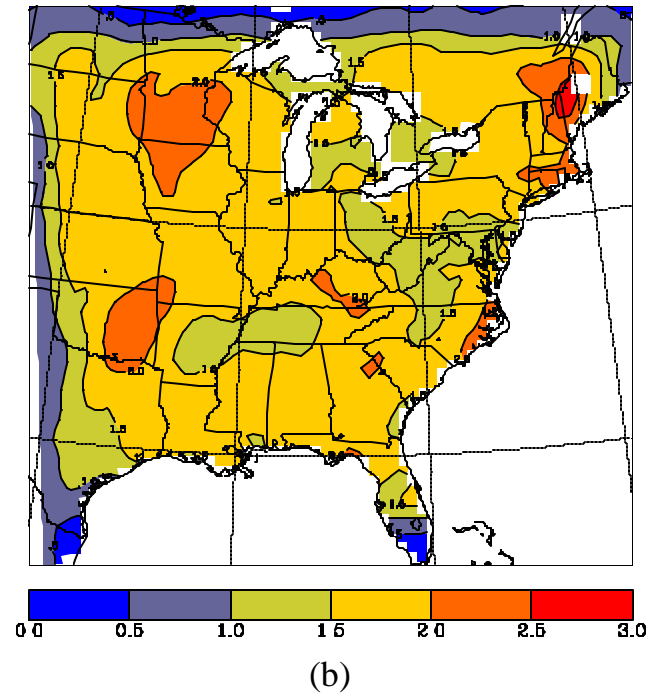
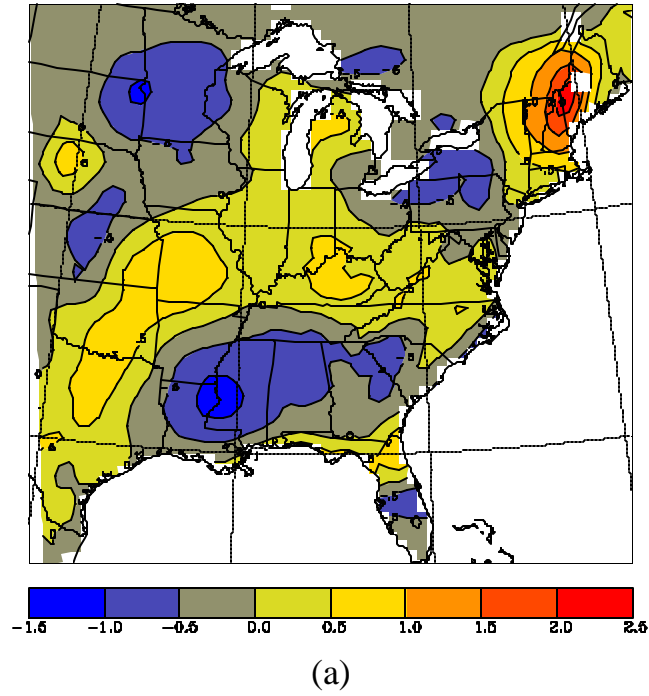


Figure 7-3. (a) Bias of the model minus the NCAR/NCEP reanalysis wind speed at 850 mb in m s^{-1} for the July 1995 episode for the 48-km grid. (b) Root mean square error (RMSE) of the same field for the same time and grid.

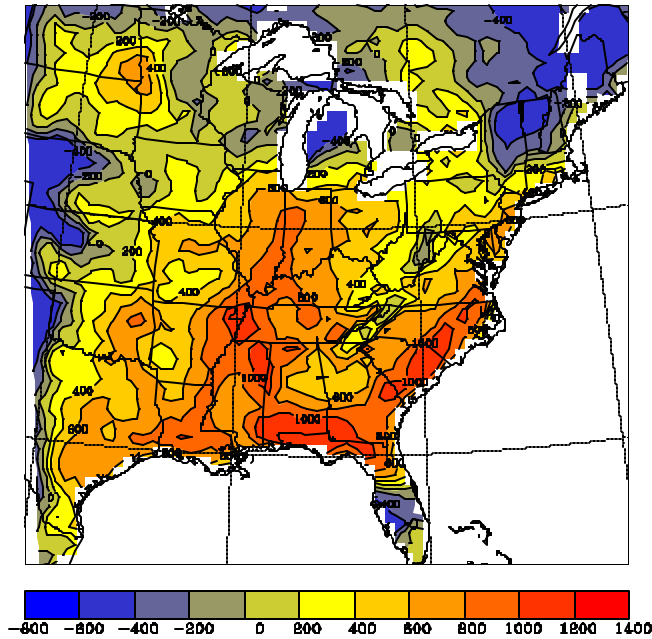
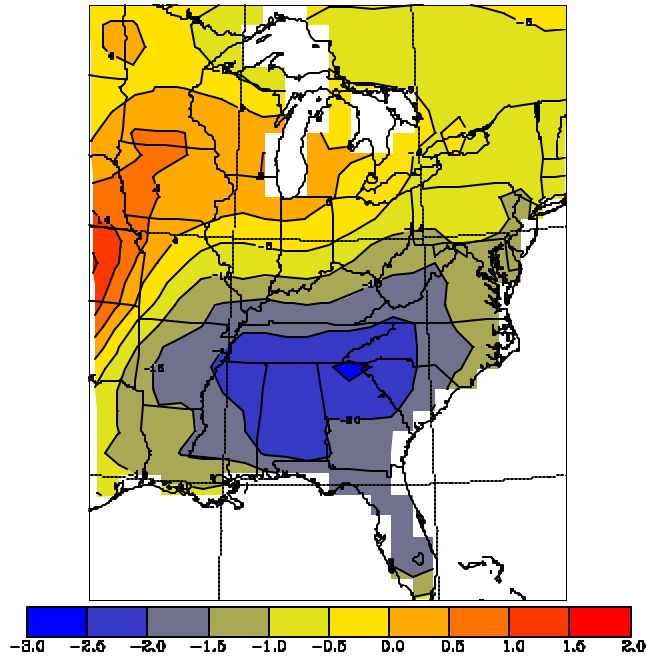


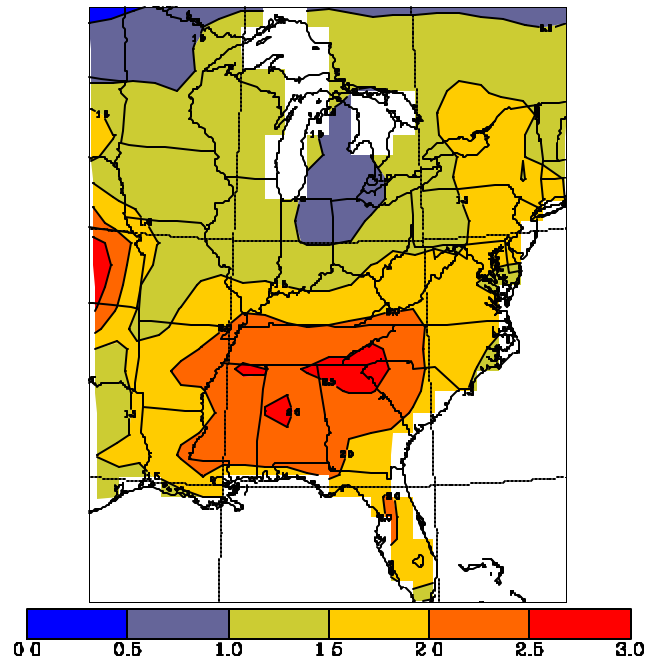
Figure 7-4. Bias of the mean model mixing height during the period 1800-000 UTC minus the observed mixing height for the period averaged over the entire July 1995 episode for the 48-km grid. Differences are in units of m. See the text for additional details.

7.2 22-30 May 1995 Episode

Figure 7-5 shows the bias and RMSE of the 850-mb temperature in $^{\circ}\text{C}$ for the May 1995 episode. A cool bias as large as -2.5°C was observed over the southeastern United States which was in contrast to a warm bias as large as $+1.5^{\circ}\text{C}$ over the central Great Plains and extending northeastward to Canada. The largest RMSE values were over the southeastern United States and approached 2.5°C . The bias and RMSE of the 850-mb water vapor mixing ratio in Figure 7-6 show a general positive bias as large as 1.5 g kg^{-1} over the central Great Plains. RMSE values were generally under 2 g kg^{-1} with a maximum along the Gulf coast of near 3.5 g kg^{-1} . Figure 7-7 shows the bias and RMSE of the 850-mb wind speed. A large area had bias values in the range of $\pm 0.50 \text{ m s}^{-1}$ and RMSE values of 2.5 m s^{-1} or less. The maximum bias and RMSE values were over an area extending northeastward from the central Great Plains and coincided in part with the area of positive bias values for temperature and mixing ratio. These coincident patterns are near the maximum of the convective precipitation (not shown) and may be related to deficiencies in the Kuo convective scheme for this case. Figure 7-8 gives the bias in the afternoon mixing heights which shows values generally in the range of $\pm 200 \text{ m}$. The large negative values over the southern Appalachians are in an area where there is little observed data.

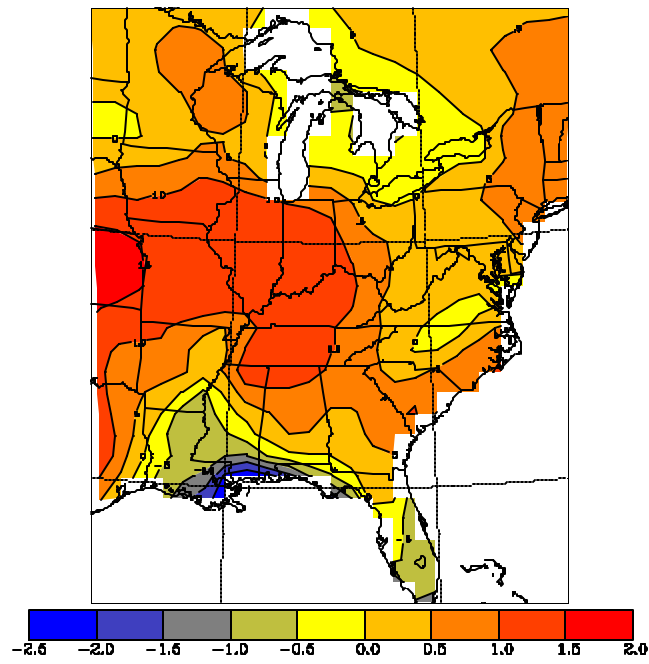


(a)

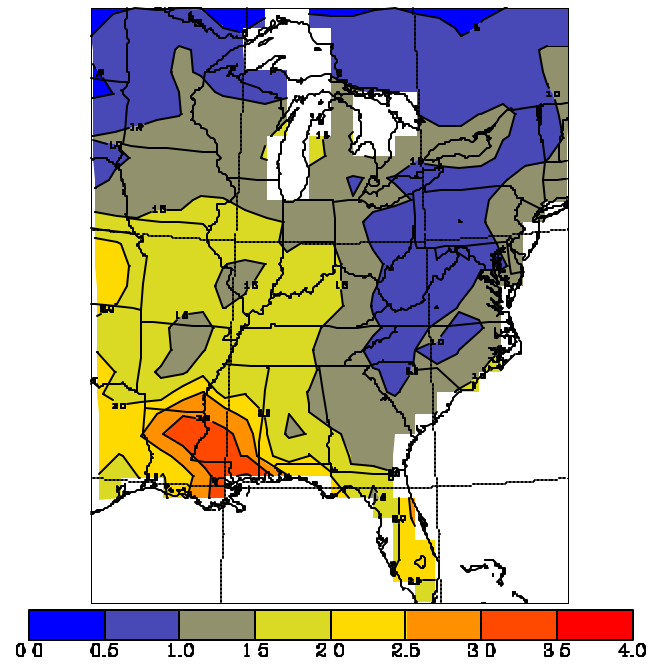


(b)

Figure 7-5. (a) Bias of the model minus the NCAR/NCEP reanalysis temperature at 850 mb in degrees C for the May 1995 episode for the 96-km grid. (b) Root mean square error (RMSE) of the same field for the same time and grid.

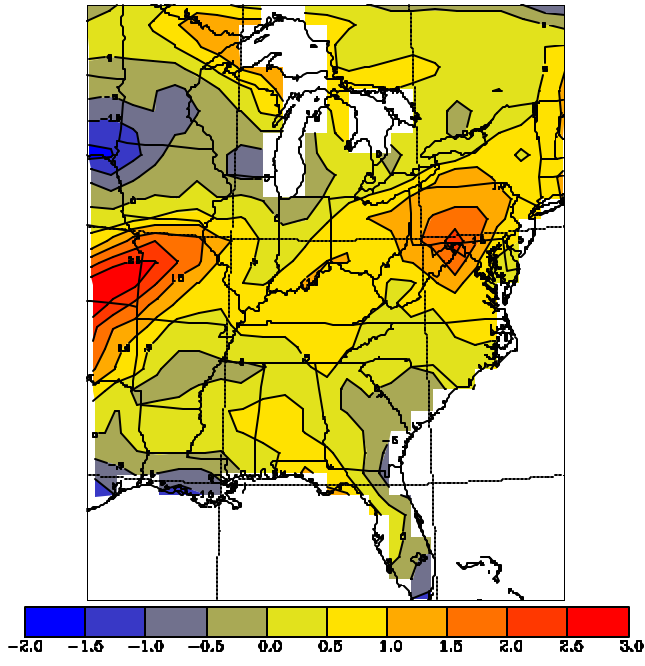


(a)

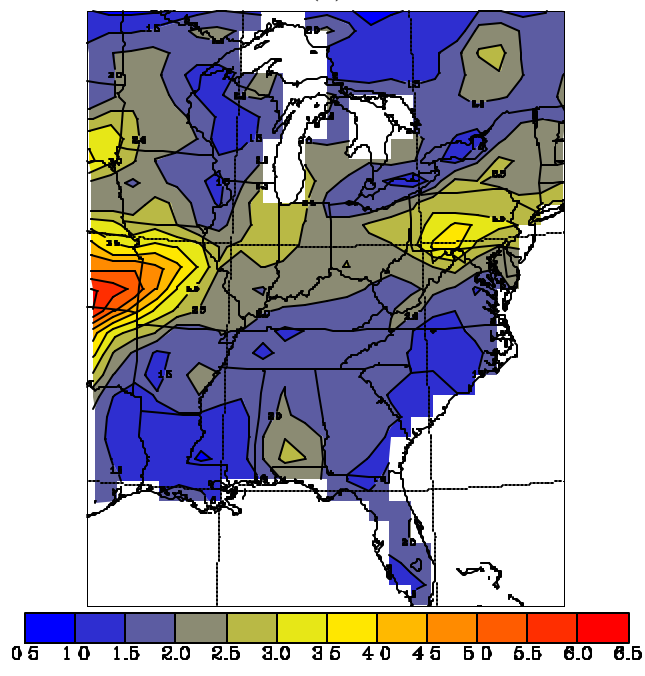


(b)

Figure 7-6. (a) Bias of the model minus the NCAR/NCEP reanalysis water vapor mixing ratio at 850 mb in g kg^{-1} for the May 1995 episode for the 96-km grid. (b) Root mean square error (RMSE) of the same field for the same time and grid.



(a)



(b)

Figure 7-7. (a) Bias of the model minus the NCAR/NCEP reanalysis wind speed at 850 mb in m s^{-1} for the May 1995 episode for the 96-km grid. (b) Root mean square error (RMSE) of the same field for the same time and grid.

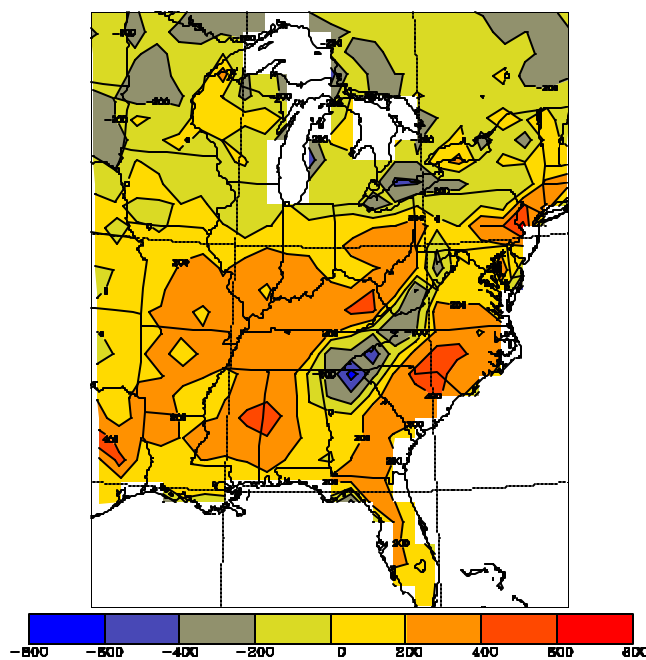
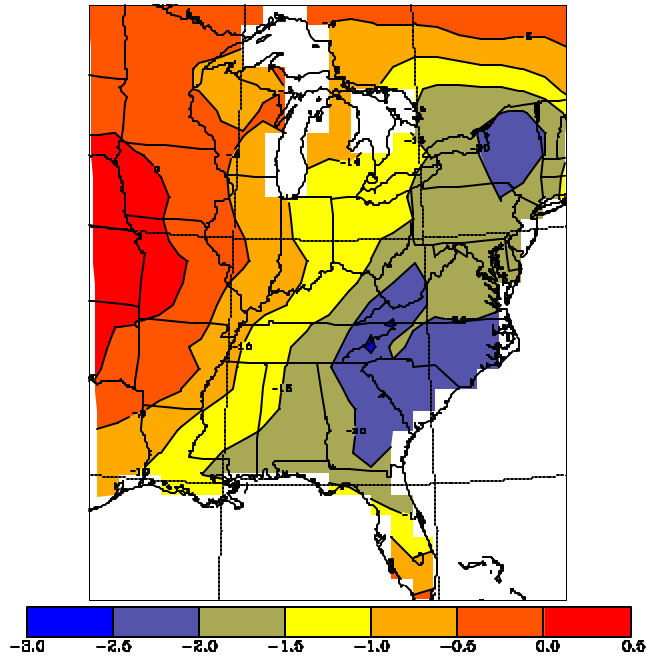


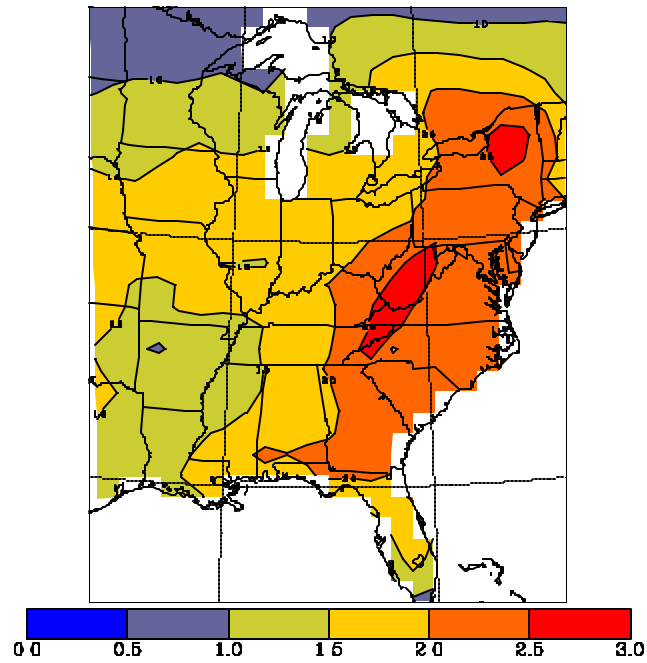
Figure 7-8. Bias of the mean model mixing height during the period 1800-000 UTC minus the observed mixing height for the period averaged over the entire May 1995 episode for the 96-km grid. Differences are in units of m. See the text for additional details.

7.3 9-18 May 1993 Episode

Figure 7-9 shows the bias and RMSE of the 850-mb temperature in $^{\circ}\text{C}$ for the May 1993 episode. A cool bias of -0.5 to -2°C was observed east of the Mississippi River. RMSE values in the same area were generally in the range of 1.5 to 2.5°C . The bias and RMSE of the 850-mb water vapor mixing ratio in Figure 7-10 reveal a general moist bias of 0.5 to 1 g kg^{-1} over much of the eastern United States with RMSE values up to 2 g kg^{-1} . Figure 7-11 shows the bias and RMSE of the 850-mb wind speed. Bias values were generally in the range of -0.5 to $+1 \text{ m s}^{-1}$ but with portions of Iowa and Kentucky having values of 1.5 m s^{-1} . RMSE of the wind speed were generally under 2 m s^{-1} except for three areas where values in excess of 3 m s^{-1} were observed: northeastern Iowa, the Kansas-Missouri border, and the Kentucky, West Virginia, and Virginia border. Figure 7-12 gives the bias in the afternoon mixing heights which shows values generally in the range of $\pm 200 \text{ m}$ with some values at or above 400 m over areas near the Great Lakes, the lower Ohio Valley, and the lower Mississippi Valley. Again the large negative values over the southern Appalachians are in an area where there is little observed data to determine an estimate of the observed mixing height. The bias patterns in this case are harder to explain than the ones for the July 1995 and May 1995 episodes. However, all the bias magnitudes are reasonable given the model capabilities and observation limitations.

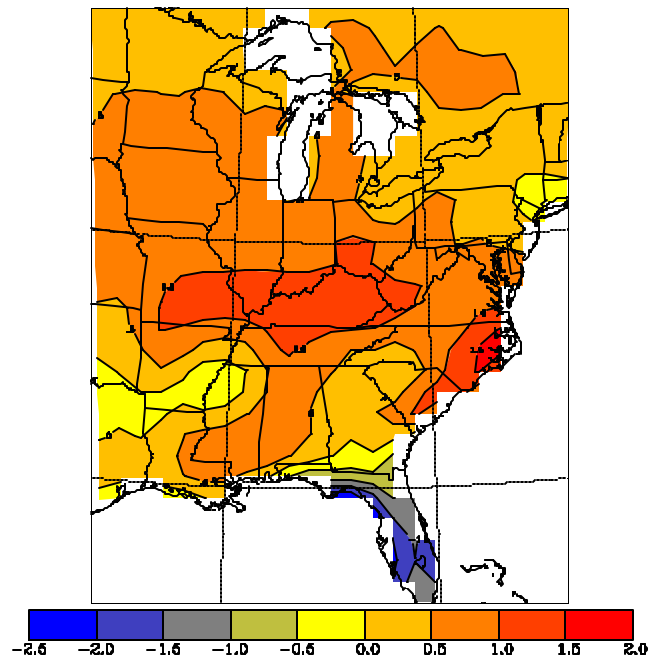


(a)

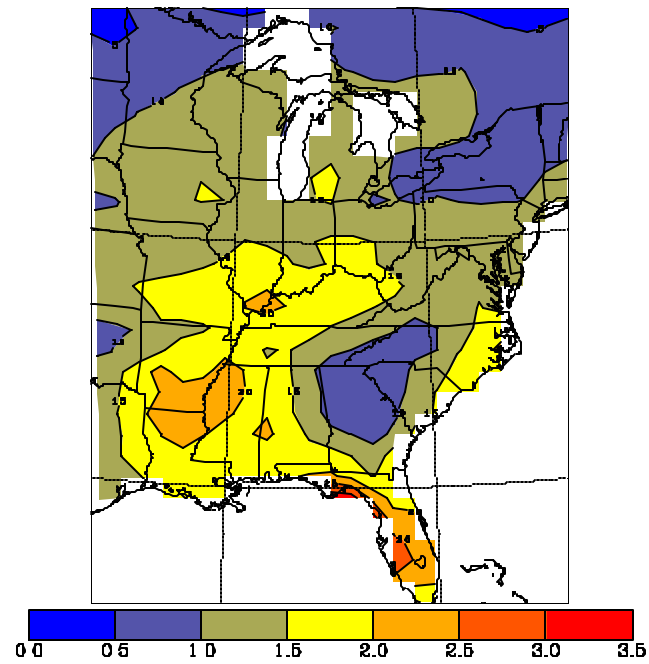


(b)

Figure 7-9. (a) Bias of the model minus the NCAR/NCEP reanalysis temperature at 850 mb in degrees C for the May 1993 episode for the 96-km grid. (b) Root mean square error (RMSE) of the same field for the same time and grid.

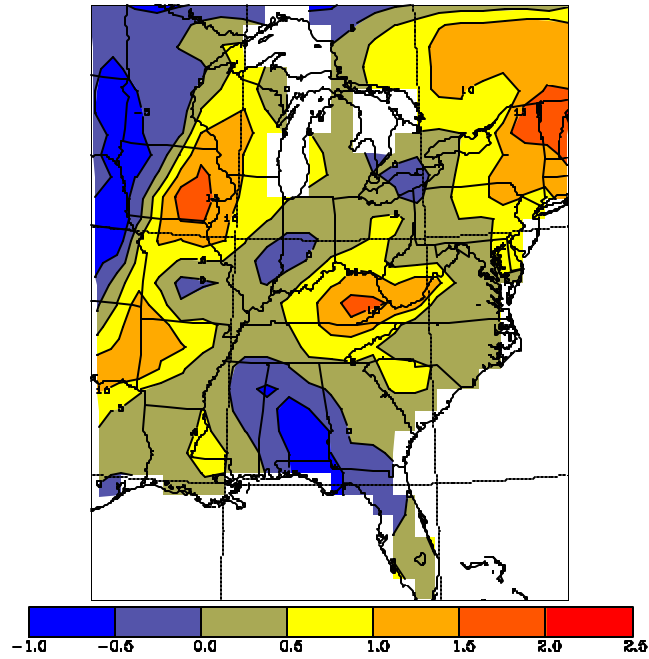


(a)

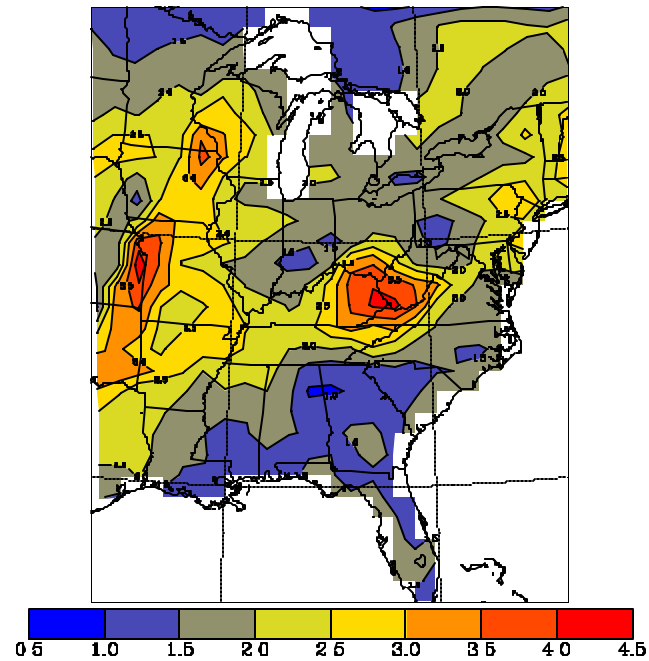


(b)

Figure 7-10. (a) Bias of the model minus the NCAR/NCEP reanalysis water vapor mixing ratio at 850 mb in g kg^{-1} for the May 1993 episode for the 96-km grid. (b) Root mean square error (RMSE) of the same field for the same time and grid.



(a)



(b)

Figure 7-11. (a) Bias of the model minus the NCAR/NCEP reanalysis wind speed at 850 mb in m s^{-1} for the May 1993 episode for the 96-km grid. (b) Root mean square error (RMSE) of the same field for the same time and grid.

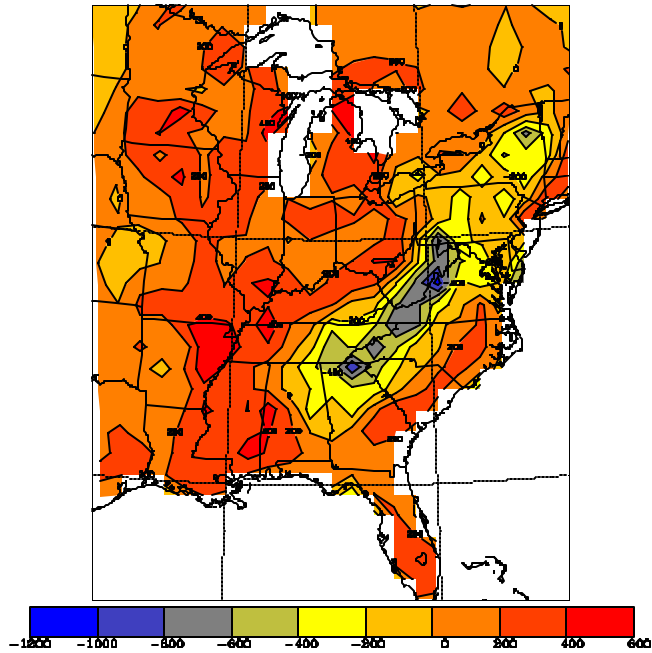
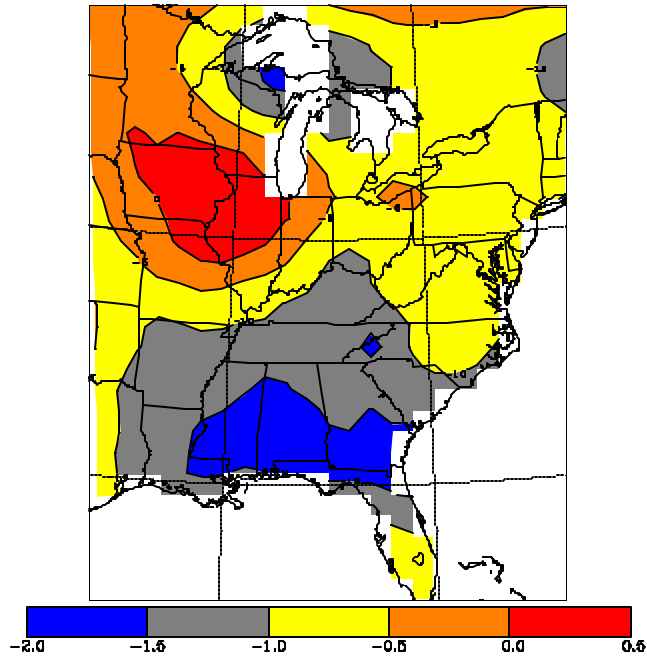


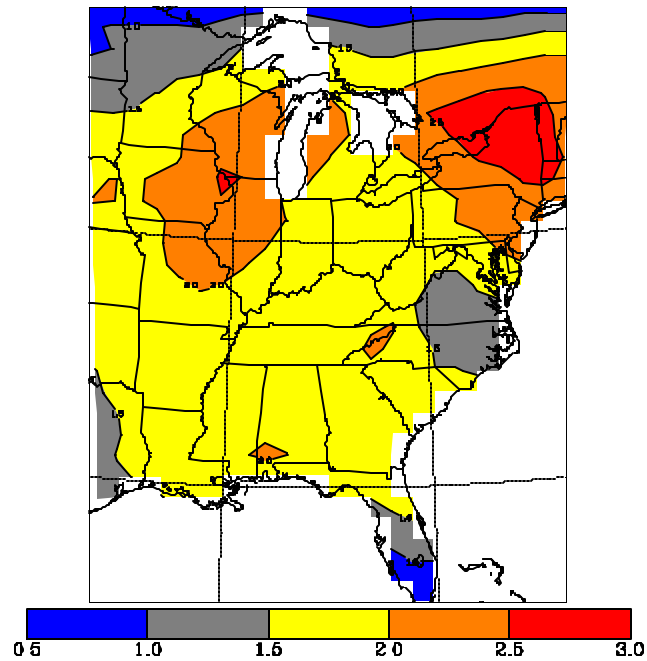
Figure 7-12. Bias of the mean model mixing height during the period 1800-000 UTC minus the observed mixing height for the period averaged over the entire May 1993 episode for the 96-km grid. Differences are in units of m. See the text for additional details.

7.4 21 March to 1 April 1993 Episode Results

Figure 7-13 shows the bias and RMSE of the 850-mb temperature in °C for the March 1993 episode. A cool bias of -0.5 to -1.5°C covered much of the eastern United States. RMSE values for temperature were 2°C or less over most areas. The bias and RMSE for water vapor mixing ratio in Figure 7-14 show a general bias of +0.5 to +1 g kg⁻¹ with RMSE values of 2 g kg⁻¹ or less. The results for wind speed in Figure 7-15 show values generally in the range of ±1 m s⁻¹ with RMSE values usually 2 m s⁻¹ or less. The mixing height bias in Figure 7-16 shows values in the range of ±200 m with the following exceptions: over the Appalachians where observations are rare, along coastal areas, and over parts of Iowa and Wisconsin.

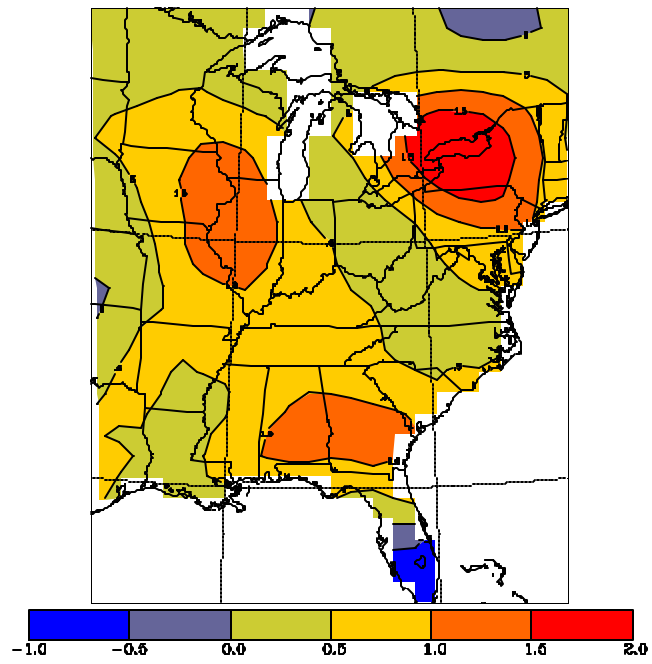


(a)

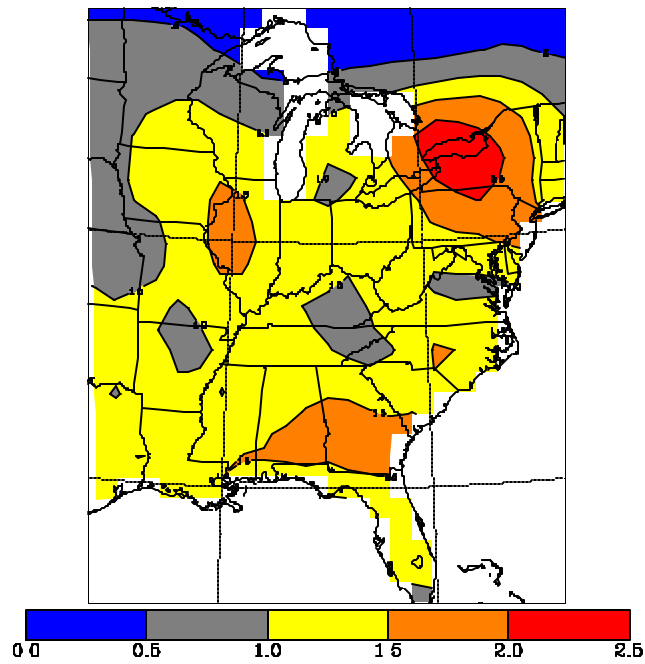


(b)

Figure 7-13. (a) Bias of the model minus the NCAR/NCEP reanalysis temperature at 850 mb in degrees C for the March 1993 episode for the 96-km grid. (b) Root mean square error (RMSE) of the same field for the same time and grid.



(a)



(b)

Figure 7-14. (a) Bias of the model minus the NCAR/NCEP reanalysis water vapor mixing ratio at 850 mb in g kg^{-1} for the March 1993 episode for the 96-km grid. (b) Root mean square error (RMSE) of the same field for the same time and grid.

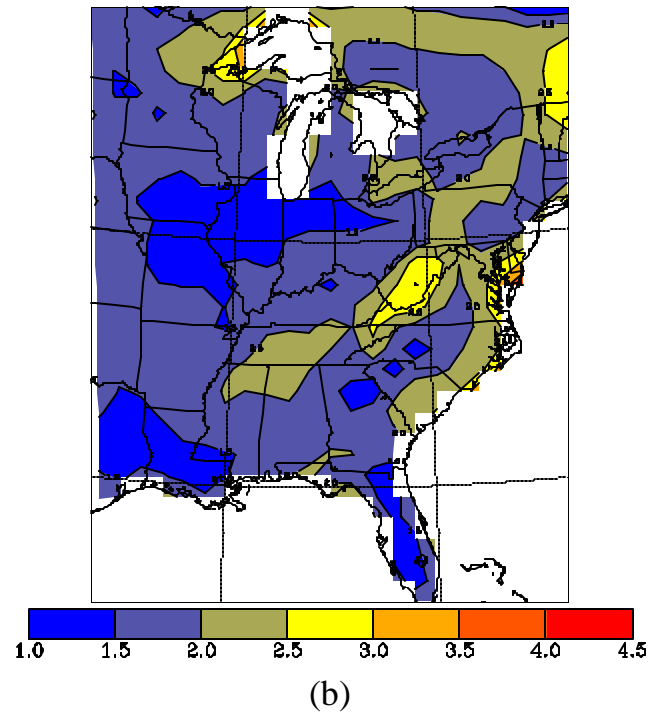
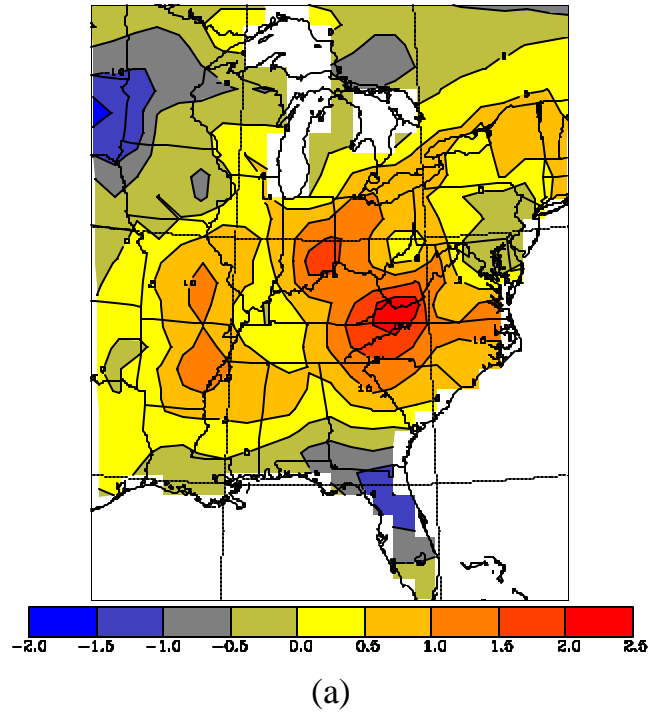


Figure 7-15. (a) Bias of the model minus the NCAR/NCEP reanalysis wind speed at 850 mb in m s^{-1} for the March 1993 episode for the 96-km grid. (b) Root mean square error (RMSE) of the same field for the same time and grid.

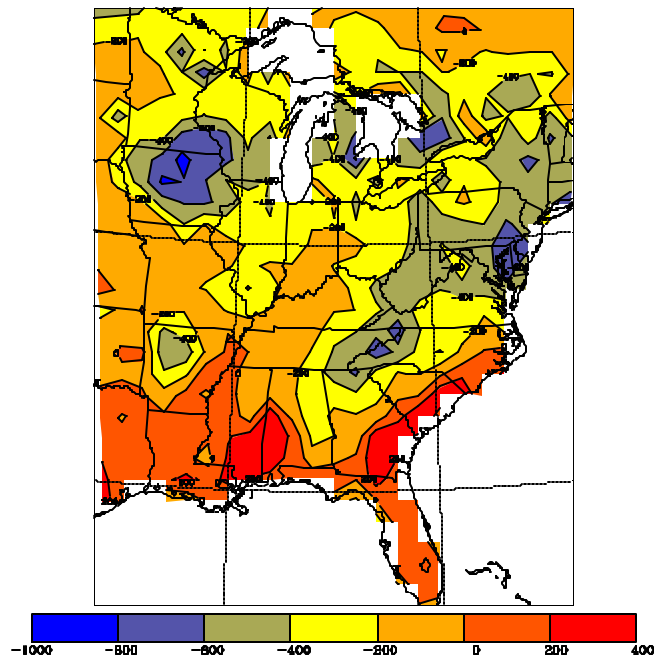
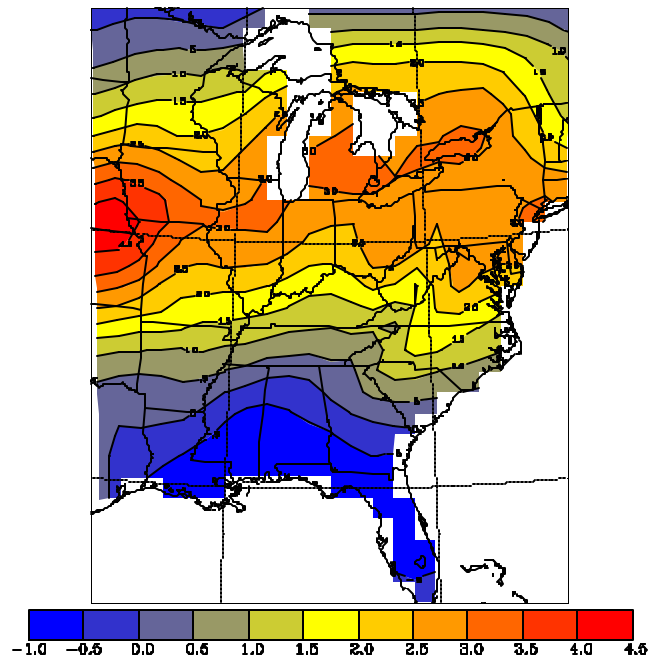


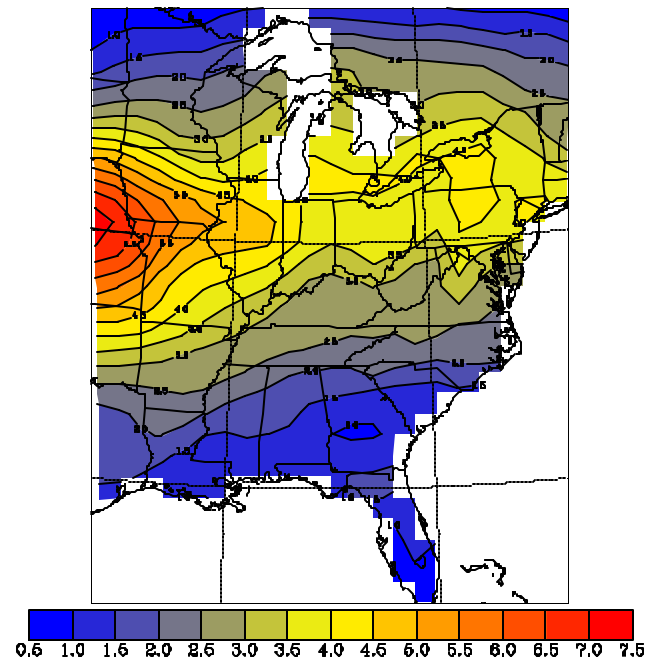
Figure 7-16. Bias of the maximum model mixing height minus the maximum observed mixing height for the period 1800-0000 UTC averaged over the entire March 1993 episode for the 96-km grid. Differences are in units of m. See the text for additional details.

7.5 6-14 February 1994 Episode Results

Figure 7-17 shows the bias and RMSE of the 850-mb temperature in $^{\circ}\text{C}$ for the February 1994 episode. A west-east band extending from the Iowa-Missouri border eastward to the mid-Atlantic had a warm bias of 2°C or more with the maximum values near 4°C over the central Mississippi Valley. The RMSE values followed the same pattern with maximum values near 7°C . Explanations for this behavior are not evident without further investigation but may be related to the need for better vertical resolution at altitudes above 5 km. This episode had the strongest average jet-stream level winds and it is in these situations that vertical resolution can be especially important. An increase in vertical resolution can affect both mass and wind fields. This issue was evident early in the creation of this simulation but time constraints did not allow for the exploration of different grids. The biases of 850-mb water vapor mixing ratio (Figure 7-18) were mostly in the range of $\pm 0.50 \text{ g kg}^{-1}$ with RMSE values of 1.5 g kg^{-1} or less. A general positive bias of $+1$ to $+3 \text{ m s}^{-1}$ was observed for wind speed (Figure 7-19). The area of largest bias was over the Great Lakes, New England, and along the Appalachians. The RMSE values for wind speed followed the same pattern with values up to 6.5 m s^{-1} . Mixing height bias (Figure 7-20) was in the range of $\pm 200 \text{ m}$ southeast of the Appalachians and values were generally -200 to -400 m to the west. The area with larger under-predictions coincides in part with the area of positive temperature biases which may imply the model created an Arctic layer which was too shallow compared with observations.

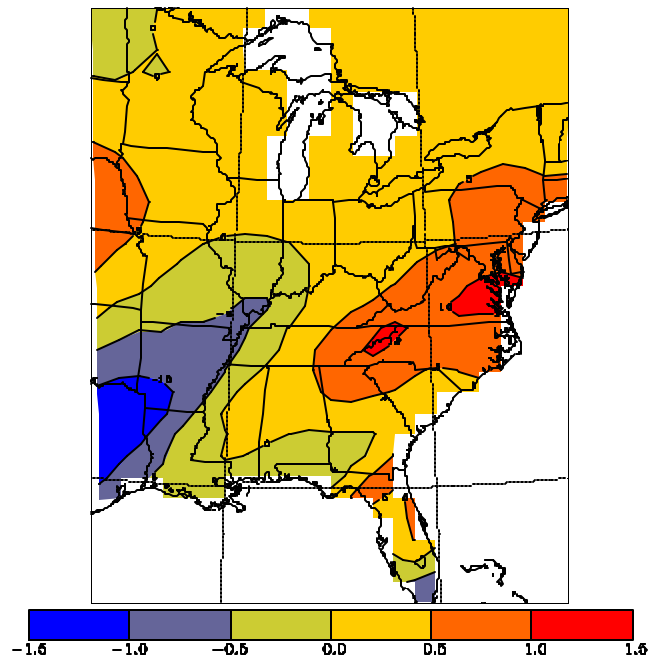


(a)

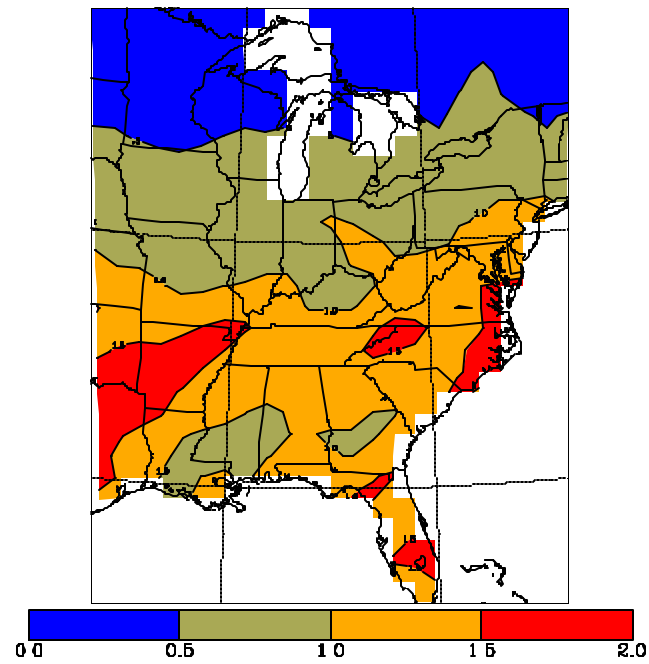


(b)

Figure 7-17. (a) Bias of the model minus the NCAR/NCEP reanalysis temperature at 850 mb in degrees C for the February 1994 episode for the 96-km grid. (b) Root mean square error (RMSE) of the same field for the same time and grid.

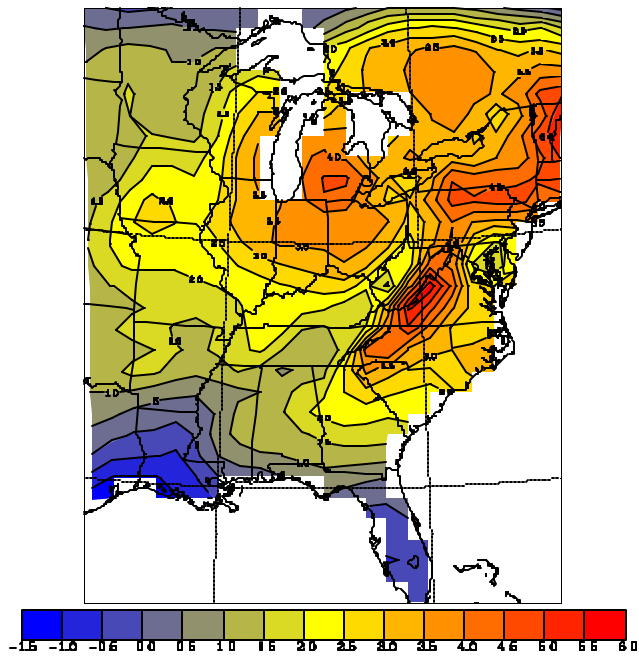


(a)

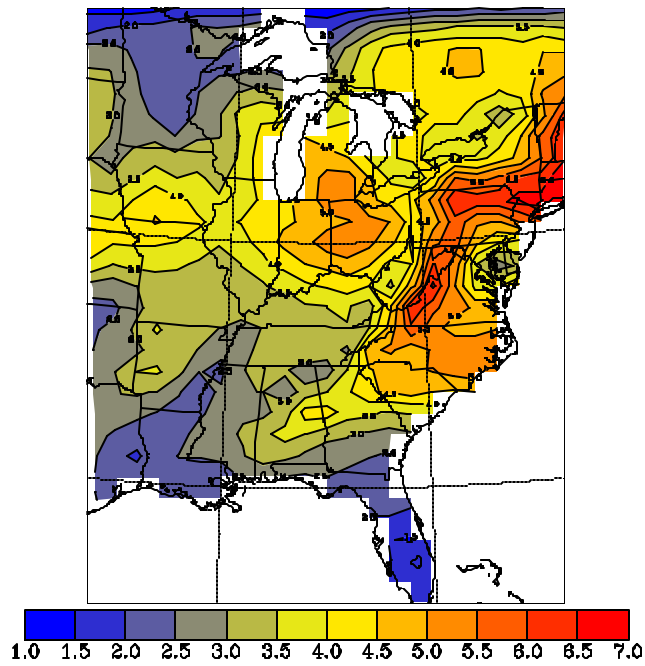


(b)

Figure 7-18. (a) Bias of the model minus the NCAR/NCEP reanalysis water vapor mixing ratio at 850 mb in g kg^{-1} for the February 1994 episode for the 96-km grid. (b) Root mean square error (RMSE) of the same field for the same time and grid.



(a)



(b)

Figure 7-19. (a) Bias of the model minus the NCAR/NCEP reanalysis wind speed at 850 mb in m s^{-1} for the February 1994 episode for the 96-km grid. (b) Root mean square error (RMSE) of the same field for the same time and grid.

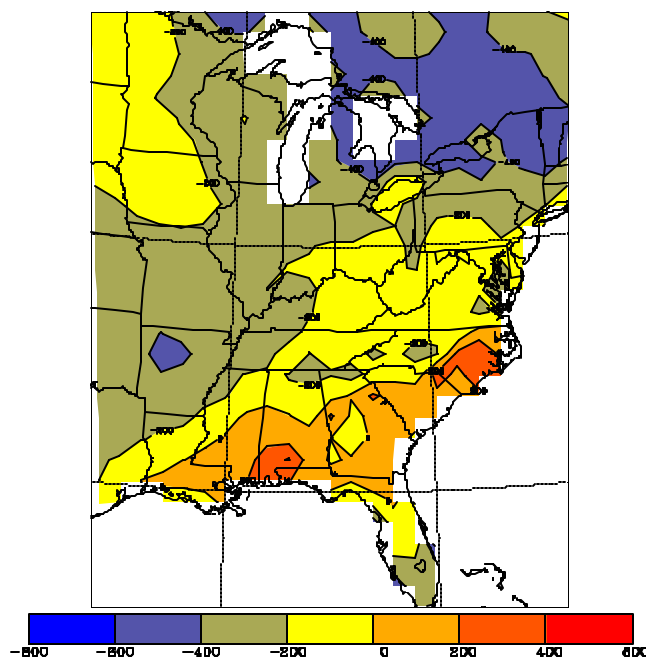


Figure 7-20. Bias of the model mixing height averaged over the period 1800-2200 UTC minus the observed mixing height averaged over the entire February 1994 episode for the 96-km grid. Differences are in units of m. See the text for additional details.

7.6 21 July - 1 August 1991 Episode Results

Figure 7-21 shows the bias and RMSE of the 850-mb temperature in $^{\circ}\text{C}$ for the July 1991 episode. A cool bias ranging from -0.50 to -1.50°C was observed over much of the eastern United States. RMSE for temperature were generally 2°C or less. Figure 7-22 shows a general moist bias at 850 mb of $+0.50$ to $+1$ g kg^{-1} with RMSE values usually 1.5 g kg^{-1} or less. The wind speed at 850 mb in Figure 7-23 had typical bias values of -0.50 to $+1.50$ m s^{-1} with higher values along the Atlantic coast. RMSE values demonstrated a similar pattern with values as large as 4.5 m s^{-1} . The bias of the mixing heights in Figure 7-24 showed values typically in the range of ± 200 m. The larger negative values over the higher terrain of the Appalachians are in areas where the observed analysis has a small observational density.

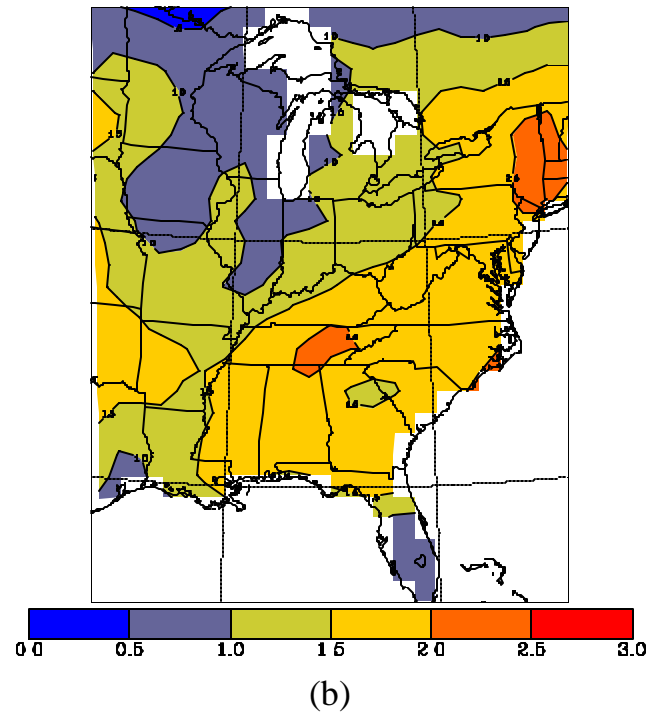
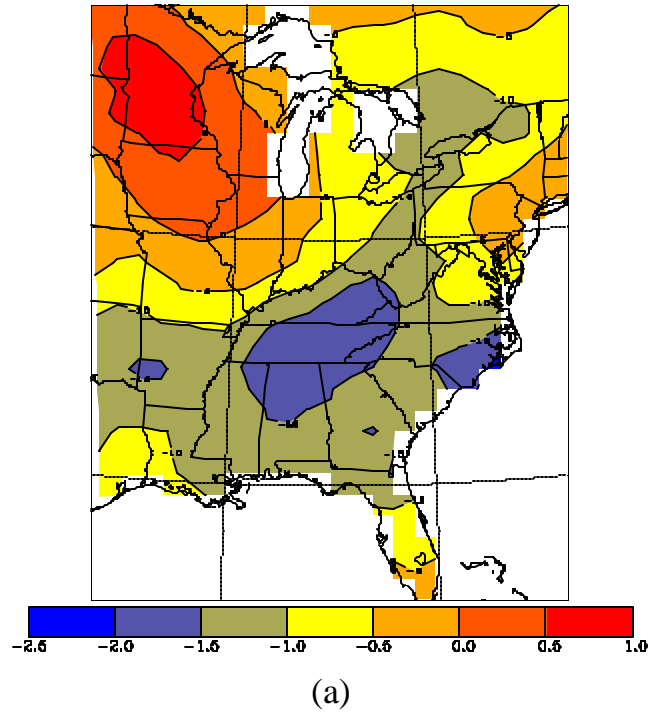
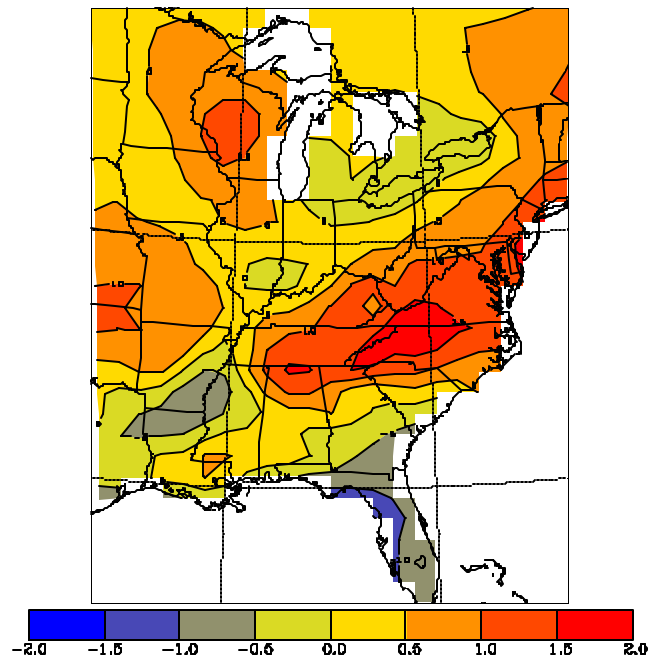
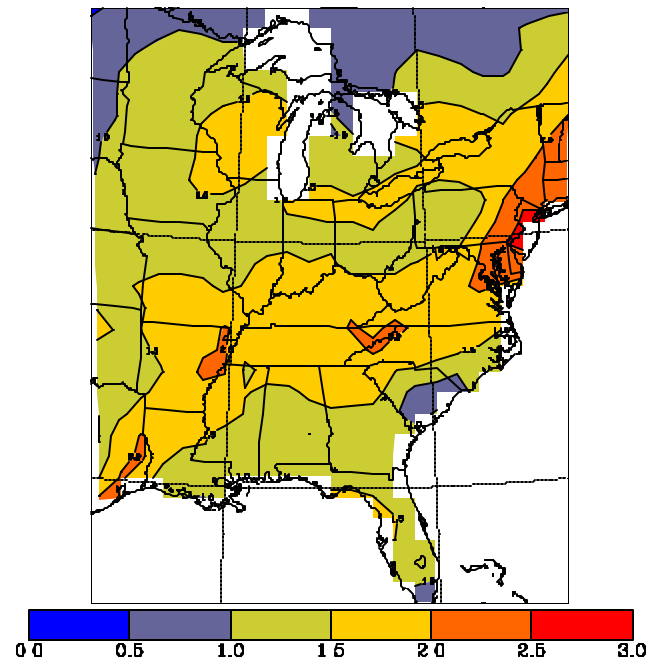


Figure 7-21. (a) Bias of the model minus the NCAR/NCEP reanalysis temperature at 850 mb in degrees C for the July 1991 episode for the 96-km grid. (b) Root mean square error (RMSE) of the same field for the same time and grid.

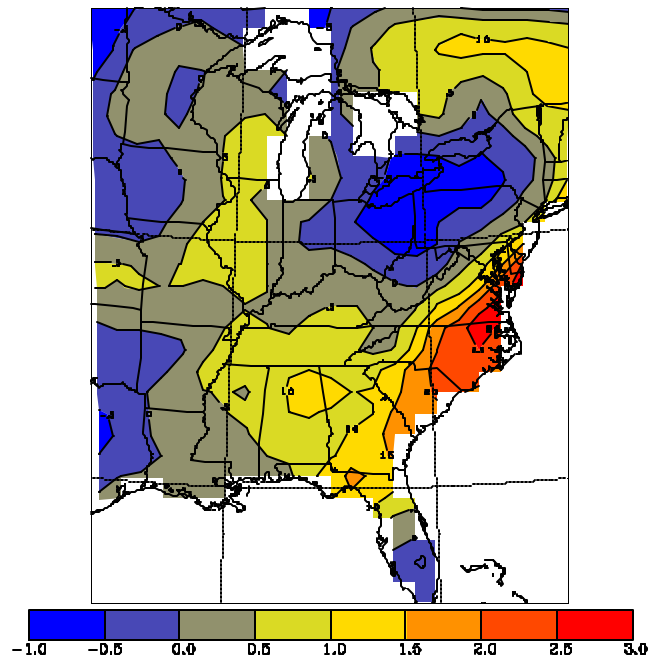


(a)

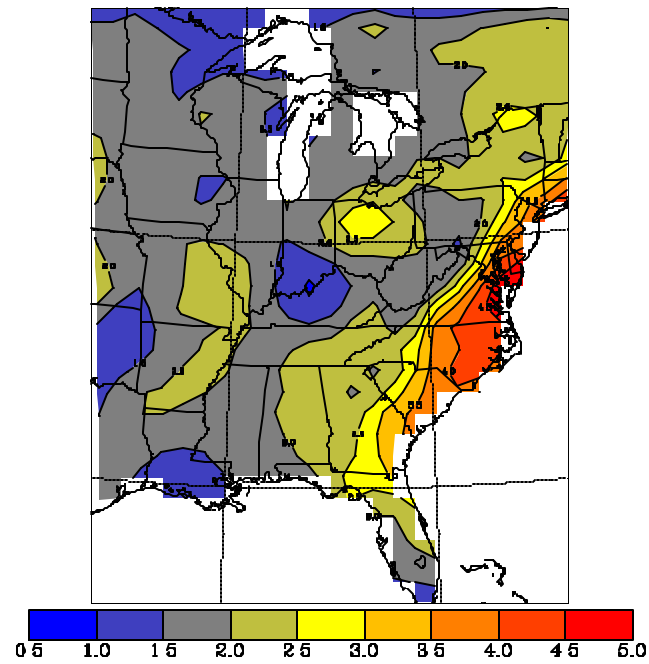


(b)

Figure 7-22. (a) Bias of the model minus the NCAR/NCEP reanalysis water vapor mixing ratio at 850 mb in g kg^{-1} for the July 1991 episode for the 96-km grid. (b) Root mean square error (RMSE) of the same field for the same time and grid.



(a)



(b)

Figure 7-23. (a) Bias of the model minus the NCAR/NCEP reanalysis wind speed at 850 mb in m s^{-1} for the July 1991 episode for the 96-km grid. (b) Root mean square error (RMSE) of the same field for the same time and grid.

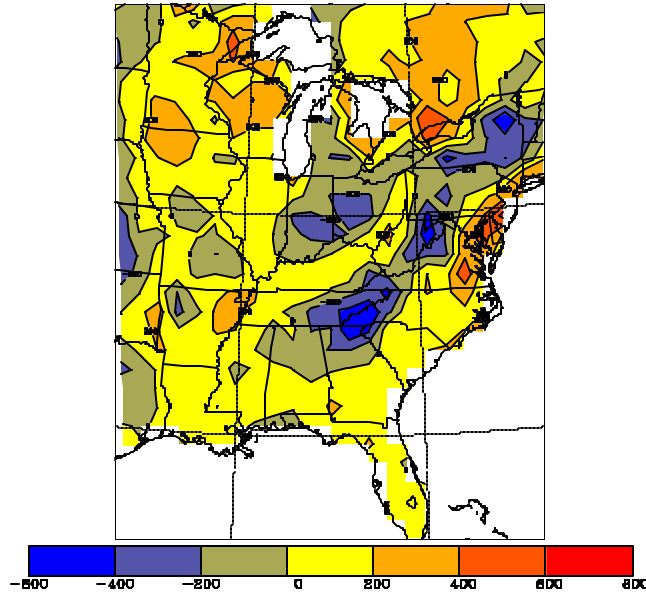


Figure 7-24. Bias of the model mixing height averaged over the period 1800-0000 UTC minus the observed mixing height averaged over the entire July 1991 episode for the 96-km grid. Differences are in units of m. See the text for additional details.

7.7 3-12 August 1993 Episode Results

7.7.1 Statistics of Aloft Predictions of Temperatures and Winds

Table 7-7 summarizes the predicted and observed, vertically-integrated horizontal winds and temperatures for the 3-12 August 1993 episode. The measurements are derived from the various NWS upper air reporting sites over the eastern U.S. From the table there is good agreement between the predicted and observed vertically averaged temperatures for each simulation day. For example, the vertically-averaged predicted and observed temperatures on the 12 km domain are 14.0°C and 12.5°C, respectively. The predicted and observed wind speeds and directions are also in very good agreement. Specifically, the mean aloft predicted and observed wind speeds are 6.9 m s⁻¹ and 6.7 m s⁻¹, yielding a net 3% discrepancy. Part of this good agreement is due to the fact that aloft temperature and wind observations from the NWS radiosondes were employed in the RAMS FDDA nudging schemes. However, the actual weighting coefficients used in the nudging were small so that the RAMS fields were not under a heavy constraint to match the observations locally. While this apparent good agreement in the estimation of aloft temperatures, wind speeds, and wind directions shown in the summary statistics of Table 7-7 is encouraging and gives some confidence that the modeled wind patterns are a reasonable approximation to the conditions that actually occurred, this evaluation is insufficient by itself to judge the reasonableness of the model predictions aloft.

7.7.2 Vertical Profiles of Mixing Ratios, Temperatures and Winds

Further insight into the aloft model performance can be developed by examining so-called ‘skew-T’ plots of the modeled and observed wind and thermodynamic profiles. Such plots were developed for the RAMS output for every available rawinsonde sounding in the SAMI domain.) The full set of plots are contained on the CD archive). Figure 7-24 is an example of a skew-T plot at the Greensboro, SC site at 1300 EST on 7 August 1993. The solid blue line represents the RAMS upper air temperature profile while the solid red line corresponds to radiosonde observations. The thin blue and red lines denote the mixing ratio predictions and observations, respectively. Modeled and observed horizontal winds are shown in the stick plots to the right.

Perusal of the results from the Greensboro site midday on 7 August reveals that there is quite good agreement between modeled and observed temperatures through the planetary boundary layer (pbl). Also, above 900 mb, there is fairly good agreement between predicted and observed winds. Within the first 1000m of the atmosphere, however, there is about a 90 degree discrepancy between the predicted and observed horizontal winds. Also, the model produced larger mixing ratios through the pbl compared with the measurements although close to the ground they are in good agreement. As noted above, a full set of these plots have been developed and archived; however, project resources have not allowed a more detailed analysis of this intriguing data set. A systematic inter-comparison of the modeled vertical structures within the lowest thousand meters would be very interesting, particularly in regions of complex topography. These data sets have been archived for SAMI and are available to parties interested in conducting further analyses.

7.8 23-29 June 1992 Episode Results

7.8.1 Statistics of Aloft Predictions of Temperatures and Winds

Table 7-8 summarizes the aloft wind comparisons for the 23-29 June 1992 episode. As with the August episode, there is good agreement between the predicted and observed vertically averaged temperatures for each simulation day. The vertically-averaged predicted and observed temperatures on the 12 km domain are 13.5°C and 13.8°C, respectively. The mean predicted and observed wind aloft wind speeds are 7.3 m s⁻¹ and 6.6 m s⁻¹, giving a 11% discrepancy.

7.8.2 Vertical Profiles of Mixing Ratios, Temperatures and Winds

Figure 7-25 gives a skew-T plot at the Greensboro, SC at 2000 EST on 25 June 1992. On this evening at Greensboro, there is good agreement between modeled and observed temperatures above about 300m agl.

At the surface, the model estimate the onset of a shallow nocturnal temperature inversion while the data show the remainder of a slightly superadiabatic layer extending to ground. Throughout the depth of the model domain, there is fairly good agreement in the modeled and observed horizontal winds. As with the August 1993 episode, RAMS gives larger mixing ratios through the pbl compared with the measurements although close to the ground they are again in good agreement.

7.9 24 April – 3 May 1995 Episode Results

7.9.1 Statistics of Aloft Predictions of Temperatures and Winds

Table 7-9 summarizes the aloft wind comparisons for the April-May 1995 episode. There is reasonably good agreement between the predicted and observed vertically averaged temperatures for each simulation day. The vertically-averaged predicted and observed temperatures on the 12 km domain are 6.6°C and 6.0°C, respectively. The mean predicted and observed wind aloft wind speeds are 10.0 m s⁻¹ and 9.1 m s⁻¹, producing a 10% discrepancy.

7.9.2 Vertical Profiles of Mixing Ratios, Temperatures and Winds

Figure 7-26 shows a skew-T plot at Greensboro at 0800 EST on 29 April 1995. On this morning at Greensboro, there is good agreement between modeled and observed temperatures at the ground and above about 2000m. Within the boundary layer, however, there is about a 3°C positive (warm) bias in the modeled temperatures. At the surface, the model estimates the remnants of the nocturnal temperature inversion and this feature is also evident in the data. Throughout the depth of the model domain, there is fairly good agreement in the modeled and observed horizontal winds. Unlike the August 1993 and June 1992 episodes, RAMS gives lower mixing in the first 2500 m of the atmosphere compared with the measurements; above this height, the RAMS fields are more moist compared with the observations.

Table 7.7. Mean of the Vertically Averaged Profiles of Modeled and Predicted Temperatures and Winds for the 3-12 August 1993 Episode—12 Km Grid.

Date	Observed Temp. (deg C)	Predicted Temp. (deg C)	Observed Wind Speed (ms ⁻¹)	Predicted Wind Speed (ms ⁻¹)	Observed Wind Direction (deg)	Predicted Wind Direction (deg)
11 Aug	13.8	13.6	3.8	4.2	191	219
10 Aug	13.7	13.5	4.5	3.5	68	127
9 Aug	13.5	13.5	4.3	3.2	25	344
8 Aug	13.0	13.2	5.5	5.1	273	265
7 Aug	12.6	13.4	9.2	10.7	282	269
6 Aug	13.2	13.4	8.2	9.6	252	243
5 Aug	13.8	14.0	8.2	8.2	284	270
4 Aug	15.6	15.4	8.8	9.1	255	244
3 Aug	16.7	16.4	7.9	8.5	251	248
AVE	12.5	14.0	6.7	6.9	--	--

Table 7.8. Mean of the Vertically Averaged Profiles of Modeled and Predicted Temperatures and Winds for the 22-29 June 1992 Episode—12 Km Grid.

Date	Observed Temp. (deg C)	Predicted Temp. (deg C)	Observed Wind Speed (ms ⁻¹)	Predicted Wind Speed (ms ⁻¹)	Observed Wind Direction (deg)	Predicted Wind Direction (deg)
23 June	10.7	11.0	5.9	7.5	262	242
24 June	13.2	13.2	8.5	10.5	248	251
25 June	14.9	14.2	8.2	9.1	261	252
26 June	15.2	14.7	7.0	8.3	258	249
27 June	13.9	13.7	6.8	6.6	300	295
29 June	14.1	13.3	5.4	4.3	331	288
29 June	14.9	14.3	4.1	4.7	219	216
AVE	13.8	13.5	6.6	7.3	--	--

Table 7.9. Mean of the Vertically Averaged Profiles of Modeled and Predicted Temperatures and Winds for the 24 April – 3 May 1995 Episode—12 Km Grid.

Date	Observed Temp. (deg C)	Predicted Temp. (deg C)	Observed Wind Speed (ms ⁻¹)	Predicted Wind Speed (ms ⁻¹)	Observed Wind Direction (deg)	Predicted Wind Direction (deg)
25 April	2.5	2.8	9.7	10.0	310	298
26 April	4.6	4.4	6.8	8.2	282	255
27 April	7.7	7.5	8.8	11.0	216	217
28 April	6.2	9.6	9.6	11.1	277	278
29 April	6.9	6.4	6.2	6.6	313	269
30 April	8.7	8.3	8.5	10.2	232	227
1 May	7.4	8.4	10.2	10.6	292	263
2 May	5.9	7.0	13.4	13.9	247	254
3 May	4.1	4.9	8.8	9.1	336	316
AVE	6.0	6.6	9.1	10.0	--	--

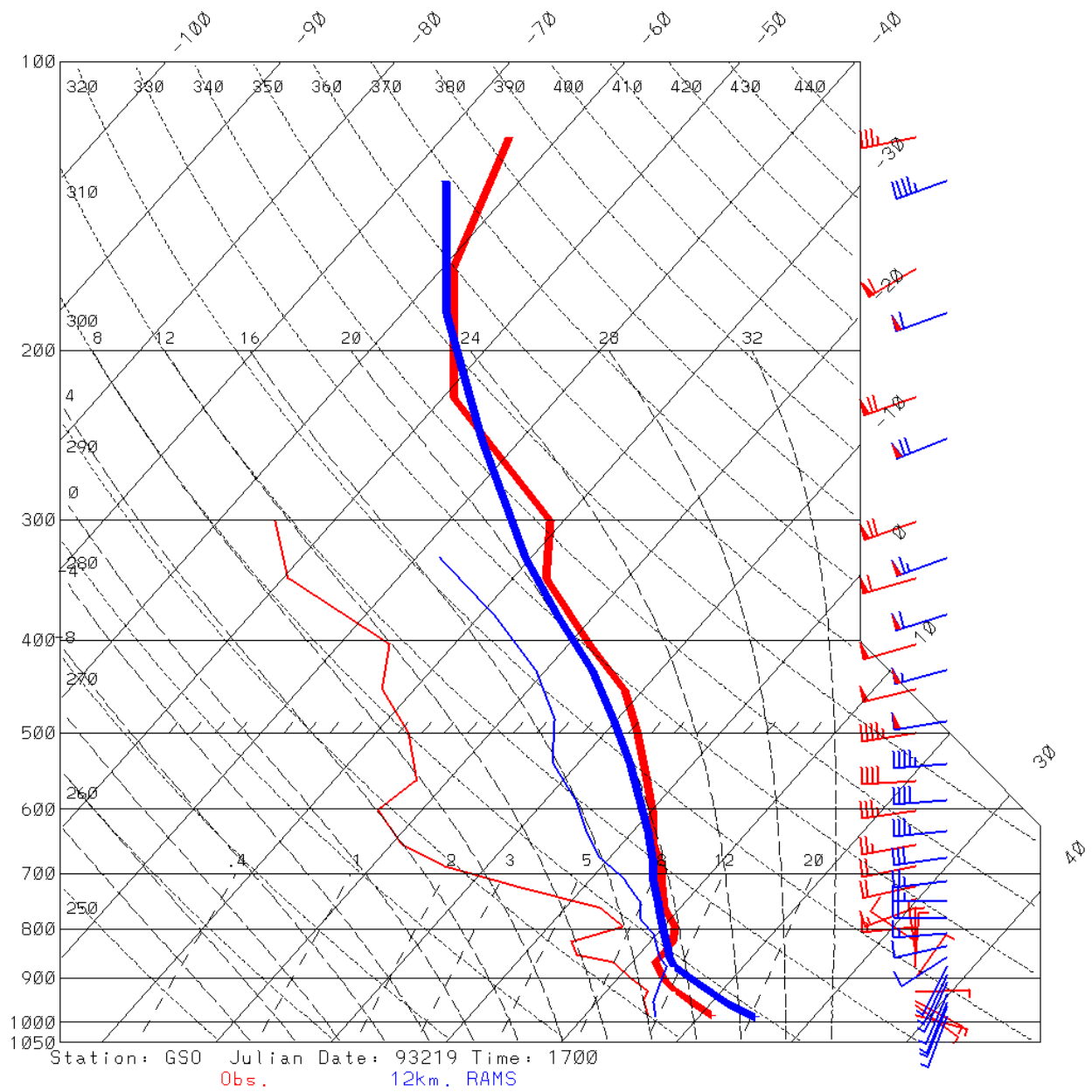


Figure 7-24. Comparison of Observed (red) and Predicted RAMS (blue) Upper Air Wind, Temperature and Mixing Ratios on 7 August 1993 at Greensboro, NC: 1300 EST.

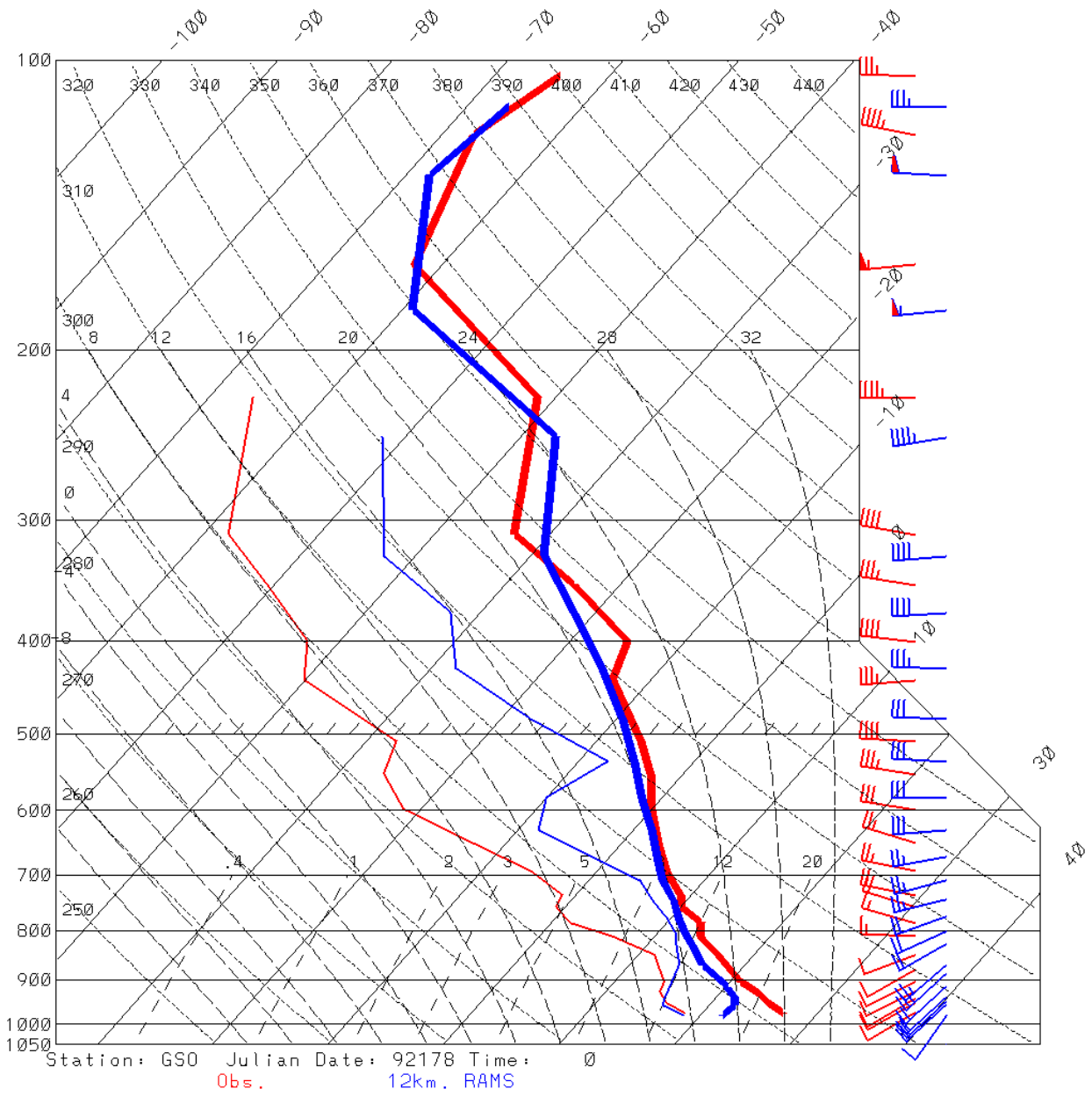


Figure 7-25. Comparison of Observed (red) and Predicted RAMS (blue) Upper Air Wind, Temperature and Mixing Ratios on 25 June 1992 at Greensboro, NC: 2000 EST UTC.

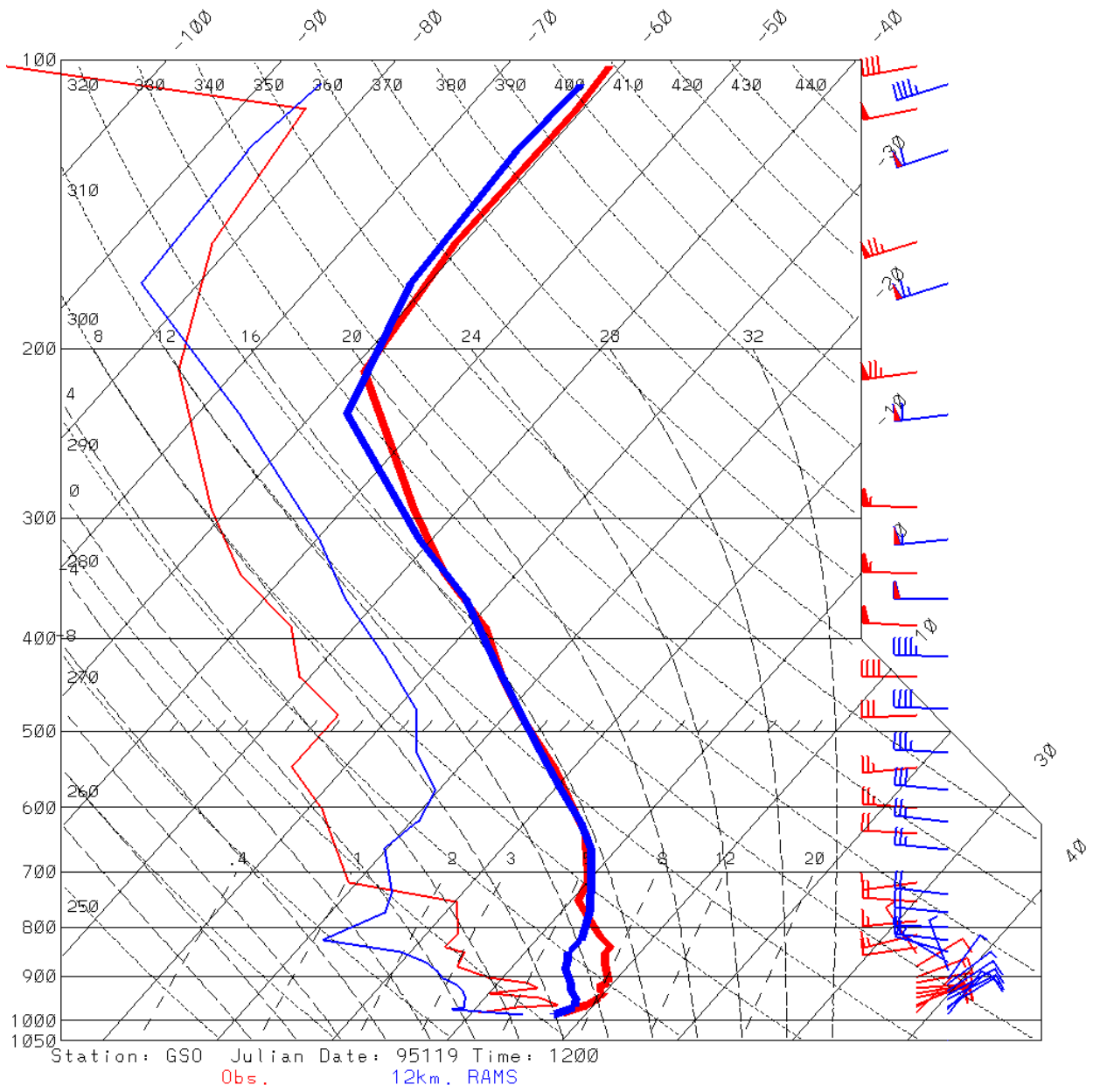


Figure 7-26. Comparison of Observed (red) and Predicted RAMS (blue) Upper Air Wind, Temperature and Mixing Ratios on 29 April 1995 at Greensboro, NC: 0800 EST.

8.0 RAMS PERFORMANCE ACROSS SAMI EPISODES

In addition to performing evaluations of RAMS model performance for the specific episodes assigned them, the UAH and AG team elected to add an additional analysis aimed at portraying model performance with a unified set of statistical and graphical procedures. Although outside the scope of UAH and AG work efforts, this supplement work was performed in order that SAMI might be able to interpret the performance of the model using a common suite of evaluation tools. This was accomplished, in part, by using AG's MAPS evaluation software, previously introduced in Chapter 5. An added benefit is that the SAMI episodes can then be compared with other RAMS and MM5 evaluations carried out by Alpine Geophysics across the U.S. over the past five years.

In this section we present the results of six (6) UAH episodes and three (3) AG episodes using two distinct software products. The first, developed by UAH, computes episode-composite near-ground level bias and error performance statistics for temperature, wind speed and mixing ratio. The UAH algorithms utilize similarity theory to develop scaling relationships to extrapolate Layer 1 RAMS temperatures, winds, and mixing ratios (at 20 m agl) to the heights at which these parameters are commonly measured (i.e. 2 m for temperatures and mixing ratios; 10 m for winds). The second product is MAPS which produces a variety of statistical and graphical evaluation products based on the model-produced output at Layer 1. MAPS is used to develop sixteen (16) different statistical measures of performance in addition to a variety of graphical displays. Finally, we present summary tables and figures that compare the SAMI RAMS evaluation results with other studies.

8.1 Episode Composite Near-Ground Level Performance Measures

Table 8-1 presents near-ground level episode composite bias and error statistics for temperature, wind speed, wind direction, and mixing ratio. These statistics were calculated by UAH using code developed to extrapolate RAMS Layer 1 output to standard measurement heights.

8.1.1 Bias and Error in Mean 2 m Temperatures

The bias and error composite statistics for 2 m temperatures for nine (9) SAMI episodes are presented in Table 8-1 and Figure 8-1. The range in overall bias in near surface temperature is -2.55°F to 1.17°F with a mean over all episodes of -1.20°F (one degree F=0.55 degrees C). For the root mean square error (RMSE), the range over the episodes is 3.82°F to 5.38°F with a mean value of 4.45°F . These bias and error statistics are displayed graphically in Figure 8-1. Only the February 1994 and July 1995 episode exhibited a tendency to overestimate near-surface temperatures and the RMSE errors for all episodes are fairly similar to the mean value.

8.1.2 Bias and Error in Mean 10 m Wind Speeds

Bias and error composites for 10 m surface winds are given in Table 8-1 and Figure 8-2. The range in bias of near surface wind speeds across the 9 SAMI episodes is 0.18 m s^{-1} to 1.33 m s^{-1} with a mean over all episodes of 0.82 m s^{-1} . Thus, RAMS overestimated surface wind speeds consistently in every SAMI

episode even when the model predictions are extrapolated down to the nominal height of the observations. For RMSE, the range over the episodes is 1.51 to 2.75 with a mean value of 2.05 m s⁻¹. The wind speed bias and error statistics are shown in Figure 8-2. There is considerable variability in the degree to which RAMS overestimates surface wind speeds across the episodes. This over-prediction is the least with the May 1995 episode and is greatest for the February 1994 and April-May 1995 episodes. Less variability across episodes is seen in the RMSE plots; interestingly, here the May 1995 episode is not the one with the lowest error even though it had the lowest speed bias, suggesting the presence of cancellation of errors in the bias calculation for this episode.

8.1.3 Bias and Error in Mean 10 m Wind Directions

Wind direction bias and error estimates for the 10 m surface winds are presented in Table 8-1 and Figure 8-3. The bias in episode composite near surface wind directions across the 9 episodes is -3.76 degrees to 12.30 degrees with a mean over all episodes of -0.76 degrees. Only the March 1993 and May 1995 episodes had positive directional biases but there is really little significance to the sign of this bias quantity given the scale of the SAMI domain. More meaningful is the RMSE in wind direction. Here the range over the episodes is 63 degrees to 83 degrees with a mean value of 72.2 degrees. As shown in Figure 8-3, there is actually very little variability in wind direction RMSE across the 9 SAMI episodes based on these near-surface wind statistics. Of course from an air quality modeling perspective, the bias needs to be examined at shorter times scales than the episode composite and this will be done in a later section.

8.1.4 Bias and Error in 2 m Mixing Ratios

The bias and error composite statistics for 2 m mixing ratios are listed in Table 8-1 and presented in Figure 8-4. The range in overall bias in near surface mixing ratio is -1.76 g/Kg to -0.00 g/Kg with a mean of -0.60 g/Kg. over all episodes. The RMSE ranges from 0.59 g/Kg to 4.12 g/Kg with a mean value of 1.55 g/Kg. As noted in the table, we suspect that the particularly large mixing ratio bias and error statistics for the April 1995 episode may be the result in a breakdown in the surface layer vertical extrapolation scheme rather than an indication of poor model performance. As noted in Section 6.7 wherein a more detailed evaluation of surface mixing ratios was carried out, we did not see performance this poor. It is also possible that the extrapolation scheme may have experienced difficulties with the July 1995 episode as well but this episode was not examined intensively with the MAPS software. Aside from the suspected problems with the bias and error statistics for these two episodes, the overall summaries in Figure 8-4 suggest good and consistent performance across all 7 remaining SAMI episodes.

8.2 Time Series of Spatial Mean Surface Winds, Temperature and Mixing Ratios

Two-thirds of the UAH RAMS modeling episodes were re-evaluated using AG's MAPS evaluation software and then compared with the three RAMS runs previously discussed in sections 6.7 through 6.9. Below, we present statistical and graphical results of these comparisons. The statistical results are presented in Tables 8-2 and 8-3 in terms of episode average statistics for the 12 km and 24 km grid domains, respectively. Here we focus on the 12 km results. Figures 8-5 through 8-10 display the hourly results in the form of spatial mean time series, first introduced in Chapter 7. Note also that the results

presented below are derived from Layer 1 RAMS predictions (~20 m) and do not exactly correspond to the height of the measured surface temperatures, winds and mixing ratios.

8.2.1 Spatial Mean Temperatures

Spatial mean ground-level temperature time series are presented in Figure 8-5 for seven (7) SAMI episodes. Three of these (3-12 August 1993, 22-29 June 1992, and 24 April-3 May 1995) have already been discussed in sections 6.7 through 6.9. Ground-level bias and gross error statistics for temperature are listed in Table 8-2a. The bias in episode average ground level temperatures across the 7 episodes ranges from -1.46°C to 0.51°C with a mean over all episodes of 0.79°C . The range in gross error over the episodes is 1.60°C to 2.24°C with a mean value of 1.94°C . As shown in Figure 8-5, RAMS matches the diurnal variation in temperature fairly well with two exceptions. First, there is a systematic tendency to underestimate the afternoon temperatures due to mismatch between 2m measurement height and the 20 m height of the lowest RAMS prediction. More obvious is the systematic underestimation of temperature in the February 1994 episode for the 8-10 February period. For these three days, the model systematically under-predicts the ground level temperatures, day and night, by 4 to 8°C . Otherwise, the time series plots are fairly consistent across the episodes and similar to other mesoscale model applications.

8.2.2 Vector Mean Wind Speeds

Hourly spatial mean ground-level wind speed time series are presented in Figure 8-6 and the episode average bias and gross error statistics are listed in Table 8-2b. The mean predicted wind speeds are all positively biased (i.e., they all overestimate the observations) and the average discrepancy between modeled and observed episode average wind speed ranges from 35% to 140% with a mean over all episodes of 67%. As shown in Figure 8-6, the hourly spatial mean wind times series for predictions and observations have large day-to-day variability with each episode and from episode to episode. RAMS tendency to over-predict the 10 m winds is evident in these plots. The greatest discrepancies occur during the early part of the 8-13 February 1994 episode (especially 9 February). Despite the seemingly large differences between predicted and observed spatial mean winds from day-to-day and episode-to-episode, these results are generally consistent across the episodes and similar to other mesoscale model applications.

8.2.3 Mean Wind Direction Differences

The spatial mean wind direction time series are shown in Figure 8-6 and the episode average bias and gross error statistics are listed in Table 8-2b. The episode mean differences between predicted and observed surface winds ranges from 4 to 103 degrees with a composite mean of 39 degrees. From Figure 8-7 there is generally good agreement in the day-to-day and hour-to-hour wind directions for most of the episodes. The greatest wind direction discrepancies occur for the March 1993 and February 1994 episodes.

8.2.4 Index of Agreement

Spatial mean index of agreement scores for the seven (7) SAMI episodes are listed in Table 8-2 and presented graphically in Figure 8-8. The index ranges from 0.72 to 0.81 with a composite mean over all

episodes of 0.76. While each of the index of agreement time series exhibit unique diurnal features, the similarity of the mean index scores is quite remarkable. There is actually very little variation in the index scores across the episodes even though the episodes themselves cover a broad range of synoptic and climatic conditions.

8.2.5 RMSE Errors

Table 8-2 presents the RMSE errors for the seven SAMI episodes. The episode average RMSE errors range from 1.90 m s^{-1} to 2.76 m s^{-1} with a mean across the seven episodes of 2.18 m s^{-1} . For all but the May 1995 episode, the systematic component exceeds the systematic component of the RMSE error and for the May episode the two components are nearly identical. Thus, there is consistency in the finding that (because the systematic component is nearly always the larger of the two) the preponderance of the RAMS modeling uncertainty tends to result from input uncertainties and the inherent difficulties in prescribing model inputs from sparse measurements. The spatial mean RMSE error plots again identify the 8-10 February 1994 period as one of concern due to the large (i.e., $>5 \text{ m s}^{-1}$) RMSE errors during the early portion of the episode.

8.2.6 Spatial Mean Mixing Ratios

Spatial mean ground-level mixing ratio time series are presented in Figure 8-10 and the episode average statistical summaries are given in Table 8-2c. The bias in episode average ground level mixing ratios across the 7 episodes ranges from -0.60 g/Kg to 0.03 g/Kg with a mean over all episodes of -0.10 g/Kg . The range in gross error over the episodes is 0.44 g/Kg to 1.10 g/Kg with a mean value of 0.78 g/Kg . As shown in Figure 8-10, RAMS provides an excellent match of the diurnal variation in mixing ratios for each episode studied.

8.3 Comparison with Other Prognostic Model Evaluation Studies

Table 8-4 summarizes episode composite temperature, wind speed, wind direction and mixing ratio statistics for nearly thirty (30) MM5 and RAMS model applications over the past five years. The table focuses on results from prognostic model applications on 12 km grid meshes since this the scale most commonly reported. Most of the studies, however, also included model evaluation at 36 km and 4 km scales as well. This information has also been compiled and is available from AG. While these statistics may be helpful in making *general* comparisons between studies and episodes, it is clear that the calculation of an episode mean statistic often conceals important day-to-day and/or hour-to-hour variations that may be quite important in judging the adequacy of a meteorological or air quality model simulation.

8.3.1 Bias and Error in Mean Temperatures

From Table 8-4a the mean bias and gross errors in the ensemble of RAMS and MM5 studies reviewed are -0.5°C and 1.9°C , respectively. The standard deviations for these quantities are 0.6°C and 0.5°C , respectively. Comparing the seven (7) SAMI episodes with the broader set of evaluations, we find that for gross error, all SAMI episodes fall within at least \pm one standard deviation (i.e., 1 sigma) of the ensemble

mean. Four of the seven SAMI episodes yield mean bias statistics just outside the, ± 1 sigma of -0.8°C to 0.4°C . However, two points are worth noting. First, a number of the studies reported in Table 8-4 employed vertical grid structures that shallower first layers compared with the 20 m first atmospheric layer in RAMS. Indeed, many of the MM5 runs used first grid cells of 9-10 m in thickness. Thus, one cannot rigorously apply the statistical summaries without recognizing the impact that the height mismatch between measurement and prediction has on the statistics. Second, the whether or not a particular episode falls within or outside of the ± 1 sigma range should not be taken as an indicator of model acceptance or rejection. This range is used here simply to facilitate comparisons between modeling studies and is explicitly not suggested as a model performance criterion to be rigidly applied.

8.3.2 Bias and Error in Mean Mixing Ratios

The mean bias and gross errors in mixing ratios are presented in Table 8-4b for the ensemble of RAMS and MM5 studies. The mean values for bias and error are -0.4 g/Kg and 1.4 g/Kg, respectively. The standard deviations for these quantities are 0.7 g/Kg and 0.5 g/Kg, respectively. For mixing ratio bias, we find that all SAMI episodes fall well within at least \pm one standard deviation (i.e., 1 sigma) of the ensemble mean. For gross error in mixing ratio, for of the seven SAMI episodes yield smaller errors that -1 sigma range of 0.9 g/Kg and the other two episodes are at the low end of the range. Thus, RAMS performs better than average to mixing ratio.

8.3.3 Average Discrepancy in Mean Wind Speed

Table 8-4c lists the average discrepancy (i.e. accuracy) of wind speed prediction for the ensemble of RAMS and MM5 studies. The mean and standard deviation of wind speeds across these studies are 44.3% and $\pm 42.8\%$, respectively. With the exception of the 3-12 August episode, all of the SAMI episodes had wind speed accuracies that were well within the 1 sigma range. One of the reasons why the 3-12 August episode produced larger percentage differences between predicted and observed winds was due to the systematically lower wind speeds that occurred during this episode and the fact that lower values in the denominator produce higher percentage values for the accuracy measure. When this fact is taken into account, we see that the RAMS performance for wind speed is also quite comparable to other recent studies.

8.3.4 RMSE Errors

The mean and standard deviations of the RMSE errors, listed in Table 8-4c, are 2.07 m s^{-1} and ± 0.38 m s^{-1} , respectively. With the exception of the 8-13 February 1994 episode, all of the SAMI episodes had wind speed RMSE errors that were well within the 1 sigma range. Even considering the February episode, we conclude that the model's performance based on the RMSE errors is also quite comparable to other recent studies. However, as discussed earlier, there remains concern over the model's performance for the 8-10 February 1994 portion of the modeling period and this interval is largely responsible for the larger than expected RMSE error for this episode.

8.3.5 Index of Agreement

The mean and standard deviations of the Index of Agreement are 0.74 and ± 0.06 , respectively. With the exception of the 24 April – 3 May 1991 episode, all of the SAMI episodes had wind speed RMSE errors that were well within the 1 sigma range. The April-May episode is just outside the ± 1 sigma range. Thus, for the index of agreement statistic as well, RAMS' performance is quite consistent with other MM5 and RAMS simulations elsewhere in the U.S.

8.3.6 Average Discrepancy in Mean Wind Direction

Table 8-4c shows that the mean and standard deviations episode average wind direction difference are 24.6 degrees and 30.7 deg, respectively. Only the 23-31 March 1993 and 8-13 February 1994 episode fall outside of the ± 1 sigma range. Each episode has a mean wind direction difference of approximately 100 degrees. The remaining six episodes are well within the range. The directional biases in these two episodes should be examined further to assess their potential impact on air quality model calculations. Recall from Figures 8-7c and 8-7d that there were several periods during each episode, lasting from 1 to 3 days, when significant biases occurred in the spatial mean predicted and observed wind directions. With these two exceptions, we believe that RAMS' performance for wind direction is consistent with other MM5 and RAMS studies.

Table 8-1. Statistical Summaries of RAMS Performance for All SAMI Episodes Using the UAH Surface Layer Algorithms: 12 Km Grid Results. (a) Bias Statistics

Performance Attribute	Feb '94	July '91	July '95	Mar '93	May '93	May '95	June '92	Aug '93	April '95	Mean Value
Surface Temperature (deg F)	0.54	-1.27	1.17	-2.28	-2.55	-1.75	-2.20	-0.80	-1.65	-1.20
Surface Mixing Ratio (gm/Kg)	-0.00	-0.37	-1.45	-0.16	-0.30	-0.29	-0.32	-1.76 ⁺	-0.77	-0.60
Surface Wind Speed (ms ⁻¹)	1.33	0.94	0.49	0.88	0.38	0.18	0.66	1.16	1.33	0.82
Surface Wind Direction (deg)	-3.76	-2.29	-8.16	12.30	-3.68	1.30	-0.08	-1.11	-1.39	-0.76

Table 8-1. Statistical Summaries of RAMS Performance for All SAMI Episodes Using the UAH Surface Layer Algorithms: 12 Km Grid Results. (b) Root Mean Square Error Statistics

Performance Attribute	Feb '94	July '91	July '95	Mar '93	May '93	May '95	June '92	Aug '93	April '95	Mean Value
Surface Temperature (deg F)	5.04	4.01	4.37	5.38	4.80	4.17	4.24	3.82	4.26	4.45
Surface Mixing Ratio (gm/Kg)	0.59	0.90	2.56	0.67	1.06	1.03	1.07	4.12 ⁺	1.96	1.55
Surface Wind Speed (ms ⁻¹)	2.75	2.26	1.51	2.15	1.73	1.75	1.85	2.08	2.35	2.05
Surface Wind Direction (deg)	73.0	77.0	83.0	70.0	67.0	63.0	74.0	78.0	65.0	72.2

⁺ Note: We suspect these particularly large mixing ratio statistics are the result of a breakdown in the surface layer vertical extrapolation scheme more than an indication of poor model performance as confirmed by the mixing ratio results for this episode described in section 6.7.

Table 8-2. RAMS Model Evaluation Statistics for Seven SAMI Episodes on the 12 Km Grid using the AG MAPS Model Evaluation Software. (a) Temperatures (deg C).

Performance Attribute	24-29 May '95	11-17 May '93	23-31 Mar '93	8-13 Feb '94	3-12 Aug '93	22-29 Jun '92	24 Ap- 3 May '95	Mean Value
Mean Bias (deg C)	-0.96	-1.46	-1.33	0.51	-0.40	-1.10	-0.80	-0.79
Gross Error (deg C)	1.88	2.12	2.24	2.13	1.60	1.80	1.80	1.94

Table 8-2. RAMS Model Evaluation Statistics for Seven SAMI Episodes on the 12 Km Grid using the AG MAPS Model Evaluation Software. (b) Winds (ms^{-1}).

Performance Attribute	24-29 May '95	11-17 May '93	23-31 Mar '93	8-13 Feb '94	3-12 Aug '93	22-29 Jun '92	24 Ap- 3 May '95	Mean Value
Mean Obs. Speed	2.15	1.56	1.89	2.37	1.11	1.54	1.86	1.78
Mean Pred. Speed	2.90	2.36	2.89	3.86	2.66	2.55	2.98	2.89
Speed Accuracy (%)	35	51	53	63	140	66	60	67
RMSE	1.90	1.90	2.27	2.76	2.18	1.89	2.35	2.18
RMSE _S	1.30	1.38	1.69	2.15	1.72	1.38	1.84	1.64
RMSE _U	1.34	1.27	1.46	1.64	1.28	1.24	1.46	1.38
Index of Agreement	0.76	0.76	0.74	0.72	0.75	0.75	0.81	0.76
Skill _E	0.63	0.68	0.68	0.69	0.75	0.66	0.64	0.68
Skill _{VAR}	0.88	0.97	1.03	1.03	1.02	0.84	1.15	0.99
Mean Obs. Dir. ($^{\circ}$)	179	234	64	344	179	250	261	--
Mean Pred. Dir. ($^{\circ}$)	192	228	164	241	204	230	257	--
Diff in Mean Dir. ($^{\circ}$)	13	6	100	103	25	20	4	39

Table 8-2. RAMS Model Evaluation Statistics for Seven SAMI Episodes on the 12 Km Grid using the AG MAPS Model Evaluation Software. (c) Mixing Ratios (gm/Kg).

Performance Attribute	24-29 May '95	11-17 May '93	23-31 Mar '93	8-13 Feb '94	3-12 Aug '93	22-29 Jun '92	24 Ap- 3 May '95	Mean Value
Mean Bias (gm/Kg)	0.00	-0.01	-0.02	0.00	-0.60	0.03	-0.10	-0.10
Gross Error (gm/Kg)	0.81	0.83	0.55	0.44	1.10	1.00	0.70	0.78

Table 8-3. RAMS Model Evaluation Statistics for Seven SAMI Episodes on the 24 Km Grid using the AG MAPS Model Evaluation Software. (a) Temperatures (deg C).

Performance Attribute	24-29 May '95	11-17 May '93	23-31 Mar '93	8-13 Feb '94	3-12 Aug '93	22-29 Jun '92	24 Ap- 3 May '95	Mean Value
Mean Bias (deg C)	-0.97	-1.24	-0.29	0.80	-0.50	-0.90	-0.70	-0.54
Gross Error (deg C)	2.11	2.28	2.08	2.46	1.80	1.90	1.80	2.06

Table 8-3. RAMS Model Evaluation Statistics for Seven SAMI Episodes on the 24 Km Grid using the AG MAPS Model Evaluation Software. (b) Winds (ms^{-1}).

Performance Attribute	24-29 May '95	11-17 May '93	23-31 Mar '93	8-13 Feb '94	3-12 Aug '93	22-29 Jun '92	24 Ap- 3 May '95	Mean Value
Mean Obs. Speed	1.68	1.21	1.09	1.81	1.08	1.05	1.29	1.32
Mean Pred. Speed	2.53	2.45	1.32	3.07	2.43	2.30	2.06	2.31
Speed Accuracy (%)	51	102	21	70	125	119	60	78
RMSE	2.60	2.50	2.57	3.43	2.41	2.17	2.51	2.60
RMSE _S	1.58	1.67	1.79	2.35	1.67	1.40	1.71	1.74
RMSE _U	2.03	1.82	1.81	2.44	1.56	1.61	1.78	1.86
Index of Agreement	0.80	0.82	0.83	0.77	0.78	0.84	0.85	0.82
Skill _E	0.77	0.74	0.68	0.82	0.84	0.72	0.65	0.75
Skill _{VAR}	1.11	1.06	1.19	1.23	1.18	1.07	1.20	1.15
Mean Obs. Dir. ($^{\circ}$)	163	255	58	1	196	252	262	--
Mean Pred. Dir. ($^{\circ}$)	187	236	140	242	210	241	248	--
Diff in Mean Dir. ($^{\circ}$)	24	19	82	119	14	11	14	40

Table 8-3. RAMS Model Evaluation Statistics for Seven SAMI Episodes on the 24 Km Grid using the AG MAPS Model Evaluation Software. (c) Mixing Ratios (gm/Kg).

Performance Attribute	24-29 May '95	11-17 May '93	23-31 Mar '93	8-13 Feb '94	3-12 Aug '93	22-29 Jun '92	24 Ap- 3 May '95	Mean Value
Mean Bias (gm/Kg)	0.07	0.12	0.21	0.26	-0.40	-0.20	0.00	0.01
Gross Error (gm/Kg)	0.89	0.86	0.66	0.65	1.10	0.90	0.70	0.82

Table 8-4. Summary of prognostic meteorological model performance evaluations by Alpine Geophysics: 12 km grid resolution results. (a) Surface Temperatures (deg C).

Modeling Domain	Model	Study	Ref	Episode	Mean Bias (deg C)	Gross Error (deg C)
Southeastern U.S.	RAMS	SAMI	7	24-29 May '95	-1.0	1.9
Southeastern U.S.	RAMS	SAMI	7	11-17 May '93	-1.5	2.1
Southeastern U.S.	RAMS	SAMI	7	23-31 Mar '93	-1.3	2.2
Southeastern U.S.	RAMS	SAMI	7	8-13 Feb '94	0.5	2.1
Southeastern U.S.	RAMS	SAMI	7	3-12 Aug '93	-0.4	1.6
Southeastern U.S.	RAMS	SAMI	7	22-29 Jun '92	-1.1	1.8
Southeastern U.S.	RAMS	SAMI	7	24 Apr-3 May '91	-0.8	1.8
Texas	MM5	COAST	11	4-11 Sept '93	0.2	1.8
Central Florida	MM5	PFOS-Episode 1	10	16-24 Apr '99	0.1	1.5
Central Florida	MM5	PFOS-Episode 2	10	2-10 May '97	0.2	1.6
Central Florida	MM5	PFOS-Episode 3	10	25-30 Aug '97	0.2	1.7
Central Florida	MM5	PFOS-Episode 4	10	4-10 April '99	-0.4	1.3
Central Florida	MM5	PFOS-Episode 5	10	17-23 Sept '97	0.1	1.6
Central Florida	MM5	PFOS-Episode 9	10	20-28 Apr '98	0.3	1.3
Midwestern U.S.	MM5	Kansas/Missouri	8	11-24 Jun '95	-0.1	1.8
Eastern U.S.	MM5	Pittsburgh SIP	1	31 July-2 Aug '95	0.8	2.4
Western U.S.	MM5	SARMAP	4	3-6 Aug '90	0.2	2.9
Upper Midwest	RAMS	CRC-LMO'S	6	26-28 Jun '91	0.1	1.4
Upper Midwest	RAMS	CRC-LMOS	6	17-19 Jul '91	-0.0	1.9
Upper Midwest	MM5	CRC-LMOS	6	26-28 Jun '91	-0.5	1.6
Upper Midwest	MM5	CRC-LMOS	6	17-19 Jun '91	-0.3	1.7
Eastern U.S.	RAMS	OTAG	3	13-21 Jul '91	1.6	2.1
Eastern U.S.	MM5	OTAG	3	13-21 Jul '91	-0.1	2.0
Eastern U.S.	MM5	OTAG	2	1-11 Jul '88	-0.6	3.3
Eastern U.S.	MM5	OTAG	1	12-15 Jul '95	-0.2	2.0
Eastern U.S.	MM5	Cincinnati SIP	5	18-22 Jun '94	-0.7	2.4
Southeastern U.S.	MM5	BAMP	9	6-11 Sep '93	-0.4	2.1
Southeastern U.S.	MM5	BAMP	9	15-19 Aug '93	-0.3	2.4
Maximum Value					-1.5	1.3
Minimum Value					1.6	3.3
Mean Value					-0.2	1.9
Standard Deviation					0.6	0.5
1 Sigma Range					-0.8 to 0.4	1.4 to 2.4

Table 8-4. Summary of prognostic meteorological model performance evaluations by Alpine Geophysics: 12 km grid resolution results. (b) Surface Mixing Ratio (gm/Kg).

Modeling Domain	Model	Study	Ref	Episode	Mean Bias (gm/Kg)	Gross Error (gm/Kg)
Southeastern U.S.	RAMS	SAMI	7	24-29 May '95	0.0	0.8
Southeastern U.S.	RAMS	SAMI	7	11-17 May '93	-0.0	0.8
Southeastern U.S.	RAMS	SAMI	7	23-31 Mar '93	-0.0	0.6
Southeastern U.S.	RAMS	SAMI	7	8-13 Feb '94	0.0	0.4
Southeastern U.S.	RAMS	SAMI	7	3-12 Aug '93	-0.6	1.1
Southeastern U.S.	RAMS	SAMI	7	22-29 Jun '92	0.0	1.0
Southeastern U.S.	RAMS	SAMI	7	24 Apr-3 May '91	-0.1	0.7
Texas	MM5	COAST	11	4-11 Sept '93	0.1	1.4
Central Florida	MM5	PFOS-Episode 1	10	16-24 Apr '99	-0.1	1.2
Central Florida	MM5	PFOS-Episode 2	10	2-10 May '97	0.1	1.2
Central Florida	MM5	PFOS-Episode 3	10	25-30 Aug '97	-2.0	2.3
Central Florida	MM5	PFOS-Episode 4	10	4-10 April '99	0.8	1.5
Central Florida	MM5	PFOS-Episode 9	10	17-23 Sept '97	-0.4	1.6
Central Florida	MM5	PFOS-	10	20-28 Apr '98	-0.2	0.9
Midwestern U.S.	MM5	Kansas/Missouri	8	11-24 Jun '95	-0.4	1.3
Eastern U.S.	MM5	Pittsburgh SIP	1	31 July-2 Aug '95	0.2	2.2
Western U.S.	MM5	SARMAP	4	3-6 Aug '90	-0.2	1.9
Upper Midwest	RAMS	CRC-LMOS	6	26-28 Jun '91	-0.1	1.2
Upper Midwest	RAMS	CRC-LMOS	6	17-19 Jul '91	0.4	1.4
Upper Midwest	MM5	CRC-LMOS	6	26-28 Jun '91	-0.1	1.2
Upper Midwest	MM5	CRC-LMOS	6	17-19 Jun '91	-0.6	1.5
Eastern U.S.	RAMS	OTAG	3	13-21 Jul '91	-0.0	1.2
Eastern U.S.	MM5	OTAG	3	13-21 Jul '91	-0.3	1.4
Eastern U.S.	MM5	OTAG	2	1-11 Jul '88	-1.4	2.0
Eastern U.S.	MM5	OTAG	1	12-15 Jul '95	-1.5	2.2
Eastern U.S.	MM5	Cincinnati SIP	5	18-22 Jun '94	-1.6	2.2
Southeastern U.S.	MM5	BAMP	9	6-11 Sep '93	-0.6	1.0
Southeastern U.S.	MM5	BAMP	9	15-19 Aug '93	-1.5	1.9
Maximum Value					-2.0	0.4
Minimum Value					0.8	2.3
Mean Value					-0.4	1.4
Standard Deviation					0.7	0.5
1 Sigma Range					-1.1 to 0.3	0.9 to 1.9

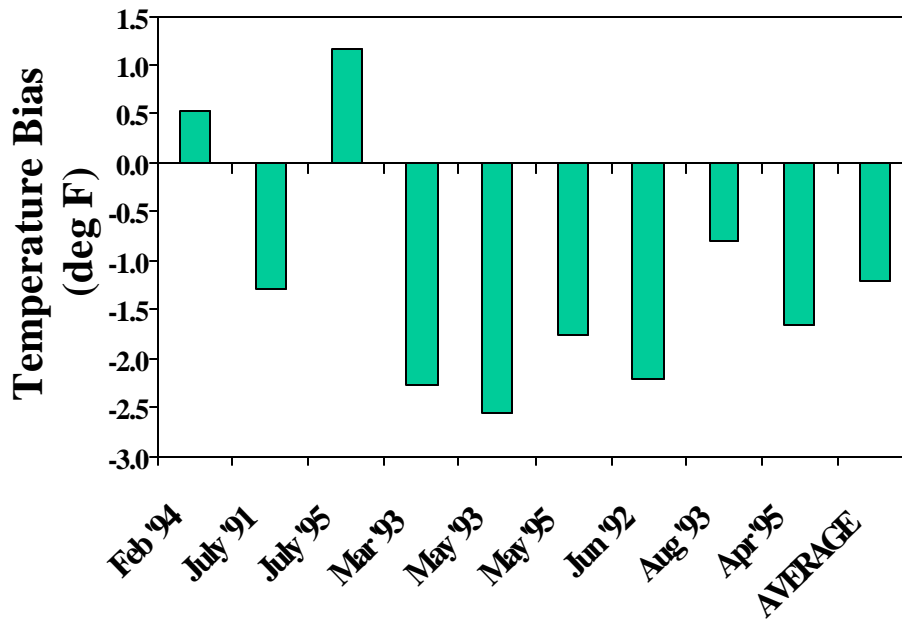
Table 8-4. Summary of prognostic meteorological model performance evaluations by Alpine Geophysics: 12 km grid resolution results. (c) Surface Wind Speeds.

Modeling Domain	Model	Study	Ref	Episode	Average Error (%)	RMSE (ms ⁻¹)	Index of Agreement	Mean Wind Dir. Diff. (deg)
Southeastern U.S	RAMS	SAMI	7	24-29 May '95	35.0	1.90	0.76	13.0
Southeastern U.S	RAMS	SAMI	7	11-17 May '93	51.0	1.90	0.76	6.0
Southeastern U.S	RAMS	SAMI	7	23-31 Mar '93	53.0	2.27	0.74	100.0
Southeastern U.S	RAMS	SAMI	7	8-13 Feb '94	63.0	2.76	0.72	103.0
Southeastern U.S	RAMS	SAMI	7	3-12 Aug '93	140.0	2.18	0.75	25.0
Southeastern U.S	RAMS	SAMI	7	22-29 Jun '92	66.0	1.89	0.75	20.0
Southeastern U.S	RAMS	SAMI	7	24 Apr-3 May '91	60.0	2.35	0.81	4.0
Texas	MM5	COAST	11	4-11 Sept '93	61.4	2.20	0.69	15.0
Central Florida	MM5	PFOS-Episode 1	10	16-24 Apr '99	20.9	1.94	0.78	10.0
Central Florida	MM5	PFOS-Episode 2	10	2-10 May '97	21.0	1.95	0.78	32.0
Central Florida	MM5	PFOS-Episode 3	10	25-30 Aug '97	30.6	1.86	0.73	32.0
Central Florida	MM5	PFOS-Episode 4	10	4-10 April '97	18.1	1.80	0.80	8.0
Central Florida	MM5	PFOS-Episode 5	10	17-23 Sept '97	27.9	1.84	0.72	9.0
Central Florida	MM5	PFOS-Episode 9	10	20-28 Apr '98	24.0	1.79	0.78	26.4
Midwestern U.S.	MM5	Kansas/Missouri	8	11-24 Jun '95	16.7	2.20	0.80	20.0
Eastern U.S.	MM5	Pittsburgh SIP	1	31 July-2 Aug '95	12.6	1.78	0.75	8.0
Western U.S.	MM5	SARMAP	4	3-6 Aug '90	22.6	2.13	0.80	3.0
Upper Midwest	RAMS	CRC-LMOS	6	26-28 Jun '91	11.9	1.82	0.69	16.7
Upper Midwest	RAMS	CRC-LMOS	6	17-19 Jul '91	3.5	1.73	0.64	7.4
Upper Midwest	MM5	CRC-LMOS	6	26-28 Jun '91	5.8	1.70	0.79	14.0
Upper Midwest	MM5	CRC-LMOS	6	17-19 Jun '91	15.6	1.65	0.77	7.4
Eastern U.S.	RAMS	OTAG	3	13-21 Jul '91	4.6	1.61	0.74	27.1
Eastern U.S.	MM5	OTAG	3	13-21 Jul '91	23.0	1.92	0.73	17.0
Eastern U.S.	MM5	OTAG	2	1-11 Jul '88	65.6	3.21	0.64	7.9
Eastern U.S.	MM5	OTAG	1	12-15 Jul '95	21.2	1.91	0.68	15.2
Eastern U.S.	MM5	Cincinnati SIP	5	18-22 Jun '94	82.4	2.69	0.80	0.1
Southeastern U.S.	MM5	BAMP	9	6-11 Sep '93	89.4	2.36	0.60	21.5
Southeastern U.S.	MM5	BAMP	9	15-19 Aug '93	193.6	2.66	0.65	120.0
Maximum Value					3.5	1.61	0.60	0.1
Minimum Value					193.6	3.21	0.81	120.0
Mean Value					44.3	2.07	0.74	24.6
Standard Deviation					42.8	0.38	0.06	30.7
1 Sigma Range					1.5 to 87.1	1.69 to 2.45	0.68 to 0.80	0.0 to 55.3

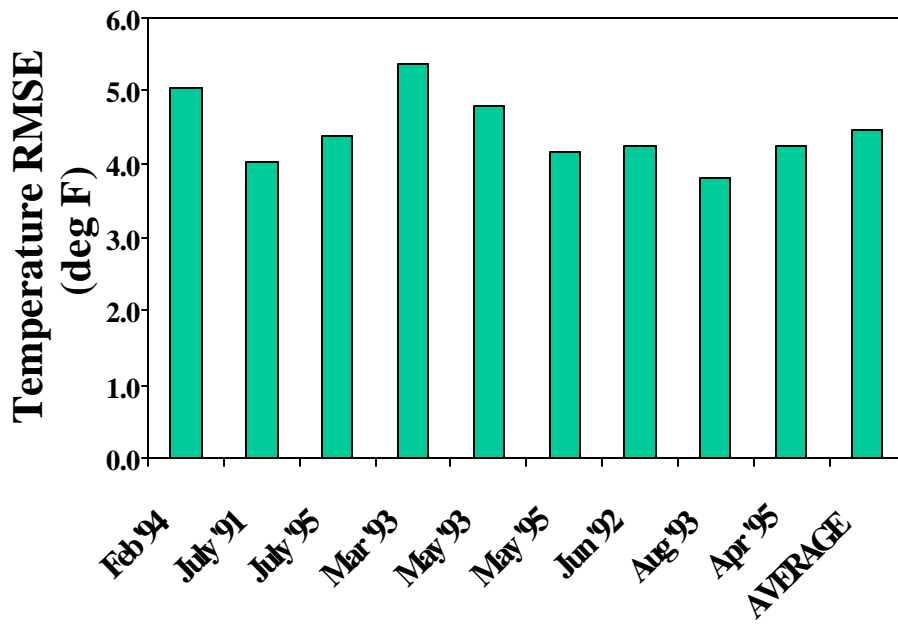
REFERENCES for Table 8-4.

1. McNally, D. E., and T. W. Tesche, 1996a. "Pittsburgh Regional Ozone Attainment Study: Evaluation of the MM5 Model for Three Episodes", prepared for the Pennsylvania Department of Environmental Protection, prepared by Alpine Geophysics, LLC, Ft. Wright, KY.
2. McNally, D. E., and T. W. Tesche, 1996b. "Evaluation of the MM5 Model for the 1-11 July 1998 OTAG Episode Over the Northeastern United States", prepared for the Pennsylvania Power and Light Company, prepared by Alpine Geophysics, LLC, Arvada, CO.

3. Tesche, T. W., and D. E. McNally, 1996. "Superregional Ozone Modeling and Analysis Study – Phase II, Work Element 5 Technical Report: Comparative Evaluation of the MM5 and RAMS Models for the July 1991 OTAG Episode", prepared for the Midwest Ozone Group, prepared by Alpine Geophysics, LLC, Ft. Wright, KY.
4. Tesche, T. W., and D. E. McNally, 1997. "The Use of the San Joaquin Valley Meteorological Model in Preparation of a Field Program in the South Coast Air Basin and Surrounding Regions of Southern California. Volume I: Final MM5 Evaluation for the 3-6 August 1990 SARMAP Episode", prepared for the California Air Resources Board, prepared by Alpine Geophysics, LLC, Ft. Wright, KY.
5. Tesche, T. W., and D. E. McNally, 1998. "Cincinnati-Hamilton Ozone Attainment Demonstration Study: Volume 5: Evaluation of the MM5 Model for the 18-22 June 1994 Episode", prepared for the Ohio Environmental Protection Agency", prepared by Alpine Geophysics, LLC, Ft. Wright, KY.
6. Tesche, T. W., and D. E. McNally, 1999. "Comparative Evaluation of the MM5 and RAMS3c Prognostic Meteorological Models over the Midwestern U.S. for Two 1991 LMOS Intensive Measurement Episodes", prepared for the Coordinating Research Council, prepared by Alpine Geophysics, LLC, Ft. Wright, KY.
7. Tesche, T. W., and D. E. McNally, 2000a. "Evaluation of the RAMS3c Prognostic Meteorological Model over the Southeastern U.S. for Three Southern Appalachian Mountain Initiative (SAMI) Episodes", draft final report prepared for the Tennessee Valley Authority and SAMI, prepared by Alpine Geophysics, LLC, Ft. Wright, KY.
8. Tesche, T. W., and D. E. McNally, 200b. "Evaluation of the MM5 Mesoscale Model Over the Central U.S. For the 11-24 June 1995 Ozone Episode", prepared for the Kansas Department of Health and Environment and the U.S. Environmental Protection Agency", prepared by Alpine Geophysics, LLC, Ft. Wright, KY.
9. Tesche, T. W., and D. E. McNally, 1998. "Evaluation of the MM5 Model for Two 1993 Regional Ozone Episodes over the Gulf Coast", prepared for the Minerals Management Service and the Offshore Operators Committee, prepared by Alpine Geophysics, LLC, Ft. Wright, KY.
10. Tesche, T. W., and D. E. McNally, 2001a. "Evaluation of the MM5 Prognostic Meteorological Model over Central Florida for Nine Peninsular Florida Ozone Study (PFOS) 8-hr Ozone Episodes", report prepared for the Florida Department of Environmental Protection Agency, prepared by Alpine Geophysics, LLC, Ft. Wright, KY.
11. Tesche, T. W., and D. E. McNally, 2001. "Application of the MM5 Prognostic Meteorological Model over the South Central U.S. for the September 1993 COAST Ozone Episode", prepared by Alpine Geophysics, LLC, Ft. Wright, KY.

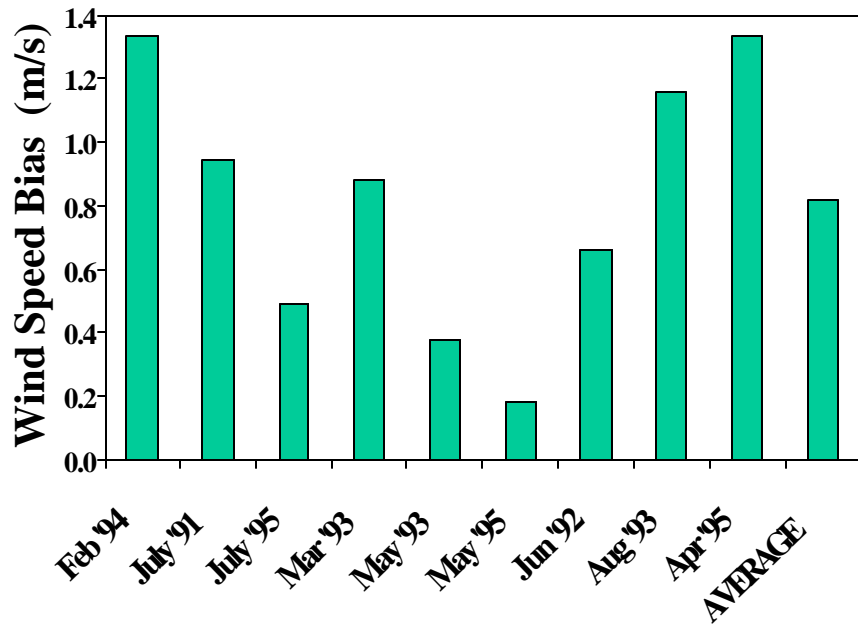


(a) Bias

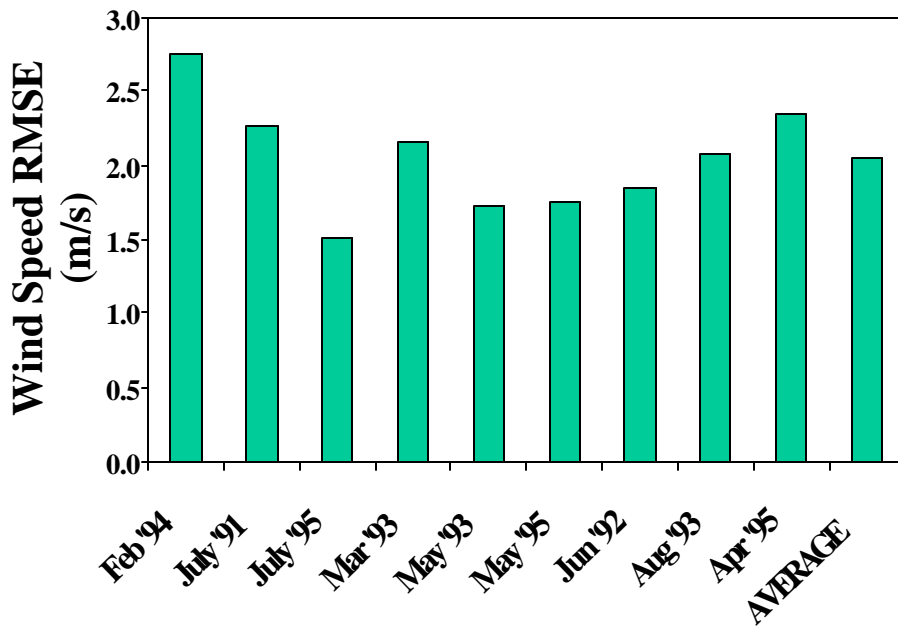


(b) RMSE

Figure 8-1. Episode Average 2m Temperature Statistics for all SAMI Episodes.

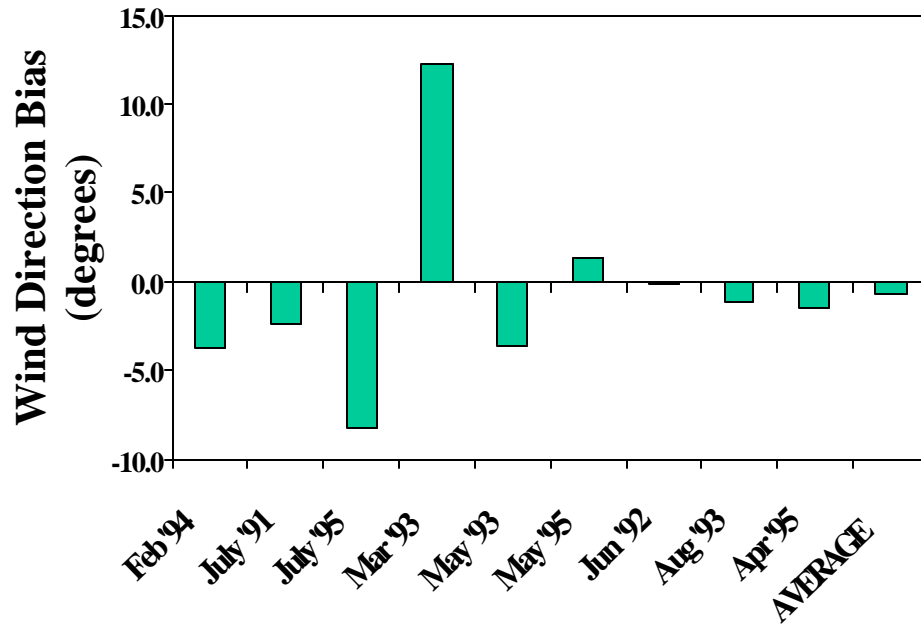


(a) Bias

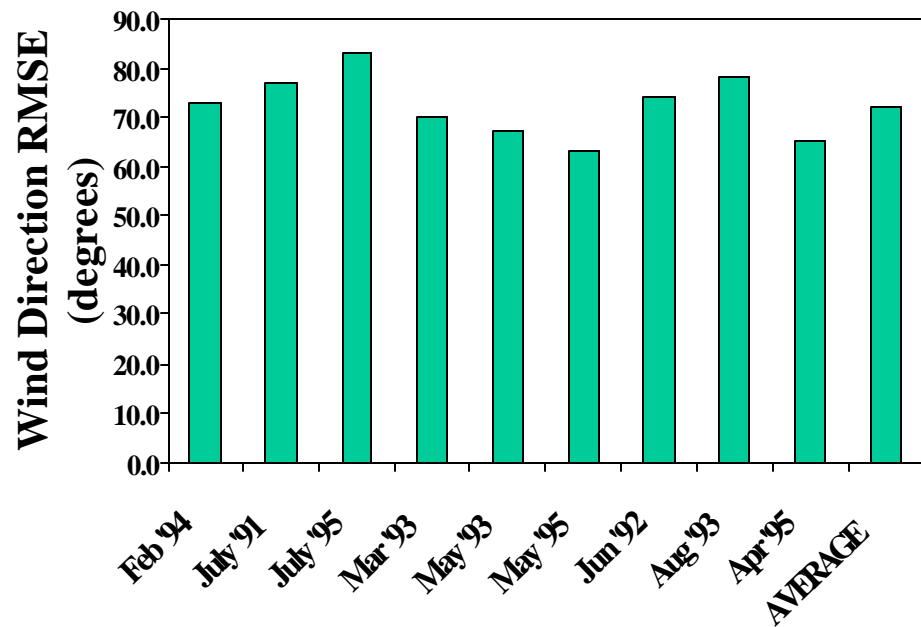


(b) RMSE

Figure 8-2. Episode Average 10 m Wind Speed Statistics for all SAMI Episodes.

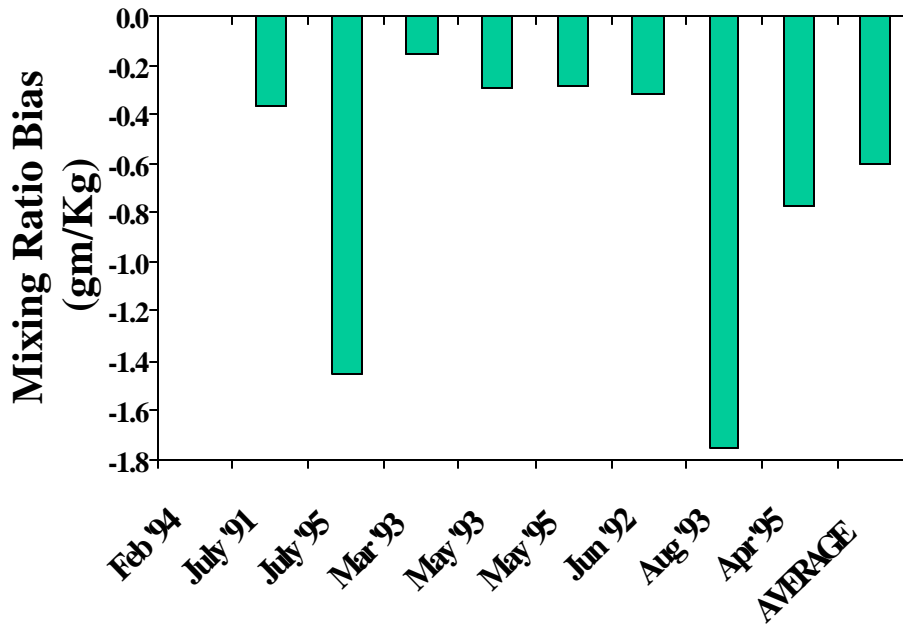


(a) Bias

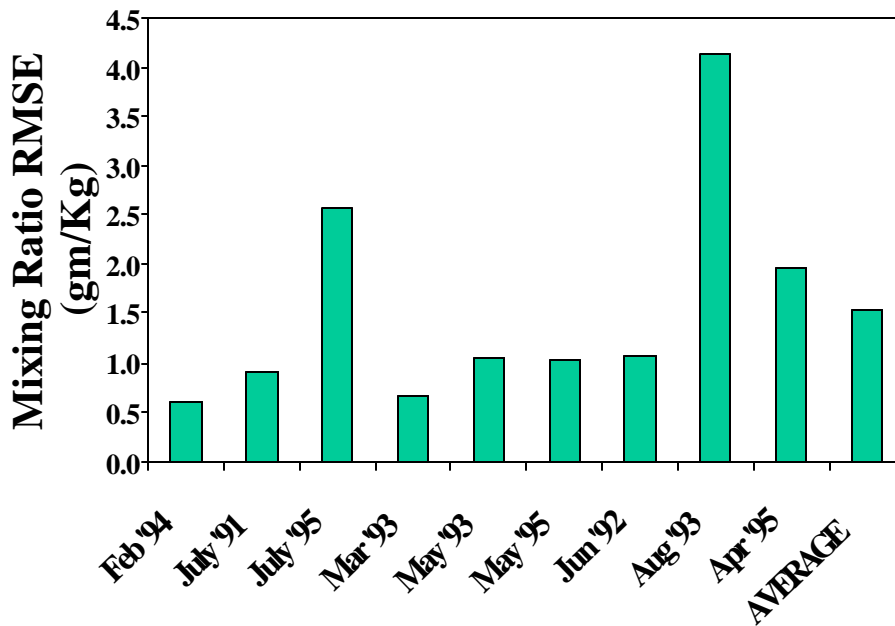


(b) RMSE

Figure 8-3. Episode Average 10 m Wind Direction Statistics for all SAMI Episodes.

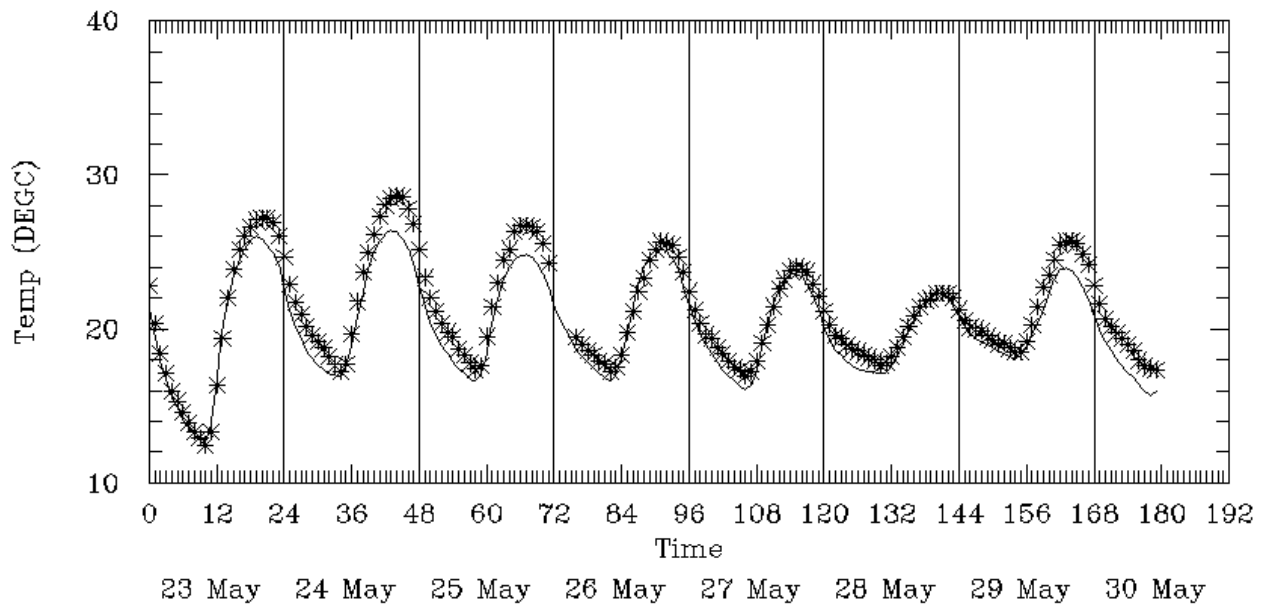


(a) Bias

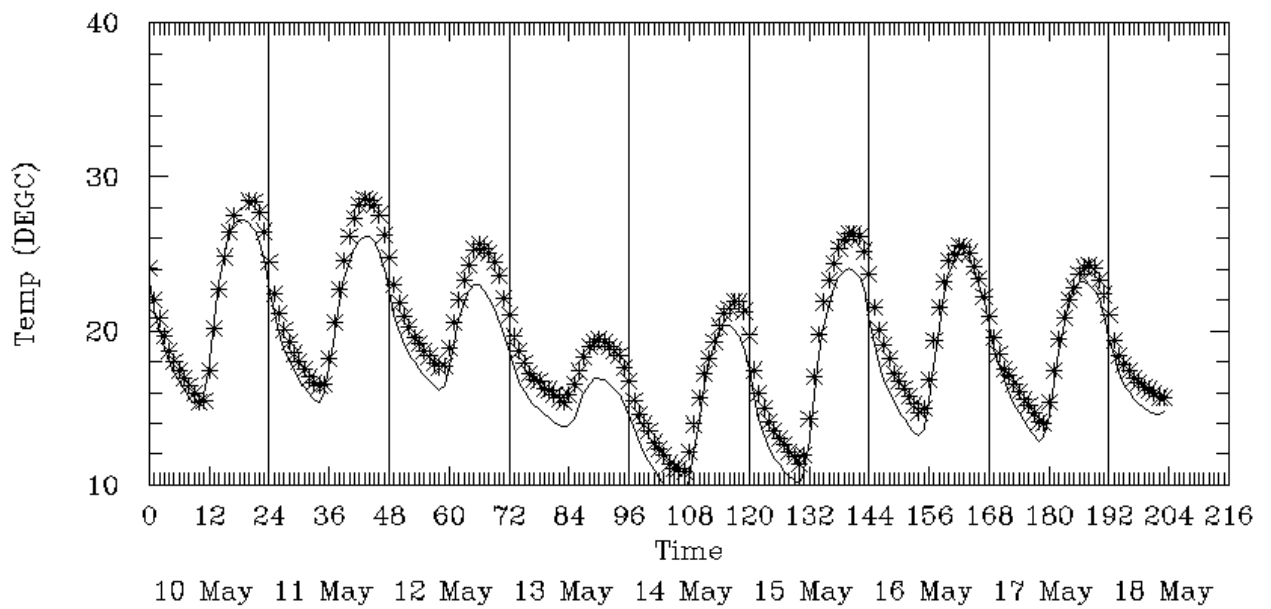


(b) RMSE

Figure 8-4. Episode Average 2m Mixing Ratio Statistics for all SAMI Episodes. (We suspect the poor mixing ratio statistics for the July 1995 and August 1993 episodes is due to a breakdown in the surface layer vertical extrapolation scheme more than an indication of poor model performance).

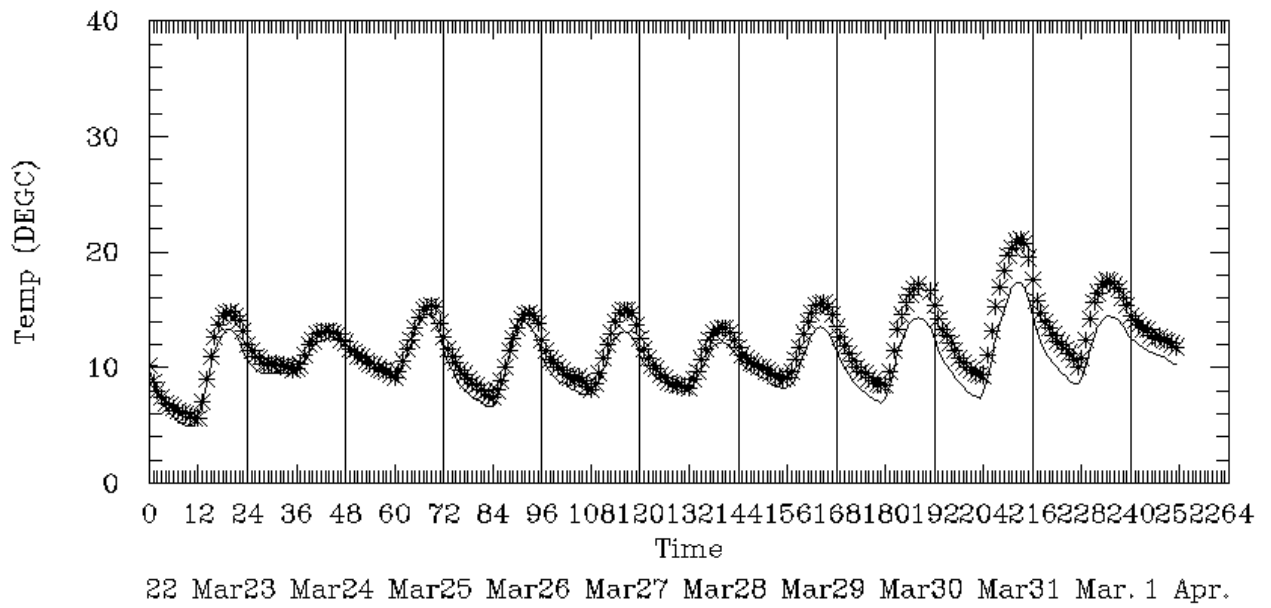


(a) 24-29 May 1995

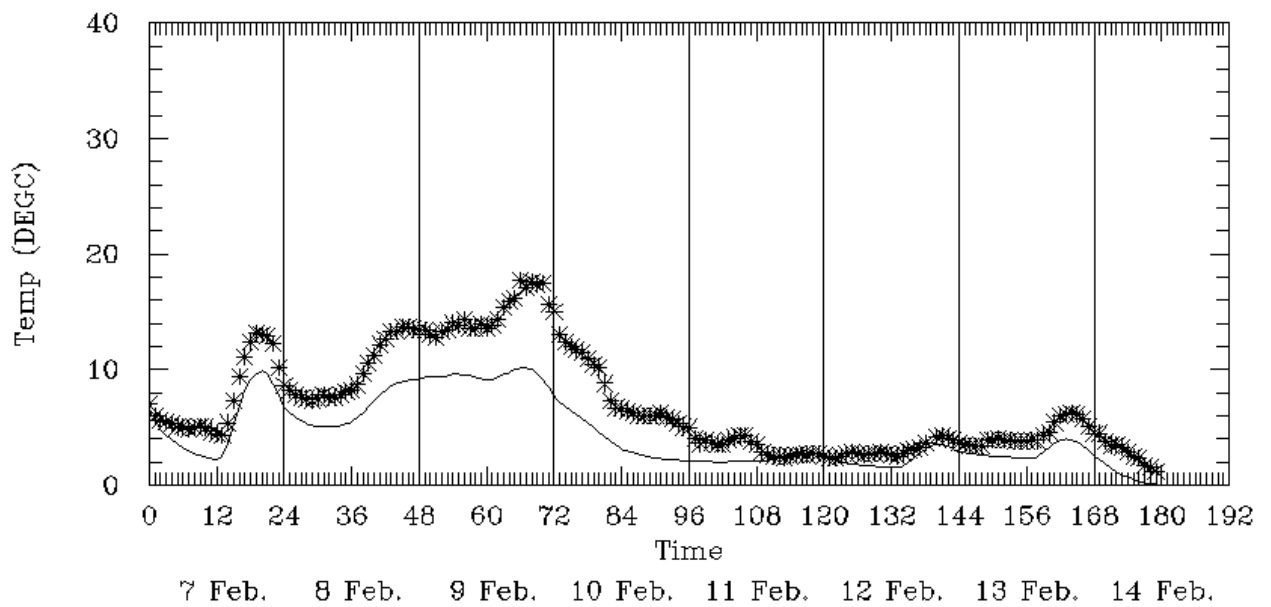


(b) 11-17 May 1993

Figure 8-5. Spatial Mean Ground-Level Temperatures for Seven SAMI Episodes.

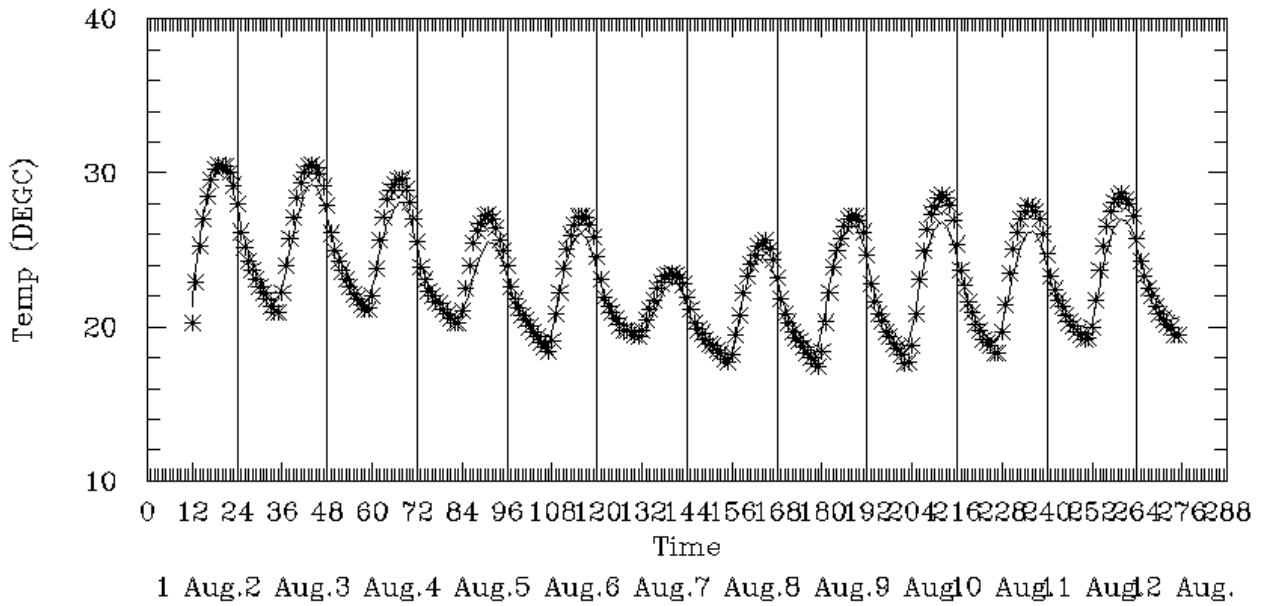


(c) 23-31 March 1993

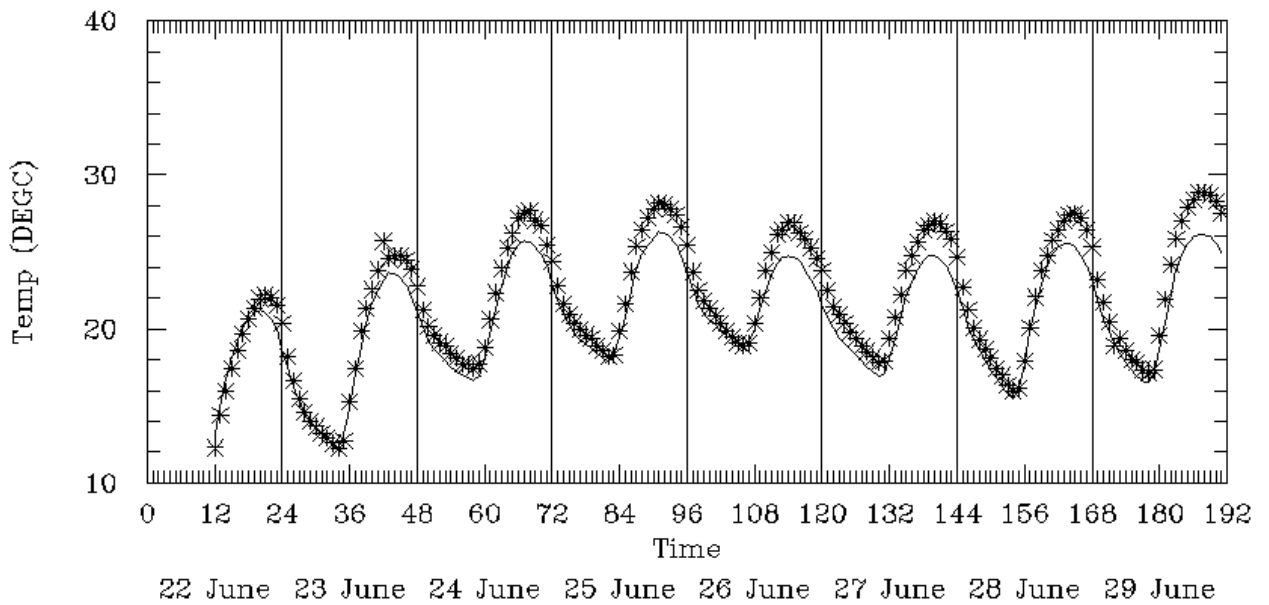


(d) 8-13 February 1994

Figure 8-5. Continued.

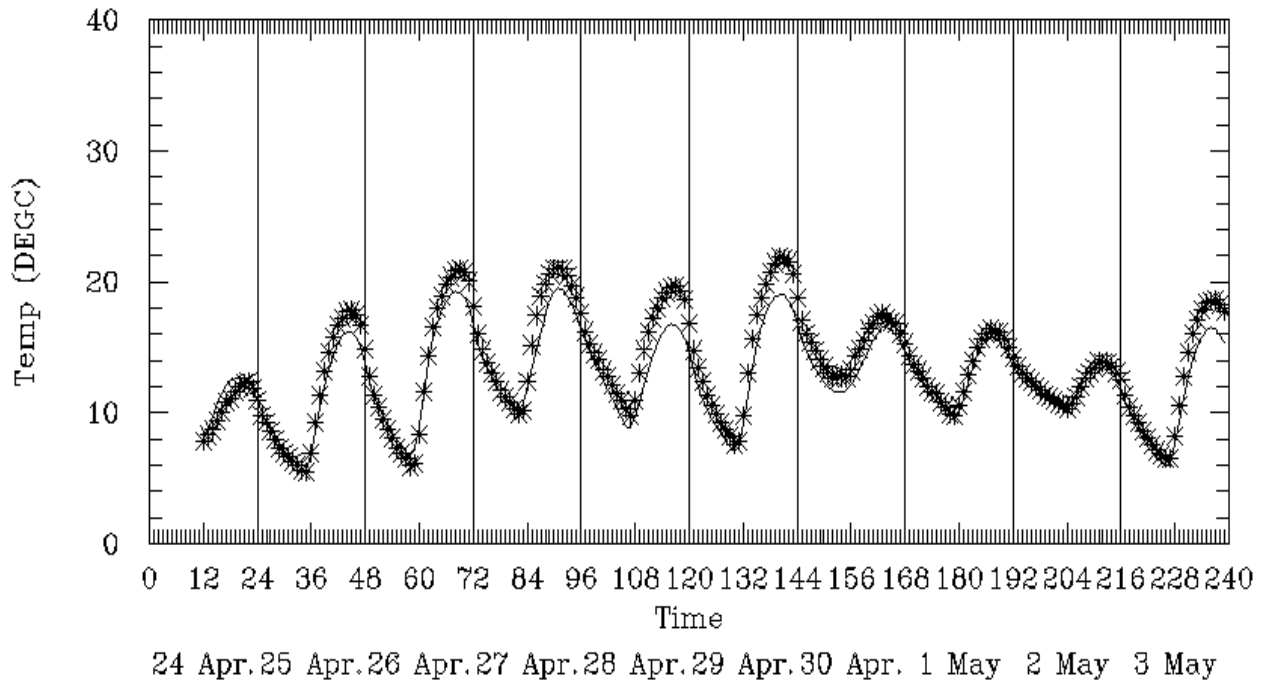


(e) 3-12 August 1993



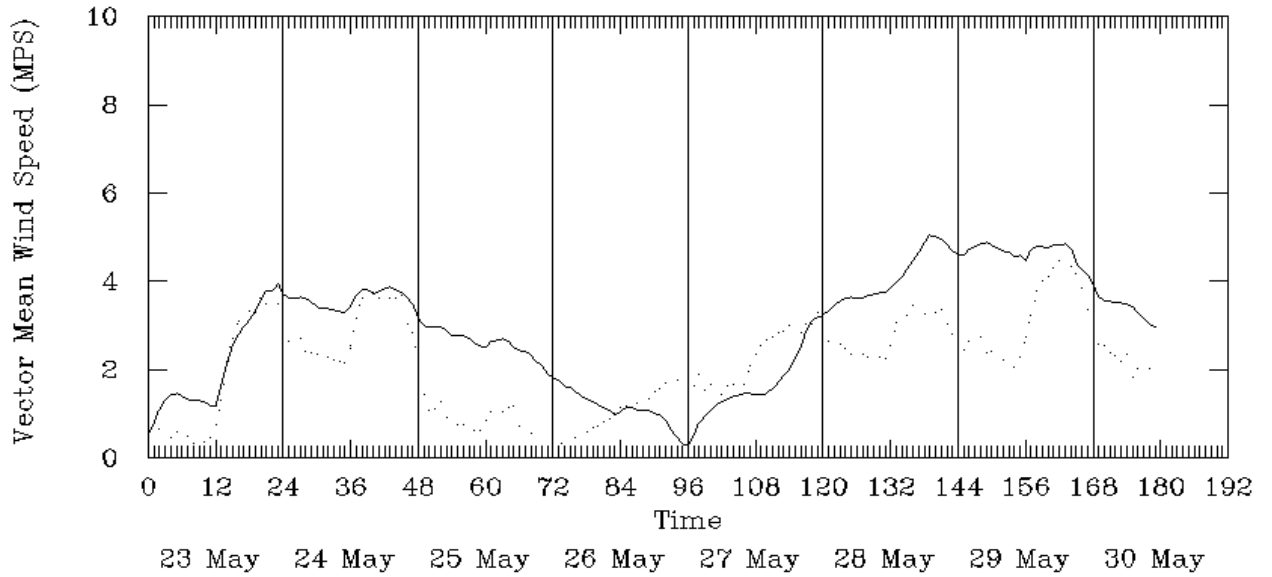
(f) 22-29 June 1992

Figure 8-5. Continued.

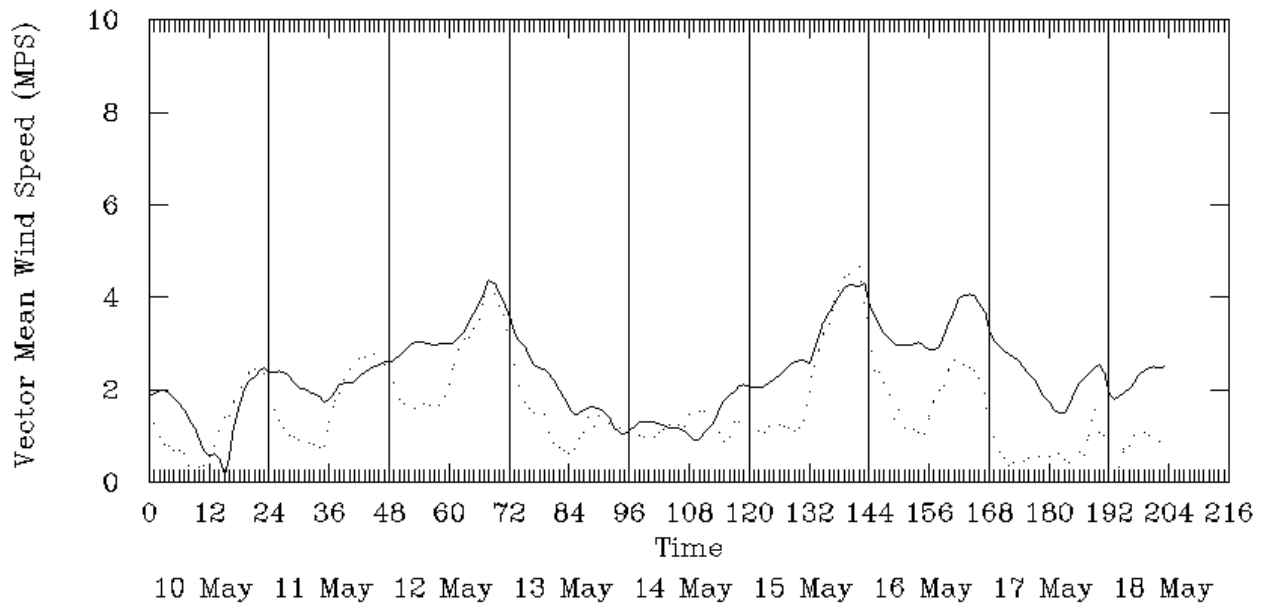


(g) 24 April – 3 May 1995

Figure 8-5. Concluded.

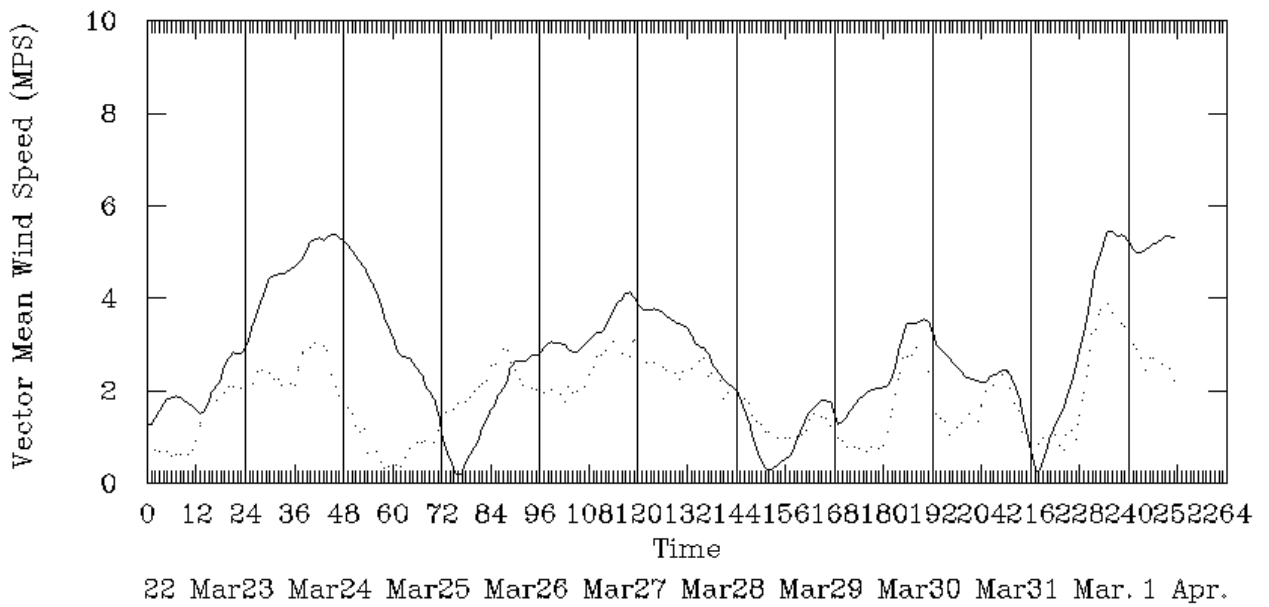


(a) 24-29 May 1995

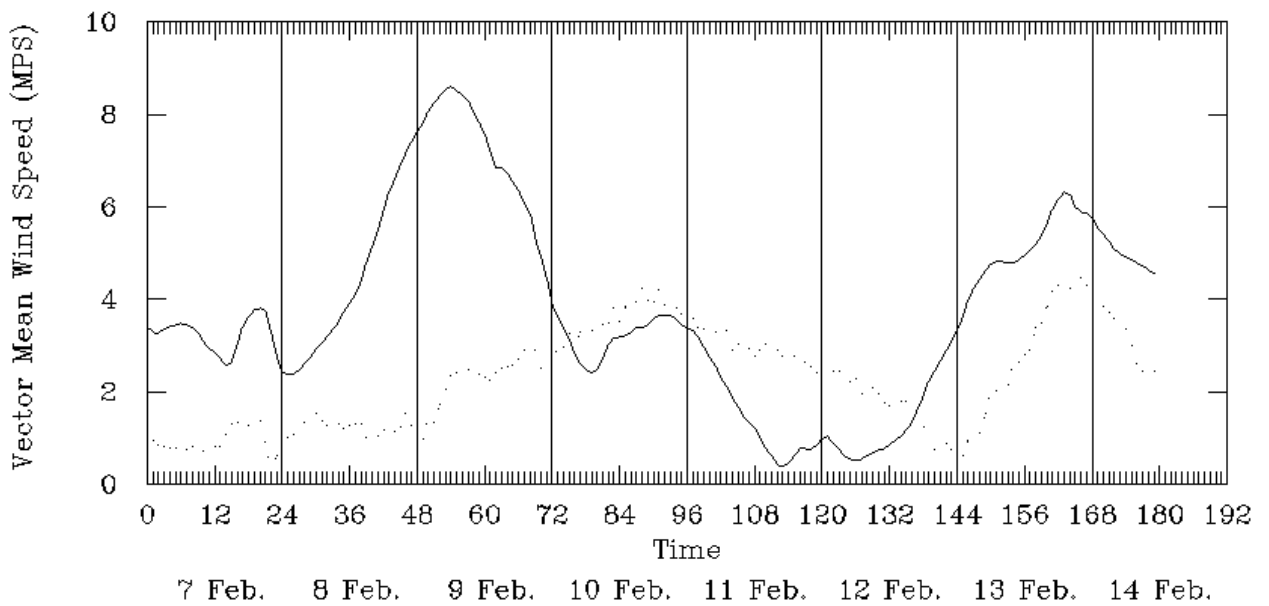


(b) 11-17 May 1993

Figure 8-6. Vector Mean Ground-Level Wind Speeds for Seven SAMI Episodes.

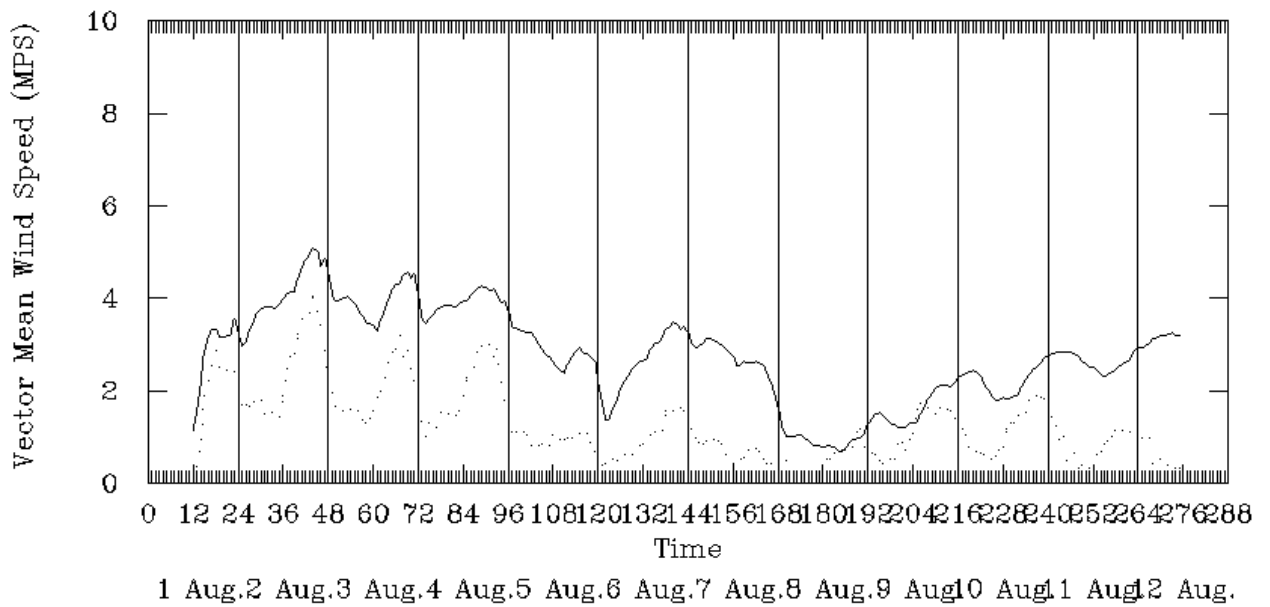


(c) 23-31 March 1993

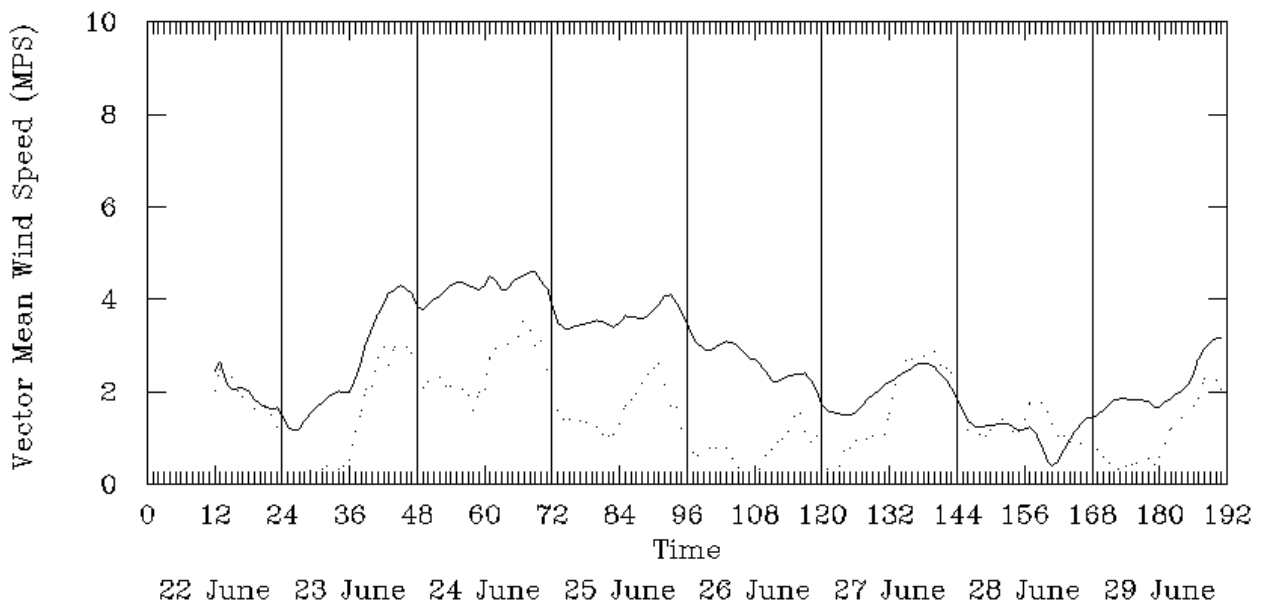


(d) 8-13 February 1994

Figure 8-6. Continued.

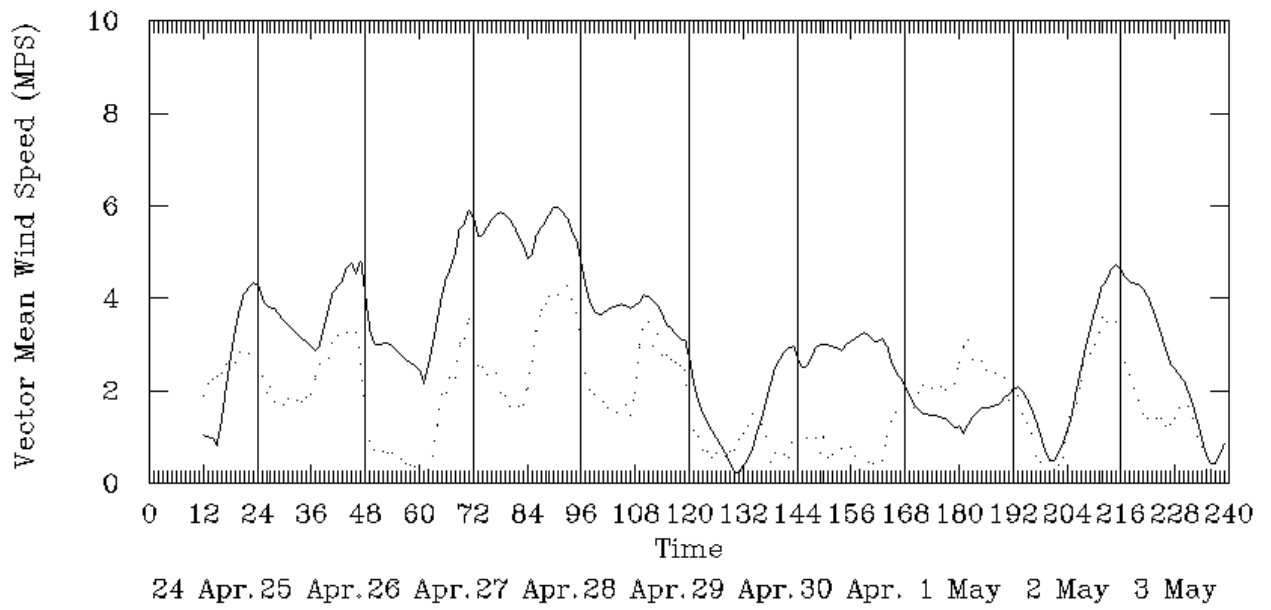


(e) 3-12 August 1993



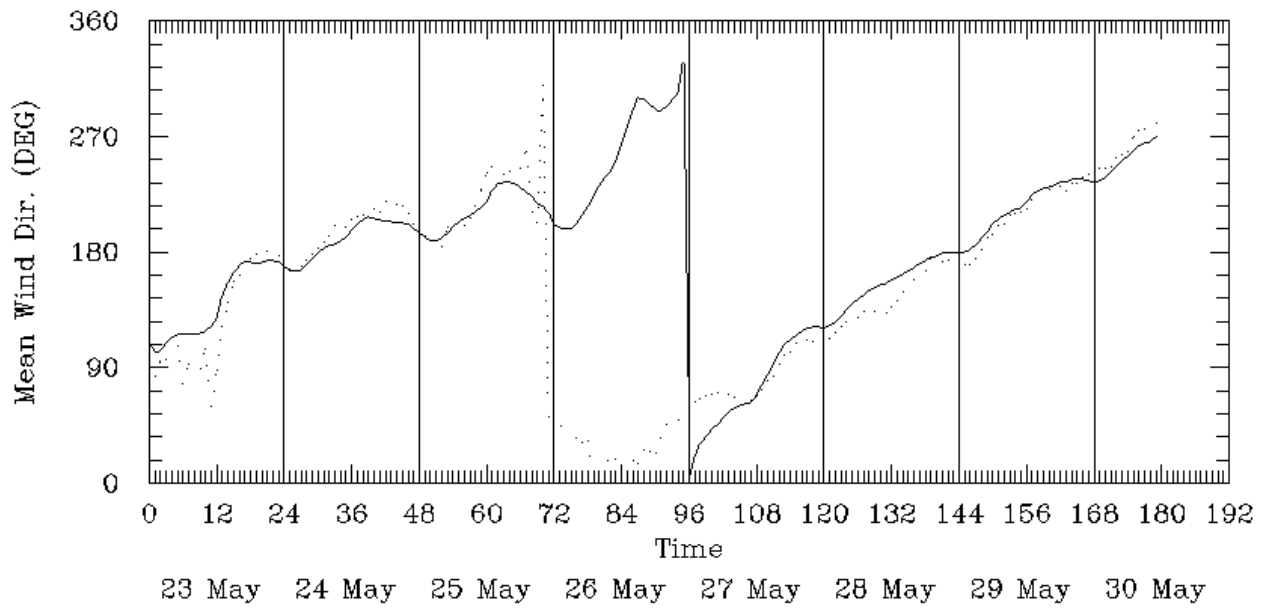
(f) 22-29 June 1992

Figure 8-6. Continued.

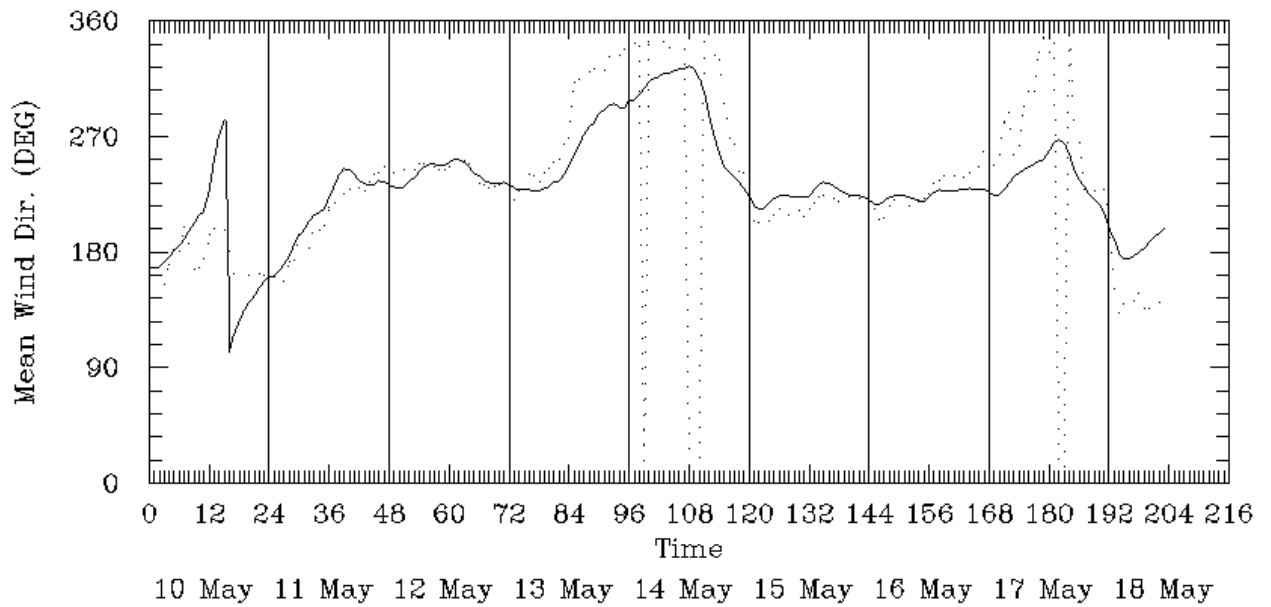


(g) 24 April – 3 May 1995

Figure 8-6. Concluded.

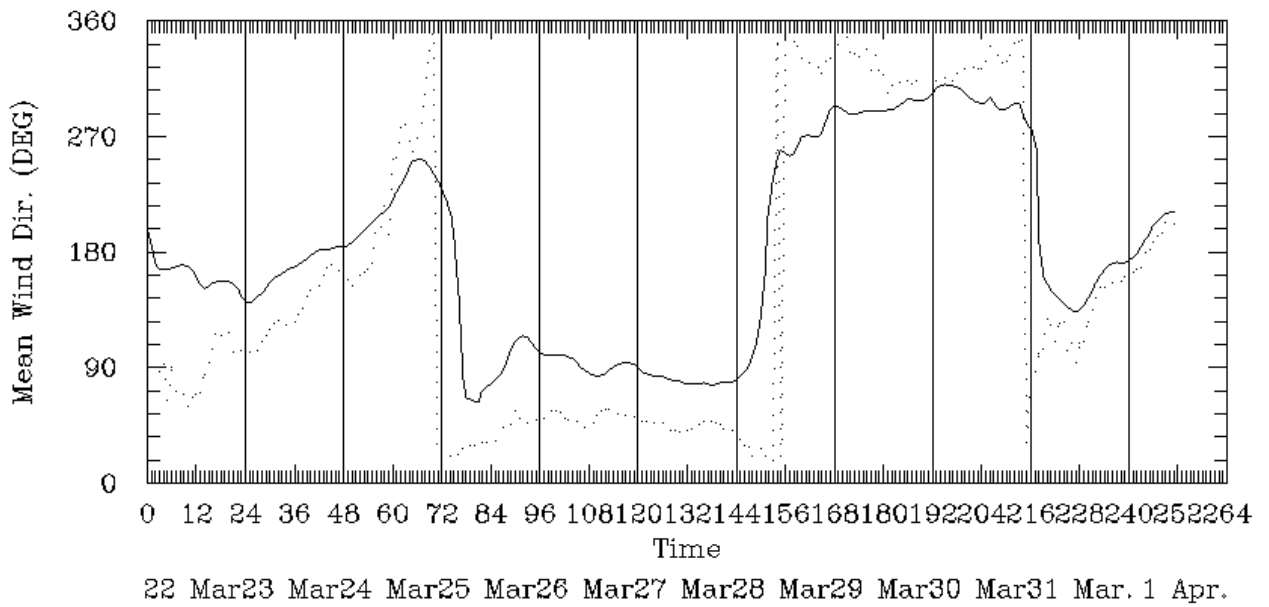


(a) 24-29 May 1995

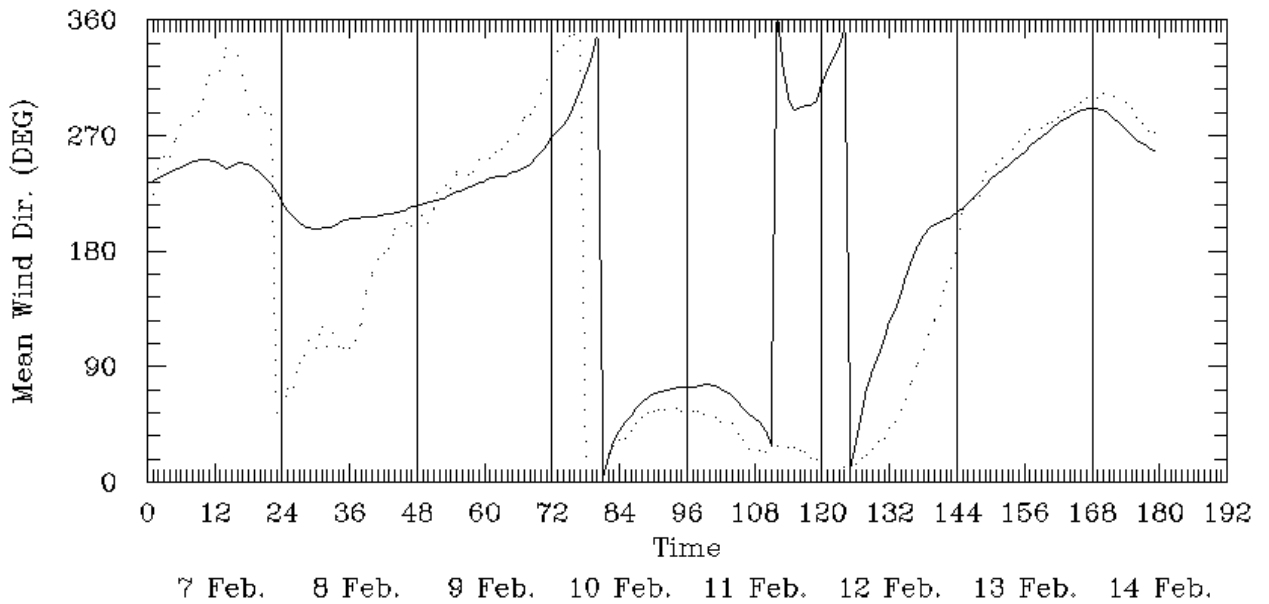


(b) 11-17 May 1993

Figure 8-7. Mean Ground-Level Wind Direction for Seven SAMI Episodes.

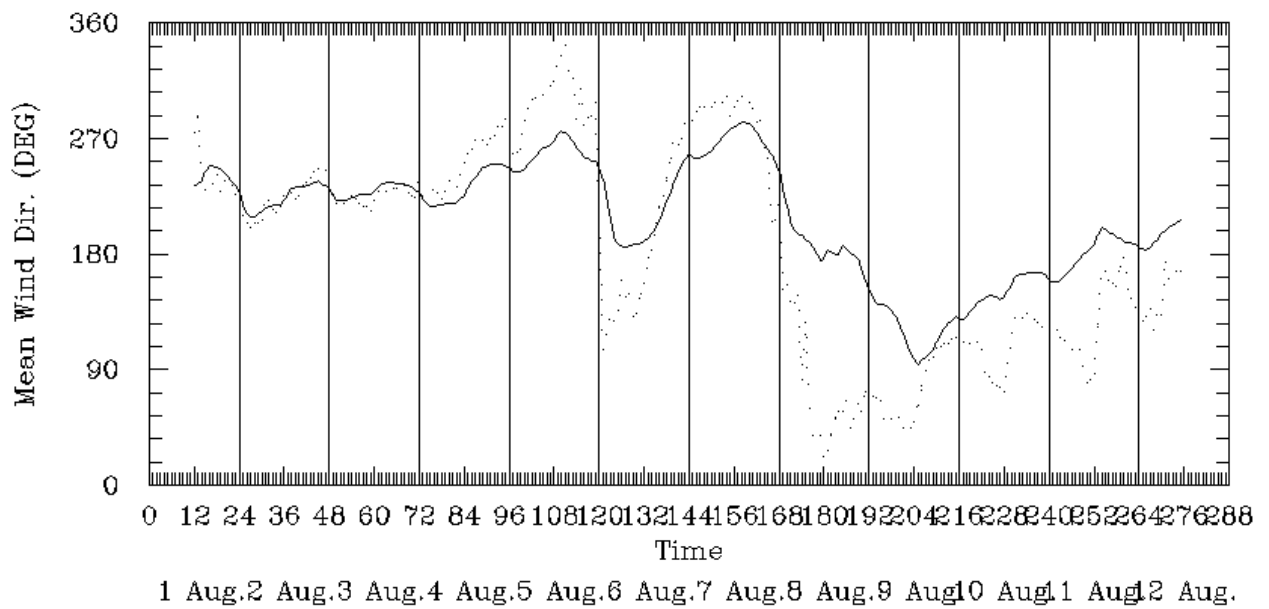


(c) 23-31 March 1993

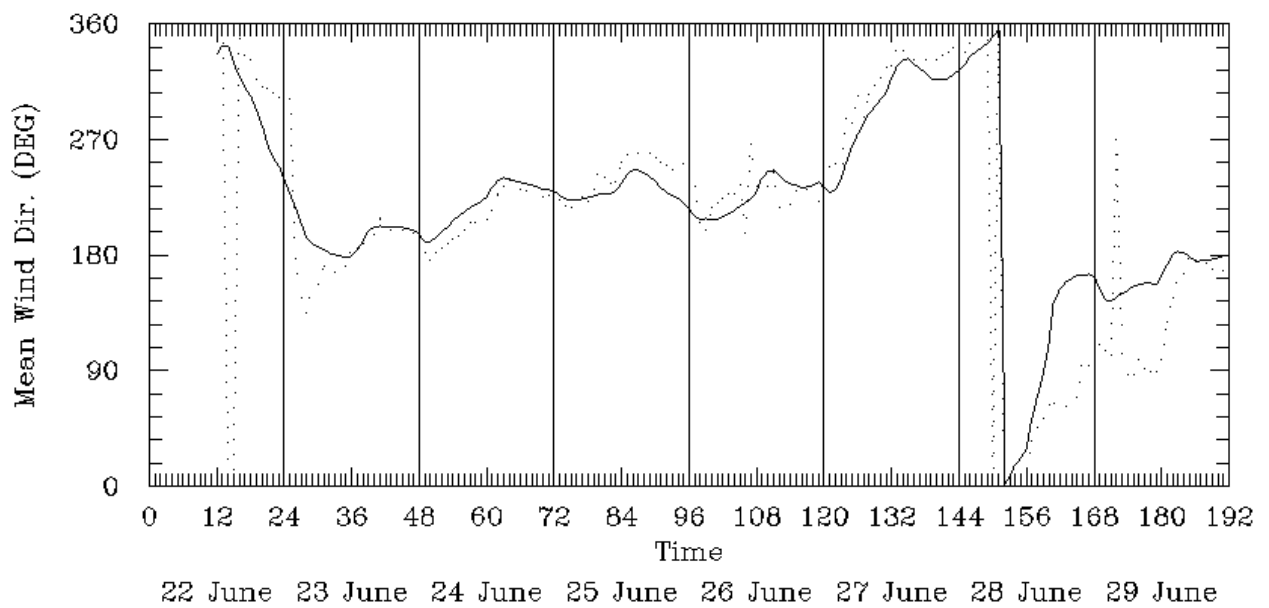


(d) 8-13 February 1994

Figure 8-7. Continued.

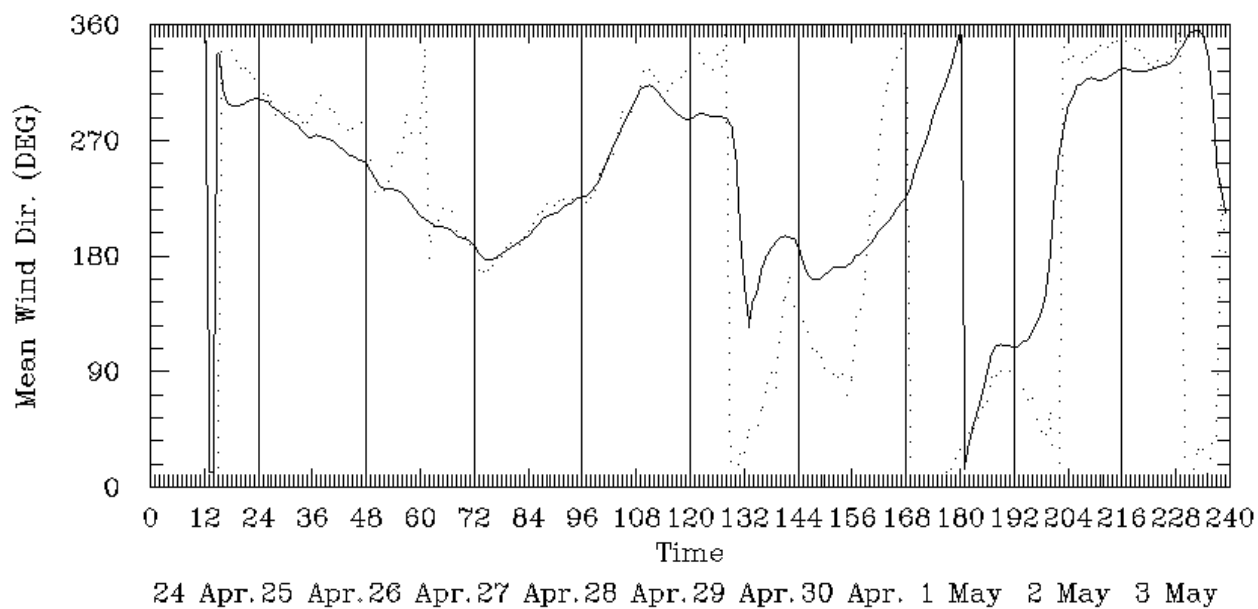


(e) 3-12 August 1993



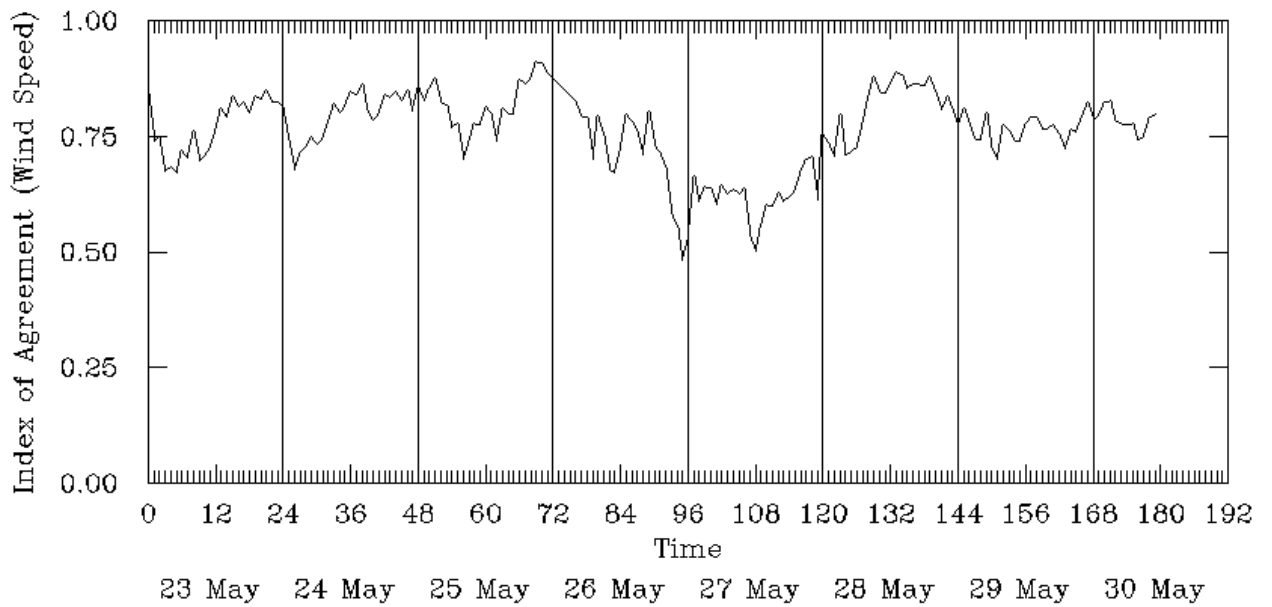
(f) 22-29 June 1992

Figure 8-7. Continued.

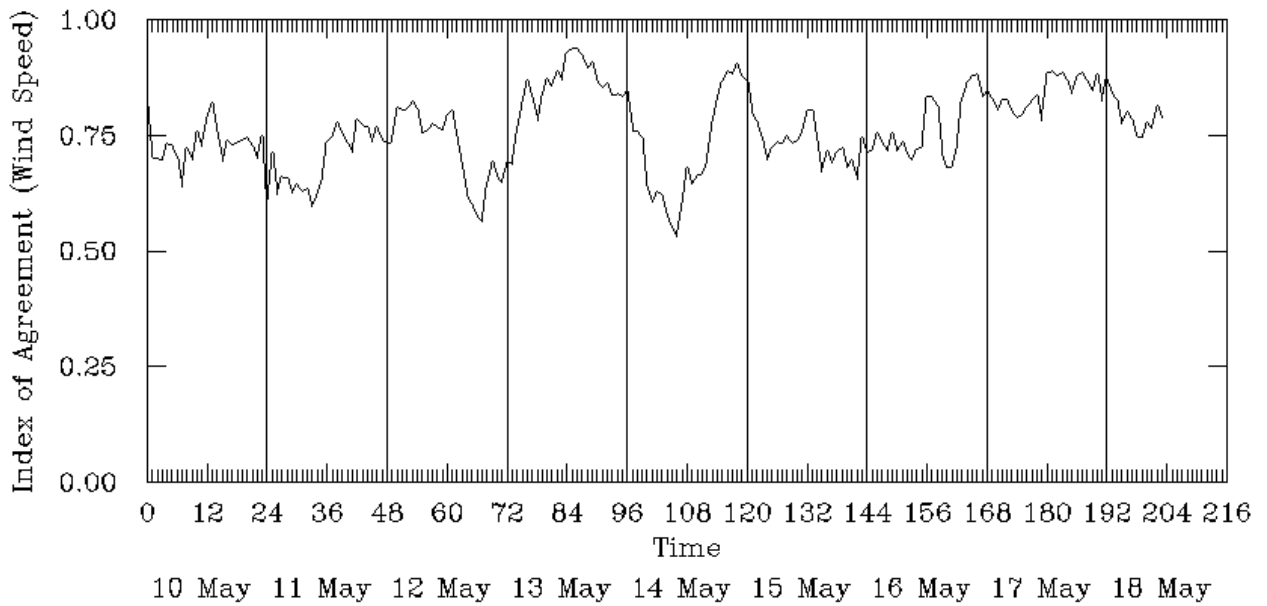


(g) 24 April – 3 May 1995

Figure 8-7. Concluded.

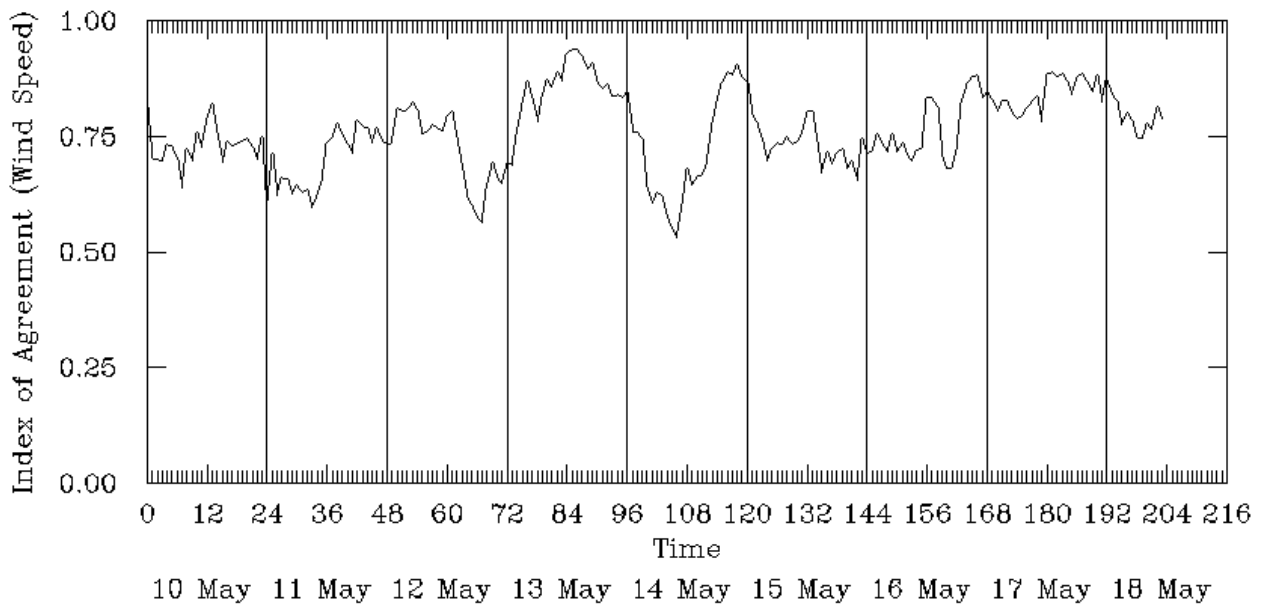


(a) 24-29 May 1995

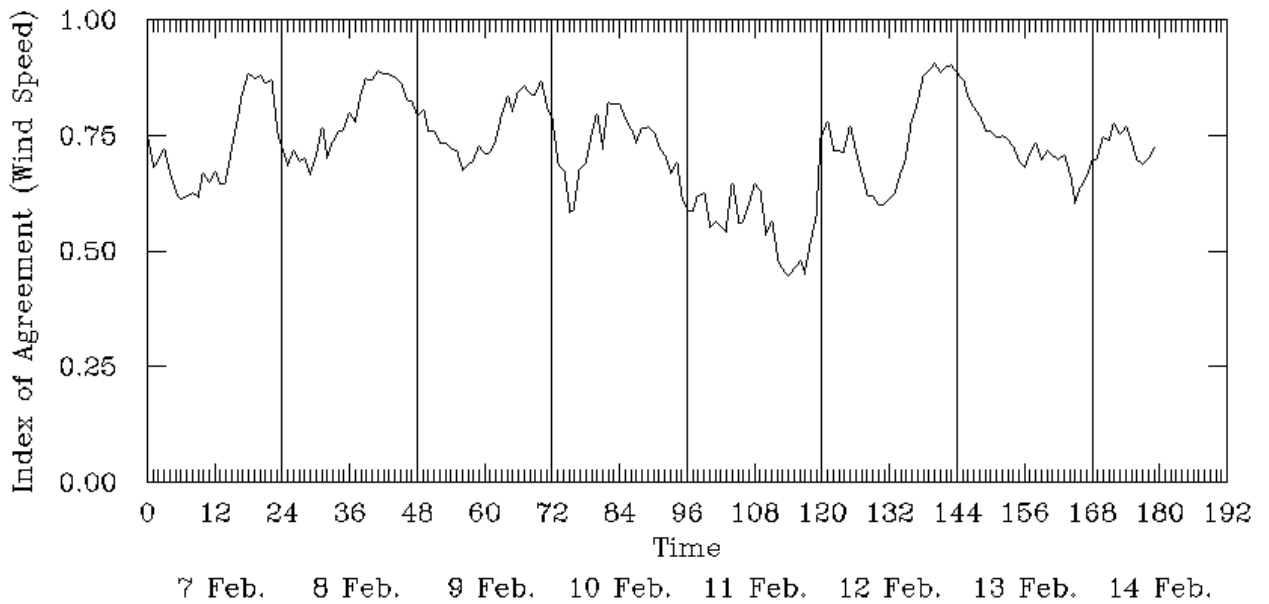


(b) 11-17 May 1993

Figure 8-8. Index of Agreement in Ground-Level Wind Speeds for Seven SAMI Episodes.

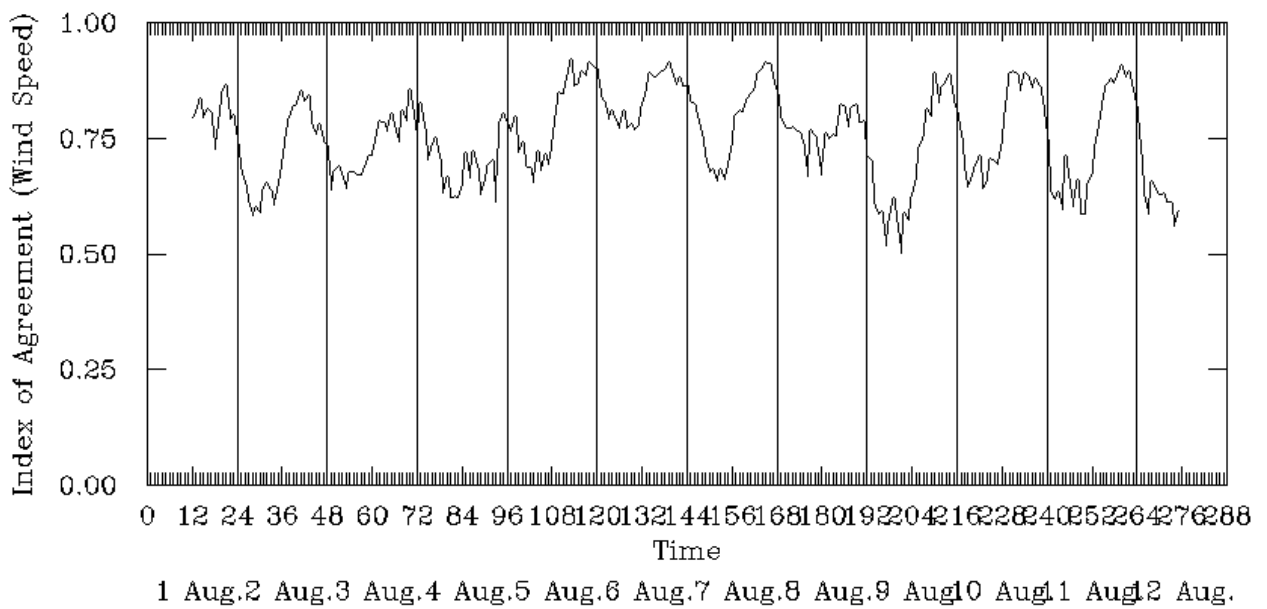


(c) 23-31 March 1993

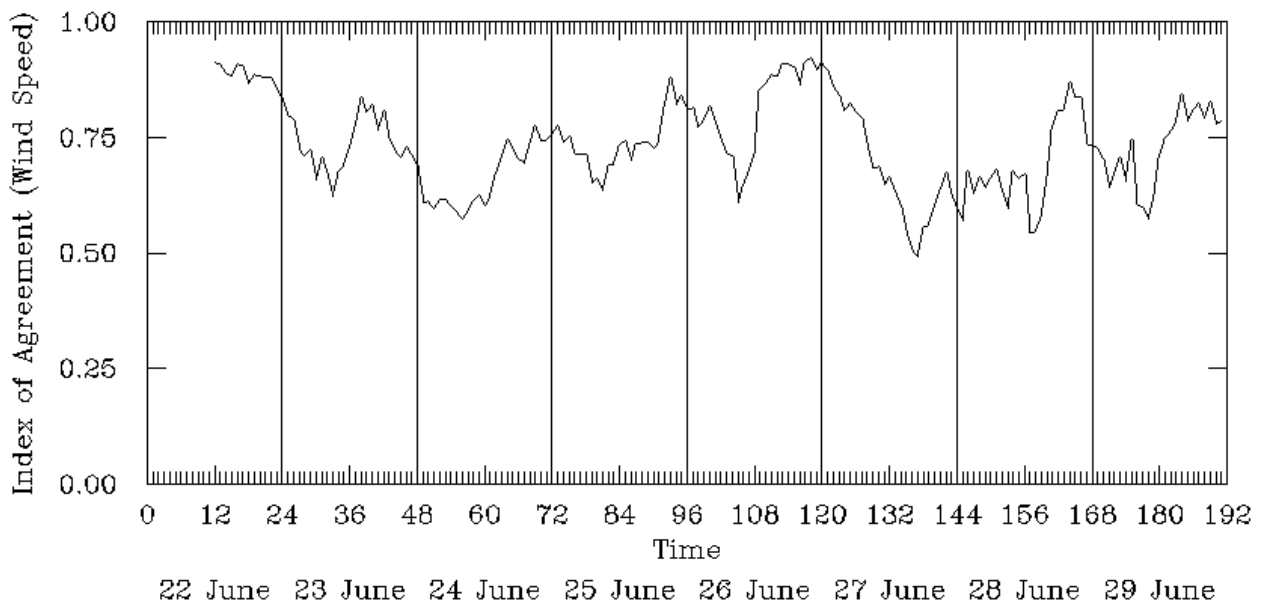


(d) 8-13 February 1994

Figure 8-8. Continued.

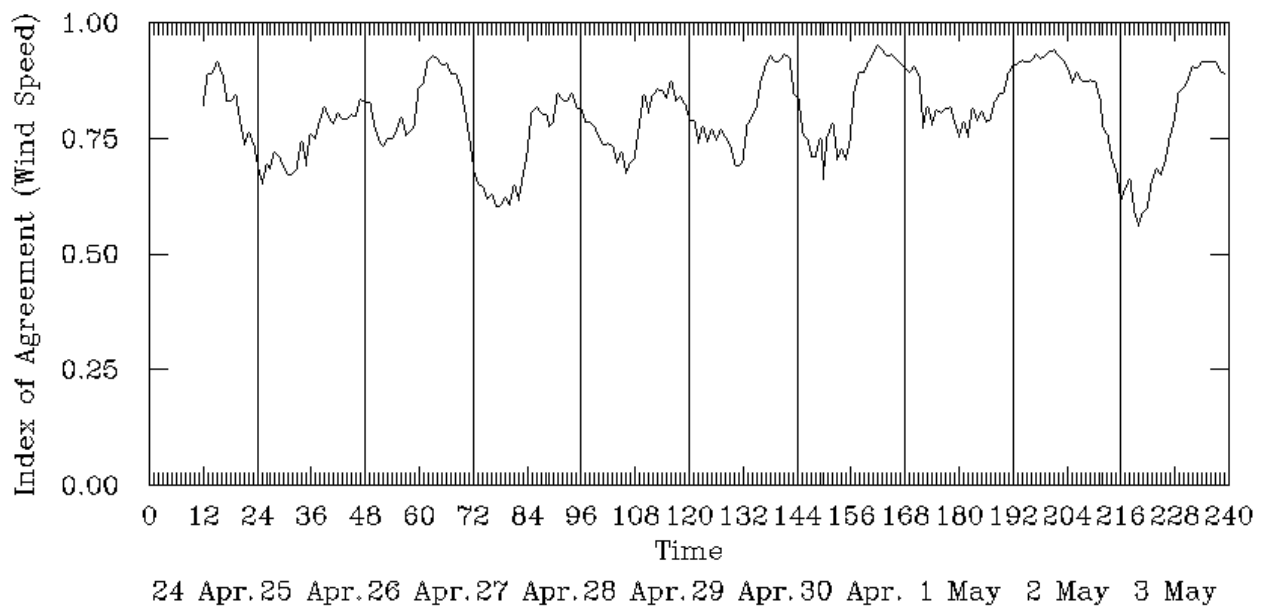


(e) 3-12 August 1993



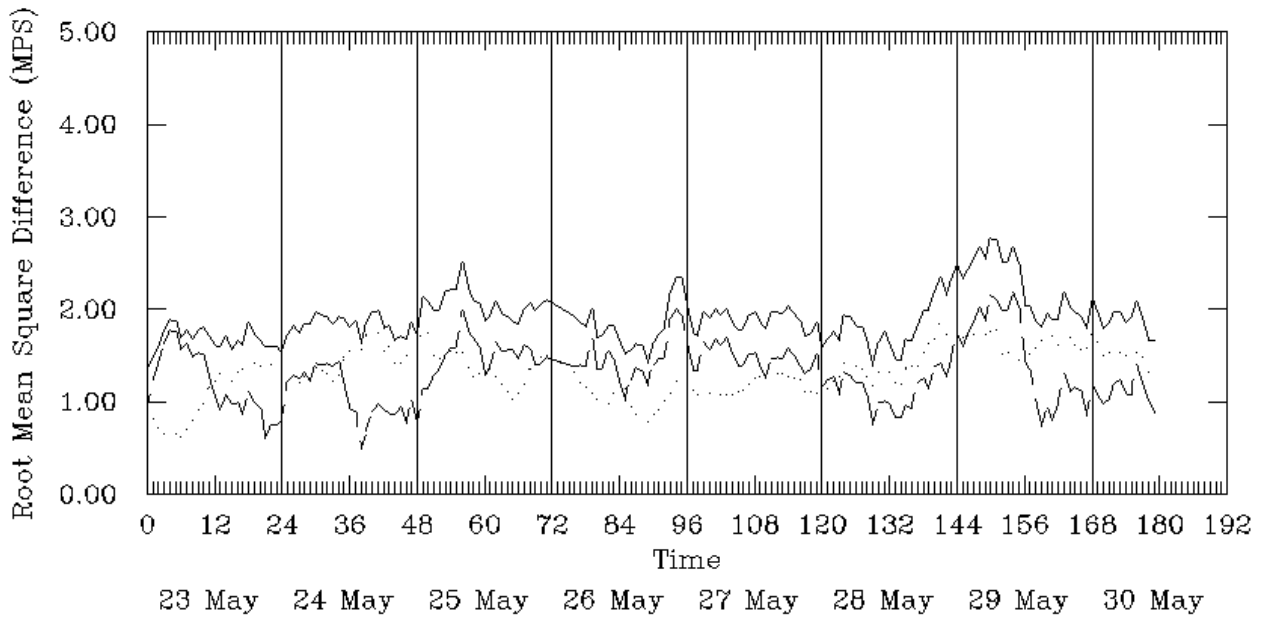
(f) 22-29 June 1992

Figure 8-8. Continued.

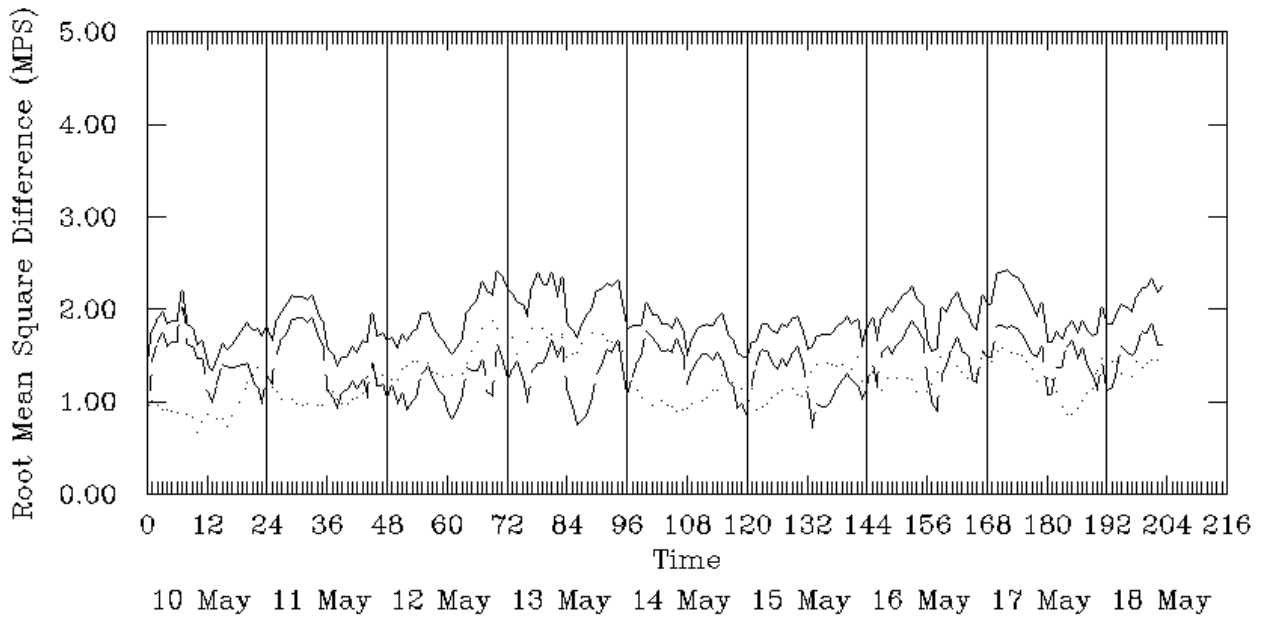


(g) 24 April – 3 May 1995

Figure 8-8. Concluded.

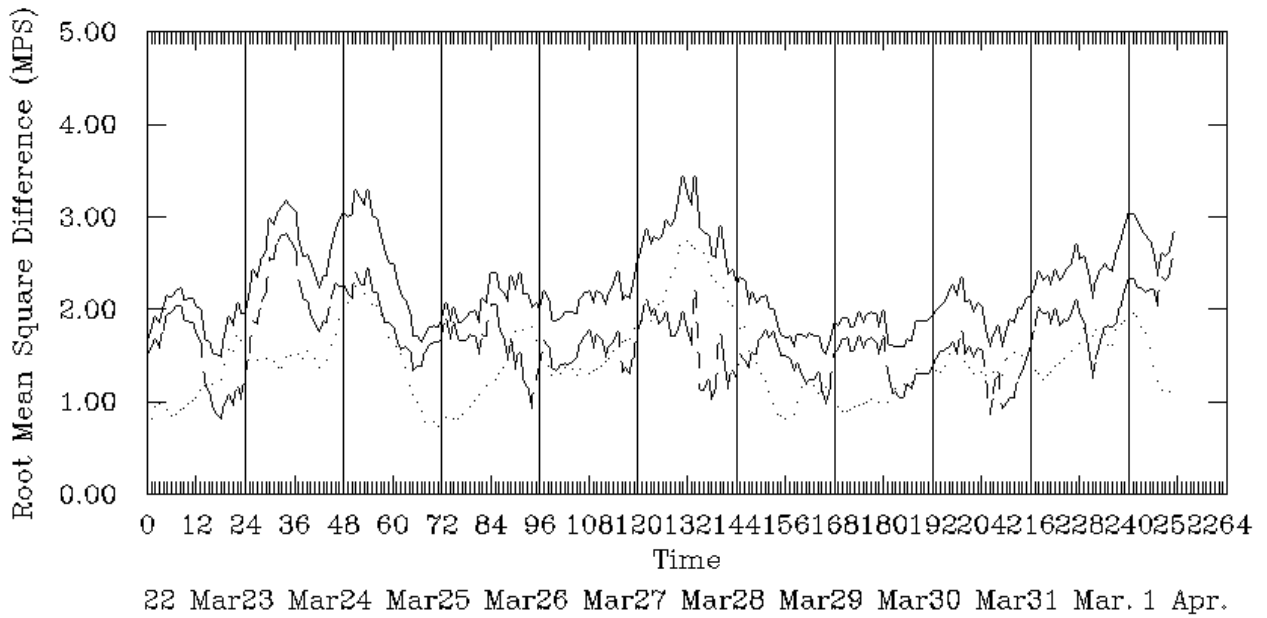


(a) 24-29 May 1995

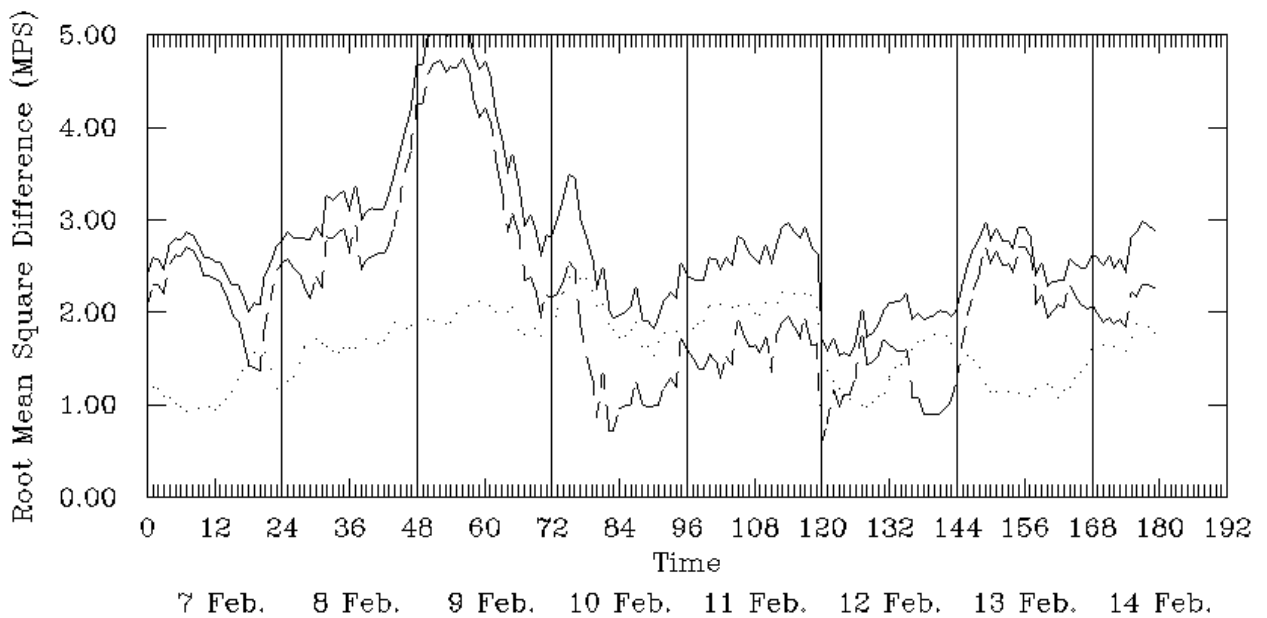


(b) 11-17 May 1993

Figure 8-9. RMSE Errors in Ground-Level Wind Speeds for Seven SAMI Episodes.

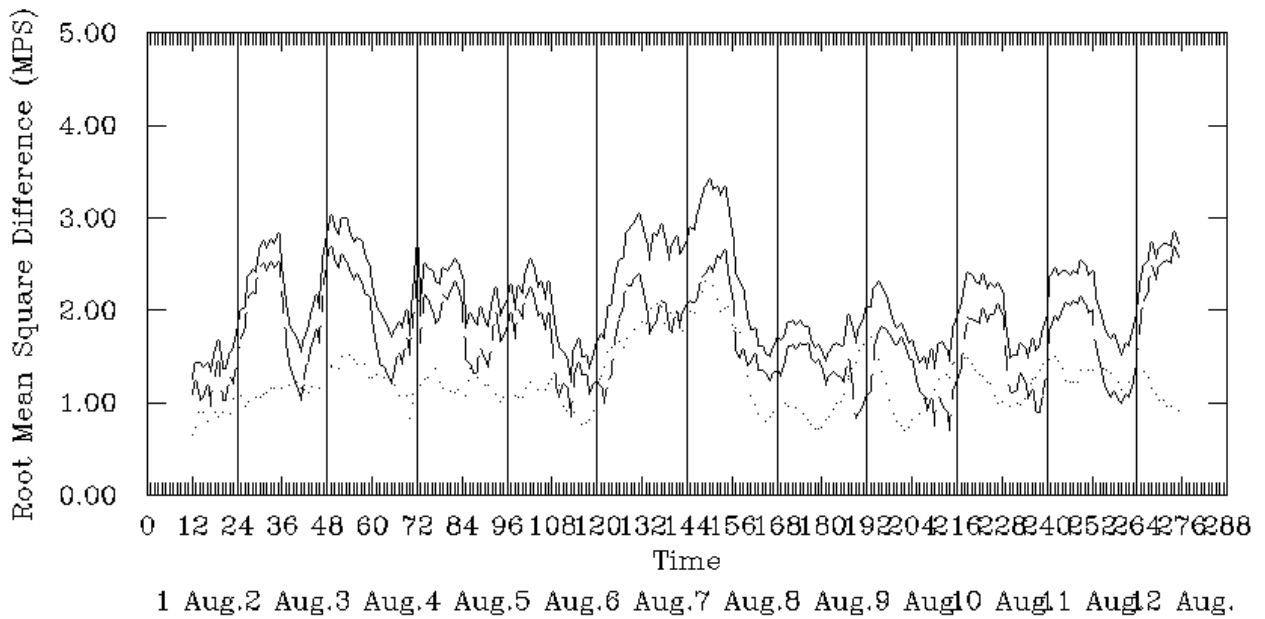


(c) 23-31 March 1993

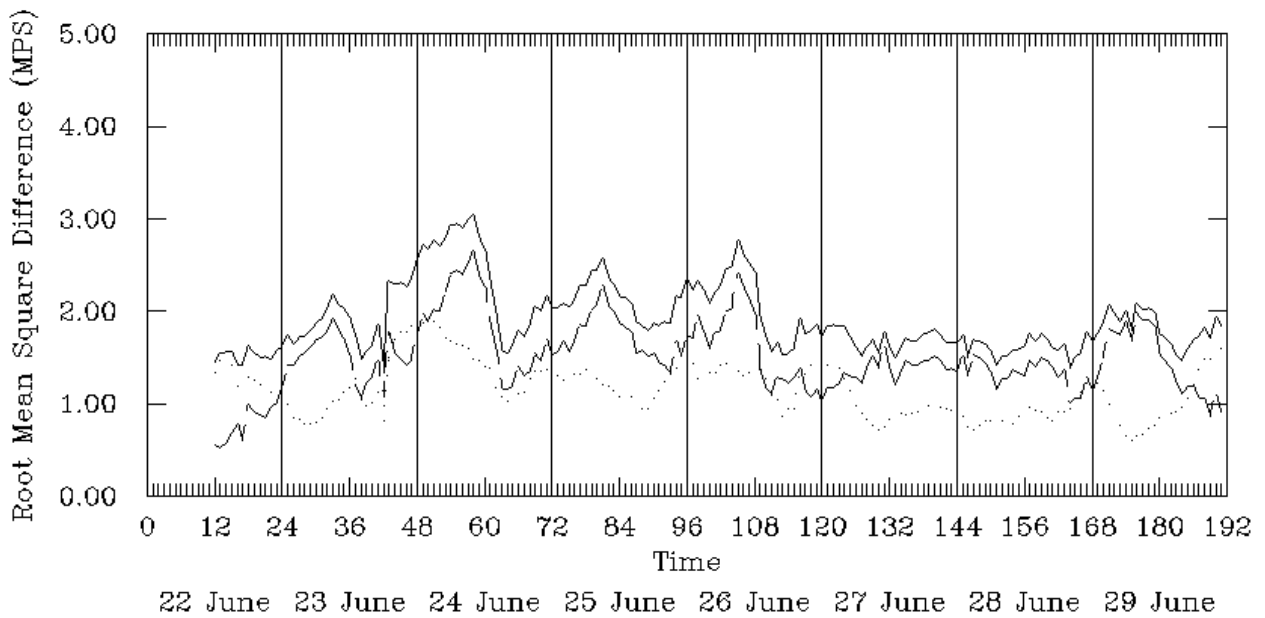


(d) 8-13 February 1994

Figure 8-9. Continued.

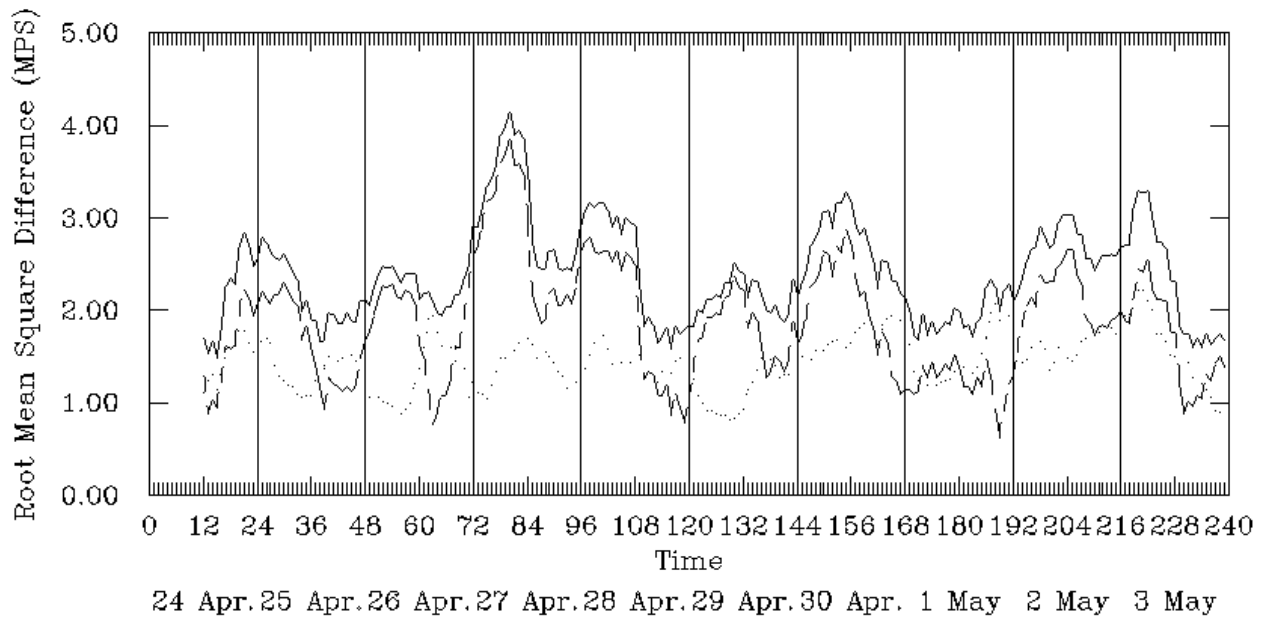


(e) 3-12 August 1993



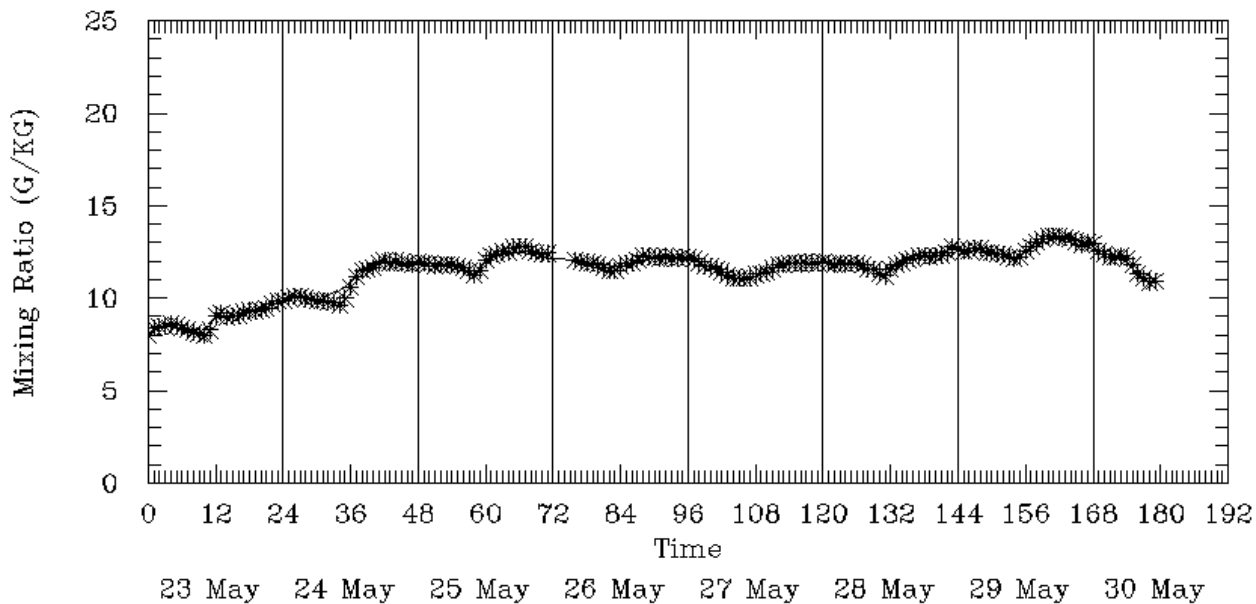
(f) 22-29 June 1992

Figure 8-9. Continued.

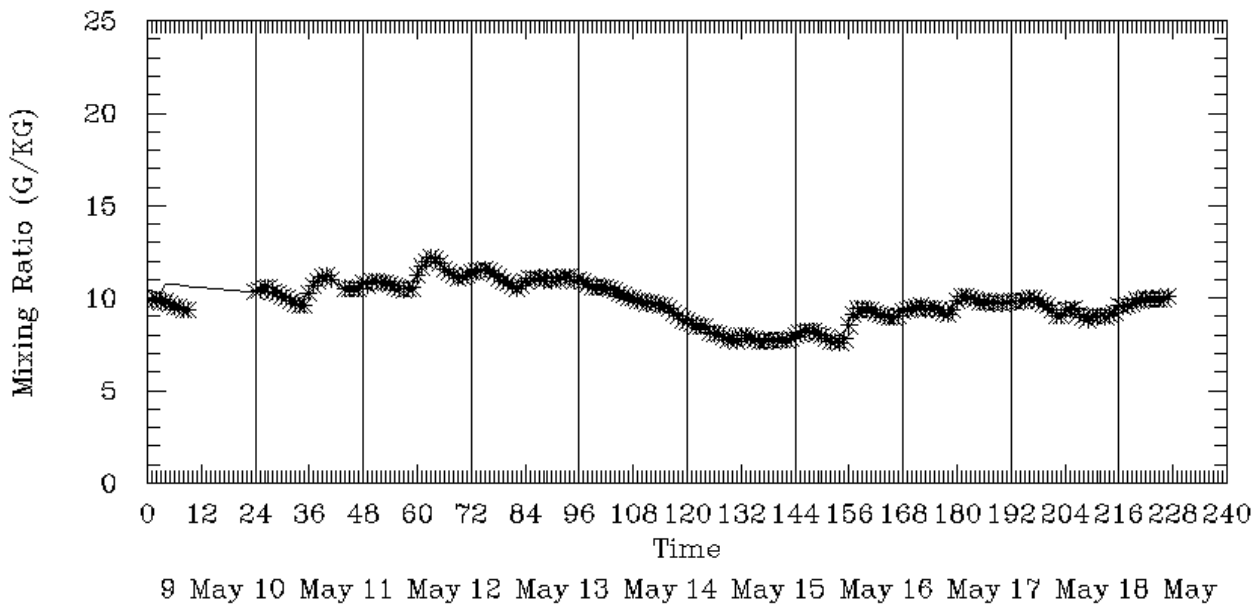


(g) 24 April – 3 May 1995

Figure 8-9. Concluded.

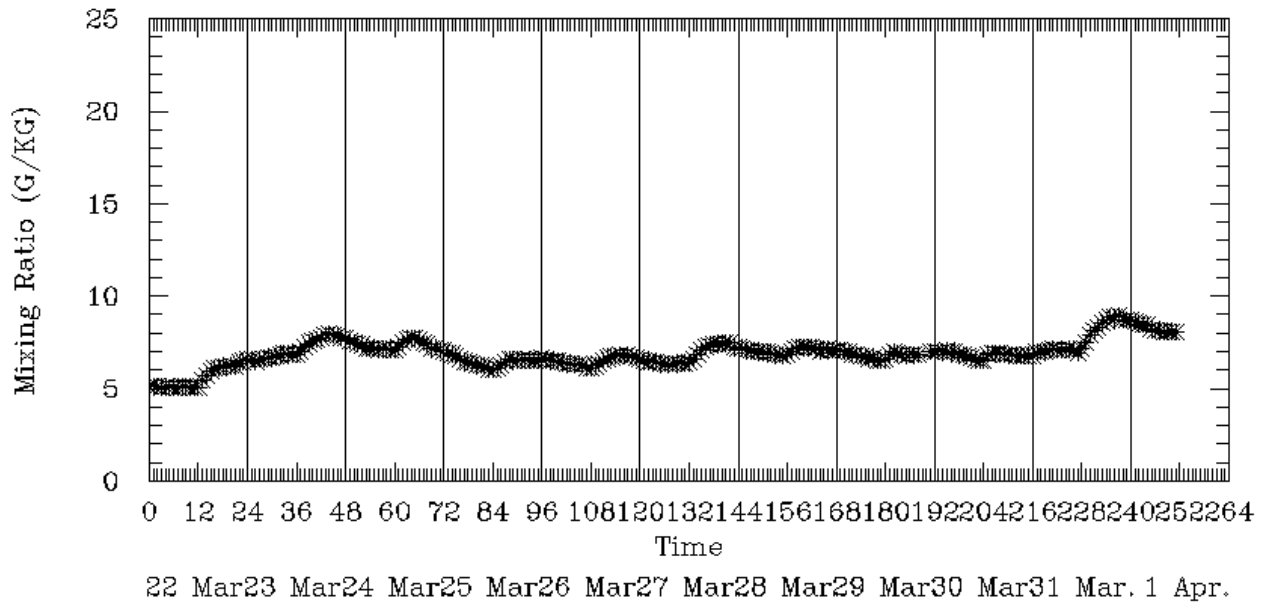


(a) 24-29 May 1995

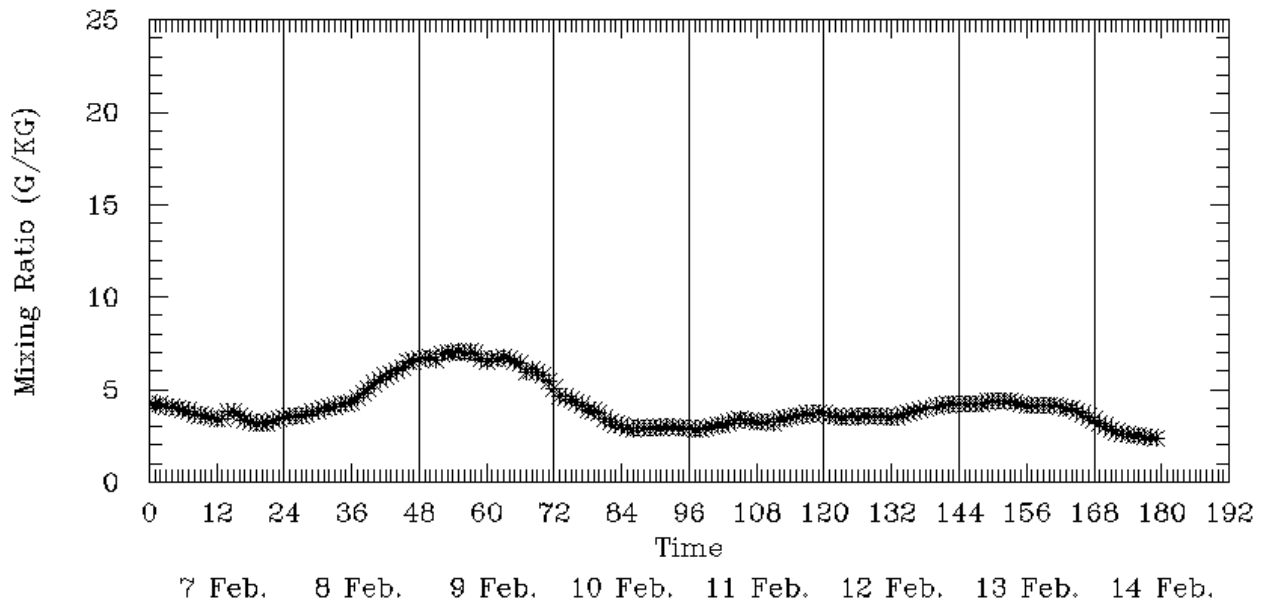


(b) 11-17 May 1993

Figure 8-10. Spatial Mean Ground-Level Mixing Ratios for Seven SAMI Episodes.

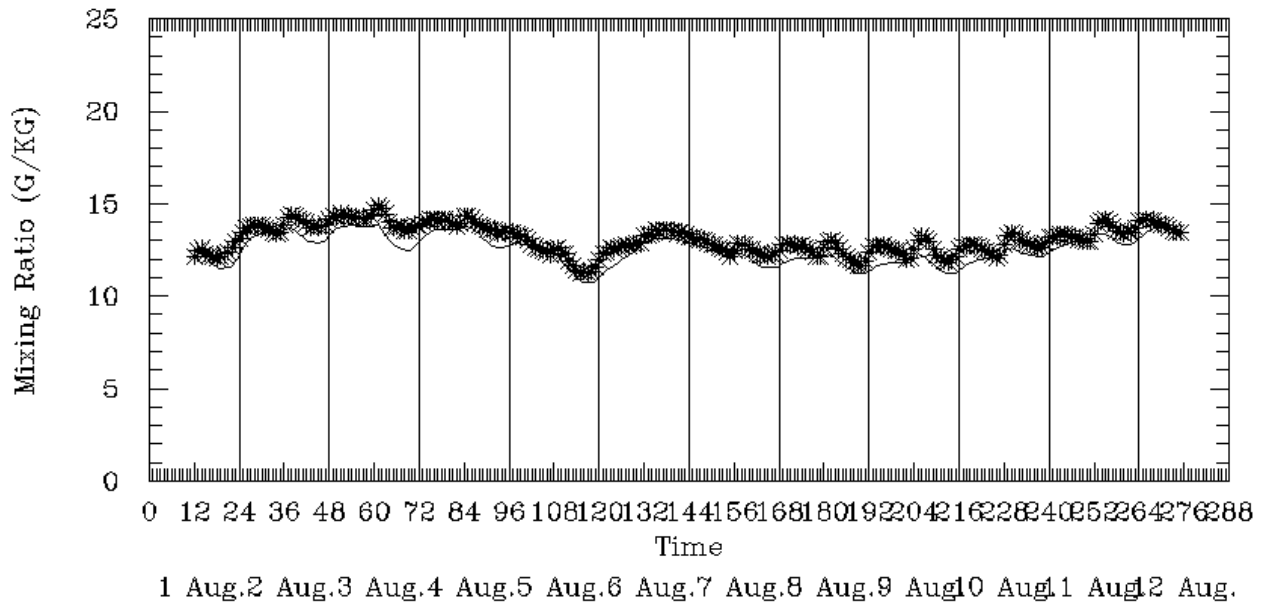


(c) 23-31 March 1993

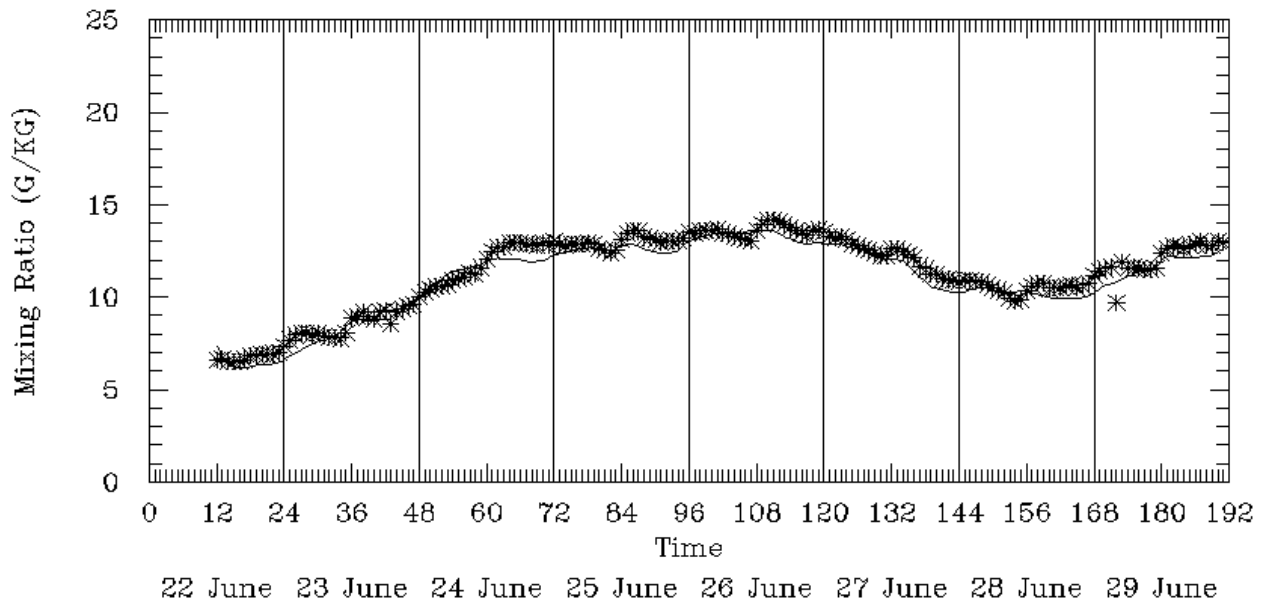


(d) 8-13 February 1994

Figure 8-10. Continued.

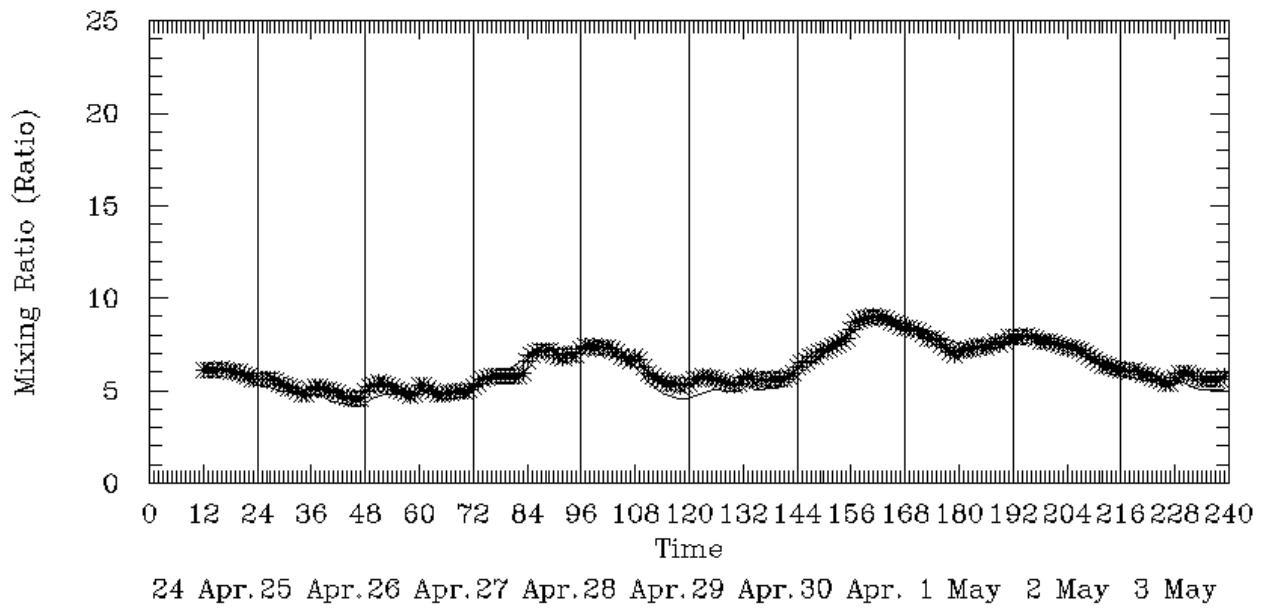


(e) 3-12 August 1993



(f) 22-29 June 1992

Figure 8-10. Continued.



(g) 24 April – 3 May 1995

Figure 8-10. Concluded.

9.0 SUMMARY AND CONCLUSIONS

This chapter presents the summary and conclusions of the RAMS model performance evaluation for nine (9) SAMI episode. We begin with a distillation of the operational evaluation results for surface winds, temperatures, mixing ratios and aloft winds and temperatures. Subsequently, we summarize the performance of the model in simulating the aloft winds and temperatures. Given the weak meteorological database available for model performance testing, the only scientific evaluation that was possible involved the comparison of modeled and observed daily average and six-hourly precipitation totals. We conclude with a formal process for assessing the suitability of the RAMS modeling episodes for air quality model applications based, in part, on comparisons with other contemporary prognostic model evaluations that have been accepted by EPA, various state governments and research groups in recent regulatory and applied research applications.

9.1. Operational Evaluation Summary

The operational summary for the six UAH episodes will utilize Tables 9-1.1-9-1.3. Table 9-1.1 is a summary of the bias and RMSE statistics for the 12-km domain. Table 9-1.2 gives the index of agreement for all the near-surface variables for each episode day. Table 9-1.3 gives the bias and RMSE statistics for the grid points of the respective coarse grid which are contained within the 12-km grid for the 850-mb values of temperature, water vapor mixing ratio, and wind speed. Although derived by different software and presented differently the same variables will be discussed here as in the operational summary for the three AG episodes.

9.1.1 9-20 July 1995

The July 1995 episode did not have the benefit of the surface nudging technique used on all the other episodes. This is demonstrated especially by the bias and RMSE of the 2-m mixing ratio of -1.45 and 2.56 g kg^{-1} , respectively, as shown in Table 9-1. The affect of the dry bias was partially mitigated by the provision of a boundary layer water vapor mixing ratio correction file to GIT for the air quality modeling phase. However, this did not change the cloud or precipitation deficiencies of this simulation. The RMSE of the wind direction at 10 m was also the largest of any of the UAH episodes at 83 degrees. This was due largely to the very light wind conditions which predominated this period. Examination of the daily index of agreement values for this episode in Table 9-2 shows the lowest mean values of all the episodes for temperature and mixing ratio of 0.69 and 0.62, respectively. Overall the index of agreement values were the lowest for the period 16-19 July when clouds and precipitation were more prevalent. The performance of the RAMS simulation at 850-mb for the 48-km grid points within the 12-km domain is given in Table 9-3. The most outstanding statistic was the RMSE for mixing ratio of 2.18 g kg^{-1} which was the largest of all the UAH episodes.

9.1.2 22-30 May 1995

Using the results of the surface performance in Table 9-1 this episode had a cool bias of about -0.98°C and relatively excellent wind results with a wind speed RMSE value of 1.75 m s^{-1} and a wind direction RMSE

value of 63 degrees. The surface wind performance is also verified by the index of agreement values in Table 9-2 where the mean values for wind speed and wind direction were 0.63 and 0.77, respectively, which were the highest or equal for any of the UAH episodes. The mean index of agreement for temperature of 0.84 had a rank of second best while the mean index of agreement for mixing ratio of 0.90 had a rank of fourth best but still at a high value. Temperature and moisture performance was diminished on 25 May when the respective daily index values dropped to 0.69 and 0.75. The most outstanding statistic of performance at 850 mb in Table 9-3 was the cool bias of -1.59°C which was the second coolest of all the episodes.

9.1.3 9-18 May 1993

This episode had the largest surface cool bias of -1.43°C but with relatively excellent wind results with a wind speed RMSE value of 1.73 m s^{-1} and a wind direction RMSE value of 67 degrees. Again the surface wind performance is verified by the index of agreement values in Table 9-2 where the mean values for wind speed and wind direction were 0.62 and 0.77, respectively, which were ranked first or second relative to the other UAH episodes. The mean index of agreement for temperature of 0.74 had a rank of fifth best while the mean index of agreement for mixing ratio of 0.87 had a rank of fifth best as well. Overall behavior with respect to the indices of agreement was reduced for the following days: for 11 May when the temperature index was 0.69 and the wind speed index was 0.57; and for 16 May when the temperature index was 0.55 and the wind direction index was 0.72. The outstanding statistics of performance at 850 mb in Table 9-3 were the temperature had a cool bias of -1.78°C which was the coolest of all the UAH episodes and a RMSE for temperature of 2.11°C which was also the largest of the UAH episodes.

9.1.4 21 March - 1 April 1993

Table 9-1 shows that this episode had the largest RMSE for temperature at 2 m of 3.01°C and also the second largest RMSE for wind speed at 10 m of 2.15 m s^{-1} . The index of agreement values in Table 9-2 show that the mean temperature and mixing ratio values of 0.82 and 0.93, respectively, were ranked third best while the wind speed and wind direction values of 0.54 and 0.76 were ranked second or third. Overall behavior relative to the daily indices of agreement was reduced for 25-26 March because of wind and for 30 March because of temperature and mixing ratio. The outstanding statistic of performance at 850 mb in Table 9-3 was the RMSE value for wind speed of 2.81 m s^{-1} which was the second largest of all the UAH episodes. The large values RMSE at the surface and at 850 mb are a reflection of the same problems revealed by the AG MAPS software as discussed in section 8. Since heavy precipitation fell over much of the 12-km grid it is likely that a major fraction of the surface temperature problems are related to cloud placement and thickness. The surface and 850-mb wind issues are harder to identify but may be related to the need for better vertical resolution for a late-winter case where the upper-level jet stream is strong.

9.1.5 6-14 February 1994

Table 9-1 shows that this episode had the second largest RMSE for temperature at 2 m of 2.82°C and also the largest RMSE for wind speed at 10 m of 2.75 m s^{-1} . The index of agreement values in Table 9-2 show that the mean temperature and mixing ratio values of 0.94 and 0.97, respectively, were ranked first while the

wind speed and wind direction values of 0.53 and 0.73 were ranked third or fourth. As mentioned in the discussion in section 8 the AG MAPS software showed that other statistical measures show significant problems with the temperatures at 2 m on the 12-km grid for portions of this episode. Examination of hourly differences between surface observations analyzed to the 12-km grid and the model values (not shown) confirmed this behavior. The model was too cold for the period 8-10 February for areas in and close to the southern Appalachians and then too warm for the period 11-13 February for an area from Georgia northeastward through the Carolinas. Reasons why the index of agreement remain high for temperature for this episode are the fortuitous location of observing sites and the fact that the index of agreement is less sensitive to model departures from observations when the observations themselves have a broad spread around the mean. The latter point is illustrated by the 1200 UTC 9 February 1994 surface analysis in the NOAA publication *Daily Weather Maps* which shows 2 m temperatures ranging from near 14°F in central Indiana to near 65°F over South Carolina. For these reasons the comparison of the daily values of the index of agreement have less value for this episode. The same trends are observed at 850 mb in Table 9-3 where the RMSE values for temperature at 2.51°C and wind speed at 4.25 m s⁻¹ were the largest of any UAH episode. As with the March 1993 simulation this episode may have required more vertical resolution at higher levels with such a strong upper-level jet. At least with respect to surface temperatures the 96-km grid appeared to perform better than the 12-km grid. Reasons for this are not clear but may involve the choice of diffusion parameters for the 12-km grid.

9.1.6 21 July - 1 August 1991

Table 9-1 shows that this episode had the second largest RMSE for wind speed at 10 m of 2.26 m s⁻¹ and as well the second largest RMSE for wind direction at 10 m of 77 degrees. This is likely the result of generally light surface winds in combination with widespread convective outflows from thunderstorms which are handled very poorly with models. Examination of the daily indices of agreement in Table 9-2 for wind direction and wind speed show the highest values were in the middle of the episode with a decrease in the same indices for the period 29-31 July. As discussed in section 4.6 this is consistent with the timing of the widespread convection east of the Appalachians. The performance at 850 mb as shown in Table 9-3 was close the mean values for the bias and RMSE for all variables.

Table 9-1. Bias and root mean square error (RMSE) for UAH episodes. Statistics based on hourly 12-km variables interpolated to all available NWS sites within the 12-km domain. Variables are: temperature at 2 m, T, °C; water vapor mixing ratio at 2 m, Q, g kg⁻¹; wind speed at 10 m, WSPD, m s⁻¹; and wind direction at 10 m, WDIR, degrees.

EPISODE	T BIAS	T RMSE	Q BIAS	Q RMSE	WSPD BIAS	WSPD RMSE	WDIR BIAS	WDIR RMSE
July 95	+0.66	2.45	-1.45	2.56	+0.49	1.51	-8.16	83.0
May 95	-0.98	2.34	-0.29	1.03	+0.18	1.75	+1.30	63.0
May 93	-1.43	2.69	-0.30	1.06	+0.38	1.73	-3.68	67.0
March 93	-1.28	3.01	-0.16	0.67	+0.88	2.15	+12.30	70.0
Feb 94	+0.30	2.82	-0.00	0.59	+1.33	2.75	-3.76	73.0
July 91	-1.27	2.25	-0.37	0.90	+0.94	2.26	-2.29	77.0

Table 9-2. Daily index of agreement statistics for temperature at 2 m (T), water vapor mixing ratio at 2 m (Q), wind direction at 10 m (WDIR), and wind speed at 10 m (WSPD) for each of the six episodes modeled by UAH. Statistics are for the day indicated ending at 1200 UTC. Statistics are based on 12-km model data interpolated to all available NWS sites within the 12-km grid domain. Cells shaded green have the highest values for a given variable, while cells shaded red have the lowest values.

July 1995 Episode												
	July 10	July 11	July 12	July 13	July 14	July 15	July 16	July 17	July 18	July 19	July 20	MEAN
T	0.86	0.78	0.76	0.75	0.65	0.64	0.64	0.62	0.60	0.57	0.70	0.69
Q	0.84	0.69	0.64	0.60	0.53	0.50	0.52	0.43	0.44	0.75	0.83	0.62
WDIR	0.73	0.71	0.69	0.65	0.73	0.69	0.62	0.71	0.66	0.62	0.62	0.68
WSPD	0.42	0.55	0.35	0.47	0.65	0.66	0.59	0.52	0.51	0.48	0.39	0.51
May 1995 Episode												
	May 23	May 24	May 25	May 26	May 27	May 28	May 29	May 30	MEAN			
T	0.90	0.79	0.69	0.87	0.92	0.88	0.87	0.85	0.84			
Q	0.95	0.90	0.75	0.81	0.93	0.95	0.93	0.94	0.90			
WDIR	0.87	0.91	0.78	0.72	0.77	0.66	0.64	0.80	0.77			
WSPD	0.61	0.70	0.71	0.47	0.53	0.62	0.70	0.73	0.63			
May 1993 Episode												
	May 10	May 11	May 12	May 13	May 14	May 15	May 16	May 17	May 18	MEAN		
T	0.78	0.69	0.64	0.79	0.82	0.66	0.55	0.86	0.90	0.74		
Q	0.83	0.74	0.78	0.85	0.97	0.93	0.83	0.90	0.97	0.87		
WDIR	0.82	0.72	0.77	0.69	0.94	0.78	0.72	0.74	0.75	0.77		
WSPD	0.60	0.57	0.72	0.66	0.55	0.68	0.67	0.59	0.55	0.62		
March 1993 Episode												
	Mar 22	Mar 23	Mar 24	Mar 25	Mar 26	Mar 27	Mar 28	Mar 29	Mar 30	Mar 31	Apr 1	MEAN
T	0.96	0.91	0.92	0.89	0.75	0.77	0.87	0.75	0.72	0.78	0.75	0.82
Q	0.95	0.99	0.97	0.95	0.94	0.96	0.92	0.88	0.85	0.89	0.94	0.93
WDIR	0.77	0.63	0.67	0.71	0.61	0.67	0.93	0.92	0.88	0.86	0.75	0.76
WSPD	0.49	0.60	0.48	0.39	0.52	0.53	0.56	0.57	0.62	0.65	0.51	0.54
February 1994												
	Feb 7	Feb 8	Feb 9	Feb 10	Feb 11	Feb 12	Feb 13	Feb 14	MEAN			
T	0.93	0.97	0.95	0.97	0.96	0.90	0.92	0.91	0.94			
Q	0.98	0.99	0.98	0.99	0.98	0.95	0.97	0.95	0.97			
WDIR	0.65	0.82	0.55	0.76	0.65	0.86	0.71	0.86	0.73			
WSPD	0.56	0.34	0.39	0.56	0.63	0.58	0.62	0.60	0.53			
July 1991 Episode												
	July 22	July 23	July 24	July 25	July 26	July 27	July 28	July 29	July 30	July 31	Aug 1	MEAN
T	0.79	0.73	0.80	0.78	0.84	0.84	0.84	0.78	0.82	0.71	0.72	0.79
Q	0.89	0.89	0.94	0.97	0.97	0.98	0.99	0.99	0.98	0.98	0.98	0.96
WDIR	0.74	0.69	0.82	0.83	0.85	0.93	0.81	0.58	0.58	0.82	0.88	0.77
WSPD	0.61	0.56	0.60	0.60	0.56	0.45	0.46	0.42	0.40	0.32	0.39	0.49

Table 9-3. Bias and root mean square error (RMSE) of the UAH episodes for variables at 850-mb for coarse grid points within the 12-km domain. Statistics based on 12-h model and NCEP/NCAR reanalysis data. Variables are: temperature, T, °C; water vapor mixing ratio, Q, g kg⁻¹; and wind speed, WSPD, m s⁻¹.

	T-BIAS	T-RMSE	Q-BIAS	Q-RMSE	W-BIAS	W-RMSE
July 95	-0.97	1.86	+1.55	2.18	-0.08	1.59
May 95	-1.59	1.83	+0.73	1.30	+0.52	1.94
May 93	-1.78	2.11	+0.80	1.41	+0.37	1.99
March 93	-1.05	1.68	+0.61	1.22	+0.84	2.81
Feb 94	+1.30	2.51	+0.49	1.25	+2.70	4.25
July 91	-1.37	1.73	+0.87	1.60	+0.96	2.55
MEAN	-0.91	1.95	+0.84	1.49	+0.89	2.52

9.1.7 22-29 June 1992

RAMS did a very job of reproducing the daily maximum temperatures on each day with the exception of 26 June where the peak was underestimated by 3.4°C. The mean bias in predicted hourly surface temperatures across the 12 km domain ranged from -1.7°C to -0.2°C with an episode mean of -1.1°C. The average gross errors in surface temperature predictions for the 8 days were 1.8°C. RAMS generally follows the hourly mean temperature measurements fairly well; however, the model systematically underestimated the afternoon spatial mean peak values on each day and this discrepancy worsened as the episode progressed. The under-prediction of the afternoon peaks was more pronounced than the August episode where RAMS clipped the afternoon peaks by a one to two degrees C. RAMS tended to slightly underestimate (~ 5% to 10%) hourly temperatures in the morning hours and on a couple of days to over predict (~ 2%-3%) midday.

RAMS estimated mean wind speeds (2.55 m s⁻¹) that were on average 66% greater than the magnitude of the episode mean observations (1.54 m s⁻¹). Mean wind speeds were higher than those encountered in the August 1993 period. Modeled wind directions showed reasonable agreement with the observations on most days. Across the 8-day episode, the mean modeled (229.7 degrees) and observed surface wind directions (250.3 degrees) differed by only 21 degrees. From day-to-day, the difference between daily average and observed wind direction varied from 10 to 150 degrees.

Episode average values of the unsystematic, systematic, and total RMSE errors were 1.24 m s⁻¹, 1.38 m s⁻¹ and 1.89 m s⁻¹, respectively. These results were an improvement over the August 1993 episode. There did not appear to be any significant error growth throughout the latter two thirds of the simulation. Slight error growth occurs during the first three days of the episode when the errors were somewhat larger than for the rest of the episode days. The preponderance of the RMSE error was from the systematic component.

The index of agreement results for the June 1992 episode were quite consistent with other prognostic model evaluations. RAMS exhibited typical hourly variation in the agreement index parameter with the lowest values occurring during the morning period when wind speeds were lowest and the directions were more variable. The index increased in the afternoon when speeds were greater. The mean value of the index of agreement varied diurnally throughout the episode; the mean over the whole period was 0.75

For near surface mixing ratios the episode mean daily maximum observed (19.3 g/Kg) and modeled (16.8 g/Kg) agreement was fairly good. RAMS systematically underestimated the maximum ratio on each day except 22 June by 2 to 4 g/Kg. The mean bias and error in mixing ratios was also quite good, with 8-day mean values of -0.3 g/Kg and 1.0 g/Kg respectively.

There was good agreement between the predicted and observed vertically averaged temperatures for each simulation day. The vertically-averaged predicted and observed temperatures on the 12 km domain were 13.5°C and 13.8°C, respectively. The mean predicted and observed wind aloft wind speeds were 7.3 m s⁻¹ and 6.6 m s⁻¹, giving a 11% discrepancy.

9.1.8 24 April – 3 May 1995

For the 24 April – 3 May 1995 SAMI episode RAMS did a very job of reproducing the daily maximum temperatures on each day. The episode-averages of the daily maximum observed and predicted temperatures were 26.9°C and 26.6°C, respectively, for a 1.1% discrepancy. The mean bias in predicted hourly surface temperatures across the 12 km domain ranged from -1.9°C to 0.7°C. On average across the episode, the mean bias in surface temperature prediction -0.8°C. The average gross errors in surface temperature predictions for the 10 days were 1.8°C, the same as the June 1992 episode. RAMS followed the hourly mean temperatures fairly well but, as with the August 1993 and June 1992 episodes, the model systematically underestimated the afternoon peaks in the latter part of April. However, the model did a good job on the 1st and 2nd of May. These discrepancies at midday were typically on the order of 2 to 3°C. The under-prediction of the afternoon peaks was more pronounced than the August 1993 episode but about the same as the June 1992 episode. The hourly temperature biases for the April-May episode were significantly larger than those for the August and June episodes. RAMS underestimated (~ 10% to 15%) hourly temperatures in the afternoon and evening hours and during the morning as well on several days.

RAMS estimated mean wind speeds (2.98 m s⁻¹) that were on average 60% greater than the magnitude of the episode mean observations (1.86 m s⁻¹). RAMS overestimated the daily average observed wind speeds during this episode by about the same amount as the June 1992 episode. Mean wind speeds were also higher than those encountered in the August 1993 period. Modeled wind directions were in reasonable agreement with the observations on the first five days of the episode and fairly poor agreement on the last five days. Across the 10-day episode, the mean modeled (257.0 degrees) and observed surface wind directions (261.4 degrees) differed by only 4 degrees. From day-to-day, however, the discrepancies between daily average and observed wind direction varied from 2 to 158 degrees. On the 29th through the 3rd of May, the mean (absolute) discrepancy between daily averaged modeled and observed wind direction was 131 degrees.

The episode average values of the unsystematic, systematic, and total RMSE errors were 1.46 m s⁻¹, 1.84 m s⁻¹ and 2.35 m s⁻¹, respectively. While there did not appear to be any significant error growth during the simulation, the RMSE errors were greater than the June and August episodes. The systematic component (model physics- related) of the RMSE error was clearly the larger contributor to the total RMSE error in this episode.

The index of agreement results for the April-May 1995 episode were quite good. This is somewhat surprising given the poorer wind direction and RMSE error performance of the model for this episode relative to the August 1993 and June 1992 periods. RAMS exhibited typical hourly variation in the agreement index parameter with the lowest values occurring during the morning period. In the afternoon when speeds were greater, the index increased. The mean value of the index of agreement varied diurnally throughout the episode; the mean over the whole period was 0.81, an improvement over the 0.75 figure obtained with the August and June episodes.

Agreement between the episode mean daily maximum observed (13.1 g/Kg) and modeled (13.5 g/Kg) mixing ratios was quite good. RAMS slightly underestimated the maximum ratio on most days. The mean bias and error in mixing ratios were also quite good, with 10-day mean values of -0.1 g/Kg and 0.7 g/Kg respectively. As with the August 1993 and June 1992 episodes, these results indicated that RAMS did a fairly good job of reproducing the daily maximum and hourly specific humidity across the 12 km domain.

From the aloft wind comparisons for the April-May 1995 episode there was reasonably good agreement between the predicted and observed vertically averaged temperatures for each simulation day. The vertically-averaged predicted and observed temperatures on the 12 km domain were 6.6°C and 6.0°C, respectively. The mean predicted and observed wind aloft wind speeds were 10.0 m s⁻¹ and 9.1 m s⁻¹, producing a 10% discrepancy.

9.2 Scientific Evaluation Summary

The precipitation evaluation of the six UAH episodes will be done for the episodes as a whole using the results shown in Figure 9-1. Figure 9-1 is a plot of the equitable threat scores taken from the rainfall statistics tables from each episode. As expected the best performance was for the February 1994 and March 1993 episodes with maximum scores of 0.20-0.30 where the synoptic situation was strongly baroclinic and convective precipitation was minimized across the 12-km domain. All the other episodes which were in the warm season had maximum scores of 0.15 or less. Regardless of the episode very little skill was observed as the threshold approached 25 mm. While these are admittedly poor scores they are consistent with the current state of mesoscale numerical weather prediction. This is discussed further in section 9.3.

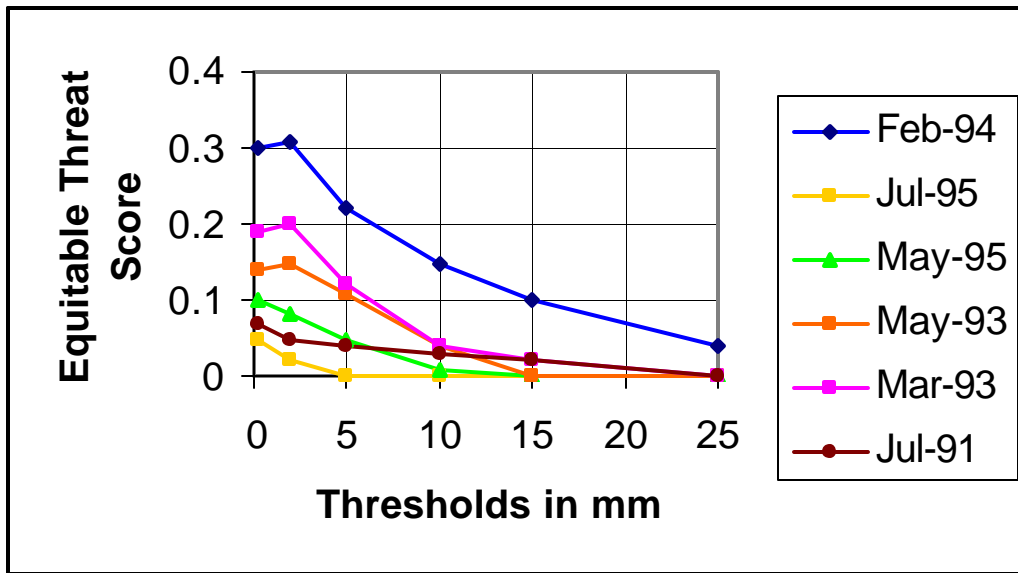


Figure 9-1. Equitable threat scores for all UAH episodes based on 6-h precipitation amounts from the 12-km grid interpolated to all NWS sites within the 12-km grid.

9.2.1 3-12 August 1993

Rain occurred on 8 of the 10 days of the August 1993 episode. The maximum observed total daily precipitation at any rain gauge varied between 9 mm and 119 mm with an episode mean of 50 mm. RAMS predicted a range of rainfall of 11.5 mm to 102.7 mm with an episode mean of 40.3 mm. The mean observed and predicted precipitation across all rain gauges was 5.3 mm and 6.7 mm, yielding an overall discrepancy of 26% which represents excellent agreement for a mesoscale prognostic model. The bias in daily rainfall predictions ranges from -0.30 mm to 10.38 mm with an episode mean of 1.9 mm. Only on 5 August did the model experience significant difficulty reproducing the daily rainfall totals. The daily gross errors in rainfall ranged between 0.41 mm and 13.91 mm with an episode mean of 5.8 mm. Overall, the model did an excellent job of simulating the daily and episode average rainfall totals. With the exception of the modest over-prediction on 5 August, the day-to-day rainfall predictions match the observations very closely in this comparison.

Scatter plots of predicted and observed daily total precipitation underscored the need for multiple statistical and graphical tools when evaluating the performance of complex atmospheric models. While the spatial time series plots suggested very good model performance based on averages across all monitoring stations, the scatter plots revealed that this good agreement came as the result of cancellation of model over- and under-predictions at the numerous individual monitors. Visual inspection of the scatter plots revealed little correlation between the various reporting sites. While RAMS did a credible job of estimating the total precipitation across the 12 km domain on each day during the August 1993 episode, the spatial distribution of rainfall events exhibited much less skill.

9.2.2 22-29 June 1992

Rain occurred on 5 of the 8 days during the June 1992 episode. The maximum daily precipitation at any rain gauge varied between 4 mm and 122 mm with an episode mean of 53.8 mm. RAMS predicted a range of daily maximum rainfall totals from 9 mm to 110.5 mm with an episode mean of 41.7 mm. The mean observed and predicted precipitation across all rain gauges was 2.9 mm and 3.9 mm, yielding an overall discrepancy of 35%. The bias in daily rainfall predictions ranges from -0.60 mm to 4.82 mm with an episode mean of 0.9 mm. Only on 27 June did the model experience significant difficulty reproducing the daily rainfall totals as evidenced by bias and error scores of 4.82 mm and 11.57 mm, respectively. The daily gross errors in rainfall ranged between 0.23 mm and 11.57 mm with an episode mean of 4 mm. Overall, the model did a good job of simulating the daily and episode average rainfall totals when averaged across all monitoring stations. With the exception of the 50% over-prediction on 27 June, the day-to-day rainfall predictions matched the observations very closely in this comparison. While the spatial time series suggested good model performance (based on averages across all monitoring stations), the scatter plots of daily precipitation at specific monitoring stations again revealed poor correlation between prediction and observation at the individual reporting sites. Thus, as with the August 1993 episode, RAMS did a credible job of estimating the total precipitation when averaged across the monitoring network on each episode day but the model's ability to predict the exact rainfall amounts paired in time and space with specific monitors was generally poor.

9.2.3 24 April – 3 May 1995

Rain occurred on 8 of the 10 days during the 24 April – 3 May 1995 episode. The maximum daily precipitation at any rain gauge varied between 3 mm and 48 mm with an episode mean of 21 mm. RAMS predicted a range of daily maximum rainfall totals from 2 mm to 38.6 mm with an episode mean of 20.1 mm. The mean observed and predicted precipitation across all rain gauges was 2.5 mm and 4.1 mm, yielding an overall discrepancy of 64% which constitutes fair agreement. RAMS' performance in predicting rainfall for this episode is poorer than for the August 1993 and July 1992 episodes. The bias in daily rainfall prediction ranges from -5.95 mm to 10.23 mm with an episode mean of 1.5 mm. On May 1st and 2nd, RAMS over-predicted the mean daily rainfall amounts by 10.5 mm and 5.9 mm, respectively. The daily gross errors in rainfall ranged between 0.02 mm and 10.63 mm with an episode mean of 3.5 mm. Overall, the model did a fair job of simulating the daily and episode average rainfall totals when averaged across all monitoring stations. With the exception of the significant over-prediction on 1 May and 2 May the day-to-day rainfall predictions matched the observations closely in this comparison even though the scatter plots suggested generally poor correlation between prediction and observation at the individual reporting sites.

9.3 Conclusions

Appendix 3 compares some of the SAMI episodes with previous MM5 and RAMS simulations they have performed. It is also instructive to compare the SAMI simulations with some statistics for current

operational numerical weather prediction models used by the National Centers for Environmental Prediction (NCEP). Figure 9-2 shows equitable threat and bias scores for precipitation for May 2000 for various models for the entire United States. The statistics are based on 48-h forecasts verifying at 0000 UTC of 3-h precipitation amounts. Maximum equitable threat scores are on the order of 0.15. Very little skill is observed as the 1 inch threshold is approached. Bias scores show an over-prediction of 0.10 inch amounts and less and then a general under-prediction of precipitation for larger values. While operational models do not have the luxury of nudging towards observations, these statistics still have relevance for evaluating the SAMI simulations. Over the 12-km domain practically no nudging was performed above the surface and even the surface nudging scheme is not able to correct for issues such as cloud location and depth. So for weak-flow conditions with convection being the dominant precipitation mode the SAMI simulations face very similar difficulties as the operational models. If one were to investigate the performance of NCEP models for other months (<http://sgi62.wwb.noaa.gov:8080/scores>) one would observe maximum equitable threat scores during the cool season on the order of 0.40 and even smaller values than the May plot in Figure 9-2 for the summer months. So, in conclusion, the equitable threat precipitation scores in Figure 9-1 for the UAH SAMI episodes are very similar to current NCEP model performance. It is likely that a similar analysis of the precipitation results for the three AG episodes would have similar conclusions.

An example of near-surface temperature performance by operational models is given by Figure 9-3 for the approximate period of 21 May to 4 June 2001. The statistics are based on 48-h forecasts verifying at 0000 UTC for the southern Midwest which covers the following region: all of Arkansas, Alabama, Mississippi, and Louisiana; most of Tennessee; and the extreme eastern portions of Oklahoma and Texas. As an example the Eta model typically had daily bias errors on the order of $\pm 3^{\circ}\text{C}$ and RMSE values of 2 to 6°C for this period. The average bias and RMSE for this period and area were near 1 and 3°C , respectively. Figure 9-4 is a similar plot for the same time period but for near-surface wind speed performance. Again as an example the Eta model had daily bias errors on the order of $\pm 3\text{ m s}^{-1}$ and RMSE values of 3 to 8 m s^{-1} . The average bias and RMSE for this period and area were near 1 and 5 m s^{-1} , respectively. The near-surface bias and RMSE values for the same variables for all the SAMI episodes were near or below these values. The operational models face similar difficulties as research models applications (SAMI, for example) including areas such as correct prediction of precipitation, soil moisture issues, and cloud location and depth.

Finally, the issue of good model performance in weak surface wind regimes has been mentioned several times in this report. Figure 9-5 shows the grand mean observed wind speed at 10 m for all of the UAH episodes. If the AG episodes had been included it is likely that the average over the southeastern United States would be even less than shown since the AG periods were warm season events. Figure 9-5 shows that a large portion of the 12-km grid had observed mean wind speeds of 2.5 m s^{-1} or less. If one considers only the surface geostrophic constraints with respect to temperature, a wind speed of 2.5 m s^{-1} corresponds to a temperature change across 12 km on the order of only 0.01°C . This is one reason why model performance is degraded during weak wind conditions.

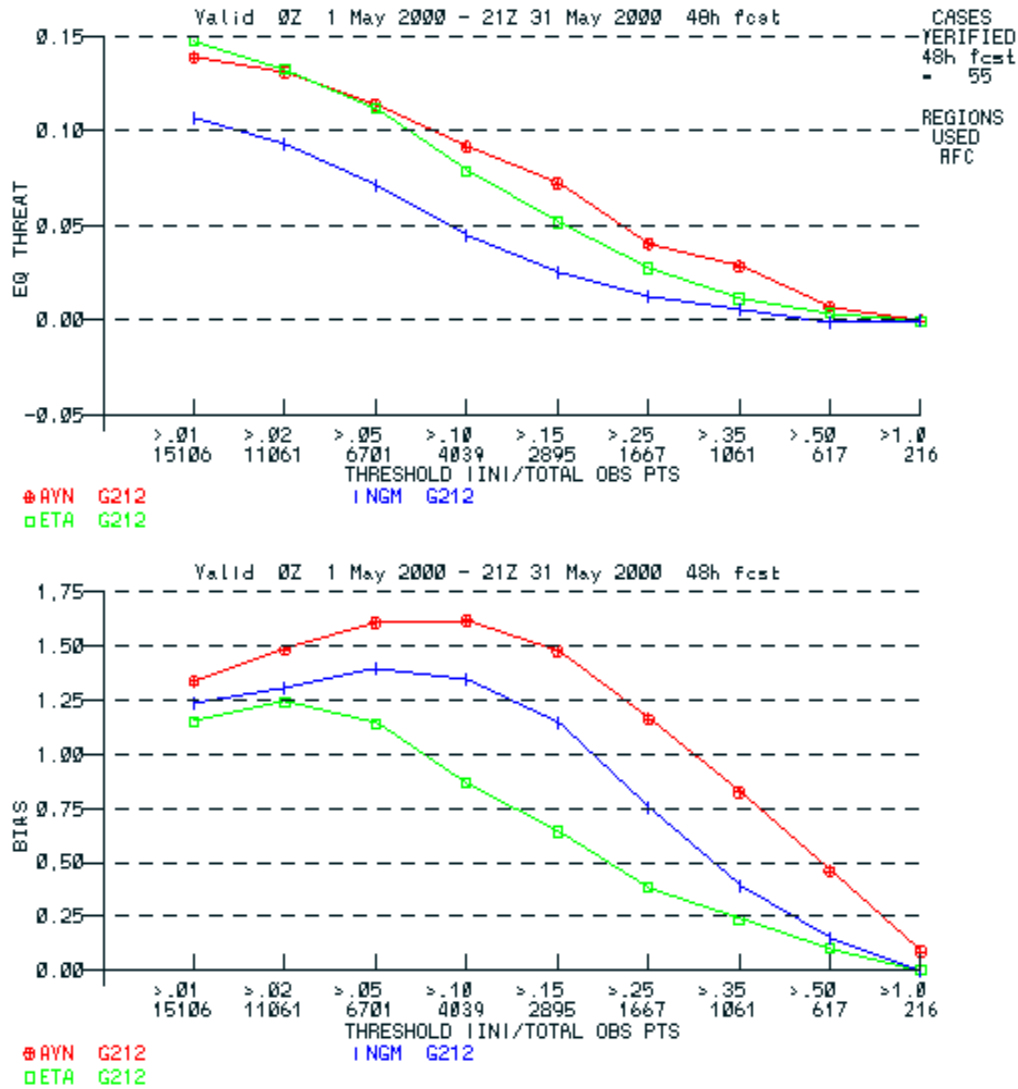


Figure 9-2. Equitable threat and bias scores for various NCEP models for May 2000. The statistics are based on 48-h forecasts verifying at 0000 UTC of 3-h precipitation amounts for the entire United States for thresholds up to 1 inch. Curves and their respective meanings and colors are: 1) the Aviation model (AVN), red; 2) the Eta model (ETA), green; and 3) the Nested grid Model (NGM), blue. This graphic was acquired at the following web site: <http://sgi62.wwb.noaa.gov:8080/scores>.

STAT=SL1L2 PARAM=T FHOURL=4H V_ANL=ANYSFC V_RGN=G104/SMW LEVEL=SFC VEHMM=0000

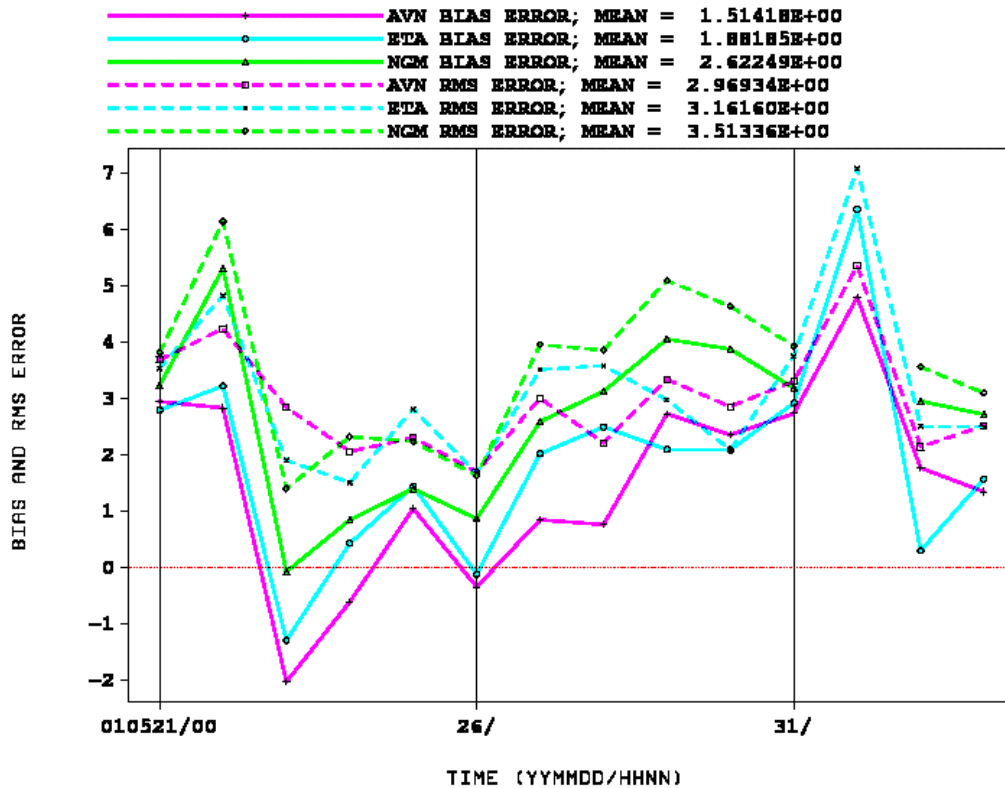


Figure 9-3 Bias and RMSE values (°C) for various NCEP models for the approximate period of 21 May to 4 June 2001 for near-surface temperatures. The statistics are based on 48-h forecasts verifying at 0000 UTC for the southern Midwest which covers the following region: all of Arkansas, Alabama, Mississippi, and Louisiana; most of Tennessee; and the extreme eastern portions of Oklahoma and Texas. Curves and their respective meanings and colors are: 1) the Aviation model (AVN), purple; 2) the Eta model (ETA), blue; and 3) the Nested grid Model (NGM), green. This graphic was acquired at the following web site: <http://sgi62.wwb.noaa.gov:8080/VSDb>.

STAT=VL1LZ PARAM=VWIND F HOUR=48 V_ANL=ANY SFC V_RGN=C104/SMW LEVEL=SFC VHHMM=0000

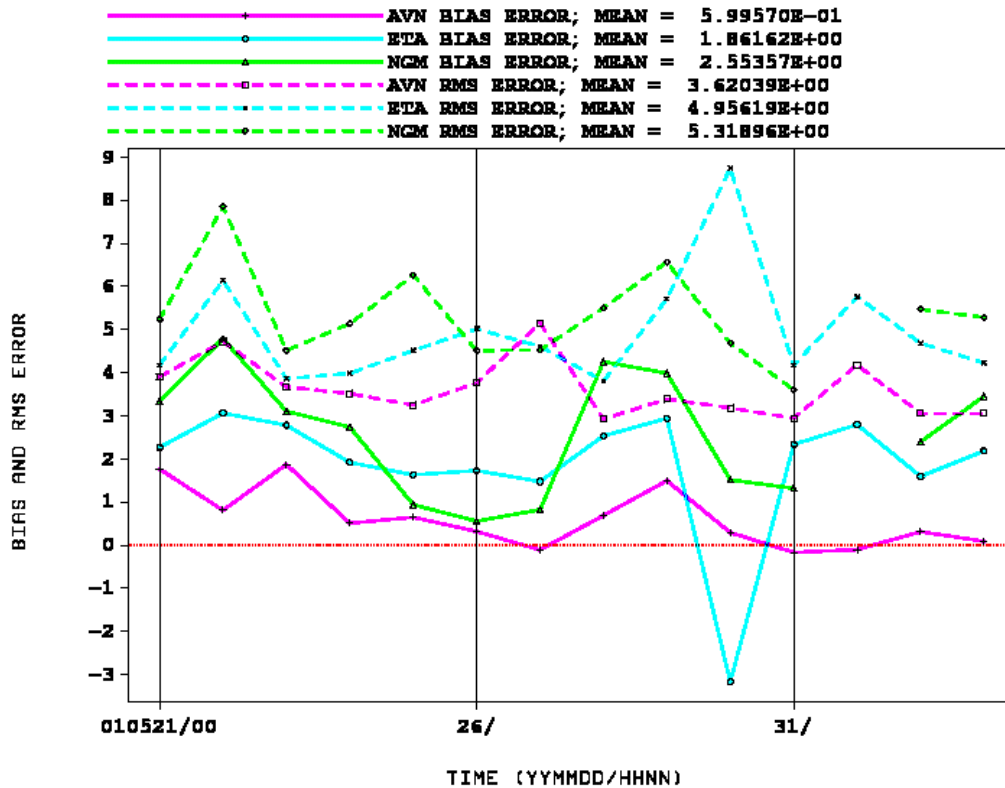


Figure 9-4. Bias and RMSE values (m s^{-1}) for various NCEP models for the approximate period of 21 May to 4 June 2001 for near-surface wind speeds. The statistics are based on 48-h forecasts verifying at 0000 UTC for the southern Midwest which covers the following region: all of Arkansas, Alabama, Mississippi, and Louisiana; most of Tennessee; and the extreme eastern portions of Oklahoma and Texas. Curves and their respective meanings and colors are: 1) the Aviation model (AVN), purple; 2) the Eta model (ETA), blue; and 3) the Nested grid Model (NGM), green. This graphic was acquired at the following web site: <http://sgi62.www.noaa.gov:8080/VSDB>.

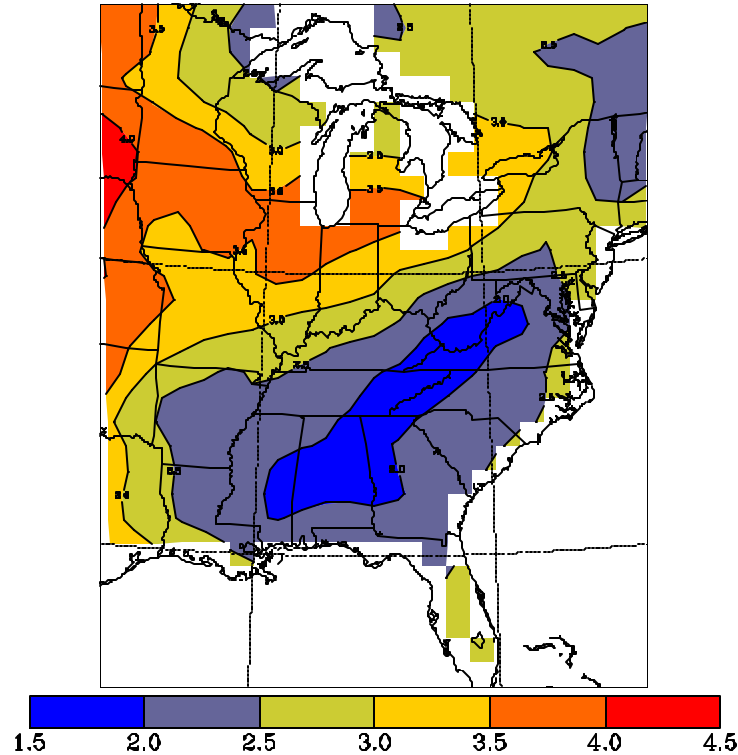


Figure 9-5. Grand average observed mean wind speed at 10 m in m s^{-1} for all UAH episodes for the 96-km grid. Hourly observations for all days and all episodes were used.

9.3.1 Aloft Winds and Temperatures

The predicted and observed vertically averaged temperatures, wind speeds and wind directions for each SAMI episode were examined and the agreement between these aloft fields was generally quite good. While part of this good agreement is simply due to the fact that aloft temperature and wind observations from the NWS radiosondes were employed in the RAMS FDDA nudging schemes, the actual weighting coefficients used in the nudging were small so that the RAMS fields were not under a heavy constraint to match the observations locally. The good agreement in aloft performance is quite consistent with several of the other MM5 and RAMS evaluation studies reported in the recent literature and gives some confidence that the modeled wind patterns are a reasonable.

Lack of high-resolution special meteorological measurements during the SAMI episodes precluded a detailed scientific evaluation of the RAMS model performance. Examination of the model's ability to simulate liquid precipitation on a daily and a six-hourly basis indicated that for virtually all of the episodes studied the model did a good to excellent job of simulating the daily and episode average rainfall totals across the 12-km domain. While the spatial time series plots suggested very good model performance based on averages across all monitoring stations, the performance of the model at individual monitoring stations and on specific days had much greater uncertainty. In most cases, scatter plots of daily averaged

precipitation at the individual monitoring stations revealed little correlation between prediction and observation. Nevertheless, the model's predictions for precipitation on daily time scales and regional spatial scales was encouraging. There did not appear to be any substantially incorrect features of the precipitation results that would suggest the presence of a seriously flawed prognostic model simulation for any of the SAMI episodes.

Based the operational and scientific evaluation results presented in this report and the findings of our review of other contemporary RAMS and MM5 evaluation studies reported in the recent literature, we find that the nine (9) SAMI RAMS simulations are easily representative of the level of performance in wind, temperature, mixing ratio and precipitation exhibited by contemporary state-of-science prognostic models. We find no reason to disqualify any of the nine meteorological episodes at this time for use in supporting regional photochemical and/or aerosol calculations with the SAMI URM-1ATM modeling system.

9.4 Adequacy of the SAMI Meteorological Modeling for Air Quality Modeling

One of the most important questions addressed in this report concerns whether the RAMS meteorological fields are adequate for their intended use in supporting the acid deposition modeling in SAMI. For the reasons discussed below, we are not able to answer this question definitively, yet a significant amount of information has been developed that, we believe, should be of use to SAMI decision-makers in their efforts to assess the overall reliability and usefulness of the RAMS meteorological modeling results for public policy making. As demonstrated below, we believe the RAMS modeling results are suitable for use in the UAM-AERO acid deposition modeling although a number of important questions remain to be answered fully.

There is no simple way to answer the question of whether the RAMS fields are adequate as input to the SAMI acid deposition model. First, there are no commonly accepted performance benchmarks for prognostic meteorological models that, if passed, would allow one to declare the RAMS fields appropriate for use. For complex atmospheric modeling problems like the ones being addressed by SAMI, it is quite doubtful that a set of quantitative performance criteria will ever be completely sufficient. The question of meteorological data set adequacy depends, at a minimum, upon the specific host emissions and air quality models (EMS-95, URM-AERO in this instance) and the nature of the modeling episodes being used. Meteorological fields that might be adequate for use in the UAM-V model for an OTAG episode, for example, may be quite deficient in an episode for SAMI since the specific needs of the air quality model and the particular chemical and physical processes that must be simulated are different. Thus, quantitative statistical and graphical performance criteria, though helpful, are inherently insufficient in aiding modelers and decision-makers in deciding whether meteorological fields are adequate for air quality modeling. Other considerations must be brought to bear. Below, we present and then work through a process whereby the adequacy of the RAMS fields for use in the SAMI acid deposition modeling can be evaluated. This process builds upon the more general evaluation process outlined by Roth, Tesche and Reynolds (1998) and recent suggestions by Tesche et al., (2001) and Emery et al., (2001) on potentially useful model performance benchmarks.

9.4.1 Framing the Questions to Be Addressed

Usually air quality simulations are quite sensitive to meteorological fields. Where this sensitivity is anticipated, it is important to make an effort to develop as accurate a representation of meteorological variables as possible. Special features of the flow fields, such as eddies, nocturnal jets, drainage flows, land-sea or land-bay breezes, and vertical circulations should be adequately characterized through the meteorological modeling. In circumstances where there are significant transitions in the meteorological variables over short distances, such as along shorelines or in areas of hilly terrain, the need for finer spatial resolution that is typically specified must be considered. If inadequate attention and care are accorded meteorological modeling, there is a significant risk of developing an inaccurate representation that will be propagated into the emissions and air quality models.

Several questions should be addressed for the specific application. Examples of these questions are as follows:

Appropriateness of Model Selection:

- > **Modeling Requirements:** Was a carefully written characterization made of the most important physical and chemical processes relevant to successful air quality modeling of each episode (e.g., a “conceptual model” of each simulation period)?
- > **Model Selection:** Did the model selection process ensure that a suitable modeling system was chosen, properly weighing the need for mature, well-tested, publicly-available model(s) against the constraints of the specific modeling problem, characteristics of the episodes to be simulated, and the limitations of schedule and resources?
- > **Model Formulation Review:** Was a rigorous evaluation and inter-comparison made between the scientific formulation of the proposed meteorological modeling system (source codes plus pre- and post-processors) versus alternative contemporary prognostic models via an open, thorough scientific review process?
- > **Code Verification:** Was the fidelity of the computer coding of the proposed model confirmed with respect to its scientific formulation, governing equations, and numerical solution procedures?

Identification of Air Quality Model Needs:

- > **Air Quality Input Needs:** Were the meteorological input needs of the host air quality model and supporting emissions models (e.g., biogenic, motor vehicle, area source processors) clearly identified including specification of the requisite averaging times and nested grid scales for the specific modeling episodes?
- > **Air Quality Model Sensitivities:** Was the air quality model’s sensitivity to key meteorological inputs established through careful consideration (including air quality model sensitivity/uncertainty

simulations) of the relevant modeling episodes over the specific domain of interest? Was the effect of uncertainty in those meteorological inputs to which the air quality model is demonstrated to be most sensitive adequately defined through appropriate numerical experiments or from previous relevant studies?

Note: Identification of air quality model needs is a crucial step in the meteorological model evaluation process, yet it is most often performed superficially if at all. Pragmatic constraints of time and resources necessitate that efforts be directed at achieving the best possible meteorological performance for those variables that matter most to the overall accuracy and reliability of the air quality model. There is little practical benefit to be gained in devoting considerable time to improving the accuracy of a particular meteorological variable if the air quality model – in the specific application at hand -- is insensitive to that variable. Particular attention should be given to those meteorological variables that have the largest uncertainty and to which the air quality model is most sensitive. This challenge can be particularly formidable when dealing with photochemical/aerosol models whose concentration and/or deposition estimates depend on several meteorological variables (mixing, transport, thermodynamic properties, precipitation) simultaneously.

Availability of Supporting Data Bases:

- > **Adequate Data Available:** Were sufficient data available to test, at the ground and aloft and over all nested grid scales of importance, the model's dynamic, thermodynamic, and precipitation-related fields?

- > **All Data Used:** Was the full richness of the available data base actually utilized in the input data file development, in FDDA, and in the evaluation of model performance?

Note: One of the main considerations underlying selection of modeling episodes for regulatory decision-making is the availability of special data collection programs to supplement the surface and aloft data routinely available from state and federal agencies. While attempts are made to select modeling episodes that coincide with intensive field measurement programs, in these situations it is common that the full set of supplemental measurements are not used thoroughly in the model input development and performance testing phases. At times, the availability of 'high-resolution' databases is touted in support of a particular episode selection choice yet when the modeling is actually performed and evaluated, only a fraction of the special studies data are actually used. This is most notably the case with air quality and meteorological data collected by aloft sampling platforms. Unless the high-resolution data are actually used to enhance the modeling and performance testing, their value is severely limited. Equally troublesome, selection of other candidate modeling days (supported by only routine information) may be overlooked which might otherwise be preferable modeling periods if a concerted effort to utilize special studies data is not made. Finally, as desirable as having supplemental meteorological measurements might be, unless the sampling was performed in the correct regions and includes the variables of primary importance to the air quality model, their potential to add meaningfully to the rigor of the modeling exercise will

be limited. Thus, when judging the value of supplemental measurement programs, it is necessary to look beyond just their mere existence (relative to non-intensively monitored days); one must establish that these intensive data set indeed contribute to improved model performance and increased reliability. This necessitates a feedback loop to the air quality modeling exercise to ensure that the times, locations, and parameters associated with the supplemental measurements truly add to the overall quality and rigor of the study.

Results of Operational, Diagnostic, and Scientific Evaluations:

- > **Full Model's Predictive Performance:** Was a full suite of statistical measures, graphical procedures, and phenomenological explorations performed with each of the models state variables and diagnosed quantities for each pertinent grid nest to portray model performance against available observations and against model estimates from other relevant prognostic simulation exercises?

- > **Performance of Individual Modules:** Was there an adequate evaluation of the predictive performance of individual process modules and preprocessor modules (e.g., advection scheme, sub-grid scale processes, closure schemes, planetary boundary layer parameterization, FDDA methodology)?

- > **Diagnostic Testing:** Were sufficient and meaningful diagnostic, sensitivity, and uncertainty analyses performed to assure conformance of the meteorological modeling system with known or expected behavior in the real world?

- > **Mapping Methods:** Were parallel evaluations made of: (a) the output from the prognostic model and (b) the output from the 'mapping' routines that interpolate the prognostic model output onto the host air quality model's grid structure? Were any important differences between the two reconciled?

- > **Quality Assurance:** Was a credible quality assurance (QA) activity implemented covering both the prognostic modeling activity as well as the mapping programs that generate air quality-ready meteorological inputs? Was the full set of hourly, three-dimensional fields examined for reasonableness even though observational data for comparison were lacking or in short supply?

Note: Such an intensive performance evaluation process is rarely, if ever, carried out due to time, resource and data base limitations. Nevertheless, it is useful to identify the *ideal* evaluation framework so that the results of the *actual* evaluation can be judged in the proper perspective. This also allows decision-makers to establish realistic expectations regarding the level of accuracy and reliability associated with the meteorological and air quality modeling process.

Comparison with Other Relevant Studies:

- > **Comparisons with Other Studies:** Were the model evaluation results (statistical, graphical, and phenomenological) compared with other similar applications of the same and alternative prognostic models to identify areas of commonality and instances of differences between modeling platforms?

Note: Reflecting limited data sets for performance testing and reliable criteria for judging a model's performance, meteorological model evaluations in recent years have emphasized comparisons with other RAMS and MM5 simulations over various modeling domains and episode types as a means of broadening the scope of the evaluation. While this insight into the model's performance – when gauged against other similar applications – is useful, caution must attend such comparisons which at times are at best anecdotal. Often the reporting of previous evaluations entails grossly composited performance statistics (episode averages or averages across episodes, for example), data bases and modeling efforts of widely varying and often unreported quality, different mathematical definitions of statistical quantities, and so on. Thus, these comparisons with other studies, while occasionally providing useful perspective, are by no means sufficient for declaring a meteorological model's performance to be reliable and acceptable in a particular application. Moreover, meteorological model evaluation benchmarks developed on the basis of such historical evaluation studies must also be applied thoughtfully with these limitations in mind.

Peer Review of Specific Modeling Exercise(s):

- > **Scope of Peer Review:** Was an adequate, properly-funded, independent, in-depth peer review of the model set-up, application, and performance evaluation efforts conducted?
- > **Findings of Peer Review:** Was the effort judged acceptable by the peer-review?

Note: Prognostic modeling requires considerable attention to detail, careful identification of options, and complete involvement in the work. Even with this commitment, critical aspects of a modeling exercise may be treated inadequately or overlooked, most often as the result of schedule or resource constraints. Consequently, an examination of the meteorological modeling effort conducted at arm's length by individuals with appropriate expertise and who have no personal involvement in the work can be essential to avoiding inadvertent oversights and problems. Such a peer review of the effort provides another check on the work as a whole. If concerns are raised about the reliability of the modeling, yet meteorological modeling results are to be used in applying air quality models despite these concerns (e.g., due to project schedule demands), the peer review can assist in suggesting to decision-makers the weight to be given the overall air quality results the planning and management context.

Often, when a professional paper is written describing the modeling study, it undergoes “peer review” by the journal. Such efforts do not constitute the review suggested here. Journal peer review usually entails a reading of the paper, thoughtful reflection, and written commentary, perhaps a 4- to 12-hour effort. Moreover, reporting in the professional literature is necessarily condensed, and much of the detail that should be scrutinized is omitted. This is especially true for complex atmospheric modeling projects.

Peer review for pre-print volumes (e.g., American Meteorological Society or Air and Waste Management Association conferences) is even less rigorous, often consisting of a cursory reading of the paper by the Session Chairperson. Peer review, as used here, refers to detailed examination and evaluation of the work conducted by experts in the field. Such experts are generally, but not limited to, those with considerable direct experience in the development, evaluation, and application of the same or very similar meteorological models. This in depth review entails the independent scientists (a) thoroughly examining the conceptual model(s) and modeling protocols prepared for the study, (b) obtaining and examining the details of the model input and output files, and (c) in many cases even running the pre- and post-processor codes and the main simulation programs to corroborate reproducibility of results and to explore inevitable technical issues that arise in such comprehensive reviews. In essence, peer review refers to immersing oneself in the materials provided. Such an effort can take *several weeks* to carry out properly.

Overall Assessment:

- > **Overall Reasonableness:** Has an adequate effort been made to evaluate the quality of representation of meteorological fields generated using the meteorological model, as revealed by the full suite of statistical, graphical, phenomenological, diagnostic, sensitivity, and uncertainty investigations? What were the strengths and limitations of the actual model performance evaluation?
- > **Fulfillment of Air Quality Model Needs:** How well are the fields represented, particularly in areas and under conditions for which the air quality model is likely to be sensitive?
- > **Appropriate Model:** Was a sound and suitable meteorological modeling system adopted?
- > **Adequate Data Base:** Was the supporting database adequate to meet input and evaluation needs?
- > **Adequate Application Procedures:** Was Four Dimensional Data Assimilation (FDDA) a part of the overall modeling approach and were sufficient data available to support the activity adequately?
- > **Quality Assurance:** Were error-checking procedures instituted, followed, and the results reported?
- > **Performance Evaluation:** Were suitable procedures specified and adopted for evaluating the quality (e.g., accuracy, precision, and uncertainty) of model estimates?
- > **Judging the Overall Process:** Were the criteria (i.e., benchmarks) used to judge performance appropriate for the specific air quality model application, rigorously applied, and properly communicated?

9.4.2 Comparison of SAMI RAMS Performance Against Newly Proposed Meteorological Model Performance Benchmarks

As discussed previously, there are no currently accepted performance criteria for prognostic meteorological models. In addition, there is valid concern that establishment of such criteria, unless accompanied with a careful evaluation process such as the one outline in this section might lead to the misuse of such goals as is occasionally the case with the accuracy, bias, and error statistics recommended by EPA for judging photochemical dispersion models. In spite of this concern, there remains nonetheless the need for some benchmarks against which to compare new prognostic model simulations.

In Table 8-4 we previously presented the RAMS episode-average temperature, wind, and mixing ratio statistics on the 12 km grid for 7 SAMI episodes and compared them with corresponding results from twenty-one (21) other RAMS and MM5 model evaluation studies we have conducted since 1995. Since the time the draft report was prepared, the MM5/RAMS model evaluation data base has been extended to forty-one (41) studies (Tesche et al., 2002). The basic conclusions drawn in Chapter 8 based on the comparisons in Table 8-4 remain valid with this larger data set.

In two recent studies (Tesche et al., 2001b; Emery et al., 2001), an attempt has been made to formulate a set meteorological model evaluation benchmarks based on the most recent model evaluation literature. The purpose of these benchmarks is not to assign a passing or failing grade to a particular meteorological model application, but rather to put its results into a useful context. These benchmarks may be helpful to decision-makers in understanding how poor or good their results are relative to the range of other model applications in other areas of the U.S. Certainly an important criticism of the EPA guidance statistics for acceptable photochemical performance is that they are relied upon much too heavily to establish an acceptable (to the EPA) model simulation of a given area and episode. Often lost in routine statistical ozone model evaluations is the need to critically evaluate all aspects of the model via the diagnostic and process-oriented approaches. The same must stressed for the meteorological performance evaluation. Thus, the appropriateness and adequacy of the following benchmarks should be carefully considered based upon the results of the specific meteorological model application being examined. Based upon these considerations, the benchmarks suggested from the studies of Emery et al, (2001) and Tesche et al., (2001) are as follows:

<i>Parameter</i>	<i>Measure</i>	<i>Benchmark</i>
<u>Wind Speed</u>	RMSE:	≤ 2 m/s
	Bias:	$\leq \pm 0.5$ m/s
	IOA:	≥ 0.6
<u>Wind Direction</u>	Gross Error:	≤ 30 deg
	Bias:	$\leq \pm 10$ deg
<u>Temperature</u>	Gross Error:	≤ 2 K

Bias: $\leq \pm 0.5 \text{ K}$
IOA: ≥ 0.8

Humidity

Gross Error: $\leq 2 \text{ g/kg}$
Bias: $\leq \pm 1 \text{ g/kg}$
IOA: ≥ 0.6

Table 9-4 presents the results of comparing the seven SAMI RAMS episode average statistical results (for those statistics that were produced in this study) with the proposed meteorological modeling benchmarks. Cells in the table colored salmon correspond to those episodes and meteorological variables that fall outside of the benchmark ranges. From the table, several of the surface temperature bias and error value lie outside the benchmark ranges as do the RMSE errors for surface winds. Compared with the benchmarks, the SAMI temperature simulations exhibit a larger under-prediction and somewhat larger errors. Also, for about half the episode, the RMSE winds are above the benchmark ranges. In only two instances (the 23-31 March '93 and 8-13 Feb '94 episodes) are the wind direction statistics noticeably poorer than the benchmarks. The mixing ratio (specific humidity) results are very good and well within the benchmark ranges. The observed temperature under-prediction bias and the over-prediction bias (discussed in Chapter 8) are perhaps the most noteworthy areas in which potential impacts on the air quality model calculations might be expected.

While one could speculate as to whether these biases and errors might have an adverse impact on the air quality model, this would actually have to be determined through air quality model sensitivity/uncertainty analyses. We are unaware of the extent to which formal exercises of this nature were conducted in the SAMI air quality modeling program. Absent this information, judgments about the impacts, if any, on the reliability of the air quality model estimates would be speculative. Ideally, these temperature and wind speed biases should be considered by the air quality modelers in their model sensitivity and uncertainty analyses.

9.4.3 Concluding Assessment of the SAMI RAMS Application

Table 9-5 presents the results of our effort to judge the adequacy of the RAMS meteorological modeling process for SAMI and the specific results for the nine (9) episodes against the set of two-dozen questions raised in the preceding section. Our overall conclusions about the adequacy of the RAMS modeling and the reliability of the meteorological fields supplied to the URM-AERO model are as follows:

- > The SAMI meteorological modeling activity clearly selected an appropriate regional prognostic model for use in the assessment;
- > The RAMS modeling was carried out in a logical, sound, well-documented manner that was consistent with good scientific principles and the procedures commonly used in the application of this sophisticated model;
- > The suite of evaluation procedures employed to test the RAMS model were comprehensive and

reflected several different model testing perspectives;

- > The data base available to test the RAMS model was extremely limited, precluding a number of meaningful, stressful tests of the model to ascertain whether it suffers from internal, compensating errors; as the result, model testing was confined principally to an operational evaluation;
- > Generally, the RAMS performance for surface and aloft winds, temperatures, mixing ratios, and precipitation are consistent with contemporary modeling experience and with new proposed evaluation benchmarks;
- > In some cases, notably the under-prediction bias for surface temperature and over-prediction bias for surface wind speed, the RAMS model exhibits (for some episodes) features that could have an effect on the air quality model estimates; however, this has not been verified through sensitivity experiments with the URM-AERO modeling system to demonstrate that these biases are indeed important. In other cases, notably mixing ratio, the RAMS performance was much better than is typically encountered with modeling of this complexity; and
- > None of the performance testing results conducted have revealed flaws in RAMS performance of such a magnitude as to clearly indicate the presence of errors that would render the model inappropriate for use as input to regional air quality models.

We conclude that the RAMS meteorological fields may be used, with appropriate cautions, to drive the regional emissions and photochemical/aerosol models for each of the episodes selected for the SAMI assessment.

Table 9-4. SAMI Modeling Results Compared with the Proposed Benchmarks.

	Episode	Temperature, (deg C)		Mix Ratio, (gm/Kg)		Surface Winds (m/s)		
		Bias	Error	Bias	Error	RMSE	Indx A	WDir Error
1	24-29 May '95	-1.0	1.9	0.0	0.8	1.90	0.76	13
2	11-17 May '93	-1.5	2.1	0.0	0.8	1.90	0.76	6
3	23-31 Mar '93	-1.3	2.2	0.0	0.6	2.27	0.74	100
4	8-13 Feb '94	0.5	2.1	0.0	0.4	2.76	0.72	103
5	3-12 Aug '93	-0.4	1.6	-0.6	1.1	2.18	0.75	25
6	22-29 Jun '92	-1.1	1.8	0.0	1.0	1.89	0.75	20
7	24Ap-3My '91	-0.8	1.8	-0.1	0.7	2.35	0.81	4
	<i>Benchmark</i>	$\leq \pm 0.5$	≤ 2.0	$\leq \pm 1.0$	≤ 2.0	≤ 2.00	≥ 0.60	≤ 30
	<i>SAMI Mean</i>	-0.8	1.9	-0.1	0.8	2.18	0.76	39
	<i>U. S. Mean</i>	-0.1	1.9	0.0	1.9	1.95	0.70	25

Table 9-5. Assessment of the RAMS Meteorological Fields As Input to the SAMI URM-AERO Acid Deposition Model.

No.	Question	Assessment
Appropriateness of Model Selection		
1	Was a careful written characterization made of the most important physical and chemical processes relevant to successful air quality modeling of each episode (e.g., a “conceptual model” of each simulation period)?	No. See the SAMI Air Quality Modeling Protocol by Russell et al. (1998).
2	Did the model selection process ensure that a suitable modeling system was chosen, properly weighing the need for mature, well-tested, publicly-available model(s) against the constraints of the specific modeling problem, characteristics of the episodes to be simulated, and the limitations of schedule and resources?	Yes. Given the fact that the episodes selected involved periods of light to heavy precipitation, the RAMS model was a sound choice. While the RAMS model was proprietary at the time SAMI began, it was possible for independent groups to obtain rights to use the code at a cost.
3	Was a rigorous evaluation and inter-comparison made between the scientific formulation of the proposed meteorological modeling system (source codes plus pre- and post-processors) versus alternative contemporary prognostic models via an open, thorough scientific review process?	No. We are not aware of any detailed comparisons being performed between RAMS and alternative models (e.g., MM5) including their respective pre- and post-processor systems. Model selection was based on general attributes of the RAMS model and the extensive experience of the SAMI contractor (UAH) in exercising this model.
4	Was the fidelity of the computer coding of the proposed model to the scientific formulation, governing equations, and numerical solution procedures adequately examined and confirmed?	The RAMS modeling system is well established with a rich development and refinement history spanning more than two decades. The model has seen extensive use worldwide by many agencies, consultants, university scientists and research groups. The current version of the model and its predecessor versions have been extensively "peer-reviewed" and considerable algorithm development and module testing has been carried out with all of the important process components.
Identification of Air Quality Model Needs		
5	Were the meteorological input needs of the host air quality model and supporting emissions models (e.g., biogenic, motor vehicle, area source processors) clearly identified including specification of the requisite average times and nested grid scales for the specific modeling episodes?	No. See the SAMI Meteorological Modeling Protocol by Norris and Doty (1998).
6	Was the air quality model’s sensitivity to key meteorological inputs established through careful consideration (including air quality model sensitivity/uncertainty simulations) of the relevant modeling episodes over the specific domain of interest? Was the effect of uncertainty in those meteorological inputs to which the air quality model is demonstrated to be most sensitive adequately defined through appropriate numerical experiments or from previous relevant studies?	No. The SAMI URM-AERO model was still undergoing final development at the time the RAMS model applications were initiated. While there was anecdotal information about the URM’s sensitivity to key model inputs, no domain- or episode-specific information was developed to help identify the subset of RAMS outputs that were most critical to the UAM-AERO gas-phase, secondary aerosol, or acid deposition predictions.
Availability of Supporting Data Bases		
7	Were sufficient data available to test, at the ground and aloft and over all nested grid scales of importance, the model’s dynamic, thermodynamic, and	No. Data were adequate to set up, operate, and evaluate (operationally) the RAMS model with standard surface and aloft NWS data sets and other information from

	precipitation-related fields?	established surface reporting networks (e.g., TVA precip. sites). No supplemental meteorological data sets, particularly for aloft processes, were available.
8	Was the full richness of the available data base actually utilized in the input data file development, in FDDA, and in the evaluation of model performance?	No. Some supplemental data sets were available.
Results of Operational, Diagnostic, and Scientific Evaluations		
9	Was a full suite of statistical measures, graphical procedures, and phenomenological explorations performed with each of the model's state variables and diagnosed quantities for each pertinent grid nest to portray performance against available observations and estimates from other relevant prognostic modeling exercises?	Yes, for the most part. An extensive set of operational evaluation statistics and graphical displays were produced focusing on point comparisons, residual analyses, and comparisons between spatial fields of measurements and predictions. The operational evaluations were carried out at all RAMS spatial scales but the level of analysis and reporting varied from one grid scale to the next. The 12 km scale received the greatest attention.
10	Was there an adequate evaluation of the predictive performance of individual process modules and preprocessor modules (e.g., advection scheme, sub-grid scale processes, closure schemes, planetary boundary layer parameterization, FDDA methodology)?	No. Lack of data to perform these experiments and SAMI schedule and resource allocations prevented these explorations from being carried out.
11	Were sufficient and meaningful diagnostic, sensitivity, and uncertainty analyses performed to assure conformance of the meteorological modeling system with known or expected behavior in the real world?	Very limited. Detailed diagnostic sensitivity experiments were performed with a few episodes (especially the first one) but subsequently, little diagnostic or sensitivity experimentation was performed as the result of schedule and budget considerations.
12	Were parallel evaluations made of: (a) the output from the prognostic model and (b) the output from the 'mapping' routines that interpolate the prognostic model output onto the host air quality model's grid structure? Were sources of differences between the two reconciled?	No. SAMI schedule and resource constraints precluded an in-depth comparison of "raw" RAMS output fields vs. the URM-ready meteorological fields resolved to the air quality model grid mesh.
13	Was a credible quality assurance activity implemented covering both the prognostic modeling activity as well as the mapping programs that generate air quality-ready meteorological inputs? Was the full set of hourly, three-dimensional fields examined for reasonableness even though observational data for comparison are lacking or in short supply?	Partially. Quality assurance activities consisted principally of routine plotting of surface fields, calculation of summary statistics (to reveal outliers or anomalies), and related graphical display methods to provide a cursory check of the model inputs and outputs. However, once the data input preparation procedures were established, the RAMS input files were constructed mostly in a hands-off manner. Quality assurance activities of the RAMS output fields was performed as an integral part of the statistical and graphical performance examinations.
Comparison with Other Relevant Studies		
14	Were the model evaluation results (statistical, graphical, and phenomenological) compared with other similar applications of the same and alternative prognostic models to identify areas of commonality and instances of differences between modeling platforms?	Partially. Episode average statistics over the 12 km grid were compared with thirty four (34) RAMS and MM5 model applications elsewhere in the U.S., primarily involving summertime ozone episodes with typical grid scales in the 4 – 16 km range. (See Table 84). No <u>detailed</u> comparisons were performed between the SAMI episodes and others reported in the literature to elucidate areas of similar performance and areas of disparate performance.
Peer Review of Specific Modeling Exercise(s)		
15	Was an adequate, properly funded, independent, in-depth peer review of the	No. SAMI schedule and resource constraints precluded a rigorous, independent

	model set-up, application, and performance evaluation efforts conducted?	peer-review of the RAMS meteorological modeling. Only a very limited-scope “peer” review was conducted as the result of Alpine Geophysics modelers engagement in the SAMI meteorological process to assist in the development of the three final episodes. This allowed an independent group to corroborate the UAH base case and modeling methods. No substantive irregularities in the UAH RAMS modeling were uncovered in the work carried out by Alpine scientists.
16	Was the effort judged acceptable by the peer-review?	Not applicable since no formal peer review was performed.
	Overall Assessment	
17	Has an adequate effort been made to evaluate the quality of representation of meteorological fields generated using the meteorological model, as revealed by the full suite of statistical, graphical, phenomenological, diagnostic, sensitivity, and uncertainty investigations? What were the strengths and limitations of the actual model performance evaluation?	Generally yes. One consequence of two different groups performing the meteorological modeling was that complimentary perspectives were brought to bear on the performance evaluation portion. This involved: (a) ‘synoptic’ or broad-scale perspective and (b) examination of the fidelity of model predictions in the vicinity of surface and aloft measurement sites within the planetary boundary layer. A rich variety of analytical procedures, statistical metrics and graphical tools employed by the two groups reflecting their particular perspective and experience in prognostic model evaluation, led to complimentary and corroborating examinations of performance and produced insights into the model’s operation that would not be as thoroughly examined via one approach alone. All of the statistical and graphical presentation methods employed were used extensively and effectively in past evaluations reported broadly in the literature.
18	How well are the fields represented, particularly in areas and under conditions for which the air quality model is likely to be sensitive?	Uncertain. The SAMI schedule and resources precluded detailed exchange between the meteorological and air quality modeling teams. The process was largely serial with the meteorology being produced, followed by the air quality modeling. With the exception of the first episode, there was very little opportunity for interaction among the meteorological and air quality modelers to produce a sustained cycle of RAMS diagnosis and performance improvement, followed by an investigation of the URM-AERO model response, producing yet another round of meteorological model diagnosis and performance improvement.
19	Was a sound and suitable meteorological modeling system adopted?	Yes. The RAMS model used in the SAMI application is clearly representative of the state-of-the-science in mesoscale prognostic modeling for air quality applications.
20	Was the supporting database adequate to meet input and evaluation needs?	No. While the available data base was sufficient to set up, exercise, and evaluate operationally the model, it was clearly deficient in supporting rigorous testing, aimed at identifying potential sources of internal, compensating errors.
21	Was Four Dimensional Data Assimilation (FDDA) a part of the overall modeling approach and were sufficient data available to support the activity adequately?	Partially. The routinely available data were sufficient to utilize data assimilation in the RAMS simulations. However, lack of high-resolution data (e.g., radar wind profilers) and budget/time constraints precluded the infusion of this information into the routine FDDA methodologies that were ultimately used.
22	Were error-checking procedures instituted, followed, and the results	Partially. The results of quality assurance activities were reported anecdotally during

	reported?	conference calls and project meetings but no formal chronology was archived of the problems encountered and solutions rendered.
23	Were suitable procedures specified and adopted for evaluating the quality (e.g., accuracy, precision, and uncertainty) of model estimates?	Partially. Very useful statistical measures and graphical procedures were employed to quantify performance for key dynamic and thermodynamic variables (e.g., bias, gross errors, root-mean-square-error, Index of Agreement, threat scores). However, little quantitative information was produced relative to model uncertainty. No formal uncertainty analysis was conducted of the RAMS simulations. Hence, the estimates of “uncertainty” in the RAMS outputs are based on the ranges in the various statistics (e.g., the range in the model’s surface temperature bias over 9 episodes) as compared to quantitative estimate of model uncertainty arising due to: (a) formulation, (b) procedures for developing inputs or processing outputs, and (c) measurement error and spatial representativeness issues.
24	Were the criteria (benchmarks) used to judge performance appropriate for the specific air quality model application, rigorously applied, and properly communicated?	Partially. A credible effort was made to identify the key components of the meteorological model evaluation process and to address each one subject to the constraints of project schedule, resources, and the information available from the meteorological and air quality modeling activities. While the present SAMI RAMS evaluation is arguably more comprehensive and systematic than any other previous prognostic model evaluation study supporting air quality applications, many areas of the evaluation were not adequately explored, principally as the result of these limitations.

9.5 In Summary

One of the most important questions addressed in this report concerns whether the RAMS meteorological fields are adequate for their intended use in supporting the acid deposition modeling in SAMI. For the reasons discussed in Chapter 9, we are not able to answer this question definitively, yet a significant amount of information was developed in this study that supports our finding that the RAMS modeling results are suitable for use in the UAM-AERO acid deposition modeling although a number of important questions remain to be answered fully.

There is no simply way to answer definitively the question of whether the RAMS fields are adequate as input to the SAMI acid deposition model. There are no universally accepted performance benchmarks that, if passed, would allow one to declare unequivocally that the RAMS fields are appropriate for use. For complex atmospheric modeling problems like the ones being addressed by SAMI, it is quite doubtful that such a set of definitive performance criteria will ever be completely sufficient. The question of meteorological data set adequacy depends, at a minimum, upon the specific host emissions and air quality models and the nature of the modeling episodes being used. Meteorological fields that might be adequate for use in one situation may be quite deficient in another if the particular chemical and physical processes that must be simulated are different. Thus, quantitative statistical and graphical performance criteria, though helpful, are inherently insufficient in telling modelers and decision-makers whether meteorological fields are adequate for air quality modeling. In this study, we developed and then applied a multi-step evaluation process whereby the adequacy of the RAMS fields for use in the SAMI acid deposition modeling was evaluated.

In addition to comparing the SAMI results with a large range of previous meteorological model evaluation studies in the U.S., we also compared the RAMS evaluation results with a recently proposed set of meteorological model evaluation benchmarks based on the most recent model evaluation literature. While these benchmarks are not aimed at assigning a passing or failing grade to a particular meteorological model application, they do help put the results into a useful context for decision-makers. Based on these and other analyses reported in Chapter 9, our overall conclusions regarding the adequacy of the RAMS modeling and the reliability of the meteorological fields supplied to the URM-AERO model are as follows:

- > The SAMI meteorological modeling activity clearly selected an appropriate regional prognostic model for use in the assessment;
- > The RAMS modeling was carried out in a logical, sound, well-documented manner that was consistent with good scientific principles and the procedures commonly used in the application of this sophisticated model;
- > The suite of evaluation procedures employed to test the RAMS model were comprehensive and reflected several different model testing perspectives;
- > The data base available to test the RAMS model was extremely limited, precluding a number of meaningful, stressful tests of the model to ascertain whether it suffers from internal, compensating errors; as the result, model testing was confined principally to an operational evaluation;
- > Generally, the RAMS performance for surface and aloft winds, temperatures, mixing ratios, and precipitation are consistent with contemporary modeling experience and with new proposed evaluation benchmarks;

- > In some cases, notably the under-prediction bias for surface temperature and over-prediction bias for surface wind speed, the RAMS model exhibits (for some episodes) features that could have an effect on the air quality model estimates; however, this has not been verified through sensitivity experiments with the URM-AERO modeling system to demonstrate that these biases are indeed important. In other cases, notably mixing ratio, the RAMS performance was much better than is typically encountered with modeling of this complexity; and
- > None of the performance testing results conducted have revealed flaws in RAMS performance of such a magnitude as to clearly indicate the presence of errors that would render the model inappropriate for use as input to regional air quality models.

We conclude that the RAMS meteorological fields may be used, with appropriate cautions, as input to the regional emissions and photochemical/aerosol models for each of the episodes selected for the SAMI assessment.

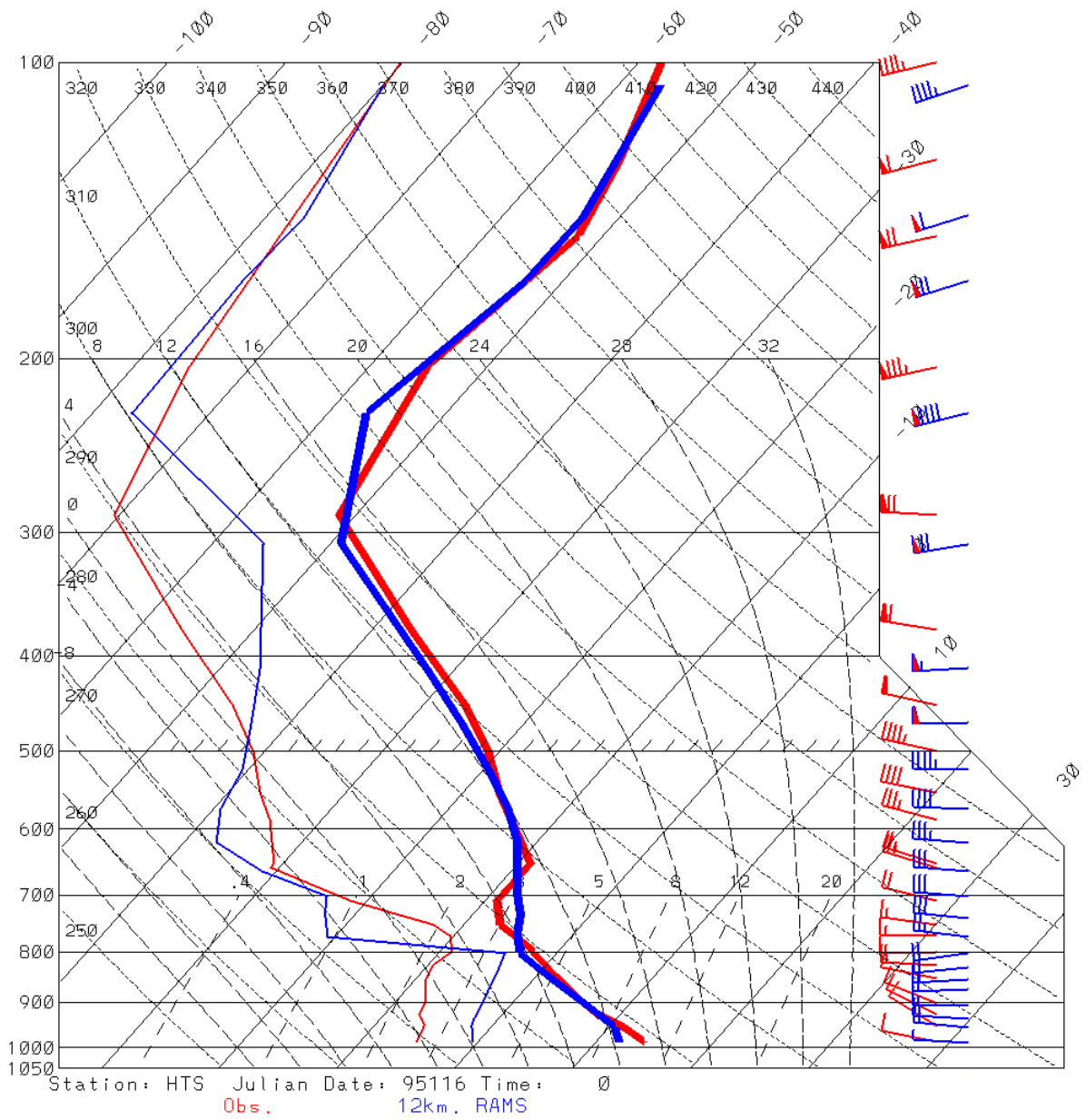


Figure 9-6. Vertical Profiles of Wind, Temperature and Mixing Ratio at Huntington, WV at 1900 EST on 25 April 1995.

9 REFERENCES

Anthes, R. A. and T. T. Warner, 1978. The Development of Mesoscale Models Suitable for Air Pollution and Other Mesometeorological Studies, Monthly Weather Review, vol. 106, pp, 1045-1078.

Anthes, R. A., 1977. A Cumulus Parameterization Scheme Utilizing a One-Dimensional Cloud Model, Monthly Weather Review, Vol. 105, pp. 270-286.

Anthes, R. A., E. Y. Hsie, and Y. H. Kao, 1987. "Description of the Penn State/NCAR Mesoscale Model Version 4 (MM4)", NCAR Technical Note 282, National Center for Atmospheric Research, Boulder, CO.

Arakawa, A. and W. Schubert, 1974. Interaction of a Cumulus Cloud Ensemble with the Large Scale Environment, Part I. J. Atmos. Sci., Vol. 31, pp. 674-701.

ARB, 1992. "Technical Guidance Document: Photochemical Modeling", prepared by the California Air Resources Board, Sacramento, CA.

Arunachalam, S., 2001. "A Comparison of EPA's Models-3/CMAQ and the MAQSIP Modeling System for Ozone Modeling in North Carolina.", 94th Annual Conference of the Air and Waste Management Association, 24-28 June 2001, Orlando, FL.

ASTeR, 1991. ARAMS: The Regional Atmospheric Modeling System, Version 2c User's Guide, ASTeR, Inc., Fort Collins, CO.

Atkinson, R., 2000. "Atmospheric Chemistry of VOCs and NOx", Atmospheric Environment, Vol. 34, pp. 2063-2100.

Avissar, R. and Y. Mahrer, 1988. Mapping Frost-Sensitive Areas with a Three-Dimensional Local-Scale Numerical Model. Part I: Physical and Numerical Aspects, Journal of Applied Meteorology, Vol. 27, pp. 400-413.

Bankov, E., et al., 1998. "A trajectory-clustering-correlation methodology for examining the long-range transport of air pollutants", Atmospheric Environment. Vol. 32, pp. 1525-1534.

Banta, R. M., et al., 1998. "Daytime buildup and nighttime transport of urban ozone in the boundary layer during a stagnation episode", Journal of Geophysical Research, 103: 22519-22544.

Barchet, W. R. and R. L. Dennis, 1990. NAPAP Model Evaluation, Volume 1: Protocol, prepared for the U.S. Environmental Protection Agency, prepared by Battelle Pacific Northwest Laboratories, Richland, WA.

Barnes, S. L., 1973: Mesoscale objective analysis using weighted time-series observations. NOAA Tech. Memo. ERL NSSL-62, National Severe Storms Laboratory, Norman, OK 73069, 60 pp, [NTIS COM-73-10781].

- Beljaars, A. C. M., and A. A. Holtslag, 1991: Flux parameterization over land surfaces for atmospheric models. J. Appl. Meteor., 30, 327-341.
- Beljaars, A. C., 1994: The parameterization of surface fluxes in large-scale models under free convection. Q. J. R. Meteorol. Soc., 121, 255-270.
- Benjamin, S. G. and N. L. Seaman, 1985. "A Simple Scheme for Objective Analyses in Curved Flow", Mon. Wea. Rev., Vol. 113, pp. 1184-1198.
- Berman, S., et al., 1997. "Uncertainties in estimating the mixing depth - Comparing three mixing-depth models with profiler measurements", Atmospheric Environment, (18) 3023-3039.
- Berman, S., et al., 1999. "Spatial and temporal variation in the mixing depth over the northeastern United States during the summer of 1995", Journal of Applied Meteorology, 38: (12) 1661-1673.
- Blackadar, A. K., 1979. High Resolution Models of the Planetary Boundary Layer, Advances in Environmental Science and Engineering, Vol. 1, No. 1, J. Pfafflin and E. Ziegler, Eds., Gordon and Breach, 50-85.
- Blanchard, C. L., 1999. "Ozone Attainment and Control Strategy Evaluation", prepared for the American Petroleum Institute, prepared by Envair, Albany, CA.
- Blanchard, C. L., 2000. "Ozone Process Insights from Field Experiments: Part III: Extent of Reaction and Ozone Formation", Atmospheric Environment, Vol. 34, pp. 2035-2044.
- Blanchard, C. L., 2001. "Trends in Ambient Concentrations of Ozone and Precursor Species in Eight Geographical Regions", 94th Annual Conference of the Air and Waste Management Association, 24-28 June 2001, Orlando, FL.
- Blanchard, C. S., 2001. "Spatial Mapping of VOC and NO_x Limitation of Ozone Formation in Six Areas", 94th Annual Conference of the Air and Waste Management Association, 24-28 June 2001, Orlando, FL.
- Blumenthal, D., et al., 1997. "Assessment of Transport and Mixing and OTAG Model Performance for Northeast U.S. Ozone Episodes: Summary of Results", prepared for the U.S. EPA, prepared by Sonoma Technology, Inc., Santa Rosa, CA.
- Bowne, N. E. and D. L. Shearer, 1991. "Lake Michigan Ozone Study: Summary of Field Measurements", First Draft, prepared by ENSR Consulting and Engineering, prepared for the Lake Michigan Air Directors Consortium, Des Plaines, IL.
- Bowne, N. E., 1992. "The Lake Michigan Ozone Study: The Data", 85th Annual Meeting of the Air and Waste Management Association, 21-26 June, Kansas City, MO.

Brieman, L., J. H. Friedman, R. A. Olshen, and C. J. Stone, 1984. *Classification and Regression Trees* Wadsworth, Belmont, California.

Brook, J. R., et al., 1999. "Description and Evaluation of a Model of Deposition Velocities for Routine Estimates of Air Pollutant Dry Deposition over North America: Part I: Model Development", Atmospheric Environment, Vol. 33, pp. 5037-5051.

Burk, S. D. and W. T. Thompson, 1989. Vertically Nested Regional Numerical Prediction Model with Second-order Closure Physics, Mon. Wea. Rev., 117, pp. 2305-2324.

Byun, D. W., 2001. "Regional, Urban, and Neighborhood Scale Air Quality Simulation with Models-3 Community Multi-Scale Air Quality (CMAQ) Model", 94th Annual Conference of the Air and Waste Management Association, 24-28 June 2001, Orlando, FL.

Casey, D. M., R. T. McNider, and A. J. Song, 1995: A quantitative analysis of the predictability of mesoscale convective activity in regions of weak synoptic forcing over the southeastern United States. Fourteenth Conference on Weather Analysis and Forecasting, Jan. 15-20, 1995, Dallas, Texas, Am. Meteor. Soc.

Chameides, W. L., et al., 2000. "An Assessment of Tropospheric Ozone: A North American Perspective NARSTO Synthesis Team", Available at the NARSTO Website. (Pages 3-11 to 3-22 are particularly informative).

Chan, D., et al., 1999. "Linking Changes in Ozone to Changes in Emissions and Meteorology", Proc. Air Pollution 99 Conf., Palo Alto, CA. Wessex Institute of Technology, pp. 663-675.

Changnon, S. A., K. E. Kunkel, and B. C. Reinke, 1996: Impacts and responses to the 1995 heat wave: A call to action. Bull. Amer. Meteor. Soc., 77, 1497-1506.

Chen, C. and W. R. Cotton, 1983: A one-dimensional simulation of the stratocumulus-capped mixed layer. Bound.-Layer Meteor., 25, 289-321.

Civerolo, K. L., et al., 2000. "The effects of land use in meteorological modeling: implications for assessment of future air quality scenarios", Atmospheric Environment, 34: (10) 1615-1621.

Colby, F. P. Jr., 1984: Convective inhibition as a predictor of convection during AVE-SESAME II. Mon. Wea. Rev., 112, 2239-2252.

Cotton, W. R., et al., 1982. The Colorado State University Three-Dimensional Cloud/Mesoscale Model C 1982, Part II: An Ice Phase Parameterization, J. Rech. Atmos., Vol. 16, pp. 295-320.

Cowling, E. B. and C. Furiness (eds), 2000. "The state of the Southern Oxidants Study (SOS): Policy7 Relevant Findings in Ozone and PM2.5 Research 1994-2000", SOS Office, Raleigh, NC. [http://www2.ncsu/CIL/southern_oxidants/] (Pages 68-78 are particularly informative.)

Cox, R., et al., 1998. Mesoscale Model Intercomparison, Bulletin of the American Meteorological Society, Vol. 79, No. 2., pp. 265-283.

Daum, P. L., et al., 2000. "Analysis of O3 formation during a stagnation episode in central Tennessee in summer 1995", Journal of Geophysical Research, 105-9107-9119.

Davis, W. T., 2001. "VMT Growth Rates in the U.S. and Their Effects on NOx and VOC Emissions.", 94th Annual Conference of the Air and Waste Management Association, 24-28 June 2001, Orlando, FL.

Dennis, R. L., et al., 1990. "Evaluation of Regional Acid Deposition Models", State-of-Science/Technology Report No. 5, National Acid Precipitation Assessment Program, Washington, D.C.

Deuel, H. P. and S. G. Douglas, 1998. "Episode Selection for the Integrated Analysis of Ozone, Visibility, and Acid Deposition for the Southern Appalachian Mountains." Systems Applications International, Inc., San Rafael, California (SYSAPP-98/07r1).

Dickinson, R. E., et al., 1986. Biosphere-Atmosphere Transfer Scheme for the NCAR Community Climate Model, Tech. Report NCAR/TN-275+STR, National Center for Atmospheric Research, Boulder, CO.

Dodge, M. C., 2000. "Chemical Oxidant Mechanisms for Air Quality Modeling: A Review", Atmospheric Environment, Vol. 34, pp. 2103-2131.

Douglas, S. G., et al., 1996. "Investigation of the Effects of Horizontal Grid Resolution on UAM-V Simulation Results for Three Urban Areas", prepared for Southern Company Services and Cinergy Corporation, prepared by Systems Applications, Int., San Rafael, CA.

Dudhia, J., 1989. "Numerical Study of Convection Observed During the Winter Monsoon Experiment Using a Mesoscale Two-Dimensional Model", J. Atmos. Sci., Vol. 46. pp. 3077-3107.

Dudhia, J., 1993. "Non-hydrostatic Version of the Penn State/NCAR Mesoscale Model: Validation Tests and Simulation of an Atlantic Cyclone and Cold Front", Mon. Wea. Rev., Vol. 121. pp. 1493-1513.

Earth Tech, 1997. "Assessment of UAM-V Model Performance in the Northeast Region for OTAG Episodes", prepared for a consortium of Utilities in the Northeast, prepared by Earth Tech, Inc., Concord, MA.

Edgerton, E., 1996. "Comparison of Modeled Versus Observed Isoprene Concentrations at Rural and Suburban Sites Across the Eastern U.S.", Atmospheric Research and Analysis, Inc., Durham, N.C.

Ek, M. and L. Mahrt, 1991: A formulation for boundary layer cloud cover. Ann. Geophys., 9, 716-724.

Emery, C., E. Tai, and G. Yarwood, 2001. "Enhanced Meteorological Modeling and Performance Evaluation for Two Texas Ozone Episodes", prepared for the Texas Natural Resources Conservation Commission, prepared by ENVIRON International Corp, Novato, CA.

Emigh, R. A., et al., 1997. "Comparison of CEM-Enhanced Emissions with OTAG Base1c Emissions and the Impact on Ozone Concentrations", Final Report prepared for the Electric Power Research Institute, prepared by Alpine Geophysics, LLC, Boulder, CO.

ENSR, 1993. "Model Code Verification of Air Quality and Meteorological Simulation Models for the Lake Michigan Ozone Study", prepared for the Lake Michigan Air Directors Consortium, prepared by ENSR Consulting and Engineering, Hartford, CN.

EPA, 1991. "Guidance for Regulatory Application of the Urban Airshed Model (UAM)", "Office of Air Quality Planning and Standards, U.S. Environmental Protection Agency, Research Triangle Park, N.C.

EPA, 1997. "Calculation of Budget Components: Technical Support Document", prepared by the Office of Air and Radiation, U.S. Environmental Protection Agency, Research Triangle Park, NC.

EPA, 1997. Byun, D. W., 2001. "Regional, Urban, and Neighborhood Scale Air Quality Simulation with Models-3 Community Multi-Scale Air Quality (CMAQ) Model", 94th Annual Conference of the Air and Waste Management Association, 24-28 June 2001, Orlando, FL.

Eskridge, R E., et al., 1997. "Separating different scales of motion in time series of meteorological variables", Bulletin of the American Meteorological Society, 78: (7) 1473-1483.

Fast, J. D., 1995. Mesoscale Modeling and Four-Dimensional Data Assimilation in Areas of Highly Complex Terrain, J of Appl. Meteorology, Vol. 34, pp. 2762-2782.

Flatau, P. J., R. L. Walko, and W. R. Cotton, 1992: Polynomial fits to saturation vapor pressure. J. Appl. Meteor., 31, 1507-1513.

Flaum, J. B., et al., 1996. "Moderating the influence of meteorological conditions on ambient ozone concentrations", Journal of the Air and Waste Management Association 46: (1) 35-46.

Gayno, G. A., 1994. Development of a Higher-Order, Fog-Producing Boundary Layer Model Suitable For Use in Numerical Weather Prediction, M. S. Thesis, The Pennsylvania State University, 104 pp.

Gayno, G. A., et al., 1994. Forecasting Visibility Using a 1.5-Order Closure Boundary Layer Scheme in a 12 Km Non-Hydrostatic Model, 10th AMS Conference on Numerical Weather Prediction, Portland, OR. 18-22 July. American Meteorological Society, Boston, MA.

Gill, D. O., 1992. User's Guide to the Penn State/NCAR Mesoscale Modeling System, NCAR Tech. Note 381 +IA, National Center for Atmospheric Research, Boulder, CO, 233 pp.

Gillani, N. V. and J. E. Pleim, 1996. "Sub-Grid-Scale Features of Anthropogenic Emissions of NO_x and VOC in the Context of Regional Eulerian Models", Atmospheric Environment, Vol. 30. No. 12, pp. 2043-2059.

Gillani, N. V., et al., 1998. "Relative Production of Ozone and Nitrates in Urban and Rural Power Plant Plumes I. Composite Results Based on Data from 10 Measurement Days", Journal of Geophysical Research, 103: 22593-22615.

Gillani, N. V., et al., 1998. "Loss Rate of NO_y from a Power Plant Plume Based on Aircraft Measurements", Journal of Geophysical Research, Vol. 103, pp. 22585-22592.

Grell, G. A., J. Dudhia, and D. R. Stauffer, 1994. "Description of the Fifth Generation Penn State/NCAR Mesoscale Model (MM5). NCAR Tech. Note, NCAR TN-398-STR, 138 pp.

Grell, G. A., et al., 1991. Semi-prognostic Tests of Cumulus Parameterization Schemes in the Middle Latitudes, Monthly Weather Review, Vol. 119, pp. 5-31.

Guinnup, D. and B. Collom, 1997. "Telling The Ozone Story With Data", Final Report, Vol. I: Executive Summary OTAG Air Quality Analysis Workgroup.

Guinnup, D. and B. Colloum, 1997. "Final Report for the OTAG Air Quality Analysis Workgroup", Final Report, Vol. II, Summary and Integration of Results.

Hallmark, S. L., 2001. "Estimating Variability Between Passenger Car Vehicle Types and the Implications for Fleet Mix Estimates on Emissions", 94th Annual Conference of the Air and Waste Management Association, 24-28 June 2001, Orlando, FL.

Haney, J. L. and S. G. Douglas, 1996. "Analysis of the Effects of Grid Resolution on UAM-V Simulation Results for the Atlanta Nonattainment Area", prepared for the Southeast Modeling Center, prepared by Systems Applications, Int., San Rafael, CA.

Hanna, S. and M. E. Fernau, 1998. Monte Carlo Estimates of Uncertainties in Predictions by a Photochemical Grid Model (UAM-IV) Due to Uncertainties in Input Variables, Atmospheric Environment, Vol. 32, No. 21. pp. 3619-3628.

Hanna, S. G., et al., 1996. "Evaluation of Photochemical Grid Models (UAM- VI, UAM- V, and the ROM-UAM-VI Couple) Using Data from the Lake Michigan Ozone Study (LMOS)", Atmospheric Environment, Vol. 30, pp. 3265-3279.

Hanna, S. R. and J. C. Chang, 1992. "Representativeness of wind measurements on a mesoscale grid with station separations of 312 m to 10 km", Boundary Layer Meteorology. 60, 309-324.

Hanna, S. R. and J. C. Chang, 1993a. Relations Between Meteorology and Ozone in the Lake Michigan

Region, Prepared for the Lake Michigan Air Directors Consortium, Prepared by Sigma Research, Inc., Concord, MA.

Hanna, S. R. and J. C. Chang, 1993b. Characterization of Mixed Layer Depths During 1991 LMOS Intensive Study Periods, Prepared for the Lake Michigan Air Directors Consortium, Prepared by Sigma Research, Inc. Concord, MA.

Hanna, S. R., 1994. Mesoscale Meteorological Model Evaluation Techniques with Emphasis on Needs of Air Quality Models, in Pielke, R. and R. Pearce, (ed). Mesoscale Modeling of the Atmosphere, Meteoro. Monogr., No. 47, American Meteorological Society, Boston, MA.

Hanna, S. R., et al., 1995. "Analysis and Evaluation of the UAM-V, UAM-IV, and ROM/UAM-IV Photochemical Grid Models for the Region Around Lake Michigan", prepared for the Coordinating Research Council, Inc., and the National Renewable Energy Laboratory, prepared by Earth Tech, Concord, MA.

Hanna, S. R., et al., 1998. "Monte Carlo estimates of uncertainties in predictions by a photochemical grid model (UAM-IV) due to uncertainties in input variables." Atmospheric Environment, 32, 3619-3628.

Hanna, S. R., et al., 1998. Evaluations of Numerical Weather Prediction (NWP) Models from the Point of View of Inputs Required by Atmospheric Dispersion Models, 5th International Conference on Harmonization within Atmospheric Dispersion Modeling for Regulatory Purposes, 18-21 May, Rhodes, Greece.

Hanna, S. R., et al., 2001. "Uncertainties in predicted ozone concentrations due to input uncertainties for the UAM-V photochemical grid model applied to the July 1995 OTAG Domain", Atmospheric Environment, Vol. 34.

Henry, R. F., et al., 2000. "Effects of changes in data reporting practices on trend assessments", Atmospheric Environment, 34: (16) 2659-2662.

Hidy, G. M., 2000. "Ozone Process Insights from Field Experiments Part I: Overview", Atmospheric Environment, Vol. 34, pp. 2001-2022.

Hogrefe, C., et al., 2000. "Interpreting the information in ozone observations and model predictions relevant to regulatory policies in the Eastern United States", Bulletin of the American Meteorological Society, 81: (9) 2083-2106.

Hudischewskyj, B. and S. G. Douglas, 2000. "Weighting SAMI Air Quality Episodes to Calculate Annual Average Dry Deposition in the SAMI Region: Methods and Results of the Weighting Factors Analysis." Systems Applications International, Inc., San Rafael, California. Technical memorandum.

Imhoff, R. E. and L. L. Gautney, 1998. "Regional Photochemical Model Estimation of the Scale of Ozone Transport in the Eastern U.S.", 10th Conference on Applications of Air Pollution Meteorology with the Air

and Waste Management Association, American Meteorological Society, 11-16 January, Phoenix, AZ.

Imhoff, R. E., et al., 2001. "NO_y Removal from the Cumberland Power Plant Plume", Atmospheric Environment, Vol. 35, pp. 179-183.

Jacko, R. B., 2001. "Aircraft Measurements of Tropospheric Ozone Within the Lake Michigan Region", 94th Annual Conference of the Air and Waste Management Association, 24-28 June 2001, Orlando, FL.

Jang, J., 2001. "Annual Application of the U.S. EPA's Third-generation Air Quality Modeling System Over the Continental United States", 94th Annual Conference of the Air and Waste Management Association, 24-28 June 2001, Orlando, FL.

Kain, J. S. and J. M. Fritsch, 1990. One-Dimensional Entraining/Detraining Plume Model and Its Application in Convective Parameterization, Journal of Atmospheric Science, Vol. 47, pp. 2784-2802.

Kain, J. S. and J. M. Fritsch, 1993. Convective Parameterization for Mesoscale Models: The Kain-Fritsch Scheme, The Representation of Cumulus Convection in Numerical Models, Meteor. Monogr., Vol. 46, American Meteorological Society, pp. 165-170.

Kalloe, G. and K. Lagouvardos, 1997. "Atmospheric Modeling Simulation over the Eastern United States with the RAMS3b Model for the Summer of 1995", prepared for the Electric Power Research Institute, Palo Alto, CA.

Kalnay, E., M. Kanamitsu, R. Kistler, W. Collins, D. Deaven, L. Gandin, M. Iredell, S. Saha, G. White, J. Woollen, Y. Zhu, M. Chelliah, W. Ebisuzaki, W. Higgins, J. Janowlak, K. C. Mo, C. Ropelewski, J. Wang, A. Leetmaa, R. Reynolds, R. Jenne, and D. Joseph, 1996: The NCEP/NCAR 40-year reanalysis project. Bull. Amer. Meteor. Soc., 77, 437-471.

Keating, T. J. and A. Farrell, 1999. "Transboundary Environmental Assessment: Lessons Learned from the Ozone Transport Assessment Group", prepared for the Office of Air Quality Planning and Standards and the National Center for Environmental Decision Making, prepared by Carnegie Mellon University.

Kessler, E., 1969: On the distribution and continuity of water substance in the atmospheric circulation. Meteor. Monogr., No. 32, Amer. Meteor. Soc., 1-84.

Kleinman, L. I., G. M., 2000. "Ozone Process Insights from Field Experiments Part II: Observation-Based Analyses for Ozone Production", Atmospheric Environment, Vol. 34, pp. 2023-2033.

Koch, S. E., M. DesJardins, and P. J. Kocin, 1983: An interactive Barnes map analysis scheme for use with satellite and conventional data. J. Climate Appl. Meteor., 22, 1487-1503.

Koerber, M., 1998. "OTAG Modeling Results", proceedings of the 10th Joint Conference on the Applications of Air Pollution Meteorology, 11-16 January, 1998, Phoenix, AZ.

Korc, M. E., et al., 1993. "Comparison of Emission Inventory and Ambient Concentration ratios of NMOC, NO_x, and CO in the Lake Michigan Air Quality Region", prepared for the Lake Michigan Air Directors Consortium, prepared by Sonoma Technology, Inc., Santa Rosa, CA.

Kunkel, K. E., S. A. Changnon, B. C. Reinke, and R. W. Arritt, 1996: The July 1995 heat wave in the central United States. Bull. Amer. Meteor. Soc., 77, 1507-1518.

Kuo, H. L., 1965. On Formation and Intensification of Tropical Cyclones Through Latent Heat Release by Cumulus Convection, J. Atmos. Sci., Vol. 22., pp. 40-63.

Kuo, H. L., 1974. Further Studies of the Parameterization of the Effect of Cumulus Convection on Large-Scale Flow, J. Atmos. Sci., Vol. 31., pp. 1232-1240.

LADCo, 1991. "Lake Michigan Ozone Study: Episode Selection Document", Report Version 3.0, prepared by the Lake Michigan Air Directors Consortium, Des Plaines, IL.

LADCo, 1994. "Evaluation of the UAM-V Photochemical Grid Model in the Lake Michigan Region", Version 2.0, prepared by the Lake Michigan Air Directors Consortium, Des Plaines, Illinois.

LADCo, 1995a. "Lake Michigan Ozone Study Project Report: Volume III - Technical Data Base", prepared by the Lake Michigan Air Directors Consortium, Des Plaines, IL.

LADCo, 1995b. "Lake Michigan Ozone Study Project Report: Volume IV - Modeling", prepared by the Lake Michigan Air Directors Consortium, Des Plaines, IL.

Lagouvardos, K., et al., 2000. "An analysis of the meteorological and air quality conditions during an extreme ozone episode over the northeastern USA", International Journal of Environmental Pollution. 14: (1-6) 581-587.

Lesht, B. M. and D. J. Brandner, 1992. Functional Representation of Great Lakes Surface Temperature, J. Great Lakes Res., Vol. 18. Pp. 98-106.

Li, S., 2001. "Quantification of Variability and Uncertainty in Natural Gas-fueled Internal Combustion Engine NO_x and Total Hydrocarbon Emissions Factors", 94th Annual Conference of the Air and Waste Management Association, 24-28 June 2001, Orlando, FL.

Lin, J., 2001. "Development of New Driving Cycles for Estimating Regional Air Quality Emissions Inventories", 94th Annual Conference of the Air and Waste Management Association, 24-28 June 2001, Orlando, FL.

Loomis, C. F., et al., 1997b. "Development of the 2007 Emissions Inventory Reflecting the EPA Section 110 SIP call Requirements for the Eastern U.S.", prepared by Alpine Geophysics, LLC, Golden, CO.

Louis, J. F., 1979. Parametric Model of Vertical Eddy Diffusivity Fluxes in the Atmosphere, Boundary Layer Meteorology, Vol. 17, pp. 187-202.

Luria, M., et al., 1992. "Lake Michigan Ozone Study (LMOS): Measurements from an Instrumented Aircraft", Atmospheric Environment, Vol. 26A, No. 18, pp. 3265-3277.

Luria, M., et al., 1999. "The Evolution of Photochemical Smog in a Power Plant Plume", Atmospheric Environment, Vol. 31, pp. 3023-3036.

Lurmann, F. and N. Kumar, 1997. "Evaluation of the UAM-V Model Performance in OTAG Simulations: Summary of Performance Against Surface Observations", Final report prepared by Sonoma Technology, Inc., Prepared for the U.S. Environmental Protection Agency and the Ozone Transport Assessment Group, Research Triangle Park, NC.

Lyons, W. A., et al., 1995. Applications of the Regional Atmospheric Modeling System (RAMS) to Provide Input to Photochemical Grid Models for the Lake Michigan Ozone Study (LMOS), Journal of Applied Meteorology, Vol. 34, No. 8, pp. 1762-1786.

Mahrer, Y. and R. A. Pielke, 1977. Numerical Study of the Airflow over Irregular Terrain, Beitr. Phys. Atmos., Vol. 50, pp. 98-113.

Main, H. and P. T. Roberts, 1993. "Validation and Analysis of the Lake Michigan Ozone Study Ambient VOC Data", prepared for the Lake Michigan Air Directors Consortium, prepared by Sonoma Technology, Inc., Santa Rosa, CA.

Majeed, M. A., 2001. "Regional Scale Modeling of PM-2.5 for Eastern U.S.", 94th Annual Conference of the Air and Waste Management Association, 24-28 June 2001, Orlando, FL.

McBride, J. L. and E. E. Ebert, 2000: Verification of quantitative precipitation forecasts from operational numerical weather prediction models over Australia. Wea. Forecasting, **15**, 103-121.

McNally, D. E., 1997. Development of Methodology for Mapping MM5 Fields onto Arbitrary Eulerian Photochemical Air Quality Simulation Models (PAQSM), Alpine Geophysics, LLC, Golden, CO.

McNally, D. E. and T. W. Tesche, 1994. "MAPS2.3 User's Guide", Alpine Geophysics, LLC, Golden, CO.

McNally, D. E. and T. W. Tesche, 1996. "Evaluation of the MM5 Model for the July 1988 and July 1995 Episodes and Comparison with the OTAG Meteorological Model, RAMS", 89th Annual Meeting of the Air and Waste Management Association, 23-28 June 1996, Nashville, TN.

McNally, D. E. and T. W. Tesche, 1996a. "Pittsburgh Regional Ozone Attainment Study: Evaluation of the MM5 Model for Three Episodes", prepared for the Pennsylvania Department of Environmental Protection, prepared by Alpine Geophysics, LLC, Ft. Wright, KY.

McNally, D. E. and T. W. Tesche, 1996b. Evaluation of the MM5 Model for the 1-11 July 1988 OTAG Episode over the Northeastern United States, prepared for Pennsylvania Power and Light Co., prepared by Alpine Geophysics, LLC, Ft. Wright, KY.

McNally, D. E. and T. W. Tesche, 1997. "Comparative Evaluation of the CAMx and UAM-V Models Over the Northeastern U.S. Using the July 1995 OTAG Episode and the NARSTO-NE Intensive Field Study Data", prepared for the Virginia Department of Environmental Quality, prepared by Alpine Geophysics, LLC, Golden, CO.

McNally, D. E. and T. W. Tesche, 1997. "Modeled Effects of Indiana Point Source NO_x Emissions Reductions on Local and Regional 1-hr and 8-hr Ground Level Ozone Concentrations in 1995 and 2007 Using Two OTAG Oxidant Episodes", prepared for the Indiana Electric Utility Air Workgroup, prepared by Alpine Geophysics, LLC, Golden, CO.

McNally, D. E. and T. W. Tesche, 1997. "Photochemical Modeling Analysis of the Northwest "Ozone Free" OTAG States Using the July 1995 OTAG Modeling Episode", prepared for Minnesota Power, prepared by Alpine Geophysics, LLC, Golden, CO.

McNally, D. E. and T. W. Tesche, 1997. "State-Specific Photochemical Modeling Analysis Using the July 1995 and July 1991 OTAG Modeling Episodes", prepared for the Ohio Environmental Protection Agency, Division of Air Pollution Control, prepared by Alpine Geophysics, LLC, Golden, CO.

McNally, D. E. and T. W. Tesche, 1998. "Effects of Indiana Point Source NO_x Emissions Reductions on Ground Level Ozone Concentrations Using the 07EPA1a Basecase Inventory", prepared for the Indiana Electric Association, prepared by Alpine Geophysics, LLC, Covington, KY.

McNally, D. E. and T. W. Tesche, 1998. "Scale of Transport Analysis Based on Sub-Regional Modeling Over the OTAG Domain in the Eastern U.S.", 91st Annual Meeting of the Air and Waste Management Association, San Diego, CA, 14-19 June 1998.

McNally, D. E. and T. W. Tesche, 1999. Impact of Stack Parameter Errors on Ground Level Ozone Metrics in the OTAG Domains", prepared for General Motors, prepared by Alpine Geophysics, LLC, Arvada, CO.

McNally, D. E., and T. W. Tesche, 1994. "MAPS2.3 User's Guide", Alpine Geophysics, LLC, Golden, CO.

McNally, D. E., and T. W. Tesche, 1996a. "Evaluation of the MM5 Model for the July 1988 and July 1995 Episodes and Comparison with the OTAG Meteorological Model, RAMS", 89th Annual Meeting of the Air and Waste Management Association, 23-28 June 1996, Nashville, TN.

McNally, D. E., and T. W. Tesche, 1996b. "Evaluation of the MM5 Model for the 1-11 July 1998 OTAG Episode Over the Northeastern United States", prepared for the Pennsylvania Power and Light Company,

prepared by Alpine Geophysics, LLC, Arvada, CO.

McNally, D. E., and T. W. Tesche, 1998. "Evaluation of the MM5 Meteorological Model over the Greater Denver Front Range Region for Two Wintertime Episodes", prepared for the Denver Regional Air Quality Council, prepared by Alpine Geophysics, LLC, Golden, CO.

McNally, D. E., et al., 1997. "Photochemical Modeling Analysis of the Pittsburgh-Beaver Valley Ozone Nonattainment Area: Volume IV: C Interim Final Report", prepared for the Southwestern Pennsylvania Clean Air Stakeholders Group, prepared by Alpine Geophysics, LLC, Covington, KY.

McNally, D. E., et al., 1998. "Nested Regional Photochemical Modeling in Support of the Pittsburgh-Beaver Valley Ozone SIP", 10th Joint Conference on the Applications of Air Pollution Meteorology with the Air and Waste Management Association, 11-16 January, Phoenix, AZ.

McNally, D. E., et al., 1998. "Photochemical Modeling of the Effects of VOC and NO_x Emissions Controls in the Baltimore-Washington Ozone Nonattainment Area", prepared for the Maryland Department of Environment, prepared by Alpine Geophysics, LLC, Covington, KY.

McNider, R. T. and R. A. Pielke, 1981: Diurnal boundary layer development over sloping terrain. J. Atmos. Sci., 38, 2198-2212.

McNider, R. T. and R. A. Pielke, 1984: Numerical simulation of slope and mountain flows. J. Climate and Appl. Meteor., 23, 1441-1453.

McNider, R. T., et al., 1998. "Meteorological conditions during the 1995 Southern Oxidants Study Nashville/Middle Tennessee field Intensive", Journal of Geophysical Research, 103: 22225-22243.

McQueen, J. T., et al., 1997. Evaluation of the RAMS Model for Estimating Turbulent Fluxes Over the Chesapeake Bay, Atmospheric Environment, Vol. 31. pp. 3803-3819.

Mellor, B. L. and T. Yamada, 1974. Hierarchy of Turbulence Closure Models for Planetary Boundary Layers, J. Atmos. Sci., Vol. 31, pp. 1791-1806.

Mellor, B. L. and T. Yamada, 1982. A Development of a Turbulence Closure Model for Geophysical Fluid Problems, Review of Geophysics and Space Physics, Vol. 20, pp. 851-875.

Milanchus, M. L., et al., 1998. "Evaluating the effectiveness of ozone management efforts in the presence of meteorological variability", Journal of the Air and Waste Management Association, 48: (3) 201-215.

Mocko, D. M. and W. R. Cotton, 1995: Evaluation of fractional cloudiness parameterizations for use in a mesoscale model. J. Atmos. Sci., 52, 2884-2901.

Monin, A. S., and A. M. Obukhov, 1954: Basic laws of turbulent mixing in the ground layer of the atmosphere. Akad. Nauk SSR Geofiz. Inst. Tr., 24, 163-187.

Morris R. E., et al., 1997. "Assessment of the Contribution of Emissions from Northern OTAG States on Elevated Ozone Concentrations", prepared for Southeast Michigan Council of Governments, prepared by ENVIRON International Corp., Novato, CA.

Morris R. E., et al., 1997. "Comparison of OTAG UAM-V/BEIS2 Modeling Results with Ambient Isoprene and Other Related Species Concentration", prepared for American Automobile Manufacturers Association, prepared by ENVIRON International Corp., Novato, CA.

Morris, R. E. and E. Tai, 1998. "Assessment of the Impact of Kentucky Sources on Downwind Nonattainment and Assessment of the Sources that Contribute to Nonattainment in Kentucky", prepared for the Utility Information Exchange of Kentucky, prepared by ENVIRON International Corp., Novato, CA.

Morris, R. E., 1997. "Review of NESCAUM Report on Long-Range Transport of Ozone and its Precursors in the Eastern U. S.", prepared for the Midwest Ozone Group, prepared by ENVIRON International Corp., Novato, CA.

Morris, R. E., 1998. "Review and Critique of the November 7, 1997 EPA Ozone Transport SIP call and Assessment of the Contribution of Emissions from Missouri on Nonattainment Using the July 1995 OTAG Database", prepared for the Missouri Electric Utility Environmental Committee, prepared by ENVIRON International Corporation, Novato, CA.

Morris, R. E., 2001. "A Methodology for Quantifying Ozone Transport and Assessing the Benefits of Alternative Control Strategies", 94th Annual Conference of the Air and Waste Management Association, 24-28 June 2001, Orlando, FL.

Morris, R. E., et al., 1996. "Assessment of the Effects of Potential Control Strategies on Emissions Sources in Ohio and Downwind Ozone Levels", The Emissions Inventory: Key to Planning, Permits, Compliance, and Reporting, Air and Waste Management Association, Pittsburgh, PA.

Morris, R. E., et al., 1997. "Area of Influence Ozone Source Apportionment Modeling for the July 1991 OTAG Episode and the Northeast Corridor and Lake Michigan Nonattainment Regions", prepared for Cinergy Corporation, prepared by ENVIRON International Corp, Novato, CA.

Morris, R. E., et al., 1997. "Ozone Source Apportionment Modeling Using the July 1991 OTAG Episode for the Northeast Corridor and Lake Michigan Regions", prepared for Cinergy Corporation, prepared by ENVIRON International Corp., Novato, CA.

Morris, R. E., et al., 2001, "Evaluation of the CAMx and Models-3/CMAQ Models over the Northeastern U.S. Region", draft final report prepared for the Coordinating Research Council, prepared by ENVIRON International, and Alpine Geophysics, LLC, Novato, CA.

Mueller, S. F., A. Song, W. B. Norris, S. Gupta, and R. T. McNider, 1996: Modeling pollutant

transport during high-ozone episodes in the southern Appalachian mountains. J. Appl. Meteor., 35, 2105-2120.

NESCAUM, 1997. "The Long-Range Transport of Ozone and Its Precursors in the Eastern United States", prepared by the Northeast States for Coordinated Air Use Management, Boston, Mass.

Nicholls, M. E., et al., 1995. Applications of the RAMS Numerical Model to Dispersion over Urban Areas, Wind Climate in Cities, eds. J. E. Cermak et al., pp. 703-732. Kluwer Academic Publishers, Dordrecht.

Norris, W. B., and K. G. Doty, 1998: Southern Appalachians Mountain Initiative: Meteorological Modeling Protocol, Version 3, 38 pp.

Norris, W. B., and K. G. Doty., 1998. "Meteorological Modeling Protocol", prepared for the Southern Appalachian Mountains Initiative (SAMI), prepared by the Georgia Institute of Technology, University of Alabama, and the University of Virginia.

Novak, D. J., et al., 2000. "A modeling study of the impact of urban trees on ozone", Atmospheric Environment, 34: (10) 1601-1613.

Odman, T. M., 2001. "Response and Sensitivity of PM_{2.5} in the Southern Appalachian Mountains", 94th Annual Conference of the Air and Waste Management Association, 24-28 June 2001, Orlando, FL.

OEC, 2000. "Ohio Valley-Ozone Alley Smog Pollution and Power Plants in the Ohio River Valley: What Can Be Done", prepared by the Ohio Environmental Council, Ohio Valley Environmental Coalition, Regional Coalition of Ohio Valley Restoration, Columbus, OH.

OTAG, 1997. "Telling the OTAG Ozone Story with Data", Final Report, Vol. I, Executive Summary, prepared by the Ozone Transport Assessment Group, Air Quality Analysis Workgroup.

OTAG, 1997. "Modeling Report", Draft Version 1.1, prepared by the Ozone Transport Assessment Group, 12 February.

OTAG, 1997b. "Ozone Transport Assessment Group Executive Report, 1997", prepared by the Ozone Transport Assessment Group.

Overcamp, T. J., 2001. "Plume Rise in a Shear Layer", 94th Annual Conference of the Air and Waste Management Association, 24-28 June 2001, Orlando, FL.

Owens, P., 2001. "Weekday/Weekend Variability and Long-term Trends in Traffic, CO, NO_y, and Ozone for the Charlotte Metropolitan Area During the 1990's", 94th Annual Conference of the Air and Waste Management Association, 24-28 June 2001, Orlando, FL.

Pielke, R. A. and M. Uliasz, 1998. Use of Meteorological Models as Input to Regional and Mesoscale Air Quality Models C Limits and Strengths, Atmospheric Environment, Vol. 32, No. 8, pp. 1455-1466.

Pielke, R. A., 1974. A Three-Dimensional Numerical Model of the Sea Breeze Over South Florida, Monthly Weather Review, Vol. 102, pp. 115-134.

Pielke, R. A., 1984. Mesoscale Meteorological Modeling, Academic Press, 612 pp.

Pielke, R. A., et al., 1992. Comprehensive Meteorological Modeling System--RAMS, Metero. Atmos. Phys., Vol. 49, pp. 69-91.

Pielke, R. and R. Pearce, 1994. Mesoscale Modeling of the Atmosphere, Meteoro. Monogr., No. 47, American Meteorological Society, Boston, MA.

Porter, C. W., 1995. Short Term High Resolution Forecasting of Fog, Cloud Ceiling Heights, and Visibilities with the PSU/NCAR Mesoscale Model, M. S. Thesis, The Pennsylvania State University, 197 pp.

Porter, P. S., et al., 1996. "Statistical Characteristics of Spatially-Decomposed Ambient Ozone Time Series Data", (Available at <http://capita.wustl.edu/otag/reports/StatChar/otagrep.htm>). New York Department of Environmental Conservation, New York, NY.

Porter, P. S., et al., 2001. "Ozone Air Quality Over North America: Part II – An Analysis of Trend Detection and Attribution Techniques", Journal of the Air and Waste Management Association, Vol. 51, pp. 273-282.

Pruppacher, H. R., and J. D. Klett, 1980: Microphysics of clouds and precipitation. D. Reidel Publishing Company, 714 pp.

Rao, S. T., et al., 1996. "Dealing with the Ozone Non-Attainment Problem in the Eastern United States", Environmental Manager, January, pp. 17-31.

Rao, S. T., et al., 1997. "Space and time scales in ambient ozone data", Bulletin of the American Meteorological Society, 78: (10) 2153-2166.

Rao, S. T., et al., 1998. "Ozone Air Quality Over North America: A Critical Review of Trend Detection Techniques and Assessments", prepared by the NARSTO Synthesis Team, Final Report available at <http://www.cgenv.com/Narsto/>

Rao, S. T., et al., 2000. "Determining the airshed for ozone and fine particle pollution in the Northeastern United States", Abstracts Papers in Atmospheric Chemistry, S 219: U628-U628 Part 1 MAR 26.

Reisner, J., R. J. Rasmussen, and R. T. Bruintjes, 1996. Explicit Forecasting of Supercooled Liquid Water

in Winter Storms using a Mesoscale Model, Quart. J. Roy, Meteor. Soc.

Reisner, J., R. T. Bruintjes, and R. J. Rasmussen, 1993. Preliminary Comparisons between MM5 NCAR/Penn. State Model Generated Icing Forecasts and Observations, Fifth Intl. Conf. On Aviation Weather Systems. Vienna, VA, Amer. Meteor. Soc., pp 65-69.

Resources Board, prepared by Alpine Geophysics, LLC, Ft. Wright, KY.

Reynolds, S. D., P. M. Roth, and T. W. Tesche, 1994. "A Process for the Stressful Evaluation of Photochemical Model Performance", prepared for the Western States Petroleum Association, prepared by Envair, San Rafael, CA and Alpine Geophysics, Crested Butte, CO.

Roberts, P. T., et al., 1995. Characteristics of VOC-Limited and NO_x Limited Areas Within the Lake Michigan Air Quality Region, prepared for the Lake Michigan Air Directors Consortium, prepared by Sonoma Technology, Inc., Santa Rosa, CA.

Roth, P. M., T. W. Tesche, and S. D. Reynolds, 1998. "A Critical Review of Regulatory Air Quality Modeling for Tropospheric Ozone", prepared for the North American Research Strategy for Tropospheric Ozone (NARSTO), prepared by Envair, and Alpine Geophysics.

Roth, P. M., 1999. "A Qualitative Approach to Evaluating the Anticipated Reliability of a Photochemical Air Quality Simulation Model for a Selected Application", Journal of the Air and Waste Management Association, Vol. 49, pp. 1050-1059.

Roth, P. M., et al., 1997. "A Critical Review of Regulatory Air Quality Modeling For Tropospheric Ozone", Critical Review Paper for the *1998 NARSTO Ozone Assessment*, 16-20 Nov., W. Palm Beach, FL.

Roth, P. M., T. W. Tesche, and S. D. Reynolds, 1995. "Protocol for Evaluating the Performance of the SARMAP Model", prepared for the SARMAP Technical Review Committee, prepared by Envair and Alpine Geophysics, LLC.

Russell, A. and R. Dennis, 2000. NARSTO Critical Review of Photochemical Models and Modeling", Atmospheric Environment, Vol. 34, pp. 2283-2324.

Russell, A. G. and R. L. Dennis, 1997. Critical Review of Photochemical Models and Modeling, NARSTO Critical Review Paper, 1998 NARSTO Ozone Assessment, submitted to Atmospheric Environment.

Russell, A. G., et al., 1998. "Air Quality Modeling Protocol", prepared for the Southern Appalachian Mountains Initiative (SAMI), prepared by the Georgia Institute of Technology, University of Alabama, and the University of Virginia.

Rutledge, S. A., and P. V. Hobbs, 1983: The mesoscale and microscale structure and organization of

clouds and precipitation in midlatitude cyclones. VIII: A model for the “seeder-feeder” process in warm-frontal rainbands. J. Atmos. Sci., 40, 1185-1206.

Ryan, W. F., et al., 1998. “Pollutant Transport During a Regional Ozone Episode in the Mid-Atlantic States”, Journal of the Air and Waste Management Association, Vol. 48, pp. 786-796.

Schaefer, J. T., 1990: The critical success index as an indicator of warning skill. Wea. Forecasting, 5, 570-575.

Schere, K. L. and R. A. Wayland, 1989. "EPA Regional Oxidant Model (ROM2.0): Evaluation on 1980 NEROS Data Bases", EPA/600/3-80/057, Atmospheric Research and Exposure Assessment Laboratory, Research Triangle Park, NC.

Schichtel, B. A. and R. A. Husar, 2001. “Eastern North American Transport Climatology During High- and Low-Ozone Days”, Atmospheric Environment, Vol. 35, pp. 1029-1038.

Schwab, D. J., et al., 1992. Satellite Measurements of Water Surface Temperature in the Great Lakes-Great Lakes Coast Watch, J. Great Lakes Res., Vol. 18, pp. 116-125.

Seaman, N. L. and D. R. Stauffer, 1996. "SARMAP Meteorological Model Final Report", prepared for the San Joaquin Valleywide Air Pollution Study Agency, prepared by the Department of Meteorology, Pennsylvania State University, University Park, PA.

Seaman, N. L. and S. A. Michelson, 1998. Mesoscale Meteorological Structure of a High-Ozone Episode During the 1995 NARSTO-Northeast Study, Journal of Applied Meteorology, (submitted).

Seaman, N. L., 1995. A Status of Meteorological Pre-Processors for Air Quality Modeling, International Conf. On Particulate Matter, Air and Waste Mgt. Assn., Pittsburgh, PA.

Seaman, N. L., 1996. A Study of Meteorological Variables Needed in Air-Quality Modeling, Annual Progress Report prepared for the Coordinating Research Council (CRC), Interim Report, Project A-11, prepared by the Department of Meteorology, Penn State University, State College, PA.

Seaman, N. L., 1998. A Meteorological Modeling for Air Quality Assessments, NARSTO Critical Review Paper, 1998 NARSTO Ozone Assessment, submitted to Atmospheric Environment.

Seaman, N. L., 2000. “Meteorological Modeling for Air Quality Assessments”, Atmospheric Environment, Vol. 34, pp. 2231-2260.

Seaman, N. L., and D. R. Stauffer, 1996. "SARMAP Meteorological Model Final Report", prepared for the San Joaquin Valleywide Air Pollution Study Agency, prepared by the Department of Meteorology, Pennsylvania State University, University Park, PA.

Seaman, N. L., D. R. Stauffer, and L. M. Lario, 1995. "MultiScale Four-Dimensional Data Assimilation

System Applied to the San Joaquin Valley During SARMAP. Part I: Modeling Design and Basic Performance Characteristics", J. Appl. Meteo., Vol. 34, pp. 1739-1761.

Seaman, N. L., D. R. Stauffer, and T. W. Tesche, 1992. "The SARMAP Meteorological Model: A Four-Dimensional Data Assimilation Technique Used to Simulate Mesobeta-Scale Meteorology During a High-Ozone Episode in California", International Specialty Conference on Tropospheric Ozone Nonattainment and Design Value Issues, U.S. EPA/AWMA, 27-30 October, Boston, MA.

Seaman, N. L., et al., 1996. "Application of the MM5-FDDA Meteorological Model to the Southern California SCAQS-1997 Domain: Preliminary Test Using the SCAQS August 1987 Case", Ninth Joint Conference on Applications of Air Pollution Meteorology, American Meteorological Society, 28 January-2 February, Atlanta, GA.

Seaman, N. L., et al., 1997. "The Use of the San Joaquin Valley Meteorological Model in Preparation of a Field Program in the South Coast Air Basin and Surrounding Regions of Southern California: Volume II-- Numerical Modeling Studies for the Development and Application of a Guidance Technique to Support of the Design of the 1997 Southern California Ozone Study Field Program, prepared for the California Air Resources Board, prepared by the Department of Meteorology, Pennsylvania State University, University Park, PA.

Sellers, P. J., Y. Mintz, Y. C. Sud, and A. Dalcher, 1986: A simple biosphere model (SiB) for use within general circulation models. J. Atmos. Sci., 43, 505-531.

Shafran, P. C. and N. L. Seaman, 1998. Comparison of Numerical Predictions of Boundary-Layer Structure Over the Midwest During the Lake Michigan Ozone Study (LMOS), 10th Joint Conference on the Applications of Air Pollution Meteorology with the Air and Waste Management Association, Phoenix, AZ. 11-16 January.

Sillman, S., 2000. "Ozone production efficiency and loss of NO_x in power plant plumes: Photochemical model and interpretation of measurements in Tennessee", Journal of Geophysical Research. 105: 9189-9202.

Sistla, G., 2001. "An Assessment of Sulfur Dioxide Emissions Reductions and the Relative Impacts of Sulfates over New York State", prepared by the Bureau of Air Resources, New York State Department of Environmental Conservation, Albany, NY.

Sistla, G., et al., 1996. "Effects of Uncertainties in Meteorological Inputs on Urban Airshed Model Predictions and Ozone Control Strategies", Atmospheric Environment, Vol. 30, NO. 12. pp. 2011-2025.

Sistla, G., et al., 2001. "A Comparison of Measured and Simulated Ozone Concentrations in Rural Areas of the Eastern United States During Summer 1995", Journal of the Air and Waste Management Association, Vol. 51. pp. 374-386.

Stauffer, D. R. and N. L. Seaman, 1990. Use of Four-Dimensional Data Assimilation in a Limited-Area Mesoscale Model. Part I: Experiments with Synoptic Data. Mon. Wea. Rev., 118, 1250-1277.

Stauffer, D. R. and N. L. Seaman, 1994. On Multi-Scale Four-Dimensional Data Assimilation, J. Appl. Meteor., 33, 416-434.

Stauffer, D. R., N. L. Seaman, and F. S. Binkowski, 1991. Use of Four-Dimensional Data Assimilation in a Limited-Area Mesoscale Model. Part II: Effects of Data Assimilation Within the Planetary Boundary Layer. Mon. Wea. Rev., 119, 734-754.

Stauffer, D. R., T. T. Warner, and N. L. Seaman, 1985. "Newtonian "Nudging" Approach to Four Dimensional Data Assimilation: Use of SESAME-IV Data in a Mesoscale Model", 7th Conference on Numerical Weather Prediction, Montreal, Canada.

Stephens, G. L., 1978: Radiation profiles in extended water clouds. II: Parameterization Schemes. J. Atmos. Sci., 35, 2123-2132.

Steyn, D. G. and I. G. McKendry, 1988. Quantitative and Qualitative Evaluation of a Three-Dimensional Mesoscale Numerical Model Simulation of a Sea Breeze in Complex Terrain, Monthly Weather Review, Vol. 116, pp. 1914-1926.

Steyn, D. G., and I. G. McKendry, 1988. "Quantitative and Qualitative Evaluation of a Three-Dimensional Mesoscale Numerical Model Simulation of a Sea Breeze in Complex Terrain", Monthly Weather Review, Vol. 116, pp. 1914-1926.

STI, 1996. "Evaluation of the UAM-V Model Performance in the OTAG Simulations: Summary of Performance Against Surface Observations", Draft, prepared for the Ozone Transport Assessment Group, prepared by Sonoma Technology, Inc., Santa Rosa, CA.

Tangirala, R. S., 2001. "Precursor Emissions and Ground-level Ozone NAAQS Exceedances in the Metropolitan Washington, DC Non-attainment Area: Day of Week Patterns", 94th Annual Conference of the Air and Waste Management Association, 24-28 June 2001, Orlando, FL.

Tesche, T. W. and D. E. McNally, 1993a. "Operational Evaluation of the CAL-RAMS Meteorological Model for LMOS Episode 1: 26-28 June 1991", prepared for the Lake Michigan Air Directors Consortium, prepared by Alpine Geophysics, Crested Butte, CO.

Tesche, T. W. and D. E. McNally, 1993b. "Operational Evaluation of the CAL-RAMS Meteorological Model for LMOS Episode 2: 17-19 July 1991", prepared for the Lake Michigan Air Directors Consortium, prepared by Alpine Geophysics, Crested Butte, CO.

Tesche, T. W. and D. E. McNally, 1993c. "Operational Evaluation of the CAL-RAMS Meteorological Model for LMOS Episode 3: 25-26 August 1991", prepared for the Lake Michigan Air Directors Consortium, prepared by Alpine Geophysics, Crested Butte, CO.

Tesche, T. W. and D. E. McNally, 1993d. "Operational Evaluation of the CAL-RAMS Meteorological Model for LMOS Episode 4: 20-21 June 1991", prepared for the Lake Michigan Air Directors Consortium, prepared by Alpine Geophysics, Crested Butte, CO.

Tesche, T. W. and D. E. McNally, 1993e. "Operational Evaluation of the SARMAP Meteorological Model (MM5) for Episode 1: 3-6 August 1990", prepared for the Valley Air Pollution Study Agency, prepared by Alpine Geophysics, Crested Butte, CO.

Tesche, T. W. and D. E. McNally, 1993. "Operational Evaluation of the SARMAP Meteorological Model (MM5) for Episodes 2: 27-29 July 1990", prepared for the Valley Air Pollution Study Agency, prepared by Alpine Geophysics, Crested Butte, CO.

Tesche, T. W. and D. E. McNally, 1994. "Evaluation of the UAM-V Over Lower Lake Michigan for Two 1991 Oxidant Episodes", prepared for the Lake Michigan Air Directors Consortium, prepared by Alpine Geophysics, Crested Butte, CO.

Tesche, T. W. and D. E. McNally, 1996. "Evaluation of the MM5 Model for Three 1995 Regional Ozone Episodes over the Northeast United States", prepared for the Southwestern Pennsylvania Clean Air Stakeholders Group, prepared by Alpine Geophysics, LLC, Covington, KY.

Tesche, T. W. and D. E. McNally, 1996. "Pittsburgh Regional Ozone Attainment Study: Volume X -- Evaluation of the MM5 Model for Three 1995 Regional Ozone Episodes over the Northeast United States", prepared for the Southwestern Pennsylvania Clean Air Stakeholders Group, prepared by Alpine Geophysics, LLC, Covington, KY.

Tesche, T. W. and D. E. McNally, 1996. "Superregional Ozone Modeling and Analysis Study – Phase II, Work Element 5 Technical Report: Comparative Evaluation of the MM5 and RAMS Models for the July 1991 OTAG Episode", prepared for the Midwest Ozone Group, prepared by Alpine Geophysics, LLC, Ft. Wright, KY.

Tesche, T. W. and D. E. McNally, 1996. "Superregional Ozone Modeling and Analysis Study C Phase I: Work Element 3: Assessment of the OTAG Data Sets -- Task 2 Technical Memorandum: Review of the OTAG Meteorological Inputs and Outputs", prepared for the Midwest Ozone Group, prepared by Alpine Geophysics, LLC, Covington, KY.

Tesche, T. W. and D. E. McNally, 1996. "Superregional Ozone Modeling and Analysis Study C Phase II: Work Element 6 Technical Report: Initial Evaluation of the SAQM Regional Model for the 13-21 July 1991 OTAG Episode", prepared for the Ohio Environmental Protection Agency and the Midwest Ozone Group, prepared by Alpine Geophysics, LLC, Covington, KY.

Tesche, T. W. and D. E. McNally, 1996. "Superregional Ozone Modeling and Analysis Study C Phase II: Status Report on SAQM/UAM-V Comparative Model Evaluation", prepared for the Midwest Ozone Group, prepared by Alpine Geophysics, LLC, Covington, KY.

Tesche, T. W. and D. E. McNally, 1996b. Evaluation of the MM5 Model for Three 1995 Regional Ozone Episodes over the Northeast United States, prepared for the Southwestern Pennsylvania Clean Air Stakeholders Group, prepared by Alpine Geophysics, LLC, Ft. Wright, KY.

Tesche, T. W. and D. E. McNally, 1997. "The Use of the San Joaquin Valley Meteorological Model in Preparation of a Field Program in the South Coast Air Basin and Surrounding Regions of Southern California. Volume I: Final MM5 Evaluation for the 3-6 August 1990 SARMAP Episode", prepared for the California Air Resources Board, prepared by Alpine Geophysics, LLC, Ft. Wright, KY.

Tesche, T. W. and D. E. McNally, 1997. Use of the MM5 Model as an Aid in Designing the 1997 Southern California Ozone Study: Part I, Final Evaluation of the MM5 Model for the 3-6 August 1990 SARMAP Episode over the Central California Region, prepared for the California Air

Tesche, T. W. and D. E. McNally, 1998. "Cincinnati-Hamilton Ozone Attainment Demonstration Study: Volume 5: Evaluation of the MM5 Model for the 18-22 June 1994 Episode", prepared for the Ohio Environmental Protection Agency", prepared by Alpine Geophysics, LLC, Ft. Wright, KY.

Tesche, T. W. and D. E. McNally, 1998. "Evaluation of the MM5 Model for Two 1993 Regional Ozone Episodes over the Gulf Coast", prepared for the Minerals Management Service and the Offshore Operators Committee, prepared by Alpine Geophysics, LLC, Ft. Wright, KY.

Tesche, T. W. and D. E. McNally, 1998. "Examination of CAMx, SAQM, and UAM-V Performance and Response to Emissions Changes Over the Eastern U.S. for Various OTAG, LMOS, and NARSTO Episodes", 91st Annual Meeting of the Air and Waste Management Association, San Diego, CA, 14-19 June 1998.

Tesche, T. W. and D. E. McNally, 1998. "Modeled Effects of Indiana Point Source NOx Emissions Reductions on Local and Regional 1-Hr and 8-Hr Ground Level Ozone Concentrations in 1995 and 2007 Using Two OTAG Oxidant Episodes", prepared for the Indiana Electric Utility Air Workgroup, prepared by Alpine Geophysics, LLC, Covington, KY.

Tesche, T. W. and D. E. McNally, 1998. "Recommendations for Air Quality Dispersion Models and Related Aerometric Data Sets in Support of the Breton Aerometric Monitoring Program (BAMP)", prepared for the Offshore Operators Committee, prepared by Alpine Geophysics, LLC, Ft. Wright, KY.

Tesche, T. W. and D. E. McNally, 1999. "Comparative Evaluation of the MM5 and RAMS3c Prognostic Meteorological Models over the Midwestern U.S. for Two 1991 LMOS Intensive Measurement Episodes", prepared for the Coordinating Research Council, prepared by Alpine Geophysics, LLC, Ft. Wright, KY.

Tesche, T. W. and D. E. McNally, 2000a. "Evaluation of the RAMS3c Prognostic Meteorological Model over the Southeastern U.S. for Three Southern Appalachian Mountain Initiative (SAMI) Episodes", draft final report prepared for the Tennessee Valley Authority and SAMI, prepared by Alpine Geophysics, LLC,

Ft. Wright, KY.

Tesche, T. W. and D. E. McNally, 2001. "Evaluation of the MM5 Prognostic Meteorological Model over Central Florida for Nine Peninsular Florida Ozone Study (PFOS) 8-hr Ozone Episodes", report prepared for the Florida Department of Environmental Protection Agency, prepared by Alpine Geophysics, LLC, Ft. Wright, KY.

Tesche, T. W. and D. E. McNally, 2001. "Evaluation of the MM5 Prognostic Meteorological Model over the Gulf Coast Region for the 6-11 September 1993 COAST Episode", report prepared for private client, prepared by Alpine Geophysics, LLC, Ft. Wright, KY.

Tesche, T. W. and D. E. McNally, 2000b. "Evaluation of the MM5 Mesoscale Model Over the Central U.S. For the 11-24 June 1995 Ozone Episode", prepared for the Kansas Department of Health and Environment and the U.S. Environmental Protection Agency", prepared by Alpine Geophysics, LLC, Ft. Wright, KY.

Tesche, T. W. et al., 2001a. "Evaluation of CAMx and Models-3/CMAQ Over the Lower Lake Michigan Region with Inputs from the RAMS3c and MM5 Models", prepared for the Coordinating Research Council, prepared by Alpine Geophysics, LLC and ENVIRON International, Ft. Wright, KY.

Tesche, T. W. et al., 2001b. "Evaluation of the MM5 Model Over the Midwestern U.S. for Three 8-Hr Oxidant Episodes", prepared for the Kansas Department of Health and Environment and the Missouri Department of Natural Resources, prepared by Alpine Geophysics, LLC and ENVIRON International, Ft. Wright, KY.

Tesche, T. W., 1991a. "Evaluation of Regional Atmospheric Models", State-of-Science Synthesis Paper, Comprehensive Modeling System Workshop, Sponsored by EPRI, U.S. DOE, NOAA, U.S. EPA, Environment Canada, API, and the Ontario Ministry of Environment, 7-8 November, Atlanta, GA.

Tesche, T. W., 1991b. "Evaluation Procedures for Using Numerical Meteorological Models as Input to Photochemical Models", 7th Joint Conference on Applications of Air Pollution Meteorology; American Meteorological Society, 14-18 January, New Orleans, LA.

Tesche, T. W., 1994. "Evaluation Procedures for Regional Emissions, Meteorological, and Photochemical Models", 86th Annual Meeting of the Air and Waste Management Association, 14-18 June, Denver, CO.

Tesche, T. W., and D. E. McNally, 1993b. "Operational Evaluation of the SARMAP Meteorological Model (MM5) for two San Joaquin Valley Ozone Episodes", prepared for the Valley Air Pollution Study Agency, prepared by Alpine Geophysics, Crested Butte, CO.

Tesche, T. W., and D. E. McNally, 1996. "Superregional Ozone Modeling and Analysis Study – Phase II, Work Element 5 Technical Report: Comparative Evaluation of the MM5 and RAMS Models for the July 1991 OTAG Episode", prepared for the Midwest Ozone Group, prepared by Alpine Geophysics, LLC, Ft. Wright, KY.

Tesche, T. W., and D. E. McNally, 1998b. "Cincinnati-Hamilton Ozone Attainment Demonstration Study: Volume 5: Evaluation of the MM5 Model for the 18-22 June 1994 Episode", prepared for the Ohio Environmental Protection Agency", prepared by Alpine Geophysics, LLC, Ft. Wright, KY.

Tesche, T. W., and D. E. McNally, 2001a. "Evaluation of the MM5 Prognostic Meteorological Model over Central Florida for Nine Peninsular Florida Ozone Study (PFOS) 8-hr Ozone Episodes", report prepared for the Florida Department of Environmental Protection Agency, prepared by Alpine Geophysics, LLC, Ft. Wright, KY.

Tesche, T. W., and D. E. McNally, 2001b. "Application of the MM5 Prognostic Meteorological Model over the South Central U.S. for the September 1993 COAST Ozone Episode", prepared by Alpine Geophysics, LLC, Ft. Wright, KY.

Tesche, T. W., D. E. McNally, and C. F. Loomis, 1999. "Estimation of Emissions Reduction Targets for the Pennsylvania Stakeholders Study", prepared for the Pennsylvania Department of Environmental Protection prepared by Alpine Geophysics, LLC, Ft. Wright, KY.

Tesche, T. W., D. E. McNally, and C. F. Loomis, 1999. "Impact of Incorrect Grid M Point Source Emissions Data on Ozone Model Performance and Year 2007 CAA and SIP Call Projections", prepared for the Indiana Electric Association, prepared by Alpine Geophysics, LLC, Ft. Wright, KY.

Tesche, T. W., D. E. McNally, and Christopher Emery, 2001. "Evaluation of the MM5 Model Over the Midwestern U.S. for Three 8-Hr Oxidant Episodes", report prepared for Kansas Department of Health and Environment and the Missouri Department of Natural Resources, prepared by Alpine Geophysics, LLC, Ft. Wright, KY and ENVIRON, International, Novato, CA.

Tesche, T. W., et al., 1990. "Improved Treatment of Procedures for Evaluating Photochemical Models", prepared for the California Air Resources Board, prepared by Alpine Geophysics, Crested Butte, CO. Contract No. A832-103.

Tesche, T. W., et al., 1997. "Photochemical Modeling Analysis of the Pittsburgh-Beaver Valley Ozone Nonattainment Area: Volume VI-- Attainment Demonstration", prepared for the Pennsylvania Department of Environmental Protection, prepared by Alpine Geophysics, LLC, Covington, KY.

Tesche, T. W., et al., 1997. "Superregional Ozone Modeling and Analysis Study C Phase II: Comparative Evaluation of the SAQM and UAM-V Models for the 13-21 July 1991 OTAG Episode", prepared for the Midwest Ozone Group, prepared by Alpine Geophysics, LLC, Covington, KY.

Tesche, T. W., et al., 1998. "Analysis of the Effects of VOC and NOx Emissions Reductions in the Eastern United States on Peak 1-hr and 8-hr Ozone Concentrations", prepared for the Midwest Ozone Group, prepared by Alpine Geophysics, LLC, Covington, KY.

Tesche, T. W., et al., 1998. "Photochemical Modeling Analysis of the Subregional Effects of the EPA

Section 110 SIP Call Within and Downwind of the State of Virginia”, prepared for AlliedSignal, Inc., prepared by Alpine Geophysics, LLC, Covington, KY.

Tesche, T. W., et al., 1998. “Application of EPA’s Flexible Attainment Demonstration Guidance to the Pittsburgh-Beaver Valley Ozone Nonattainment Area”, 10th Conference on Applications of Air Pollution Meteorology with the Air and Waste Management Association, American Meteorological Society, 11-16 January, Phoenix, AZ.

Tesche, T. W., et al., 1998. “Assessment of the Reliability of the OTAG Modeling System”, proceedings of the 10th Joint Conference on the Applications of Air Pollution Meteorology, 11-16 January, 1998, Phoenix, AZ.

Tesche, T. W., et al., 1998. “Cincinnati-Hamilton Ozone Attainment Demonstration Study: Volume 3: Interim Attainment Demonstration Results”, prepared for the Ohio Environmental Protection Agency and the Kentucky Natural Resources and Environmental Protection Cabinet, prepared by Alpine Geophysics, LLC, Covington, KY.

Tesche, T. W., et al., 1998. “Final Evaluation of the MM5 Model for the 3-6 August 1990 SARMAP Episode over Central California”, 10th Joint Conference on Applications of Air Pollution Meteorology, Phoenix, AZ.

Tesche, T. W., et al., 1998. “Review of the EPA Ozone Transport SIP Call and Recent Post-OTAG Modeling and Analysis Studies”, prepared for the Ohio EPA, prepared by Alpine Geophysics, LLC, Ft. Wright, KY.

Tesche, T. W., et al., 1998. “Tri-State Regional Ozone Modeling Study: Results of the Sub-Regional Modeling of the EPA Section 110 SIP call”, prepared for the Greater Cincinnati Chamber of Commerce, prepared by Alpine Geophysics, LLC, Covington, KY.

Tesche, T. W., et al., 2000. “Evaluation of the CAMx and Models-3/CMAQ Models over the Lake Michigan Region with Inputs from the MM5 and RAMS3c Models”, draft final report prepared for the Coordinating Research Council, prepared by Alpine Geophysics and ENVIRON International, Ft. Wright, KY.

Tesche, T. W., D. E. McNally, C. F. Loomis, and J. G. Wilkinson, 2002. “Regional Photochemical Modeling over Central Florida for Nine 8-hr Ozone Episodes”, Final Report prepared for the Florida Department of Environmental Protection, prepared by Alpine Geophysics, LLC, Ft. Wright, KY.

Thompson, A. M. and R. W. Stewart, 1991. “Effect of Chemical Kinetic Uncertainties on Calculated Constituents in a Tropospheric Photochemical Model”, Journal of Geophysical Research, Vol. 96, pp. 13089-13108.

Thompson, M. L., et al., 2001. “A Review of Statistical Methods for the Meteorological Adjustment of Tropospheric Ozone”, Atmospheric Environment, Vol. 35, pp. 617-630.

Tonneson, G. S., et al., 1998. "Estimating the Area of Influence of Ozone Produced by Local Precursor Emissions for a Summer Period with a Range of Photochemical Activity", 10th Joint Conference on the Applications of Air Pollution Meteorology, American Meteorological Society, Phoenix, AZ. 11-16 January.

Tremback, C. J. and R. Kessler, 1985. Surface Temperature and Moisture Parameterization for Use in Mesoscale Numerical Models, Seventh Conf. On Numerical Weather Prediction, Montreal, Quebec, Canada, American Meteorological Society, pp. 355-358.

Tremback, C. J., 1990. Numerical Simulation of a Mesoscale Convective Complex: Model Development and Numerical Results, Ph.D. dissertation, Atmospheric Science Paper no. 465, Colorado State University, Fort Collins, CO.

Tremback, C. J., et al., 1997. Development of Meteorological Inputs for the Urban Airshed Model: LMOS Episode 1: 22-28 June 1991, prepared for the Illinois Environmental Protection Agency, prepared by Mission Research Corporation, Fort Collins, CO, Project ACA-695.

Tripoli, G. J. and W. R. Cotton, 1982. The Colorado State University Three-Dimensional Cloud/Mesoscale Model C 1982, Part I: General Theoretical Framework and Sensitivity Experiments, J. Rech. Atmos., Vol. 16, pp. 185-220.

Turner, D. B., 1986. A Comparison of Three Methods for Calculating the Standard Deviation of the Wind Directions, Journal of Climate and Applied Meteorology, Vol. 25. pp. 703-707.

Turner, J. S., 1962: The starting plume in neutral surroundings. J. Fluid Mech., 13, 356-368.

U.S.-Canada Air Quality Committee, 1999. "Ground-Level Ozone: Occurrence and Transport in Eastern North America", Report by Subcommittee 1: Program Monitoring and Reporting, United States-Canada Air Quality Committee. March 1999.

Ulrickson, B. L., and C. F. Mass, 1990. "Numerical Investigation of Mesoscale Circulations Over the Los Angeles Basin, Part I: A Verification Study", Monthly Weather Review, Vol. 118, pp. 2138-2161.

Uthe, E. E., et al., 1992. "Airborne Lidar Mapping of Ozone Concentrations During the Lake Michigan Ozone Study", Journal of the Air and Waste Management Association, Vol. 42, pp. 1313-1318.

Valente, R. J., et al., 1998. "Ozone production during an urban air stagnation episode over Nashville, Tennessee", Journal of Geophysical Research, 103: 22,555-22,568.

Vukovich, F. M., 1995. "Regional-Scale Boundary Layer Ozone Variations in the Eastern United States and the Association with Meteorological Variations", Atmospheric Environment, Vol. 29, pp. 2250-2273.

Vukovich, F. M., 1997. "Time Scales of Surface Ozone Variations in the Regional, Non-urban Environment", Atmospheric Environment, Vol. 31, pp. 1513-1530.

Walko, R. L. and C. J. Tremback, 1991. "RAMS: The Regional Atmospheric Modeling System, Version 2c: User's Guide", prepared by ASTeR, Inc., Fort Collins, CO.

Wesley, M. L. and B. B. Hicks, 2000. "A Review of the Current Status of Knowledge on Dry Deposition", Atmospheric Environment, Vol. 34, pp. 2261-2282.

Wheeler, N. J., et al., 1997. "Assessment of the OTAG Modeling Studies and Urban Boundary Conditions", prepared for the American Petroleum Institute, prepared by MCNC-Environmental Programs, Research Triangle Park, N.C.

Wilkinson, J. G., et al., 1994. *Technical Formulation Document: SARMAP/LMOS Emissions Modeling System (EMS-95)*. AG-90/TS26 & AG-90/TS27. Prepared for the Lake Michigan Air Directors Consortium, Des Plaines, IL & The Valley Air Pollution Study Agency, Technical Support Division, Sacramento, CA. Prepared by Alpine Geophysics, Pittsburgh, PA.

Wilkinson, J. G., et al., 1998. "Emissions Modeling Protocol", prepared for the Southern Appalachian Mountains Initiative (SAMI), prepared by the Georgia Institute of Technology, University of Alabama, and the University of Virginia.

Wilmont, C. J., 1981. "On the Validation of Models", Phys. Geogr., Vol. 2, No. 2, pp. 168-194.

Wishinski, P. R., 2001. "An Evaluation of an Operational Mesoscale Meteorological Model in Predicting Surface Wind Fields and Temperatures Over Complex Terrain and Coastal Regions of the Northeastern U.S.", 94th Annual Conference of the Air and Waste Management Association, 24-28 June 2001, Orlando, FL.

Wolf, G. T., et al., 2001. "Ozone Air Quality Over North America: Part I – A Review of Reported Trends", Journal of the Air and Waste Management Association, Vol. 51, pp. 273-282.

Yamartino, R. J., 1984. "A Comparison of Several 'Single-Pass' Estimators of the Standard Deviation of Wind Direction", Journal of Climate and Applied Meteorology, Vol. 23. Pp. 1362-1366.

Yamazaki, T., J. Kondo, T. Watanabe, and T. Sato, 1992: A heat-balance model with a canopy of one or two layers and its application to field experiments. J. Appl. Meteor., 31, 86-103.

Zhang J., et al., 1998. "Meteorological processes and ozone exceedances in the Northeastern United States during the 12-16 July 1995 episode". Journal of Applied Meteorology, 37: (8) 776-789.

Zhang, D. L. and R. A. Anthes, 1982. High-Resolution Model of the Planetary Boundary Layer Sensitivity Tests and Comparisons with SESAME-79 Data, Journal of Applied Meteorology, Vol. 21. pp. 1594-1609.

Zhang, J. and S. T. Rao, 1999. "The role of vertical mixing in the temporal evolution of ground-level ozone concentrations", Journal of Applied Meteorology, (12) 1674-1691.

Zheng, A. "Quantification of Variability and Uncertainty in Emissions Inventories: A Prototype Software Tool with Application to Utility NOx Emissions", 94th Annual Conference of the Air and Waste Management Association, 24-28 June 2001, Orlando, FL.

Zurbenko, I. G., et al., "Mapping Ozone in the Eastern United State", Environmental Manager, February 24-30.

10. APPENDIX 1:
OUTPUT FROM EPISODE SELECTION SOFTWARE

The following is the episode software output for the 68 day Case 15 set of episode days. In order to get the correct output for all 3 pollutants, the software has to be run twice. The 68 days should be input to get the errors and outputs for ozone and visibility. Then the full 80 days (68 days plus 11 non-rain days plus 940212) must be input to get the correct errors for the acid deposition episodes (the software will only provide acid deposition outputs if each 8 day deposition period is entered). The following output has been cut and pasted so that the correct values are displayed for all 3 pollutants.

```
Use all days = false
fin[1][1]= .\run\gsmacid.run3.1.rerun
fin[1][2]= .\run\snpacid.run3.2.rerun
fin[2][1]= .\run\gsmvis.run1.8.rerun
fin[2][2]= .\run\snpvis.run1.2.rerun
fin[3][1]= .\run\gsm126.run2.rer
fin[3][2]= .\run\snp126.run2.4.rerun
Day list file = .\run\out5\case25t1.txt
Tolerance = 0.800000
actual days per data day for each set: 8 ,1 ,1 ,
Observation based metric [1][1] = 30.225004, # seasons = 6
Observation based metric [1][2] = 23.948332, # seasons = 6
Observation based metric [2][1] = 892574.375000, # seasons = 5
Observation based metric [2][2] = 829570.812500, # seasons = 6
Observation based metric [3][1] = 68817.117188, # seasons = 5
Observation based metric [3][2] = 66109.351562, # seasons = 5
Number of initial days input: 68
This represents 68 actual modeling days and 10 episodes.
Of these days, 1.5% are in episodes of length 2 or less.
910723
910724
910725
910726
910727
910728
910729
910730
910731
920624
920625
920626
920627
920628
920629
```

930323
930324
930325
930326
930327
930328
930329
930330
930331
930511
930512
930513
930514
930515
930516
930517
930803
930804
930805
930806
930807
930808
930809
930810
930811
940208
940209
940210
940211
940213
950426
950427
950428
950429
950430
950501
950502
950503
950524
950525
950526
950527
950528
950529

950711
950712
950713
950714
950715
950716
950717
950718
950719

ERRORS FOR EACH TREE WITH THIS SET OF DAYS:

fin[1][1]:

bin= 1, class=1, WA/WP= 1.093, n(j)/m(j)=61.000, dates= 950523
bin= 2, class=3, WA/WP= 0.000, n(j)/m(j)= 0.000, dates=
bin= 3, class=2, WA/WP= 0.000, n(j)/m(j)= 0.000, dates=
bin= 4, class=2, WA/WP= 1.186, n(j)/m(j)= 8.000, dates= 930323 940208
bin= 5, class=1, WA/WP= 0.000, n(j)/m(j)= 0.000, dates=
bin= 6, class=2, WA/WP= 0.000, n(j)/m(j)= 0.000, dates=
bin= 7, class=1, WA/WP= 1.081, n(j)/m(j)=25.000, dates= 950425
bin= 8, class=2, WA/WP= 0.000, n(j)/m(j)= 0.000, dates=
bin= 9, class=4, WA/WP= 0.000, n(j)/m(j)= 0.000, dates=
bin=10, class=4, WA/WP= 0.000, n(j)/m(j)= 0.000, dates=
bin=11, class=2, WA/WP= 0.000, n(j)/m(j)= 0.000, dates=
bin=12, class=3, WA/WP= 1.268, n(j)/m(j)= 4.000, dates= 930511 930803
bin=13, class=2, WA/WP= 0.000, n(j)/m(j)= 0.000, dates=
bin=14, class=3, WA/WP= 0.000, n(j)/m(j)= 0.000, dates=
bin=15, class=2, WA/WP= 1.122, n(j)/m(j)=17.000, dates= 920623
bin=16, class=3, WA/WP= 0.000, n(j)/m(j)= 0.000, dates=
bin=17, class=3, WA/WP= 0.000, n(j)/m(j)= 0.000, dates=
bin=18, class=2, WA/WP= 0.000, n(j)/m(j)= 0.000, dates=
bin=19, class=4, WA/WP= 1.000, n(j)/m(j)= 5.000, dates= 910723
910723, class=4, val= 5.49
920623, class=2, val= 0.89
930323, class=2, val= 1.13
930511, class=3, val= 1.64
930803, class=3, val= 1.89
940208, class=2, val= 1.17
950425, class=1, val= 0.69
950523, class=1, val= 0.17
B[1]= 1.136, B[2]= 2.023, B[3]= 1.846, B[4]= 1.600,
rescaled Ar=31.588583, S=6.000000, N= 221, sum P(j)= 221
usedays=8, distance error=0.045114, biased error=-0.370603

fin[1][2]:

bin= 1, class=1, WA/WP= 1.000, n(j)/m(j)=38.000, dates= 920623 950711
bin= 2, class=1, WA/WP= 0.000, n(j)/m(j)= 0.000, dates=
bin= 3, class=2, WA/WP= 1.541, n(j)/m(j)=11.000, dates= 950425
bin= 4, class=3, WA/WP= 0.000, n(j)/m(j)= 0.000, dates=
bin= 5, class=2, WA/WP= 0.000, n(j)/m(j)= 0.000, dates=
bin= 6, class=3, WA/WP= 1.403, n(j)/m(j)=14.000, dates= 930323
bin= 7, class=2, WA/WP= 0.000, n(j)/m(j)= 0.000, dates=
bin= 8, class=2, WA/WP= 1.619, n(j)/m(j)= 4.500, dates= 940208 950523
bin= 9, class=4, WA/WP= 0.000, n(j)/m(j)= 0.000, dates=
bin=10, class=3, WA/WP= 0.000, n(j)/m(j)= 0.000, dates=
bin=11, class=3, WA/WP= 0.000, n(j)/m(j)= 0.000, dates=
bin=12, class=4, WA/WP= 1.130, n(j)/m(j)= 2.500, dates= 910723 930511
910723, class=4, val= 5.12
920623, class=1, val= 0.21
930323, class=3, val= 1.97
930511, class=4, val= 2.84
940208, class=2, val= 1.24
950425, class=2, val= 1.02
950523, class=2, val= 1.41
950711, class=1, val= 0.15

B[1]= 1.474, B[2]= 1.186, B[3]= 1.286, B[4]= 1.286,
rescaled Ar=23.702814, S=6.000000, N= 208, sum P(j)= 208
usedays=8, distance error=-0.010252, biased error=-0.224372

fin[2][1]:

bin= 1, class=1, WA/WP= 2.743, n(j)/m(j)=13.000, dates= 930327
bin= 2, class=2, WA/WP= 0.000, n(j)/m(j)= 0.000, dates=
bin= 3, class=3, WA/WP= 0.000, n(j)/m(j)= 0.000, dates=
bin= 4, class=2, WA/WP= 1.156, n(j)/m(j)=11.000, dates= 950426
bin= 5, class=3, WA/WP= 0.000, n(j)/m(j)= 0.000, dates=
bin= 6, class=3, WA/WP= 1.894, n(j)/m(j)=16.000, dates= 950429
bin= 7, class=2, WA/WP= 1.872, n(j)/m(j)=50.000, dates= 930324
bin= 8, class=1, WA/WP= 0.000, n(j)/m(j)= 0.000, dates=
bin= 9, class=1, WA/WP= 1.904, n(j)/m(j)=27.000, dates= 940209
bin=10, class=3, WA/WP= 0.000, n(j)/m(j)= 0.000, dates=
bin=11, class=5, WA/WP= 0.000, n(j)/m(j)= 0.000, dates=
bin=12, class=5, WA/WP= 0.000, n(j)/m(j)= 0.000, dates=
bin=13, class=4, WA/WP= 0.000, n(j)/m(j)= 0.000, dates=
bin=14, class=5, WA/WP= 0.000, n(j)/m(j)= 0.000, dates=
bin=15, class=3, WA/WP= 1.445, n(j)/m(j)=16.000, dates= 930515
bin=16, class=4, WA/WP= 1.404, n(j)/m(j)= 9.000, dates= 920624 930811 950527 950712
bin=17, class=3, WA/WP= 1.521, n(j)/m(j)=10.000, dates= 930804 930807

bin=18, class=5, WA/WP= 1.000, n(j)/m(j)= 1.000, dates= 910731
 bin=19, class=3, WA/WP= 0.000, n(j)/m(j)= 0.000, dates=
 bin=20, class=4, WA/WP= 0.000, n(j)/m(j)= 0.000, dates=
 bin=21, class=5, WA/WP= 0.000, n(j)/m(j)= 0.000, dates=
 bin=22, class=5, WA/WP= 1.031, n(j)/m(j)= 3.500, dates= 910727 950715
 bin=23, class=4, WA/WP= 0.000, n(j)/m(j)= 0.000, dates=
 bin=24, class=4, WA/WP= 0.000, n(j)/m(j)= 0.000, dates=
 bin=25, class=2, WA/WP= 0.000, n(j)/m(j)= 0.000, dates=
 bin=26, class=5, WA/WP= 0.000, n(j)/m(j)= 0.000, dates=
 910727, class=5, val= 26605.00
 910731, class=5, val= 31824.00
 920624, class=4, val= 20918.00
 930324, class=2, val= 8223.00
 930327, class=1, val= 4505.00
 930515, class=3, val= 15464.00
 930804, class=3, val= 10029.00
 930807, class=3, val= 9338.00
 930811, class=4, val= 19024.00
 940209, class=1, val= 3919.00
 950426, class=2, val= 6538.00
 950429, class=3, val= 9766.00
 950527, class=4, val= 17516.00
 950712, class=4, val= 17785.00
 950715, class=5, val= 25882.00
 B[1]= 1.263, B[2]= 1.223, B[3]= 1.311, B[4]= 1.383, B[5]= 1.667,
 rescaled Ar=885440.500000, S=5.000000, N= 414, sum P(j)= 414
 usedays=15, distance error=-0.007992, biased error=-0.252793

fin[2][2]:

bin= 1, class=2, WA/WP= 1.736, n(j)/m(j)=21.333, dates= 950426 950429 950503
 bin= 2, class=3, WA/WP= 0.000, n(j)/m(j)= 0.000, dates=
 bin= 3, class=1, WA/WP= 0.000, n(j)/m(j)= 0.000, dates=
 bin= 4, class=3, WA/WP= 0.000, n(j)/m(j)= 0.000, dates=
 bin= 5, class=1, WA/WP= 0.000, n(j)/m(j)= 0.000, dates=
 bin= 6, class=2, WA/WP= 0.000, n(j)/m(j)= 0.000, dates=
 bin= 7, class=3, WA/WP= 1.174, n(j)/m(j)=10.000, dates= 950527
 bin= 8, class=1, WA/WP= 0.000, n(j)/m(j)= 0.000, dates=
 bin= 9, class=2, WA/WP= 1.000, n(j)/m(j)= 5.000, dates= 930324
 bin=10, class=3, WA/WP= 0.000, n(j)/m(j)= 0.000, dates=
 bin=11, class=1, WA/WP= 0.000, n(j)/m(j)= 0.000, dates=
 bin=12, class=1, WA/WP= 2.805, n(j)/m(j)=18.000, dates= 930331 940209
 bin=13, class=4, WA/WP= 1.609, n(j)/m(j)= 7.000, dates= 930512 930807
 bin=14, class=3, WA/WP= 1.246, n(j)/m(j)=13.000, dates= 930515

bin=15, class=2, WA/WP= 0.000, n(j)/m(j)= 0.000, dates=
 bin=16, class=2, WA/WP= 0.000, n(j)/m(j)= 0.000, dates=
 bin=17, class=3, WA/WP= 0.000, n(j)/m(j)= 0.000, dates=
 bin=18, class=4, WA/WP= 0.000, n(j)/m(j)= 0.000, dates=
 bin=19, class=2, WA/WP= 0.000, n(j)/m(j)= 0.000, dates=
 bin=20, class=5, WA/WP= 1.568, n(j)/m(j)= 7.000, dates= 950712 950715
 bin=21, class=4, WA/WP= 0.000, n(j)/m(j)= 0.000, dates=
 bin=22, class=4, WA/WP= 0.000, n(j)/m(j)= 0.000, dates=
 bin=23, class=4, WA/WP= 1.392, n(j)/m(j)= 5.000, dates= 930811
 bin=24, class=4, WA/WP= 1.613, n(j)/m(j)= 6.000, dates= 910731
 bin=25, class=4, WA/WP= 1.000, n(j)/m(j)= 3.500, dates= 920624 920627
 bin=26, class=3, WA/WP= 0.000, n(j)/m(j)= 0.000, dates=
 bin=27, class=3, WA/WP= 1.414, n(j)/m(j)= 7.500, dates= 930804 950719
 bin=28, class=2, WA/WP= 0.000, n(j)/m(j)= 0.000, dates=
 bin=29, class=4, WA/WP= 1.157, n(j)/m(j)= 8.000, dates= 910724 950524
 910724, class=4, val= 16610.00
 910731, class=4, val= 23289.00
 920624, class=4, val= 16664.00
 920627, class=4, val= 18077.00
 930324, class=2, val= 5580.00
 930331, class=1, val= 3892.00
 930512, class=4, val= 23834.00
 930515, class=3, val= 9576.00
 930804, class=3, val= 13994.00
 930807, class=4, val= 16282.00
 930811, class=4, val= 18647.00
 940209, class=1, val= 3715.00
 950426, class=2, val= 5548.00
 950429, class=2, val= 9031.00
 950503, class=2, val= 6745.00
 950524, class=4, val= 16746.00
 950527, class=3, val= 11944.00
 950712, class=5, val= 26001.00
 950715, class=5, val= 38917.00
 950719, class=3, val= 12226.00
 B[1]= 1.900, B[2]= 1.467, B[3]= 1.490, B[4]= 1.215, B[5]= 1.000,
 rescaled Ar=833232.812500, S=6.000000, N= 467, sum P(j)= 467
 usedays=20, distance error=0.004414, biased error=-0.251605

fin[3][1]:

bin= 1, class=1, WA/WP= 1.138, n(j)/m(j)=94.800, dates= 930513 930806 950501 950502 950529
 bin= 2, class=2, WA/WP= 1.882, n(j)/m(j)= 7.000, dates= 930808 950503 950527
 bin= 3, class=1, WA/WP= 1.349, n(j)/m(j)=30.000, dates= 910728 930807

bin= 4, class=3, WA/WP= 0.000, n(j)/m(j)= 0.000, dates=
 bin= 5, class=2, WA/WP= 1.623, n(j)/m(j)=15.750, dates= 930515 930805 930811 950426
 bin= 6, class=3, WA/WP= 0.000, n(j)/m(j)= 0.000, dates=
 bin= 7, class=2, WA/WP= 1.207, n(j)/m(j)= 5.333, dates= 910727 910731 930809
 bin= 8, class=2, WA/WP= 0.000, n(j)/m(j)= 0.000, dates=
 bin= 9, class=4, WA/WP= 0.000, n(j)/m(j)= 0.000, dates=
 bin=10, class=2, WA/WP= 1.162, n(j)/m(j)= 6.000, dates= 930511 930516
 bin=11, class=3, WA/WP= 0.000, n(j)/m(j)= 0.000, dates=
 bin=12, class=3, WA/WP= 1.494, n(j)/m(j)= 2.500, dates= 950429 950525
 bin=13, class=2, WA/WP= 1.442, n(j)/m(j)= 3.000, dates= 930517
 bin=14, class=3, WA/WP= 0.000, n(j)/m(j)= 0.000, dates=
 bin=15, class=2, WA/WP= 0.000, n(j)/m(j)= 0.000, dates=
 bin=16, class=4, WA/WP= 1.081, n(j)/m(j)= 9.000, dates= 920624
 bin=17, class=4, WA/WP= 0.000, n(j)/m(j)= 0.000, dates=
 bin=18, class=3, WA/WP= 0.000, n(j)/m(j)= 0.000, dates=
 bin=19, class=3, WA/WP= 0.000, n(j)/m(j)= 0.000, dates=
 bin=20, class=4, WA/WP= 0.000, n(j)/m(j)= 0.000, dates=
 bin=21, class=1, WA/WP= 1.263, n(j)/m(j)=23.000, dates= 920626
 bin=22, class=2, WA/WP= 0.000, n(j)/m(j)= 0.000, dates=
 bin=23, class=3, WA/WP= 1.056, n(j)/m(j)= 8.000, dates= 910726
 bin=24, class=2, WA/WP= 0.000, n(j)/m(j)= 0.000, dates=
 bin=25, class=3, WA/WP= 1.473, n(j)/m(j)= 5.000, dates= 920628 950524 950712 950713
 bin=26, class=3, WA/WP= 0.000, n(j)/m(j)= 0.000, dates=
 bin=27, class=2, WA/WP= 0.000, n(j)/m(j)= 0.000, dates=
 bin=28, class=4, WA/WP= 0.000, n(j)/m(j)= 0.000, dates=
 bin=29, class=3, WA/WP= 1.438, n(j)/m(j)= 1.500, dates= 950526 950715
 bin=30, class=3, WA/WP= 1.000, n(j)/m(j)= 3.000, dates= 950711
 bin=31, class=4, WA/WP= 1.281, n(j)/m(j)=10.500, dates= 950714 950719
 bin=32, class=3, WA/WP= 1.327, n(j)/m(j)= 4.000, dates= 950717
 910726, class=3, val= 871.80
 910727, class=2, val= 499.30
 910728, class=1, val= 243.40
 910731, class=2, val= 620.70
 920624, class=4, val= 1396.50
 920626, class=1, val= 83.30
 920628, class=3, val= 763.80
 930511, class=2, val= 638.30
 930513, class=1, val= 89.00
 930515, class=2, val= 488.60
 930516, class=2, val= 551.90
 930517, class=2, val= 703.60
 930805, class=2, val= 385.80
 930806, class=1, val= 104.20
 930807, class=1, val= 290.80

930808, class=2, val= 558.20
 930809, class=2, val= 549.60
 930811, class=2, val= 568.50
 950426, class=2, val= 540.60
 950429, class=3, val= 807.60
 950501, class=1, val= 168.60
 950502, class=1, val= 78.50
 950503, class=2, val= 548.40
 950524, class=3, val= 820.40
 950525, class=3, val= 771.70
 950526, class=3, val= 767.10
 950527, class=2, val= 658.40
 950529, class=1, val= 87.90
 950711, class=3, val= 1017.00
 950712, class=3, val= 874.60
 950713, class=3, val= 1086.40
 950714, class=4, val= 1351.10
 950715, class=3, val= 1012.20
 950717, class=3, val= 824.20
 950719, class=4, val= 1161.20
 B[1]= 1.000, B[2]= 1.217, B[3]= 1.747, B[4]= 1.178, B[5]=0,
 rescaled Ar=68429.140625, S=5.000000, N=1052, sum P(j)=1052
 usedays=35, distance error=-0.005638, biased error=-0.200580

fin[3][2]:

bin= 1, class=1, WA/WP= 1.089, n(j)/m(j)=52.875, dates= 910730 930513 930806 950501 950502
 950503 950528 950529
 bin= 2, class=1, WA/WP= 1.452, n(j)/m(j)=37.000, dates= 950428
 bin= 3, class=2, WA/WP= 1.356, n(j)/m(j)=23.000, dates= 950429
 bin= 4, class=1, WA/WP= 1.134, n(j)/m(j)=53.000, dates= 920625 930805
 bin= 5, class=2, WA/WP= 0.000, n(j)/m(j)= 0.000, dates=
 bin= 6, class=4, WA/WP= 1.477, n(j)/m(j)= 2.000, dates= 950427
 bin= 7, class=2, WA/WP= 0.000, n(j)/m(j)= 0.000, dates=
 bin= 8, class=3, WA/WP= 0.000, n(j)/m(j)= 0.000, dates=
 bin= 9, class=3, WA/WP= 0.000, n(j)/m(j)= 0.000, dates=
 bin=10, class=3, WA/WP= 1.497, n(j)/m(j)= 9.333, dates= 930512 950524 950711
 bin=11, class=2, WA/WP= 0.000, n(j)/m(j)= 0.000, dates=
 bin=12, class=4, WA/WP= 0.000, n(j)/m(j)= 0.000, dates=
 bin=13, class=2, WA/WP= 0.000, n(j)/m(j)= 0.000, dates=
 bin=14, class=3, WA/WP= 0.000, n(j)/m(j)= 0.000, dates=
 bin=15, class=2, WA/WP= 1.577, n(j)/m(j)=19.000, dates= 950719
 bin=16, class=4, WA/WP= 0.000, n(j)/m(j)= 0.000, dates=
 bin=17, class=4, WA/WP= 0.000, n(j)/m(j)= 0.000, dates=

bin=18, class=2, WA/WP= 1.688, n(j)/m(j)= 5.818, dates= 910726 910728 910731 920624 920626
 920628 930809 930810 930811 950525 950718
 bin=19, class=3, WA/WP= 0.000, n(j)/m(j)= 0.000, dates=
 bin=20, class=3, WA/WP= 0.000, n(j)/m(j)= 0.000, dates=
 bin=21, class=4, WA/WP= 0.000, n(j)/m(j)= 0.000, dates=
 bin=22, class=3, WA/WP= 1.323, n(j)/m(j)=12.000, dates= 920629
 bin=23, class=2, WA/WP= 1.379, n(j)/m(j)=12.000, dates= 950717
 bin=24, class=3, WA/WP= 0.000, n(j)/m(j)= 0.000, dates=
 bin=25, class=4, WA/WP= 0.000, n(j)/m(j)= 0.000, dates=
 bin=26, class=4, WA/WP= 1.013, n(j)/m(j)= 5.000, dates= 950713
 bin=27, class=3, WA/WP= 1.554, n(j)/m(j)= 3.000, dates= 950712
 bin=28, class=4, WA/WP= 1.181, n(j)/m(j)= 7.000, dates= 950715
 bin=29, class=3, WA/WP= 1.174, n(j)/m(j)= 1.000, dates= 930511 910723
 bin=30, class=4, WA/WP= 1.108, n(j)/m(j)=13.000, dates= 950714
 bin=31, class=3, WA/WP= 0.000, n(j)/m(j)= 0.000, dates=
 bin=32, class=4, WA/WP= 0.000, n(j)/m(j)= 0.000, dates=
 910723, class=3, val= 1143.10
 910726, class=2, val= 658.90
 910728, class=2, val= 737.80
 910730, class=1, val= 62.80
 910731, class=2, val= 638.50
 920624, class=2, val= 391.50
 920625, class=1, val= 224.50
 920626, class=2, val= 547.00
 920628, class=2, val= 449.00
 920629, class=3, val= 1022.10
 930511, class=3, val= 1019.60
 930512, class=3, val= 958.40
 930513, class=1, val= 72.40
 930805, class=1, val= 70.40
 930806, class=1, val= 89.80
 930809, class=2, val= 745.40
 930810, class=2, val= 567.90
 930811, class=2, val= 549.30
 950427, class=4, val= 1167.80
 950428, class=1, val= 250.60
 950429, class=2, val= 428.70
 950501, class=1, val= 65.80
 950502, class=1, val= 85.60
 950503, class=1, val= 140.60
 950524, class=3, val= 1121.60
 950525, class=2, val= 620.00
 950528, class=1, val= 72.00
 950529, class=1, val= 58.10

950711, class=3, val= 935.80
950712, class=3, val= 901.70
950713, class=4, val= 1162.60
950714, class=4, val= 1456.60
950715, class=4, val= 1334.70
950717, class=2, val= 527.30
950718, class=2, val= 430.60
950719, class=2, val= 545.20
B[1]= 1.000, B[2]= 1.191, B[3]= 1.425, B[4]= 1.205, B[5]=0,
rescaled Ar=66196.039062, S=5.000000, N=1066, sum P(j)=1066
usedays=36, distance error=0.001311, biased error=-0.166249

Total Error (average unsigned) = 12.257393
Total Error (sqrt sum squared) = 67.399037
Total Error (optimized cost) = 0.000000
Total Error (average biased) = 32.433480

The following is the episode software output for Case 15 dry deposition only. The full 80 days were run through the software to get the correct outputs (similar to wet deposition).

Use all days = false
fin[1][1]= snp121.forwt.dat
fin[1][2]= gsm22.forwt.dat
Day list file = case15f.out
Tolerance = 0.800000
actual days per data day for each set: 8 ,
Observation based metric [1][1] = 536.409973, # seasons = 6
Observation based metric [1][2] = 316.571991, # seasons = 5
Number of initial days input: 80
This represents 80 actual modeling days and 9 episodes.
Of these days, 0.0% are in episodes of length 2 or less.
910723
910724
910725
910726
910727
910728
910729
910730
910731
920623
920624
920625
920626
920627
920628
920629
920630
930323
930324
930325
930326
930327

930328
930329
930330
930331
930511
930512
930513
930514
930515
930516
930517
930518
930519
930803
930804
930805
930806
930807
930808
930809
930810
930811
930812
940208
940209
940210
940211
940212
940213
940214
940215
940216
950425
950426
950427
950428
950429
950430
950501
950502
950503
950523
950524
950525

950526
950527
950528
950529
950530
950711
950712
950713
950714
950715
950716
950717
950718
950719

ERRORS FOR EACH TREE WITH THIS SET OF DAYS:

fin[1][1]:

bin= 1, class=3, WA/WP= 0.000, n(j)/m(j)= 0.000, dates=
bin= 2, class=4, WA/WP= 0.000, n(j)/m(j)= 0.000, dates=
bin= 3, class=1, WA/WP= 0.000, n(j)/m(j)= 0.000, dates=
bin= 4, class=3, WA/WP= 0.000, n(j)/m(j)= 0.000, dates=
bin= 5, class=1, WA/WP= 0.000, n(j)/m(j)= 0.000, dates=
bin= 6, class=2, WA/WP= 0.000, n(j)/m(j)= 0.000, dates=
bin= 7, class=3, WA/WP= 0.000, n(j)/m(j)= 0.000, dates=
bin= 8, class=2, WA/WP= 0.000, n(j)/m(j)= 0.000, dates=
bin= 9, class=2, WA/WP= 0.000, n(j)/m(j)= 0.000, dates=
bin=10, class=3, WA/WP= 0.000, n(j)/m(j)= 0.000, dates=
bin=11, class=1, WA/WP= 1.087, n(j)/m(j)=18.000, dates= 940208
bin=12, class=3, WA/WP= 0.000, n(j)/m(j)= 0.000, dates=
bin=13, class=2, WA/WP= 0.000, n(j)/m(j)= 0.000, dates=
bin=14, class=1, WA/WP= 0.000, n(j)/m(j)= 0.000, dates=
bin=15, class=1, WA/WP= 0.000, n(j)/m(j)= 0.000, dates=
bin=16, class=2, WA/WP= 0.000, n(j)/m(j)= 0.000, dates=
bin=17, class=1, WA/WP= 1.273, n(j)/m(j)=19.000, dates= 910723 930323 930803 950425
950523 950711
bin=18, class=4, WA/WP= 0.000, n(j)/m(j)= 0.000, dates=
910723, class=1, val= 8.97
930323, class=1, val= 9.58
930803, class=1, val= 13.55
940208, class=1, val= 13.42
950425, class=1, val= 6.31
950523, class=1, val= 7.49
950711, class=1, val= 13.68

B[1]= 1.171, B[2]=0, B[3]=0, B[4]=0,
rescaled Ar=455.885895, S=6.000000, N= 244, sum P(j)= 178
usedays=7, distance error=-0.150117, biased error=-0.470564

```

fin[1][2]:
bin= 1, class=4, WA/WP= 0.000, n(j)/m(j)= 0.000, dates=
bin= 2, class=3, WA/WP= 0.000, n(j)/m(j)= 0.000, dates=
bin= 3, class=3, WA/WP= 0.000, n(j)/m(j)= 0.000, dates=
bin= 4, class=2, WA/WP= 0.000, n(j)/m(j)= 0.000, dates=
bin= 5, class=2, WA/WP= 1.000, n(j)/m(j)= 2.000, dates= 930511
bin= 6, class=2, WA/WP= 0.000, n(j)/m(j)= 0.000, dates=
bin= 7, class=1, WA/WP= 1.068, n(j)/m(j)=12.000, dates= 930323 940208
bin= 8, class=2, WA/WP= 0.000, n(j)/m(j)= 0.000, dates=
bin= 9, class=2, WA/WP= 0.000, n(j)/m(j)= 0.000, dates=
bin=10, class=3, WA/WP= 0.000, n(j)/m(j)= 0.000, dates=
bin=11, class=1, WA/WP= 0.000, n(j)/m(j)= 0.000, dates=
bin=12, class=2, WA/WP= 0.000, n(j)/m(j)= 0.000, dates=
bin=13, class=4, WA/WP= 0.000, n(j)/m(j)= 0.000, dates=
bin=14, class=1, WA/WP= 0.000, n(j)/m(j)= 0.000, dates=
bin=15, class=2, WA/WP= 0.000, n(j)/m(j)= 0.000, dates=
bin=16, class=1, WA/WP= 1.019, n(j)/m(j)=19.750, dates= 910723 920623 930803 950523
bin=17, class=2, WA/WP= 0.000, n(j)/m(j)= 0.000, dates=
bin=18, class=2, WA/WP= 0.000, n(j)/m(j)= 0.000, dates=
bin=19, class=2, WA/WP= 0.000, n(j)/m(j)= 0.000, dates=
bin=20, class=3, WA/WP= 0.000, n(j)/m(j)= 0.000, dates=
bin=21, class=2, WA/WP= 1.135, n(j)/m(j)= 6.000, dates= 950711
bin=22, class=2, WA/WP= 0.000, n(j)/m(j)= 0.000, dates=
bin=23, class=1, WA/WP= 0.000, n(j)/m(j)= 0.000, dates=
bin=24, class=2, WA/WP= 0.000, n(j)/m(j)= 0.000, dates=
910723, class=1, val= 3.62
920623, class=1, val= 7.16
930323, class=1, val= 6.73
930511, class=2, val= 9.65
930803, class=1, val= 6.02
940208, class=1, val= 3.41
950523, class=1, val= 6.17
950711, class=2, val= 8.14
B[1]= 1.314, B[2]= 5.667, B[3]=0, B[4]=0,
rescaled Ar=287.421631, S=5.000000, N= 226, sum P(j)= 189
usedays=8, distance error=-0.092081, biased error=-0.578595

```

```

Total Error (average unsigned) = 12.109898
Total Error (sqrt sum squared) = 17.610785
Total Error (optimized cost) = 0.000000
Total Error (average biased) = 52.457958

```

11. APPENDIX 2: EPISODE SELECTION PROCESS IN DETAIL

11.1 Running the Episode Selection Software

The episode selection software was run at least a hundred times to get the final list of SAMI episode days. There was a great deal of experimentation in learning how the software worked, as well as learning its strengths and weaknesses. The software generally did a good job of selecting a set of episode days that could be used as a starting point. But it was clear that a great deal of “user intervention” would be required to get a final set of acceptable episode days.

The software was designed to allow the user to specify whether the priority should be given to minimization of error or maximization of episode length. It is more efficient to run a small set of long episodes than a large set of short episodes. Long episodes minimize the total number of ramp-up days needed and it is generally easier to create meteorological inputs for long continuous time periods. Therefore the episode length was the primary consideration. It was envisioned that somewhere between 5 and 10 week long episodes would be selected.

It was noted earlier that the selection of episode days is limited by the availability of ambient data. The acid deposition data consists of 8 day periods and the ozone and visibility data are single day periods. The ozone data is available every day during the April-October growing season and the visibility data is only available on Wednesdays and Saturdays.

Initial runs of the episode software produced a number of 2-4 day ozone and visibility episodes and a number of 8 day acid deposition episodes. The goal of the episode selection was to minimize the total number of episodes and days, and to minimize the unscaled error at the same time. It was quickly realized that the most efficient way to select a limited number of episodes would be to select ozone and visibility episodes that were embedded within a series of 8 day acid deposition episodes. Essentially, a full 8 day period⁸ had to be selected to represent each acid deposition episode. If most (or all) of the ozone and visibility days fell within the same 8 day periods then shorter episodes could be eliminated.

Since we wanted the software to select mostly 8 day episode periods, acid deposition was made first in the user selected “pollutant order”. The software was run many times with different combinations of pollutant order and park order. It was found to be important for acid deposition to be first. Visibility was selected second and ozone third. The order of the parks was not found to be important. Great Smokies was selected first. The complete order is as follows:

⁸ After the episodes were selected, several days at the beginning and end of acid deposition episodes were eliminated if they were non-rain days since the episode classification was based on wet deposition. The eliminated days were also screened to make sure they were not ozone or visibility days. A total of 11 days out of 80 were removed as non-rain days.

- 1) Acid deposition- GSM
- 2) Acid deposition- SNP
- 3) Visibility- GSM
- 4) Visibility- SNP
- 5) Ozone- GSM
- 6) Ozone- SNP

The episode software can be run in 2 modes. In the first mode the user specifies the pollutant and park order, the tolerance⁹, the default number of days to select, and a distance and cost factor¹⁰. The software returns a full list of episode days that is “optimized” across the 3 pollutants and 2 parks (based on the user specified inputs). The software calculates the errors associated with the episode days and provides the scaling factors necessary to recreate the annual and /or seasonal averages. In the second mode, the user specifies a complete set of episode days and the software simply calculates the errors and the scaling factors. The first mode can be used to select an initial “optimized” set of days and then the second can be used to hand edit the episode days and recalculate the errors.

11.2 SAMI Episode Selection

Round 1

The episode selection process began around the same time that GA Tech was selected as the main SAMI modeling contractor. When GA Tech started their initial testing of the URM- 1ATM model they needed to prepare input data for at least one episode to use as a test case. In some of the initial testing of the episode software, the “July 1995 “ episode (approximately July 10th-15th) was frequently selected as both a high ozone and high (poor) visibility episode. Since this was likely to be good episode for SAMI to use and since it had also been an OTAG episode, SAMI decided to choose July 10th-15th¹¹ as its first episode.

The episode selection was run several times to let the software select the episode days. It was found that several 2 or 3 day episodes were almost always selected. The short episodes often contained days representing bins with high weights for one or more pollutant. The high weight days often represent a significant fraction of the annual or seasonal metric, but selecting those days would make it difficult to maintain the goal of modeling long episodes. Therefore it was important to attempt to replace these days with alternative days from the same bin which may fall within an 8 day acid deposition episode.

⁹ Tolerance is the allowed distance from the bin mean for a day to be able to be selected. SAMI used of tolerance of 0.80 (80%).

¹⁰ A larger distance factor minimizes the error and a larger chain factor minimizes the number of short episodes. SAMI set both factors to 1 which equally weights for error and episode length.

¹¹ The July '95 episode was later extended to July 11th-19th (plus ramp-up days) in order to make it an acid deposition episode and to include July 17, 18, and 19 as ozone days and July 19th as a visibility day.

As expected, the unscaled error was well correlated with the number of days selected. As part of the final round of episode selection, different cases (set of days) were developed which began with 48, 56, and 70 episode days. These cases were hand edited in different ways to become possible episode selection candidates.

The initial round of episode selection contained cases ranging from 8-10 episodes and 46-71 episodes days. The following is a summary of the first six cases that were considered by SAMI. The tables contain the number of days and episodes in each case; the biased (unscaled) and scaled errors for each pollutant and park; and the number of properly classified days for each pollutant and park, sorted by class.

Table 4-8								
			Ozone	Ozone	Annual Vis.	Annual Vis.	Acid Dep.	Acid Dep.
			GSM	SNP	GSM	SNP	GSM	SNP
Case 1	46 days	biased error %	-43.3	-45.1	-43.1	-42.5	-47.7	-56.3
8 episodes		scaled error %	-4.7	-14.2	5.2	-0.2	-8.5	-23.1
		class 1 days	5	7	0	1	1	1
Started with 48 days		class 2 days	5	1	2	2	2	0
		class 3 days	4	5	4	3	1	2
		class 4 days	4	3	2	1	2	4
		class 5 days	N/A	N/A	1	2	N/A	N/A
		Total Days	18	16	9	9	6	7
Case 2	52 days	biased error %	-38.2	-33.6	-36.5	-55.1	-61.5	-24.4
8 episodes		scaled error %	-8.2	-0.5	8.5	2.4	-20.9	7.6
		class 1	6	5	0	1	1	2
Started with 56 days		class 2	7	3	1	3	2	1
		class 3	6	5	5	3	0	1
		class 4	1	4	6	1	1	1
		class 5	N/A	N/A	1	3	N/A	N/A
		Total Days	20	17	13	11	4	5
Case 3	59 days	biased error %	-34.3	-25.1	-28.9	-49.3	-50.4	-12.5
9 episodes		scaled error %	-6.5	0.9	10.3	9.6	-9.2	3.9
Derived from case 2		class 1	6	5	0	2	1	2
		class 2	8	6	1	3	2	2
		class 3	6	5	6	3	1	1
		class 4	2	5	6	2	1	1
		class 5	N/A	N/A	1	3	N/A	N/A
		Total Days	22	21	14	13	5	6
Case 4	67 days	biased error %	-19.1	-24.3	-28.9	-31.9	-47.3	-27.9
10 episodes		scaled error %	0.9	1.4	0.1	-6.6	13.5	2.1
		class 1	9	14	3	2	1	2
Started with 70 days		class 2	11	8	2	1	2	2
		class 3	11	6	4	4	3	1
		class 4	3	4	6	8	1	1
		class 5	N/A	N/A	1	2	N/A	N/A
		Total Days	34	32	16	17	7	6
Case 5	66 days	biased error %	-23.7	-16	-33.7	-33	-47.3	-29.5
9 episodes		scaled error %	-1.9	2.1	-0.8	-8.2	13.5	0.5
		class 1	9	13	3	2	1	3
Derived from case 4		class 2	10	11	2	1	2	2
		class 3	9	6	4	5	3	1
		class 4	3	3	4	6	1	1
		class 5	N/A	N/A	1	2	N/A	N/A
		Total Days	31	33	14	16	7	7
Case 6	71 days	biased error %	-18.3	-17.2	-28.9	-32.2	-47.3	-29.5
10 episodes		scaled error %	0.4	0.9	0.1	-7	13.5	0.5
		class 1	9	14	3	2	1	3
Derived from case 5		class 2	11	11	2	1	2	2
		class 3	12	7	4	5	3	1
		class 4	4	4	6	8	1	1
		class 5	N/A	N/A	1	2	N/A	N/A

		Total Days	36	36	16	18	7	7
--	--	------------	----	----	----	----	---	---

Case 1 started with 48 days selected by the software. A short 2 day episode was removed to arrive at the final 46 day total. It can be seen from cases 1-3 that the biased errors for ozone were generally in the -30-45% range; the biased errors for visibility ranged from -30-55% and the biased errors for acid deposition were in the -40-60% range. It was not known if these errors were “acceptable”. But by increasing the number of episode days, it was shown that the errors could be reduced considerably. Cases 4-6 increased the starting number of episode days to 70. With 9 or 10 episodes and 67-71 days, the ozone errors were reduced to around -20%; the visibility errors were reduced to around -30%; and the acid deposition errors were reduced to -30% at SNP and -50% at GSM.

Round 2

The next 3 cases represented the second set of possible episodes. Case 7 was derived from Case 1 and Cases 8 and 9 were both derived from Case 5. Case 5 contained fewer days and episodes than Cases 4 and 6. Therefore it became the default set of episode days. The objective of Cases 8 and 9 was to reduce the number of episodes and days even further without increasing the errors.

			Ozone	Ozone	Annual Vis.	Annual Vis.	Acid Dep.	Acid Dep.
			GSM	SNP	GSM	SNP	GSM	SNP
Case 7	42 days	biased error %	-60.9	-59.9	-45.8	-47.1	-56.2	-66.3
6 episodes		scaled error %	-35.6	-27.6	9.1	-5.4	42.1	99.9
		class 1	5	8	0	1	0	0
Derived from case 1		class 2	6	1	1	3	2	0
		class 3	0	3	4	3	1	2
		class 4	0	0	1	1	2	1
		class 5	N/A	N/A	1	1	N/A	N/A
		Total Days	11	12	7	9	5	3
Case 8	63 days	biased error %	-24.6	-19.9	-32.9	-33.6	-55.3	-29.7
8 episodes		scaled error %	-2.8	-0.2	0.9	-6.9	-16.9	0.3
		class 1	7	10	4	3	1	3
Derived from case 5		class 2	9	11	1	2	3	2
		class 3	9	6	4	4	2	1
		class 4	3	3	4	6	1	1
		class 5	N/A	N/A	1	2	N/A	N/A
		Total Days	28	30	14	17	7	7
Case 9	62 Days	biased error %	-24.7	-15.5	-26.2	-30.9	-45.2	-16.8
8 Episodes		scaled error %	-2.8	1.1	-1.4	-3	-8.7	-1
		class 1	8	13	2	1	2	3
Derived from case 5		class 2	11	12	2	4	2	2
		class 3	10	6	5	4	2	1
		class 4	3	4	4	6	1	1
		class 5	N/A	N/A	1	2	N/A	N/A
		Total Days	32	35	14	17	7	7

It can be seen in Case 7 that decreasing the number of episodes to 6 with only 42 episode days, drastically increases the biased errors, especially for ozone and visibility. Cases 8 and 9 show that the number of episodes from Case 5 can be decreased from 9 to 8 without a large increase in error. In fact, in some cases the errors in Cases 8 and 9 are even lower than Case 5. Since the errors in Case 9 were slightly lower than Case 8 (and there was one less day), Case 9 was proposed as the final set of modeling days.

Round 3

At this point in the process Case 9 had been established as a “benchmark” set of episode days. The associated biased and scaled errors were reasonable compared to other selected sets of episode days. Soon after this leg of the episode selection process was completed, several groups within SAMI wanted to explore the possibility of reducing the number of episodes and episode days. It was unknown whether SAMI’s schedule and budget would support modeling 8 episodes and 62 episode days.

Cases 9b, 9c, and 9d were derived from Case 9 in an effort to illustrate the effects of reducing the number of episodes. As was expected, in all 3 cases, the biased errors increased. By limiting the number of episode days to less than 50, it was not possible to sufficiently reduce the errors to a level that satisfied the modeling subcommittee. It was therefore argued that more episodes and episode days were needed in order to effectively represent the seasonal and annual metrics for all three 3 pollutants. The episode selection process continued.

Table 4-10								
			Ozone	Ozone	Annual Vis.	Annual Vis.	Acid Dep.	Acid Dep.
			GSM	SNP	GSM	SNP	GSM	SNP
Case 9b	48 Days	biased error %	-28.2	-31.5	-35.5	-47.8	-64.9	-30.4
6 Episodes		scaled error %	3.5	-4.9	0.1	-9.6	-12.4	0.8
		class 1	7	9	2	1	1	2
Derived from case 9		class 2	9	8	1	1	1	1
		class 3	8	5	4	4	2	1
Removed 950425		class 4	2	3	3	4	1	1
and 920623		class 5	N/A	N/A	1	2	N/A	N/A
		Total Days	26	25	11	12	5	5
Case 9c	45 Days	biased error %	-34.1	-21.8	-34.7	-46.6	-56.2	-28.8
8 Episodes		scaled error %	-7.2	-2.5	1.3	-4.6	-18.7	2.4
		class 1	5	9	2	1	1	2
Derived from case 9		class 2	5	7	1	1	2	1
		class 3	9	6	2	2	1	1
Removed 950425		class 4	3	3	3	4	1	1
and 930803		class 5	N/A	N/A	1	2	N/A	N/A
		Total Days	22	25	9	10	5	5
Case 9d	47 Days	biased error %	-37.8	-29.2	-27.4	-33.2	-65.6	-18.3
6 Episodes		scaled error %	-8	-4.7	-3.1	2	-13.7	-2.5
		class 1	6	13	2	1	1	2
Derived from case 9		class 2	7	12	2	4	1	2
		class 3	9	6	3	2	1	1
Removed 930803		class 4	2	4	2	2	1	1
and 920623		class 5	N/A	N/A	1	2	N/A	N/A
		Total Days	24	35	10	11	4	6

Round 4

At this point, Case 9 was still the best combination of episode days selected to date. Both the number of days and magnitude of errors were reasonable. The biggest weakness of Case 9 was its limited representation of class 1 visibility days (cleanest 20% of days). This was important for several reasons. First, the committee wanted to be able to adequately represent the full range of conditions from clean to dirty for all pollutants. They wanted to be sure that the future change in air quality could be quantified on clean days as well as dirty days (since the goal was to capture the annual average visibility). Second, the proposed regional haze rules required a demonstration that visibility does not degrade on the cleanest 20% of visibility days at each Class 1 area.

In Case 9 there was only one class 1 visibility day at SNP and two class 1 day at GSM. Therefore, in an effort to increase the number of class 1 visibility days, it was decided to add a ninth episode which contained relatively clean days. A February '94 episode (940208) was selected which contained two (properly classified) class 1 days in each park. The episode could also be extended to be 8 days long to pick up an additional class 2 acid deposition episode for each park. Case 10 shows the errors associated with adding the period from 940209-940212. This covers the visibility days only (940209 and 940212). The errors barely change compared to Case 9 because the new clean episode days represent days with small weights. But the number of class 1 visibility days increases to 4 at GSM and 3 at SNP. Case 11 adds a couple more days to make the new episode both a visibility and acid deposition episode. This brings the total number of episodes to 9 and the number of episode days to 68.

As an alternative, Case 12 adds another summer episode (930724) instead of the winter '94 episode. The summer episode has a larger effect on error, but doesn't add any other clean days. Cases 13 and 14 add both the winter and summer episodes. While the errors are improved slightly compared to Case 11, the modeling committee decided that the number of episodes needed to be limited 9. Case 11 was deemed to be the most efficient combination of episodes and errors. The SAMI operations committee subsequently approved the decision to model 9 episodes (and 68 episode days).

Table 4-11								
			Ozone	Ozone	Annual Vis.	Annual Vis.	Acid Dep.	Acid Dep.
			GSM	SNP	GSM	SNP	GSM	SNP
Case 11	68 Days	biased error %	-24.7	-15.5	-24.4	-29.5	-45	-17.6
9 Episodes		scaled error %	-2.8	1.1	-1.6	-0.2	-8.2	-2
		class 1	8	13	4	3	2	3
Derived from case 9		class 2	11	12	2	4	3	3
(Add 940208-940213)		class 3	10	6	5	4	2	1
Vis. and Acid		class 4	3	4	4	6	1	1
		class 5	N/A	N/A	1	2	N/A	N/A
		Total Days	32	35	16	19	8	8
Case 12	67 Days	biased error %	-19.5	-16.7	-21.4	-28.6	-45.2	-16.8
9 Episodes		scaled error %	-0.6	0	-0.4	0.8	-8.7	-1
		class 1	8	14	2	1	2	3
Derived from case 9		class 2	12	12	2	4	2	2
(Add 930724-930728)		class 3	13	7	5	4	2	1
ozone and vis.		class 4	4	5	6	8	1	1
		class 5	N/A	N/A	1	2	N/A	N/A
		Total Days	37	38	16	19	7	7
Case 13	71 Days	biased error %	-19.5	-16.7	-19.6	-30.1	-45.2	-16.8
10 Episodes		scaled error %	-0.6	0	-0.6	-1.8	-8.7	-1
		class 1	8	14	4	3	2	3
Derived from case 9		class 2	12	12	2	4	2	2
(Add 930724-930728		class 3	13	7	5	4	2	1
and 940209-940212)		class 4	4	5	6	8	1	1
ozone and vis.		class 5	N/A	N/A	1	2	N/A	N/A
		Total Days	37	38	18	21	7	7
Case 14	73 Days	biased error %	-19.5	-16.7	-19.6	-30.1	-45	-17.6
10 Episodes		scaled error %	-0.6	0	-0.6	-1.8	-8.2	-2
		class 1	8	14	4	3	2	3
Derived from case 9		class 2	12	12	2	4	3	3
(Add 930724-930728		class 3	13	7	5	4	2	1
and 940208-940213)		class 4	4	5	6	8	1	1
ozone, vis., and acid		class 5	N/A	N/A	1	2	N/A	N/A
		Total Days	37	38	18	21	8	8

Round 5

Naturally, the episodes were selected before the meteorological modeling could take place. The episode selection process assumed that the meteorological and air quality models would be able to successfully reproduce the historical episodes. The meteorology associated with one of the episodes in Case 11 proved to be particularly difficult. The 940405 episode was a class 4 acid deposition for GSM and represented a

significant fraction of the annual deposition (it had a high weight). There was a large amount of observed precipitation at GSM during the episode. RAMS was not able to adequately reproduce the observed precipitation. It was therefore decided to drop this episode in favor of another class 4 acid deposition episode at GSM.

Several other GSM class 4 episodes were identified. Cases 15 and 16 show the errors when the 940405 episode is replaced by the 910723 and 91806 episodes respectively. The overall error in Case 15 is generally lower than either Case 16 or the original Case 11. Additionally, 910723 is a class 4 acid deposition episode at SNP and contains several additional visibility and ozone days at each park. The subcommittee decided to use the 910723 episode as the replacement. **Case 15 became the final set of episode days with 9 episodes and 69 days¹².**

			Ozone	Ozone	Annual Vis.	Annual Vis.	Acid Dep.	Acid Dep.
			GSM	SNP	GSM	SNP	GSM	SNP
Case 15	69 Days	biased error %	-20	-16.6	-23.6	-26.4	-37.1	-22.4
9 Episodes		scaled error %	-0.5	0.1	-1.2	-1.9	4.5	-1
		class 1	8	11	3	3	2	3
Derived from case 11		class 2	13	14	2	4	3	3
deleted 940405 and		class 3	11	7	4	4	2	1
added 910723		class 4	3	4	4	8	1	2
		class 5	N/A	N/A	3	2	N/A	N/A
		Total Days	35	36	16	21	8	9
Case 16	68 Days	biased error %	-20.5	-17.6	-23.9	-30.7	-39.6	-26.9
9 Episodes		scaled error %	-0.9	-1.1	-1	-2.7	0.4	-6.8
		class 1	9	12	3	3	2	2
Derived from case 11		class 2	11	11	2	4	3	3
deleted 940405 and		class 3	12	6	5	4	2	1
added 910806		class 4	3	4	4	8	1	1
		class 5	N/A	N/A	1	2	N/A	N/A
		Total Days	35	33	15	21	8	7

The Final Round

Following the approval of the Case 15 episode days, one more addition was made to the episode selection process. In the original development of the CART database, only wet deposition measurements were used to characterize acid deposition. After the episode selection was completed (and the base case modeling was well on its way), the modeling subcommittee decided to look at estimating the annual total for dry deposition. SAI was hired to run CART again for GSM and SNP using the same meteorological information as the original classification. The details of the analysis can be found in (Hudischewskyj, 2000).

¹² The subsequent air quality model performance for visibility for day 940212 was judged to be deficient. This day was later thrown out of the episode selection statistics for visibility for both parks, but the total number of modeled days is still 69.

Since the 69 episode days were already selected, SAMI needed to determine how the already selected episodes would be classified for dry deposition. Since the wet deposition episodes were heavily influenced by the amount of precipitation at the Class I areas, it was no surprise that dry deposition during most of the selected episodes was low. At GSM there were 6 class 1 dry deposition episodes and 2 class 2 episodes. At SNP all 7 selected episodes fell into class 1 bin. Due to the under-representation of the medium and high dry deposition periods, the unscaled dry deposition errors are relatively high. For the same reason the uncertainty associated with the dry deposition weightings is likely to be higher than for the other pollutants.

An additional source of uncertainty results from the removal of the 11 “non-rain” days from the original 80 day episode total. These days were removed at a time in the selection process when only wet deposition was being considered. It was thought to be reasonable to remove these days (at the beginning and end of episode period) because wet deposition cannot occur on days without precipitation. But dry deposition obviously occurs on non-rain days. In fact, dry deposition is likely to be highest on those days. It was too late in the process to add the non-rain days back into the episodes. The following table summarizes the dry deposition results.

Table 4-13				
			Dry Dep.	Dry Dep.
			GSM	SNP
Case 15	69 Days	biased error %	-57.8	-47.0
9 Episodes		scaled error %	-9.2	-15.0
		class 1	6	7
		class 2	2	0
		class 3	0	0
		class 4	0	0
		class 5	N/A	N/A
		Total Days	8	7

**12. APPENDIX 3:
DETAILED COMPARISONS WITH OTHER PROGNOSTIC MODEL EVALUATION
STUDIES**

Table 10-1 and Figure 10-1 summarize statistically and graphically the performance evaluation results of nearly thirty (30) MM5 and RAMS model applications over the past five years. Results for 12 km model applications are listed since this the scale most commonly reported in recent studies. Most of the studies, however, have also examined prognostic model skill at 36 km and 4 km scales; this information has also been compiled by AG.

Table 10-1 presents episode-mean statistics for surface temperature, mixing ratio, and winds. While these statistics may be helpful in making general comparisons between studies and episodes, the calculation of an episode mean statistic often conceals important day-to-day and/or hour-to-hour variations that may be quite important in judging the adequacy of a meteorological or air quality model simulation.

Table 12-1. Summary of Prognostic Meteorological Model Performance Evaluations by Alpine Geophysics: 12 Km Grid Resolution Results. (a) Surface Temperatures (deg C).

Modeling Domain	Model	Study	Ref	Episode	Mean Bias(deg C)	Gross Error (deg C)
St. Louis	MM5	Kansas/Missouri	12	11-24 June '95	-0.3	1.6
St. Louis	MM5	Kansas/Missouri	12	8-15 July '95	0.2	1.7
St. Louis	MM5	Kansas/Missouri	12	14-21 Aug '98	2.0	2.3
Kansas City	MM5	Kansas/Missouri	12	11-24 June '95	-0.7	1.5
Kansas City	MM5	Kansas/Missouri	12	8-15 July '95	-0.8	1.7
Kansas City	MM5	Kansas/Missouri	12	14-21 Aug '98	0.9	1.6
Texas	MM5	COAST	11	4-11 Sept '93	0.2	1.8
Central Florida	MM5	PFOS-Episode 1	10	16-24 Apr '99	0.1	1.5
Central Florida	MM5	PFOS-Episode 2	10	2-10 May '97	0.2	1.6
Central Florida	MM5	PFOS-Episode 3	10	25-30 Aug '97	0.2	1.7
Central Florida	MM5	PFOS-Episode 4	10	4-10 April '99	-0.4	1.3
Central Florida	MM5	PFOS-Episode 5	10	17-23 Sept '97	0.1	1.6
Central Florida	MM5	PFOS-Episode 9	10	20-28 Apr '98	0.3	1.3
Eastern U.S.	MM5	Pittsburgh SIP	1	31 July-2 Aug '95	0.8	2.4
Western U.S.	MM5	SARMAP	4	3-6 Aug '90	0.2	2.9
Southeastern U.S.	RAMS	SAMI	7	3-12 Aug '93	-0.4	1.6
Southeastern U.S.	RAMS	SAMI	7	22-29 Jun '92	-1.1	1.8
Southeastern U.S.	RAMS	SAMI	7	24 Apr-3 May '91	-0.8	1.8
Upper Midwest	RAMS	CRC-LMO'S	6	26-28 Jun '91	0.1	1.4
Upper Midwest	RAMS	CRC-LMOS	6	17-19 Jul '91	-0.0	1.9
Upper Midwest	MM5	CRC-LMOS	6	26-28 Jun '91	-0.5	1.6
Upper Midwest	MM5	CRC-LMOS	6	17-19 Jun '91	-0.3	1.7
Eastern U.S.	RAMS	OTAG	3	13-21 Jul '91	1.6	2.1
Eastern U.S.	MM5	OTAG	3	13-21 Jul '91	-0.1	2.0
Eastern U.S.	MM5	OTAG	2	1-11 Jul '88	-0.6	3.3
Eastern U.S.	MM5	OTAG	1	12-15 Jul '95	-0.2	2.0
Eastern U.S.	MM5	Cincinnati SIP	5	18-22 Jun '94	-0.7	2.4
Southeastern U.S.	MM5	BAMP	9	6-11 Sep '93	-0.4	2.1
Southeastern U.S.	MM5	BAMP	9	15-19 Aug '93	-0.3	2.4
Mean Value					-0.0	1.9

Table 12-1. Summary of Prognostic Meteorological Model Performance Evaluations by Alpine Geophysics: 12 Km Grid Resolution Results. (a) Surface Mixing Ratio (gm/Kg).

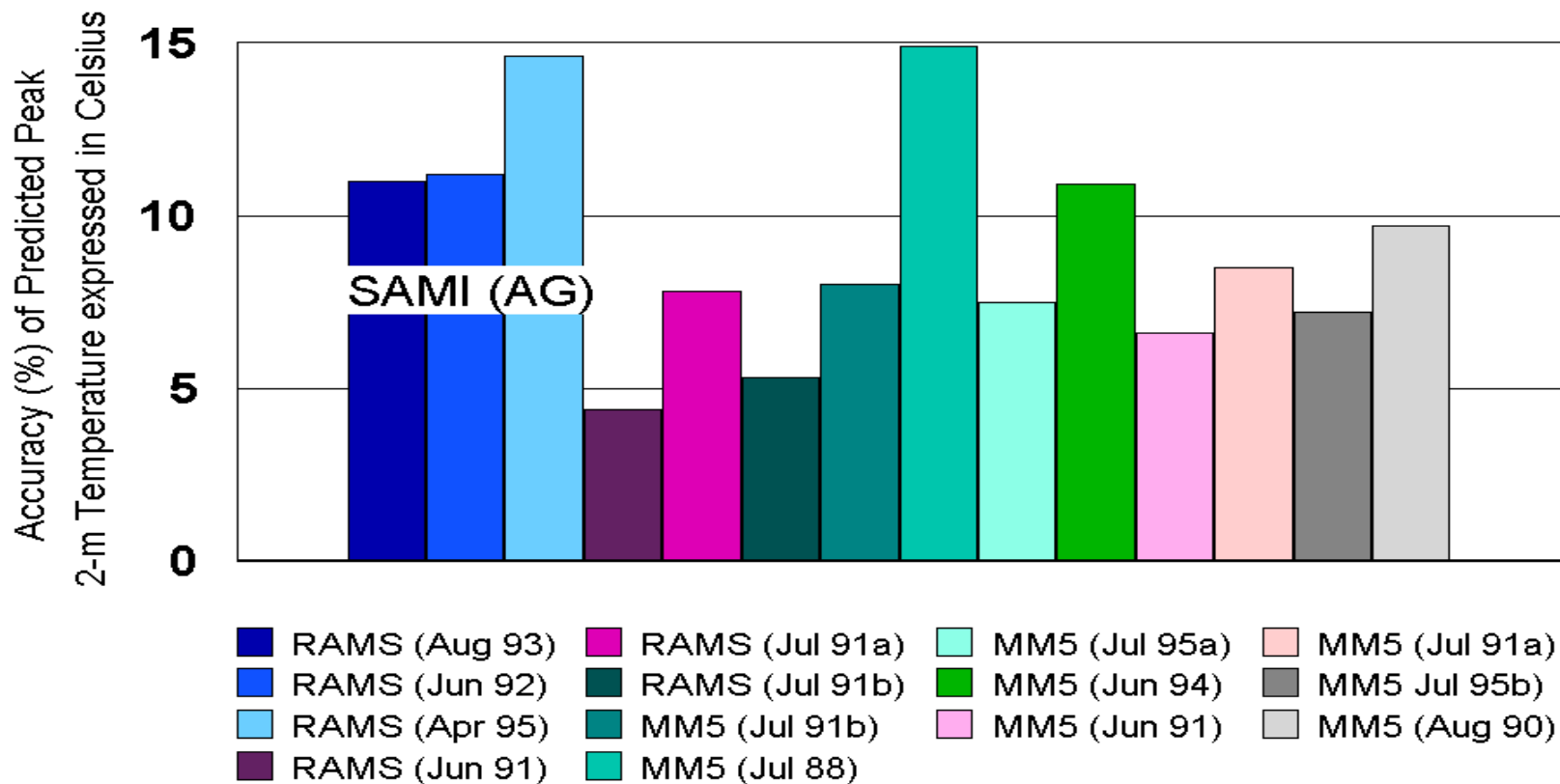
Modeling Domain	Model	Study	Ref	Episode	Mean Bias (gm/Kg)	Gross Error (gm/Kg)
St. Louis	MM5	Kansas/Missouri	12	11-24 June '95	-0.9	1.3
St. Louis	MM5	Kansas/Missouri	12	8-15 July '95	-0.6	1.6
St. Louis	MM5	Kansas/Missouri	12	14-21 Aug '98	2.4	2.6
Kansas City	MM5	Kansas/Missouri	12	11-24 June '95	-0.5	1.2
Kansas City	MM5	Kansas/Missouri	12	8-15 July '95	0.2	1.5
Kansas City	MM5	Kansas/Missouri	12	14-21 Aug '98	-2.3	2.5
Texas	MM5	COAST	11	4-11 Sept '93	0.1	1.4
Central Florida	MM5	PFOS-Episode 1	10	16-24 Apr '99	-0.1	1.2
Central Florida	MM5	PFOS-Episode 2	10	2-10 May '97	0.1	1.2
Central Florida	MM5	PFOS-Episode 3	10	25-30 Aug '97	-2.0	2.3
Central Florida	MM5	PFOS-Episode 4	10	4-10 April '99	0.8	1.5
Central Florida	MM5	PFOS-Episode 9	10	17-23 Sept '97	-0.4	1.6
Central Florida	MM5	PFOS-	10	20-28 Apr '98	-0.2	0.9
Eastern U.S.	MM5	Pittsburgh SIP	1	31 July-2 Aug '95	0.2	2.2
Western U.S.	MM5	SARMAP	4	3-6 Aug '90	-0.2	1.9
Southeastern U.S.	RAMS	SAMI	7	3-12 Aug '93	-0.6	1.1
Southeastern U.S.	RAMS	SAMI	7	22-29 Jun '92	-0.3	1.0
Southeastern U.S.	RAMS	SAMI	7	24 Apr-3 May '91	-0.1	0.7
Upper Midwest	RAMS	CRC-LMOS	6	26-28 Jun '91	-0.1	1.2
Upper Midwest	RAMS	CRC-LMOS	6	17-19 Jul '91	0.4	1.4
Upper Midwest	MM5	CRC-LMOS	6	26-28 Jun '91	-0.1	1.2
Upper Midwest	MM5	CRC-LMOS	6	17-19 Jun '91	-0.6	1.5
Eastern U.S.	RAMS	OTAG	3	13-21 Jul '91	-0.0	1.2
Eastern U.S.	MM5	OTAG	3	13-21 Jul '91	-0.3	1.4
Eastern U.S.	MM5	OTAG	2	1-11 Jul '88	-1.4	2.0
Eastern U.S.	MM5	OTAG	1	12-15 Jul '95	-1.5	2.2
Eastern U.S.	MM5	Cincinnati SIP	5	18-22 Jun '94	-1.6	2.2
Southeastern U.S.	MM5	BAMP	9	6-11 Sep '93	-0.6	1.0
Southeastern U.S.	MM5	BAMP	9	15-19 Aug '93	-1.5	1.9
Mean Value					-0.4	1.5

Table 12-1. Summary of Prognostic Meteorological Model Performance Evaluations by Alpine Geophysics: 12 Km Grid Resolution Results. (a) Surface Wind Speeds

Modeling Domain	Model	Study	Ref	Episode	Average Error (%)	RMSE (ms ⁻¹)	Index of Agreement	Mean Wind Dir. Diff. (deg)
St. Louis	MM5	Kansas/Missouri	12	11-24 June '95	31.6	1.88	0.48	20
St. Louis	MM5	Kansas/Missouri	12	8-15 July '95	10.3	1.86	0.41	1
St. Louis	MM5	Kansas/Missouri	12	14-21 Aug '98	47.5	1.83	0.45	4
Kansas City	MM5	Kansas/Missouri	12	11-24 June '95	38.9	2.03	0.45	2
Kansas City	MM5	Kansas/Missouri	12	8-15 July '95	28.5	1.97	0.47	12
Kansas City	MM5	Kansas/Missouri	12	14-21 Aug '98	45.1	1.90	0.47	0
Texas	MM5	COAST	11	4-11 Sept '93	61.4	2.20	0.69	15.0
Central Florida	MM5	PFOS-Episode 1	10	16-24 Apr '99	20.9	1.94	0.78	10.0
Central Florida	MM5	PFOS-Episode 2	10	2-10 May '97	21.0	1.95	0.78	32.0
Central Florida	MM5	PFOS-Episode 3	10	25-30 Aug '97	30.6	1.86	0.73	32.0
Central Florida	MM5	PFOS-Episode 4	10	4-10 April '97	18.1	1.80	0.80	8.0
Central Florida	MM5	PFOS-Episode 5	10	17-23 Sept '97	27.9	1.84	0.72	9.0
Central Florida	MM5	PFOS-Episode 9	10	20-28 Apr '98	24.0	1.79	0.78	26.4
Eastern U.S.	MM5	Pittsburgh SIP	1	31 July-2 Aug '95	12.6	1.78	0.75	8.0
Western U.S.	MM5	SARMAP	4	3-6 Aug '90	22.6	2.13	0.80	3.0
Southeastern U.S.	RAMS	SAMI	7	3-12 Aug '93	139.6	2.18	0.75	25.6
Southeastern U.S.	RAMS	SAMI	7	22-29 Jun '92	65.6	1.89	0.75	20.6
Southeastern U.S.	RAMS	SAMI	7	24 Apr-3 May '91	60.2	2.35	0.81	4.4
Upper Midwest	RAMS	CRC-LMOS	6	26-28 Jun '91	11.9	1.82	0.69	16.7
Upper Midwest	RAMS	CRC-LMOS	6	17-19 Jul '91	3.5	1.73	0.64	7.4
Upper Midwest	MM5	CRC-LMOS	6	26-28 Jun '91	5.8	1.70	0.79	14.0
Upper Midwest	MM5	CRC-LMOS	6	17-19 Jun '91	15.6	1.65	0.77	7.4
Eastern U.S.	RAMS	OTAG	3	13-21 Jul '91	4.6	1.61	0.74	27.1
Eastern U.S.	MM5	OTAG	3	13-21 Jul '91	23.0	1.92	0.73	17.0
Eastern U.S.	MM5	OTAG	2	1-11 Jul '88	65.6	3.21	0.64	7.9
Eastern U.S.	MM5	OTAG	1	12-15 Jul '95	21.2	1.91	0.68	15.2
Eastern U.S.	MM5	Cincinnati SIP	5	18-22 Jun '94	82.4	2.69	0.80	0.1
Southeastern U.S.	MM5	BAMP	9	6-11 Sep '93	89.4	2.36	0.60	21.5
Southeastern U.S.	MM5	BAMP	9	15-19 Aug '93	193.6	2.66	0.65	120.0

Mean Value	42.2	2.02	0.68	16.8
------------	------	------	------	------

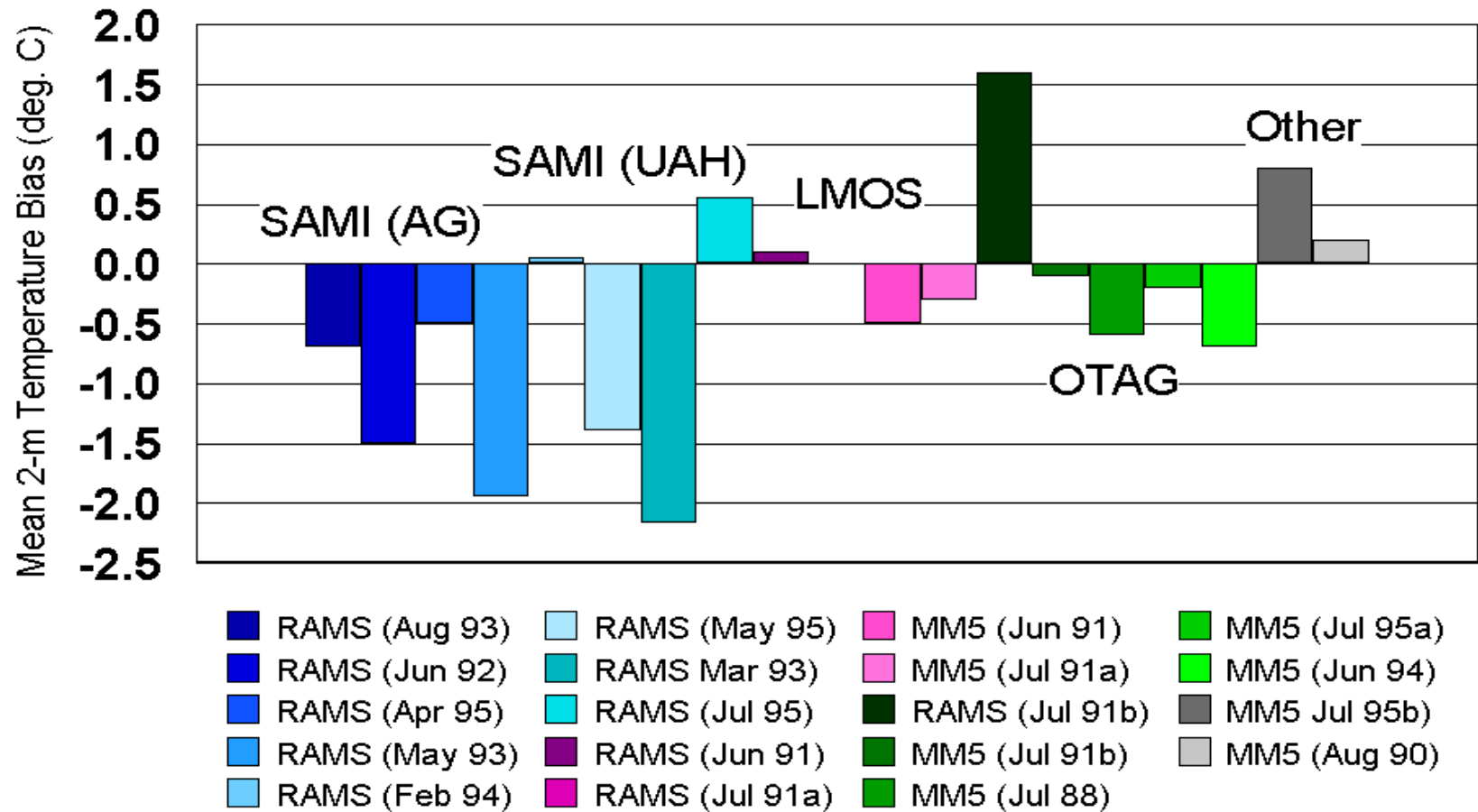
Meteorological Model Performance at 12-km Grid Resolution



SAMI=bluish; LMOS=purple & pink; OTAG=greenish; Other=gray

Figure 12-1. Accuracy of Predicted Peak 2m Temperatures From Recent Prognostic Meteorological Models.

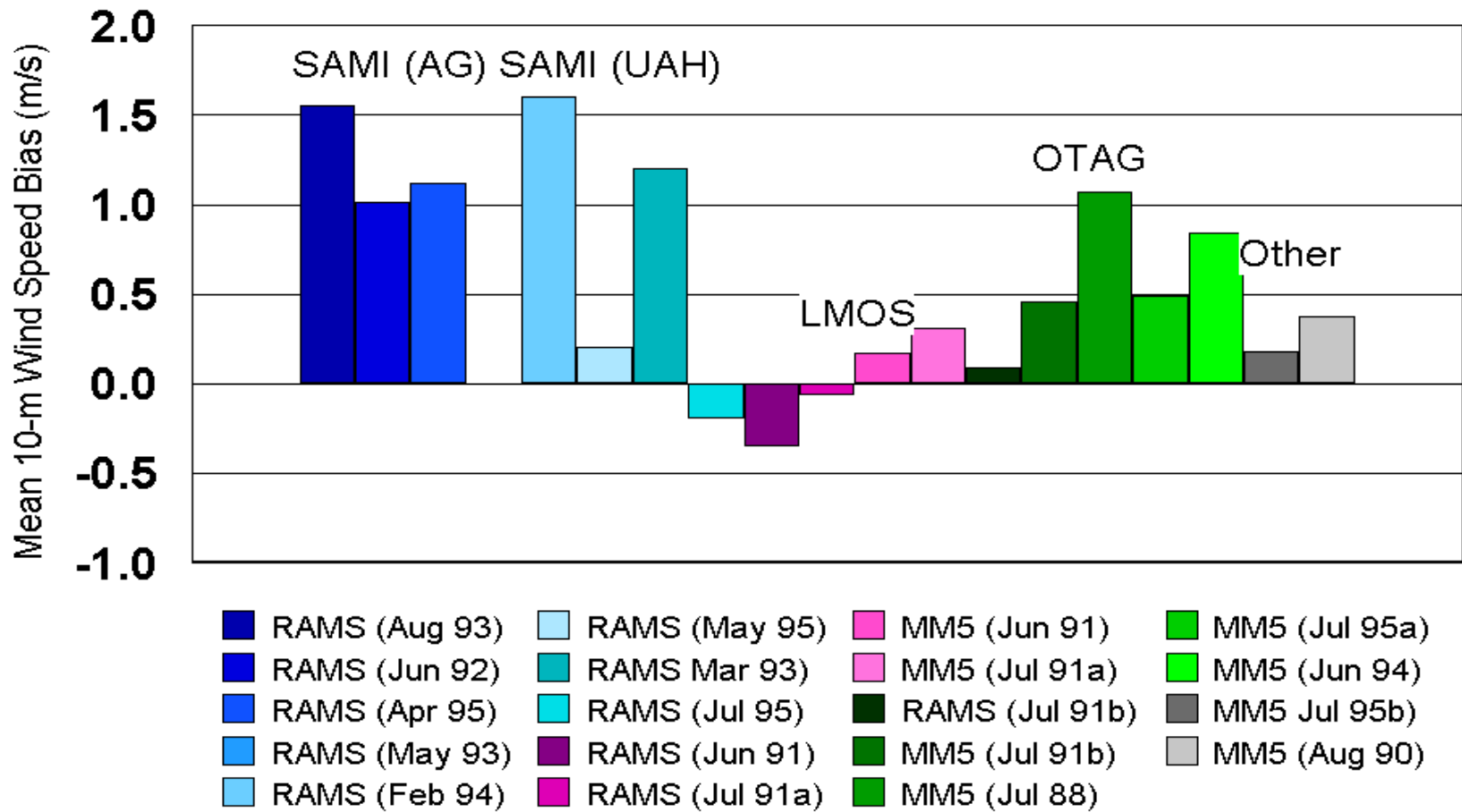
Meteorological Model Performance at 12-km Grid Resolution



SAMI=bluish; LMOS=purple & pink; OTAG=greenish; Other=gray

Figure 12-2. Mean Bias in Predicted Hourly Temperatures at 2 m From Recent Prognostic Meteorological Models.

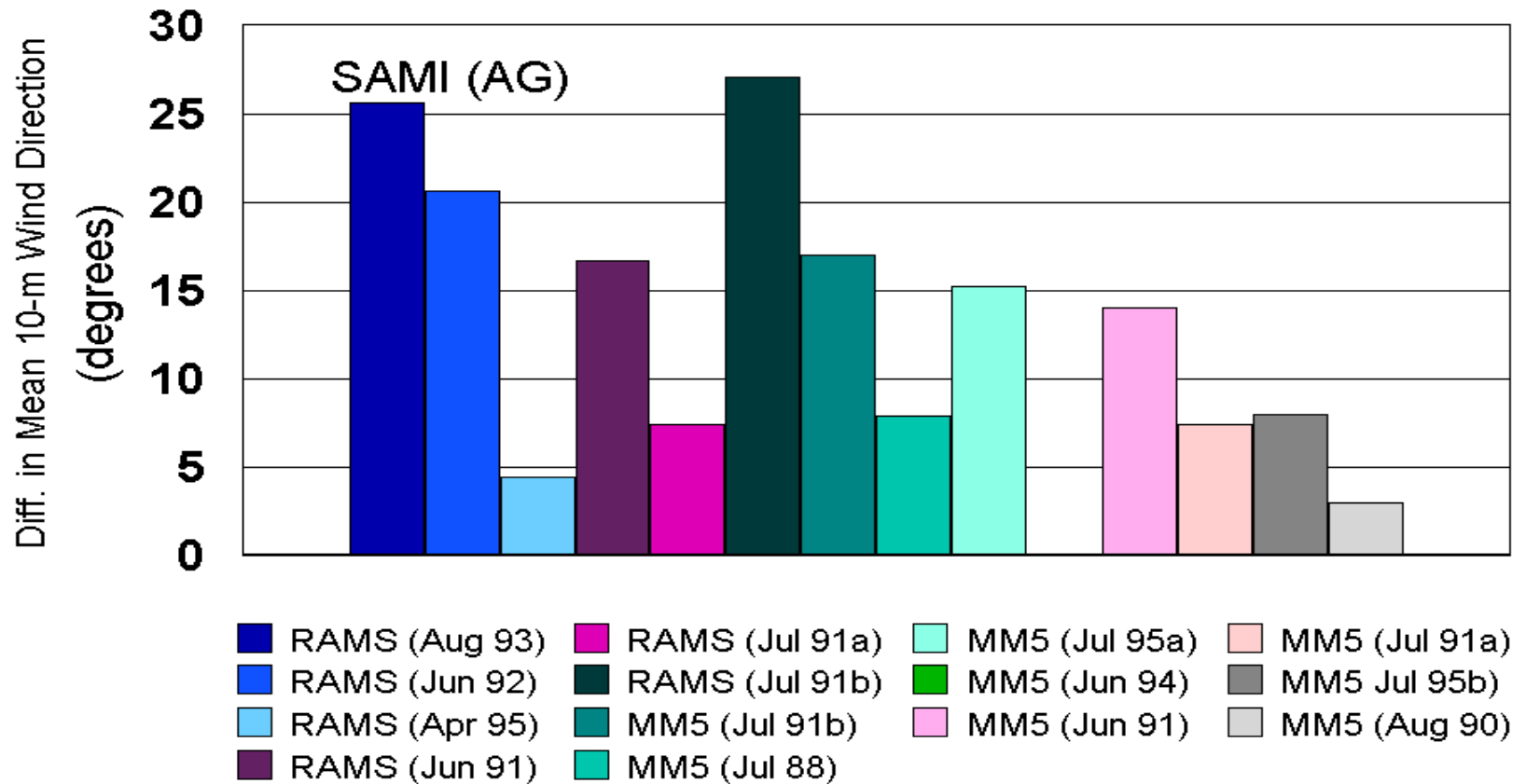
Meteorological Model Performance at 12-km Grid Resolution



SAMI=bluish; LMOS=purple & pink; OTAG=greenish; Other=gray

Figure 12-3. Bias in Hourly Wind Speeds at 10 m From Recent Prognostic Meteorological Models.

Meteorological Model Performance at 12-km Grid Resolution



SAMI=bluish; LMOS=purple & pink; OTAG=greenish; Other=gray

Figure 12-4. Difference in Mean Wind Direction at 10-m From Recent Prognostic Meteorological Models.

13. APPENDIX 4:

Southern Appalachian Mountains Initiative

**METEOROLOGICAL MODELING
PROTOCOL**

**Version 3
May 6, 1998**

Prepared By
William B. Norris and Kevin G. Doty
University of Alabama in Huntsville

Meteorological Modeling Protocol

1. Introduction

The Georgia Institute of Technology (GIT) plans to simulate a series of episodes selected for the Southern Appalachian Mountains Initiative (SAMI). The episodes have been chosen so that important metrics of ambient ozone concentration, acid deposition, and visibility impairment can be statistically constructed from the model results and used to assess future air quality in the Southern Appalachian Mountains. GIT will use the Urban-to-Regional Multiscale model (URM-1ATM) to carry out the air-quality simulations. Among the inputs required by URM-1ATM are fields of meteorological variables such as wind components, temperature, and moisture. The University of Alabama in Huntsville (UAH) will use a mesoscale meteorological model to provide the required meteorological input for URM-1ATM.

This document describes the technical choices in the design of the meteorological model simulations and serves the following purposes:

- It commits UAH to a set of data sources and procedures for conducting the meteorological simulations.
- It clarifies the interface between the UAH and GIT models.
- It provides SAMI with a basis for reviewing, evaluating, and approving the meteorological modeling activities.

Nevertheless, the document should be viewed more as guidance than law. Each episode will undoubtedly possess unique features that may require adjustments to the prescribed modeling approach. The modeling process should be left flexible enough to allow for adaptation to situations that may be perceived only as the model simulations are conducted.

The primary model for producing the meteorological fields is the Regional Atmospheric Modeling System (RAMS), Version 3a, developed by scientists at Colorado State University. To a lesser extent UAH will use the Pennsylvania State University - National Center for Atmospheric Research (PSU-NCAR) mesoscale model, version 5, (MM5). The technical attributes of these models are described in Appendix A (RAMS) and Appendix B (MM5). RAMS has been used in previous air-quality evaluations to provide meteorological fields to photochemical models (Lyons et al., 1991; Ozone Transport Assessment Group (OTAG), 1996). Likewise, MM5 has been used for these types of applications (Seaman *et al.*, 1995).

The main body of the document is organized into nine topics. Following this introduction Sections 2-4 describe the overall design and approach to the meteorological simulations. Sections 5-7 describe processing and evaluating the data produced by the model runs. Section 8 pertains to computational issues such as the hardware to be used and the estimated amount of time needed to perform the simulations. Section 9 pertains to quality assurance.

- Section 1: Introduces the protocol.
- Section 2: Defines the model domain and grid structures.
- Section 3: Describes the kinds of inputs RAMS will use for initialization and assimilation.
- Section 4: Discusses the choices to be made among available subgrid-scale parameterizations.
- Section 5: Lists the variables for which output will be available from RAMS either directly or as derived values.
- Section 6: Lists and discusses activities that will be carried out for a subset of the simulations to evaluate model performance.
- Section 7: Describes the major difficulties that will be encountered in exporting the meteorological fields to URM-1ATM and how these difficulties will be approached.
- Section 8: Describes the computational resources to be used and provides estimates of the run times for standardized simulations so that actual run times can be predicted.
- Section 9: Outlines quality-assurance activities that will be carried out to promote the accuracy and reproducibility of the meteorological modeling.

2. Meteorological Model Domain and Grid Configuration

Important initial decisions in designing the simulations are selecting the size and location of the meteorological model domain and its system of nested grids. The aim of these choices is to ensure that the data supplied to URM-1ATM is appropriate as possible for air-quality modeling in the SAMI region subject to the constraints of available resources.

2.1 Meteorological Model Domain

Horizontally the domain must be large enough to supply meteorological fields for the entire URM-1ATM domain. Vertically the domain must be high enough to model the meteorological processes that could significantly affect air-quality levels in the Southern Appalachians.

2.1.1 Horizontal Extent of Meteorological Domain

The meteorological model domain must be at least as large as the air-quality model domain. For comparison with the meteorological domain, a horizontal view of the air-quality domain is shown in Figure 1-1 in a Mercator projection with the true latitude at 26° N and central longitude of 99° W. The domain extends east to west from about 66° W to 99° W, and south to north from about 26° N to about 47° N. This domain was selected to encompass all the major source regions which potentially have a significant

impact on the Southern Appalachians.

The bounds of the meteorological model domain are shown in Figure 2. The size and location ensures that at every point in URM-1ATM the applicable meteorological values can be obtained by interpolation (with subsequent adjustment to conserve mass between the two domains [see Section 7]).

2.1.2 Vertical Extent of Domain

The top of the meteorological domain is approximately 17 km . With this vertical extent RAM permits the development of deep convection and can capture the vertical motions associated with stratospheric intrusions into the troposphere which may be important in relation to ozone transport.

2.2 Grid Configuration

The characteristics of the physical problem and the demands on computer resources have been considered in determining the horizontal and vertical resolution of the grid structures to be used. Independent of the resolution, RAMS uses the Arakawa C grid (Messinger and Arakawa, 1976; Arakawa and Lamb, 1977) as the basis of its numerical integrations. In this arrangement scalar variables are defined at grid-cell centers and wind components are defined on grid-cell faces (Figure 3)

2.2.1 Horizontal Grid Configuration

Before describing the horizontal grid system to be used in RAMS, the grid system of URM-1ATM will be described. The URM-1ATM grid structure has five levels of resolution. The outermost grid has a resolution of 192 km with successive grids having resolutions of 96, 48, 24, and 12 km. The grids having the coarser resolutions are used to resolve emissions in major source regions away from the Southern Appalachians. The finer grids are used to resolve both emissions and pollutant levels in or near the complex topography of the Southern Appalachians. These features are depicted in Figure 1-1.

The RAMS horizontal grid configuration differs from that of URM-1ATM. Both models carry out their respective calculations in a Cartesian coordinate system but use different map projections. URM-1ATM maps its domain from the surface of a spherical earth into a plane using a Mercator projection while RAMS uses an oblique stereographic projection.

The coarse, intermediate, and fine grids for RAMS have resolutions of 96, 24, and 12 km, respectively, as shown in Figure 2. The details about the locations of the three grids are listed in Tables 1-3. The purpose of the 96-km grid is to capture the synoptic-scale meteorology that influences mesoscale processes in and near the Southern Appalachians. The RAMS intermediate grid (horizontal resolution of 24 km) covers the Southeast, and the fine grid (horizontal resolution 12 km) covers portions of the Southern Appalachians. The choice of 12 km for the RAMS fine-grid resolution was largely based on the use of the URM-1ATM 12-km fine-grid resolution for URM-1ATM. Aside from the need to limit excessive model run times, the rationale was that the meteorological details resulting from using a finer grid, such as 4 km, would be smoothed out when the meteorological fields were interpolated into the coarser URM-1ATM domain. The location of the 12-km grid required that it include the Great Smoky Mountains National Park and the

Shenandoah National Park.

2.2.2 Feasibility of an Ultra-Fine Grid Resolution for Complex Terrain

An ultra-fine resolution of 4 km will significantly improve the resolution of complex terrain. Finer resolution of the terrain will in turn lead to better resolution of slope-induced meteorological fields. The question is whether the higher resolution will significantly affect the outcome of the air-quality modeling. Therefore, UAH will make two preliminary model runs on a selected episode. The first will use the nest of the 96, 24 and 12 km just described, while the second will add the ultra-fine resolution of 4 km.

The ultra-fine resolution consists of two grids--one near the Great Smoky Mountain National Park and the other near the Shenandoah National Park as shown in Figure 4. The grid covering Shenandoah has been extended to the west to include the nearby front range of the Allegheny Mountains which is expected to affect the meteorology that occurs in Shenandoah. The topography of the region is shown in Figure 5. The details about the characteristics of the ultra-fine grids are listed in Table 4.

The output fields from the two preliminary model runs will be passed to GIT for input to URM-1ATM. If the ultra-fine resolution leads to air-quality model results which are significantly different then the UAH/GIT team will seek guidance from SAMI in resolving the conflict between unacceptably long model run times and the possible degradation of modeling quality from using a maximum resolution of 12 km. "Significantly" is intentionally not defined here in order to permit discussion of this point among SAMI modeling subcommittee members when the test results become available.

2.2.3 Vertical Grid Configuration

RAMS and URM-1ATM differ in their vertical coordinate systems. RAMS uses a sigma-h system. At the surface the model's lowest level assumes nearly the shape of the underlying terrain. The upper levels become progressively flatter as they approach the domain top. The thickness of the RAMS vertical layers increases from 40 m near the surface to a maximum of 1000 m. The spacing of the vertical levels is listed in Table 5.

3. Model Inputs

The required input data for RAMS can be divided into two main groups. One is the atmospheric data for the initial, boundary condition, and nudging fields. The other is the various fields which are required to specify the surface characteristics.

3.1 Atmospheric Data

Atmospheric data are needed to initialize model fields, to provide time-dependent boundary conditions as the simulations proceed, and to furnish values interior to the model domain toward which the model solution can be nudged (see 4.3).

The National Centers for Environmental Prediction (NCEP)/National Center for Atmospheric Research

(NCAR) reanalysis data (Kalnay et al., 1996) was chosen as the main data source for the atmospheric data. The procedures used to transform the reanalysis data into a form useful in RAMS is described in Appendix C. The required three-dimensional variables needed for an initial state are the horizontal wind components, water vapor mixing ratio, potential temperature, and a scaled pressure (the Exner function).

3.2 Surface Characteristics

Topography for the 96-km grid will be obtained from a 10-minute resolution dataset compiled by the U.S. Navy (Global Terrain Height Data) and for the other grids from a 30-second resolution dataset (NCAR Contiguous U.S. Terrain Height Data).

Among the important variables in regional modeling, soil moisture is one of the most intractable because of its spatial and temporal variability and the absence of routine measurements. Values can be deduced from infrared satellite images, but because of expense and time, that approach is not being considered for this project (although see 6.3). Initial soil moisture fields will be obtained from the reanalysis dataset even though they are highly influenced by the model component of the reanalysis system as opposed to observations.

Soil temperature will be initialized as a function of the atmospheric temperature. This is accomplished in RAMS by specifying a profile of departures from the lowest air temperature. Sea-surface temperatures (specifically for the Atlantic Ocean and the Gulf of Mexico) will be obtained again from the reanalysis dataset.

Soil type data are derived from the STATSGO dataset developed by the National Cooperative Soil Survey and distributed by the National Resources Conservation Service. Raw data resolution is on the order of 1 km horizontally and with 11 layers in the vertical over most of the continental United States. The current soil model in RAMS is not designed to allow variable soil types in the vertical so the predominant or modal value was chosen from the STATSGO data for each soil model column.

Vegetation indices and 18 land-use types are supplied with RAMS by the model distributor. These values will be used in each simulation.

4. Model Configuration

RAMS is a versatile modeling system capable of simulating flows from the scale of a global hemisphere to the scale of a building (Pielke *et al.*, 1992). Nearly 200 options are available to RAMS users to allow them to tailor the model configuration to best fit the problem to be studied. This section discusses the most important of these choices for SAMI modeling.

4.1 Nesting vs. Stand-Alone Domains

Preliminary work in running the different resolution grids independently and in a sequential fashion in a one-way nested approach has not been successful. Therefore, future simulations will run the nested grids simultaneously in a two-way approach which is the default and intended mode of the RAMS model.

4.2 Moist Processes

For each type of impact of interest to SAMI--ozone concentrations, acid deposition, and visibility impairment--clouds and precipitation are important and therefore the various choices which govern the moisture physics are important as well.

4.2.1 Cumulus Parameterization

The generation of cumulus clouds presents a special problem for mesoscale modeling. A number of cumulus parameterizations have been devised to approximate subgrid-scale convection by using the grid-scale values as the environment for the convection. A modified version of the Kuo parameterization (Kuo, 1974), is available in RAMS and will be activated for the 96- and 24-km grids but probably not the 12-km grid. This version of the Kuo scheme has a simple downdraft with the precipitation efficiency being made a function of vertical wind shear.

4.2.2 Grid-scale Moist Processes

One of SAMI's purposes for modeling the Southern Appalachians is to determine the relationship between emissions and acid deposition in the region. In order for the air-quality model to simulate wet deposition properly, the meteorological model will need to provide variables such as three-dimensional fields of cloud and rain water mixing ratio and two-dimensional fields such as cloud base and cloud top and the surface precipitation rate. RAMS provides several levels of moist physics of which the most complex allows for five prognostic condensate types: rain, snow, pristine ice, ice aggregates, graupel, and hail. Cloud water values are obtained diagnostically by subtracting the total condensate plus water vapor from the total water. UAH is proposing to use the minimum level of the moist physics which will allow for only cloud and rain water but no ice microphysics.

4.3 Four-Dimensional Data Assimilation (FDDA)

FDDA is a technique for incorporating external data into a model so that it influences the model solution while maintaining time continuity and dynamic coupling among the modeled fields. The external data may consist of observations, if the model is being used to reconstruct past events, or of forecasts. Also, the data may be available for all or only a few of the model domain's grid points, either on the boundaries or in the interior.

RAMS uses the method of Newtonian relaxation, or nudging, to incorporate external data. With this method the model state is relaxed toward the state defined by the external data by adding artificial tendency terms to one or more of the models prognostic equations. In RAMS the artificial tendency term is given by

$$(a_e - a_m)/T \quad (1)$$

where a_e is the external value, a_m is the corresponding model value, and T is a time scale controlling the strength of the nudging term. The time scale T can be allowed to vary from a typical minimum value near the

domain walls in order to maximize nudging there and then increased to the maximum value, T_{\max} , in the center of the domain. The time scale T can also be held constant everywhere and this will be the initial approach taken in this study. Nudging will be performed on the 96-km grid but not on the finer meshes. For the SAMI simulations the external data will be the analyses obtained from the reanalysis dataset. The FDDA will be performed with $T_{\max}=1$ h. In tests conducted by the Tennessee Valley Authority less bias was found in the simulated wind speeds and directions when $T_{\max}=1$ h. However, the standard error in these variables increased compared to results when $T_{\max}=3$ h. The optimal choice may be episode dependent.

4.4 Other Configuration Considerations

Other choices must be made before RAMS can be run. Some of these are summarized in this section.

4.4.1 Model Physics

The equations used by RAMS are the nonhydrostatic, quasi-Boussinesq set described by Tripoli and Cotton (1982). Although the hydrostatic version of RAMS could be used on the coarser grids, the nonhydrostatic model will be used throughout to maintain consistency.

4.4.2 Finite-Difference Formulation

The finite-difference formulation is second order in space and a hybrid combination in time. In the hybrid temporal scheme in the nonhydrostatic mode the u, v , and w wind components and pressure use centered in time differencing (i.e., the leapfrog scheme) whereas all other scalars use forward in time differencing. The advection terms are written in flux form so that mass, momentum, and energy are conserved.

4.4.3 Diffusion

The horizontal diffusion is handled as a first-order eddy viscosity based on a local exchange coefficient that is a function of velocity deformation and static stability derived from Smagorinski (1963) with modifications. The vertical diffusion calculations include a Mellor and Yamada (1982) scheme to allow for the prognostic determination of the turbulent kinetic energy.

4.4.4 Radiation

RAMS includes two schemes for radiation calculations. The Mahrer-Pielke (1977) scheme accounts for sloping terrain, forward Rayleigh scattering, and the absorption of shortwave radiation by oxygen, ozone, carbon dioxide, and water vapor, but it does not allow for the presence of any kind of condensate. The Chen and Cotton (1983) scheme does account for condensate and is the scheme UAH will use for SAMI modeling initially. UAH is aware that a potential problem has been identified in the Chen and Cotton (1983) scheme having to do with solar heating rates in stratiform clouds. If the problem appears in the SAMI modeling, UAH may switch to the Fu et al. (1995) scheme which is not supplied with RAMS but which has been added to RAMS by researchers in the Global Hydrology and Climate Center in Huntsville, Alabama. A drawback of the Fu et al. (1995) scheme is its high computational demands.

4.4.5 Soil Model

The boundary values at the bottom of the domain are supplied by a soil model. The model was first developed by McCumber and Pielke (1981) and later modified by Tremback and Kessler (1985). A layer of finite depth at the soil-atmosphere is assumed, and prognostic equations are formulated for fluxes of heat and water vapor through the layer. The model assumes eleven layers from the surface down to 0.50 m below the surface.

4.4.6 Model Physics Changes

The original RAMS-3a model uses the Louis (1979) parameterization in determining the surface fluxes which eliminates the need for any iterative calculations to determine the Obukhov length. Beljaars and Holtslag (1991) provide evidence that the difference between the Louis (1979) approach and an exact calculation can be large in stable situations. Therefore, an efficient iterative approach which explicitly solves for the Obukhov length as a function of the surface Richardson number has been implemented using the general recommendations of Beljaars and Holtslag (1991). The transition of the surface fluxes to the free convection regime is implemented in a fashion similar to Beljaars (1994).

The original cloud fraction approach in RAMS-3a was to designate it either as zero or one but no values in between. The Ek and Mahrt (1991) cloud fraction scheme has been introduced as described by Mocko and Cotton (1995). It has been implemented in a way such that cloud fractions in the unstable boundary layer are a function of the horizontal mesh size, the surface moisture flux, and the standard deviation of the vertical velocity.

5. Model Output

Hourly average values of all needed variables will be saved for each episode. The biogenic emission model and URM-1ATM require certain meteorological fields that RAMS does not compute directly but which can be derived from the basic state variables. Table 7 gives a list of the variables which will be delivered to GIT, classifies it as “basic” or “derived,” specifies its dimension, and gives the units in which it is expressed.

6. Evaluation of Meteorological Fields

Since externally available data is blended into RAMS solutions via FDDA, finding independent data sets to evaluate RAMS performance is a potential problem. However, certain routinely observed and independent surface variables exist, and two types of remotely sensed data sets are available that are relevant and useful.

These data sets will provide a reasonable measure of RAMS performance. A relative measure comes from comparing RAMS output with the corresponding output of another meteorological model, such as MM5. Also, comparisons can be made with observations toward which RAMS has been nudged to ascertain how well the model is assimilating the external values. Finally, a subjective method for evaluating RAMS is to examine trajectories generated by a Lagrangian particle model. These matters are discussed in this section.

The quantitative statistical measures that will be used to compare predicted and observed values are described in Appendix D.

6.1 Routine Observations

Three possible categories of routine observations could be used to verify model simulations. The first category is the hourly surface airways dataset which provides surface or near-surface measurements of temperature, pressure, wind, and precipitation at several hundred locations across the United States. Software has been developed which interpolates a given variable to an observed station location and computes error statistics such as the standard deviation and bias. This dataset will likely be the predominant one used for the verification of near-surface variables. The second category is the cooperative network of observations which has a much higher spatial density but which suffers from considerable asynoptic temporal characteristics which make it difficult to use. The third category is the network of rawinsondes which are available every 12 h. Again software has been developed to compare model soundings interpolated to the rawinsonde locations.

6.2 Comparison with Wind/Temperature Profiler Measurements

From June 19 - July 28, 1995, the Southern Oxidant Study (SOS) conducted an intensive field study of the transport of ozone and its precursors in Nashville and the surrounding region of Middle Tennessee. Measurements were taken on both surface and airborne platforms using both direct and remote-sensing methods. Among the instruments used in the study were five wind and temperature profilers. These were located at various points in the Nashville area (Figure 6). Using radar, these devices were able to observe wind speeds and directions from near the surface to about 6 km above the surface. Using sodar, they were able to observe temperatures from near the surface to about 0.7 km above the surface. The resulting profiles are generally available every hour for the entire study period.

To take advantage of the rich set of observations with which model output can be compared, RAMS will be run initially over the SAMI domain for the period July 11-19, 1995. For each hour of this period the RAMS velocity components will be compared with the corresponding values from the profilers at various levels. Figure 7 shows how wind speeds calculated by RAMS compared with wind speeds measured by the three profilers closest to Nashville for four vertical layers during July 9-18, 1995. The winds were taken from a RAMS run made by the Wisconsin Department of Natural Resources for OTAG. Figures of this type can assist in revealing biases in RAMS predictions and will be used in this manner to evaluate modeling carried out for SAMI. Similarly, comparisons will be made of RAMS and observed temperature profiles in the first few hundred meters of the atmosphere.

6.3 Comparison of Cloud Fields with Satellite Images

Modeled cloud fields can be compared with satellite images to determine how well the moist physics of the model are working. Visible and infrared images are available hourly from NOAA geostationary satellites. Techniques are available for mapping these cloud fields into modeling domains so that grid-cell comparisons can be made of location, height, and optical thickness of clouds. This technique will be used to evaluate the performance of RAMS for one episode for which precipitation or extensive cloud cover is known to have occurred and for which satellite images are readily available. A summary of the techniques for processing satellite images for comparison with model results is given in Appendix E.

6.4 Comparison with MM5 Output

One of the ways in which MM5 is potentially superior to RAMS is the number of available cumulus parameterizations (seven in MM5 compared to one in RAMS). MM5 will be run for a wet, convective episode using the Kain-Fritsch parameterization (Kain and Fritsch, 1993) to provide a comparison against the Kuo scheme of RAMS. In a comparison of several cumulus parameterizations Wang and Seaman (1997) found that no particular one exhibited superior behavior in all simulations but the Kain-Fritsch parameterization had several desirable characteristics including relatively good performance in warm-season events.

A comparison of MM5 and RAMS output for the same episode cannot be a pure comparison of cumulus parameterization schemes. Aside from the differences in the two schemes, MM5 and RAMS are based on somewhat different implementations of atmospheric physics and are initialized according to different procedures. However, using observed precipitation amounts at stations across the modeling domain judgments can be made about the performance of each model.

The modeling protocol for RAMS as described in Sections 2, 3, and 4 of this document will also apply to MM5 simulations except that data to initialize and provide time-dependent boundary values for the model will come from MM5's own data analysis package.

6.5 Lagrangian Particle Model Trajectory Visualizations

A subjective but useful means of examining the flow fields produced by RAMS is by flow visualization. One way to do this is by driving a Lagrangian particle model (LPM) with the output of RAMS. UAH has a LPM (McNider, 1981; McNider et al., 1988) that can be used for this purpose.

The LPM releases fictitious particles sequentially anywhere within the domain. Once released, the particles are subjected to the grid-scale flow fields of the meteorological model and may also be subjected to turbulent transport from subgrid-scale flows. The results are displayed graphically, either as single frames or as animations. Use of the LPM is straightforward and consumes little extra computer time. Therefore, the LPM will be used with every episode using major source regions and selected locations in complex terrain as release points.

7. Post-Processing of Meteorological Fields

RAMS was not designed for the purpose of providing input to URM-1ATM nor was URM-1ATM designed to receive the output of RAMS. Therefore, a number of post-processing steps will have to be performed before the output from RAMS can be used in URM-1ATM. These steps include transformations between different map projections and adjustments to insure conservation of mass.

7.1 Map Projections

The horizontal wind components in RAMS are Cartesian components and are not components relative to a

spherical earth. The RAMS wind components will be rotated to "true" north-south and west-east components by UAH for use by GIT.

7.2 Interpolation of RAMS Fields to the URM-1ATM Grid

GIT will perform the necessary horizontal and vertical interpolations on the RAMS output data to the URM-1ATM model grids as well as rotation of the "true" horizontal wind components to the Cartesian components on the URM-1ATM grid. Further details are contained in the SAMI Air Quality Modeling Protocol (Russell *et al.*, 1997).

7.3 Conservation of Mass

The final step in converting RAMS fields to appropriate URM-1ATM input is to correct for a loss of conservation of mass. The combination of spatial interpolation and different continuity equations between RAMS and URM-1ATM can give rise to mass conservation errors in the URM-1ATM model. A common technique for rectifying the problem is to adjust the vertical velocity in the "new" model (here, URM-1ATM) so that mass conservation is enforced. The details of how GIT will do this can be found in the SAMI Air Quality Modeling Protocol (Russell *et al.*, 1997).

8. Computational Considerations

Table 7 gives estimates for the total run time for 78 days on three machine configurations: a 75 MHZ SGI, one 500 MHZ DEC-ALPHA, and two 500 MHZ DEC-ALPHAs. The total run time of 78 days is based on 62 chosen days plus 16 "ramp-up" days needed on the basis of 2 "ramp-up" days for 8 episodes. The time estimates given are purely computer time and do not reflect the time costs needed for run initialization, debugging, etc.

9. Quality Assurance

The model simulations carried out by UAH will make use of either RAMS or MM5, models recognized by atmospheric scientists as incorporating currently acceptable technology for representing atmospheric processes. The role of quality assurance in the modeling efforts of UAH will be to ensure that the critical steps in the modeling process can be accounted for, and if necessary, duplicated. To this end the program of quality assurance described below will be implemented.

9.1 Appropriateness of Input Data Sets

Meteorological and air-quality models must be appropriately initialized and be supplied with appropriate boundary values if the results of a model simulation are to be meaningful. For the same reason the input files used to establish a model configuration for a simulation must be appropriate to the problem under investigation. Often differences of opinion exist on the suitability of the data to be used for these purposes. Traditionally the issue has been settled by opening the modeling process up to peer review and allowing experts to pass judgment on the matter by independently critiquing the papers and presentations of their colleagues. This approach, which has a long-standing history of utility and success in the modeling

community, will be employed by UAH. Input data sets for each episode will be available for inspection for anyone on the SAMI Modeling sub-committee or for any other expert the sub-committee chooses.

9.2 File Documentation

Five main groups of files are associated with each model run: the atmospheric data for the initial and nudging fields, the surface characteristics files for fields such as terrain, input file(s) specifying model options, the output of the model itself, and the model source code. Three copies of each file group will be maintained: one on the machine where it was produced, one on the long-term disk storage on the local Cray, and one on a workstation backup tape. In addition, the input file(s) specifying model options will be appended to each model output file. The final measure to insure file documentation will be a careful log file which will show the date of the simulation and the names of the input data sets. The logs will make use of a consistent system of identification codes for associating the files with the simulation.

ACKNOWLEDGEMENTS

The first four authors would like to acknowledge and thank Stephen F. Mueller and his staff at Tennessee Valley Authority who assembled and edited this report. Plots for most of the UAH diagrams were created by the National Center for Atmospheric Research (NCAR) Graphics package. NCAR is supported by the National Science Foundation. The 500-mb geopotential height anomaly plots were obtained from the National Oceanic and Atmospheric Administration - Cooperative Institute for Research in Environmental Sciences (NOAA-CIRES) Climate Diagnostics Center (CDC) web page. Much of the data required to run and verify the meteorological simulations was obtained from NCAR's Scientific Computing Division's (SCD) Data Support Section. Other important datasets were obtained from the Earth System Science Center (ESSC) of the Pennsylvania State University and the International Satellite Land Surface Climatology Project (ISLSCP).

References

- Anthes, R. A. and T. T. Warner, 1978. Development of hydrodynamic model suitable for air pollution and other mesometeorological studies. Mon. Wea. Rev. **106**, 1045-1078.
- Arakawa, A. and V. R. Lamb, 1977. Computational design of the basic dynamical process of the UCLA general circulation model. In Methods of Computational Physics, **Vol. 17**, 174-265. 337 pp.
- Arritt, R. W., R. T. McNider, and R. A. Pielke, 1987. Numerical model evaluation of the extension of the critical dividing streamline hypothesis to mesoscale two-dimensional terrain. Atmos. Environ., **30**, 1905-1913.
- Atwater, M. A. and P. S. Brown, Jr., 1974. Numerical calculation of the latitudinal variation of solar radiation for an atmosphere of varying opacity. J. Appl. Meteor., **13**, 289-297.
- Barnes, S. L., 1973. Mesoscale objective analysis using weighted time-series observations. NOAA Tech. Memo. ERL NSSL-62, National Severe Storms Laboratory, Norman, OK 73069, 60 pp, [NTIS COM-73-10781].
- Beljaars, A. C., 1994. The parameterization of surface fluxes in large-scale models under free convection. Q. J. R. Meteorol. Soc., **121**, 255-270.
- Beljaars, A. C. M. and A. A. M. Holtslag, 1991. Flux parameterization over land surfaces for atmospheric models. J. Appl. Meteor., **30**, 327-341.
- Casey, D. M., R. T. McNider, and A. J. Song, 1995. A quantitative analysis of the predictability of mesoscale convective activity in regions of weak synoptic forcing over the southeastern United States. *Fourteenth Conference on Weather Analysis and Forecasting*, Jan. 15-20, 1995, Dallas, Texas, Am. Meteor. Soc.
- Chang, J. S., R. A. Brost, I. S. A. Isaksen, S. Madronich, P. Middleton, W. R. Stockwell, and C. J. Walcek, 1987. A three-dimensional eulerian acid deposition model: physical concepts and formulation. J. Geophys. Res., **92**, D12, 14681-14700.
- Chen, C. and W. R. Cotton, 1983. A one-dimensional simulation of the stratocumulus-capped mixed layer. Bound.-Layer Meteor., **25**, 289-321.
- Diak, G. R., C. Gautier, and S. Masse, 1982. An operational system for mapping insolation from GOES satellite data. Solar Energy, **28**:371-376.
- Diak, G. R. and C. Gautier, 1983. Improvements to a simple physical model for estimating insolation from GOES data. J. Appl. Meteor., **22**: 505-508.
- Ek, M. and L. Mahrt, 1991. A formulation for boundary layer cloud cover. Ann. Geophys., **9**, 716-724.

- Fast, J. D., 1995. Mesoscale modeling and four-dimensional data assimilation in areas of highly complex terrain. J. Appl. Meteor., **34**, 2762-2782.
- Fast, J. D., S. Zhong, and C. D. Whiteman, 1996. Boundary layer evolution within a canyonland basin. Part II: Numerical simulations of nocturnal flows and heat budgets. J. Appl. Meteor., **35**, 2162-2178.
- Fu, Q., S. K. Krueger, and K. N. Liou, 1995. Interactions of radiation and convection in simulated tropical cloud clusters. J. Atmos. Sci., **52**, 1310-1328.
- Gautier, C., G. Diak, and S. Masse, 1980. A simple physical model to estimate incident solar radiation at the surface from GOES satellite data. J. Appl. Meteor., **19**: 1005-1012.
- Gautier, C., 1982. Mesoscale insolation variability derived from satellite data. J. Appl. Meteor., **21**: 51-58.
- Grell, G. A., J. Dudhia, and D. R. Stauffer, 1994. *A Description of the Fifth-Generation Penn State/NCAR Mesoscale Model (MM5)*. NCAR Technical Note NCAR/TN-398+STR, National Center for Atmospheric Research, Boulder, Colorado.
- Kain, J. S. and J. M. Fritsch, 1993. Convective parameterization for mesoscale models: The Kain-Fritsch scheme. *The Representation of Cumulus Convection in Numerical Models*, Meteor. Mono., No. 46, Amer. Meteor. Soc., 165-170.
- Kalnay, E., M. Kanamitsu, R. Kistler, W. Collins, D. Deaven, L. Gandin, M. Iredell, S. Saha, G. White, J. Woollen, Y. Zhu, M. Chelliah, W. Ebisuzaki, W. Higgins, J. Janowlak, K. C. Mo, C. Ropelewski, J. Wang, A. Leetmaa, R. Reynolds, R. Jenne, and D. Joseph, 1996. The NCEP/NCAR 40-year reanalysis project. Bull. Amer. Meteor. Soc., **77**, 437-471.
- Koch, S. E., M. DesJardins, and P. J. Kocin, 1983. An interactive Barnes map analysis scheme for use with satellite and conventional data. J. Climate Appl. Meteor., **22**, 1487-1503.
- Kondratyev, K. Y., 1969. Radiation in the Atmosphere. (New York: Academic Press).
- Kuo, H. L., 1974. Further studies of the parameterization of the influence of cumulus convection on large scale flow. J. Atmos. Sci., **31**, 1231-1240.
- Louis, J. F., 1979. A parametric model of vertical eddy fluxes in the atmosphere. Bound.-Layer Meteor., **17**, 187-202.
- Lynch, P., 1989. Partitioning the wind in a limited domain. Mon. Wea. Rev., **117**, 1492-1500.
- Lyons, W. A., C. J. Tremback, and T. W. Tesche, 1991. Model Performance Evaluation and Sensitivity Testing. Prognostic meteorological modeling protocol for the Lake Michigan Ozone Study, Version 2. Lake Michigan Air Directors Consortium, 2350 East Devon Ave., Des Plaines, Illinois 60018.

- MacDonald, J. E., 1960. Direct absorption of solar radiation by atmospheric water vapor. J. of Meteor., **17**, 319-328.
- Mahrer Y. and R. A. Pielke, 1977. A numerical study of the air flow over irregular terrain. Contrib. Atmos. Phys., **50**, 89-113.
- McCumber, M. C. and R. A. Pielke, 1981. Simulation of the effects of surface fluxes of heat and moisture in a mesoscale numerical model. Part I: Soil layer. J. Geophys. Res., **86**, 9929-9938.
- McNider, R. T., 1981. Investigation of the impact of topographic circulations on the transport and dispersion of air pollutants. Ph.D. dissertation, Dept. of Environmental Sciences, University of Virginia, 210 pp.
- McNider, R. T. and R. A. Pielke, 1981. Diurnal boundary layer development over sloping terrain. J. Atmos. Sci., **38**, 2198-2212.
- McNider, R. T. and R. A. Pielke, 1984. Numerical simulation of slope and mountain flows. J. Climate and Appl. Meteor., **23**, 1441-1453.
- McNider, R. T., M. Moran and R. A. Pielke, 1988. Influence of Diurnal and Inertial Boundary Layer Oscillations on Long-Range Dispersion. Atmos. Environ., **22**, 2445-2462.
- McNider, R. T., A. J. Song, D. M. Casey, P. J. Wetzel, W. L. Crosson, and R. M Rabin, 1994. Toward a dynamic-thermodynamic assimilation of satellite surface temperature in numerical atmospheric models. Mon. Wea. Rev., **122**, 2784-2803.
- McNider, R. T., J. A. Song, and S. Q. Kidder, 1995. Assimilation of GOES-derived solar insolation into a mesoscale model for studies of cloud shading effects. Int. J. Remote Sensing, **16**, 2207-2231.
- McNider, R. T, W. B. Norris, D. M. Casey, J. E. Pleim, S. J. Roselle, and W. M. Lapenta, 1997. Assimilation of satellite data in regional air quality models. Twenty-Second NATO/CCMS International Technical Meeting on Air Pollution Modeling and Its Application in Clermont-Ferrand, France, June 2-6, 1997.
- Mellor, G. L. and T. Yamada, 1982. Development of the turbulent closure model for geophysical fluid problems. Rev. Geophys. Space Phys., **20**, 851-875.
- Messinger, F. and A. Arakawa, 1976. Numerical Methods Used in Atmospheric Models. GARP Publication Series, No. 14, WMO/ICSU Joint Organizing Committee, 64 pp.
- Mocko, D. M. and W. R. Coton, 1995: Evaluation of fractional cloudiness parameterizations for use in a mesoscale model. J. Atmos. Sci., **52**, 2884-2901.
- Mueller, S. F., A. Song, W. B. Norris, S. Gupta, and R. T. McNider, 1996. Modeling pollutant transport

- during high-ozone episodes in the southern Appalachian mountains. J. Appl. Meteor., **35**, 2105-2120.
- O'Brien, J. J., 1970. Alternative solutions to the classical vertical velocity problem. J. Appl. Meteor., **9**, 197-203.
- Ozone Transport Assessment Group, 1996. Modeling Protocol, Version 3.0.
- Pielke, R. A., 1974. A three-dimensional numerical model of the sea breeze over south Florida. Mon. Wea. Rev., **102**, 115-134.
- Pielke R. A., W. R. Cotton, R. L. Walko, C. J. Tremback, W. A. Lyons, L. D. Grasso, M. E. Nicholls, M. D. Moran, D. A. Wesley, T. J. Lee, and J. H. Copeland, 1992. A comprehensive meteorological modeling system--RAMS. Meteor. Atmos. Phys., **49**, 69-91.
- Poulos, G. S. and J. E. Bossert, 1995. An observational and prognostic numerical investigation of complex terrain dispersion. J. Appl. Meteor., **34**, 650-669.
- Ruggaber, A., R. Dlugi, and T. Nakajima, 1994. Modelling radiation quantities and photolysis frequencies in the troposphere. J. Atmos. Chem., **18**, 171-210.
- Russell, A. G., R. McNider, J. Moody, and J. Wilkinson, 1997. Air Quality Modeling Protocol. Southern Appalachian Mountains Initiative, Asheville, North Carolina.
- Seaman, N. L., 1992. Meteorological modeling applied to regional air-quality studies using four-dimensional data assimilation. In Environmental Modeling, ed. P. Melli and P. Zanetti (Southampton: Computational Mechanics Publications), 65-88.
- Seaman, N. L., D. R. Stauffer, and A. M. Lario-Gibbs, 1995. A multiscale four-dimensional data assimilation system applied in the San Joaquin Valley during SARMAP. Part I: Modeling design and basic performance characteristics. J. Appl. Meteor., **34**, 1739-1761.
- Smagorinski, J., 1963. General circulation experiments with the primitive equations, Part I, The basic experiment. Mon. Wea. Rev., **91**, 99-164.
- Tremback, C. J. and R. Kessler, 1985. A surface temperature and moisture parameterization for use in mesoscale numerical models. Preprints, *Seventh Conf. on Numerical Weather Prediction*, Montreal, Que., Canada, Amer. Meteor. Soc., 17-20.
- Tripoli, G. J. and W. R. Cotton, 1982. The Colorado State University three-dimensional cloud/mesoscale model--1982, Part I, General theoretical framework and sensitivity experiments. J. Rech. Atmos., **16**, 185-219.
- Wang, W. and N. L. Seaman, 1997. A comparison study of convective parameterization schemes in a mesoscale model. Mon. Wea. Rev., **125**, 252-278.

Zaveri, R. A., R. D. Saylor, L. K. Peters, R. T. McNider, A. Song, 1995. A model investigation of summertime diurnal ozone behavior in rural mountainous locations. Atmos. Environ., **29**, 1043-1065.

Appendix A. RAMS

A.1 Description of RAMS

RAMS is a three-dimensional, primitive-equation model that uses terrain-following coordinates. It represents the merger of a hydrostatic model originally developed at the University of Virginia (Pielke, 1974; Mahrer and Pielke, 1977; McNider and Pielke, 1981, 1984) and a nonhydrostatic model developed by Tripoli and Cotton (1982) at Colorado State University. The surface energy budget is maintained using radiative fluxes, latent and sensible heat fluxes, and subsurface heat conduction. Shortwave parameterization is by Mahrer and Pielke (1977); longwave parameterization, by Chen and Cotton (1983). Subsurface heat conduction is provided by a soil temperature model (Tremback and Kessler, 1985). Turbulence is parameterized using a 1.5-closure scheme developed by Mellor and Yamada (1982). RAMS provides for the inclusion of terrain elevations, land use, and land-water fractions. RAMS also provides for four-dimensional data assimilation (FDDA). This feature allows large-scale evolution to be incorporated through the domain boundaries and observations within the domain to be blended with the model-calculated tendencies to control error growth.

There is no limit either on RAMS domain size or on its cell mesh size. The model can be used to simulate large-scale atmospheric systems on the order of a planetary hemisphere, mesoscale flows over subcontinental regions, microscale phenomena such as tornadoes, and submicroscale turbulent flow over buildings. In view of the complexity of mountain flows, RAMS' ability to resolve small-scale phenomena is advantageous. RAMS employs two-way grid nesting that allows large-scale and small-scale phenomena to be modeled simultaneously.

A.2 Previous RAMS Applications

A considerable amount of the use of RAMS and its predecessor models by UAH investigators has centered around a study of flows affected by topography. McNider developed the first three-dimensional simulations of small-scale slope and valley flows (McNider, 1981; McNider and Pielke, 1984) and investigated large-scale sloping terrain (McNider, 1981). Using mesoscale models, Arritt *et al.* (1987) also carried out an analysis of the role of thermally driven topographic flow in altering Froude-number dependent plume-impact models, such as CTDMPLUS. Recently the role of the Great Smoky Mountains in influencing the regional circulation and in initiating convection has been investigated using models and satellite data (Casey *et al.*, 1995). The UAH efforts most directly related to this work have been modeling studies which investigated the role of terrain in ozone exposure at high elevations and the impact on modulating the diurnal ozone profile (Zaveri *et al.*, 1995). For six weeks under the SOS program, UAH also carried out real-time RAMS simulations over the Southeast during the Nashville field intensive campaign. The model was initialized and nudged at the boundaries using the Eta model forecasts. The ozone field was initialized using noon observations from state monitoring sites and transported in the simulations as a passive scalar.

Pielke *et al.* (1992) have conducted a survey of the range of RAMS applications. These extend from large-eddy simulations to synoptic-scale weather systems and from mid-latitude tornadoes to subtropical thunderstorms. In particular in very recent studies, Poulos and Bossert (1995), Fast (1995), Fast *et al.* (1996), and Mueller *et al.* (1996) describe studies in which RAMS is used to simulate flows over complex

terrain including FDDA.

RAMS has been applied to locations in the SAMI region. In an unpublished study, UAH used the hydrostatic predecessor of RAMS (UVA/CSU) to model the Southern Appalachians. The simulation was able to reproduce the grid scale updrafts over the elevated terrain and the subsidence over the surrounding regions. Mueller *et al.* (1996) employed RAMS, along with a Lagrangian particle dispersion model, to identify a meteorological modeling methodology that can be used in regional photochemical modeling and to identify large regional ozone precursor sources that may impact the southern Appalachians during periods having high ozone levels. With respect to the first goal, a number of approaches were tested. A hydrostatic model with homogeneous initialization, RAMS run nonhydrostatically with homogeneous initialization, and RAMS run nonhydrostatically with nonhomogeneous initialization and FDDA were evaluated against observations. The last method best reproduced observed wind patterns.

Appendix B. MM5

MM5 is the fifth generation of the Penn State/NCAR Mesoscale Model originally developed by Anthes in the early 1970's and later documented by Anthes and Warner (1978). The current version has been documented by Grell *et al.* (1994).

MM5 is a grid-point model with finite differences centered in space and time. Second-order finite differences are used for the advection terms, and an Asselin time filter is applied to all prognostic variables. The model can be run either in a hydrostatic or nonhydrostatic mode. The hydrostatic option uses split semi-explicit time integration for efficient treatment of the fast gravity modes. The nonhydrostatic option uses semi-implicit time integration for the sound-wave modes. The horizontal grid uses the Arakawa-Lamb B staggering in which scalars are defined at the center of a grid square and eastward and northward velocity components are defined at the corners. MM5 uses normalized pressure differences (sigma coordinates) for its vertical coordinate system. Vertically, all variables are carried at half-sigma levels except for vertical velocity, which is carried at full-sigma levels.

MM5 is capable of both one-way and two-way nesting up to nine domains with nests at the same level being allowed to overlap. Options are provided for initializing nests. MM5 is also capable of FDDA to allow observations to be input to the model over an extended period of time using forcing terms that nudge the solution toward the observations while maintaining realistic continuity of flow and geostrophic and thermal-wind balances. The model is able to modify flows according the shape of the terrain underlying the model domain. It also allows for thirteen land-use categories that account for seasonal changes in climatological values of albedo, roughness length, longwave emissivity, heat capacity, and moisture availability. Calculations can be carried out on model grids that are either in the Lambert conformal, polar stereographic, or Mercator projections.

Appendix C. Initialization Procedures

The National Centers for Environmental Prediction (NCEP)/National Center for Atmospheric Research (NCAR) reanalysis data (Kalnay et al., 1996) (hereafter referred to as "data" or "reanalysis data") was chosen as the main data source for the initial and boundary condition files for the 96-km meteorological grid for two reasons: 1) it provides a consistent, easily available dataset for any episode chosen for this study, and 2) it provides a source for variables such as soil moisture which are not synoptically available over large areas. The reanalysis product used for the three-dimensional fields was the data on a Gaussian horizontal grid and a sigma grid vertically with respect to pressure (i.e., sigma-p). The horizontal resolution is on the order of 1.9° while the vertical resolution has 28 levels.

The important points of the process required to convert the reanalysis data into a form compatible for the RAMS model will now be discussed briefly. This involves three basic steps: a horizontal interpolation, a vertical interpolation, and a wind adjustment. The horizontal step uses a Barnes (1973) analysis scheme implemented in a manner similar to Koch et al. (1983) to obtain the values of the required variables on the reanalysis sigma-p surfaces at the horizontal locations of the RAMS horizontal grid. A weighted-average of a Barnes (1973) analysis of the surface airways observations of the wind at 10-m and the reanalysis winds at 10-m provides the lowest level of data for the vertical interpolation of the wind data.

The vertical interpolation involves three heights: the reanalysis terrain height, the model terrain height, and an estimate of the mixed layer depth. A stability dependent function with respect to the reanalysis data, F , is defined in (C.1),

$$F = \left| r^2 (z-E)^{-2} \frac{\rho q \rho^2 q}{\rho z \rho z^2} \right| \quad (C.1)$$

where r is density, q is the potential temperature, and z and E are the height above sea level and terrain height for the reanalysis data, respectively. An estimate of the top of the mixed layer, Z_m , is then defined by the highest level where $F \geq 10.0 \text{ kg K}^3 \text{ m}^{-8}$ with a potential temperature lapse rate $\leq 1.0\text{e-}03 \text{ K m}^{-1}$. The height differences dz_1 , dz_2 , and dz_g are then defined by (C.2)-(C.4), where E^* is the model terrain height.

$$dz_1 = Z_m - E \quad (C.2)$$

$$dz_2 = |E^* - E| \quad (C.3)$$

$$dz_g = \max [dz_1, dz_2] \quad (C.4)$$

For variables other than the wind components and for the situation where the model terrain is less than or equal to the data terrain, i.e., $E^* < E$, the vertical profile is divided into three regions using the heights Z_c and Z_p as defined in (C.5) and (C.6).

$$Z_c = E + dz_g \quad (C.5)$$

$$Z_p = E^* + dz_g \quad (C.6)$$

For heights with respect to the model terrain, z^* , which are at or above Z_c , the model values are obtained by simple linear interpolation with respect to height from the data values. For the region $Z_p \leq z^* \leq Z_c$, the model values are obtained from a linear regression using data values between the heights Z_p and Z_c . For the region below Z_p , the data gradient values are utilized according the descriptions given in (C.7)-(C.10), where the index "k" refers to data vertical levels and the index "l" refers to model vertical levels. The

difference between the data and model terrain heights is added to the data heights as in (C.7) so that they can be referenced with regard to the model height values. The bottom and top weights for the linear interpolation of the data gradient values to the model level "l" are described in (C.8). The estimated gradient value at model level "l" is then given by (C.9), where "A" can be any scalar data variable. The actual model value of "A" at level "l" is then calculated by extrapolating downward from the value above as in (C.10).

$$Z_a = z + E^* - E \quad (C.7)$$

$$\left\{ \begin{array}{l} \text{for } z_a(k) \leq z^*(l) \leq z_a(k+1), \\ w_b = \frac{z_a(k+1) - z^*(l)}{z_a(k+1) - z_a(k)}, \\ w_t = 1 - w_b \end{array} \right. \quad (C.8)$$

$$\left. \frac{\nabla A}{\nabla z} \right)_l = w_b \left. \frac{\nabla A}{\nabla z} \right)_k + w_t \left. \frac{\nabla A}{\nabla z} \right)_{k+1} \quad (C.9)$$

$$A^*(l) = A^*(l+1) - \left. \frac{\nabla A}{\nabla z} \right)_l [Z_a(k+1) - z^*(l)] \quad (C.10)$$

For the wind components for the situation where the model terrain is less than or equal to the data terrain, the vertical profile is divided into only two regions. For model heights which are at or above Z_c , the model values are obtained by simple linear interpolation. For model heights below Z_c , the model values are obtained by expanding or contracting the equivalent reanalysis data layer using regression of the data wind values with respect to the natural logarithm of height. Some of the details of this procedure will now be discussed. The heights of the wind 10 m above the data and model terrain are denoted as in (C.11) and (C.12). Using the slope and intercept defined in (C.13) equation (C.14) is the linear relationship or mapping between the reanalysis data heights z and the corresponding heights Z_a on the model vertical grid. Three different linear regressions are then performed on the data wind components in the layer between Z_c and Z_{10}^* using the adjusted heights Z_a . The three regressions are shown in (C.15)-(C.17), where "B" is a u or v wind component. The slope \mathbf{b} remains the same for the three regressions but the intercept values change. In (C.15) the regression line for the estimated wind component is forced to match the data value at the level Z_c . In (C.16) the estimated wind component is forced to match the data value with the largest magnitude in the layer from Z_c to Z_{10}^* at level Z_{\max} . Finally, in (C.17) the estimated wind component is forced to match the data value at Z_{10} . The actual model value at a model grid level is then a weighted average of two of the three estimates. The determination of which two estimates are used depends on whether z^* is between Z_c and Z_{\max} or whether z^* is between Z_{\max} and Z_{10}^* . This approach has three advantages: it allows for continuity of the wind components relative to the layer above where direct interpolation of the wind data are performed, it allows any wind maximum in the layer to be captured, and it allows for matching the data winds at the 10-m level.

$$Z_{10}^* = E^* + 10 \text{ meters} \quad (\text{C.11})$$

$$Z_{10} = E + 10 \text{ meters} \quad (\text{C.12})$$

$$S_z = \frac{Z_c - Z_{10}^*}{Z_c - Z_{10}}, \quad b_z = (1 - S_z)Z_c \quad (\text{C.13})$$

$$Z_a = S_z z + b_z \quad (\text{C.14})$$

$$B_t = \mathbf{b} \ln(z^*) + b_t \quad (\text{C.15})$$

$$B_b = \mathbf{b} \ln(z^*) + b_b \quad (\text{C.16})$$

$$B_m = \mathbf{b} \ln(z^*) + b_m \quad (\text{C.17})$$

For the situation where the model terrain is greater than the data terrain, i.e., $E^* > E$, the vertical profile is divided into only two regions for all variables. For model heights which are at or above Z_c , the model values are again obtained by simple linear interpolation. For variables other than the wind components the region below Z_c , the data gradient values are utilized according the descriptions given in (C.7)-(C.10) as described above. The wind components in the region below Z_c are handled in the same way as described above as well.

Barnes (1973) analyses of temperature and specific humidity at 2-m from the surface observations are used to adjust the temperature and moisture fields on the RAMS grid after the vertical interpolation just described. The depth over which this adjustment occurs is the largest of either the mixing depth Z_m or a specified minimum depth, which is usually on the order of 500-1000 m. The profiles of temperature and specific humidity are changed over this depth in a linear fashion to match the observed analyses at 2 m. The stability of each column is then checked and corrected to remove any layers above the bottom layer where potential temperature decreases with height.

The bulk of the computational time is spent in the third and final step which is the wind adjustment. The combination of horizontal and vertical interpolation and the differences in the terrain between the reanalysis data and the RAMS terrain introduce small changes in the divergent component of the wind which if left uncorrected generally lead to large, unrealistic vertical velocities at the top of the model domain. First the divergence and the relative vorticity are calculated on the RAMS grid. The divergence in each column is then adjusted as a function of height after O'Brien (1970) in order to obtain a vertical velocity near zero at the top of the model domain which is consistent with the top boundary condition used in RAMS. The subsequent approach to the wind calculations is then essentially after Lynch (1989). The total wind is divided into divergent, rotational, and harmonic components. The harmonic wind is defined such that it has neither vorticity or divergence. The velocity streamfunction and potential fields are obtained by solving Poisson's-type equations with the known relative vorticity and adjusted divergence by simultaneous over-relaxation with a Dirichlet boundary condition of zero. Gradients of the streamfunction and potential fields then give the rotational and divergent wind components, respectively. The sum of the derived rotational and divergent wind components is then subtracted from the total wind on the domain border to obtain the first-guess of the border values of the harmonic wind. These perimeter values of the harmonic wind

are then adjusted such that their line integral around the perimeter is zero which insures the nondivergence of the harmonic component. The velocity potential for the harmonic component is then calculated in the same way using simultaneous over-relaxation with a Neumann boundary condition provided by the perimeter values of the harmonic wind. Gradients of the velocity potential then give the harmonic wind over the entire domain. The final wind field is then obtained by summing the divergent, rotational, and harmonic components over the entire three-dimensional domain.

Appendix D. Statistical Measures for Model Evaluation

Bias: The average of the differences between modeled and observed values.

$$Bias = \frac{1}{n} \sum_{i=1}^n (M_i - O_i)$$

A positive (negative) bias indicates the model is overpredicting (underpredicting) on the average.

Standard Error: The standard deviation of the differences between modeled and observed values.

$$Standard\ Error = \sqrt{\frac{1}{n} \sum [(M_i - O_i) - Bias]^2}$$

The standard error is a measure of the dispersion of the modeled values from the observed values.

Correlation: The normalized covariance of modeled and observed values.

$$Correlation = \frac{Cov(M, O)}{\mathbf{s}_M \mathbf{s}_O}$$

where

$$Cov(M, O) = \frac{1}{n} \sum_{i=1}^n (M_i - \bar{M})(O_i - \bar{O})$$

\bar{M} and \bar{O} (\mathbf{s}_M and \mathbf{s}_O) are the means (standard deviations) of the modeled and observed values.

Appendix E. Satellite Image Processing Techniques

Three satellite data-processing techniques that will be needed for carrying out work of meteorological model evaluation are described.

E.1 Method 1: Surface Insolation from Satellite Images

The GOES-7 (GOES-8) satellite returns the magnitude of upwelling radiation as brightness counts in the range 0-63 (0-1023). Relative to land and water, cloud tops are highly reflective and usually result in larger brightness counts. In general, the deeper the cloud, the greater its ability to reflect radiation in the visible range. Counts of intermediate magnitude indicate a mixture of radiation reflected from both cloud top and the earth's surface. The lowest counts arise when little or no cloud is present and the reflection is primarily, if not entirely, from the earth's surface. Our insolation model has been developed to compute surface albedo and insolation values from visible images observed by GOES satellites (McNider *et al.*, 1995; McNider *et al.*, 1997). The heart of the model is a radiative-transfer technique patterned after that of Gautier *et al.* (1980), Gautier (1982), Diak *et al.* (1982), and Diak and Gautier (1983), which is used to convert hourly GOES brightness data into surface insolation.

The technique requires hourly surface albedo obtained from clear-sky brightness counts. If a single, cloud-free image were available for each hour of daylight, the brightness counts could be obtained directly from them. However, because cloudy skies are so common, a single, cloud-free image is usually not available. Our experience has shown that for a given daylight hour images over a period of 20-30 days are needed to obtain a stable minimum brightness count for that hour, especially in the Southeast during summer when cumulus clouds are ubiquitous. Brightness counts are converted into reflectances using a formula unique to each satellite. This approach has the inherent ability to account for both spatial and temporal differences in albedo due to soil type, vegetation, and time of day and year.

Once the clear-sky albedo and the brightness count are known for a given satellite-image pixel, surface insolation at the pixel can be calculated from the radiative-transfer model of Gautier *et al.* (1980). The model assumes a single cloud layer. Above the cloud layer, radiation is Rayleigh scattered and absorbed by water vapor. In the cloud layer, radiation is scattered and absorbed. Below the cloud layer, radiation is absorbed by water vapor. For the scattering coefficients, we use the parameterization originally presented by Kondratyev (1969) and modified by Atwater and Brown (1974). For the water-vapor absorption coefficients, we use an empirical formulation of MacDonald (1960). For in-cloud absorption we use a step function that depends on brightness count (McNider *et al.*, 1995). This results in a quadratic equation in cloud albedo. Once known, cloud albedo can be used to calculate downwelling solar radiation and insolation at the surface. The procedure yields surface insolation at each pixel in an image. Such images can be gridded and values for all pixels within a grid cell averaged to produce hourly input fields for assimilation into photochemical models, or, as for the case we are proposing, for comparing with the hourly insolation fields predicted by a meteorological model.

E.2

Method 2: Cloud-Top Altitudes from Satellite Images

Photochemical modeling systems differ in their sources of photodissociation constants. In some cases these are obtained from radiative transfer models that include the scattering, absorbing, or reflecting properties of atmospheric aerosols and clouds (e.g., Ruggaber *et al.* 1994). In other cases radiative transfer models assume clear skies, and correction factors are later applied to the results to obtain the desired cloudy-sky values (e.g., Chang *et al.*, 1987). In either approach cloud information is essential. Cloud information is sometimes obtained directly from National Weather Service observations. In other cases it is obtained from meteorological models that handle moisture dynamically and thermodynamically either through parameterizations or microphysics.

We have already mentioned the shortcomings of these data sources--the sparseness, lack of frequency, and subjectivity of the National Weather Service observations, and the errors in cloud placement, extent, and timing of the meteorological-model predictions--and have pointed out how satellite observations can overcome many of these weaknesses. Calculating the effect of clouds on photolysis frequencies requires a knowledge of cloud altitude and thickness. For example, RADM approximates the cloud optical depth t with the parameterization

$$t = 3L_{con}\Delta z_{cld}/2r_{H_2O}r$$

where L_{con} is the mean condensed water content, Δz_{cld} is the mean depth of the cloud layer, r is the mean cloud drop radius, and r_{H_2O} is the density of water (Chang *et al.*, 1987). In RADM, constant values are assumed for each factor except Δz_{cld} , which is obtained from the meteorological model.

Cloud-top elevations can be estimated using infrared satellite images. Just as with visible images, GOES-7 (GOES-8) returns infrared measurements in discrete counts in the range 0-63 (0-1023). These values can be transformed into temperatures using radiative transfer equations. If the area corresponding to a pixel is covered with clouds, the temperature associated with the pixel is that of the top of the clouds. If a temperature sounding is available near the location of the pixel at the time of the satellite measurement, the pressure level, and hence the elevation, at cloud top can be determined. At this point in the development of the technique, for a given pixel we are using the sounding from the closest rawinsonde station and are linearly interpolating in time between successive soundings.

A potential shortcoming of the method is using the sparse and relatively infrequent NWS soundings. Another potential shortcoming arises from the relatively low resolution of infrared pixels. The 8 x 8 km (4 x 4-km) area of a GOES-7 (GOES-8) infrared pixel may be only partially covered by clouds so that the temperature value returned by the satellite for that pixel is a weighted mean of the surface and cloud-top temperatures, T_{avg} . In such cases the method, without further modification, would produce a cloud-top elevation lower than that of the actual cloud top. Because the horizontal resolution of GOES-7 and GOES-8 visible images (1 x 1 km) exceeds that of GOES-7 (GOES-8) infrared images by a factor of 64 (16), the visible image corresponding to an infrared image can be used to quantify the fraction a of an infrared pixel covered by cloud. If the surface temperature T_{sfc}

for the pixel is known or can be estimated (perhaps directly from a surface measurement or from a neighboring clear pixel), then the temperature of the cloud top T_{cld} can be estimated by solving the following equation:

$$T_{avg} = (1 - \sqrt{a})T_{sfc} + \sqrt{a}T_{cld}$$

We have found that the square-root weighting provides more consistent results than a linear weighting. A third possible shortcoming arises from the fact that the infrared sensor sees only the top of the uppermost cloud layer. We compute the elevation of the cloud base as the lifting condensation level, which is the elevation of the cloud base for the lowest cloud layer. If cloud thickness is computed as the difference between cloud top and cloud base, too large a thickness will be calculated when multiple cloud layers are present in the troposphere. The problem can be particularly troublesome when lower cloud decks are shielded from the satellite sensor by cirrus.

E.3 Method 3. Surface (Skin)-Temperature Changes from Satellite Images

Biogenic and soil NO_x emissions rates depend on surface temperature. The ability of atmospheric models to predict surface temperatures would be improved if concurrent surface-temperature observations could be successfully assimilated into the calculations. We have developed a method, employing infrared satellite images, that is capable of assimilating surface temperature rates of change into boundary-layer models. The method allows us to calculate surface temperatures that are completely consistent with values calculated for all other variables in the model. We have tested the method in one- and three-dimensional models for cases not involving photochemical modeling (McNider *et al.*, 1994; McNider *et al.*, 1997).

In principle, the performance of atmospheric models should be improved if observations are blended at appropriate times into the models' calculations via FDDA. FDDA has not worked well for surface temperatures because they are not always compatible with the calculated vertical profiles of either the air or soil. By altering the slopes of temperature profiles near the surface, the approach may cause predicted dispersion rates and other variables depending on the temperature gradient to be significantly affected (Seaman, 1992). Our method for assimilating temperature observations overcomes the difficulty.

Surface temperature is produced from the interplay of a number of processes. Among these are those that govern net radiation, sensible and latent heat flux at the earth-air interface, and heat flux through the top few centimeters of soil. Some of these variables vary widely over space and time. For example, even if latent-heat flux is correctly initialized throughout the domain of a photochemical model, it is difficult for the model to accurately predict future values since it depends on the "friction humidity" of similarity theory, which is intrinsically difficult to measure or calculate. Our method allows us to skirt the need for knowing the value of friction humidity. By assimilating observed temperature *rates of change* into the model, we automatically account for the combined effect of all processes affecting surface temperature, including those pertaining to heat flux. Other types of satellite data can also be assimilated into the models.

Table 1. Specifications of the RAMS Coarse Grid System	
Horizontal Resolution:	96 km
Number of East/West Cells	35
Number of North/South Cells	31
Number Vertical Cells:	35
Center Latitude:	37.800° N
Center Longitude:	85.100° W
Northwest Corner	
Latitude:	48.742° N
Longitude:	107.289° W
Southwest Corner	
Latitude:	23.858° N
Longitude:	100.902° W
Southeast Corner	
Latitude:	23.858° N
Longitude:	69.298° W
Northeast Corner	
Latitude:	48.742° N
Longitude:	62.911° W

Table 2. Specifications of the RAMS Intermediate Grid System	
Horizontal Resolution:	24 km
Number of East/West Cells	62
Number of North/South Cells	58
Number Vertical Cells:	35
Center Latitude:	36.484° N
Center Longitude:	82.951° W
Northwest Corner	
Latitude:	42.477° N
Longitude:	91.679° W
Southwest Corner	
Latitude:	30.227° N
Longitude:	90.699° W
Southeast Corner	
Latitude:	29.973° N
Longitude:	75.547° W
Northeast Corner	
Latitude:	42.133° N
Longitude:	73.895° W

Table 3. Specifications of the RAMS Fine Grid System	
Horizontal Resolution:	12 km
Number of East/West Cells	84
Number of North/South Cells	68
Number Vertical Cells:	35
Center Latitude:	36.578° N
Center Longitude:	82.276° W
Northwest Corner	
Latitude:	40.194° N
Longitude:	87.997° W
Southwest Corner	
Latitude:	32.725° N
Longitude:	87.734° W
Southeast Corner	
Latitude:	32.725° N
Longitude:	77.093° W
Northeast Corner	
Latitude:	39.904° N
Longitude:	76.302° W

Table 4. Specifications of the RAMS Ultra-Fine Grid System		
Horizontal Resolution	4 km	
	Great Smoky Mt. NP	Shenandoah NP
Number of East/West Cells	71	68
Number of North/South Cells	44	32
Number Vertical Cells:	35	35
Center Latitude	35.733°N	38.495°N
Center Longitude	83.014°W	79.503°W
Northwest Corner		
Latitude	36.478°N	39.024°N
Longitude	84.603°W	81.079°W
Southwest Corner		
Latitude	34.931°N	37.909°N
Longitude	84.572°W	81.055°W
Northeast Corner		
Latitude	36.479°N	39.025°N
Longitude	81.469°W	77.974°W
Southeast Corner		
Latitude	34.932°N	37.909°N
Longitude	81.499°W	77.998°W

Table 5. Specification of Vertical Grid Spacing		
Cell Level No.	u,v and scalar vertical grid	w vertical grid
35	16866.71	17366.71
34	15866.71	16366.71
33	14866.71	15366.71
32	13866.71	14366.71
31	12866.71	13366.71
30	11866.71	12366.71
29	10866.71	11366.71
28	9866.71	10366.71
27	8866.71	9366.71
26	7866.43	8366.71
25	6859.91	7366.71
24	5923.04	6371.05
23	5115.68	5505.26
22	4413.64	4752.40
21	3803.16	4097.74
20	3272.32	3528.47
19	2810.71	3033.45
18	2409.31	2603.00
17	2060.27	2228.70
16	1756.76	1903.22
15	1492.83	1620.19
14	1263.33	1374.08
13	1063.77	1160.07
12	890.23	973.97
11	739.33	812.15
10	608.12	671.43
9	494.01	549.07
8	394.79	442.67
7	308.52	350.15
6	233.49	269.70
5	168.26	199.73
4	111.53	138.90
3	62.20	86.00
2	19.30	40.00
1	-18.00	0.00

Variable	Type	Dimension	Units
u wind component	Basic	3	m s^{-1}
v wind component	Basic	3	m s^{-1}
vertical wind component	Basic	3	m s^{-1}
density	Basic	3	N m^{-2}
pressure	Basic	3	mb
temperature	Basic	3	K
water vapor mixing ratio	Basic	3	g kg^{-1}
vertical turbulent exchange coeff.	Basic	3	$\text{m}^2 \text{s}^{-2}$
u wind component at 10 m	Basic	2	m s^{-1}
v wind component at 10 m	Basic	2	m s^{-1}
temperature at 2 m	Basic	2	K
water vapor mixing ratio at 2 m	Basic	2	g kg^{-1}
grid-scale cloud base	Derived	2	m
grid-scale cloud top	Derived	2	m
convective cloud base	Derived	2	m
convective cloud top	Derived	2	m
convective cloud area	Derived	2	%
liquid precipitable water	Derived	2	mm
convective fraction of total precipitation rate	Derived	2	%
mixing height	Derived	2	m
surface shortwave radiative flux	Basic	2	W m^{-2}
total precipitation rate	Basic	2	mm s^{-1}

The second row labeled "Ratio" is the ratio of CPU time divided by the simulation time for a two-way nested run with the 96, 24, and 12 km grids. The total simulation time is derived from the minimum number of days to be modeled by current estimates which are 62 actual days over 8 episodes plus 2 "ramp-up" days per episode which gives a total simulation time of 78 days. The columns then give the actual estimated time to run all days with the UAH SGI machine, one DEC-ALPHA, and two DEC-ALPHA machines. See the text for further details.

Table 7. Estimated RAMS Execution Times			
Parameter	75 MHZ SGI	500 MHZ DEC-ALPHA	Two 500 MHZ DEC-ALPHA
Ratio	4.16	1.04	1.04
Time for 78 days	324 days	81 days	41 days